Facultad de Ciencias

Departamento de Biologia Molecular

DESARROLLO DE NUEVAS TÉCNICAS DE DILUCIÓN ISOTÓPICA ESTABLE Y ANÁLISIS MASIVO POR ESPECTROMETRÍA DE MASAS APLICADAS AL ESTUDIO MOLECULAR DE ENFERMEDADES CARDIOVASCULARES Y AL ESTADO DINÁMICO DEL REDOXOMA TIOL

Memoria presentada para optar al grado de

Doctor en Ciencias por el licenciado

Pablo Martínez Acedo

Director de Tesis:

Prof. Jesús Vázquez Cobos

Co-directora de Tesis:

Dra. Estefanía Núñez Sánchez

Madrid, 2012

A mi esposa Naiara y mi hijo Pablo.

A mis padres.

A mis hermanos y mis sobrinos.

Sois los picos más intensos del espectro de mi vida.....

AGRADECIMIENTOS

Permettez-moi d'inscrire votre nom en tête de ce livre et au-dessus de sa dédicace; car c'est à vous, surtout, que j'en dois la publication ... Acceptez donc ici l'hommage de ma gratitude, qui, si grande qu'elle puisse être, ne sera jamais à la hauteur de votre éloquence et de votre dévouement. Gustave Flaubert 'Madame Bovary'

Los que me conocen saben que soy hombre de pocas palabras. Pero en esta ocasión, llegando al cruce de caminos en el que me encuentro y mirando hacia atrás, me doy cuenta de que me faltan palabras y espacio para darles las gracias a todas esas personas que han compartido conmigo este caminar *tésico*. Todo lo que me han enseñado, como persona y como científico.

Jesús. JV. ¿Cómo no iba a ser el Prof. Jesús Vázquez, director de esta tesis doctoral y "*el jefe*", primero de esta lista? Tú creíste en mí hace 5 años y me diste la oportunidad cuando llegué de Francia para emprender aquí mi camino científico. Has conseguido trasmitirme tu pasión por la Proteómica y la Espectrometría de Masas. Nunca aprendí tanto como cuando te apartabas de la estadística y del ordenador para "*trastear*" con los equipos... Has seguido creyendo en mí día tras día, "*dándome caña*" para sacar lo mejor que tengo. No sé si lo habrás conseguido, no soy quién para decirlo, pero te estaré eternamente agradecido por ello.

A todos los que han sido mis compañeros de batalla en el C-001 de Biológicas de la UAM, el 311 del Centro de Biología Molecular Severo Ochoa, o en el Centro Nacional de Investigaciones Cardiovasculares: ha sido un privilegio y un gran honor compartir tantas horas a vuestro lado. No hubiese podido aterrizar en un laboratorio mejor. Quiero darle las gracias de manera especial a la Dra. Estefanía Núñez, co-directora de este trabajo. Steffy, además de tu amistad, me llevo en mi bagaje tu rigor en el trabajo y tu calidad científica. Siempre me has apoyado y dado buenos consejos (aunque yo siempre tenga razón...) ¿Qué va a pasar con el jersey que estábamos tricotando? A la Dra Inma Jorge, con quién empecé mi aventura proteómica y que puso las bases de mi formación. A Daniel Pérez, compañero de faena doctoral, siempre dispuesto a ayudar y a compartir sus conocimientos. Por cierto, ¿3+2? A la Dra. Elena Bonzón, que con su afán de conocimiento, siempre aporta innovación al trabajo y buenos consejos. A Marco, que temblaba cada vez que lo llamaba: ¡la de bugs que he visto! Gracias por facilitarme el trabajo. A Raquel, que sin saberlo es *lab manager* del equipo: no sé qué sería de nosotros si no estuvieras en el laboratorio; gracias por la confianza que trasmites y tu amistad. A Pilar y Fernando, los novatos que han tomado el relevo: estoy convencido de que hubiese aprendido mucho a vuestro lado; gracias por vuestra amistad, vuestra alegría y vuestras ganas de aprender. Y a las nuevas incorporaciones con las que, desgraciadamente, poco he compartido: Juan-Carlos, tu buen humor y saber hacer me han ayudado mucho en este *sprint* final, siempre dispuesto a ayudar; Mariano, seguro que hubiese aprendido mucho y disfrutado aún más discutiendo de orgánica...

No puedo ni quiero olvidarme de todos los que han pasado por el laboratorio. De manera especial, quiero agradecerle al Dr. Pedro Navarro su amistad, sus numerosos conocimientos compartidos, las risas que nos echamos, y las calibraciones y pulguitas compartidas. También por facilitarme la vida con ese software tan maravilloso y "*completamente automático*"... Al Dr. Horacio Serrano que me acompañó en los inicios de este caminar: gracias por la paciencia inicial y tus grandes consejos (¡todavía hay frases que recuerdo y digo!). De manera especial quiero dar las gracias a la Dra. Elena Burillo: ¡qué gran fichaje hubieses sido para el laboratorio! Gracias por tu gran amistad y por tu positividad, por tu rigor y espíritu crítico y científico.

Al personal de los servicios de Proteómica del CBMSO y del CNIC: Anabel, Yoli, Espe, Merche, Sandra, Inés, Carlos y Nuria, Emilio, Enrique y Juan Antonio. Todos habéis participado en mi formación proteómica, aunque de manera más cariñosa, quiero agradecerle a Anabel sus trucos de secuenciación y sus conocimientos de trampas, y a Espe y Yoli por sus trucos para el día a día con cualquier protocolo. ¡Y también por lo mucho que nos hemos reído juntos! A Enrique, por transmitirme una parte de lo que sabe de Orbis y de HPLC-nano.

Son muchos los colaboradores que han participado en este trabajo. Quiero darles las gracias a la Dra. Arántzazu Alfranca y al Prof. Juan-Miguel Redondo del CNIC por haber sido los primeros "en sufrir" nuestro análisis de datos... Al Prof. Santiago Lamas del CBMSO, por compartir sus conocimientos y sus buenos y numerosos consejos, así como a los Dres. Patricia Rodríguez, Mariano Redondo-Horcajo y Francisco J Sánchez en especial: del gran trabajo colaborativo ha surgido una amistad, y no hemos terminado ni "*oxidados*" ni "*estresados*" (bueno, no mucho...). En el mundo redox también tengo que darle las gracias a Antonio Martínez-Ruíz por su paciencia y por las numerosas conversaciones químicas de las que siempre ha salido una loca idea... También agradecerles al Prof. Dr. José Antonio Bárcena y el Dr. Brian McDonagh de la Universidad de Córdoba por su ciencia y amistad, por sus conocimientos y buen humor. Por último, y no por ello menos importante, quiero agradecerles de corazón a los Dres. David García-Dorado, Marisol Ruiz-Meana y Elisabet Miró-Casas del Hospital Universitari Vall d'Hebron por su amistad y su visión mitocondrial de los problemas biológicos

Bien évidemment, je ne pouvais oublier mon passé français... Nombreux sont ceux avec qui j'ai partagé d'excellents moments d'amitié été de Science. En premier lieu, je tiens à me souvenir de mes compagnons de fac, sans qui ces années à Jussieu n'auraient pas été si bonnes, tout particulièrement mon bon ami Jacques Peuscet. La camaraderie universitaire est devenue amitié sincère : merci pour tous tes bons conseils et pour ton exemple de courage et de motivation. C'est toujours un plaisir de prendre un café avec toi et d'apprendre de ton expérience. Finalement, je tiens à remercier de tout cœur la famille Bourgeois (Sam et Gene) et Florence : j'ai vécu des moments inoubliables à vos côtés et je ne vous ai jamais remercié pour votre amitié, votre patience et vos excellents conseils. Vous avez tous les 4 une place dans ma vie.

A todas las personas fuera del ambiente del laboratorio que he conocido y que me han brindado ayuda y amistad. A Bernabé Bodas de Thermo, por ser tan atento y siempre generoso. A Mada de la UAM, gracias porque siempre que te he solicitado, has respondido presente con una sonrisa y una efectividad inigualable. A Predes, siempre con una sonrisa, dispuesta a escuchar y ayudar, dando unos consejos inigualables...

Pero si hoy estoy aquí, si he llegado adónde he llegado y soy la persona que soy hoy, las gracias se las tengo que dar a mi familia. A mi esposa Naiara, razón principal de mi venida a Madrid. Te he dicho muchísimas veces (y lo seguiré haciendo) lo mucho que te quiero, pero nunca te he dado las gracias por estar cada día a mi lado, comprendiéndome, apoyándome, animándome y dándome fuerzas, motivándome. Sencillamente, eres la mejor. A mi hijo Pablo: ya leerás estas líneas dentro de unos años y quiero que sepas que, desde que naciste, has llenado mi vida de alegría y serenidad, de ternura y amor. Por ti, todo ha merecido y merece la pena. A mis padres, que siempre han confiado en mí sin dudar ni un solo segundo. Si soy quién soy y como soy, es gracias a vosotros: gracias por vuestro sacrificio y vuestro ejemplo. A mis hermanos Yolanda y Jorge, *ma sœur et mon beau-frère*: siempre me habéis apoyado en todas mis

decisiones y me habéis dado los mejores consejos, incluso motivándome cuando las dudas me acechaban. Gracias a vosotros aprendí que nunca hay que rendirse. Sois modelos para mí en todos los aspectos. Y como no darles las gracias a mis sobrinos Jorge y Teresa (Jaime, aún eres muy pequeño...) por su inocencia, su ternura y sus miradas: sin saberlo ni quererlo, me habéis ayudado y transmitido la energía que necesitaba en los malos momentos y que sólo vosotros podías hacer. A vosotros, mi familia: gracias por estar ahí.....

La Proteómica cuantitativa, que se define como el estudio de los cambios de expresión de un proteoma determinado, ha experimentado un gran desarrollo en los últimos años. Los métodos cuantitativos basados en espectrometría de masas constituyen una alternativa robusta frente a las técnicas basadas en electroforesis bidimensional. En este trabajo, presentamos un método de cuantificación masiva basado en el marcaje enzimático con $^{16}O/^{18}O$ y en un modelo estadístico novedoso que permite un análisis profundo de una gran variedad de proteomas. Esta tecnología se ha aplicado al estudio de los mecanismos moleculares implicados en la angiogénesis en el endotelio vascular, mediante el análisis de los cambios de expresión producidos por la estimulación de células endoteliales del cordón umbilical humano con el factor pro-angiogénico VEGF durante 4 y 8 h. Los resultados obtenidos sugieren que la técnica de marcaje con ^{18}O y análisis posterior mediante espectrometría de masas en trampa iónica lineal, en combinación con un algoritmo que permite el control de la eficiencia de marcaje y un modelo estadístico robusto, constituye una alternativa semi-automática y prometedora para la realización de estudios de expresión diferencial de proteínas a gran escala mediante marcaje isotópico estable.

La Proteómica cuantitativa aplicada al estudio de las modificaciones redox (PTMOs) constituye aún un reto a nivel tecnológico, debido a la naturaleza lábil de algunas de las principales PTMOs a nivel de los grupos tiol, así como a la falta de herramientas para la identificación de los residuos modificados y el desarrollo tardío de los espectrómetros de masas de alta resolución. En esta tesis, se ha desarrollado un método simple y directo para el análisis de los cambios dinámicos que tienen lugar en el redoxoma, GELSILOX. Brevemente, los proteomas se someten a un proceso de doble alquilación que permite diferenciar el estado de oxidación de los residuos de cisteína, digestión en gel, marcaje diferencial con $^{16}O/^{18}O$ y separación mediante IEF seguido del análisis mediante espectrometría de masas en trampa iónica lineal. La técnica GELSILOX permite la cuantificación de los cambios de oxidación de los grupos tiol en un elevado número de péptidos utilizando un modelo estadístico novedoso, así como la identificación de la cisteína modificada y el análisis y cuantificación simultáneos del resto del proteoma en un mismo experimento. El método GELSILOX nos ha permitido caracterizar las principales dianas redox del peróxido de hidrógeno en células endoteliales y revela un aumento del estado de oxidación de los grupos tiol tras un período de hipoxia. Además, utilizando esta técnica, hemos detectado dianas redox modificadas tras procesos de isquemia-reperfusión en mitocondrias de corazón de rata, demostrando que dichas modificaciones son revertidas en animales que son sometidos previamente a precondicionamiento isquémico. Por otro lado, también se puede abordar el estudio del papel fisiológico de las especies reactivas de nitrógeno y oxígeno mediante el uso de técnicas de proteómica dirigida sobre la proteína de interés. En este trabajo, se aplicó la técnica de monitorización de iones de fragmentación específicos utilizando una trampa iónica lineal para demostrar que la CsA induce la nitración de la Tyr en posición 34 de la enzima MnSOD, ofreciendo una explicación bioquímica a la inactivación de la enzima y al efecto tóxico de la CsA.

Quantitative proteomics, which may be defined as the study of global changes in the expression level of proteins, is a field that has experimented a great development in the last years. MS-based quantitative proteomic methods are a very solid alternative to the well-established gel-based techniques. However, reliable MS-based high-throughput quantification is still a challenge. Here, we present a high-throughput quantitative proteomics method based on enzymatic $^{16}O/^{18}O$ labeling, that allows a rapid, solid and deep analysis of a wide variety of proteomes on the basis of a recently developed statistical model. This technology was applied to the study of molecular mechanisms underlying angiogenesis in vascular endothelium, analyzing expression changes in the protein profile of human umbilical vein endothelial cells (HUVEC) in culture in response to the pro-angiogenic factor VEGF after 4- and 8-h incubation. A quantitative study was also performed with liver cell cultures to analyze the effect of a pharmacological agent at two different concentrations. Results obtained in these model suggest that the ^{18}O labeling protocol and analysis by linear ion trap mass spectrometry, in conjunction with a computational algorithm that allows a precise control of labeling efficiency and a robust and validated statistical model, provides a promising and semi-automated alternative to perform large-scale studies of differential expression of proteins by stable isotope labeling.

Quantitative redox proteomics still remains a technical challenge, mainly because of the labile nature of some thiol-redox modifications, the lack of tools to directly detect the modified residues and the relatively late development of highly sensitive analytical instruments. A simple and straightforward method for the analysis of the dynamic redox proteome has been developed, GELSILOX. Briefly, proteomes are subjected to double alkylation to differentially label the oxidation state of Cys, in-gel digestion, differential $^{18}O/^{16}O$-labeling and IEF fractionation followed by LC-LIT-MS/MS analysis. GELSILOX allows the precise quantification of oxidative thiol modifications in several hundreds of peptides using a new statistical approach and determining the exact Cys modified, as well as the simultaneous differential quantification of the whole proteome in the same experiment. GELSILOX permits the characterization of the major endothelial redox targets of hydrogen peroxide in endothelial cells and reveals that hypoxia induces a significant increase in the status of oxidized thiols. GELSILOX also detected thiols that are redox-modified by ischemia-reperfusion in heart mitochondria and demonstrated that these alterations are abolished in ischemic-preconditioned animals. The study of the physiological role of reactive nitrogen and oxygen species can also be achieved using targeted proteomics on a protein of interest. The Selected MS/MS Ion Monitoring technique using a linear ion trap mass spectrometer was used to demonstrate that CsA induced specific MnSOD tyrosine 34 nitration both in the recombinant protein and in endothelial cells overexpressing the protein, offering a biochemical explanation for the enzyme inactivation and the toxic effect of CsA.

ACN Acetonitrilo

amu Unidades atómicas de masa

BAEC Células endoteliales de aorta bovina

CsA Ciclosporina A

EDTA Ácido etilendiaminotetraacético

EGTA Ácido etilenglycoltetraacético

ETC Cadena de transporte de electrones mitocondrial

FDR Tasa de error

HPLC Cromatografía líquida de alta prestación

HUVEC células de cordón umbilical humano

IAM yodoacetamida

ICAT Etiquetas de afinidad codificadas por isótopos

IEF Isoeletroenfoque

IFM Mitocondrias intermiofibrilares

IP Precondicionamiento isquémico

IR Isquemia-reperfusión

iTRAQ Etiquetas isobáricas para cuantificación relativa y absoluta

LIT Trampa iónica lineal

LTQ Cuadrupolo de confinamiento lineal

MMTS Metil metanotiosulfonato

MnSOD Superóxido dismutasa de manganeso

MS Espectro de masas

MS/MS o MS^2 Espectro de masas en tándem o espectro de fragmentación

m/z masa / carga

NEM N-etil maleimida

PBS Tampón fosfato salino

PTMs Modificaciones postraduccionales

PTMOs Modificaciones postraduccionales oxidativas

pRatio Razón de probabilidades

RP Cromatografía líquida de fase reversa

SCX Cromatografía de intercambio catiónico fuerte

SDS-PAGE Electroforesis en gel poliacrilamida con dodecilsulfato sódico

SIL Marcaje con isótopos estables

SILAC Marcaje isotópico estable con aminoácidos en cultivos celulares

SMIM Monitorización de iones de fragmentación específicos

SRM Monitorización selectiva de reacción

SSM Mitocondrias subsarcolemales

TFA Ácido trifluoroacético

VEGF Factor de crecimiento endotelial vascular

INTRODUCCIÓN

I.1.- Definición de la Proteómica

El término "Proteoma" apareció en 1995 y fue definido como el conjunto de PROTeínas expresadas por el genOMA de una línea celular, un tejido o un organismo [1, 2], aunque los primeros estudios globales de las proteínas, que bajo la perspectiva actual podrían ser considerados como trabajos de Proteómica, se remontan a 1975 con la introducción de la electroforesis bidimensional [3-5].

Como elemento perteneciente a las tecnologías –ómicas, la Proteómica se puede definir como una disciplina que comprende un conjunto de metodologías orientadas al análisis de proteínas a gran escala con el objetivo de caracterizar globalmente y desde un punto de vista dinámico todas las proteínas expresadas por un sistema biológico en un entorno y condiciones determinadas, incluyendo sus isoformas, sus modificaciones y sus interacciones. Mientras que el genoma define los actores potenciales de la actividad celular, el proteoma representa los efectores de dicha función [6]. El campo de la Proteómica se ha organizado clásicamente en tres áreas principales:

- Proteómica de expresión, cuya finalidad es la caracterización a gran escala de todas las proteínas contenidas en un tejido, una célula o un orgánulo. La información obtenida en este área de la proteómica permite identificar nuevas proteínas implicadas en la transducción de señales o en el desarrollo de ciertas enfermedades.
- Proteómica de expresión diferencial, cuyo objetivo es estudiar de forma comparativa los cambios dinámicos de expresión del perfil proteico, ya sean estables o transitorios, entre un estado celular normal y patológico, o como consecuencia del tratamiento con fármacos u otros estímulos [7].
- Proteómica de interacción proteína-proteína (o de mapa celular), que surge de la constatación de que, en los organismos eucariotas, las proteínas normalmente actúan formando complejos con otras proteínas y de que numerosos procesos biológicos están regulados por este tipo de interacciones.

En Proteómica aún no se dispone de una metodología tan estándar y robusta como la que se aplica en los proyectos de Genómica, que ha permitido la secuenciación completa de distintos genomas de gran importancia en Biología como el de *Drosophila Melanogaster*, el de *Arabidopsis Thaliana* o el del *Homo Sapiens*. Tampoco se dispone aún de reacciones y metodologías análogas para el análisis, la secuenciación y la amplificación de proteínas. La

principal dificultad del estudio del proteoma, si lo comparamos con los análisis del genoma o del transcriptoma, se debe a la falta de desarrollo de las metodologías para la secuenciación automática y los *arrays* de proteínas. Aun así, las herramientas en tecnología de proteínas han conocido grandes avances, lo que ha contribuido al auge de la Proteómica.

I.2.- Espectrometría de masas y Proteómica

La espectrometría de masas es una técnica analítica que emergió a finales de los años 80 como la más adecuada para el análisis de proteínas [8, 9], aunque se introdujo en el ámbito del análisis de biomoléculas al final de la década de los años 70 [10], convirtiéndose rápidamente en uno de los métodos más utilizados en química analítica. Los desarrollos en los últimos 20 años en este campo han impactado en el área del análisis de proteínas, desplazando totalmente a los métodos tradicionales como la secuenciación de Edman o el análisis de aminoácidos. Estos avances han permitido los estudios a gran escala de investigación del proteoma, que, a su vez, han contribuido a acuñar el concepto de Proteómica. Con la espectrometría de masas, y por primera vez en la historia de la biomedicina, se dispone de una herramienta para el análisis sistemático de las proteínas, que, a fin de cuentas, son los agentes fundamentales de la vida. La espectrometría de masas se revela, por tanto, como una de las tecnologías clave de la ciencia del siglo XXI.

Los espectrómetros de masas miden la relación masa-carga (m/z) de iones generados a partir de un analito, permitiendo la caracterización de un gran número de moléculas a partir de su espectro de masas (MS). Las operaciones básicas de un espectrómetro de masas son la ionización, la separación de iones por su relación m/z en el analizador y su posterior detección midiendo intensidades de flujos iónicos [11].

I.2.1.- La Proteómica "clásica" o de Primera Generación

La estrategia experimental en la que se ha basado la Proteómica desde sus comienzos a principios de los años 90 se basa en la separación previa de las proteínas mediante electroforesis mono o bidimensional en geles de poliacrilamida. En el primer caso, las proteínas se separan atendiendo a su peso molecular y en el segundo caso, primero en función de su punto isoeléctrico y posteriormente en función de su peso molecular [4]. Esta segunda estrategia tiene la ventaja de ser muy resolutiva, permitiendo visualizar más de 1.000 especies proteicas diferentes en un mismo gel. La identificación de las proteínas se lleva a cabo por digestión directa en el mismo gel donde se han separado, usando proteasas altamente específicas y analizando los péptidos obtenidos mediante espectrometría de masas. El análisis

de dichos péptidos utilizando un espectrómetro de masas de tipo MALDI-TOF y la identificación de las proteínas en las bases de datos a partir del mapa o "huella peptídica" [12, 13] permite una identificación rápida y directa de las proteínas mediante la detección precisa de las masas de los péptidos [14, 15]. Cuando la identificación a partir de la huella peptídica no es inequívoca, los péptidos producidos se analizan mediante espectrometría de masas en tándem, que permite obtener espectros de fragmentación (MS/MS o MS^2) [16], los cuales son altamente específicos de la secuencia peptídica. La identificación de los espectros MS/MS se lleva a cabo comparando el espectro obtenido con espectros teóricos generados a partir de bases de datos [14, 17]. Ambas aproximaciones (mapa de péptidos y fragmentación) son complementarias y sinérgicas, y su combinación permite la identificación prácticamente universal de cualquier proteína. Aunque esta estrategia es muy potente, tiene ciertas limitaciones: por ejemplo, las proteínas pequeñas y las muy grandes no son fáciles de analizar mediante electroforesis bidimensional, así como las proteínas de membrana debido a su hidrofobicidad; además, las proteínas poco abundantes, que por lo general juegan un papel fisiológico importante, son difíciles de detectar [18]. Las técnicas electroforéticas sólo permiten la separación y la detección de una parte muy limitada del proteoma, y resultan, en general, poco reproducibles y difíciles de estandarizar [19].

I.2.2.- La Proteómica de Segunda Generación

Una serie de avances recientes ha cambiado el panorama hasta el punto de que hoy en día se habla de una "Proteómica de Segunda Generación" [20]. Estas técnicas se basan en la digestión directa de proteomas en disolución y la identificación a escala masiva de péptidos mediante espectros MS^2, la cual permite una identificación muy fiable en las bases de datos (un único péptido es suficiente para identificar una proteína) [17, 21]. Por una parte, el fraccionamiento por cromatografía líquida bidimensional (intercambio catiónico fuerte y fase reversa) previo al análisis en línea por espectrometría de masas permite la identificación masiva de mezclas complejas de proteínas, de complejos macromoleculares e incluso de proteomas de forma rápida, automática, reproducible y con una cobertura y un rango dinámico superiores a la estrategia electroforética [22, 23]. Por otra parte, el desarrollo de técnicas para el marcaje isotópico de péptidos y la purificación selectiva de los péptidos modificados, han permitido aplicar esta tecnología al análisis de expresión diferencial de proteomas [24, 25] y al análisis sistemático de modificaciones postraduccionales (PTMs) [26, 27]. Estas tecnologías son relativamente estandarizables y asequibles a una completa automatización, y muchos autores ven en ellas el futuro de la Proteómica.

I.3.- Proteómica de expresión diferencial mediante técnicas de segunda generación

Uno de los retos principales de la Proteómica de Segunda Generación es la necesidad de poder realizar estudios cuantitativos de las muestras para el análisis de los cambios dinámicos que afectan al proteoma. El análisis de la expresión diferencial de proteínas es fundamental para entender los procesos biológicos y tiene un papel cada vez más relevante en las investigaciones biomédicas. En paralelo al desarrollo de las técnicas de segunda generación, en los últimos años ha habido un progreso notable en la incorporación de estrategias cuantitativas, fundamentalmente usando dilución isotópica estable. En este tipo de aproximaciones, se comparan dos estados de interés de un mismo proteoma, como por ejemplo la presencia o ausencia de estímulo, marcando los péptidos producidos en cada una de las condiciones con diferentes isótopos de un mismo reactivo y analizando conjuntamente las muestras. De esta forma, en el análisis de la mezcla de los péptidos de la muestra control (A) y de la muestra problema (B), la pareja de péptidos da lugar a un doblete detectado en el MS, cuya intensidad relativa evalúa la proporción exacta de proteína presente en las muestras originales. Este método es enormemente robusto y posee numerosas ventajas frente a los métodos clásicos, fundamentalmente en términos de implementación y aplicabilidad. En las técnicas de marcaje con isótopos estables (SIL), dicho isótopo estable puede ser introducido mediante la incorporación metabólica de aminoácidos isotópicamente marcados en cultivos celulares (SILAC), mediante la utilización de reactivos químicos (ICAT, iTRAQ o TMT), o mediante marcaje enzimático con la introducción de átomos de ^{18}O en el extremo C-terminal de los péptidos producidos mediante digestión tríptica [28].

I.3.1.- El marcaje metabólico o SILAC

El marcaje metabólico ha sido descrito como una técnica cuantitativa muy robusta [29]. Este método se basa en la incorporación de los isótopos de manera metabólica *in vivo* en todas las proteínas, y recibió el nombre de SILAC (Stable Isotope Labeling by Amino acids in Cell culture), aunque originalmente se denominaba AACT (Amino Acid Coded mass Tagging) [30, 31]. En esta aproximación, uno o varios aminoácidos con isótopos pesados (^{13}C y/o ^{15}N) se añaden al medio de cultivo de las células, permitiendo, después de varias generaciones de crecimiento, la incorporación del aminoácido pesado a todas las proteínas durante el proceso anabólico. Posteriormente, se mezcla una misma cantidad de células proveniente de los dos estados biológicos a comparar, se extraen y digieren las proteínas, y los péptidos obtenidos son

cuantificados por espectrometría de masas. Los primeros trabajos publicados utilizando la técnica SILAC se desarrollaron utilizando leucina marcada con deuterio, al ser la leucina el aminoácido esencial más abundante (está presente en más del 50 % de los péptidos trípticos) y el marcaje con deuterio poco costoso [29, 32]. Sin embargo, y debido al efecto isotópico del deuterio en los perfiles de elución cromatográfica que modifica las propiedades del péptido e impide la coelución de los péptidos marcados y sin marcar, a día de hoy se utilizan mayoritariamente la lisina y la arginina marcadas, que ofrecen la ventaja de estar presentes en todos los péptidos trípticos; aunque también se puedan utilizar isótopos de la tirosina para estudiar rutas de señalización [33]. La diferencia de masa entre el péptido marcado y sin marcar depende de la combinación isotópica utilizada ($^{12}C_6{}^{14}N_4$-Arg, $^{13}C_6{}^{14}N_4$-Arg, $^{13}C_6{}^{15}N_4$-Arg, etc.). Existen también otros métodos de marcaje metabólico alternativos, como el enriquecimiento del medio de cultivo con ^{15}N [25]. La técnica SILAC tiene la ventaja de presentar la menor variabilidad debida al tratamiento de la muestra, ya que son las células y no las proteínas o los péptidos los que se mezclan inmediatamente después del marcaje. Esto implica que cualquier pérdida de proteína debida a la lisis celular o la extracción, así como los artefactos que puedan falsear los datos de cuantificación, afectan por igual a las muestras marcada y sin marcar. Sin embargo, como el marcaje de las proteínas tiene lugar de forma metabólica durante su síntesis, la técnica SILAC no es aplicable a ciertos tipos de muestras, como muestras clínicas o de tejidos. En un intento de paliar ese defecto, un estudio reciente ha demostrado que se puede extender la tecnología SILAC a modelos *in vivo* de ratones, suplementando la dieta libre de lisinas de dichos animales con lisina pesada [34], basándose en los trabajos pioneros de Hayter *et al.* en los que obtuvieron una línea de pollos marcados parcialmente tras someterlos a una dieta que contenía valina marcada isotópicamente [35]. Combinando el ratón SILAC con las técnicas de silenciamiento génico, se dispone hoy en día de una estrategia muy potente para realizar estudios de proteómica cuantitativa *in vivo*. Sin embargo, y a pesar de haber aplicado el concepto de "animal SILAC" a otros organismos como *Drosophila melanogaster* [36], esta técnica tiene un elevado coste de generación del modelo así como de su mantenimiento, lo que la hace prohibitiva para la mayoría de los laboratorios de proteómica. Además, esta técnica no se puede aplicar a modelos humanos.

I.3.2.- El marcaje químico

Los métodos de marcaje *in vitro* constituyen una segunda clase de técnicas de dilución isotópica estable utilizadas en proteómica cuantitativa en los que el marcaje se realiza utilizando reactivos químicos marcados isotópicamente que se unen covalentemente a las proteínas o a los

péptidos. Tienen la ventaja de poder utilizarse con cualquier tipo de muestra, pero la variabilidad experimental suele ser mayor que con la técnica SILAC, ya que las muestras marcadas y no marcadas se combinan post-digestión; por lo tanto, las pérdidas de material o los artefactos que ocurran durante la manipulación de la muestra y la generación de péptidos a partir de las proteínas pueden falsear los datos de cuantificación. Se han desarrollado numerosas estrategias para introducir isótopos a nivel de proteínas o de péptidos por reacción química; sin embargo, la aplicabilidad de estas estrategias se ve algo limitada por el coste de los reactivos. La técnica basada en el reactivo ICAT (Isotope Code Affinity Tag) es uno de los métodos de marcaje isotópico químico que más se ha usado [37]. El ICAT se compone de un grupo reactivo específico de Cys (yodoacetamida), de biotina y de un espaciador que contiene el isótopo "ligero" (8 átomos de hidrógeno) o "pesado (8 átomos de deuterio). El reactivo ICAT se une a las Cys de las proteínas en una etapa pre-digestión. A continuación, las dos muestras se mezclan y se digieren con proteasas (tripsina o EndoLys-C) y los péptidos resultantes son purificados por cromatografía de afinidad con avidina, obteniendo fracciones enriquecidas en péptidos que contienen Cys, lo cual simplifica el análisis al ser éste un amino-acido poco abundante en el proteoma (representa el 1.42 % de los aminoácidos presentes en las proteínas [38]). La cantidad relativa de cada proteína presente en las muestras es determinada midiendo la intensidad de cada pico de masa, difiriendo en 8 Da entre las muestras marcada y no marcada, coincidiendo con los ocho hidrógenos intercambiables del reactivo. A pesar de ser uno de los métodos más utilizados originalmente, el ICAT tiene ciertos inconvenientes, como reacciones químicas secundarias debido a la reactividad del reactivo con los extremos N-terminal de las proteínas y con los residuos de Lys, efectos isotópicos en los perfiles de elución de los péptidos con deuterio, problemas de ionización por el gran tamaño de la biotina, así como dificultades a la hora de interpretar los espectros MS/MS al no tener la biotina un patrón definido de fragmentación, además de pérdida de información por la cuantificación exclusiva de los péptidos con cisteína (se estima que entre un 10 y un 13 % de las proteínas no contienen Cys, y, por lo tanto, no son cuantificables con ICAT [39]). Para intentar paliar algunos de estos defectos, se ha desarrollado una nueva generación de reactivos ICAT basados en el ^{13}C, el cICAT, que, además de carecer de los efectos isotópicos del deuterio, contiene una extremidad hidrolizable en medio ácido que separa el reactivo de la biotina, lo que aumenta la calidad de los espectros MS/MS así como el número de péptidos identificados [40].

Más recientemente, se ha desarrollado una aproximación alternativa análoga al marcaje químico de las proteínas con ICAT basada en el reactivo iTRAQ (Isobaric Tags for Relative and Absolute Quantification) [41]. Esta técnica utiliza cuatro reactivos, todos ellos con la misma masa, que reaccionan con las aminas del extremo N-terminal de los péptidos y de las lisinas con un reactivo de grupo (NHS-ester), permitiendo la cuantificación relativa de las proteínas en cuatro muestras biológicas diferentes de forma simultánea ("*multiplexing*"). A diferencia de los métodos SILAC e ICAT, son los péptidos y no las proteínas los que se marcan con el reactivo iTRAQ. Una vez finalizada la reacción química, se mezclan las distintas muestras y se procede a un análisis masivo por espectrometría de masas. En el espectro MS, los péptidos marcados con cualquiera de los reactivos iTRAQ tienen el mismo peso molecular y aparecen como un único pico cromatográfico y, por tanto, se fragmentan a la vez. Durante la fragmentación de los péptidos, la ruptura del reactivo iTRAQ libera iones reporteros mono-cargados (con masas de 114, 115, 116 y 117 Da, respectivamente) que son específicos de cada una de las muestras, permitiendo la cuantificación relativa en función de la intensidad de los mismos. Entre las ventajas de esta técnica cabe destacar la posibilidad de comparar varias muestras en un solo experimento, el hecho de que la cuantificación se lleva a cabo en el espectro de fragmentación, donde la razón señal/ruido es muy superior, y el efecto aditivo que supone sumar la intensidad de las diferentes especies en un único espectro de fragmentación, lo que aumenta su sensibilidad y permite la utilización de una cantidad de muestra menor. Existe otro reactivo iTRAQ que permite comparar 8 muestras [42] y también se ha desarrollado otro basado en la misma química, el TMT, que permite la comparativa de 2 o 6 muestras en un mismo experimento [43].

I.4.- Proteómica de expresión diferencial utilizando marcaje isotópico estable con agua ^{18}O y espectrometría de masas con trampa iónica lineal

La utilización de oxígeno 18 (^{18}O) para la cuantificación de proteínas tiene su origen en los trabajos de Sprinson y Rittenberg de 1951, en los cuales se estudia el mecanismo de retroinhibición en la hidrólisis del enlace peptídico catalizada por quimiotripsina, demostrando que uno de los productos de la reacción (H_2O) es también substrato de la reacción de intercambio de oxígeno [44]. El marcaje con ^{18}O es un marcaje a nivel de péptido que consiste en la incorporación de átomos de ^{18}O en el extremo C-terminal de los péptidos generados por digestión enzimática de las proteínas de una de las dos muestras biológicas a comparar, siendo la tripsina la enzima de mayor uso, aunque se pueden usar otras enzimas de la familia de las serín proteasas, como la proteasa Glu-C, la proteasa Lys-C o la quimiotripsina [28]. El

mecanismo enzimático implica un ataque nucleófilo de $H_2{}^{18}O$ sobre el grupo carbonilo del extremo C-terminal de los péptidos generados por digestión tríptica para la incorporación de un átomo de ^{18}O; la incorporación del segundo átomo de ^{18}O se efectúa por el mismo tipo de mecanismo hasta que se establece un equilibrio entre los péptidos y el $H_2{}^{18}O$ (Fig. I.1).

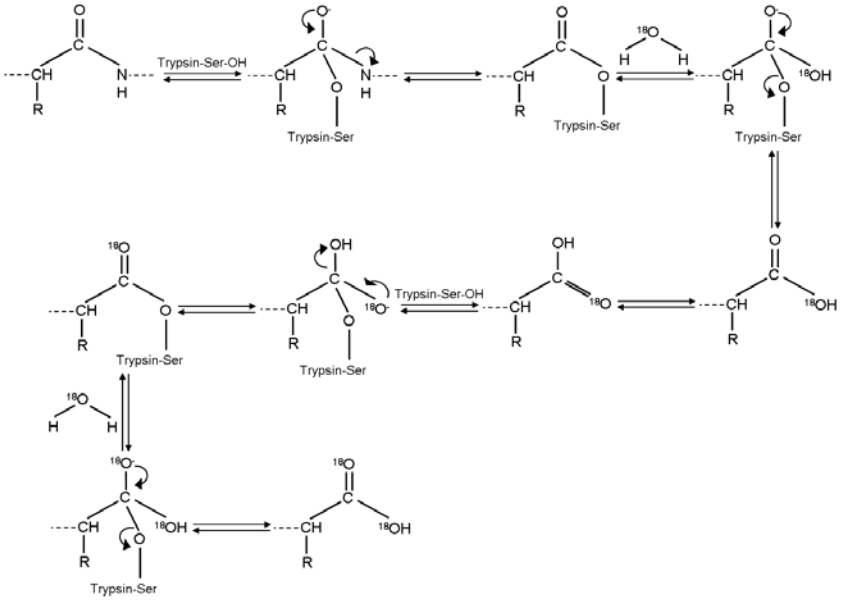

Fig. I.1.- Esquema de la reacción enzimática de incorporación de dos átomos de ^{18}O catalizada por tripsina. El mecanismo requiere que la tripsina reconozca los extremos C-terminal de la lisina o de la arginina en cada péptido como substrato de la reacción. Después de la formación de un aducto acil-enzima entre el péptido y la proteasa, una molécula de agua hidroliza el intermediario e introduce el átomo de ^{18}O.

Una vez marcados los péptidos, éstos se mezclan con los péptidos de la muestra no marcada y se analizan por espectrometría de masas. Las dos especies del péptido (que contienen ^{16}O y ^{18}O, respectivamente) son químicamente idénticas, por lo que coeluyen en un único pico cromatográfico y se detentan simultáneamente en el mismo espectro MS.

La primera aplicación proteómica de esta técnica para cuantificar proteínas a gran escala se llevó a cabo en el año 2001, comparando el perfil proteico de dos serotipos de adenovirus [45]. A partir de ese trabajo pionero, esta técnica llamó mucho la atención de la comunidad científica, debido a una serie de ventajas que ofrecía respecto a otras técnicas SIL:

- A diferencia de SILAC, la técnica es aplicable a todo tipo de muestras: proteomas virales, de cultivos celulares, de suero, de tejidos
- Se marcan todos los péptidos trípticos de la muestra
- Se puede utilizar cuando la cantidad de analito es muy limitada, del orden del µg o para marcar muestras a gran escala

- El marcaje se hace mediante reacción enzimática, y por lo tanto, tiene una especificidad muy alta, evitando reacciones secundarias que falsearían los datos de cuantificación, así como la contaminación de la muestra con los productos de la reacción (el péptido marcado y H_2O)
- El reactivo ($H_2{}^{18}O$) es el menos costoso y se trata de un compuesto altamente estable por lo que no es necesario emplear la totalidad del reactivo en cada reacción.

Sin embargo, y a pesar del interés de la técnica, hoy en día el uso del marcaje con ^{18}O para los estudios de proteómica cuantitativa no está tan extendido como el de las técnicas SILAC o iTRAQ. Este hecho se pone de manifiesto al consultar el número de entradas en las bases de datos bibliográficas para las distintas estrategias de marcaje (71 para ^{18}O, 297 para SILAC y 447 para iTRAQ según una búsqueda de Dic. 2011). Esta falta de popularidad se debe en gran medida al hecho de que, por norma general y hasta el momento, la cuantificación relativa mediante marcaje con ^{18}O se ha considerado una técnica compleja, delicada y de difícil implementación. Si no se controlan de manera muy minuciosa las condiciones de marcaje, la incorporación del ^{18}O a los péptidos puede no ser completa. Además, el etiquetado de ^{18}O es sensible a pH, por lo que no todas las etapas de manipulación de péptidos son compatibles con esta estrategia de marcaje. Estos problemas han impedido el uso generalizado de esta técnica en comparación con los otros métodos SIL. Por tanto, en contra de lo cabría esperar, no existe un protocolo estándar para el marcaje enzimático con tripsina y que exista una gran variedad de aproximaciones experimentales para el marcaje con ^{18}O en la literatura [45-54].

Las diferencias entre los distintos protocolos publicados residen en:

- Las etapas de preparación de la muestra antes del marcaje
- El pH de la reacción a la que se lleva a cabo el intercambio de oxígenos
- La presencia o no de sales de calcio
- La incubación de la mezcla reactiva con o sin solventes orgánicos
- El uso de tripsina en disolución o inmovilizada
- La estrategia seguida para inactivar la tripsina y garantizar la permanencia de la marca.

La diferencia de masa entre las especies marcada y no marcada de un mismo péptido es pequeña (+ 2 Da si el marcaje es incompleto con la incorporación de un solo átomo de ^{18}O, + 4 Da si es completo). Esto ha condicionado previamente el uso de esta técnica de forma exclusiva a espectrómetros de alta resolución debido al solapamiento de las envolturas isotópicas de la

especie no marcada y las especies marcadas con uno y con dos átomos de ^{18}O. Sin embargo, en un trabajo reciente de nuestro laboratorio, se ha demostrado que la espectrometría de masas de baja resolución en una trampa iónica lineal también permite una cuantificación muy precisa de péptidos marcados con ^{18}O [55], aprovechando su alta velocidad de barrido y la posibilidad que ofrece de introducir barridos de media-alta resolución sobre intervalos estrechos de m/z (espectros "*ZoomScan*") (Fig. I.2a).

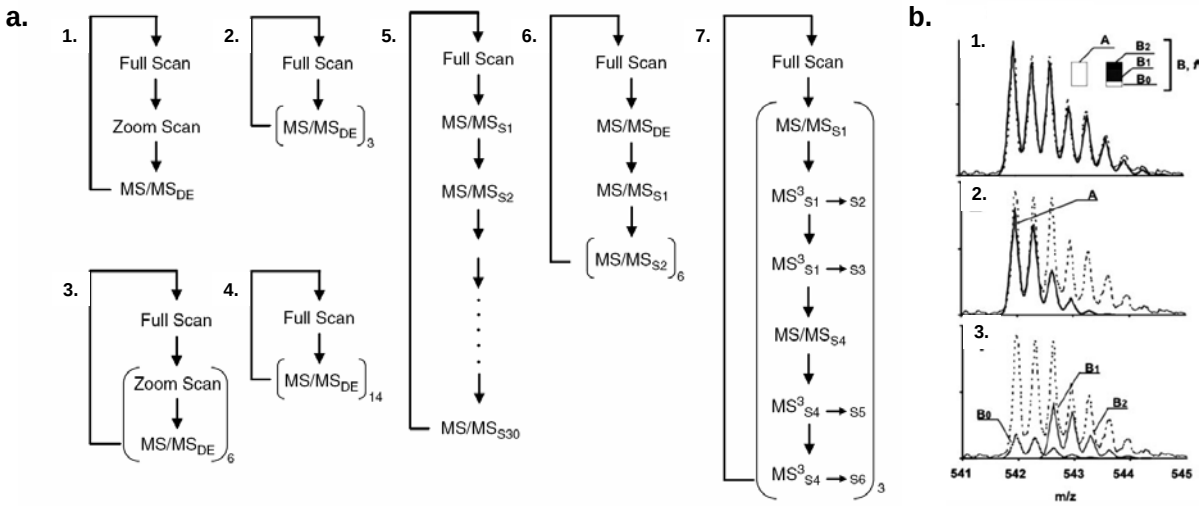

Fig. I.2.- Desarrollo de la técnica de marcaje isotópico en nuestro laboratorio. **(a.)** Ejemplos de modos de barrido en una trampa iónica lineal [56]. El modo de barrido (3.), en la que se alternan 6 *ZoomScans* con 6 MS/MS por ciclo, es el método utilizado para la cuantificación masiva con SIL: los espectros *ZoomScans* se utilizan para obtener la envoltura isotópica de los péptidos que permite calcular su cantidad relativa, y los espectros MS/MS sirven para identificar dichos péptidos. De ese modo, la cuantificación y la identificación se llevan a cabo al mismo tiempo. **(b.)** Estimación de la eficiencia de marcaje con ^{18}O [57]. Se señala la contribución a la envoltura isotópica de cada una de las especies del péptido (A: especie proveniente de la muestra no marcada; B_0, B_1 y B_2, especies provenientes de la muestra sometida a marcaje en la que se han incorporado ninguno, uno o dos átomos de ^{18}O, respectivamente). El algoritmo descompone la envoltura isotópica total en la suma de los cuatro componentes, que se relacionan entre sí por la eficiencia de marcaje.

La abundancia relativa de los dos péptidos puede ser determinada comparando la intensidad de los picos de las especies no marcada y marcada, teniendo en cuenta que la incorporación de ^{18}O puede ser incompleta, incorporándose un solo átomo de ^{18}O [58], siendo necesario corregir los errores introducidos por la superimposición de las envolturas isotópicas de las especies marcadas y no marcadas. En nuestro laboratorio, se ha desarrollado recientemente un método para el cálculo de la eficiencia de marcaje a nivel de péptido y para corregir la incorporación incompleta que aumenta considerablemente la robustez y la automatización de la técnica de marcaje con ^{18}O (Fig. I.2b) [57].

Teniendo en cuenta todas estas consideraciones, nos propusimos en esta tesis continuar los trabajos de nuestro laboratorio, poniendo a punto un protocolo robusto y riguroso de

marcaje con ^{18}O que fuera de aplicabilidad universal y de fácil integración en la rutina de un laboratorio de proteómica, aprovechando la capacidad de cuantificación de la trampa lineal (Fig. I.2a) y el método de cálculo de la eficiencia de marcaje que permite monitorizar en todo momento el porcentaje de incorporación de ^{18}O (Fig. I.2b).

I.5.- Análisis estadístico de experimentos de cuantificación diferencial por marcaje isotópico a gran escala

La proteómica cuantitativa a gran escala genera una gran cantidad de datos y su análisis es considerado un problema que todavía no se ha resuelto satisfactoriamente. Uno de los cuellos de botella principales de dichas aproximaciones es determinar si los cambios de abundancia de las proteínas son reales o artefactuales. Los métodos analíticos existentes para la determinación de la significatividad de los cambios de abundancia de las proteínas en estudios cuantitativos mediante SIL son escasos [59]. La mayoría de estos métodos asumen un muestreo independiente así como una distribución normal de las proporciones relativas de proteínas, sin que ésta haya sido demostrada en un contexto general. Sólo algunos estudios recientes han empezado a estudiar la fiabilidad y las fuentes de error en experimentos de iTRAQ [60, 61], y se han desarrollado algoritmos que estiman los intervalos de confianza de las proporciones de abundancia de proteína determinados por marcaje metabólico $^{14}N/^{15}N$ [62, 63]. La idoneidad de un método de cuantificación utilizando SIL sólo puede establecerse con el análisis de la precisión con la que las proteínas son cuantificadas dentro de un marco estadístico apropiado. Con objeto de desarrollar dicho marco estadístico para el análisis masivo de cambios de expresión de péptidos marcados con ^{18}O, se realizó en el laboratorio un experimento de hipótesis nula a gran escala en el cual una misma muestra se comparó contra sí misma [64]. Este trabajo demostró que los datos de cuantificación masiva no pueden describirse usando métodos estadísticos clásicos basados en distribuciones normales y que la varianza en la población completa de medidas de cuantificaciones relativas no es homogénea [65]. El experimento de hipótesis nula, en el cual no deberían detectarse cambios, reveló que 72 proteínas cambiaban su abundancia de manera estadísticamente significativa con un *p-value* < 0.05, siendo éste un criterio comúnmente utilizado en proteómica cuantitativa; dicho número disminuyó hasta 20 proteínas usando como criterio de significancia la FDR. Estos datos resultan inaceptables desde el punto de vista estadístico, ya que un gran número de los cambios de abundancia que se detectarían en experimentos reales utilizando estos criterios serían falsos. Para paliar estos defectos, se diseñó un modelo estadístico jerárquico novedoso que, por

primera vez, considera por separado los errores a nivel de espectro, de péptido y de proteína, asignando una varianza específica para cada cuantificación [64, 65]. Este modelo estadístico tiene en cuenta cuatro factores que contribuyen al error de la cuantificación:

- Un error sistemático debido a la mezcla de dos muestras para su comparación.
- Un error de medida del espectrómetro de masa, que, sumado al error del ajuste del espectro experimental a la curva teórica de cada medida utilizado para cuantificar, refleja la varianza a nivel de espectro.
- Los errores generados por las etapas de digestión tríptica y de marcaje enzimático, que se reflejan en la varianza a nivel de péptido.
- La variabilidad biológica y el error que se comete en la etapa de extracción proteica [65], reflejados en la varianza a nivel de proteína.

Aplicando el modelo estadístico mencionado al experimento de hipótesis nula, se detectó un sólo valor atípico entre las más de 1.200 proteínas cuantificadas (Fig. I.3), el cual tiene que asignarse a un artefacto y no a un cambio de abundancia. Este resultado nos permitió concluir que disponíamos de un modelo estadístico que describía correctamente la hipótesis nula. Dicho modelo estadístico se aplicó a los distintos proyectos de proteómica cuantitativa descritos en esta tesis doctoral.

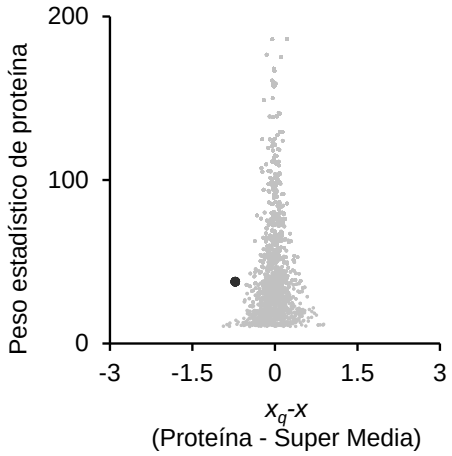

Fig. I.3.- Análisis de los valores atípicos a nivel de proteína en el experimento de hipótesis nula. Representación del peso estadístico de proteína en función del $\log_2$ (A/B) en los que el punto negro representa la única proteína que se desvía de la distribución con una FDRq < 5 %.

I.6.- Angiogénesis y Proteómica

Los vasos sanguíneos constituyen el primer órgano en desarrollarse en el embrión y forman la mayor red en el cuerpo humano en comparación con las redes linfáticas o nerviosas, llevando a los distintos órganos el oxígeno necesario para la vida. La angiogénesis, o formación

de nuevos vasos sanguíneos a partir de otros preexistentes, es un proceso complejo que requiere un equilibrio cuantitativo, cualitativo y temporal fino entre numerosas señales estimuladoras e inhibidoras implicadas en proliferación, migración y diferenciación celulares, como integrinas, angiopoietinas, quimioquinas o sensores de oxígeno [66]. En los últimos 15 años, los estudios genéticos en ratón y pez-cebra han mejorado considerablemente el conocimiento de los mecanismos y de los actores moleculares que regulan el crecimiento vascular, entre los cuales se encuentra el factor de crecimiento endotelial vascular (VEGF), mitógeno específico de las células endoteliales que estimula la angiogénesis. El proceso de angiogénesis tiene lugar durante el desarrollo embrionario y también está implicado en la cicatrización de heridas y procesos relacionados con funciones reproductoras en el adulto [67]. Por otro lado, la angiogénesis está implicada en el establecimiento y progresión de diversas situaciones fisiopatológicas en el adulto; así, tiene un papel clave en la patogénesis de la retinopatía diabética, en enfermedades inflamatorias crónicas como la artritis reumatoide, y es esencial para el desarrollo de tumores sólidos y la formación de metástasis [68]. Por otro lado, la neovascularización es importante para minimizar los efectos de la oclusión arterial causada por la aterosclerosis. La angiogénesis comprende una serie de procesos finamente regulados, en los que participan de forma fundamental las células endoteliales: tras su activación por estímulos proangiogénicos, dichas células son capaces de degradar la matriz extracelular, migrar hacia los tejidos circundantes, proliferar y ensamblarse para formar nuevos vasos sanguíneos, que, posteriormente, sufrirán procesos de remodelación y estabilización, mediante el reclutamiento de células perivasculares [67]. Debido a la implicación de la angiogénesis en la formación de tumores y en la neovascularización, el desarrollo de fármacos diseñados para actuar sobre este proceso reviste un enorme interés biomédico. Sin embargo, para permitir el uso seguro de terapias basadas en el control de los procesos angiogénicos, es fundamental disponer de un conocimiento detallado de los mecanismos moleculares que lo regulan, sobre todo el inherente a la acción de VEGF, cuya inhibición parece necesaria, aunque insuficiente, para frenar el proceso angiogénico en numerosas patologías. Sin embargo, los estudios masivos existentes en la bibliografía son todavía muy escasos, y se han llevado a cabo principalmente utilizando técnicas de transcriptómica [69-72]. Estos estudios han utilizado preferentemente las células HUVEC (Human Umbilical Vein Endotelial Cells) como modelo *in vitro* de células endoteliales humanas.

El estudio del proteoma de las células HUVEC se inició en 1995 mediante técnicas clásicas (electroforesis bidimensional e identificación de las bandas proteínicas mediante

espectrometría de masas), habiéndose conseguido la identificación de 53 proteínas partiendo de 30 µg de proteína y con tres rangos de pH [73]. En un trabajo posterior, este estudio se extendió a 162 proteínas partiendo de 60 µg de proteína [74]; estas técnicas también permitieron la identificación de 8 proteínas que cambiaban de abundancia en respuesta a estímulos proapoptóticos durante 24 h. En claro contraste, la aplicación de las técnicas de segunda generación utilizando el reactivo ICAT y tratando las células HUVEC con sulfato de sokotrasterol (droga de origen marino con efectos potencialmente proangiogénicos [75]) durante 24 h, permitió la identificación de 1.019 proteínas partiendo de 500 µg de proteínas de células HUVEC, así como la determinación de 93 proteínas que aumentaban su abundancia en respuesta al tratamiento frente a 37 proteínas que la disminuían de manera significativa [76].

En un trabajo preliminar del laboratorio, se probaron a pequeña escala varias de las aproximaciones de marcaje mencionadas anteriormente con el objetivo de diseñar un protocolo estándar de marcaje con ^{18}O [55]. Introduciendo mejoras en la tecnología de proteómica de segunda generación, se identificaron más de 1.500 proteínas del proteoma nuclear de células HUVEC (datos no publicados). Basándonos en estos resultados previos y dada la importancia de la angiogénesis en la fisiopatología cardiovascular, nos propusimos estudiar los cambios dinámicos en el proteoma de células HUVEC en respuesta a estímulos proangiogénicos tales como el mediado por VEGF a distintos tiempos de incubación como modelo biológico para validar la puesta a punto de las nuevas tecnologías de marcaje isotópico a gran escala.

I.7.- Proteómica redox y su importancia en el ámbito cardiovascular

Las especies reactivas oxidantes se conocen desde el punto de vista químico desde hace más de 30 años, y desde entonces, se ha hecho cada vez más patente su importancia biológica [77]. En el momento actual, se distinguen dos grandes grupos de especies reactivas, no todas ellas radicalarias, las derivadas del oxígeno (ROS) y las derivadas del nitrógeno (RNS). Su importancia radica en su capacidad para oxidar macromoléculas biológicas como el ADN, las proteínas, los carbohidratos y los lípidos.

El descubrimiento de los denominados interruptores moleculares reguladores mediados por tioles, o Cys susceptibles de oxidación reversible, tanto en organismos procariotas como eucariotas, ha establecido un papel fundamental de la oxidación de Cys en Biología [78, 79], proporcionando un mecanismo flexible de regulación para numerosos procesos celulares [80] y dando lugar a un nuevo paradigma en transducción de señales [81]. La capacidad de los residuos de Cys de actuar como interruptores moleculares se basa en la

química redox específica de ese aminoácido [82], ya que su cadena lateral está compuesta de un átomo de azufre polarizable, rico en electrones y muy nucleófilo. Su reactividad es aún mayor en su forma desprototonada o tiolato RS^-. En ese sentido, el grupo tiol de la Cys es medianamente ácido, siendo su p*Ka* dependiente de la estructura tridimensional de la proteína y del entorno local (en un péptido, el p*Ka* de la Cys suele estar alrededor de 8,5, pero en una proteína, puede alcanzar valores tan bajos como 3.5 [82]). Debido a su alta reactividad, el grupo tiol de la Cys desempeña un papel biológicamente relevante en procesos catalíticos o de unión a metales (Zn^{2+} y Fe^{2+}). Las proteínas que contienen Cys son particularmente susceptibles a la oxidación por las especies reactivas del nitrógeno y del oxígeno (RNOS), aunque las modificaciones oxidativas no sólo afecten a estos residuos, pudiendo modificar también metioninas, tirosinas y triptófanos [83]. Las RNOS pueden dañar las biomoléculas generando un desequilibrio entre su producción y su eliminación por los sistemas detoxificantes: se habla entonces de estrés nitroxidativo. Esta condición patológica tiene un papel relevante en numerosas alteraciones, como la disfunción endotelial [84] y el daño por isquemia-reperfusión [85]. En concreto, se ha asociado el estrés oxidativo a numerosas enfermedades como la aterosclerosis, la hipertensión, la diabetes, el cáncer o ciertos desórdenes neurodegenerativos [86-89]. Sin embargo, se ha descubierto que esas RNOS pueden también actuar como segundos mensajeros en procesos fisiológicos [90, 91], y numerosos estudios en la última década han demostrado que una gran variedad de estímulos externos, como los factores de crecimiento o las interleucinas, pueden activar la producción controlada de RNOS en células sanas contribuyendo a las rutas de señalización intracelulares [92], siendo las Cys los moduladores de la señal a través de su oxidación. Este mecanismo regulador ha sido comparado con el de la fosforilación [93].

Las enfermedades cardiovasculares isquémicas son la causa más frecuente de muerte en el mundo, alcanzando el 23 % de las defunciones en los países más desarrollados según datos de la Organización Mundial de la Salud. El miocardio posee mecanismos complejos que favorecen el mantenimiento del equilibrio entre consumo y aporte de oxígeno necesarios para su función contráctil fisiológica; estos mecanismos pueden actuar como defensa contra distintas patologías como la hipoxia (una reducción de aporte de O_2) o la isquemia, entre otras (Fig. I.4). Las PTMs redox de las proteínas cardiacas pueden afectar su conformación y su estabilidad, así como la actividad de diversos receptores, transportadores de iones, quinasas y fosfatasas, de factores de crecimiento o de proteínas contráctiles [94].

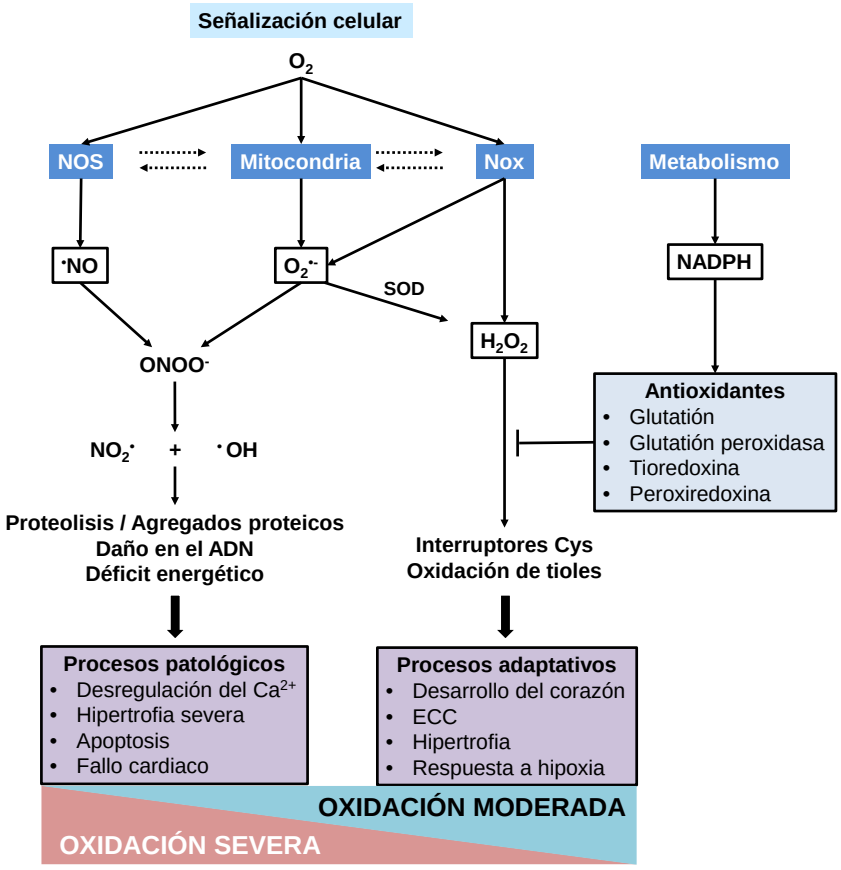

Fig. I.4.- Principales fuentes de RNOS en cardiomiocitos y sus efectos (modificado a partir de [94]). Una gran variedad de estímulos pueden iniciar la señalización mediada por eventos redox, como factores de crecimiento o hipoxia, produciendo un aumento de la generación de RNOS (sobre todo de ˙NO, de $O2^{\cdot-}$ y de H_2O_2) por las NO sintasas (NOS), las NADPH oxidasas (Nox) o por las mitocondrias. Los niveles moderados de RNOS están implicados en procesos adaptativos a través de la oxidación reversible de Cys en respuesta a la hipoxia o modulando el acoplamiento excitación-contracción (ECC). Por otro lado, los niveles altos de RNOS se traducen en procesos patológicos como resultado del daño macromolecular que generan.

La hipoxia afecta la función cardiaca y es uno de los iniciadores principales de numerosos procesos patológicos crónicos como por ejemplo el infarto de miocardio, el daño por isquemia-reperfusión o la hipertrofia cardiaca. Por una parte, la hipoxia severa o isquemia se traduce en muerte celular por necrosis y/o apoptosis debida a la falta de oxígeno [95, 96], en una ruptura de la homeostasis del calcio y del sodio [97], así como del pH [98], en daño mitocondrial [99] y en un aumento de la producción de RNOS [100]. La reperfusión, o re-abastecimiento de los tejidos isquémicos con O_2 mediante el flujo sanguíneo, es necesaria para la supervivencia de los cardiomiocitos para re-establecer la homeostasis metabólica e iónica, pero también está asociada a daño celular [101]. Durante la reperfusión, especialmente en los primeros minutos, las proteínas intracelulares, pero sobre todo las mitocondriales [100, 102], se pueden alterar en parte por mecanismos dependientes de RNOS [103]. Debido a la abundancia de las mitocondrias en corazón, la pérdida de la función mitocondrial tiene un gran

impacto en los cardiomiocitos al ser necesario el ATP para su actividad contráctil [104]; por ello, y teniendo en cuenta que son una de las fuentes principales de producción de RNOS [105], se considera que las mitocondrias son las dianas principales del daño por isquemia-reperfusión (I/R) [106] y uno de los objetivos centrales de los tratamientos de prevención del daño cardiaco como el precondicionamiento isquémico (IP). El IP, que se produce cuando se llevan a cabo ciclos breves y repetitivos de I/R antes de la isquemia prolongada, se describió por primera vez en 1986 [107] y tiene un efecto protector sobre el miocardio preservando las funciones mitocondriales y reduciendo el daño oxidativo producido por la I/R. Por último, se ha descrito que los cardiomiocitos son relativamente resistentes a la hipoxia moderada [108], un mecanismo que se debe en parte a numerosos procesos adaptativos desencadenados por el factor de transcripción sensible a redox Hif [109, 110]. Además de la activación por la disminución de los niveles de O_2, un incremento de RNOS también activa las vías dependientes de Hif [111, 112].

Una consecuencia importante a nivel bioquímico de la generación de RNOS es la nitración de las tirosinas de las proteínas, en la que se substituye un átomo de hidrógeno por un grupo nitro (-NO_2) en uno de los dos átomos de carbono equivalentes en posición orto con respeto al grupo –OH del anillo fenólico de los residuos de Tyr [113]. Esta PTMO se ha detectado en numerosos compartimentos del sistema cardiovascular como el plasma, el endotelio o el miocardio, y puede afectar la función de la proteína modificada por inactivación o ganancia de función, convirtiéndose en biomarcador de disfunción cardiovascular [114]. En trabajos previos del laboratorio del Prof. Santiago Lamas, se demostró que la ciclosporina A (CsA), utilizada como agente inmunosupresor para reducir la actividad del sistema inmunitario del paciente y el riesgo de rechazo de trasplante de órgano, promovía la generación de superóxido y de peroxinitrito en el endotelio vascular [115]. Ese efecto está asociado a un aumento de la nitración de proteínas, siendo la superóxido dismutasa de manganeso (MnSOD) uno de los candidatos más probables [116]. La Tyr34 de la MnSOD ha sido identificada como diana crítica de nitración *in vitro* y como responsable de la inactivación de la proteína con consecuencias funcionales también *in vivo* [113, 117].

La Proteómica Redox se puede definir como el conjunto de herramientas proteómicas utilizadas para la detección y la cuantificación de PTMs oxidativas (PTMOs) que modulan el proteoma en condiciones de estrés oxidativo o de señalización. Esta definición engloba todas las PTMOs, las cuales se pueden dividir en dos categorías, reversibles e irreversibles. Las modificaciones en Cys son las que, a día de hoy, se consideran más relevantes, ya que

intervienen en el plegamiento de las proteínas, en su actividad, en el reconocimiento celular y en el tráfico intracelular, entre otras funciones. Dada su reactividad, las Cys son susceptibles de oxidación por H_2O_2, $O_2^{\cdot -}$, $^{\cdot}OH$, $ONOO^-$, N_2O_3, $^{\cdot}NO$, ó $^{\cdot}NO_2$, dando lugar a modificaciones con distintos grados de reversibilidad (S-nitrosilación, puentes disulfuro intra- e intermoleculares, sulfenación y S-glutationilación) o completamente irreversibles (sulfinación y sulfonación) (Fig. I.5), aunque recientemente se ha demostrado que la sulfinación puede ser revertida por un mecanismo enzimático dependiente de ATP catalizado por sulfiredoxinas [118].

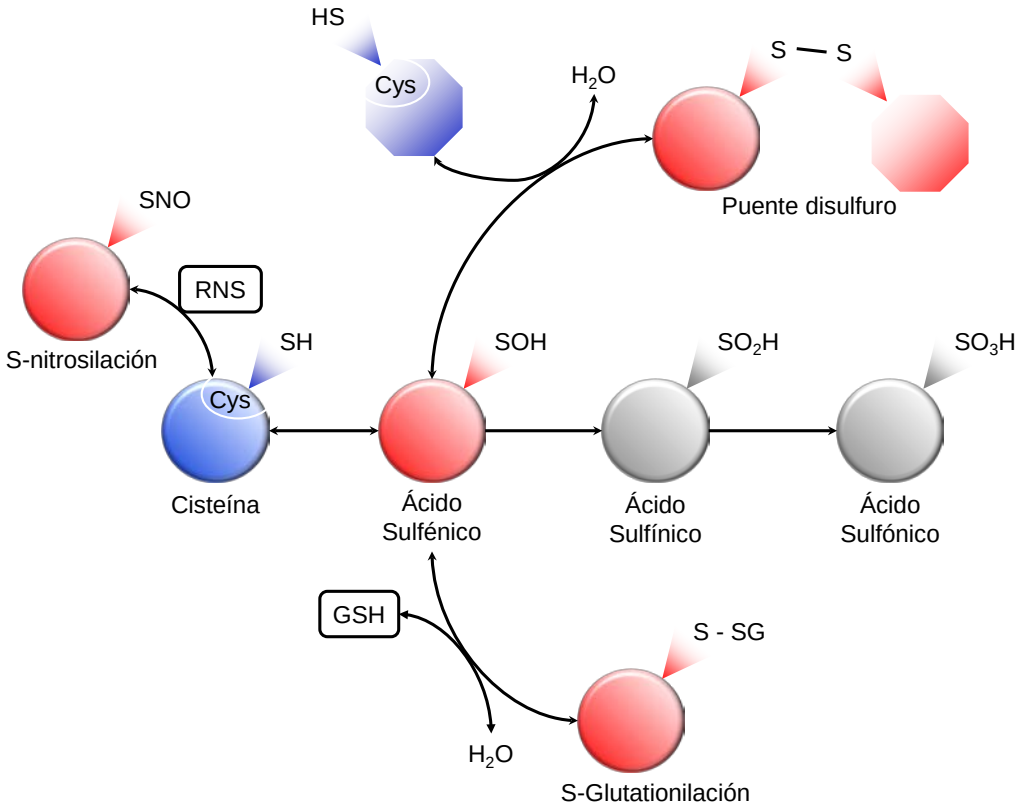

Fig. I.5.- Esquema de las modificaciones oxidativas más frecuentes en Cys. Los grupos tioles de las Cys, especialmente los que poseen un p*Ka* bajo, reaccionan con las RNOS. Se piensa que el producto de oxidación inicial es la formación de ácido sulfénico. Esta PTMO puede estabilizarse por el micro-entorno de la proteína o condensarse con una segunda Cys formando puentes disulfuro intra- o inter-moleculares. El ácido sulfénico puede también condensarse con el tripéptido glutatión (GSH) para formar S-glutationilación. Bajo condiciones severas de estrés oxidativo, el grado de oxidación del grupo tiol aumenta y se pueden formar ácidos sulfínicos y/o sulfónicos. La reacción de los grupos tioles con RNS genera también S-nitrosilaciones.

La determinación de la función exacta de la oxidación de Cys en procesos fisiopatológicos se ha visto obstaculizada por la dificultad de detectar de manera específica y selectiva las distintas formas oxidadas del grupo tiol en entornos biológicos complejos. Por otra parte, los detalles moleculares relacionados con la formación de esas modificaciones y los residuos de Cys específicos modificados *in vivo* son muy poco conocidos. En la última década,

y con el objetivo de aportar nuevos datos que respondan al interés creciente de la comunidad científica acerca del papel de las PTMOs en Cys, se han desarrollado numerosas aproximaciones proteómicas [119, 120]. Debido a las limitaciones de la detección directa de esas modificaciones en los espectros MS/MS (la S-nitrosilación se rompe con la ionización por láser y la S-glutationilación tiene un perfil aleatorio de fragmentación complicando mucho la interpretación de los espectros), la mayoría de las estrategias desarrolladas se basan en la derivatización de la Cys en sus distintos estados de oxidación, siendo los reactivos específicos de grupos tioles más utilizados la yodoacetamida (IAM), la N-etilmaleimida (NEM) o el Metil-metanotiosulfonato (MMTS) (Fig. I.6).

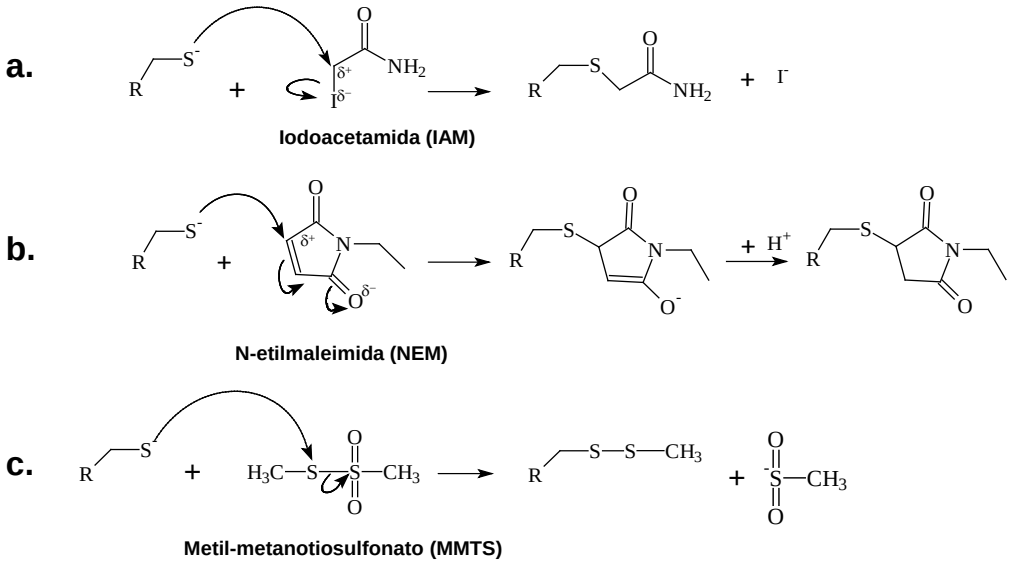

Fig. I.6.- Esquema de las distintas reacciones de derivatización de la Cys con los agentes químicos más comúnmente utilizados. a.- Reacción de la IAM con el tiolato de la Cys (alquilación por substitución de tipo S_N2). b.- Alquilación de la Cys por la NEM (alquilación por adición de Michael). c.- Reacción del MMTS (formación de un puente disulfuro con la Cys).

La mayoría de los estudios proteómicos encaminados al estudio del redoxoma se han basado en técnicas de primera generación [121] o en técnicas de afinidad dirigidas contra modificaciones específicas como la S-nitrosilación [122] o la S-glutationilación [123]. Sin embargo, y exceptuando algunos trabajos recientes [85, 124-129], estas modificaciones apenas se han estudiado utilizando técnicas de proteómica de segunda generación. Las estrategias de análisis cuantitativo utilizando SIL han sido poco aplicadas en proteómica redox, y se basan en los trabajos pioneros de Sethuraman *et al.* [130], en los que utilizan el reactivo ICAT para marcar, purificar y analizar las Cys reducidas en proteínas de membrana de corazón de conejo tratados con 10 mM de peróxido de hidrógeno. Recientemente, esta aproximación se ha modificado para permitir cuantificar en una misma muestra el ratio de Cys oxidadas frente al de Cys reducidas en un método denominado OxICAT (Fig. I.7) [127].

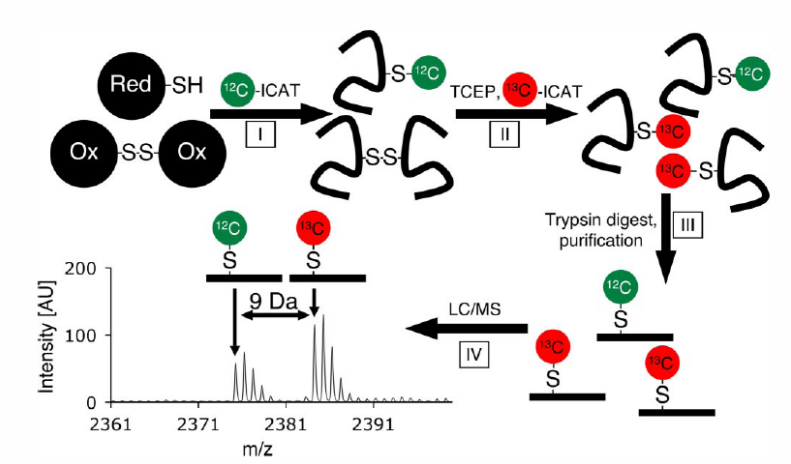

Fig. I.7.- Determinación del estado de oxidación de las Cys utilizando la tecnología OxICAT [127]. Las proteínas se incuban en condiciones desnaturalizantes con el reactivo ligero de ICAT-^{12}C (puntos verdes) que se unen de manera irreversible a las Cys reducidas (etapa I). En la etapa II y tras precipitar las proteínas, se reducen con TCEP todas las Cys oxidadas de forma reversible y se modifican con el ICAT-^{13}C (puntos rojos). Después de una nueva etapa de precipitación para eliminar el exceso de reactivo, las proteínas se digieren con tripsina y los péptidos modificados con ICAT se purifican en columnas de avidina. Los péptidos eluidos se analizan por MS, determinando la proporción de péptido oxidado por el tratamiento en una misma muestra.

Sin embargo, la mayoría de las técnicas existentes diseñadas para la cuantificación relativa del estado de oxidación de las Cys en diferentes situaciones solo analizan la población de Cys reducidas (libres) u oxidadas, pero no las dos en conjunto. Además, ningún método permite discernir si los cambios observados se deben a alteraciones en la abundancia de proteínas o si reflejan realmente un cambio del estado de oxidación de las Cys. Por último, y debido a la ausencia de un modelo estadístico adecuado para el análisis global de los datos cuantitativos, los métodos actuales carecen de la precisión y sensibilidad necesarias para detectar alteraciones moderadas inducidas por condiciones suaves de oxidación características de ambientes fisiológicos. Para paliar estos defectos, y como trabajo central de esta tesis doctoral, nos propusimos, por un lado, el desarrollo de la tecnología GELSILOX (GEL-based Stable Isotope Labeling of OXidized Cys), un método para el estudio cuantitativo y simultáneo de los proteomas total y redox tiólico que introduce un análisis estadístico innovador para la interpretación de los datos y hace uso de desarrollos técnicos recientes de nuestro laboratorio. Esta técnica se aplicó a un conjunto de modelos, entre los comentados anteriormente, de alta relevancia desde el punto de vista fisiopatológico y de la proteómica cardiovascular redox. Simultáneamente, y en paralelo con este método de análisis masivo y "libre de hipótesis", nos propusimos continuar avanzando en el desarrollo de técnicas que permitieran la caracterización pormenorizada y selectiva de dianas potenciales de modificación por estímulos oxidativos, utilizando técnicas de proteómica dirigida.

OBJETIVOS

Con objeto de paliar las limitaciones de los métodos de proteómica cuantitativa convencional y redox existentes, en esta tesis doctoral nos propusimos diseñar una estrategia robusta de marcaje con ^{18}O, de aplicabilidad universal y que también permitiera el estudio dinámico de alteraciones producidas por situaciones de estrés oxidativo. Por otro lado, nos propusimos continuar avanzando en el desarrollo de técnicas para la monitorización altamente selectiva de dianas concretas de daño oxidativo. Para validar las nuevas técnicas se seleccionaron una serie de modelos *in vitro* e *in vivo* y de alta relevancia biológica.

Los objetivos concretos planteados en esta tesis fueron los siguientes:

1. Desarrollar una tecnología robusta y de validez universal para llevar a cabo experimentos de cuantificación de cualquier tipo de proteoma mediante marcaje isotópico con ^{18}O.
2. Demostrar la robustez y potencial de la técnica determinando los cambios dinámicos que tienen lugar en el proteoma de células endoteliales tras la estimulación pro-angiogénica mediada por VEGF.
3. Desarrollar una tecnología robusta para el estudio cuantitativo sistemático y a gran escala de los cambios oxidativos que tienen lugar en Cys específicas.
4. Utilizar los desarrollos tecnológicos para caracterizar los cambios dinámicos que producen situaciones de estrés oxidativo moderado en el proteoma del endotelio vascular y determinar cuáles son los residuos de cisteína que alteran su estado de oxidación durante este proceso.
5. Determinar el daño oxidativo producido en el proteoma mitocondrial por episodios de isquemia-reperfusión en corazón y el efecto del precondicionamiento isquémico.
6. Caracterizar la potencial modificación oxidativa inducida por ciclosporina A sobre la superóxido dismutasa de manganeso.

MATERIALES Y MÉTODOS

Modelos experimentales

Muestras utilizadas para la optimización del protocolo de marcaje con ^{18}O en disolución

Los extractos proteicos de células HUVEC (1.5 x 10^6 células) fueron cedidos generosamente por la Dra. Arantza Alfranca y el Prof. Juan-Miguel Redondo, del laboratorio de "Regulación de la expresión génica en el endotelio vascular" del Centro Nacional de Investigaciones Cardiovasculares (CNIC). La estimulación con VEGF (Peprotech, London, UK) se llevó a cabo incubando las células durante 0, 4 u 8 h con el factor de crecimiento a una concentración de 50 ng/ml en medio 199 (BioWhittaker, Walkersville, MD) conteniendo 20 % de FCS (Invitrogen), 50 µg/ml de extractos cerebrales bovinos y 100 µg/ml de heparina (Sigma). Las células en estado de confluencia se despegaron y se resuspendieron en el tampón de lisis (Tris 50 mM pH 7,5, NaCl 400 mM, EDTA 1 mM, EGTA 2,5 mM, Triton X-100 al 1 %, DTT 1 mM, inhibidores de proteasas y fosfatasas), se incubaron 15 min en hielo, y se centrifugaron a 10.000 g durante 15 min a 4 ºC. A continuación, se recogieron los sobrenadantes y se cuantificaron las proteínas utilizando el reactivo de Bradford (Bio-Rad). Para los experimentos de confirmación por Western blot, las proteínas (8 µg/carril) fueron separadas por SDS-PAGE y transferidas a membrana de nitrocelulosa, las cuales fueron incubadas con los anticuerpos anti-anexina A1 (Santa Cruz Biotechnology, Santa Cruz, CA), anti-triosa fosfato isomerasa (Abcam, Cambridge, UK), anti-reticulocalbina (Bethyl, Montgomery, TX), y anti-β-tubulina (Sigma). Las bandas inmunoreactivas se detectaron mediante substrato potenciador de quemolominescencia (ECL, GE Healthcare).

Muestras utilizadas para el desarrollo de la estrategia GELSILOX para el estudio masivo de los cambios de oxidación producidos en células en cultivo como modelos endoteliales

Las células EA.hy296 (cedidas generosamente por la Dra. Cora-Jean S. Edgell, UNC, NC, USA) fueron procesadas en el laboratorio del Dr. Antonio Martínez-Ruiz en el servicio de Inmunología del Hospital La Princesa. Las células fueron cultivadas en DMEM suplementado con HAT, 10 % de suero fetal bovino inactivado por calor, 100 U/mL de penicilina y 100 µg/mL de estreptomicina a 37 ºC, con 5 % CO_2. El tratamiento con diamida se hizo durante 10 min a una concentración final de 2 mM. El tratamiento por hipoxia se llevó a cabo en una cámara Invivo2 200 (Ruskinn) con 0,5 % de O_2, 5 % de CO_2, a 37ºC durante 2 h. Las células se lavaron 2 veces con suero fisiológico y la proteínas se extrajeron con un tampón TENT (Tris 50

mM pH 7,5, EDTA 1 mM, neocuproina 100 µM, Triton X-100 1%) conteniendo inhibidores de proteasas y NEM 50 mM como agente alquilante 1 (ver apartado "*3.1.- Optimización del protocolo de cuantificación masiva de proteomas y de estado de oxidación de Cys"* para más detalles). El debris celular fue eliminado por centrifugación, se añadió SDS al 2 % al sobrenadante y se incubó 30 min a 37 ºC. Las células BAEC fueron cultivadas en el laboratorio del Prof. Santiago Lamas en el Centro de Biología Molecular Severo Ochoa (CBMSO – CSIC/UAM) en gelatina en RPMI complementado con suero fetal bovino al 10 % hasta el 80 % de confluencia. Las células fueron tratadas con 1 mM de H_2O_2 (Sigma) durante 10 min a 37 ºC, lavadas con PBS y sometidas a extracción proteica en tampón de lisis (Tris-HCl 50 mM pH 7,2, EDTA 1 mM y Triton X-100 1 %) suplementado con NEM 50 mM como primer agente alquilante.

Muestras utilizadas para el estudio mediante GELSILOX del daño oxidativo producido en tejidos por isquemia/reperfusión

Los corazones de ratas macho de la raza Sprague-Dawley se extrajeron rápidamente y se sometieron a perfusión retrógrada durante 15 min a 37 ºC con una solución oxigenada de Krebs (NaCl 118 mM, HCO_3 25 mM, $MgCl_2$ 1,2 mM, H_2PO_4 1,2 mM, KCl 4,7 mM, $CaCl_2$ 1,8 mM, glucosa 11 mM, pH 7,4) en un aparato de Languendorff. Después del equilibrado, los corazones se sumergieron en una solución de Krebs a 37ºC y fueron sometidos a 20 min de isquemia global y 5 min de reperfusión, precedidos por 20 min de perfusión normóxica para las muestras IR o por dos ciclos de 5 min de isquemia para las muestras IP_IR. Los corazones fueron removidos de la cánula y las mitocondrias cardíacas subsarcolemales e intermiofibrilares se obtuvieron por centrifugación diferencial y ultracentrifugaciones en gradiente de Percoll, como se ha descrito con anterioridad [131]. Las mitocondrias se hirvieron en el tampón de carga para el SDS-PAGE (Tris-HCl 0,9 M, pH 8,45, glicerol 24 % (w/v), SDS 8 % (w/v)) durante 5 min y fueron tratadas con IAM 50 mM durante 30 min en oscuridad. La pureza de las preparaciones mitocondriales fue estimada por análisis proteómicos en un 95 %.

Muestras utilizadas para la validación por proteómica dirigida de la modificación por nitración de un residuo Tyr de la MnSOD

Para los experimentos de nitración de la MnSOD recombinante humana, la proteína se incubó con el medio condicionado de cultivo de células BAEC tratadas con CsA (10 µM, 2 h), su vehículo o el tampón nitrante [132] y se procesaron como ha sido descrito por el grupo del Prof. S. Lamas [115]. Para los experimentos de nitración de la MnSOD celular, las células

BAEC fueron deplecionadas de suero durante 16 h e infectadas con el vector adenoviral de la MnSOD (Gene Transfer Vector Core, University of Iowa) a una multiplicidad de infección de 100 durante 2 h. Las células se incubaron en un medio completo durante 22 h. Por último, se trataron las células con CsA (10 µM, 2 h) o su vehículo y se extrajeron las proteínas.

Desarrollo de la estrategia de marcaje con ^{18}O en disolución

Los extractos de proteínas (1 mg de muestra control y 1 mg de muestra tratada con VEGF) se desalaron y el detergente fue eliminado usando columnas PD-10 (Amersham Biosciences, Piscataway, NJ), eluyendo con bicarbonato amónico 25 mM pH 8,8 y urea 9 M. Las muestras se redujeron con DTT 10 mM a 57 ºC durante 30 min. Las cisteínas se alquilaron con IAM a 50 mM de concentración final durante 60 min a temperatura ambiente y en oscuridad. Posteriormente, las muestras se diluyeron con bicarbonato amónico 25 mM pH 8,8 para disminuir la concentración de urea hasta 1,4 M; la tripsina (Promega, Madison, WI) se añadió a una proporción enzima:sustrato de 1:20 (w/w) y las muestras se digirieron durante la noche a 37 ºC [133]. Después de acidificar las muestras con TFA al 1 % para parar la reacción, éstas se desalaron con columnas Oasis® (Waters, Milford, MA, USA) eluyendo con ACN al 80 % conteniendo TFA al 1 %. Los péptidos se secaron por centrifugación en vacío (SPD121P de Savant) y se incubaron durante la noche a 37 ºC con tripsina inmovilizada (Pierce, Erembodegem, Belgium) en una solución conteniendo ACN al 20 %, acetato amónico 100 mM (pH 6,0), tripsina inmovilizada en proporción 200:1 (v/w) y agua normal ^{16}O (muestra control) o agua marcada ^{18}O (muestra tratada con VEGF) en proporción 1:1 (p/p).

Los péptidos provenientes de la muestra marcada y no marcada se mezclaron y desalaron por HPLC utilizando una columna C18 de RP (250 x 4,6 mm, 5 µm, Vydac, Deerfield, IL, USA); la elución se hizo por escalones (fase móvil A: formiato amónico 5 mM; fase móvil B: ACN al 80 %, formiato amónico 5 mM) a 400 µl/min: 5 % B durante 5 min seguidos de 9 min a 40 % B y 9 min a 95 % B. Los péptidos se eluyeron en tres fracciones, que se mezclaron para el fraccionamiento por HPLC-SCX utilizando una columna BioBasic SCX (200 x 2,2 mm, 5 µm, ThermoFischer, Waltham, MA); la elución se hizo en gradiente (fase móvil A: ACN al 25 %, formiato amónico 5 mM; fase móvil B: ACN al 25 %, formiato amónico 500 mM) a 200 µl/min: después de una fase isocrática de 5 min en 100 % A, se aumentó linealmente hasta 10 % B durante 36 min, 40 % B durante 40 min y 100 % B durante 2 min. Finalmente, los péptidos se recogieron en 92 fracciones de 200 µl cada una, las cuales fueron liofilizadas y analizadas directamente por espectrometría de masas.

Optimización del método robusto de digestión en gel y de marcaje con ^{18}O

Los extractos de proteínas binarios (control y tratado) de 500 µg se resuspendieron en 300 µl de tampón de carga, y se cargaron en pocillos de 2,8 cm en un gel convencional SDS-PAGE (grosor de 1,5 mm, concentrador del 4 %, y separador del 10 %). La carrera se paró en el momento en que las muestras penetraron 3 mm en el gel separador, de manera que todo el proteoma quedó concentrado en una sola banda en la interfaz entre los geles concentrador y separador [134]. La banda de proteínas se visualizó mediante tinción con azul de Coomassie (Bio-Rad. CA, USA), se recortó y se troceó en cubos (2 x 2 mm). Los trozos de gel se sometieron a un proceso de reducción/alquilación con DTT 10 mM e IAM 54 mM respectivamente, previos a la digestión con tripsina a una proporción proteína:proteasa de 5:1 (w/w) en un tampón compuesto por bicarbonato amónico 50 mM, pH 8,8 conteniendo ACN 10 % (v/v) y 5-cyclohexyl- 1-pentyl--D-maltosida 0,01 % (w/v) [135] durante toda la noche a 37 ºC. Los péptidos trípticos resultantes se extrajeron mediante incubación de los trozos de gel con bicarbonato amónico 12 mM, pH 8,8 durante 1 h. Después de acidificar las muestras con TFA al 1 % para parar la reacción, éstas se desalaron con columnas Oasis® como se ha descrito en el apartado anterior.

Los péptidos se marcaron de manera diferencial con $^{16}O/^{18}O$ como ya se ha descrito en el apartado *"Optimización de la estrategia de marcaje con ^{18}O en disolución"*. La eficacia de la reacción de marcaje se monitorizó en este punto con la mezcla de 2 alícuotas de 5 µg de cada una de las muestras y analizándolas por HPLC-MS/MS. La reacción de marcaje se paró con un doble tratamiento: en un primer paso, se eliminaron las bolas de tripsina usando un filtro físico (Wizard minicolumns, Promega) y después se inhibió la actividad residual de la tripsina incubando 1 h a 37 ºC las muestras con TLCK (Tosyl-L-Lysine Chloromethyl Ketone), un inhibidor irreversible de la proteasa, a una concentración final de 1 mM a partir de un stock de 50 mg/ml diluido en metanol. En este punto, se controló la eficacia de la inactivación de la tripsina comprobando que, al mezclar 2 alícuotas de 5 µg de cada una de las muestras y analizándolas por HPLC-MS/MS, no se observaba desmarcaje. Las 2 muestras se mezclaron, se diluyeron hasta un 2 % de ACN, el pH se ajustó a 3 con formiato amónico 1 M, pH 3, y se desalaron en cartuchos de fase reversa C18 Oasis®, eluyendo con ACN 50 % en formiato amónico 5 mM, pH 3. Los péptidos desalados se secaron por centrifugación en vacío, y la mezcla de los mismos se resuspendió en un tampón de enfoque (glicerol 5 % y tampón IPG 2 % pH 3–10 o 4–7 (GE Healthcare)), se cargó en 24 pocillos en tiras de isoelectroenfoque de 24 cm (Immobiline DryStrip, pH3–10 or 4–7 (GE Healthcare)) y los péptidos se separaron por

punto isoeléctrico en un fraccionador OFFgel modelo 3100 (Agilent, Santa Clara, CA), utilizando el método estándar recomendado por el fabricante. Las fracciones recuperadas se acidificaron con 20 µl de formiato amónico 1 M, pH 3, y cada una de ellas se desaló con puntas OMIX C18 (Varian, Inc, Agilent, USA) acopladas a pipeta. Por último, los péptidos se eluyeron con ACN 50 % en formiato amónico 5 mM, pH 3, se secaron por centrifugación en vacío y se analizaron por RP-HPLC-LIT.

Análisis masivo por espectrometría de masas

Los péptidos se analizaron por medio de un sistema Surveyor LC acoplado a un espectrómetro de masas modelo LTQ (ThermoFischer, San Jose, CA). Los péptidos se concentraron utilizando una pre-columna BioBasic-18 (30 x 0,32 mm, ThermoFischer) y se separaron por RP utilizando una columna analítica BioBasic-18 (150 x 0,18 mm, 5 µm, ThermoFischer), a un flujo de 2 µl/min y utilizando un gradiente de 155 min desde el 14 % al 30 % B (fase móvil A: acido fórmico al 0,1 % (v/v); fase móvil B: ACN al 80 % (v/v), acido fórmico al 0,1 % (v/v)). La trampa lineal se programó para efectuar un espectro de sondeo de 400 a 1.600 Th, seguido de seis ciclos compuestos por un espectro de media-alta resolución (*ZoomScan*) y un espectro de fragmentación (MS/MS) por ciclo sobre los seis iones más intensos detectados. Los parámetros del espectrómetro de masas, el número de microscans, la energía de colisión normalizada y los parámetros de exclusión dinámica usados han sido descritos previamente [55, 65].

La identificación de proteínas se llevó a cabo usando SEQUEST como ya se ha descrito [136] frente a la base de datos de proteínas Swiss-Prot; dependiendo de la naturaleza de la muestra, se usaron bases de datos de proteínas humanas, de mamífero o mixta rata-ratón. Los parámetros de búsqueda incluyeron como modificaciones variables la oxidación de la Met (+ 15.9949 Da), una modificación de + 4 Da en lisina y arginina correspondiente a la incorporación de ^{18}O, y como modificación fija, la carboxiamidometilación de la Cys (+ 57.034 Da). Para los experimentos de estudio de la oxidación en Cys, los parámetros de búsqueda sólo incluyeron modificaciones variables, siendo estas la oxidación de la Met, la incorporación de ^{18}O a los residuos Lys y Arg, así como las modificaciones de la Cys por IAM, NEM (+ 125.0477 Da) o MMTS (+ 71.0371 Da). Se permitió que el motor de búsqueda se saltara dos sitios de corte, con una tolerancia de 2 ó 1,2 amu para los precursores y los iones fragmento, respectivamente.

El análisis estadístico y la determinación de las tasas de error se han llevado a cabo después de hacer una búsqueda frente a la base de datos normal y otra frente a una base de datos invertida

y usando el método del pRatio [137]. La FDR de las identificaciones de los péptidos se calcularon usando un método refinado previamente publicado por el grupo [138].

Análisis de datos de proteómica cuantitativa mediante marcaje isotópico con ^{18}O

La cuantificación de los péptidos a partir del *ZoomScan* se realizó según un método descrito previamente [55, 57] utilizando QuiXoT, un programa desarrollado en el laboratorio escrito en C#, que abre automáticamente los datos crudos del espectrómetro de masas y los resultados de identificación, mostrando únicamente los *ZoomScan* correspondientes a cada péptido [139, 140]. La cuantificación en QuiXoT se realiza mediante un algoritmo descrito previamente [57]. Se utilizan para la cuantificación sólo los *ZoomScan* pertenecientes a identificaciones de péptidos con una tasa de error menor o igual al 5 %. Los espectros *ZoomScan* se ajustan a una curva teórica, permitiendo un cálculo simultáneo de la concentración de proteína en las dos muestras, así como de la eficiencia de marcaje *f*. El resultado de la cuantificación de un espectro *s* correspondiente al péptido *p* que proviene de la proteína *q* se expresa cómo $x_{qps} = \log_2(A/B)$, dónde A y B son las cantidades de péptido expresadas en unidades de área en las muestras control y tratada, respectivamente. Cuando la cantidad de péptido es la misma en las dos muestras, $x_{qps} = 0$. Se asume que los errores experimentales de esta medida provienen de un error sistemático, μ, en la razón en la que están mezcladas las dos muestras; de las desviaciones que se producen en la concentración de proteína debidas a la variabilidad biológica y durante el proceso de preparación de los extractos de proteína ρ_q; de desviaciones en la concentración de los péptidos generadas por digestión tríptica de su proteína correspondiente así como por la etapa de marcaje isotópico, β_{qp}; y del error de cuantificación de la pareja peptídica, ξ_{qps}, que puede ser debido, por una parte, al error de medida inherente al espectrómetro de masas utilizado, y por otra al ajuste del espectro experimental a una curva teórica (evaluado por el peso estadístico de espectro), es decir:

$$x_{qps} = \mu + \rho_q + \beta_{qp} + \xi_{qps} \qquad \textbf{(Eq. 1)}$$

Se asume que β_{qp} y ρ_q siguen distribuciones normales, es decir $\beta_{qp} \sim N(0, \sigma_{\mathbf{P}}^2)$ y $\rho_q \sim N(0, \sigma_{\mathbf{Q}}^2)$, y que las varianzas de péptido y proteína, $\sigma_{\mathbf{P}}^2$ y $\sigma_{\mathbf{Q}}^2$ respectivamente, son constantes. También se asume que ξ_{qps} se distribuye normalmente como $\xi_{qps} \sim N(0, \sigma_{\mathbf{S}}^2 + k/v_{qps})$, donde $\sigma_{\mathbf{S}}^2$ es la varianza de la cuantificación de los espectros debida al

error de medida del espectrómetro de masas, v_{qps} es el peso estadístico asociado al ajuste a una curva teórica y k es una constante que depende del espectrómetro de masas y de las condiciones de barrido. Como la cuantificación de cada proteína se lleva a cabo por varios péptidos, y cada péptido a su vez se cuantifica por varios espectros, se escoge una media ponderada para cada uno de estos valores, donde el peso estadístico w a nivel de espectro s, péptido p y proteína q es la inversa de su varianza local, y la varianza local a cada nivel se calcula, de acuerdo a la teoría estadística, como la inversa de la suma de las inversas de las varianzas de las medidas en el nivel anterior, es decir:

$$w_{qps} = \frac{1}{\frac{k}{v_{qps}} + \sigma_{\mathbf{S}}^2} \qquad w_{qp} = \frac{1}{\frac{1}{\sum_s w_{qps}} + \sigma_{\mathbf{P}}^2} \qquad w_q = \frac{1}{\frac{1}{\sum_p w_{qp}} + \sigma_{\mathbf{Q}}^2} \qquad \textbf{(Eq. 2)}$$

De manera que las medias ponderadas para péptido, proteína, y media global – que es una estimación del valor μ y se calcula como la media ponderada de los valores de proteína– se calculan, respectivamente, de la siguiente manera

$$x_{qp} = \frac{\sum_s w_{qps} x_{qps}}{\sum_s w_{qps}} \qquad x_q = \frac{\sum_p w_{qp} x_{pq}}{\sum_p w_{qp}} \qquad x = \frac{\sum_q w_q x_q}{\sum_q w_q} \qquad \textbf{(Eq. 3)}$$

Para tener en cuenta el error sistemático μ para cada experimento, se substrae la media global del experimento al ratio de las proteínas.

El modelo estadístico permite determinar cuál es la varianza local de cada una de las medidas o de cada uno de los péptidos o proteínas, que viene dada por la inversa de los respectivos pesos, calculados de acuerdo a las ecuaciones Eq. 2. Estas varianzas locales pueden utilizarse para estimar si un valor determinado – un espectro, un péptido o una proteína – se desvía significativamente de la media correspondiente – el péptido, la proteína o la media global, respectivamente – ya que de acuerdo al modelo, a todos los niveles las medidas se comportan como distribuciones normales locales. Si $P(\mu, \sigma^2, x_t)$ es la probabilidad de que el valor x_t correspondiente a la medida t se desvíe de la distribución normal con media μ y varianza σ^2, la probabilidad de que una medida a nivel de espectro, péptido o proteína se desvíe de la media correspondiente viene dada por

$$p_{qps} = P(x_{qp}, w_{qps}^{-1}, x_{qps}) \qquad p_{qp} = P(x_q, w_{qp}^{-1}, x_{qp})$$

$$p_q = P(x, w_q^{-1}, x_q) \quad \textbf{(Eq. 4)}$$

La presencia de valores atípicos se detecta utilizando una prueba de hipótesis múltiple y controlando la tasa de error FDR [141-144], definida como la proporción de valores que se espera que se desvíen de la distribución normal al azar dentro de la población de valores atípicos. Ya que el número de cambios aleatorios esperados es el producto de la probabilidad, definida en las ecuaciones Eq. 4, multiplicada por el número total de eventos a cada nivel, la FDR para cada uno de los tres niveles de estudio se define como

$$FDR_{qps} = \frac{p_{qps} \cdot NS}{O(p_{qps})} \qquad FDR_{qp} = \frac{p_{qp} \cdot NP}{O(p_{qp})} \qquad FDR_q = \frac{p_q \cdot NQ}{O(p_q)} \quad \textbf{(Eq. 5)}$$

en las cuales *NS*, *NP* y *NQ* son el número total de espectros, de péptidos y de proteínas, respectivamente, y $O(p)$ es el número de eventos observados con una probabilidad igual o menor.

Análisis dirigido de modificaciones postransduccionales por espectrometría de masas

Para caracterizar de manera específica la nitración en la Tyr34 de la MnSOD, las muestras se separaron mediante electroforesis SDS-PAGE y las bandas correspondientes al peso molecular esperado de la MnSOD fueron recortadas y digeridas con tripsina como se ha descrito en varias publicaciones del grupo [145, 146]. La digestión se paró añadiendo TFA al 1 %, y el análisis MS de los péptidos se llevó a cabo usando un sistema HPLC Surveyor acoplado a un espectrómetro de masas modelo LTQ (ThermoScientific, San Jose, CA, USA). Brevemente, los péptidos son concentrados y desalados en una pre-columna de fase reversa (0,32 x 30 mm, BioBasic-18, ThermoScientific) y eluidos en línea en una columna analítica de fase (0,18 x 150 mm BioBasic-18, ThermoScientific), operando a 2 µl/min y usando un gradiente de 40 min del 0 % al 40 % de solvente B [solvente A: ácido fórmico al 0,1 % (v/v), solvente B: ácido fórmico al 0,1 % (v/v), ACN al 80 % (v/v)]. El LTQ se programó en modo SMIM [56, 146]. Previamente, se realizó un barrido de amplio rango de m/z de 400-1600 Th para identificar de manera global los péptidos presentes en la muestra. Los espectros de fragmentación posteriores se programaron sobre el ión 580.3, correspondiente al ión precursor triplemente cargado del péptido HHAAYVNNLNVTEEK y sobre el ión 595.3,

correspondiente al ión precursor triplemente cargado de la forma nitrada en Tyr del mismo péptido (Δm = + 45 Da). Dos espectros MS^3 adicionales fueron programados sobre los iones 510.7 and 533.20, productos de la fragmentación de los péptidos no modificados y nitrado, respectivamente. El grupo de barridos se repite dos veces por ciclo.

RESULTADOS

R.1.- Optimización de la estrategia de marcaje con ^{18}O

R.1.1.- Optimización de la eficiencia de marcaje

En este tipo de aproximaciones experimentales, optimizar la eficiencia de incorporación de los átomos de ^{18}O de cada péptido es crítico para lograr cuantificaciones fiables en experimentos a gran escala y evitar así resultados erróneos. Ello es debido a que si la incorporación de ^{18}O no fuera completa o parte de los péptidos de la muestra tratada con $H_2{}^{18}O$ perdiera la marca isotópica, su concentración se subestimaría generando falsos cambios de abundancia. Con objeto de desarrollar un protocolo robusto de marcaje, analizamos las distintas estrategias existentes en la bibliografía. Las diferentes técnicas se diferencian fundamentalmente en la adición de solvente orgánico, el pH durante la etapa de marcaje, el tiempo de reacción, así como la estrategia para la inactivación de la tripsina tras el marcaje.

En una primera aproximación, decidimos realizar una batería de experimentos a pequeña escala utilizando los distintos protocolos anteriormente comentados. En todas estas pruebas, optamos por realizar el marcaje enzimático una vez digeridas las muestras, al considerar que de esta manera tanto la digestión como el marcaje se llevan a cabo en condiciones óptimas de pH y concentración salina [147]. En estos ensayos, partimos de las condiciones establecidas en trabajos previos de nuestro grupo [55, 57], en los que la reacción de intercambio de oxígeno se hizo a pH 6,75 en presencia de $CaCl_2$, utilizando tripsina soluble y parando la reacción mediante la adición de ácido fórmico. Para cada condición experimental testada, estudiamos la estabilidad de la marca de ^{18}O analizando por espectrometría de masas de trampa iónica lineal las muestras marcadas con las distintas estrategias (Fig. R.1). Para ello, representamos el $\log_2$-ratio ($^{16}O/^{18}O$) frente a la eficiencia de marcaje *f*; en este gráfico, si las condiciones de marcaje son correctas, la eficiencia de marcaje debería ser próxima a la unidad, no detectándose cambios en la ratio.

La primera condición que se probó fue modificar el porcentaje de acetonitrilo (ACN) de la mezcla reactiva, ya que se ha descrito que la presencia de ACN aumenta la actividad de la tripsina en comparación con los medios puramente acuosos [148]. Como se ve en la Fig. R.1a, observamos que el aumento excesivo de la proporción de ACN impide que la reacción de marcaje tenga lugar al tener todos los péptidos identificados una eficiencia de incorporación de ^{18}O menor de 0,5. El aumento del volumen de reacción (Fig. R.1b) mejoró considerablemente la eficiencia de marcaje (*f*), mientras que disminuyendo el tiempo de la reacción de marcaje, sólo conseguimos mejorar moderadamente *f* (Fig. R.1c). Hervir e incubar la muestra con ácido fórmico (Fig. R.1d) no impidió que la muestra se desmarcara;

observamos también una reversión lenta de la reacción hirviendo únicamente la muestra (Fig. R.1e). Estos efectos de desmarcaje no se detectaban o era despreciables en experimentos en los que el análisis por espectrometría de masas se realizaba inmediatamente después de mezclar las muestras marcadas y sin marcar, indicando que todo los efectos observados se debían efectivamente a un desmarcaje gradual y no a un marcaje incompleto. Finalmente, cuando la muestra marcada se secaba y resuspendía en formiato amónico pH 3, observamos que la mayoría de los péptidos permanecían marcados con una eficiencia del 80-90 % (Fig. R.1f), independientemente del tiempo transcurrido entre el marcaje y el análisis por espectrometría de masas. Por lo tanto, como la estrategia de análisis inmediato por espectrometría de masas no era viable para experimentos a gran escala, era necesario mejorar las condiciones de marcaje para mantener un etiquetado que fuese estable incluso durante meses.

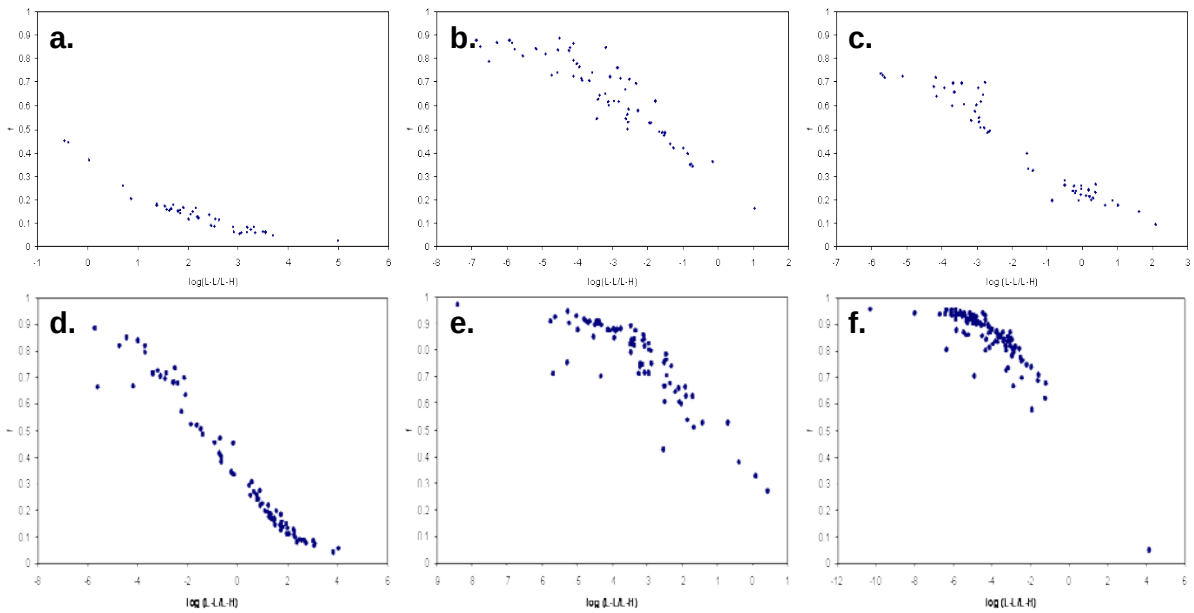

Fig. R.1.- Análisis de la eficiencia de marcaje en los experimentos de optimización del protocolo de marcaje con ^{18}O. Las distintas condiciones probadas incluyeron el aumento de la proporción de solvente orgánico en la mezcla de reacción **(a.)**, el aumento del volumen de manipulación de la muestra **(b.)**, la disminución del tiempo de la etapa de marcaje **(c.)**, hervir e incubar la muestra con ácido fórmico durante 48 h **(d.)**, hervir solamente la muestra después de la etapa de marcaje **(e.)**, secar y resuspender la muestra en formiato amónico a pH 3 **(f.)**, siendo esta última la estrategia óptima para obtener una eficiencia de marcaje de la mayoría de los péptidos > 0,8.

Se ha descrito que la actividad residual de la tripsina utilizada para marcar los péptidos con ^{18}O es en parte responsable del intercambio del oxígeno cuando los péptidos marcados se

resuspenden en un medio conteniendo agua no marcada. Por todas estas razones, desarrollamos un método en el que, una vez digeridas las proteínas a un pH óptimo de 8,8, los péptidos se marcan en presencia de $H_2{}^{18}O$ en acetato amónico pH 6 con 20 % de ACN durante toda la noche. En el nuevo protocolo utilizamos tripsina inmovilizada en bolas de agarosa, las cuales pueden ser retiradas del medio utilizando un filtro físico, y las muestras se sometieron a una nueva etapa de reducción-alquilación, con objeto de asegurarnos de que la enzima queda completamente inactivada. Esta desnaturalización es posible porque la tripsina es una proteína cuya estructura tridimensional está altamente estabilizada por puentes disulfuro [149], y evita una posible actividad tríptica residual que pudiese existir tras la eliminación de las bolas de tripsina al romperse la unión agarosa-proteasa. Esta última etapa es fundamental al haberse descrito que el intercambio inverso puede ocurrir incluso aunque se baje el pH a valores en los que la tripsina supuestamente no es activa [49]. Para asegurarnos de que no se producen pérdidas de material por la unión inespecífica de los péptidos a la agarosa como ya ha sido descrito [150], el protocolo incluye el análisis de alícuotas de 5 µg de péptidos antes y después de la etapa de marcaje, asegurándonos de la reproducibilidad de los cromatogramas así como de una misma eficiencia de identificación de los péptidos. Finalmente, para evitar el desmarcaje por hidrólisis ácida, observado al utilizar ácido fórmico o ácido trifluoroacético como estrategia para inactivar la tripsina, el pH se mantuvo a 3 durante todas las etapas posteriores al marcaje, incluyendo las etapas de desalado y fraccionamiento por HPLC-SCX. Los péptidos se analizaron en un medio conteniendo 5 mM de formiato amónico a pH 3, lo que garantiza por un lado que el pH sea suficientemente bajo para favorecer la unión de los péptidos a la matriz C18 de la columna de cromatografía de fase reversa (RP) en línea con el espectrómetro de masas sin desmarcar los péptidos, y, por otro lado, que la concentración de formiato amónico sea lo suficientemente alta para mantener tamponado el medio sin que las sales interfieran en el análisis por masas. Este paso es crítico para mantener un marcaje estable y unas cuantificaciones fiables en cualquier experimento masivo.

Como se puede observar en la Fig. R2, utilizando el protocolo optimizado de marcaje con ^{18}O, todos los péptidos de una serie de experimentos de cuantificación por marcaje isotópico usando varios proteomas mantuvieron su marca durante todo el procesamiento de las muestras, y se estimó que, para cada experimento y para la mayoría de los péptidos, f era superior a 0,8. Por consiguiente, y puesto que la eficiencia de marcaje es la proporción de átomos de oxígeno que están en forma del isótopo ^{18}O en el grupo carboxilo C-terminal, la proporción de péptidos no marcados provenientes de la muestra marcada, que corresponde a $(1 - f)^2$ en ningún caso es superior al 4 %, que sería el error máximo que se cometería al

calcular la abundancia relativa. A estos altos niveles de eficiencia de marcaje, por tanto, el efecto de un marcaje incompleto sobre la cuantificación es despreciable y, en todo caso, se puede corregir teniendo en cuenta el factor de corrección del marcaje [57].

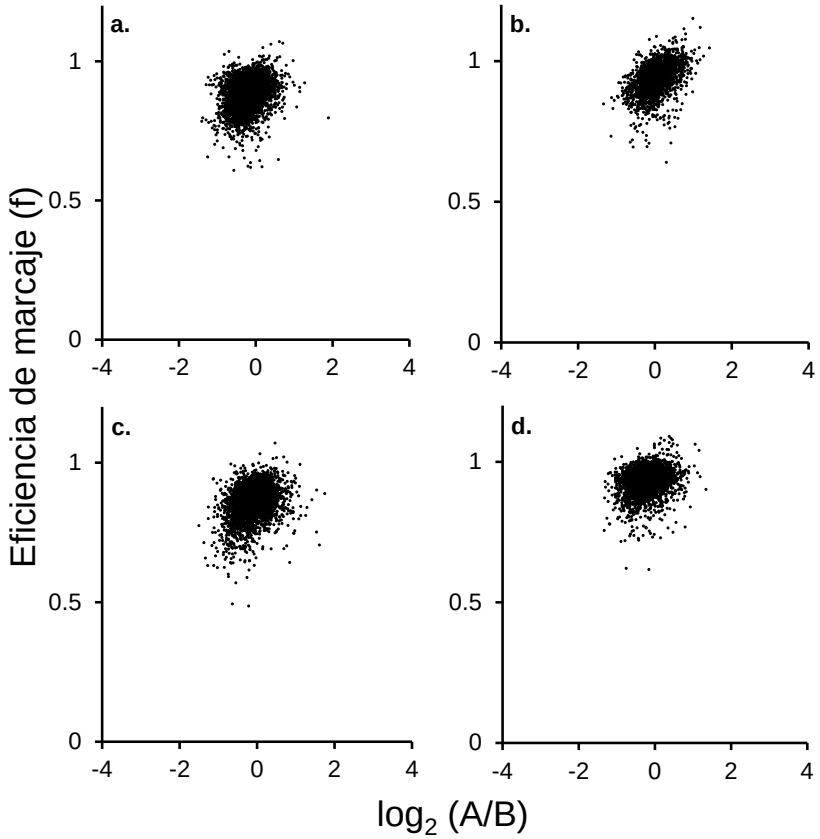

Fig. R.2.- Distribución de la eficiencia de marcaje (*f*) con ^{18}O frente al $\log_2$ del ratio de A/B. A corresponde a la concentración de péptido en la muestra no marcada, y B a la concentración de los péptidos marcados con ^{18}O. Representación de las distribuciones para los distintos experimentos de análisis de los cambios de abundancia del proteoma de HUVEC: **(a.)** hipótesis nula, **(b.)** réplica a pequeña escala, experimento de 4 h **(c.)** y de 8 h **(d.)** de tratamiento con VEGF, respectivamente.

R.1.2.- Aplicación al estudio de los cambios de abundancia del proteoma de HUVEC inducidos por VEGF

Con objeto de validar el nuevo método de marcaje, lo aplicamos al estudio de los cambios generados en el proteoma de células HUVEC por el factor de crecimiento VEGF a 4 y 8 h de estimulación. Este trabajo se realizó en colaboración con la Dra. Inmaculada Jorge y el laboratorio del Prof. Juan-Miguel Redondo del CNIC. Como se ha comentado en la introducción, el VEGF es un agente mitógeno específico de las células endoteliales, implicado en la cicatrización, en la angiogénesis, en el crecimiento tumoral, en la permeabilidad

microvascular y en la hemostasis [151]. Se ha demostrado que este factor activa varias vías de señalización intracelular, pero los cambios inducidos en las células a nivel de proteoma en este modelo *in vitro* de angiogénesis apenas se conocen.

R.1.2.1.- Aproximación experimental

Se realizaron tres análisis por espectrometría de masas de un extracto crudo de proteínas de HUVEC (1 mg de muestra control y 1 mg de muestra tratada). En el primero de ellos, el experimento 0, o experimento test, se compararon dos alícuotas idénticas de una misma muestra con el objetivo de testar la hipótesis nula y comprobar la robustez del modelo estadístico desarrollado para la interpretación de los datos cuantitativos [64, 65]. En los siguientes análisis, las células fueron incubadas en presencia de VEGF durante 4 u 8 h, respectivamente. Finalmente, también se hizo una réplica a pequeña escala del experimento de 4 h analizando 100 µg de extracto proteico con el fin de validar los resultados obtenidos a escala masiva.

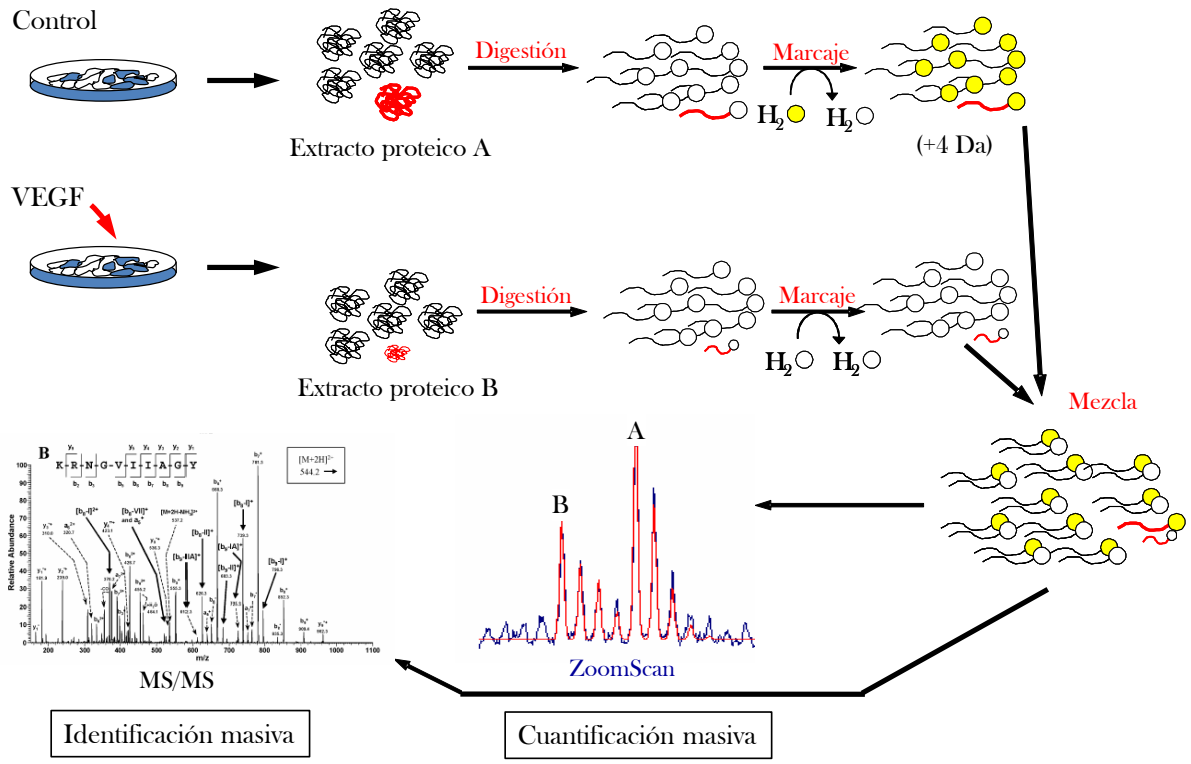

Fig. R.3.- Estrategia experimental de marcaje con ^{18}O en disolución y su aplicación al estudio del efecto del VEGF en el proteoma de células HUVEC. Las proteínas de los cultivos control y tratado con VEGF se digirieron con tripsina y se marcaron con ^{18}O. Tras inactivar la tripsina y mantener las muestras a pH 3, los péptidos se mezclaron y se analizaron por espectrometría de masas previa separación multidimensional por HPLC.

Las muestras control y tratada se digirieron primero con tripsina y, posteriormente, se expusieron a la reacción de intercambio de ^{16}O por ^{18}O utilizando el protocolo optimizado descrito en el apartado anterior. Los péptidos de la muestra tratada con VEGF se marcaron con ^{18}O, mientras que los de la muestra control se incubaron con agua normal $H_2{}^{16}O$. Las muestras se mezclaron, se fraccionaron por intercambio iónico fuerte (SCX) en HPLC y se analizaron por espectrometría de masas utilizando gradientes de 170 min. En estas condiciones, cada experimento dura varias semanas, de forma que por cada análisis masivo, el espectrómetro de masas está funcionando durante un mes ininterrumpidamente. Como se ha descrito en un trabajo anterior del laboratorio [55], la trampa lineal se programó para realizar un espectro de media-alta resolución (*ZoomScan*) seguido de un espectro de fragmentación MS/MS en los 6 iones más intensos detectados en el espectro de barrido *FullScan*. Utilizamos el espectro *ZoomScan* para cuantificar los dobletes péptidicos marcados con ^{16}O / ^{18}O y los espectros MS^2 para identificar el péptido en una base de datos de proteínas (Fig. R.3). Los espectros *ZoomScan* se analizaron utilizando QuiXoT, un software desarrollado previamente en el laboratorio [64, 139, 140], que ajusta la envoltura isotópica completa a la suma de las envolturas isotópicas teóricas de cuatro especies: la especie no marcada proveniente de la muestra no marcada, y las especies no marcada, la marcada con un solo átomo de ^{18}O y la que ha incorporado dos ^{18}O en la muestra marcada [57]. La determinación de la eficiencia de marcaje se llevó a cabo utilizando el modelo cinético descrito anteriormente (Fig. R.4) [57].

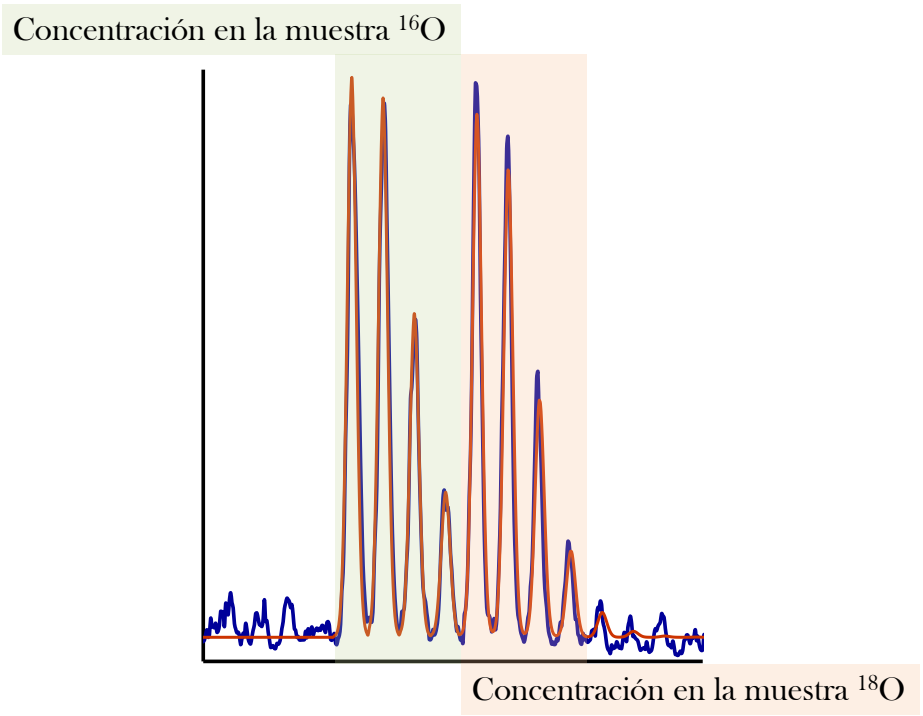

Fig. R.4.- Cuantificación de los péptidos por el software QuiXoT. El programa permite el control de la eficiencia de marcaje de todos y cada uno de los péptidos cuantificados, mediante un ajuste del espectro (línea azul) a una curva teórica (línea roja) definida simultáneamente por las concentraciones de péptido (en unidades de área) de las dos muestras analizadas, la eficiencia de marcaje, y otros factores que definen este tipo de espectros como por ejemplo la señal de fondo o el ancho de pico. En verde se representa la parte del espectro correspondiente a la muestra no marcada, y en naranja, la de la muestra con ^{18}O.

En cada uno de los experimentos masivos, alrededor de 10.000 espectros de fragmentación fueron asignados a una secuencia peptídica con una FDR del 5 % utilizando el método de la razón de probabilidades [137]. Estos espectros de fragmentación se asignaron a aproximadamente 4.000 péptidos únicos y 2.000 proteínas únicas para cada experimento (Tabla T.1), haciendo un total de 3.878 proteínas únicas si se combinan los cuatro experimentos.

Tabla T.1
Estadística de identificación y de cuantificación en los 3 experimentos masivos

	Test	VEGF	
		4 h	8 h
Fracciones de SCX	71	64	92
Espectros de fragmentación MS/MS	142.585	134.59	149.713
Espectros MS/MS identificados (1)	13.701	9.171	12.196
Péptidos únicos	4.878	4.806	3.876
Proteínas únicas	2.461	1.982	2.085
Espectros cuantificados	7.640	5.097	4.391
Péptidos únicos cuantificados	2.271	2.556	1.218
Proteínas únicas cuantificadas	1.246	1.278	890
Varianza a nivel de espectro (s^2_S) (95% C.I.)	0,018 (0,016-0,020)	0,024 (0,022 - 0,026)	0,031 (0,028 - 0,034)
Varianza a nivel de péptido (s^2_P) (95% C.I.)	0,021 (0,014-0,028)	0,019 (0,014 - 0,026)	0,014 (0,006 - 0,023)
Varianza a nivel de proeína (s^2_Q) (95% C.I.)	0,0007 (0-0,009)	0,004 (0 - 0,12)	0,003 (0 - 0,011)
Cambios de abundancia significativos (2)	1	26	37

(1) con una FDR de identificación igual o menor del 5 %, calculada usando pRatio [137]
(2) Valores atípicos a nivel de proteína con una FDRq menor del 5 %

R.1.2.2.- Estudio de los cambios de abundancia generados por el VEGF en el proteoma de células HUVEC a distintos tiempos de incubación

Desde el punto de vista puramente estadístico, los valores que se desvían más de lo esperado de la media de las cuantificaciones a nivel de proteína ("supermedia") representan cambios de abundancia. Las cuantificaciones de proteínas con FDRq < 10 % se inspeccionaron manualmente. La relación de proteínas que cambian su abundancia a 4 y 8 h de tratamiento se muestra en las tablas T.2 y T.3, respectivamente.

Tabla T.2
Cambios de abundancia significativos del proteoma de HUVEC tras 4 h de tratamiento con VEGF

Proteína	Nº Acceso	(X_q-X) ±SD (n)	-Fold Change	p_q	FDR_q (%)
Calreticulin [Precursor]	P27797	1.03 ± 0.14 (2)	2.04 down	3.3E-14	0.00%
Cofilin-2	Q9Y281	1.86 ± 0.26 (1)	3.62 down	2.1E-12	0.00%
Tyrosyl-tRNA synthetase, cytoplasmic	P54577	1.53 ± 0.22 (1)	2.88 down	8.9E-12	0.00%
Triosephosphate isomerase	P60174	1.03 ± 0.16 (2)	2.04 down	3.3E-11	0.00%
Calumenin [Precursor]	O43852	0.96 ± 0.15 (2)	1.94 down	4.3E-10	0.00%
von Willebrand factor [Precursor]	P04275	0.41 ± 0.08 (12)	1.33 down	4.3E-07	0.01%
UDP-glucose:glycoprotein glucosyltransferase 1 [Precursor]	Q9NYU2	1.13 ± 0.23 (1)	2.20 down	4.8E-07	0.01%
Multifunctional protein ADE2	P22234	1.18 ± 0.23 (1)	2.27 down	4.0E-07	0.01%
Rho GTPase-activating protein 29	Q52LW3	1.22 ± 0.26 (1)	2.33 down	2.1E-06	0.04%
Annexin A1	P04083	0.44 ± 0.10 (5)	1.36 down	8.3E-06	0.1%
Eukaryotic translation initiation factor 5B	O60841	0.61 ± 0.14 (3)	1.53 down	7.7E-06	0.1%
Reticulocalbin-1 [Precursor]	Q15293	0.55 ± 0.13 (3)	1.46 down	2.5E-05	0.3%
Heat shock protein HSP 90-alpha	P07900	0.36 ± 0.09 (9)	1.28 down	3.0E-05	0.3%
Gamma-interferon-inducible protein Ifi-16	Q16666	0.77 ± 0.20 (1)	1.71 down	7.6E-05	0.6%
YTH domain family protein 2	Q9Y5A9	0.97 ± 0.25 (1)	1.97 down	8.7E-05	0.7%
Flotillin-1	O75955	0.92 ± 0.24 (1)	1.89 down	9.7E-05	0.7%
Lupus La protein	P05455	0.75 ± 0.20 (1)	1.68 down	0.0002	1.1%
RRP1-like protein B	Q14684	0.91 ± 0.25 (1)	1.88 down	0.0002	1.3%
T-complex protein 1 subunit theta	P50990	0.47 ± 0.13 (3)	1.38 down	0.0002	1.5%
Obg-like ATPase 1	Q9NTK5	0.56 ± 0.16 (2)	1.48 down	0.0004	2.4%
Coatomer subunit beta'	P35606	0.59 ± 0.17 (2)	1.50 down	0.0006	3.4%
Phosphoglycerate mutase 1	P18669	0.63 ± 0.19 (1)	1.55 down	0.0009	4.5%
Cation-dependent mannose-6-phosphate receptor [Precursor]	P20645	0.77 ± 0.23 (1)	1.70 down	0.0011	5.1%
Cytochrome b-c1 complex subunit 1, mitochondrial [Precursor]	P31930	0.54 ± 0.17 (2)	1.45 down	0.0014	5.9%
tRNA (cytosine-5-)-methyltransferase NSUN2	Q08J23	0.80 ± 0.25 (1)	1.74 down	0.0014	6.1%
Carbonyl reductase [NADPH] 1	P16152	0.76 ± 0.25 (1)	1.69 down	0.0021	8.3%
Staphylococcal nuclease domain-containing protein 1	Q7KZF4	0.41 ± 0.13 (3)	1.33 down	0.0022	8.7%
Proteasome subunit alpha type-3	P25788	-0.76 ± 0.19 (1)	1.70 up	7.6E-05	0.6%
Replication protein A 14 kDa subunit	P35244	-0.81 ± 0.24 (1)	1.75 up	0.0006	3.1%
Alpha-endosulfine	O43768	-0.80 ± 0.24 (1)	1.75 up	0.0009	4.3%
Squamous cell carcinoma antigen recognized by T-cells 3	Q15020	-0.76 ± 0.23 (1)	1.69 up	0.0010	4.6%
Methionine adenosyltransferase 2 subunit beta	Q9NZL9	-0.73 ± 0.23 (1)	1.65 up	0.0017	6.7%

X_q: $\log_2$-ratio de la proteína
X: "supermedia" del experimento
SD: desviación estándar
(n) número de péptidos cuantificados por proteína
p_q: probabilidad de que una proteína se desvíe de la media de las proteínas
FDR_q: tasas de error a nivel de proteína

Tabla T.3
Cambios de abundancia significativos del proteoma de HUVEC tras 8 h de tratamiento con VEGF

Proteína	Nº Acceso	(X_q-X) ±SD (n)	-Fold Change	p_q	FDR_q (%)
Tryptophanyl-tRNA synthetase, cytoplasmic	P23381	1.22 ± 0.14 (1)	2.34 down	0.0E+00	0.00%
Purine nucleoside phosphorylase	P00491	0.97 ± 0.14 (1)	1.95 down	2.7E-12	0.00%
Echinoderm microtubule-associated protein-like 3	Q32P44	1.16 ± 0.19 (1)	2.23 down	2.0E-09	0.00%
Ubiquitin carboxyl-terminal hydrolase 5	P45974	1.40 ± 0.24 (1)	2.63 down	4.3E-09	0.00%
High mobility group protein B2	P26583	0.99 ± 0.16 (1)	1.99 down	1.8E-09	0.00%
Lamin-B1	P20700	1.01 ± 0.17 (1)	2.01 down	7.8E-09	0.00%
Mitochondrial inner membrane protein	Q16891	0.74 ± 0.16 (1)	1.68 down	1.7E-06	0.02%
Probable palmitoyltransferase ZDHHC13	Q8IUH4	1.29 ± 0.27 (1)	2.45 down	2.0E-06	0.03%
Nucleolin	P19338	0.94 ± 0.20 (1)	1.92 down	2.9E-06	0.03%
Interferon-induced transmembrane protein 3	Q01628	0.88 ± 0.19 (1)	1.84 down	2.5E-06	0.03%
Myotrophin	P58546	1.00 ± 0.23 (1)	1.99 down	1.4E-05	0.1%
Cofilin-2	Q9Y281	0.81 ± 0.19 (1)	1.75 down	2.4E-05	0.2%
Nuclear receptor-binding factor 2	Q96F24	0.94 ± 0.23 (1)	1.92 down	5.0E-05	0.3%
Casein kinase II subunit beta	P67870	0.70 ± 0.17 (1)	1.62 down	4.9E-05	0.4%
CDGSH iron sulfur domain-containing protein 2	Q8N5K1	0.86 ± 0.22 (1)	1.81 down	8.5E-05	0.5%
Zinc transporter 1	Q9Y6M5	0.88 ± 0.23 (1)	1.84 down	0.0001	0.7%
Pirin	O00625	0.84 ± 0.23 (1)	1.79 down	0.0002	1.3%
Glutaredoxin-3	O76003	0.61 ± 0.18 (1)	1.53 down	0.0005	2.3%
Transcription intermediary factor 1-beta	Q13263	0.65 ± 0.19 (1)	1.57 down	0.0005	2.4%
Serpin H1 [Precursor]	P50454	0.48 ± 0.14 (1)	1.40 down	0.0007	3.0%
Superoxide dismutase [Cu-Zn]	P00441	0.98 ± 0.29 (1)	1.97 down	0.0009	3.1%
UBX domain-containing protein 8	Q96CS3	0.57 ± 0.17 (1)	1.48 down	0.0009	3.2%
Ran GTPase-activating protein 1	P46060	0.49 ± 0.15 (1)	1.41 down	0.0009	3.3%
Interleukin enhancer-binding factor 2	Q12905	0.54 ± 0.17 (1)	1.45 down	0.0012	3.5%
40S ribosomal protein S14	P62263	0.48 ± 0.15 (1)	1.39 down	0.0011	3.5%
Protein FADD	Q13158	0.74 ± 0.23 (1)	1.67 down	0.0017	4.5%
ATP-dependent RNA helicase DDX39	O00148	0.40 ± 0.13 (2)	1.32 down	0.0019	4.8%
Enoyl-CoA hydratase, mitochondrial [Precursor]	P30084	0.47 ± 0.15 (1)	1.39 down	0.0023	5.2%
Protein-L-isoaspartate(D-aspartate) O-methyltransferase	P22061	0.76 ± 0.25 (1)	1.70 down	0.0022	5.2%
Translation initiation factor eIF-2B subunit delta	Q9UI10	0.76 ± 0.26 (1)	1.69 down	0.0045	8.9%
Leucine-rich repeat flightless-interacting protein 1	Q32MZ4	-0.66 ± 0.18 (1)	1.58 up	0.0003	1.3%
Eukaryotic translation initiation factor 2A	Q9BY44	-0.45 ± 0.13 (3)	1.37 up	0.0003	1.4%
Patatin-like phospholipase domain-containing protein 2	Q96AD5	-1.06 ± 0.31 (1)	2.09 up	0.0005	2.3%
Succinate dehydrogenase [ubiquinone] flavoprotein subunit, mitochondrial	P31040	-0.57 ± 0.17 (2)	1.48 up	0.0008	3.0%
Delta-1-pyrroline-5-carboxylate synthetase	P54886	-0.59 ± 0.18 (2)	1.51 up	0.0010	3.1%
Eukaryotic translation initiation factor 3 subunit E	P60228	-0.60 ± 0.18 (1)	1.51 up	0.0010	3.1%
Palmdelphin	Q9NP74	-0.99 ± 0.31 (1)	1.99 up	0.0012	3.5%
Periodic tryptophan protein 1 homolog	Q13610	-0.60 ± 0.19 (1)	1.52 up	0.0015	4.2%
Matrin-3	P43243	-0.61 ± 0.20 (1)	1.53 up	0.0017	4.5%
Protein ERGIC-53 [Precursor]	P49257	-0.54 ± 0.18 (1)	1.46 up	0.0020	4.6%
Vacuolar protein sorting-associating protein 4A	Q9UN37	-0.46 ± 0.15 (2)	1.37 up	0.0020	5.0%
Mitofusin-2	O95140	-0.49 ± 0.16 (1)	1.40 up	0.0027	6.0%
Protein disulfide-isomerase A4 [Precursor]	P13667	-0.39 ± 0.13 (2)	1.31 up	0.0034	7.2%
Myosin-Id	O94832	-0.39 ± 0.13 (2)	1.31 up	0.0038	8.1%
Heat shock 70 kDa protein 1	P08107	-0.66 ± 0.23 (1)	1.58 up	0.0040	8.5%
Synaptic vesicle membrane protein VAT-1 homolog	Q99536	-0.39 ± 0.14 (2)	1.31 up	0.0044	8.7%

Algunos cambios de abundancia detectados son pequeños aunque estadísticamente significativos; esas proteínas suelen tener un peso estadístico muy alto debido a que se cuantifican con varios péptidos diferentes [65]. El peso estadístico a nivel de proteína, que se define como la inversa de la varianza de la proteína, refleja la calidad y la precisión de la cuantificación[64], de manera que las mediciones más precisas (con una varianza menor) tienen una significatividad estadística mayor que las de baja calidad (con una varianza mayor). El peso estadístico tiene en cuenta, entre otras cosas, el hecho de que las cuantificaciones de proteína son más fiables cuanto mayor es el número de péptidos cuantificados para esa

proteína. Un claro ejemplo se representa en la Fig R.5A, en la que se observa que el factor von Willebrand disminuye únicamente 1,33 veces a 4 h de estimulación. Este cambio es muy pequeño pero detectable y consistente para cada uno de sus 12 péptidos únicos cuantificados, hasta el punto de que está asociado a una FDRq menor del 0,01 %. Sin embargo, a 8 h de estimulación con VEGF, la abundancia del factor von Willebrand no se ve alterada por el tratamiento (Fig R.5b). En claro contraste, y como control de cuantificación, representamos los espectros *ZoomScan* de 4 péptidos de la tubulina β, proteína también muy abundante, y observamos que tanto a 4 como a 8 h de tratamiento con el factor de crecimiento, la abundancia de la proteína no cambia por el tratamiento (Fig. R.5C y R.5D). Otras proteínas, como por ejemplo la cofilina-2, fueron cuantificadas por un número menor de péptidos únicos, aunque su cambio de abundancia era mayor (Tabla T.2).

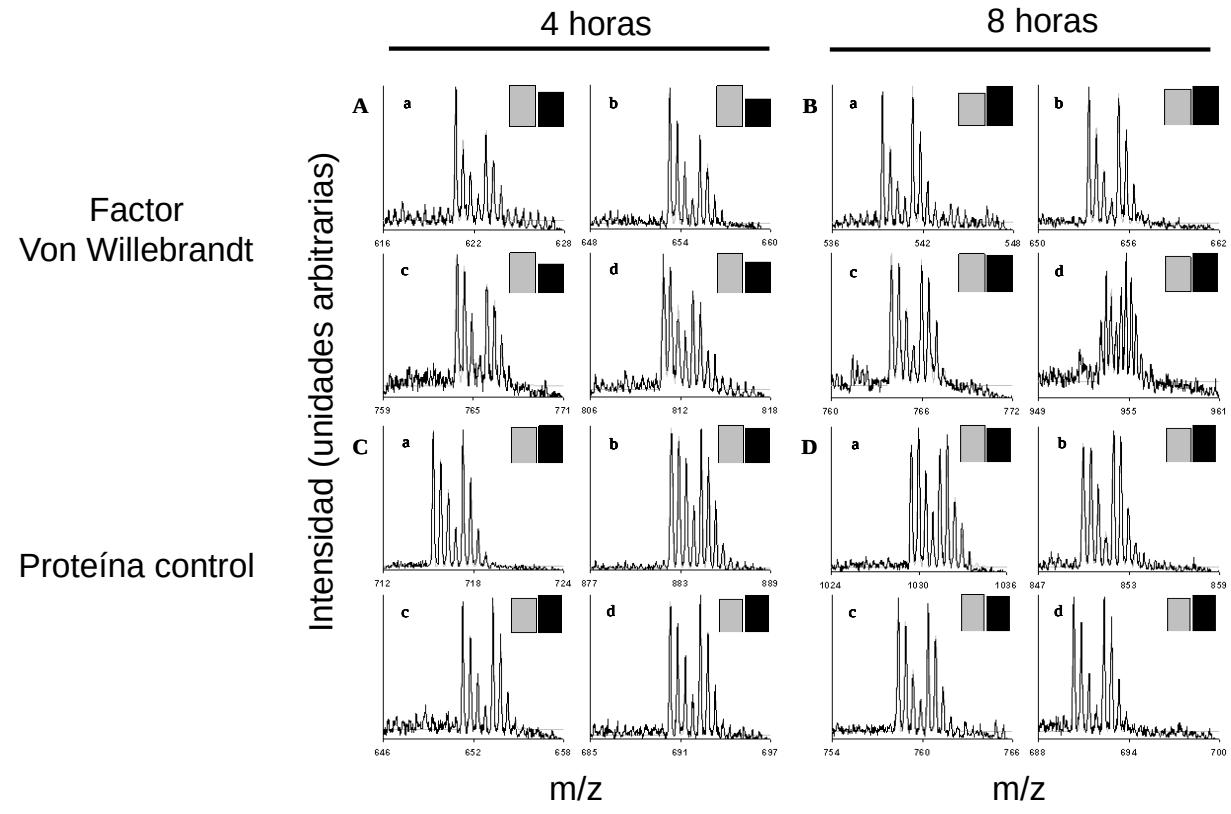

Fig. R.5.- Sensibilidad del modelo estadístico. El modelo estadístico jerárquico permite detectar cambios de abundancia muy leves como el del factor von Willebrandt (**A** y **B**) así como demostrar de forma robusta que otras proteínas no ven su abundancia alterada por el tratamiento, como la tubulina β (**C** y **D**). Los diagramas de barras traducen los datos de cuantificación del *ZoomScan* correspondiente (en gris se representa la concentración del péptido en la muestra no marcada y en negro la del péptido con ^{18}O).

En este estudio, se detectaron 32 y 46 proteínas con cambios en su abundancia estadísticamente significativos tras el tratamiento con VEGF durante 4 y 8 h, respectivamente (Tablas T.2 y T.3). La mayoría de las proteínas del proteoma de células HUVEC que cambian (84 %) tienen una abundancia disminuida tras 4 h de estimulación por el factor de crecimiento (Fig. R.6a), mientras que la diferencia entre disminuciones y aumentos de abundancia (65 y 35 %, respectivamente) es menor cuando el tratamiento se lleva a cabo durante 8 h (Fig. R.6b). Este resultado sugiere que el perfil de expresión del proteoma de HUVEC en respuesta al VEGF es bifásico, lo cual sería consistente con el hecho de que casi todos los cambios de abundancia de las proteínas son diferentes entre 4 y 8 h de tratamiento. De acuerdo con las anotaciones de la base de datos *Gene Onthology (GO)*, la mayoría de las proteínas con abundancia alterada tras 4 h de tratamiento son citoplásmicas y están implicadas en el plegamiento de proteínas, mientras que a 8 h de estimulación, la mayoría de las proteínas son citosólicas o asociadas a las membranas de diferentes orgánulos, implicadas principalmente en la respuesta celular a distintos estímulos.

Entre los distintos experimentos, se cuantificaron un total de 1.319 proteínas únicas. Si comparamos nuestros resultados con otros estudios del proteoma de HUVEC existentes en la literatura, observamos que la mayoría de las proteínas que identificamos con una abundancia alterada se han descrito con técnicas basadas en geles bidimensionales como sensibles al VEGF a tiempos largos de incubación (24 h [152] o 48 h [153]) o sensibles al sulfato de sokotrasterol [76], factor de origen marino descrito como activador de la angiogénesis [154]. Sin embargo, pocos de los cambios detectados en esos estudios han sido corroborados en nuestros modelos. Entre las proteínas que hemos detectado con cambio de abundancia, la anexina A1 [153], la reticulocalbina [152], así como la proteína activadora de Ran y la triosa fosfato isomerasa [76] han sido descritas previamente, pero con un cambio que va en el sentido contrario al que nosotros hemos cuantificado. Sin embargo, el cambio detectado para la proteína activadora de Ran coincide con dos trabajos publicados anteriormente [152, 153]; junto con la proteína 70 de choque térmico, éstas dos proteínas son las dos únicas que coinciden en la bibliografía con nuestros resultados.

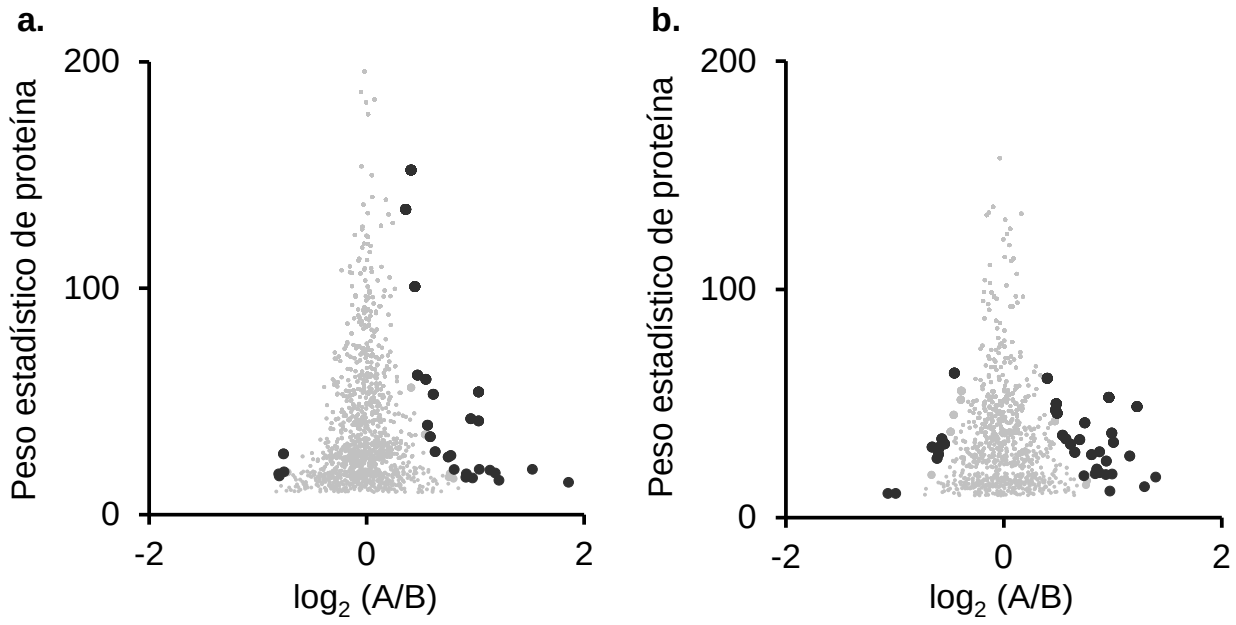

Fig. R.6.- Análisis de los cambios de abundancia estadísticamente significativos a nivel de proteína. Representación del peso estadístico en función del $\log_2$(ratio) a nivel de proteína correspondientes a los experimentos de tratamiento de HUVEC con VEGF durante 4h (**a.**) y 8h (**b.**). Los cambios de abundancia (puntos negros) se detectan utilizando como criterio aquellas desviaciones atípicas a nivel de proteína con FDRq < 5 %.

La coherencia de los resultados se estudió realizando una réplica técnica a pequeña escala del efecto del VEGF en células HUVEC a 4 h de estimulación y comparando los resultados con el experimento masivo (Fig. R.7). Como cabría esperar, no todas las proteínas detectadas en el experimento masivo se identificaron a pequeña escala. Sin embargo, todas las proteínas que cambiaban de abundancia en el experimento a pequeña escala cambiaban con la misma tendencia en el experimento masivo.

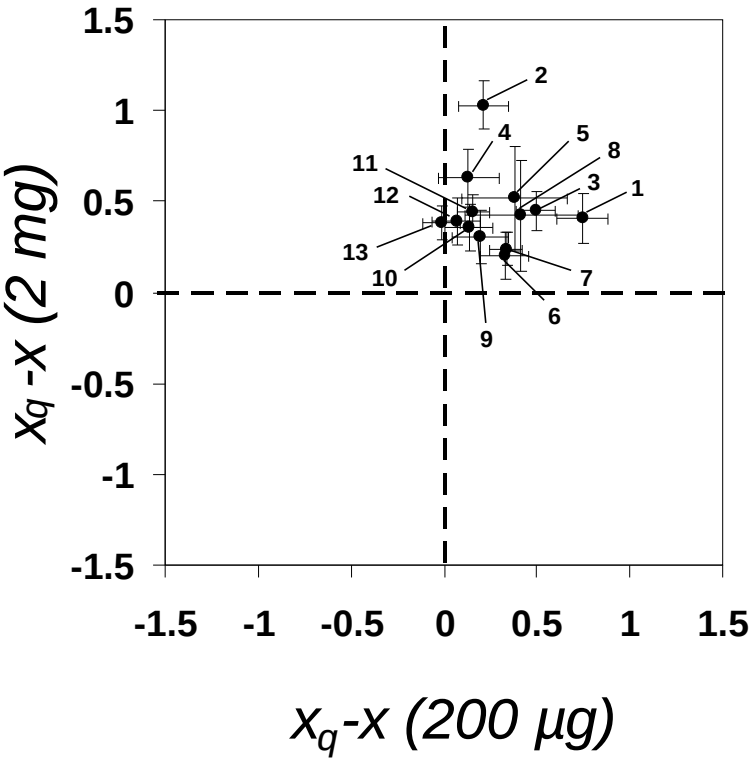

Fig. R.7.- Consistencia de los cambios de abundancia en los dos experimentos de 4 h de tratamiento con VEGF. La lista de proteínas que muestran un cambio de abundancia significativo a un nivel de FDRq < 35% (p_q < 0.02) en el experimento VEGF 4h a gran escala es comparada con las mismas proteínas cuantificadas en el experimento de réplica a pequeña escala, y los valores de x_q de un experimento son representados frente a los observados en el otro. Las barras de error representan las desviaciones estándar de las medias de las cuantificaciones de proteína ($\sqrt{w_q^{-1}}$). Los números hacen referencia a las siguientes proteínas: [1] factor von Willebrand (P04275), [2] calreticulina (P27797), [3] proteína 14-3-3 ζ/δ (P63104), [4] fosfoglicerato mutasa 1 (P18669), [5] inhibidor alfa de la disociación de GDP de la proteína Rab (P31150), [6] enzima activadora de uniquitina E1 (P22314), [7] vimentina (P08670), [8] reductasa mitocondrial de peróxido dependiente de tioredoxina (P30048), [9] proteína de choque térmico hsp90 β (P08238), [10] proteína de choque térmico hsp90 α (P07900), [11] anexina A1 (P04083), [12] proteína 14-3-3 theta (P27348) y [13] triosa fosfato isomerasa (P60174).

Con el objetivo de validar algunos de los cambios de abundancia detectados por marcaje isotópico, decidimos analizar por *Western-blot*, en colaboración con la Dra. Arantza Alfranca y el Prof. Juan-Miguel Redondo, el comportamiento de las tres proteínas que, de acuerdo a los datos bibliográficos, se comportan de manera opuesta a la que nosotros hemos descrito. Para ello, se incubaron células HUVEC con VEGF durante 4 y 8 h, así como durante 16 y 24 h para determinar el comportamiento de esas proteínas a tiempos de incubación largos, monitorizando los niveles de tubulina β como control interno (Fig. R.8). A pesar de que los cambios detectados por espectrometría de masas eran pequeños (2-fold o menos) y, por

tanto, difíciles de analizar por *Western-blot*, fuimos capaces de observar una disminución de las bandas correspondientes a la reticulocalbina-1 y a la anexina A1 frente al control tras 4 h de tratamiento. Sin embargo, en el examen directo del *Western-blot*, no se apreciaba ningún cambio en la banda correspondiente a la triosa fosfato isomerasa. A continuación, se realizó un estudio de densitometría de todas las bandas y a todos los tiempos de incubación, el cual reveló que el patrón de expresión relativa detectado era consistente con el análisis por espectrometría de masas (Fig. R.8b): las tres proteínas siguen un mismo patrón de expresión, en el que su abundancia baja a 4 h de tratamiento, recuperando el nivel basal cuando el tratamiento se extiende en el tiempo. Considerando que los cambios detectados en la triosa fosfato isomerasa y en la anexina A1 se confirmaron también en el experimento réplica a pequeña escala (Fig. R.7), estos resultados nos indican que la maquinaria celular responde de manera específica al tratamiento a tiempos cortos de incubación lo cual no permite hacer una comparación exacta con los resultados bibliográficos, realizados a distintos tiempos de incubación. Por último, observamos que algunas de las proteínas alteradas a 4 u 8 h de tratamiento con VEGF y que no se detectaron en estudios anteriores tienen un papel importante en la angiogénesis, como la triglicérido lipasa adiposa [155], la hsp90 [156, 157], la nucleolina [158], la cofinila-2 [159, 160], y las tirosil-ARNt y triptofanil-ARNt sintetasas [161, 162].

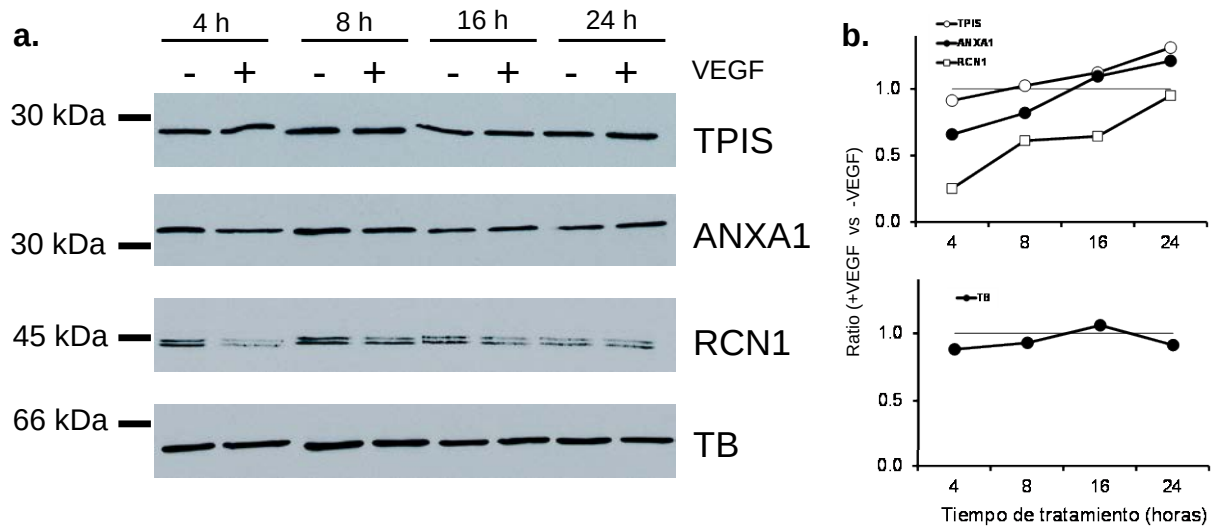

Fig. R.8.- Validación por Western-blot de algunos de los cambios de abundancia detectados por MS/MS en este estudio. (a.) Los extractos de proteínas de células control de HUVEC o tratadas con VEGF a distintos tiempos se separaron en un gel SDS-PAGE, se transfirieron a membrana y se analizaron utilizando anticuerpos específicos dirigidos contra la triosa fosfato isomerasa (TPIS), la anexina A1 (ANXA1) y la reticulocalbina-1 (RCN1), así como contra la tubulina β (TB) utilizada como control de carga. La posición de los estándares de peso molecular se indica a la izquierda. **(b.)** Las bandas detectadas por los anticuerpos se cuantificaron por densitometría, y se representó el ratio de las intensidades de las bandas de los extractos tratados con VEGF y sin tratar en función del tiempo de incubación. El análisis estadístico por los métodos convencionales de regresión indica una correlación significativa ($p < 0,02$) entre el ratio de proteínas y el tiempo de incubación para la TPIS, la ANXA1 y la RCN1, pero no para la TB ($p > 0,3$).

R.1.2.3.- Problemas asociados a la estrategia experimental

Esta estrategia de digestión en disolución, marcaje con ^{18}O y fraccionamiento por intercambio catiónico fuerte (SCX) nos permitió realizar el estudio más profundo hasta la fecha del proteoma de células HUVEC. No obstante, durante la optimización del protocolo de marcaje, observamos que los péptidos con digestiones parciales (definidos como los péptidos que contienen en su secuencia al menos un sitio de corte de tripsina) o metionina oxidada se desviaban del ratio esperado 1:1, ya que se trata de procesos que no ocurren con la misma extensión en las dos muestras a comparar. Este hecho nos sugirió que dichos péptidos no reflejaban la concentración real de la proteína al poderse identificar un mismo péptido bajo dos especies distintas (por ejemplo con Met ox y sin oxidar) con valores de cuantificación diferentes para cada una. Por esa razón, los péptidos con Met ox y sin ox, y los péptidos parcialmente digeridos, así como sus sub-péptidos, fueron considerados como no fiables para la cuantificación de las proteínas y tuvieron que ser eliminados del análisis. Como se observa

en la Tabla T.1, una vez eliminados los espectros de mala calidad (aproximadamente un 20 % de los espectros [64]), así como los péptidos con digestión parcial o con Met, el número de espectros utilizados para la cuantificación es mucho menor que el número de espectros de fragmentación identificados: únicamente cuantificamos la mitad de los péptidos previamente identificados.

Por otra parte, en un análisis posterior de los datos, constatamos que utilizando el protocolo descrito, una gran proporción de grupos amino de las Lys y de los extremos N-terminal de los péptidos sufrieron una reacción de alquilación con la yodoacetamida utilizada para la alquilación de Cys en la doble etapa de reducción-alquilación a la que las muestras son sometidas. Como se ha comentado anteriormente, la primera etapa es necesaria para obtener una digestión homogénea entre muestras y aumentar el rendimiento de generación de péptidos, mientras que la segunda se introdujo para la inactivación de la actividad residual de la tripsina que puede perdurar tras la etapa de marcaje. Los reactivos alquilantes como la IAM utilizada para alquilar los grupos tioles generados por la reducción con DTT y que, a su vez, mantienen las proteínas desnaturalizadas (Eq. 1.1), pueden reaccionar en cierta proporción con los grupos amino de los extremos N-terminal y de los residuos Lys (Eq. 1.2), produciendo una sobre-alquilación.

- $\text{Proteína-S}^- + \text{I-CH}_2\text{-CO-NH}_2 \longrightarrow \text{Proteína-S-CH}_2\text{-CO-NH}_2 + \text{I}^-$ (1)
- $\text{Proteína-NH}_2 + \text{I-CH}_2\text{-CO-NH}_2 \longrightarrow \text{Proteína-NH-CH}_2\text{-CO-NH}_2 + \text{I}^-$ (2)

Eq. 1.- Reacción de la IAM con Cys o con los grupos amino N-ter y de la Lys

Este efecto se detectó repitiendo las búsquedas de los datos crudos contra la base de datos añadiendo como modificación variable la carboxiamidometilación en Lys y en los extremos N-terminal de los péptidos [163]. Los resultados nos permitieron detectar una proporción relativamente elevada de péptidos con grupos amino modificados por IAM (20 %) que eran detectados en su gran mayoría como valores atípicos de cuantificación, con ratios significativamente diferentes al resto de péptidos sin modificar que formaban parte de la misma proteína (Fig. R.9). Además, observamos que el comportamiento de los péptidos con Lys modificada (Fig. R.9, puntos negros) y sin modificar (Fig. R.9, puntos blancos) era diferente (disminución y aumento de abundancia, respectivamente), sugiriendo que la reacción de sobre-

alquilación no fue homogénea en las dos muestras comparadas y que esos péptidos con Lys falseaban los datos de cuantificación de manera artefactual.

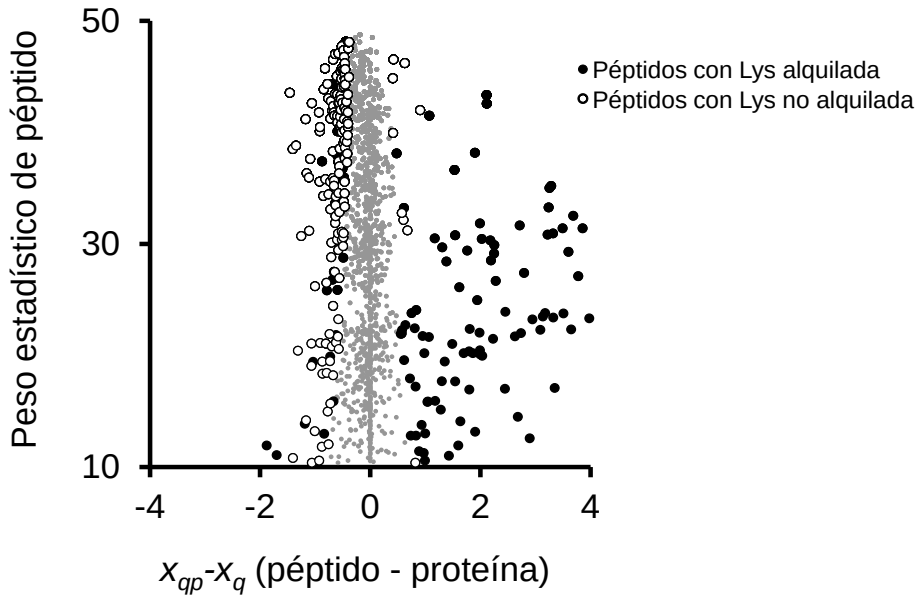

Fig. R.9.- Efecto de la sobre alquilación en la cuantificación relativa a nivel de péptido utilizando una etapa de reducción/alquilación para inactivar la tripsina post-marcaje. Se representa el peso estadístico de cada péptido frente a la diferencia entre el péptido y la media de la proteína de la que proviene. Los péptidos con Lys modificada por IAM (puntos negros) se desvían de la media de sus proteínas en sentido contrario a los péptidos con Lys no alquilada (puntos blancos), generando así datos de cuantificación erróneos.

En este punto es importante resaltar el hecho de que esta pérdida de datos de cuantificación respecto a los datos de identificación no se debe a la técnica de marcaje con ^{18}O en sí, ya que, como se muestra en la Fig. R.2, la eficiencia de marcaje está muy controlada en estos experimentos. Del mismo modo, esta disminución no se debe al modelo estadístico utilizado para analizar los datos, al ser el número valores atípicos a nivel de espectro y de péptido despreciable [64, 65]. La mayoría de los espectros de mala calidad eliminados se deben al poder resolutivo limitado de los *ZoomScan* utilizados para cuantificar en una trampa iónica lineal, mientras que los efectos de la digestión parcial, así como la oxidación de Met se debe a la excesiva manipulación de los péptidos y es inherente a las técnicas de marcaje isotópico post-digestión. Por esta razón nos propusimos desarrollar un método de cuantificación más robusto que evitara en lo posible este tipo de artefactos.

R.2.- Desarrollo de un método robusto para la cuantificación con ^{18}O

En este apartado se describe el desarrollo de un protocolo de marcaje masivo con ^{18}O que sea universal y robusto, que mantenga el marcaje durante todo el tiempo que dure la manipulación de la muestra y su análisis por espectrometría de masas, minimizando los artefactos generados durante el protocolo. El método fue desarrollado en colaboración con Daniel Pérez, quién optimizó la etapa de digestión de las proteínas.

R.2.1.- Optimización de un método robusto de digestión y de marcaje con ^{18}O

En el nuevo protocolo, esquematizado en la Fig. R.10, la digestión se lleva a cabo en gel y no en disolución, ya que, como se ha comentado antes, esta estrategia comúnmente utilizada en proteómica [65, 148, 164], demostró no ser homogénea produciendo grados de digestión parcial diferente entre las muestras a comparar. Además, la digestión en disolución no permite el uso de detergentes para solubilizar las proteínas de membrana, por lo que en ese tipo de aproximación, no es posible analizar todos los componentes del proteoma. En el nuevo método, se reemplaza la etapa de reducción-alquilación para inhibir la tripsina por un tratamiento con TLCK, inhibidor irreversible de esta enzima, evitando los efectos de sobrealquilación. Finalmente, para optimizar el rendimiento de identificación y de cuantificación, se sustituyó el fraccionamiento de los péptidos por SCX (que generaba alrededor de 90 fracciones) por una separación por isoelectroenfoque (IEF) en disolución (OFFGel) en la que todo el proteoma se separa en 24 fracciones, técnica que se posiciona como una alternativa a la cromatografía SCX (menos reproducible y resolutiva) en los estudios de análisis masivo de proteómica [164, 165]

En el nuevo método, las dos muestras que se comparan se resuspenden en un tampón de carga con SDS y se someten a una electroforesis monodimensional SDS-PAGE convencional. El voltaje se para cuando el frente de migración penetra 3 mm en el gel separador, concentrando todo el proteoma en una única banda en la interfaz de los geles concentrador y separador (Fig. R.10a). Las bandas de cada muestra se visualizan tiñéndolas con azul de Coomassie y se recortan en porciones iguales. La matriz de acrilamida se utiliza como cámara de reacción para eliminar el SDS, así como para reducir y alquilar las proteínas. Esta misma matriz permite la digestión de las proteínas en condiciones controladas al mantenerse las mismas geometría y concentración de proteína, así como un mismo volumen y una misma proporción proteína:proteasa para cualquier proteoma (Fig. R.10b). La digestión en gel permite la eliminación de cualquier detergente o contaminante de la muestra de forma muy

efectiva, cuya presencia podrían dificultar la digestión de las muestras o interferir con el análisis por espectrometría de masas. Tras la digestión, los péptidos se someten a la reacción de intercambio ^{16}O / ^{18}O catalizada por tripsina inmovilizada en bolas de agarosa en un tampón de acetato amónico que mantiene el pH en 6 (Fig. R.10d). La inactivación de la tripsina se logra eliminando las bolas de agarosa con un filtro físico e incubando las muestras con TLCK, un inhibidor específico e irreversible de la tripsina (Fig. R.10e). Esta estrategia nos garantiza que los grupos amino de las Lys y de los extremos N-terminal de los péptidos no se sobrealquilan con la IAM, eliminando de esta manera una fuente de artefactos con el muevo protocolo. En este punto, y antes de juntar las muestras marcada y sin marcar, se controla la eficiencia de incorporación de ^{18}O (Fig. R.10.2). Tras desalar las muestras manteniendo el pH en 3 para evitar el desmarcaje de las muestras (Fig. R.10f), los péptidos se separan en 24 fracciones por isoelectroenfoque en disolución utilizando la técnica de OFFGel (Fig. R.10g). Después de una nueva etapa de desalado (Fig. R.10h), las diferentes fracciones se analizan por espectrometría de masas de trampa iónica lineal, y los péptidos identificados en las bases de datos de proteínas se cuantifican mediante el software desarrollado en el laboratorio QuiXoT (Fig. R.10i) [64, 139, 140].

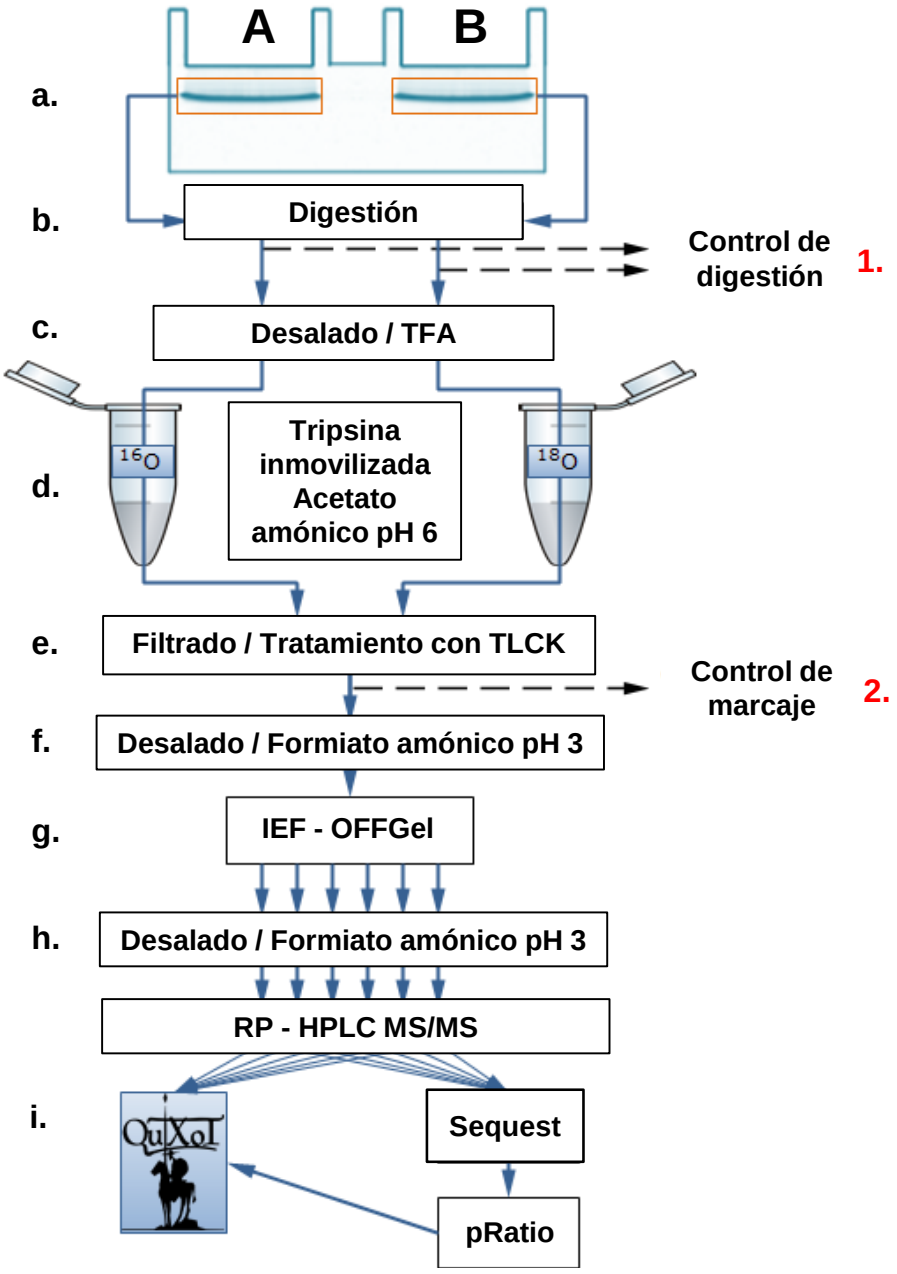

Fig. R.10.- Esquema del protocolo robusto de cuantificación con ^{18}O (por cortesía de Fernando J García-Marqués). Las proteínas se concentran en una única banda en gel SDS-PAGE (**a.**) y se utiliza la matriz de acrilamida como cámara de reacción para la digestión controlada de las proteínas (**b.**). Después de controlar la eficiencia de digestión (1.) y de una etapa de desalado con TFA (**c.**), los péptidos generados se someten al marcaje enzimático con $H_2{}^{18}O$ a un pH controlado de 6 (**d.**). La tripsina inmovilizada se elimina utilizando un filtro físico y las muestras se tratan con TLCK para inhibir una actividad residual de la tripsina (**e.**). Una vez comprobada que la reacción de marcaje ha sido efectiva (2.), las dos muestras se mezclan y se desalan utilizando formiato amónico como tampón de pH (**f.**). Tras la separación de los péptidos por IEF-OFFGel (**g.**), los péptidos se vuelven a desalar controlando el pH a 3 (**h.**). Las 24 fracciones obtenidas se analizan por espectrometría de masas en un LTQ, utilizando el flujo de tratamiento de los datos optimizado en el laboratorio para la identificación de los péptidos contra las bases de datos de proteínas, la validación de los resultados de identificación utilizando el método de la razón de probabilidades y la cuantificación de las proteínas con el software QuiXoT (**i.**).

R.2.2.- Análisis de la eficiencia de marcaje utilizando el método robusto

El protocolo robusto se aplicó al análisis de dos extractos proteicos de células de carcinoma hepático humano (HepG2), control y tratado con un fármaco de origen desconocido. Este trabajo se realizó en colaboración con los laboratorios Neuron Bio. Los péptidos marcados se fraccionaron por OFFGel en tiras de gradiente de pH de 4 a 7. La figura Fig. R.11a muestra el número de péptidos identificados en cada fracción, y permite observar la existencia de dos zonas ricas en péptidos y dos zonas más pobres. Esta distribución se ha confirmado con todos los proteomas analizados en el laboratorio utilizando este protocolo robusto demostrando la reproducibilidad del mismo así como de la técnica OFFGel. Nuestros datos muestran que más del 65 % de los péptidos identificados se encuentran en una única fracción y más del 75 % en una o dos fracciones (Fig. R.11b). Además, la redundancia de péptidos, definida como el cociente entre la suma del número de péptidos únicos identificados en todas las fracciones y el número total de péptidos únicos identificados, es menor de 2, lo que implica que cada péptido se identifica en un máximo de dos fracciones.

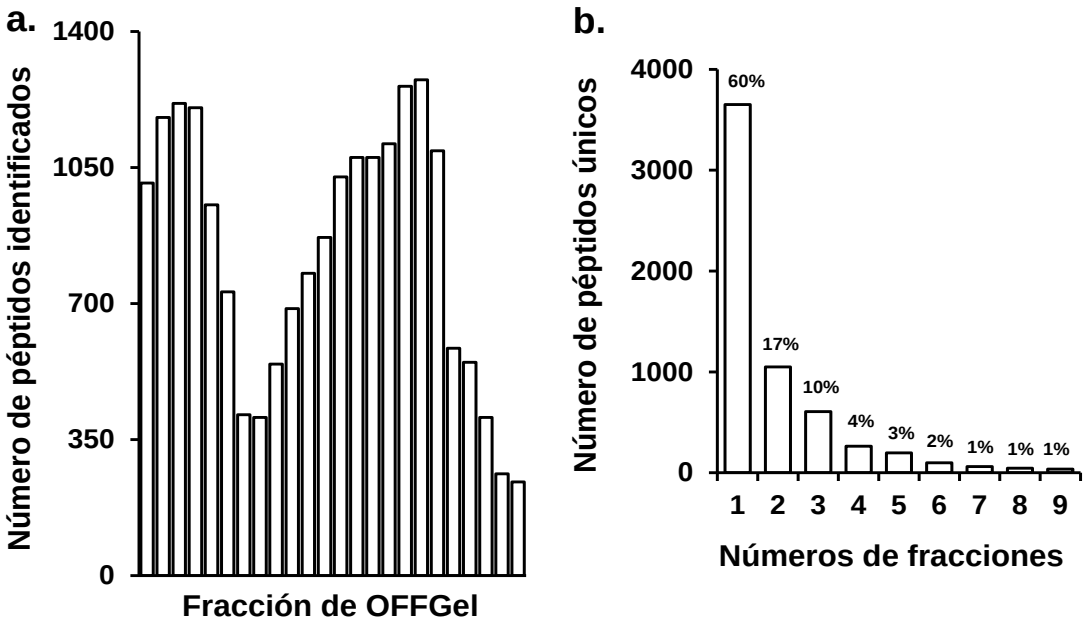

Fig. R.11.- Análisis de las identificaciones de péptidos utilizando la técnica de IEF-OFFGel. (a.) Perfil representativo del fraccionamiento de los péptidos en un rango de pH de 4 a 7. (b.) Distribución del número de péptidos en función del número de fracciones en los que fueron identificados. Estos resultados corresponden al análisis del proteoma de células HepG2 en los que se identificaron 6.128 péptidos únicos correspondientes a 2.342 proteínas únicas.

Esta técnica de separación por IEF en disolución en un rango de pH de 3 a 11 ha sido aplicada previamente por el grupo de Fenselau para péptidos marcados con ^{18}O [165]. Sin embargo, en el trabajo mencionado no se analizó la estabilidad del marcaje con ^{18}O de los péptidos en todo el rango de pH. Por esta razón, nos propusimos estudiar si la inhibición de la tripsina por el TLCK así como la técnica OFFGel eran completamente compatibles con nuestra estrategia de marcaje y cuantificación con ^{18}O sin producir desmarcaje de los péptidos. Para ello, analizamos la eficiencia de marcaje a nivel individual de cada péptido cuantificado usando el algoritmo previamente diseñado en el laboratorio [57]. Como se muestra la Fig.R.12a, la eficiencia de marcaje para cada uno de los péptidos de las 24 fracciones de OFFGel es del 95 %, incluso para los rangos extremos de pH (3-10), y se mantiene también después de las dos etapas de desalado y del tiempo relativamente largo que dura un experimento de OFFGel (típicamente, 2 ó 3 días). Estos resultados demuestran por primera vez la compatibilidad de la separación por IEF y el marcaje isotópico con ^{18}O. Aplicando este protocolo de marcaje optimizado al análisis de varios proteomas de diferente origen, como pueden ser células endoteliales humanas (Fig. R.12b) o mitocondrias de corazón de rata (Fig. R.12c) hemos sido capaces de mantener una alta eficiencia de marcaje (alrededor del 90 %). Estos resultados se han confirmado sistemáticamente en numerosos proteomas que no forman parte de esta tesis doctoral, incluyendo extractos de cerebro de ratón o secretoma de células Jurkat [134].

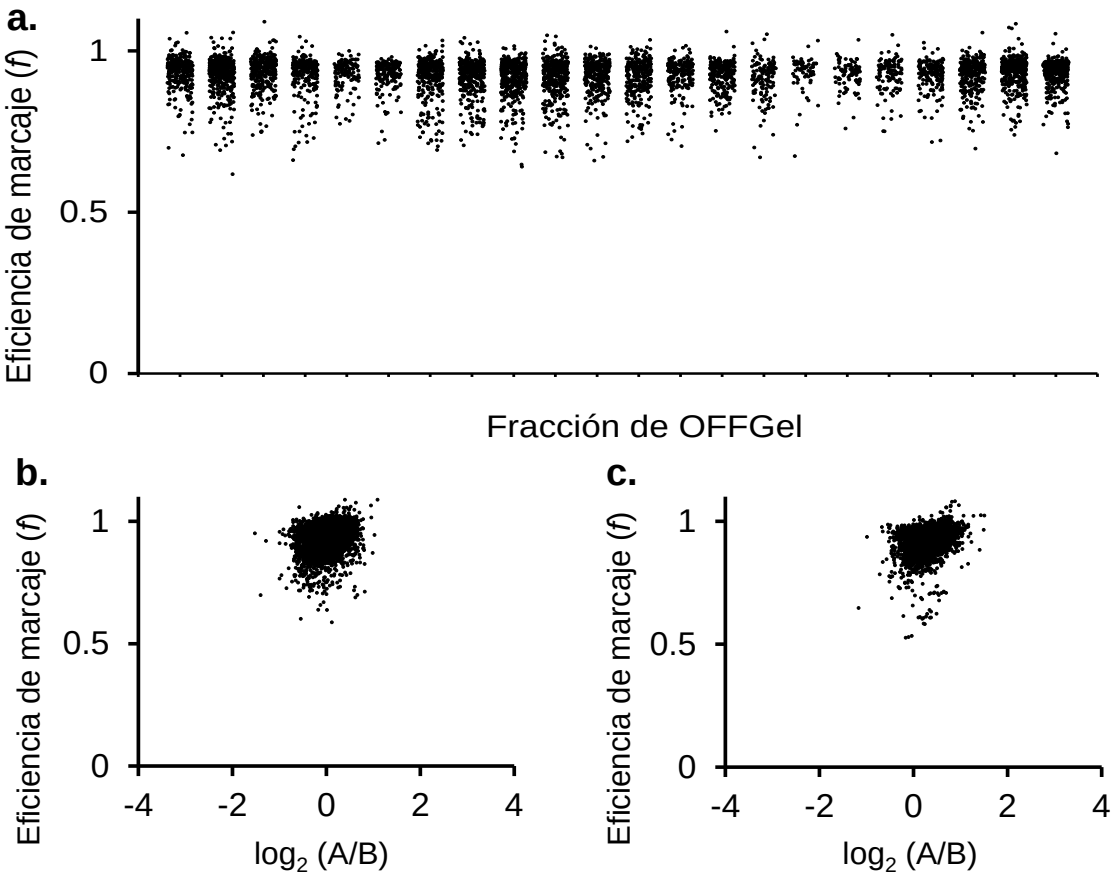

Fig. R.12.- Análisis de la eficiencia de marcaje con ^{18}O de los péptidos separados por IEF-OFFGel. (a.) Distribución de la eficiencia de marcaje individual para cada una de las 24 fracciones de OFFGel obtenidas en un experimento masivo con tiras de pH de 3 a 10. Observamos que incluso para los valores extremos de pH (las primeras y las últimas fracciones, respectivamente), la eficiencia se mantiene por encima del 95 % para la gran mayoría de los péptidos. (**b.** y **c.**) Distribución de la eficiencia de marcaje frente al log_2-(A/B). Comprobamos que la eficiencia se mantiene por encima del 90 % antes de analizar cualquier proteoma, y que dicha eficiencia es independiente del tipo de muestra estudiada (**b.** células endoteliales EA.hy296; **c.** mitocondrias de cardiomiocitos de rata).

R.2.3.- Valores atípicos de cuantificación a nivel de péptido: artefactos de Metionina oxidada

La robustez del nuevo método y la presencia de artefactos a nivel de péptido, tales como la digestión parcial, la oxidación de Met o la sobrealquilación, pueden analizarse utilizando el modelo estadístico. Los artefactos a nivel de péptido producen un aumento de la varianza a este nivel (σ^2_p) y se detectan utilizando la variable FDR_{qp}, que refleja la proporción de péptidos que se espera que se desvíen al azar de la distribución normal dentro de la población de valores atípicos a nivel de péptido [64]. El efecto de la digestión parcial forma parte de la tesis doctoral de Daniel Pérez y no se discutirá en esta tesis.

La oxidación de la Met es un proceso espontáneo y puede producirse en distinta magnitud en las dos muestras que se están comparando, por lo que la proporción relativa de péptidos oxidados y no oxidados en Met se puede desviar del ratio real del péptido. Para comprobar dicho efecto, estudiamos la dispersión de los péptidos con y sin Met ox frente a la media de las proteínas en un experimento en el que la digestión se realizó en disolución (Fig. R.13a) y la comparamos con la dispersión obtenida en un experimento en el que se utilizó el protocolo optimizado de digestión (Fig. R.13b). En el caso de la digestión en disolución, observamos que el comportamiento de los péptidos con Met ox (Fig. 13a, puntos blancos) era diferente al de los péptidos sin Met ox (Fig. 13b, puntos negros), desviándose ambas poblaciones de péptidos de la media de la proteína correspondiente. Por lo contrario, este efecto es despreciable cuando la etapa de digestión se realizó en gel, debido principalmente a una mayor reproducibilidad y control de las condiciones cuando el proteoma se encuentra retenido en la matriz de acrilamida.

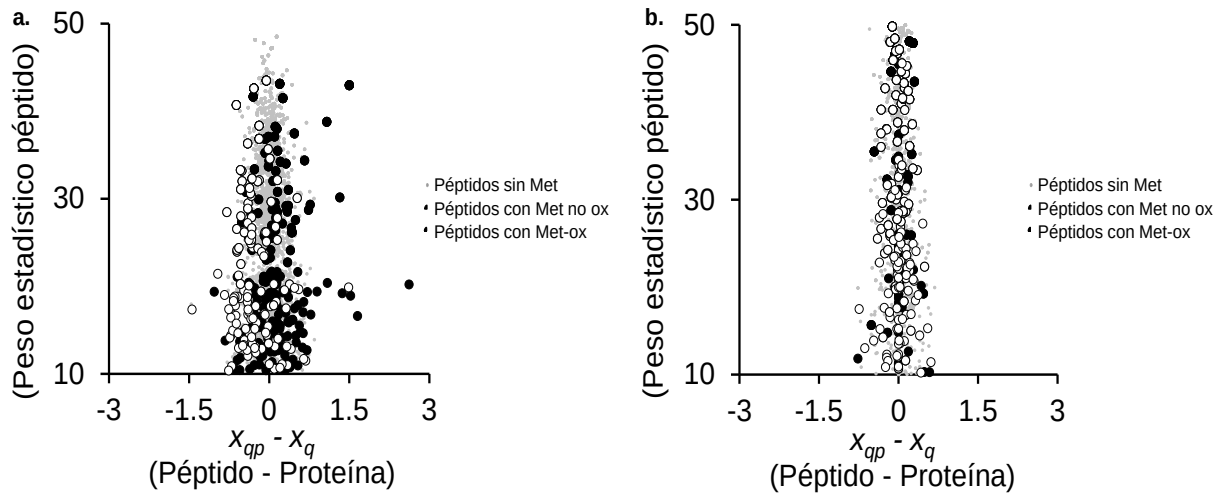

Fig. R.13.- Efecto de la metionina oxidada en la cuantificación relativa a nivel de péptido utilizando el protocolo de digestión en disolución para el análisis del proteoma de células HUVEC (**a.**) o el protocolo optimizado de digestión en gel concentrante para el estudio del proteoma de mitocondrias de cardiomiocitos de rata (**b.**). El comportamiento de los péptidos con Met oxidada (puntos blancos) y sin oxidar (puntos negros) frente al resto de los péptidos es diferente si la digestión se hace en disolución (**a.**); sin embargo, si la digestión se hace en gel concentrador, los péptidos con Met ox o Met sin oxidar no se desvían de la media de los péptidos (**b.**) y, por lo tanto, no influyen negativamente en los datos de cuantificación.

R.2.4.- Validación del nuevo método robusto

Este nuevo método de aplicación universal para el marcaje de péptidos con ^{18}O permite un control completo sobre las fuentes de varianza, permite el marcaje de cualquier tipo de muestra (incluyendo tejidos), así como la cuantificación de cualquier cantidad de muestra, evitando reacciones secundarias que produzcan artefactos en la cuantificación, y controlando de forma rigurosa todas la fuentes de error. Como podemos comprobar en la Tabla T.4, las varianzas a nivel de espectro obtenidas en el análisis de numerosos proteomas de diferentes orígenes utilizando el protocolo robusto son muy similares entre sí y similares a la varianza obtenida en el proteoma de HUVEC descrito con anterioridad y analizado con el protocolo de digestión en disolución. También comprobamos que, para ninguno de los proteomas analizados, la varianza a nivel de proteína es significativamente diferente de cero, indicando que las diferencias entre cultivos celulares o entre las aproximaciones para fraccionar subproteomas no introducen errores apreciables para la comparación relativa a nivel de proteína.

Tabla T.4
Eficiencias de digestión estadística de cuantificación de varios proteomas analizados mediante el método robusto

Proteoma	H1	H2	Mit	HUVEC
% de digestión parcial (a)	5,3	4,2	8,0	12,9-39,8
Varianza a nivel de espectro (s^2_S) (95% C.I.)	0,011 (0,010-0,012)	0,019 (0,018 - 0,020)	0,019 (0,017 - 0,021)	0,018-0,031
Varianza a nivel de péptido (s^2_P) (95% C.I.)	0,024 (0,019-0,031)	0,018 (0,015 - 0,021)	0,031 (0,020 - 0,040)	0,014-0,021
Varianza a nivel de proeína (s^2_Q) (95% C.I.)	0,005 (0-0,011)	0,005 (0 - 0,009)	0,006 (0 - 0,019)	0,0007-0,004

(a) Se asume que los péptidos con digestión parcial contienen al menos un sitio de corte tríptico diferente a Lys-Pro ó Arg-Pro.
H1 y H2: extracto celular de HepG2
Mit: mitocondrias de corazón de rata
HUVEC: proteoma digerido en disolución.

El análisis de la varianza a nivel de péptido resulta el parámetro más importante para juzgar la idoneidad del protocolo diseñado al realizarse la etapa de marcaje después de la digestión de las proteínas. Esta nueva aproximación de digestión en gel concentrante produce menos del 10 % de digestiones parciales, las cuales se controlan de rutina para cada análisis antes de continuar con el protocolo (Fig. R.10.1), porcentaje mucho menor que el obtenido en la digestión en disolución con urea utilizada en los experimentos de HUVEC (Tabla T.4) [65]. Además, hemos demostrado en el apartado anterior que, utilizando el método robusto, la oxidación de Met no genera artefactos de cuantificación. De manera consistente con estas

demostraciones, las varianzas calculadas a nivel de péptido para los diferentes proteomas listados en la tabla T.4 son muy similares y prácticamente idénticas a la varianza de péptido obtenida utilizando la aproximación de digestión en disolución y marcaje.

Como último punto de validación de la aproximación experimental desarrollada, analizamos la precisión de la hipótesis nula asociada al modelo estadístico en los distintos proteomas estudiados. Para ello, basándonos en un trabajo publicado por el grupo [65], representamos la distribución del $\log_2$-ratio de las proteínas estandarizado según sus varianzas estimadas (valores z_q) y ajustando las curvas a funciones gaussianas (Fig. R.14). Como cabría esperar, en ninguno de los casos estudiados, la desviación estándar es significativamente diferente de uno; además, ninguna desviación de la normalidad se detectó para ninguno de los modelos (recuadros en la Fig. R.14). Por lo tanto, los errores producidos por el método robusto son reproducibles, controlados, y correlacionan con la hipótesis nula del modelo estadístico utilizado y con las varianzas calculadas (Tabla T.4).

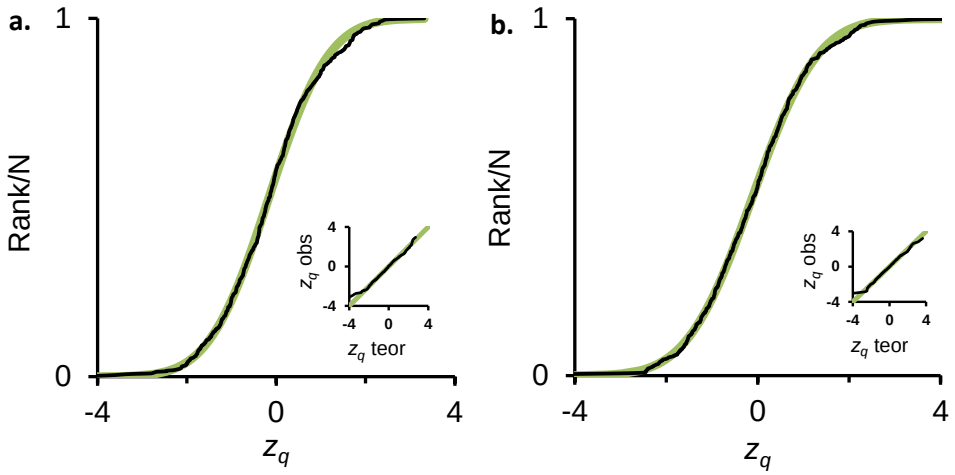

Fig. R.14.- Análisis de la normalidad de la distribución de cuantificaciones a nivel de proteína. Los datos corresponden al análisis del proteoma de células HepG2 tratadas con 2 dosis de un fármaco de origen desconocido. Se representan las distribuciones acumulativas de la variable estandarizada z_q (línea negra), así como los gráficos de probabilidad normal correspondientes (recuadros). Las curvas se ajustaron por mínimos cuadrados a una distribución normal (línea verde). La desviación estándar correspondiente al mejor ajuste fue de 1.05 (**a.**) y de 1.12 (**b.**), confirmando que los datos experimentales se ajustan al modelo teórico esperado con varianza unidad.

R.3.- Estrategia GELSILOX para la cuantificación simultanea del estado de oxidación de Cys y del proteoma

Los casos de valores atípicos que hemos comentado son un buen ejemplo de la utilidad de las FDR y de las varianzas a los tres niveles de análisis (espectro, péptido y proteína), que permiten detectar errores generados por el protocolo a todos los niveles. De la misma manera que el análisis de las cuantificaciones a nivel de péptido permite detectar valores atípicos debidos a artefactos, nos planteamos la posibilidad de utilizar este nivel de análisis para detectar estadísticamente alteraciones en los niveles de modificaciones postraduccionales (PTMs) con relevancia biológica. Aprovechando esta propiedad del modelo estadístico, nos propusimos desarrollar un método que aprovechara el método robusto de cuantificación y el modelo estadístico a nivel de péptido para detectar cambios en el estado de oxidación de Cys producidos por condiciones de estrés oxidativo.

R.3.1.- Desarrollo de un método para la cuantificación masiva y simultánea de proteomas y del estado de oxidación de Cys

En este apartado, describimos la tecnología GELSILOX o de marcaje isotópico estable basado en gel de las Cys oxidadas (*GEL-based Stable Isotope Labeling of OXidized Cys*), un método para el estudio cuantitativo simultáneo de los proteomas total y redox que introduce un nuevo análisis estadístico para la interpretación de los resultados a nivel de péptido [166].

R.3.1.1.- Estrategia experimental

En la técnica GELSILOX, las proteínas se extraen en presencia de SDS y de un reactivo alquilante convencional (NEM o IAM) que reacciona con los tioles libres o reducidos (Fig. R.15a). Los extractos se someten a una electroforesis monodimensional SDS-PAGE concentrante, de manera que todo el proteoma está condensado en una sola y única banda en la interfaz de los geles concentrador y separador [134], tal y como se ha comentado en apartados anteriores. Una vez inmovilizadas las proteínas en el gel (Fig. R.15b), se utiliza la matriz de acrilamida como cámara de reacción para manipular la muestra: este procedimiento limita las pérdidas de proteínas evitando etapas de precipitación de las mismas o de purificación de péptidos. Tras eliminar el SDS con diversos pasos de lavados con agua y acetonitrilo, se reducen con ditiotreitol (DTT) todas las Cys oxidadas de forma reversible y los tiolatos liberados se modifican con un agente alquilante diferente al de la extracción (IAM o MMTS), de manera que cada población de Cys (reducida y oxidada) tiene una etiqueta diferente (Fig. R.15c). Finalmente, las proteínas se digieren con tripsina en condiciones bien

controladas (Fig. R.15d). Durante el desarrollo de este trabajo, hemos observado que estas condiciones experimentales son críticas para obtener cuantificaciones fiables que puedan ser descritas por nuestro modelo estadístico [134]. Los péptidos generados son sometidos a un marcaje diferencial con ^{18}O y, tras separarlos en 24 fracciones por isoelectroenfoque, se analizan por LC-MS/MS en una trampa iónica lineal (Fig. R.15d).

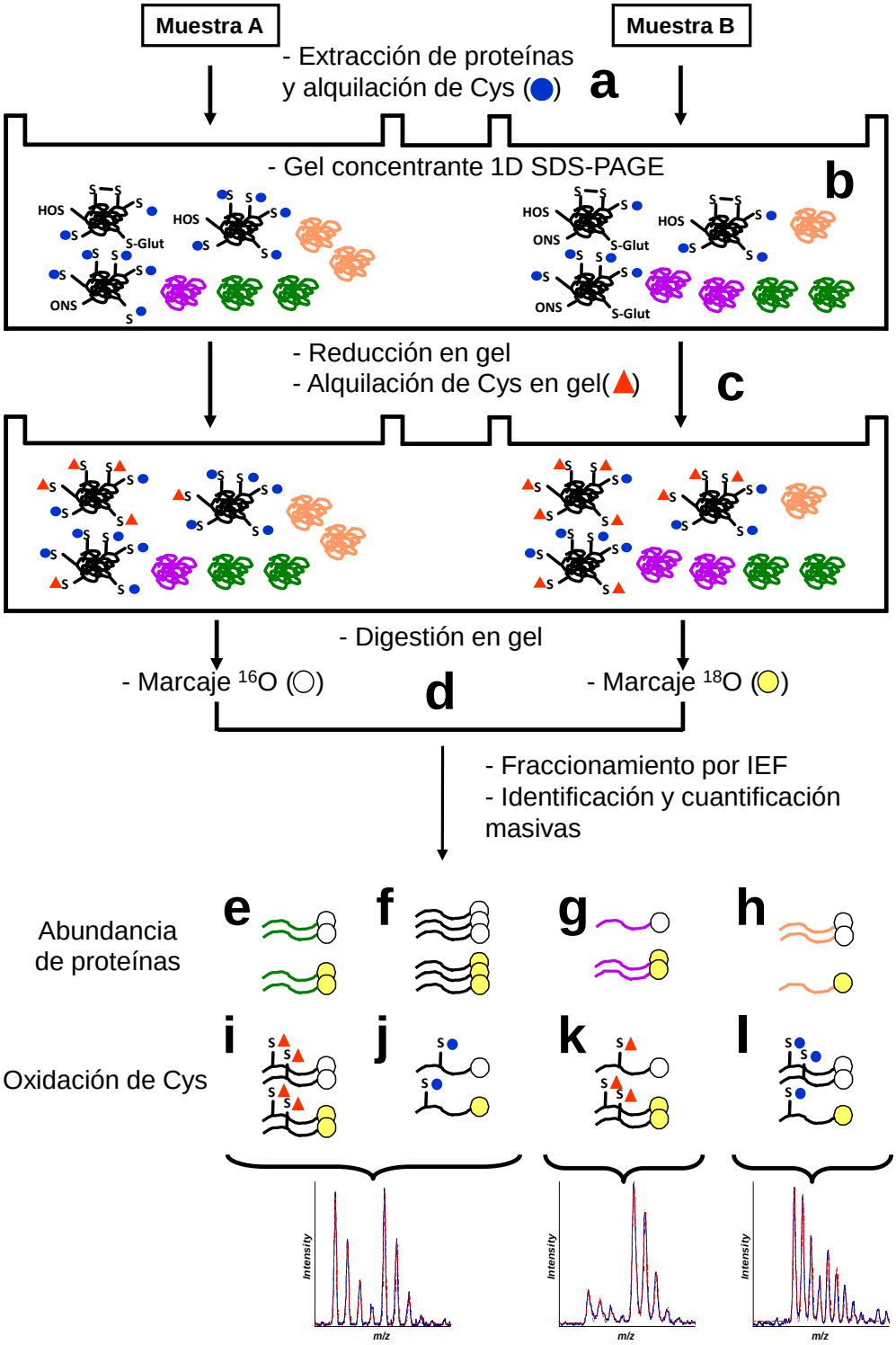

Fig. R.15.- Esquema del protocolo GELSILOX. (a) Extracción proteica y bloqueo de las Cys reducidas. (b) Electroforesis en gel concentrante SDS-PAGE. (c) Reducción en gel y alquilación de las Cys oxidadas. (d) Digestión tríptica en gel, marcaje con $^{16}O/^{18}O$, fraccionamiento por isoelectroenfoque en disolución y análisis cuantitativo por espectrometría de masas de los péptidos resultantes. El método permite cuantificar péptidos de proteínas que no cambian (e, f), aumentan (g) o disminuyen su abundancia relativa (h), así como la cuantificación de péptidos con Cys oxidadas de forma reversible (i, k) o con Cys reducidas (j, l) que no cambian (i, j,) aumentan (k) o disminuyen su estado de oxidación de forma estadísticamente significativas (l) en relación a los demás péptidos cuantificados de la misma proteína (f).

Los péptidos que no contienen Cys (noCys) se utilizan para cuantificar la abundancia relativa de las proteínas (Fig. R.15e-h), mientras que los péptidos con Cys son cuantificados en su estado original de oxidación o reducción, el cual se diferencia por el incremento característico de masa introducido por los diferentes reactivos alquilantes (Fig. R.15i-l). Para tener en cuenta el efecto de los cambios de abundancia de proteínas y para cuantificar al mismo tiempo los péptidos de los proteomas total y redox tiólico, se utiliza un método estadístico novedoso para el análisis de la varianza a nivel de péptido. Dicho algoritmo se basa en las tres fuentes de error de nuestro modelo (espectro, péptido y proteína) que se han descrito en apartados anteriores [65]. La robustez estadística está determinada por el análisis global de las varianzas y no de cada proteína o péptido individualmente. Dicho análisis global consigue una descripción completa y precisa del experimento utilizando únicamente cuatro parámetros estadísticos.

R.3.1.2.- Análisis estadístico de los datos a nivel de péptido

La estrategia GELSILOX requiere la realización de dos análisis estadísticos. En un primer análisis, se ignoran los péptidos con residuos de Cys en su secuencia, y se utiliza el resto de los péptidos del proteoma para calcular las varianzas a nivel de espectro, de péptido y de proteína, así como para determinar las proteínas con cambios en su abundancia estadísticamente significativos. El segundo análisis estadístico incluye la población entera de péptidos del proteoma, con Cys y sin Cys, y se utilizan las varianzas calculadas en el primer análisis para caracterizar los péptidos con Cys que se desvían de la distribución esperada de péptidos pertenecientes a una misma proteína. Para ello se introduce en el análisis estadístico una variable estandarizada a nivel de péptido, definida en la población de los péptidos no únicos (o lo que es lo mismo, péptidos pertenecientes a proteínas identificadas por más de dos péptidos) por:

$$z_{qp} = \frac{x_{qp} - x_q}{\left(\frac{1}{\sum_s w_{qps}} + \sigma_{\mathbf{P}}^2 \right)^{1/2}} \cdot \left(\frac{n_q}{n_q - 1} \right)^{1/2} \quad , \quad n_q > 1 \quad (Eq\ 2.1)$$

Esta variable expresa la desviación entre el $\log_2$-ratio de la cuantificación del péptido p y el de la cuantificación de la proteína q en unidades de desviación estándar, y constituye una estimación no sesgada que se obtiene mediante la corrección de la cantidad de péptidos de la

proteína q (n_q). En la hipótesis nula, se espera que esta variable siga una distribución normal con media 0 y varianza 1. Los valores atípicos a nivel de péptido se detectan calculando la probabilidad de que las medidas de las cuantificaciones de péptido se desvíen de la media de proteínas utilizando la variable estandarizada definida por la ecuación (Eq 2.1) y controlando la tasa de error (FDR_{qp}). La cuantificación de los péptidos así como el análisis de los datos se hizo utilizando QuiXoT, un programa escrito en C# en nuestro laboratorio para la identificación y cuantificación masiva de proteomas marcados con ^{18}O [64, 139, 140].

R.3.1.3.- Prueba de concepto de la tecnología GELSILOX: análisis de los cambios de oxidación producidos por un estímulo oxidante inespecífico

Como parte de un trabajo colaborativo con el grupo del Prof. Santiago Lamas en el CBMSO y el Dr. Antonio Martínez-Ruíz del Hospital de la Princesa, y como experimento de validación del método, decidimos estudiar el efecto producido por 10 minutos de tratamiento con diamida a una concentración de 2 mM en células EA.hy296 en cultivo, como modelo de células endoteliales humanas La diamida es un reactivo oxidante específico de tioles, permeable a membranas y ampliamente utilizado para estudiar la oxidación de proteínas [167, 168]. Por el contrario, este reactivo no se ha usado en experimentos masivos de detección de residuos Cys redox-sensibles. En este estudio, cuantificamos 3.260 péptidos únicos, de los cuales 254 contienen al menos una Cys en estado oxidado o reducido (Fig. R.16a). El análisis estadístico de la varianza a nivel de péptido de las cuantificaciones de los péptidos noCys frente a las medias de sus proteínas correspondientes revela que la distribución experimental está perfectamente descrita por la distribución de hipótesis nula predicha por el modelo (Fig. R.16b), demostrando la reproducibilidad de la técnica y la precisión de las cuantificaciones, así como la ausencia total de artefactos a nivel de péptido, como la oxidación de Met o las digestiones parciales que se han descrito en apartados anteriores. El tratamiento con diamida aumentó la abundancia de la mayoría de los péptidos con Cys oxidada (oxCys, Fig. R.16c, puntos rojos) y produjo el efecto opuesto en los péptidos con Cys reducida (redCys, Fig. R.16c, puntos azules).

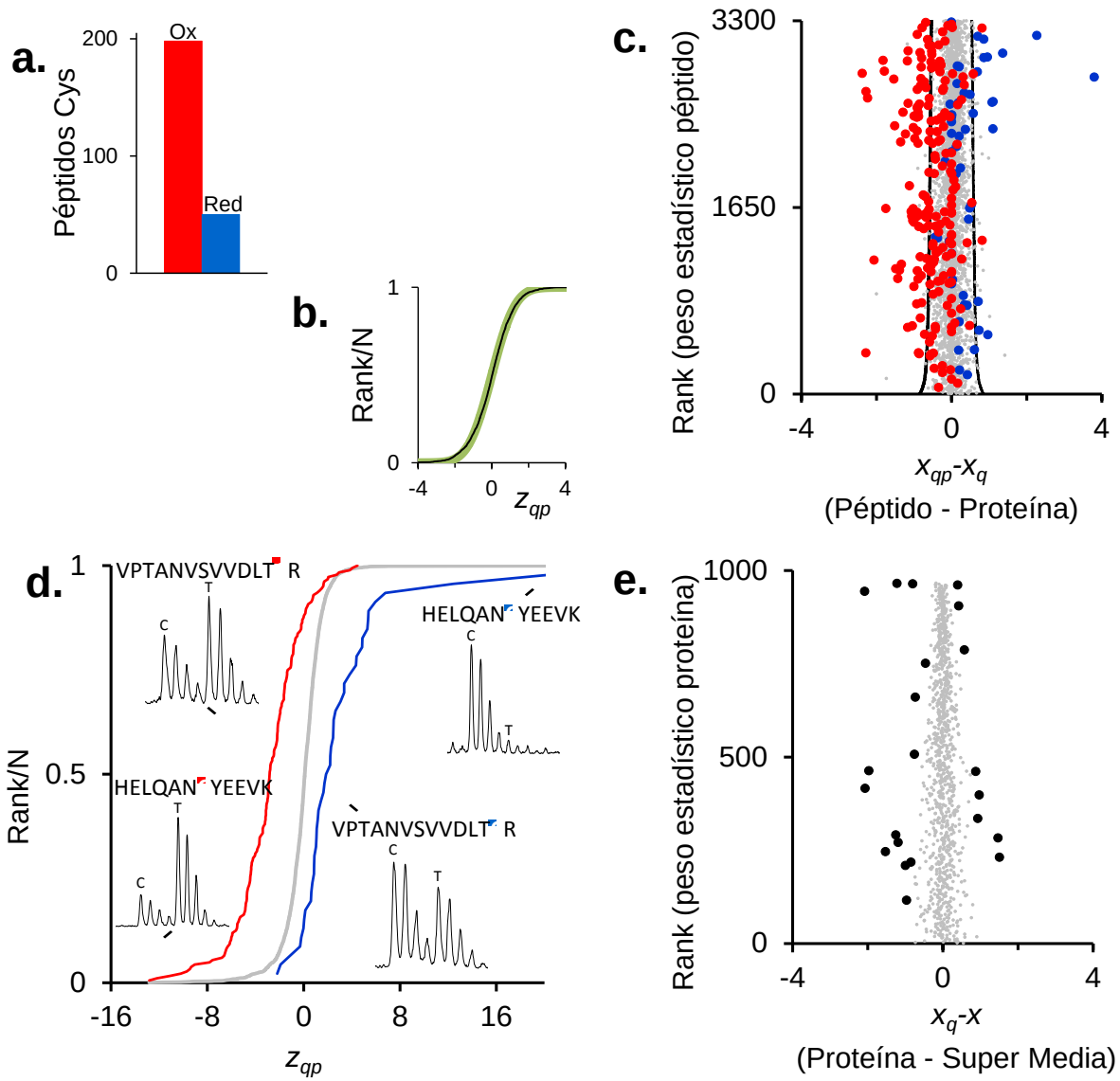

Fig. R.16.- Validación de la técnica GELSILOX con el análisis de los cambios de oxidación de Cys y de abundancia de proteínas producidos por la diamida. (a.) Número de péptidos cuantificados que contienen Cys oxidadas (rojo) o reducidas (azul). (b.) Distribuciones acumulativas de la variable estandarizada a nivel de péptido, calculada sin tener en cuenta los péptidos con Cys, que demuestra la concordancia entre los datos experimentales (puntos negros) y la curva teórica (puntos verdes). (c.) Distribución del $\log_2$-ratio de las cuantificaciones de los péptidos frente a la media de sus proteínas correspondientes (puntos rojos: péptidos con oxCys; puntos azules: péptidos con redCys); los valores negativos (hacia la izquierda) indican un aumento de abundancia, mientras que los valores positivos (hacia la derecha) traducen una disminución de abundancia. (d.) Distribuciones acumulativas de la variable estandarizada a nivel de péptido de los péptidos con oxCys (rojo), redCys (azul) o noCys (gris); recuadros: espectros de masas representando la intensidad de los péptidos en las muestras control (C) y tratada (T). Estos péptidos pertenecen a la cofilina-1 y a la gliceraldehído-3-fosfato deshidrogenasa (Anexo A.1). (e.) Distribución del $\log_2$-ratio de las cuantificaciones de las proteínas frente a la supermedia del experimento; los puntos negros indican las cambios significativos de abundancia con una tasa de error del 5 %.

El efecto global de la diamida en el redoxoma (o población de Cys sensibles a redox) se refleja en el desplazamiento opuesto de las distribuciones de los péptidos oxCys y redCys frente a la hipótesis nula (Fig. R.16d), que sirvió para detectar el aumento significativo de abundancia de 104 péptidos oxCys y la disminución de 17 péptidos redCys (Anexo A.1). Es interesante notar que estas curvas tienen una pendiente central menos acusada que la hipótesis nula y la sigmoide está ensanchada hacia los extremos, lo que sugiere que los grupos tioles tienen un rango de sensibilidad muy amplio en respuesta al tratamiento con diamida (Fig. R.16d). En paralelo, los péptidos nonCys permitieron la cuantificación de 976 proteínas únicas, de las cuales 14 aumentaron de manera significativa su abundancia en respuesta a la diamida y 9 la disminuyeron (Fig. R.16e y Anexo A2). Las distribuciones de las cuantificaciones de las proteínas para todos los modelos analizados con la técnica GELSILOX siguieron una distribución normal de media cero y desviación estándar uno (Fig. R.17), confirmando de nuevo la robustez del método y la precisión con la que el modelo estadístico describe los datos cuantitativos a este nivel.

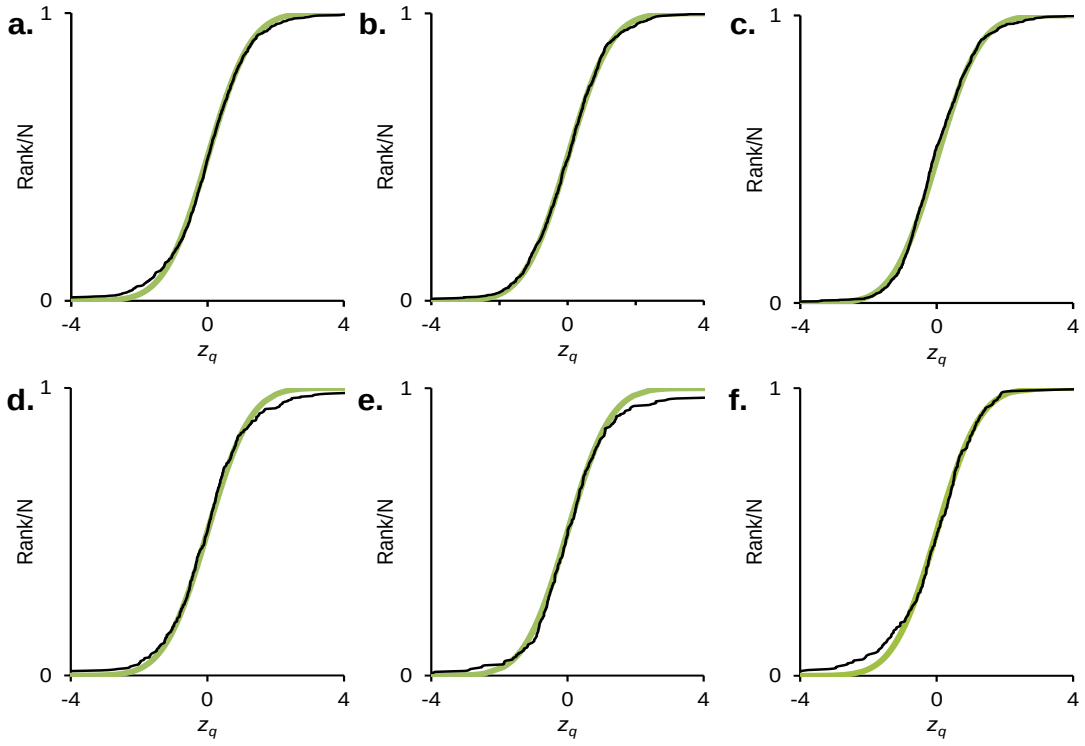

Fig. R.17.- Análisis de la normalidad de las cuantificaciones a nivel de proteína. Los datos corresponden al análisis de los distintos proteomas analizados mediante la técnica GELSILOX. (**a.**) Células EA.hy296 tratadas con diamida. (**b.**) Células BAEC estimuladas con H2O2. (**c.**) Células EA.hy296 sometidas a hipoxia. (**d.**) SSM de corazón de rata sometidas a IR. (**e.**) IFM de corazón de rata sometidas a IR. (**f.**) SSM de corazón de rata sometidas a IP previamente a IR. Se representan las distribuciones acumulativas de la variable estandarizada z_q (línea negra),ajustadas por mínimos cuadrados a una distribución normal (línea verde).

Entre las proteínas que cambian de abundancia, algunas contienen péptidos oxCys que, por los métodos convencionales de purificación de péptidos con Cys, hubiesen sido identificados de manera errónea como sensibles a diamida, porque el cambio de estado de oxidación de la Cys identificado refleja en realidad un cambio de abundancia de la proteína. Ese efecto se muestra en la Fig. R.18, en la que representamos la dispersión de todos los péptidos de la plectina-1 en relación a los demás péptidos del proteoma (Fig. R.18b). La plectina-1 es una proteína que sufre un cambio de abundancia estadísticamente significativo en respuesta a diamida (Fig. R.18a); sin embargo, y a pesar de ello, todos los péptidos de la proteína, incluyendo los nonCys, los oxCys y los péptidos redCys, muestran los mismos valores de cuantificación relativa frente a la media de la propia proteína, sin que éstos se desvíen de la media de todos los péptidos del proteoma. Los péptidos oxCys de la plectina-1, como por ejemplo el péptido FLEGTSCAGVFVDATK, hubiesen sido identificados y cuantificados como cambios de su estado de oxidación mediante técnicas de purificación de péptidos, cuando en realidad reflejan un cambio de abundancia de la proteína. Este resultado demuestra por primera vez la necesidad de realizar los dos análisis (cambios de abundancia de proteína y cambios en el estado de oxidación de los péptidos) de manera simultánea.

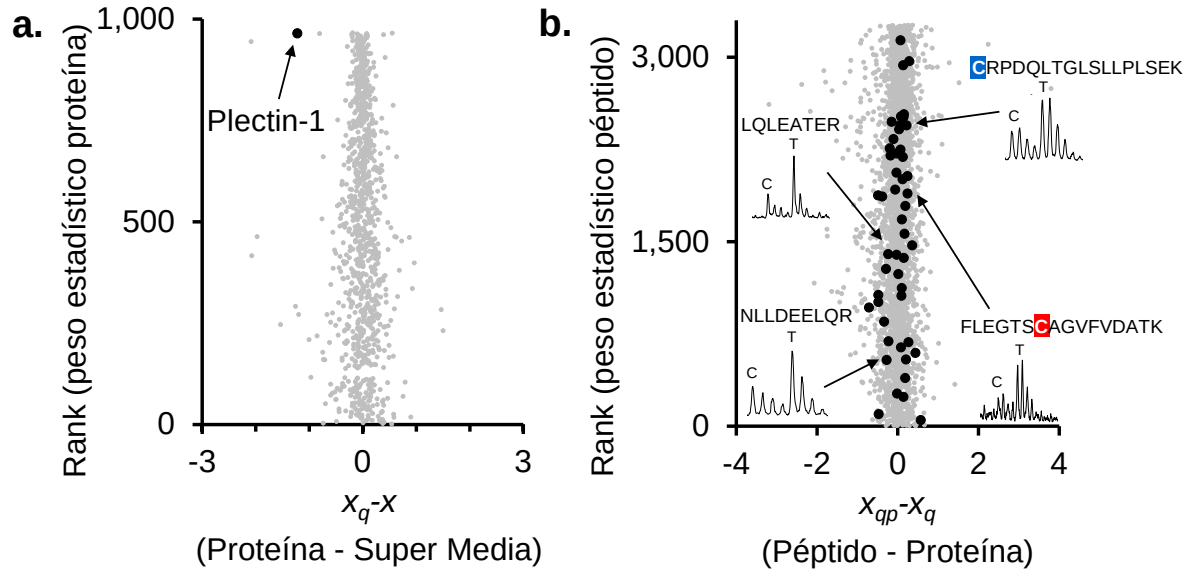

Fig. R.18.- Ejemplo de proteína que cambia de abundancia por el tratamiento con diamida y que contiene péptidos oxCys y redCys que no cambian de abundancia a nivel de péptido. (a.) Distribución del $\log_2$-ratio de las cuantificaciones de las proteínas frente a la súper media del experimento, mostrando el comportamiento de la plectina-1 (punto negro). (b.) Distribución del $\log_2$-ratio de las cuantificaciones de los péptidos, mostrando los péptidos correspondientes a la plectina-1 (puntos negros). Los recuadros muestran los espectros de masa utilizada para cuantificar los péptidos de la plectina-1 indicados. Todos los péptidos, incluso los que contienen péptidos oxCys o redCys, tienen los mismos valores de cuantificación.

R.3.2- Estudio del proteoma y de las alteraciones redox producidas en dos modelos de estrés oxidativo en células endoteliales en cultivo

Para demostrar la eficacia del GELSILOX, una vez validada la técnica, decidimos analizar las alteraciones en los proteomas total y redox generados por dos modelos de estrés oxidativo en células endoteliales en cultivo. Estas células fueron seleccionadas al ser la disfunción endotelial [84] un factor predominante en una serie de situaciones fisiopatológicas en las que se ha implicado el estrés oxidativo [169].

R.3.2.1.- Análisis de los proteomas total y redox tiólico de células BAEC tratadas con H_2O_2

Decidimos en primer lugar aplicar el protocolo de GELSILOX al estudio del efecto de concentraciones moderadas de H_2O_2 en células endoteliales primarias de aorta bovina (BAEC). A pesar de sus efectos tóxicos, el H_2O_2, una de las ROS más documentada y estudiada, puede actuar como segundo mensajero [170], y está implicado en la transducción de señales, así como en procesos patológicos como la aterosclerosis, la hipertensión o el daño por isquemia-reperfusión [171]. Las células se incubaron durante 15 min con agua oxigenada a una concentración de 1 mM en el medio extracelular. Se predijo que esa concentración, de 4 a 10 veces menor que la que se ha utilizado en estudios anteriores de oxidación de Cys [127-129], genera una concentración intracelular de H_2O_2 de 100 µM [170], que está en el límite del rango de concentraciones estimadas para que el agua oxigenada ejerza su acción de segundo mensajero [172]. En este estudio, se cuantificaron 429 péptidos con Cys (Fig. R.19a), y a partir de la distribución de los péptidos nonCys, que se ajustó a la hipótesis nula esperada (Fig. R.19b), fue posible detectar de manera consistente el cambio de 13 péptidos oxCys cuya abundancia aumentaba de forma significativa y de 12 péptidos redCys que disminuían su abundancia con respecto a los péptidos nonCys de la misma proteína (Fig. R.19c). El efecto de esa dosis semi-fisiológica es mucho más evidente en las distribuciones globales de los péptidos oxCys y redCys (Fig. R.19d), lo que sugiere que los péptidos oxCys con cambios de abundancia significativos son los residuos de Cys más sensibles a H_2O_2 en el proteoma. En ese mismo experimento, fuimos capaces de detectar un cambio de abundancia en 10 proteínas (Fig. R.19e).

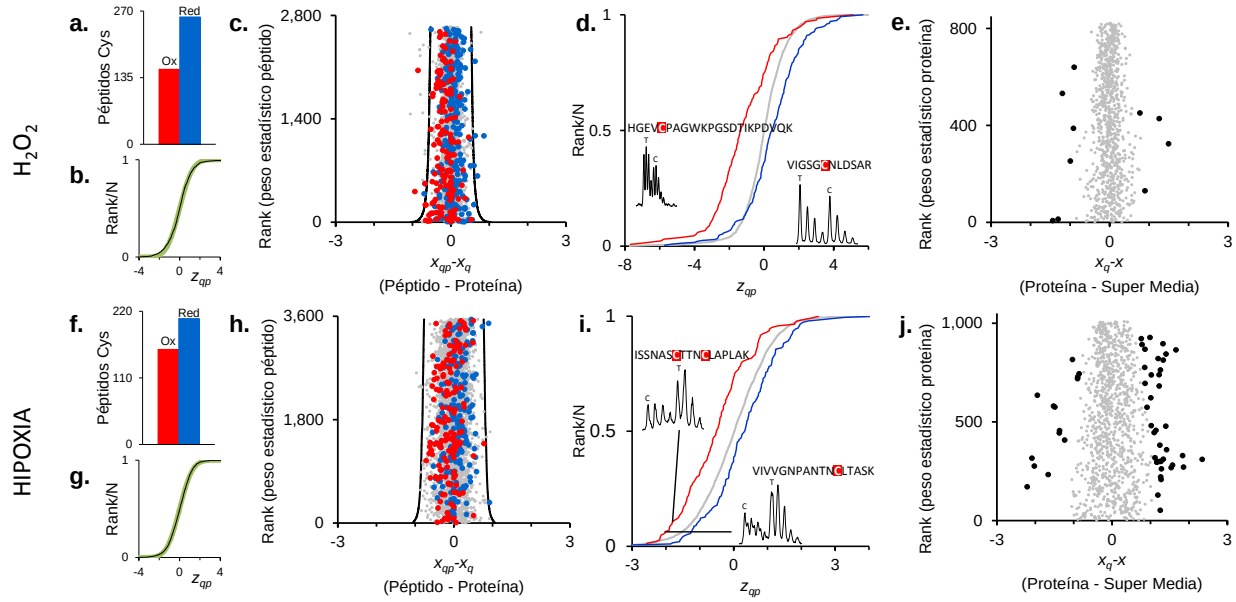

Fig. R.19.- Aplicación del GELSILOX a modelos endoteliales sometidos a tratamientos oxidativos moderados. (**a-e**) Células BAEC tratadas con H_2O_2. (**f-j**) Células EA.hy296 cultivadas en condiciones de hipoxia. Las figuras representan los mismos conceptos estadísticos que en la Fig. R.15. Los péptidos de los recuadros corresponden a la peroxiredoxina-1 y a la L-lactato deshidrogenasa (**d**), así como a la gliceraldehído-3-fosfato deshidrogenasa y a la malato deshidrogenasa (**i**).

R.3.2.2.- Análisis del efecto de la hipoxia en los proteomas total y redox tiólico de células endoteliales humanas

Dada la sensibilidad mostrada por el GELSILOX en el estudio anterior, usamos esa misma estrategia para determinar las Cys específicas alteradas por periodos cortos de hipoxia en células endoteliales humanas. La hipoxia está asociada a la producción de ROS en procesos de señalización [173], así como en la angiogénesis y enfermedades cardíacas isquémicas [174]. Sin embargo, no existen estudios masivos que hayan abordado este proceso por técnicas de proteómica redox. En este modelo, y a pesar de que cuantificamos 376 péptidos con al menos una Cys (Fig. R.19f) y que la distribución de los péptidos nonCys fue la esperada (Fig. R.19g), no se detectó ningún aumento significativo en ningún péptido oxCys (Fig. R.19h). Sin embargo, la sensibilidad del método fue suficiente para detector un aumento general en la población de los péptidos oxCys y una disminución de los péptidos redCys (Fig. R.19i), así como cambios en la abundancia de más de 50 proteínas (Fig. R.19j).

R.3.3- Estudio del daño oxidativo producido por isquemia/reperfusión y del efecto protector del precondicionamiento isquémico en corazón de rata

A continuación, decidimos utilizar la aproximación GELSILOX para elucidar los posibles mecanismos implicados en el daño producido en el corazón por isquemia-reperfusión (IR) así como los efectos del precondicionamiento isquémico (IP), un mecanismo de protección que disminuye el impacto de la IR [175-177]. En colaboración con el laboratorio del Dr. David García-Dorado del Hospital Universitari Vall d'Hebron, analizamos los cambios inducidos en los proteomas total y redox en mitocondrias subsarcolemales (SSM) de cardiomiocitos de rata sometidas a IR (SSM_IR), así como el efecto de la IR en mitocondrias interfibrilares (IFM_IR). Además, estudiamos el efecto de la IR en SSM aisladas de corazones sometidos a IP previo a la IR (SSM_IPIR) para poder determinar el efecto del precondicionamiento sobre el daño producido por IR.

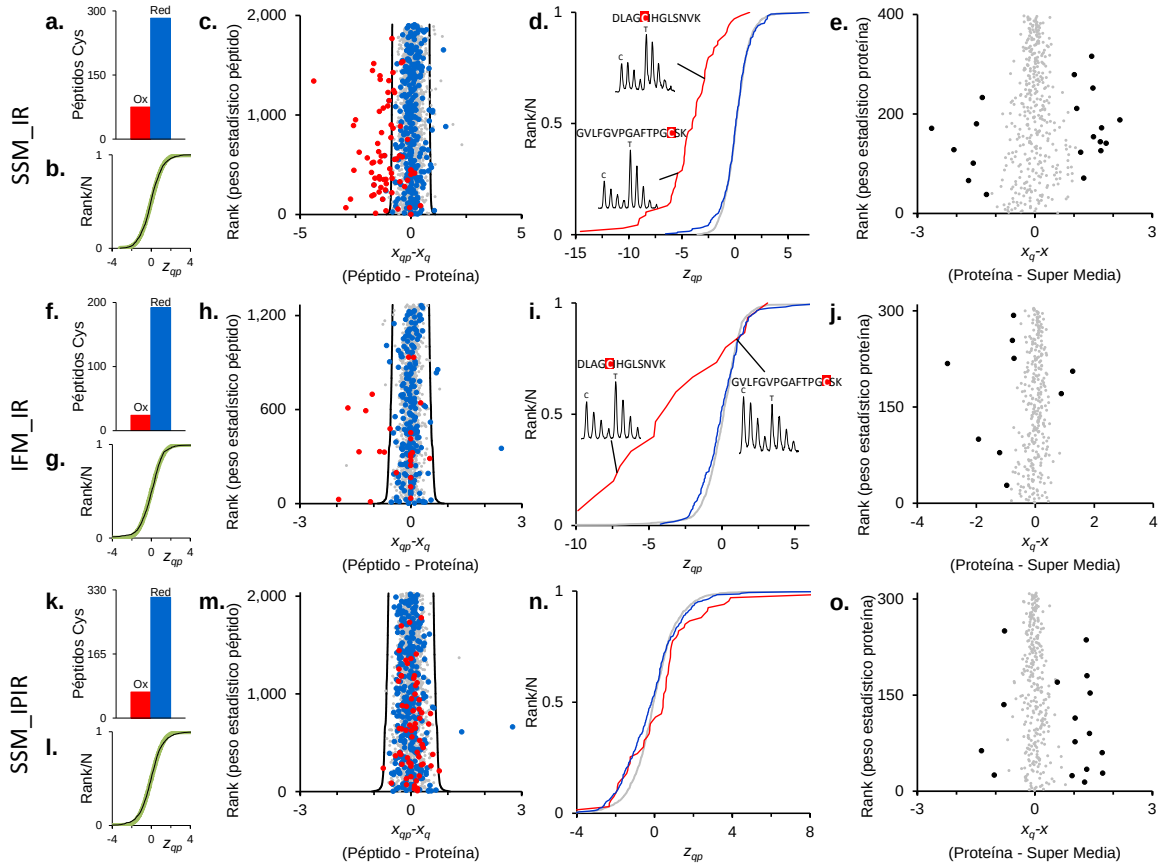

Fig. R.20.- Análisis cuantitativo con GELSILOX del proteoma mitocondrial en respuesta al precondicionamiento isquémico y a la reperfusión en corazones de rata: SSM_IR (**a-f**), IFM_IR (**g-l**), SSM_IPIR (**m-r**). Las figuras representan los mismos conceptos estadísticos que en las Figs. R.15 y R.18. Los péptidos de los recuadros corresponden a la isocitrato deshidrogenasa y a la peroxiredoxina-5.

En todos estos modelos *in vivo*, la proporción de oxCys es menor que en los experimentos de GELSILOX en cultivos celulares (Fig. R.20a, f, k), lo cual podría deberse a una menor manipulación de la muestra que la que tiene lugar en las células en cultivo, de forma que las proteínas de células en cultivo están basalmente más oxidadas. Después de comprobar las distribuciones de los péptidos nonCys (Fig. R.20b, g, l) y de calcular las varianzas, fuimos capaces de cuantificar 388 péptidos con al menos una Cys, de los cuales 49 péptidos oxCys aumentaban de manera significativa su abundancia en SSM_IR (Fig. R.20c y Anexo A.3). La distribución global de estos péptidos está claramente desplazada hacia la izquierda, hacia el aumento de abundancia (Fig. R.20d). Esos efectos son menos apreciables en IFM_IR, en las cuales únicamente 9 péptidos oxCys aumentan su abundancia (Fig. R.20h). La desviación frente a la hipótesis nula de la distribución de los péptidos oxCys en IFM es menor que para las mitocondrias SSM, aunque sigue siendo detectable debido a la sensibilidad del método y, de manera consistente con los resultados individuales, desplazada hacia el aumento de abundancia (Fig. R.20i). Dichos cambios están, sin embargo, inhibidos completamente en SSM_IPIR, de forma que ningún péptido oxCys aumenta su abundancia si se estudian de manera individual (Fig. R.20m) y la distribución global de los mismos se ajusta de forma casi perfecta a la hipótesis nula (Fig. R.20n). De los 36 péptidos oxCys que aumentan, observados en al menos dos de las tres condiciones utilizadas, todos menos uno de los que aumentan en IFM_IR también lo hacen en SSM_IR, y la gran mayoría de los cambios de estado de oxidación detectados en SSM_IR son revertidos por el tratamiento precondicionante (Tabla T.5).

Tabla T.5
Comparativa de los cambios en el estado de oxidación de las Cys en los 3 modelos de mitocondria

Nº acceso	Proteína	Secuencia	IFM_IR	SSM_IR	SSM_IP_IR
Q6P6R2	Dihydrolipoyl dehydrogenase, mitochondrial	NETLGGTC@LNVGC@IPSK		-15.13	0.83
Q5XIH3	NADH dehydrogenase (Ubiquinone) flavoprotein 1	HESC@GQC@TPC@R		-9.15	0.84
Q66HF1	NADH-ubiquinone oxidoreductase 75 kDa subunit, mitochondrial	VVAAC@AMPVMK		-8.26	-1.40
P45953	Very long-chain specific acyl-CoA dehydrogenase, mitochondrial	VASGQALAAFC@LTEPSSGSDVASIR		-6.38	0.59
P81155	Voltage-dependent anion-selective channel protein 2	PIC@IPPPYADLGK		-6.02	-0.25
P85834	Elongation factor Tu, mitochondrial	HYAHTDC@PGHADYVK		-5.79	1.66
P56574	Isocitrate dehydrogenase [NADP], mitochondrial	SSGGFVVAC@K	1.56	-5.76	-1.80
Q66HF1	NADH-ubiquinone oxidoreductase 75 kDa subunit, mitochondrial	VVAAC@AMPVM*K		-5.64	2.49
D3ZLT1	NADH dehydrogenase (Ubiquinone) 1 beta subcomplex, 7	HEQHDWDYC@EHQDYVK		-5.60	0.49
Q80W89	NADH dehydrogenase [ubiquinone] 1 alpha subcomplex subunit 11	FFEAYNETPDGTQC@HR		-4.99	-0.90
P09605	Creatine kinase S-type, mitochondrial	LGYILTC@PSNLGTGLR	0.52	-4.80	1.62
P21913	Succinate dehydrogenase [ubiquinone] iron-sulfur subunit, mitochondrial	C@GPMVLDALIK		-4.79	0.61
Q9ER34	Aconitate hydratase, mitochondrial	DFAPGKPLNC@IIK		-4.75	0.48
Q9ER34	Aconitate hydratase, mitochondrial	VGLIGSC@TNSSYEDMGR		-4.72	
D4A311	NADH dehydrogenase (Ubiquinone) 1 alpha subcomplex, 8	FDEC@VLDK		-4.69	-1.91
P56574	Isocitrate dehydrogenase [NADP], mitochondrial	DLAGC@IHGLSNVK	-6.98	-4.42	0.08
D3ZD09	Cytochrome c oxidase subunit 6B1	NC@WQNYLDFHR		-3.93	-1.81
Q9R063	Peroxiredoxin-5, mitochondrial	GVLFGVPGAFTPGC@SK	0.24	-3.71	0.59
P09650	Mast cell protease 1	GDSGGPLVC@AGVAHGIVSYGR		-3.70	0.83
P04636	Malate dehydrogenase, mitochondrial	GC@DVVVIPAGVPR	-4.66	-3.68	
Q9ER34	Aconitate hydratase, mitochondrial	C@TTDHISAAGPWLK		-3.62	1.17
Q9R1Z0	Voltage-dependent anion-selective channel protein 3	VC@NYGLIFTQK	-0.37	-3.53	0.46
D3ZLT1	NADH dehydrogenase (Ubiquinone) 1 beta subcomplex, 7	DSFPNFVAC@K	0.00	-3.11	-0.22
B0K020	CDGSH iron-sulfur domain-containing protein 1	FPFC@DGAHIK		-3.08	-1.64
P04636	Malate dehydrogenase, mitochondrial	GYLGPEQLPDC@LK	-7.43	-2.96	1.38
Q920L2	Succinate dehydrogenase [ubiquinone] flavoprotein subunit, mitochondrial	VGSVLQEGC@EK	-8.93	-2.83	
P04636	Malate dehydrogenase, mitochondrial	TIIPLISQC@TPK	-6.23	-2.73	1.22
Q66HF1	NADH-ubiquinone oxidoreductase 75 kDa subunit, mitochondrial	FC@YHER		-2.72	
Q05962	ADP/ATP translocase 1	EFNGLGDC@LTK	-4.55	-2.67	
Q66HF1	NADH-ubiquinone oxidoreductase 75 kDa subunit, mitochondrial	M*C@LVEIEK		-2.45	1.26
Q9ER34	Aconitate hydratase, mitochondrial	VGLIGSC@TNSSYEDM*GR		-2.09	3.64
D4A311	NADH dehydrogenase (Ubiquinone) 1 alpha subcomplex, 8	LVNGC@ALNFFR	3.03	-1.63	-1.96
Q68FY0	Cytochrome b-c1 complex subunit 1, mitochondrial	LC@TSATESEVTR	-3.82		2.82
P56574	Isocitrate dehydrogenase [NADP], mitochondrial	C@ATITPDEAR	-3.16		2.89
P00507	Aspartate aminotransferase, mitochondrial	EYLPIGGLADFC@K	-9.87		-1.26
P00507	Aspartate aminotransferase, mitochondrial	TC@GFDFSGALEDISK	-2.01		1.06

Se listaron los péptidos presentes en al menos 2 de los 3 experimentos y con un valor de z_{qp} menor que -1,96 en al menos uno de los tres experimentos. Los péptidos que aumento de su abundancia están representados en verde, y las disminuciones en rojo, según una escala de colores (z_{qp}: -5 0 5). El estado de oxidación de las Cys se representa con el símbolo "@" (oxCys) o "^" (redCys). (*) Metionina oxidada.

R.4.- Proteómica dirigida para el estudio de modificaciones postraduccionales: aplicación a la identificación de la nitración de la superóxido dismutasa de manganeso en su Tyr 34

R.4.1.- Optimización de los parámetros de espectrometría de masas para la identificación dirigida de la nitración de la Tyr34 de la MnSOD

El peroxinitrito ($ONOO^-$) es un potente agente oxidante que resulta de la reacción entre el anión superóxido ($O_2^{\cdot -}$) y el óxido nítrico ($NO^{\cdot}$) [178] y ha sido descrito como mediador en numerosos procesos patológicos como la diabetes [179, 180], desórdenes neurodegenerativos [181, 182], así como enfermedades cardiovasculares [183-186] y daño endotelial [187]. El $ONOO^-$ ejerce sus efectos citotóxicos mediante modificaciones oxidativas de lípidos, ADN o proteínas, siendo la nitración de Tyr uno de esos efectos. Se ha demostrado que el tratamiento con la CsA inducía la generación de $ONOO^-$ así como la inactivación de la MnSOD [115]. Por lo tanto, resulta interesante saber si el tratamiento de células endoteliales con CsA afecta a la Tyr catalítica de la MnSOD de manera específica. En primer lugar, establecimos las condiciones de análisis del espectrómetro de masas para caracterizar la nitración de dicha Tyr directamente en la proteína recombinante humana rHuMnSOD exponiéndola a un tampón nitrante [132]. Para ello, realizamos una monitorización de iones de fragmentación (SMIM) en una trampa iónica lineal acoplada a un HPLC utilizando técnicas optimizadas previamente en nuestro laboratorio [56, 145, 146]. El equipo se programó para realizar fragmentaciones múltiples sobre los iones correspondientes a las formas no nitradas y nitradas del péptido tríptico que contiene la Tyr catalítica de la MnSOD, de secuencia HHAAY^{34}VNNLNVTEEK. Del análisis de los datos concluimos que monitorizando la fragmentación de los dos iones precursores así como la subfragmentación de uno de los iones fragmento más intensos, era posible demostrar de forma inequívoca la nitración en la Tyr34 de la proteína (Fig. R.21).

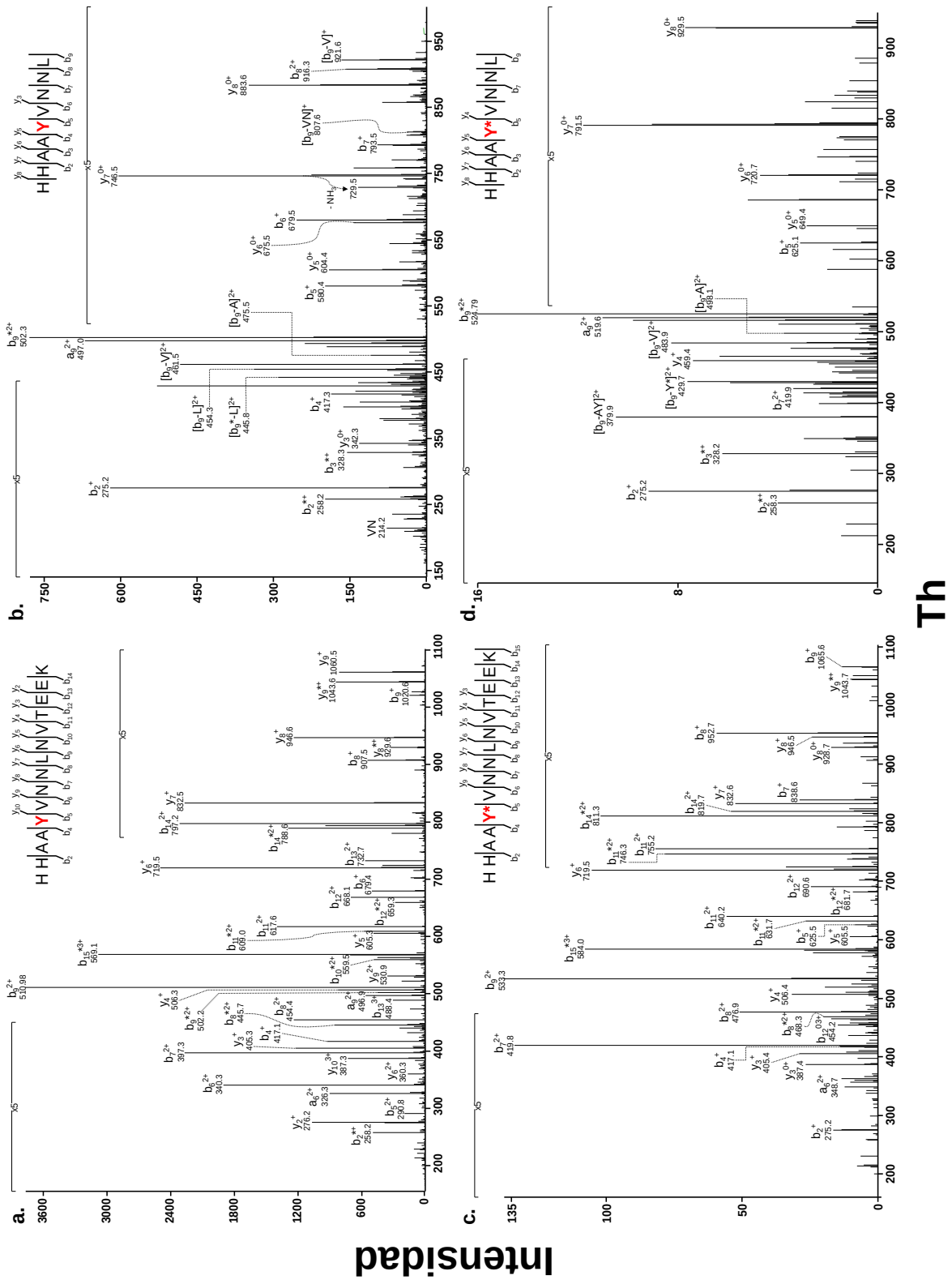

Fig. R.21.- Espectros MS/MS (**a. – b.**) y MS^3 (**c. – d.**) de las especies no modificadas (**a. – c.**) y nitradas (**b. – d.**) del péptido HHAAYVNNLNVTEEK de la MnSOD recombinante humana tratada con el generador exógeno de peroxinitrito SIN-1. Los espectros MS^3 se generaron a partir de la fragmentación de ión doblemente cargado b_9^{2+} detectado en el espectro MS/MS.

Una vez optimizadas las condiciones para la detección específica de la Tyr34-NO_2 por SMIM, aplicamos la técnica al análisis de la rHuMnSOD incubada con medio condicionado de células tratadas con CsA. El patrón de fragmentación y la presencia de fragmentos específicos de las formas no modificada y nitrada demuestran que el medio condicionado induce la nitración del residuo Tyr34 de la MnSOD (Fig R.22).

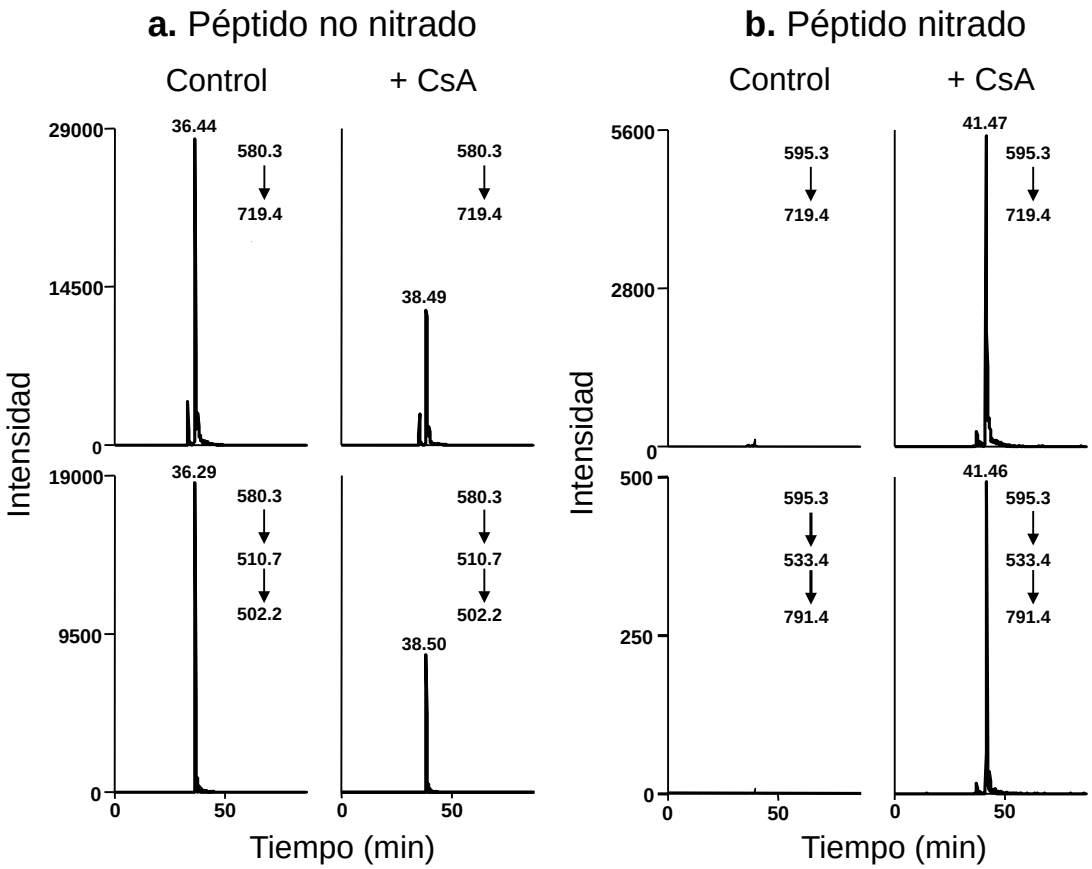

Fig. R.22.- La CsA induce la nitración de la Tyr34 de la MnSOD recombinante. Trazas cromatográficas virtuales MS/MS (paneles superiores) y MS^3 (paneles inferiores) de la de la forma no modificada (**a.**) y nitrada (**b.**) del péptido HHAAYVNNLNVTEEK identificado en la MnSOD humana recombinante tratada con el medio condicionado de células BAEC tratadas con el vehículo (control) o con CsA. Los paneles superiores corresponden a la traza del fragmento y_6^+ y los paneles inferiores a la traza del subfragmento b_9^{*2+} generado a partir del fragmento b_9^{2+} en el caso del péptido no modificado, y la traza del subfragmento y_7^{0+} generado a partir del fragmento y_7^+ en el caso del péptido nitrado.

R.4.2.- Aplicación a la identificación de la ^{34}Tyr-NO_2 de la MnSOD en células endoteliales

Una vez optimizado el flujo de trabajo y las condiciones experimentales de análisis por espectrometría de masas, utilizamos esa aproximación para caracterizar la nitración de la Tyr34

de la MnSOD en células endoteliales tratadas con CsA. Para ello, se llevó a cabo el mismo análisis por SMIM con un extracto de proteínas total de células BAEC infectadas con construcciones adenovirales que sobre-expresaban la MnSOD que no modifican la capacidad de la CsA de inducir nitración [146]. Como se muestra en la Figura R.23B, la traza cromatográfica de iones fragmento específicos demuestra que el péptido nitrado está presente en una proporción muy baja cuando el extracto proviene de células tratadas únicamente con el medio condicionado vehículo, lo que implica que la gran mayoría del péptido se encuentra en su forma sin modificar. Sin embargo, cuando se trata las células con CsA, la intensidad del péptido no modificado disminuye (Fig. R.23A), mientras que su forma modificada aumenta (Fig. R.23B).

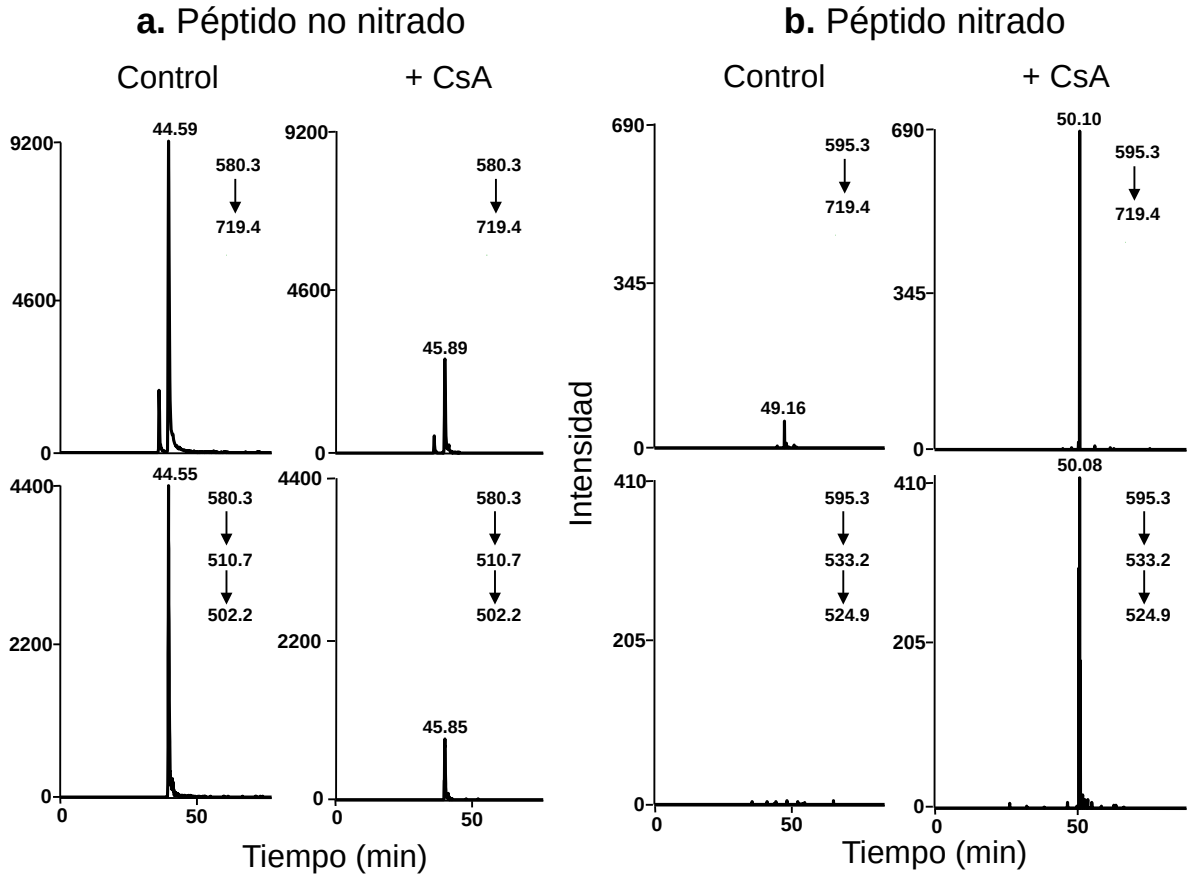

Fig. R.23.- La CsA induce la nitración de la Tyr34 de la MnSOD sobre-expresada en células endoteliales. Trazas cromatográficas virtuales MS/MS (paneles superiores) y MS^3 (paneles inferiores) de la de la forma no modificada (**A.**) y nitrada (**B.**) del péptido HHAAYVNNLNVTEEK identificado en un extracto de proteínas de células BAEC infectadas con construcciones adenovirales expresando la MnSOD humana y tratadas con el vehículo (control) o con CsA. Los paneles superiores corresponden a la traza del fragmento y_6^+ y los paneles inferiores a la traza del subfragmento b_9^{*2+} generado a partir del fragmento b_9^{2+}.

Los espectros de fragmentación MS/MS y MS^3 obtenidos a los tiempos de elución de los picos anteriores identifican de manera inequívoca nuestro péptido de interés y la presencia de una modificación de 45 Da en la Tyr34, consistentes con una modificación por nitración (Fig. R.24). De manera que, utilizando la espectrometría de masas y la proteómica dirigida, hemos obtenido datos que sugieren que la CsA es capaz de inducir la nitración de la MnSOD en células endoteliales, concretamente en el residuo esencial para la actividad catalítica de la proteína. Por lo tanto, por aproximaciones de proteómica dirigida, hemos identificado una diana específica de la citotoxicidad inducida por la CsA.

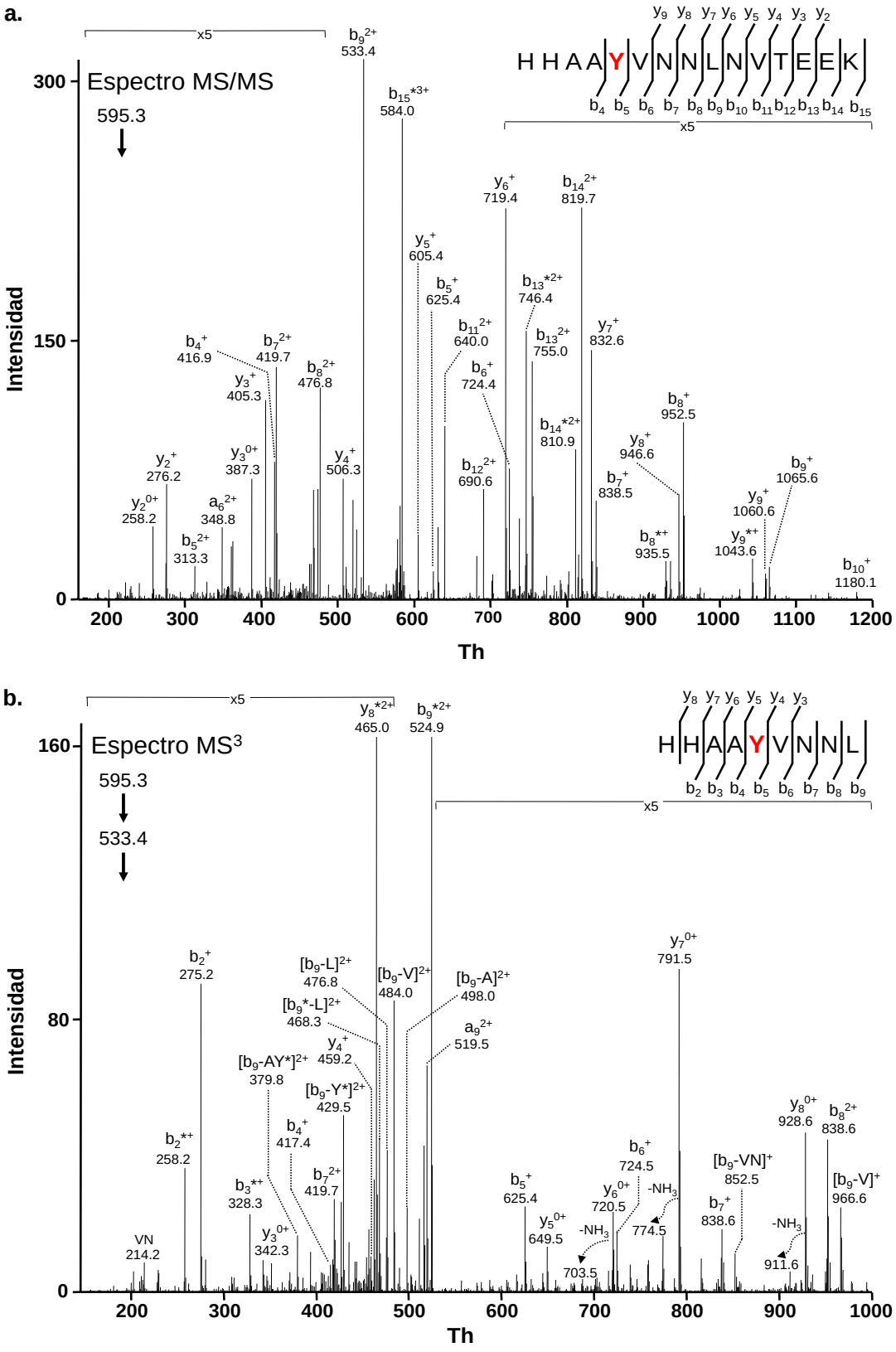

Fig. R.24.- Espectros MS/MS **(a.)**y MS^3 **(b.)** de las especies peptídicas obtenidos al tiempo de elución de los picos de la Fig. R.24B. El espectro MS^3 se generó a partir de la fragmentación de ión doblemente cargado b_9^{2+} detectado en el espectro MS/MS. Los fragmentos correspondientes a la pérdida interna de aminoácidos a partir de iones de la serie b se indican usando la nomenclatura utilizada en trabajos anteriores del grupo [188].

DISCUSIÓN

D.1.- Desarrollo de una tecnología robusta para análisis cuantitativos masivos utilizando ^{18}O

En esta tesis, describimos el análisis más extenso a día de hoy del proteoma de células HUVEC, en el cual se identificaron más de 3.800 proteínas únicas entre los cuatro experimentos, de las cuales fuimos capaces de cuantificar más de 1300 proteínas únicas utilizando marcaje isotópico con ^{18}O en una trampa iónica lineal LTQ. Estos resultados demuestran la validez del uso de los espectros de media-alta resolución de un LTQ para la cuantificación relativa de péptidos. Las condiciones de barrido necesarias para obtener datos de cuantificación y de identificación de manera alternativa en un mismo análisis por espectrometría de masas fueron descritas en un trabajo anterior del laboratorio [55], y el algoritmo diseñado para controlar y corregir la eficiencia de marcaje también fue publicado previamente [57]. El control de la eficiencia de marcaje de cada uno de los péptidos cuantificados resultó crítico para desarrollar un protocolo de marcaje adecuado para estudios largos de cuantificación masiva y poder obtener resultados cuantitativos consistentes. Cabe destacar que el rendimiento de incorporación del isótopo también ha sido considerado problemático para otros métodos de marcaje isotópico. Por ejemplo, la eficiencia de la técnica SILAC necesita una comprobación minuciosa del grado de incorporación metabólica de los aminoácidos marcados en el medio de cultivo así como otros efectos adversos como la conversión de arginina en prolina [189]. En otro trabajo reciente, se ha propuesto un algoritmo para calcular la eficiencia de marcaje utilizando los reactivos iTRAQ [190], y su aplicación reveló que, además de detectar la presencia de una proporción notable de péptidos marcados parcialmente, la reactividad de los cuatro compuestos iTRAQ con los péptidos era diferente. Sin embargo, el análisis de la eficiencia de marcaje para estas dos técnicas sólo puede hacerse de forma global en la población entera de péptidos, mientras que el algoritmo diseñado en el laboratorio para determinar la eficiencia de marcaje utilizando $H_2{}^{18}O$ la calcula para cada péptido individualmente aprovechando el hecho de que el marcaje con ^{18}O es una reacción cinética en dos etapas [57]. A pesar de que la reacción con los reactivos iTRAQ pueda ser considerada un proceso en dos etapas para los péptidos que contengan un grupo reactivo adicional al extremo N-terminal de los péptidos, como puede ser la Lys, la cantidad de péptido no marcado no puede ser cuantificada con esta aproximación, por lo que no es posible usar un algoritmo cinético semejante al utilizado en el caso del ^{18}O.

La detección de los cambios de abundancia en células endoteliales en respuesta al factor VEGF fue posible gracias al desarrollo de un modelo estadístico novedoso para el análisis caracterizado por tres factores principales:

- El modelo considera que todas las cuantificaciones relativas no tienen la misma precisión, y por lo tanto la varianza no puede ser considerada homogénea en la población entera de medidas.
- El modelo tiene en cuenta tres fuentes adicionales de error correspondientes a cada uno de los niveles de cuantificación: el error cometido durante la medida en el espectrómetro de masas, el error con que diferentes péptidos cuantifican la proteína de la que se generan, y la dispersión con que cada una de las proteínas se desvía del valor promedio esperado.
- El modelo supone que las varianzas asociadas a las fuentes de error de cada uno de los tres niveles – espectro, péptido, proteína – son constantes y comunes para todo el experimento, lo que contrasta con la aproximación típica realizada en geles bidimensionales en los estudios clásicos de proteómica cuantitativa en los que se asume que cada medida a nivel de proteína tiene una varianza diferente.

Por otro lado, en este trabajo de tesis doctoral, se presenta un protocolo general robusto para el marcaje con ^{18}O, que ha sido validado con numerosas muestras de distinta naturaleza [134]. Durante todo el proceso de optimización de las condiciones experimentales, y con el objetivo de minimizar los artefactos causados por la etapa de digestión, por la oxidación aleatoria y no controlada de las Met, así como de un marcaje incompleto, el protocolo se sometió a un profundo análisis basado en el modelo estadístico [65]. Como primera etapa de optimización, se realizó un análisis estadístico detallado de la digestión en geles SDS-PAGE, siendo parte de la tesis doctoral de Daniel Pérez y, por lo tanto, no se ha discutido en este manuscrito. Además, se demostró que la etapa de reducción-alquilación utilizada en el protocolo clásico para inhibir la actividad residual de la tripsina tras la etapa de marcaje [65] modificaba una proporción significativa de los grupos amino presentes en los péptidos, introduciendo una fuente adicional de error de cuantificación a nivel de péptido. Dicho efecto se debe principalmente al hecho de que la reacción química de modificación de los grupos amino por el reactivo alquilante utilizado es una reacción menor y secundaria y, por lo tanto, es muy improbable que tenga lugar en la misma proporción en las dos muestras analizadas.

Teniendo en cuenta todos estos factores, diseñamos un protocolo mejorado de cuantificación masiva basado en la concentración de todo el proteoma en una sola y única

banda en un gel SDS-PAGE, seguida de una etapa de digestión en gel, en la cual las condiciones son más controlables que en los protocolos clásicos de digestión en disolución y de una etapa de marcaje isotópico con agua pesada. La reproducibilidad y la eficiencia de la etapa de digestión son críticas para obtener cuantificaciones robustas y libres de artefactos; para ello, se optimizó dicha etapa y se obtuvo un mayor rendimiento y reproducibilidad en la eficiencia de digestión en comparación con proteomas digeridos en disolución. Otra mejora introducida en esta nueva aproximación experimental es la substitución de la etapa de reducción-alquilación post-marcaje para inactivar la tripsina por el tratamiento de las muestras con TLCK, un inhibidor irreversible de la tripsina. Este cambio reveló ser efectivo para inhibir el intercambio inverso del ^{18}O durante todo el tiempo experimental. Además, esta etapa reduce la manipulación de la muestra y evita modificaciones químicas no controladas que introducen artefactos de cuantificación. Por último, se mejoró la etapa de preparación de muestra previa al análisis por espectrometría de masas reemplazando el fraccionamiento por intercambio catiónico en HPLC por la separación de los péptidos marcados por isoelectroenfoque (IEF) en disolución, un método más reproducible y con un rendimiento muy alto de cuantificación como se ha descrito en trabajos recientes [189, 191, 192]. Esta técnica, denominada OFFGel, se ha introducido recientemente y utiliza las tiras convencionales de gradiente inmovilizado de pH (IPG) que se usan comúnmente para la separación de proteínas por electroforesis bidimensional, manteniendo los péptidos separados por punto isoeléctrico en disolución [193]. El fraccionamiento OFFGel ha demostrado ser altamente eficiente y muy reproducible para la separación de péptidos en muestras complejas [189, 191, 192]. Este método también tiene la ventaja de proporcionar la información del pI de los péptidos, siendo éste un criterio suplementario muy útil para la validación de la identificación de los péptidos [144], que permite aumentar el número de péptidos identificados en un 5-7 % [134]. Analizando la eficiencia de marcaje de cada uno de los péptidos cuantificados, demostramos que la separación por OFFGel es completamente compatible con el marcaje por ^{18}O, incluso a valores extremos de pH (3 y 10). A pesar de que está descrito que el etiquetado con ^{18}O es sensible al pH [49, 65] y de que la técnica de separación por IEF en disolución haya sido utilizada en trabajos anteriores para fraccionar péptidos marcados con ^{18}O [165], a día de hoy, no se había estudiado la estabilidad del marcaje como fuente potencial de artefactos de cuantificación ni se había tenido en cuenta en estudios previos de cuantificación por técnicas de marcaje isotópico estable.

Un problema que encontramos en los experimentos de proteómica cuantitativa es la presencia de valores atípicos de cuantificación a nivel de péptido debidos a las distintas etapas de manipulación de las muestras. Dos de las fuentes principales de generación de valores

atípicos de cuantificación a nivel de péptido son la oxidación de la Met y variaciones en el proceso de digestión. La oxidación de Met es técnicamente muy difícil de controlar al ser éste un amino ácido muy reactivo y su oxidación un proceso que puede ocurrir en diferentes proporciones en las muestras comparadas. De igual forma, los péptidos provenientes de digestión parcial (es decir, conteniendo al menos un sitio de corte trípico en su secuencia) indican que la digestión tríptica ha sido incompleta, proceso que también puede ser diferente entre las muestras a comparar. Sin embargo, aunque estas dos potenciales fuentes de error sean obvias y falseen los datos de cuantificación, no se han analizado con anterioridad y, aparentemente, no se han tenido en cuenta en estudios de cuantificación de proteínas con SIL. En este trabajo, y en conjunto con la tesis doctoral de Daniel Pérez, hemos demostrado que con esta nueva aproximación experimental optimizada, estas dos fuentes de error no aumentaban la variabilidad de las cuantificaciones de los péptidos, lo cual queda demostrado por la homogeneidad de las varianzas a nivel de péptido entre los distintos proteomas analizados. Una posible explicación es que la manipulación de la muestra es menor, ya sea durante la etapa de digestión en gel utilizando la cámara de reacción que constituye la matriz de acrilamida o en la etapa de inactivación de la tripsina post-marcaje. Por lo tanto, el protocolo robusto permitió incluir en el análisis estadístico todas aquellas cuantificaciones desechadas correspondientes a digestiones parciales y oxidaciones de Met, aumentando en casi un 25 % el número de péptidos totales cuantificados, consiguiendo una mayor profundidad de análisis y un mayor poder estadístico sin comprometer la calidad de las cuantificaciones. Por otro lado, cabe destacar que la mejora del protocolo ha permitido también disminuir el tiempo de estudio masivo de un proteoma, reduciendo el tiempo de preparación de la muestra, el análisis por espectrometría de masas y el análisis cuantitativo de los datos a dos semanas.

El protocolo general y robusto para la cuantificación por marcaje isotópico estable constituye la tecnología proteómica de cuantificación diferencial con la validación estadística más rigurosa publicada hasta la fecha. Esta aproximación, así como el modelo estadístico diseñado en este trabajo, se ha aplicado a más de una veintena de proteomas de distinta naturaleza [134], lo cual ha permitido estimar unas varianzas de referencia para futuros estudios cuantitativos masivos con las que se pueden detectar fuentes de error o artefactos. Así, una varianza a nivel de espectro más elevada en comparación con la varianza de referencia es indicativa de un mal funcionamiento del espectrómetro de masas, mientras que una varianza a nivel de péptido más elevada revela problemas en las etapas de digestión y/o marcaje. Por último, una varianza a nivel de proteína demasiado elevada nos sugiere una manipulación excesiva de la muestra en las etapas previas a la obtención del extracto proteico, indicándonos

que hay demasiada heterogeneidad entre los extractos proteicos y entonces el experimento tendrá poca potencia estadística para detectar cambios significativos. El diseño experimental desarrollado en esta tesis, junto con las herramientas estadísticas y computacionales desarrolladas en el laboratorio [57, 65, 137, 138] podría convertirse en una aproximación general para estudios masivos de proteómica semi-cuantitativa utilizando ^{18}O y una trampa iónica lineal. Con estos avances, podemos considerar que el desarrollo de la técnica de marcaje con ^{18}O ha alcanzado en este punto su madurez y ha adquirido los mismos niveles de reproducibilidad y estabilidad que las otras técnicas de SIL, pero con la ventaja frente a SILAC de permitir el análisis cuantitativo de cualquier tipo de muestra (plasma, orina e incluso tejidos) proveniente de cualquier origen (muestras de plantas, animales y humanas). Además, el método robusto posée el valor añadido de que su análisis ha sido validado con el diseño de un modelo estadístico para la hipótesis nula.

D.2.- Estudio de la angiogénesis inducida por el factor de crecimiento endotelial vascular en células endoteliales humanas

Considerados conjuntamente, los resultados obtenidos en el análisis del efecto del factor proangiogénico VEGF en células endoteliales son consistentes con otros estudios con el mismo tipo celular. En estos trabajos, se estimulan las células HUVEC con el medio condicionado de células cancerígenas, modelo que describe de manera más exacta la angiogénesis tumoral que el tratamiento con VEGF en sí mismo, y en el cual la mayoría de las proteínas (88 %) disminuyen su abundancia por el tratamiento [153]. Además, al comparar nuestros resultados con los cambios observados en trabajos de otros grupos [76, 152, 153], en los cuales el tratamiento proangiogénico de las células era más largo, comprobamos que la mayoría de las proteínas que cambian de abundancia en nuestro estudio no coincidían con los datos publicados. Si tenemos en cuenta los resultados obtenidos por *Western-Blot* en los que se estudió el comportamiento de un grupo de proteínas seleccionadas a distintos tiempos de incubación, nuestros datos son consistentes con un patrón de expresión proteica dinámico que modula la respuesta angiogénica. El tratamiento con estímulos proangiogénicos podría manifestarse con la modificación postraduccional de proteínas pre-existentes o en la síntesis *de novo* de reguladores de la angiogénesis, que actuarían de manera autocrina, ampliando la respuesta angiogénica a tiempos largos. Sin embargo, no podemos descartar la posibilidad de que las diferencias entre nuestro estudio y los trabajos publicados se deban, en parte, a un mayor rigor estadístico para determinar la significatividad de los cambios que utiliza nuestro

modelo, que, además de incluir un modelado de la hipótesis nula, utiliza la FDR como criterio para determinar los cambios reales de abundancia.

Por otro lado, cabe destacar que la mayoría de los cambios de abundancia significativos detectados en este trabajo no han sido descritos previamente, incluso con aproximaciones de *microarrays*, y por lo tanto, aportan datos novedosos sobre los procesos moleculares generados en respuesta al VEGF a tiempos cortos de tratamiento. Algunas de las proteínas cuantificadas han sido descritas como implicadas de manera directa o indirecta en procesos de angiogénesis. Además de la hsp70, chaperona cuya abundancia disminuye por el tratamiento de células HUVEC con VEGF [152, 153], también hemos cuantificado una disminución en la abundancia de la hsp90, de la que se ha descrito que su inhibición tiene efectos antiangiogénicos *in vivo* [156, 157]. La disminución de la abundancia de la lipasa adiposa de triglicéridos también es consistente con un proceso proangiogénico al ser un receptor del factor derivado del epitelio pigmentario [155], que ha sido descrito como un potente inhibidor endógeno de la angiogénesis [194]. De manera similar, la proteína activadora de Ran-GTPasa regula la localización nuclear de PTEN, supresor tumoral que también se ha descrito como inhibidor de procesos de angiogénesis [195], de forma que la menor abundancia de la proteína activadora de Ran-GTPasa debida al VEGF podría inhibir la translocación de PTEN. De las dos aminoacil-ARNt-sintetasas identificadas con abundancia alterada en este estudio, se ha descrito que la tirosil-ARNt, detectada tras 4 h de tratamiento con VEGF, puede actuar como factor proangiogénico en células HUVEC [162, 196]; mientras que se ha demostrado que la triptofanil-ARNt sintetasa, detectada a las 8 h de estimulación, podría inhibir la migración y la angiogénesis de las células HUVEC [162]. Por último, estudios previos coinciden con la implicación de la nucleolina y la caseína quinasa 2 en la angiogénesis, en los cuales se describe que la localización de la nucleolina en la superficie celular está modulada por VEGF en procesos angiogénicos [158] además de tener un papel fundamental en la organización nucleolar de la cromatina en la cual también está implicada la caseína quinasa 2 [197].

D.3.- GELSILOX: nueva estrategia para el análisis global del proteoma tiólico redox

D.3.1.- Desarrollo de nueva estrategia de análisis de los proteomas total y redox tiólico

A pesar de un interés creciente en los últimos años por las modificaciones oxidativas en Cys, el cual queda patente en el elevado número de publicaciones (el 70 % de las entradas en la base de datos *Pubmed* para "*Cys oxidation*" se han publicado a partir del año 2000), quedan aún por responder numerosas preguntas acerca de esas PTMs, incluyendo su alcance, su estequiometria, su especificidad, y, sobre todo, su relevancia fisiopatológica. Para ello, se han desarrollado numerosas aproximaciones proteómicas, la mayoría de ellas basadas en técnicas de purificación o de geles bidimensionales, dando lugar a la denominada proteómica redox. La mayor facilidad de manipular los péptidos que las proteínas de las que provienen hace que los métodos ya establecidos y validados de la proteómica moderna hayan abierto el camino al estudio masivo de las PTMOs. Por lo tanto, las nuevas aproximaciones proteómicas, bajo condiciones de análisis masivo de péptidos similares a las que se han desarrollado para el análisis profundo de los proteomas [134], y acoplándolas a aproximaciones de marcaje isotópico, ofrecen una oportunidad extraordinaria para el estudio sistemático de esas PTMs desde un punto de vista dinámico. Basándonos en todas estas consideraciones, diseñamos la aproximación GELSILOX, que aprovecha los desarrollos del laboratorio en el área de la cuantificación masiva con ^{18}O, así como su validación estadística [55, 57, 65], para determinar de manera simultánea el patrón de cambios de abundancia en el proteoma total y en el proteoma redox tiólico o redoxoma, siendo necesarios su análisis e interpretación conjunta. La técnica GELSILOX es un método robusto que se puede aplicar a estudios de proteómica cuantitativa rutinarios y que proporciona el poder estadístico necesario para detectar pequeñas alteraciones del estado redox generadas por condiciones biológicamente relevantes. Demostramos sus prestaciones identificando cambios en la abundancia relativa de proteínas, así como las Cys exactas que aumentan su estado de oxidación en varios tipos celulares y animales como modelos de estrés oxidativo poco estudiados desde el punto de vista de la proteómica masiva. A día de hoy, este estudio es el primero que aplica un modelo estadístico al análisis de la variación de los péptidos frente a la cuantificación de sus proteínas para la detección altamente sensible de los cambios dinámicos de PTMs.

La técnica GELSILOX tiene numerosas ventajas frente a otros métodos utilizados en proteómica redox. Por un lado, sigue un método robusto cuyas fuentes de error se describen

con precisión por un modelo de hipótesis nula que ha sido validado con el análisis cuantitativo masivo de numerosas muestras de diferentes orígenes [134]. El método permite llevar a cabo experimentos de proteómica cuantitativa convencional que, con una pequeña modificación en el protocolo permite además obtener información de proteómica redox. Por otro lado, utiliza reactivos comúnmente usados en proteómica de bajo coste (IAM, NEM, MMTS), incluyendo el agua pesada utilizada en la etapa de marcaje, y permite potencialmente la utilización de cualquier pareja de reactivos alquilantes (IAM, NEM, MMTS, pero también ácido yodoacético, N-metilmaleimida o yodoacetonilida [198]). Además GELSILOX podría llevarse a cabo con cualquier estrategia de SIL y con cualquier tipo de espectrómetro de masas, incluyendo los de baja resolución como se ha demostrado en este trabajo. Pero la mayor ventaja del método GELSILOX reside en su capacidad para diferenciar los cambios en el estado de oxidación de los péptidos de los cambios de abundancia de las proteínas, lo cual resulta posible al basar el análisis de los resultados en la validación de la hipótesis nula tanto a nivel de péptido como a nivel de proteína, permitiendo el cálculo de la significatividad de los cambios en el redoxoma y en el proteoma total. Otra gran ventaja que ofrece la técnica, conjuntamente al modelo estadístico, es la capacidad de analizar globalmente las alteraciones en la pauta de las PTMOs diferenciando las distintas poblaciones de péptidos oxCys y redCys, y analizar el comportamiento de cada población en relación a la hipótesis nula representada por la población de péptidos sin Cys. Con este tipo de análisis, fuimos capaces de determinar que la hipoxia aumentaba el estado de oxidación global de la población de péptidos oxCys del proteoma de células endoteliales sin que el análisis individual de cada péptido oxCys permitiera detectar dicho aumento. Además, el análisis de la varianza a nivel de péptido controla la presencia de artefactos durante la manipulación de los péptidos con Cys, ya que se procesan y se cuantifican con el conjunto de péptidos que no contienen Cys.

D.3.2.- Análisis de los proteomas totales y redox tiólicos en el endotelio vascular sometido a estrés oxidativo

La aproximación por GELSILOX se validó utilizando un modelo forzado de oxidación que consiste en el tratamiento de células endoteliales con diamida, un reactivo oxidante inespecífico. La eficacia del método se demostró analizando modelos más fisiológicos como el efecto del peróxido de hidrógeno o de la hipoxia en células endoteliales. El estudio comparativo de los cambios en las poblaciones de péptidos oxCys alterados por los tres tratamientos muestra unos perfiles muy similares (Tabla T.4), lo que podría sugerir un efecto común predominante sobre el estado de oxidación del proteoma, independiente del estrés

oxidativo al que es sometido. Además, dicha comparativa nos revela cuáles son las dianas principales de un estrés oxidativo moderado en el endotelio. Entre los péptidos comunes, todos los péptidos oxCys que aumentan por el tratamiento por H_2O_2, excepto uno, también lo hacen con la diamida, y la mayoría de los péptidos más alterados por la hipoxia también aumentan con los otros dos tratamientos. De todos los péptidos alterados en su estado de oxidación, al menos un tercio han sido descritos previamente como centros activos de proteínas, como los sitios más reactivos, oxidados o nitrosilados, incluyendo:

- la Cys173 de la peroxiredoxina-1, que forma el puente disulfuro intramolecular sensible a peróxido de hidrogeno que regula la actividad de la enzima [80, 172].
- la Cys599 de la hsp-90α, implicada en la regulación negativa de la actividad ATPasa de la proteína y en la inhibición de su unión a la eNOS por S-nitrosilación [199].
- la Cys139 de la cofilina 1, de la que se ha demostrado que su oxidación por H_2O_2 induce apoptosis [200].
- la Cys163 de la L-lactato deshidrogenasa, detectada previamente como sitio nitrosilable [126].
- la Cys152, que forma el sitio activo de la gliceraldehído-3-fosfato deshidrogenasa [201].

En claro contraste, el patrón de los cambios de abundancia de proteínas inducidos por los tres estímulos oxidativos muestra poca coincidencia entre ellos (Anexo A.2), lo cual podría sugerir que la respuesta de la maquinaria proteica es dependiente del estímulo aplicado. A pesar de todo lo mencionado anteriormente, y de manera consistente con estudios previos, todos los tratamientos producen una disminución de las proteínas asociadas con procesos de crecimiento celular, como son la síntesis de proteínas, la replicación de ADN, el procesamiento y la transcripción del ARNm, así como reorganización del citoesqueleto.

D.3.3.- Análisis de los proteomas totales y redox tiólicos en mitocondrias de cardiomiocitos de rata sometidas a IR y efecto protector del IP

Por otro lado, decidimos analizar mediante la técnica GELSILOX las alteraciones en el proteoma redox tiólico de mitocondrias aisladas de corazón de rata sometidas a IR y analizar el efecto del IP, proceso protector que atenúa los efectos de la IR [175-177]. Se considera que las mitocondrias desempeñan un papel central en la generación de RNOS [202, 203] y que están implicadas en el IP así como en el daño producido por IR [85]. Además, las proteínas mitocondriales son dianas importantes de daño oxidativo [146, 204]. Sin embargo, los sitios de Cys afectados por ROS en este subproteoma, en el que las proteínas de membrana son

abundantes, no han sido investigados previamente por técnicas de análisis masivo. Por lo tanto, este modelo resulta altamente relevante desde el punto de vista biológico para probar el rendimiento del nuevo método. Con el fin de evaluar la especificidad del tratamiento, utilizamos dos poblaciones diferentes de mitocondrias, las SSM y las IFM, que muestran una sensibilidad diferente a la apertura inducida por Ca^{2+} del poro de transición mitocondrial [205], un mecanismo descrito como fundamental en los procesos de muerte celular inducidos por IR [206, 207]. Nuestros resultados concuerdan con la bibliografía existente, ya que demostramos que la IR produce un aumento en la abundancia en una amplia población de péptidos oxCys en SSM, mientras que ese efecto es mucho más suave en IFM. Aún más interesante, es la constatación de que el IP previa a un episodio de IR inhibe los efectos de la IR en la población de péptidos oxCys en SSM, lo que sugiere una relación directa entre el IP y la inhibición del daño oxidativo. El análisis de los péptidos oxCys alterados por el tratamiento isquémico resulta también consecuente cuando los efectos de la IR se comparan entre IFM y SSM: excepto uno, todos los péptidos que aumentan su abundancia en IFM por la IR lo hacen también en SSM. Además, la gran mayoría de los péptidos oxCys detectados (72 %) han sido descritos previamente en otros modelos como centros activos sensibles a redox, centros de unión a metales o dianas de la tiorredoxina 1, incluyendo:

- la Cys385 de la aconitasa 2, que forma parte del centro de unión hierro-azufre, cuya desestructuración por daño oxidativo ha sido propuesta para explicar la inactivación de la enzima que se observa en episodios de IR cardiaca [208].
- la Cys99 de la peroxiredoxina 5, que forma el sitio activo de la proteína [209].
- las Cys89 y Cys212 de la malato deshidrogenasa, dianas de la tiorredoxina 1 [210].
- la Cys528 de la succinato deshidrogenasa y la Cys379 de la isocitrato deshidrogenasa, que han sido descritas como dianas de S-nitrosilación [85, 126].

La gran mayoría de las Cys alteradas por los tratamientos, a pesar de su relevancia fisopatológica al pertenecer a proteínas de la cadena de transporte de electrones (ETC) o a enzimas metabólicas, no se han descrito en estudios anteriores en el contexto del daño por IR. En claro contraste, el patrón de cambios de abundancia de proteínas inducidos por IR es bastante diferente (Table T.6), siendo las proteínas de la ETC las más numerosas en SSM, y las que resultan menos alteradas en IFM. Por otra parte, la mayoría de los cambios de abundancia de proteínas detectados en SSM_IR están notablemente revertidos en SSM_IPIR. Nuestros resultados sugieren que la IR desestabiliza la estructura de los complejos mitocondriales de la ETC en SSM, aumentando la generación de RNOS y así el daño oxidativo en proteínas

mitocondriales [96]. Las alteraciones en proteínas de la ETC son menos pronunciadas en IFM y muy tenues en las SSM de los corazones de ratas sometidas a precondicionamiento, lo que explicaría la disminución o la inhibición del daño oxidativo detectadas, respectivamente. La técnica GELSILOX proporciona pues las herramientas necesarias para evaluar y comprender los mecanismos fisiopatológicos subyacentes al IP, así como el efecto protector del precondicionamiento sobre el daño oxidativo, al cubrir las dos alteraciones dinámicas (cambio de abundancia de proteínas y de estado de oxidación de péptidos) que modulan la respuesta celular a corto, medio y largo plazo del tratamiento por IR.

D.4.- La CsA induce la nitración de la Tyr 34 de la MnSOD

La espectrometría de masas es una técnica de primordial importancia en proteómica, y los desarrollos en este campo han sido posibles gracias a la mejora de los instrumentos de medida, de las estrategias experimentales y de las herramientas bioinformáticas. A día de hoy, es posible identificar y determinar la abundancia relativa de miles de proteínas en un sistema biológico por el análisis por espectrometría de masas de los péptidos generados tras la digestión de un proteoma con una proteasa. Sin embargo, en ciertos casos, es necesaria la caracterización específica de un péptido concreto en una muestra compleja. Esta aproximación dirigida se está convirtiendo en una herramienta de validación de resultados obtenidos por análisis cuantitativos masivos y consiste en concentrar toda la potencia del espectrómetro de masas en monitorizar el péptido de interés. La monitorización selectiva de reacción (SRM) es el método más usado para identificar un péptido de forma altamente específica y precisa [211], y se basa en la selección del ión precursor de nuestro péptido de interés, su fragmentación y la monitorización de un fragmento específico de ese péptido [56]. A pesar de ser la técnica más sensible para la identificación de un péptido, la SRM no permite obtener los espectros de fragmentación ni la validación por fragmentación múltiple MS^n. Por esta razón, para aplicar dicha técnica, es necesario haber identificado el péptido con anterioridad y comprobar que los iones fragmento monitorizados son específicos de nuestro péptido de interés. Sin embargo, en muestras biológicas complejas, es muy difícil encontrar fragmentos específicos de un péptido de interés, ya que carecemos de la información estructural del péptido y la masa que se detecta en un MS puede pertenecer a varios péptidos. En estos casos, el espectro de fragmentación del péptido de interés es imprescindible para confirmar la naturaleza de la especie identificada o para determinar el residuo exacto en la secuencia que puede ser modificado postraducionalmente. Sin embargo, la obtención de un espectro de fragmentación de un

péptido concreto no siempre es posible cuando se realiza un experimento de análisis masivo en los que únicamente se identifican los iones más intensos que eluyen a un tiempo determinado durante la cromatografía HPLC. Para paliar este defecto, se puede programar el detector MS para que realice espectros MS/MS continuos en unas determinadas masas seleccionadas a lo largo del gradiente de elución de la cromatografía. Esta técnica, desarrollada en el laboratorio y bautizada SMIM (monitorización de iones de fragmentación específicos) [56], se ha aplicado a la identificación de proteínas presentes en un proteoma en muy baja abundancia [212], a la caracterización de modificaciones postraduccionales en residuos concretos como la fosforilación [145] o la S-nitrosilación [199]. La técnica SMIM tiene varias ventajas frente a los modos de barrido convencionales: el promedio de un número elevado de espectros MS/MS durante una ventana corta de tiempo de elución aumenta considerablemente la sensibilidad de la medida y, además, se pueden determinar las trazas cromatográficas obteniendo espectros de monitorización selectiva de iones virtuales. Estas ventajas se deben sobre todo a la velocidad de barrido que caracteriza las trampas iónicas lineales como las que disponemos en nuestro laboratorio. En este trabajo, utilizando la técnica SMIM y en colaboración con el grupo del Prof. Santiago Lamas, demostramos de manera inequívoca, que la CsA induce la nitración de la MnSOD en su Tyr34, validando los resultados con la fragmentación MS^3 altamente específica de nuestro péptido de interés.

La MnSOD es una enzima mitocondrial considerada como esencial en la primera línea de defensa de detoxificación de superóxido. En la pared vascular, se ha demostrado que esta enzima juega un papel crucial en la protección vascular [213]. La MnSOD cataliza la reacción de conversión del superóxido en peróxido de hidrógeno y agua. El objetivo de esta conversión es múltiple, incluyendo la protección de la inactivación del óxido nítrico o de proteínas mitocondriales (aconitasa y fumarasa entre otras) [213]. El átomo de manganeso es crítico para la actividad de la enzima, y la Tyr34 se encuentra próxima a dicho átomo y, por lo tanto, de su centro activo [214]. La nitración de dicho residuo de Tyr se demostró hace ya 10 años y está ampliamente aceptado por la comunidad científica que esa modificación implica la inactivación de la enzima [114]. Por otra parte, el peroxinitrito es el único agente oxidante fisiológico conocido capaz de inactivar la actividad enzimática de la MnSOD [214]. Numerosos estudios han destacado la importancia fisiopatológica de la nitración de la MnSOD así como su implicación en numerosas patologías, como puede ser el rechazo crónico del trasplante renal [116], la lesión traumática del cerebro [215], la edad [216], o la hipertensión inducida por angiotensina-II [217]. En este estudio, y por primera vez, demostramos que la nitración de la MnSOD inducida por la CsA se produce específicamente en su Tyr34, proporcionándonos

una explicación bioquímica a la inactivación de la enzima. Además, en este mismo trabajo y en colaboración con el Dr. Mariano Redondo-Horcajo y el Prof. Santiago Lamas, se demostró que el tratamiento de células endoteliales con ácido úrico, un compuesto anti-nitrante que elimina los radicales derivados del peroxinitrito [218, 219], inhibe la inactivación de la MnSOD [146], resultado que refuerza la idea de unión directa entre la toxicidad de la CsA y el estrés nitroxidativo mitocondrial. Por último, cabe destacar que las concentraciones de CsA utilizadas en este trabajo (1–10 mM) están ligeramente por encima del límite superior del rango terapéutico de las concentraciones en pacientes con trasplante renal tratados con estos agentes, y, por lo tanto, son las que se espera encontrar en el contexto de la toxicidad vascular. Por tanto, se puede especular que la disminución de la actividad catalítica de la MnSOD endotelial contribuye a la amplificación del estrés nitroxidativo así como a la propagación del daño endotelial por un mecanismo de retro-amplificación.

D.5.- Perspectivas de futuro

Un punto que aún queda por estudiar es si la aproximación de varianza global, y de manera más general, el modelo estadístico utilizado en esta tesis doctoral, puede aplicarse a experimentos de proteómica cuantitativa utilizando otros métodos de marcaje como SILAC o iTRAQ, además de su aplicabilidad a datos obtenidos con espectrómetros de masas de alta resolución. Otra gran meta que debe alcanzar la proteómica cuantitativa es la integración de la biología de sistemas que permita discernir cambios de expresión de grupos de proteínas que realicen una misma función, de forma que aumente nuestra comprensión sobre los cambios producidos a nivel celular. Ello sería posible introduciendo niveles superiores en el modelo estadístico jerárquico, de manera que la integración de la información se haría en un mismo marco estadístico. Esos trabajos ya se están realizando, y son los temas centrales de la tesis de Marco Trevisan Herraz.

Asimismo, estos desarrollos se podrían aplicar a la estrategia GELSILOX para combinar cualquier tipo de marcaje isotópico y cualquier espectrómetro de masas con cualquier combinación de agentes alquilantes para derivatizar las Cys. La técnica GELSILOX se podría también implementar con una etapa de purificación de péptidos para aumentar el rendimiento de cuantificación del redoxoma, utilizando la parte no retenida en la etapa de purificación para cuantificar el proteoma total. Además, la aproximación GELSILOX podría discriminar las distintas PTMOs en Cys acoplando una etapa de tipo *"biotin-switch"* en gel utilizando ascorbato para marcar específicamente las Cys S-nitrosiladas [122] o utilizando compuestos determinados que reaccionarían de manera específica con las diferentes formas oxidadas de la

Cys (como por ejemplo la dimedona o derivados de dimedona para marcar la sulfenilación [220, 221], así como introducir una etapa de tratamiento con de glutaredoxinas para revertir la S-glutationilación [222]) aprovechando la matriz de acrilamida como cámara de reacción.

Recientemente, se ha descrito un método elegante, el OxMRM, para la cuantificación del estado de oxidación de las Cys basado también en la alquilación diferencial de las Cys, pero combinándola con una etapa de purificación por inmunoafinidad y procesando los péptidos por MRM. Aplicando esta aproximación a una línea celular de cáncer de mama tratadas con diamida o con H_2O_2, monitorizando el estado de oxidación de 7 de las 10 Cys de la proteína p53, así como 8 de las 10 Cys de la fosfatasa PTP1B [223]. La mayor limitación de esta aproximación experimental es la necesidad de seleccionar *a priori* las proteínas candidatas para el estudio así como una especificidad muy alta de los anticuerpos utilizados para la purificación. Sin embargo, los recientes avances en las técnicas de proteómica dirigida [224] ofrecen nuevas posibilidades de validación a gran escala de los datos obtenidos por proteómica cuantitativa que se podrían desarrollar para confirmar los cambios en el estado de oxidación cuantificados por la técnica GELSILOX.

CONCLUSIONES

1. Las tecnologías desarrolladas en este trabajo, en combinación con las herramientas de cuantificación masiva desarrolladas en nuestro grupo, permiten el análisis de los patrones de cambios de abundancia de los proteomas total y redox tiólico de cualquier muestra, identificando los residuos específicos de cisteína que se modifican, y controlando las distintas fuentes de error.
2. La angiogénesis inducida por VEGF es un proceso bifásico en el tiempo que refleja una respuesta compleja, específica y a corto plazo de las células endoteliales de cordón umbilical humano.
3. Una concentración moderada de agua oxigenada induce en células endoteliales un aumento significativo en la concentración de la forma oxidada de una serie de residuos de cisteína.
4. Un periodo corto de hipoxia no produce cambios significativos apreciables en la concentración de la forma oxidada de residuos de cisteína, pero produce un aumento significativo cuando se considera globalmente la población de cisteínas en su forma oxidada.
5. Diferentes estímulos oxidativos parecen producir en endotelio vascular una pauta común de aumentos en la forma oxidada de las cisteínas, sugiriendo un mecanismo compartido de acción.
6. El proceso de isquemia-reperfusión llevado a cabo *in vivo* en corazón de rata produce un aumento en la concentración de cisteínas oxidadas en proteínas mitocondriales, sobre todo en las que pertenecen a complejos de la cadena de transporte de electrones. Este efecto es más acusado en mitocondrias subsarcolemmales que en mitocondrias intermiofibrilares.
7. El efecto producido por la isquemia-reperfusión desaparece cuando los corazones de rata se someten a un proceso previo de precondicionamiento isquémico.
8. El tratamiento de células endoteliales con ciclosporina A induce la nitración de la tirosina situada en el centro catalítico de la superóxido dismutasa dependiente de manganeso, que podría deberse a la generación de peroxinitrito mitocondrial. Esta modificación estructural podría explicar la citotoxicidad vascular observada durante los tratamientos con ciclosporina A.

BIBLIOGRAFÍA

1. Wasinger, V.C., et al., *Progress with gene-product mapping of the Mollicutes: Mycoplasma genitalium.* Electrophoresis, 1995. **16**(7): p. 1090-4.

2. Wilkins, M.R., et al., *Progress with proteome projects: why all proteins expressed by a genome should be identified and how to do it.* Biotechnol Genet Eng Rev, 1996. **13**: p. 19-50.

3. Klose, J., *Protein mapping by combined isoelectric focusing and electrophoresis of mouse tissues. A novel approach to testing for induced point mutations in mammals.* Humangenetik, 1975. **26**(3): p. 231-43.

4. O'Farrell, P.H., *High resolution two-dimensional electrophoresis of proteins.* J Biol Chem, 1975. **250**(10): p. 4007-21.

5. Scheele, G.A., *Two-dimensional gel analysis of soluble proteins. Charaterization of guinea pig exocrine pancreatic proteins.* J Biol Chem, 1975. **250**(14): p. 5375-85.

6. Kinter, M. and N.E. Sherman, *Protein Sequencing and Identification Using Tandem Mass Spectrometry.* Wiley-Interscience Publications, 2000.

7. Corthals, G.L., et al., *The dynamic range of protein expression: a challenge for proteomic research.* Electrophoresis, 2000. **21**(6): p. 1104-15.

8. Karas, M. and F. Hillenkamp, *Laser desorption ionization of proteins with molecular masses exceeding 10,000 daltons.* Anal Chem, 1988. **60**(20): p. 2299-301.

9. Fenn, J.B., et al., *Electrospray ionization for mass spectrometry of large biomolecules.* Science, 1989. **246**(4926): p. 64-71.

10. Roepstorff, P. and W.J. Richter, *Status of, and developments in, mass spectrometry of peptides and proteins.* Int J Mass Spectrom Ion Process, 1992. **118/119**: p. 789-809.

11. Chapman, J.R., *Protein and Peptide Analysis by Mass Spectrometry.* Methods in Molecular Biology, 2006.

12. Henzel, W.J., et al., *Identifying proteins from two-dimensional gels by molecular mass searching of peptide fragments in protein sequence databases.* Proc Natl Acad Sci U S A, 1993. **90**(11): p. 5011-5.

13. James, P., et al., *Protein identification by mass profile fingerprinting.* Biochem Biophys Res Commun, 1993. **195**(1): p. 58-64.

14. Perkins, D.N., et al., *Probability-based protein identification by searching sequence databases using mass spectrometry data.* Electrophoresis, 1999. **20**(18): p. 3551-67.

15. Pandey, A. and M. Mann, *Proteomics to study genes and genomes.* Nature, 2000. **405**(6788): p. 837-46.

16. Mortz, E., et al., *Sequence tag identification of intact proteins by matching tanden mass spectral data against sequence data bases.* Proc Natl Acad Sci U S A, 1996. **93**(16): p. 8264-7.

17. Eng, J.K., A.L. McCormack, and J.R.r. Yates, *An approach to correlate tandem mass spectral data of peptides with amino acid sequences in a protein database.* J Am Soc Mass Spectrom, 1994. **5**: p. 976-989.

18. Shevchenko, A., et al., *Linking genome and proteome by mass spectrometry: large-scale identification of yeast proteins from two dimensional gels.* Proc Natl Acad Sci U S A, 1996. **93**(25): p. 14440-5.

19. Gygi, S.P., et al., *Correlation between protein and mRNA abundance in yeast.* Mol Cell Biol, 1999. **19**(3): p. 1720-30.

20. Griffin, T.J. and R. Aebersold, *Advances in proteome analysis by mass spectrometry.* J Biol Chem, 2001. **276**(49): p. 45497-500.

21. Yates, J.R., 3rd, et al., *Method to correlate tandem mass spectra of modified peptides to amino acid sequences in the protein database.* Anal Chem, 1995. **67**(8): p. 1426-36.

22. Link, A.J., et al., *Direct analysis of protein complexes using mass spectrometry.* Nat Biotechnol, 1999. **17**(7): p. 676-82.

23. Washburn, M.P., D. Wolters, and J.R. Yates, 3rd, *Large-scale analysis of the yeast proteome by multidimensional protein identification technology.* Nat Biotechnol, 2001. **19**(3): p. 242-7.

24. Gygi, S.P., et al., *Quantitative analysis of complex protein mixtures using isotope-coded affinity tags.* Nat Biotechnol, 1999. **17**(10): p. 994-9.

25. Conrads, T.P., et al., *Quantitative analysis of bacterial and mammalian proteomes using a combination of cysteine affinity tags and 15N-metabolic labeling.* Anal Chem, 2001. **73**(9): p. 2132-9.

26. Oda, Y., T. Nagasu, and B.T. Chait, *Enrichment analysis of phosphorylated proteins as a tool for probing the phosphoproteome.* Nat Biotechnol, 2001. **19**(4): p. 379-82.

27. Zhou, H., J.D. Watts, and R. Aebersold, *A systematic approach to the analysis of protein phosphorylation.* Nat Biotechnol, 2001. **19**(4): p. 375-8.

28. Fenselau, C. and X. Yao, *Proteolytic labeling with 18O for comparative proteomics studies: preparation of 18O-labeled peptides and the 18O/16O peptide mixture.* Methods Mol Biol, 2007. **359**: p. 135-42.

29. Ong, S.E., et al., *Stable isotope labeling by amino acids in cell culture, SILAC, as a simple and accurate approach to expression proteomics.* Mol Cell Proteomics, 2002. **1**(5): p. 376-86.

30. Oda, Y., et al., *Accurate quantitation of protein expression and site-specific phosphorylation.* Proc Natl Acad Sci U S A, 1999. **96**(12): p. 6591-6.

31. Chen, X., L.M. Smith, and E.M. Bradbury, *Site-specific mass tagging with stable isotopes in proteins for accurate and efficient protein identification.* Anal Chem, 2000. **72**(6): p. 1134-43.

32. Jiang, H. and A.M. English, *Quantitative analysis of the yeast proteome by incorporation of isotopically labeled leucine.* J Proteome Res, 2002. **1**(4): p. 345-50.

33. Amanchy, R., et al., *Phosphoproteome analysis of HeLa cells using stable isotope labeling with amino acids in cell culture (SILAC).* J Proteome Res, 2005. **4**(5): p. 1661-71.

34. Kruger, M., et al., *SILAC mouse for quantitative proteomics uncovers kindlin-3 as an essential factor for red blood cell function.* Cell, 2008. **134**(2): p. 353-64.

35. Hayter, J.R., et al., *The subunit structure and dynamics of the 20S proteasome in chicken skeletal muscle.* Mol Cell Proteomics, 2005. **4**(9): p. 1370-81.

36. Sury, M.D., J.X. Chen, and M. Selbach, *The SILAC fly allows for accurate protein quantification in vivo.* Mol Cell Proteomics, 2010. **9**(10): p. 2173-83.

37. Wasinger, V.C. and G.L. Corthals, *Proteomic tools for biomedicine.* J Chromatogr B Analyt Technol Biomed Life Sci, 2002. **771**(1-2): p. 33-48.

38. Gevaert, K., et al., *Stable isotopic labeling in proteomics.* Proteomics, 2008. **8**(23-24): p. 4873-85.

39. Leitner, A. and W. Lindner, *Current chemical tagging strategies for proteome analysis by mass spectrometry.* J Chromatogr B Analyt Technol Biomed Life Sci, 2004. **813**(1-2): p. 1-26.

40. Han, D.K., et al., *Quantitative profiling of differentiation-induced microsomal proteins using isotope-coded affinity tags and mass spectrometry.* Nat Biotechnol, 2001. **19**(10): p. 946-51.

41. Ross, P.L., et al., *Multiplexed protein quantitation in Saccharomyces cerevisiae using amine-reactive isobaric tagging reagents.* Mol Cell Proteomics, 2004. **3**(12): p. 1154-69.

42. Choe, L., et al., *8-plex quantitation of changes in cerebrospinal fluid protein expression in subjects undergoing intravenous immunoglobulin treatment for Alzheimer's disease.* Proteomics, 2007. **7**(20): p. 3651-60.

43. Thompson, A., et al., *Tandem mass tags: a novel quantification strategy for comparative analysis of complex protein mixtures by MS/MS.* Anal Chem, 2003. **75**(8): p. 1895-904.

44. Sprinson, D. and D. Rittenberg, *Nature of the activation process in enzymatic reactions.* Nature, 1951. **167**: p. 484.

45. Yao, X., et al., *Proteolytic 18O labeling for comparative proteomics: model studies with two serotypes of adenovirus.* Anal Chem, 2001. **73**(13): p. 2836-42.

46. Stewart, II, T. Thomson, and D. Figeys, *18O labeling: a tool for proteomics.* Rapid Commun Mass Spectrom, 2001. **15**(24): p. 2456-65.

47. Heller, M., et al., *Trypsin catalyzed 16O-to-18O exchange for comparative proteomics: tandem mass spectrometry comparison using MALDI-TOF, ESI-QTOF, and ESI-ion trap mass spectrometers.* J Am Soc Mass Spectrom, 2003. **14**(7): p. 704-18.

48. Bantscheff, M., B. Dumpelfeld, and B. Kuster, *Femtomol sensitivity post-digest (18)O labeling for relative quantification of differential protein complex composition.* Rapid Commun Mass Spectrom, 2004. **18**(8): p. 869-76.

49. Staes, A., et al., *Global differential non-gel proteomics by quantitative and stable labeling of tryptic peptides with oxygen-18.* J Proteome Res, 2004. **3**(4): p. 786-91.

50. Zang, L., et al., *Proteomic analysis of ductal carcinoma of the breast using laser capture microdissection, LC-MS, and 16O/18O isotopic labeling.* J Proteome Res, 2004. **3**(3): p. 604-12.

51. Qian, W.J., et al., *Quantitative proteome analysis of human plasma following in vivo lipopolysaccharide administration using 16O/18O labeling and the accurate mass and time tag approach.* Mol Cell Proteomics, 2005. **4**(5): p. 700-9.

52. Liu, H., et al., *Non-gel-based dual 18O labeling quantitative proteomics strategy.* Anal Chem, 2007. **79**(20): p. 7700-7.

53. Broedel, O., et al., *In-Gel 18O labeling for improved identification of proteins from 2-DE Gel spots in comparative proteomic experiments.* J Proteome Res, 2009. **8**(7): p. 3771-7.

54. Lopez-Ferrer, D., et al., *Evaluation of a high-intensity focused ultrasound-immobilized trypsin digestion and 18O-labeling method for quantitative proteomics.* Anal Chem, 2009. **81**(15): p. 6272-7.

55. Lopez-Ferrer, D., et al., *Quantitative proteomics using 16O/18O labeling and linear ion trap mass spectrometry.* Proteomics, 2006. **6 Suppl 1**: p. S4-11.

56. Jorge, I., et al., *High-sensitivity analysis of specific peptides in complex samples by selected MS/MS ion monitoring and linear ion trap mass spectrometry: application to biological studies.* J Mass Spectrom, 2007. **42**(11): p. 1391-403.

57. Ramos-Fernandez, A., D. Lopez-Ferrer, and J. Vazquez, *Improved method for differential expression proteomics using trypsin-catalyzed 18O labeling with a correction for labeling efficiency.* Mol Cell Proteomics, 2007. **6**(7): p. 1274-86.

58. Miyagi, M. and K.C. Rao, *Proteolytic 18O-labeling strategies for quantitative proteomics.* Mass Spectrom Rev, 2007. **26**(1): p. 121-36.

59. Lau, K.W., et al., *Capture and analysis of quantitative proteomic data.* Proteomics, 2007. **7**(16): p. 2787-99.

60. Gan, C.S., et al., *Technical, experimental, and biological variations in isobaric tags for relative and absolute quantitation (iTRAQ).* J Proteome Res, 2007. **6**(2): p. 821-7.

61. Boehm, A.M., et al., *Precise protein quantification based on peptide quantification using iTRAQ.* BMC Bioinformatics, 2007. **8**: p. 214.

62. Pan, C., et al., *ProRata: A quantitative proteomics program for accurate protein abundance ratio estimation with confidence interval evaluation.* Anal Chem, 2006. **78**(20): p. 7121-31.

63. Pan, C., et al., *Robust estimation of peptide abundance ratios and rigorous scoring of their variability and bias in quantitative shotgun proteomics.* Anal Chem, 2006. **78**(20): p. 7110-20.

64. Navarro, P., *Desarrollo de nuevas metodologías informáticas aplicadas a la espectrometría de masas y al análisis masivo de datos generados en proyectos de proteómica utilizando técnicas de segunda generación.* Tesis Doctoral - UAM, 2010.

65. Jorge, I., et al., *Statistical model to analyze quantitative proteomics data obtained by 18O/16O labeling and linear ion trap mass spectrometry: application to the study of vascular endothelial growth factor-induced angiogenesis in endothelial cells.* Mol Cell Proteomics, 2009. **8**(5): p. 1130-49.

66. Carmeliet, P., *Angiogenesis in health and disease.* Nat Med, 2003. **9**(6): p. 653-60.

67. Carmeliet, P., *Angiogenesis in life, disease and medicine.* Nature, 2005. **438**(7070): p. 932-6.

68. Alfranca, A., et al., *Prostanoid signal transduction and gene expression in the endothelium: role in cardiovascular diseases.* Cardiovasc Res, 2006. **70**(3): p. 446-56.

69. McCormick, S.M., et al., *DNA microarray reveals changes in gene expression of shear stressed human umbilical vein endothelial cells.* Proc Natl Acad Sci U S A, 2001. **98**(16): p. 8955-60.

70. Abe, M. and Y. Sato, *cDNA microarray analysis of the gene expression profile of VEGF-activated human umbilical vein endothelial cells.* Angiogenesis, 2001. **4**(4): p. 289-98.

71. Yang, S., et al., *Vascular endothelial growth factor-induced genes in human umbilical vein endothelial cells: relative roles of KDR and Flt-1 receptors.* Arterioscler Thromb Vasc Biol, 2002. **22**(11): p. 1797-803.

72. Minami, T., et al., *Thrombin stimulation of vascular adhesion molecule-1 in endothelial cells is mediated by protein kinase C (PKC)-delta-NF-kappa B and PKC-zeta-GATA signaling pathways.* J Biol Chem, 2003. **278**(9): p. 6976-84.

73. Bruneel, A., et al., *Proteomic study of human umbilical vein endothelial cells in culture.* Proteomics, 2003. **3**(5): p. 714-23.

74. Bruneel, A., et al., *Proteomics of human umbilical vein endothelial cells applied to etoposide-induced apoptosis.* Proteomics, 2005. **5**(15): p. 3876-84.

75. Murphy, S., et al., *Identification of sokotrasterol sulfate as a novel proangiogenic steroid.* Circ Res, 2006. **99**(3): p. 257-65.

76. Karsan, A., et al., *Quantitative proteomic analysis of sokotrasterol sulfate-stimulated primary human endothelial cells.* Mol Cell Proteomics, 2005. **4**(2): p. 191-204.

77. Winterbourn, C.C., *Reconciling the chemistry and biology of reactive oxygen species.* Nat Chem Biol, 2008. **4**(5): p. 278-86.

78. Kumsta, C., M. Thamsen, and U. Jakob, *Effects of oxidative stress on behavior, physiology, and the redox thiol proteome of Caenorhabditis elegans.* Antioxid Redox Signal, 2011. **14**(6): p. 1023-37.

79. Antelmann, H. and J.D. Helmann, *Thiol-based redox switches and gene regulation.* Antioxid Redox Signal, 2011. **14**(6): p. 1049-63.

80. Klomsiri, C., P.A. Karplus, and L.B. Poole, *Cysteine-based redox switches in enzymes.* Antioxid Redox Signal, 2011. **14**(6): p. 1065-77.

81. Martinez-Ruiz, A. and S. Lamas, *S-nitrosylation: a potential new paradigm in signal transduction.* Cardiovasc Res, 2004. **62**(1): p. 43-52.

82. Reddie, K.G. and K.S. Carroll, *Expanding the functional diversity of proteins through cysteine oxidation.* Curr Opin Chem Biol, 2008. **12**(6): p. 746-54.

83. Roeser, J., et al., *Oxidative protein labeling in mass-spectrometry-based proteomics.* Anal Bioanal Chem, 2010. **397**(8): p. 3441-55.

84. Deanfield, J.E., J.P. Halcox, and T.J. Rabelink, *Endothelial function and dysfunction: testing and clinical relevance.* Circulation, 2007. **115**(10): p. 1285-95.

85. Kohr, M.J., et al., *Simultaneous measurement of protein oxidation and S-nitrosylation during preconditioning and ischemia/reperfusion injury with resin-assisted capture.* Circ Res, 2011. **108**(4): p. 418-26.

86. Hirooka, Y., et al., *Oxidative stress and central cardiovascular regulation. - Pathogenesis of hypertension and therapeutic aspects.* Circ J, 2010. **74**(5): p. 827-35.

87. Koh, C.H., et al., *Chronic exposure to U18666A is associated with oxidative stress in cultured murine cortical neurons.* J Neurochem, 2006. **98**(4): p. 1278-89.

88. Visconti, R. and D. Grieco, *New insights on oxidative stress in cancer.* Curr Opin Drug Discov Devel, 2009. **12**(2): p. 240-5.

89. Wei, W., et al., *Oxidative stress, diabetes, and diabetic complications.* Hemoglobin, 2009. **33**(5): p. 370-7.

90. Oktyabrsky, O.N. and G.V. Smirnova, *Redox regulation of cellular functions.* Biochemistry (Mosc), 2007. **72**(2): p. 132-45.

91. Janssen-Heininger, Y.M., et al., *Redox-based regulation of signal transduction: principles, pitfalls, and promises.* Free Radic Biol Med, 2008. **45**(1): p. 1-17.

92. Paulsen, C.E. and K.S. Carroll, *Orchestrating redox signaling networks through regulatory cysteine switches.* ACS Chem Biol, 2010. **5**(1): p. 47-62.

93. Spickett, C.M., et al., *Proteomic analysis of phosphorylation, oxidation and nitrosylation in signal transduction.* Biochim Biophys Acta, 2006. **1764**(12): p. 1823-41.

94. Santos, C.X., et al., *Redox signaling in cardiac myocytes.* Free Radic Biol Med, 2011. **50**(7): p. 777-93.

95. Maulik, N., T. Yoshida, and D.K. Das, *Regulation of cardiomyocyte apoptosis in ischemic reperfused mouse heart by glutathione peroxidase.* Mol Cell Biochem, 1999. **196**(1-2): p. 13-21.

96. Murphy, E. and C. Steenbergen, *Mechanisms underlying acute protection from cardiac ischemia-reperfusion injury.* Physiol Rev, 2008. **88**(2): p. 581-609.

97. Murata, M., et al., *Mitochondrial ATP-sensitive potassium channels attenuate matrix Ca(2+) overload during simulated ischemia and reperfusion: possible mechanism of cardioprotection.* Circ Res, 2001. **89**(10): p. 891-8.

98. Jennings, R.B., et al., *Development of cell injury in sustained acute ischemia.* Circulation, 1990. **82**(3 Suppl): p. II2-12.

99. Chen, Q., et al., *Ischemic defects in the electron transport chain increase the production of reactive oxygen species from isolated rat heart mitochondria.* Am J Physiol Cell Physiol, 2008. **294**(2): p. C460-6.

100. Tompkins, A.J., et al., *Mitochondrial dysfunction in cardiac ischemia-reperfusion injury: ROS from complex I, without inhibition.* Biochim Biophys Acta, 2006. **1762**(2): p. 223-31.

101. Angelos, M.G., et al., *Hypoxic reperfusion of the ischemic heart and oxygen radical generation.* Am J Physiol Heart Circ Physiol, 2006. **290**(1): p. H341-7.

102. Kim, N., et al., *Potential biomarkers for ischemic heart damage identified in mitochondrial proteins by comparative proteomics.* Proteomics, 2006. **6**(4): p. 1237-49.

103. Zweier, J.L. and M.A. Talukder, *The role of oxidants and free radicals in reperfusion injury.* Cardiovasc Res, 2006. **70**(2): p. 181-90.

104. Suleiman, M.S., A.P. Halestrap, and E.J. Griffiths, *Mitochondria: a target for myocardial protection.* Pharmacol Ther, 2001. **89**(1): p. 29-46.

105. Chen, Q., et al., *Production of reactive oxygen species by mitochondria: central role of complex III.* J Biol Chem, 2003. **278**(38): p. 36027-31.

106. Boudina, S., et al., *Alteration of mitochondrial function in a model of chronic ischemia in vivo in rat heart.* Am J Physiol Heart Circ Physiol, 2002. **282**(3): p. H821-31.

107. Murry, C.E., R.B. Jennings, and K.A. Reimer, *Preconditioning with ischemia: a delay of lethal cell injury in ischemic myocardium.* Circulation, 1986. **74**(5): p. 1124-36.

108. Malhotra, R. and F.C. Brosius, 3rd, *Glucose uptake and glycolysis reduce hypoxia-induced apoptosis in cultured neonatal rat cardiac myocytes.* J Biol Chem, 1999. **274**(18): p. 12567-75.

109. Aragones, J., et al., *Oxygen sensors at the crossroad of metabolism.* Cell Metab, 2009. **9**(1): p. 11-22.

110. Schofield, C.J. and P.J. Ratcliffe, *Oxygen sensing by HIF hydroxylases.* Nat Rev Mol Cell Biol, 2004. **5**(5): p. 343-54.

111. Loor, G. and P.T. Schumacker, *Role of hypoxia-inducible factor in cell survival during myocardial ischemia-reperfusion.* Cell Death Differ, 2008. **15**(4): p. 686-90.

112. Rey, S. and G.L. Semenza, *Hypoxia-inducible factor-1-dependent mechanisms of vascularization and vascular remodelling.* Cardiovasc Res, 2010. **86**(2): p. 236-42.

113. Radi, R., *Nitric oxide, oxidants, and protein tyrosine nitration.* Proc Natl Acad Sci U S A, 2004. **101**(12): p. 4003-8.

114. Peluffo, G. and R. Radi, *Biochemistry of protein tyrosine nitration in cardiovascular pathology.* Cardiovasc Res, 2007. **75**(2): p. 291-302.

115. Navarro-Antolin, J., et al., *Role of peroxynitrite in endothelial damage mediated by Cyclosporine A.* Free Radic Biol Med, 2007. **42**(3): p. 394-403.

116. MacMillan-Crow, L.A., et al., *Nitration and inactivation of manganese superoxide dismutase in chronic rejection of human renal allografts.* Proc Natl Acad Sci U S A, 1996. **93**(21): p. 11853-8.

117. Quijano, C., N. Romero, and R. Radi, *Tyrosine nitration by superoxide and nitric oxide fluxes in biological systems: modeling the impact of superoxide dismutase and nitric oxide diffusion.* Free Radic Biol Med, 2005. **39**(6): p. 728-41.

118. Lowther, W.T. and A.C. Haynes, *Reduction of cysteine sulfinic acid in eukaryotic, typical 2-Cys peroxiredoxins by sulfiredoxin.* Antioxid Redox Signal, 2011. **15**(1): p. 99-109.

119. Giron, P., L. Dayon, and J.C. Sanchez, *Cysteine tagging for MS-based proteomics.* Mass Spectrom Rev, 2011. **30**(3): p. 366-95.

120. Leonard, S.E. and K.S. Carroll, *Chemical 'omics' approaches for understanding protein cysteine oxidation in biology.* Curr Opin Chem Biol, 2011. **15**(1): p. 88-102.

121. Izquierdo-Alvarez, A. and A. Martinez-Ruiz, *Thiol redox proteomics seen with fluorescent eyes: The detection of cysteine oxidative modifications by fluorescence derivatization and 2-DE.* J Proteomics, 2011. **75**(2): p. 329-38.

122. Martinez-Ruiz, A. and S. Lamas, *Detection and identification of S-nitrosylated proteins in endothelial cells.* Methods Enzymol, 2005. **396**: p. 131-9.

123. Brennan, J.P., et al., *The utility of N,N-biotinyl glutathione disulfide in the study of protein S-glutathiolation.* Mol Cell Proteomics, 2006. **5**(2): p. 215-25.

124. Greco, T.M., et al., *Identification of S-nitrosylation motifs by site-specific mapping of the S-nitrosocysteine proteome in human vascular smooth muscle cells.* Proc Natl Acad Sci U S A, 2006. **103**(19): p. 7420-5.

125. Hao, G., et al., *SNOSID, a proteomic method for identification of cysteine S-nitrosylation sites in complex protein mixtures.* Proc Natl Acad Sci U S A, 2006. **103**(4): p. 1012-7.

126. Doulias, P.T., et al., *Structural profiling of endogenous S-nitrosocysteine residues reveals unique features that accommodate diverse mechanisms for protein S-nitrosylation.* Proc Natl Acad Sci U S A, 2010. **107**(39): p. 16958-63.

127. Leichert, L.I., et al., *Quantifying changes in the thiol redox proteome upon oxidative stress in vivo.* Proc Natl Acad Sci U S A, 2008. **105**(24): p. 8197-202.

128. Sethuraman, M., et al., *Isotope-coded affinity tag (ICAT) approach to redox proteomics: identification and quantitation of oxidant-sensitive cysteine thiols in complex protein mixtures.* J Proteome Res, 2004. **3**(6): p. 1228-33.

129. McDonagh, B., et al., *Shotgun redox proteomics identifies specifically modified cysteines in key metabolic enzymes under oxidative stress in Saccharomyces cerevisiae.* J Proteomics, 2009. **72**(4): p. 677-89.

130. Sethuraman, M., et al., *Isotope-coded affinity tag approach to identify and quantify oxidant-sensitive protein thiols.* Mol Cell Proteomics, 2004. **3**(3): p. 273-8.

131. Boengler, K., et al., *Connexin 43 in cardiomyocyte mitochondria and its increase by ischemic preconditioning.* Cardiovasc Res, 2005. **67**(2): p. 234-44.

132. Yamakura, F., et al., *Inactivation of human manganese-superoxide dismutase by peroxynitrite is caused by exclusive nitration of tyrosine 34 to 3-nitrotyrosine.* J Biol Chem, 1998. **273**(23): p. 14085-9.

133. Shevchenko, A., et al., *In-gel digestion for mass spectrometric characterization of proteins and proteomes.* Nat Protoc, 2006. **1**(6): p. 2856-60.

134. Bonzon-Kulichenko, E., et al., *A robust method for quantitative high-throughput analysis of proteomes by 18O labeling.* Mol Cell Proteomics, 2011. **10**(1): p. M110 003335.

135. Katayama, H., et al., *Efficient in-gel digestion procedure using 5-cyclohexyl-1-pentyl-beta-D-maltoside as an additive for gel-based membrane proteomics.* Rapid Commun Mass Spectrom, 2004. **18**(20): p. 2388-94.

136. Lopez-Ferrer, D., et al., *Statistical model for large-scale peptide identification in databases from tandem mass spectra using SEQUEST.* Anal Chem, 2004. **76**(23): p. 6853-60.

137. Martinez-Bartolome, S., et al., *Properties of average score distributions of SEQUEST: the probability ratio method.* Mol Cell Proteomics, 2008. **7**(6): p. 1135-45.

138. Navarro, P. and J. Vazquez, *A refined method to calculate false discovery rates for peptide identification using decoy databases.* J Proteome Res, 2009. **8**(4): p. 1792-6.

139. Navarro, P., et al., *A full automated and integrated bioinformatic toolset for large-scale peptide identification and quantification by stable 18O isotope labeling.* Joint SEProt-EuPA Congress, Valencia, Spain, February 10-14, 2007.

140. Trevisán-Herraz, M., et al., *Quixot, a powerful software platform to perform quantification and statistical analysis of SIL experiments using different MS instruments.* HUPO 10th Annual World Congress: Translational Proteomics, February 4-7, Geneva-Switzerland, 2011.

141. Choi, H. and A.I. Nesvizhskii, *False discovery rates and related statistical concepts in mass spectrometry-based proteomics.* J Proteome Res, 2008. **7**(1): p. 47-50.

142. Kall, L., et al., *Assigning significance to peptides identified by tandem mass spectrometry using decoy databases.* J Proteome Res, 2008. **7**(1): p. 29-34.

143. Tabb, D.L., *What's driving false discovery rates?* J Proteome Res, 2008. **7**(1): p. 45-6.

144. Fitzgibbon, M., Q. Li, and M. McIntosh, *Modes of inference for evaluating the confidence of peptide identifications.* J Proteome Res, 2008. **7**(1): p. 35-9.

145. Villar, M., et al., *Systematic characterization of phosphorylation sites in NFATc2 by linear ion trap mass spectrometry.* Proteomics, 2006. **6 Suppl 1**: p. S16-27.

146. Redondo-Horcajo, M., et al., *Cyclosporine A-induced nitration of tyrosine 34 MnSOD in endothelial cells: role of mitochondrial superoxide.* Cardiovasc Res, 2010. **87**(2): p. 356-65.

147. Hajkova, D., K.C. Rao, and M. Miyagi, *pH dependency of the carboxyl oxygen exchange reaction catalyzed by lysyl endopeptidase and trypsin.* J Proteome Res, 2006. **5**(7): p. 1667-73.

148. Blonder, J., et al., *Quantitative profiling of the detergent-resistant membrane proteome of iota-b toxin induced vero cells.* J Proteome Res, 2005. **4**(2): p. 523-31.

149. Liener, I.E., *The essentiality of the disulfide linkages in trypsin.* J Biol Chem, 1957. **225**(2): p. 1061-9.

150. Petritis, B.O., et al., *A simple procedure for effective quenching of trypsin activity and prevention of 18O-labeling back-exchange.* J Proteome Res, 2009. **8**(5): p. 2157-63.

151. Minami, T., et al., *Vascular endothelial growth factor- and thrombin-induced termination factor, Down syndrome critical region-1, attenuates endothelial cell proliferation and angiogenesis.* J Biol Chem, 2004. **279**(48): p. 50537-54.

152. Pawlowska, Z., et al., *Heat shock proteins and other components of cellular machinery for protein synthesis are up-regulated in vascular endothelial cell growth factor-activated human endothelial cells.* Proteomics, 2005. **5**(5): p. 1217-27.

153. Katanasaka, Y., et al., *Proteomic characterization of angiogenic endothelial cells stimulated with cancer cell-conditioned medium.* Biol Pharm Bull, 2007. **30**(12): p. 2300-7.

154. Makarieva, T.N., et al., *Steroids in Porifera. II. Steroid derivatives from two sponges of the family Halichondriidae. Sokotrasterol sulfate, a marine steroid with a new pattern of side chain alkylation.* Steroids, 1983. **42**(3): p. 267-81.

155. Notari, L., et al., *Identification of a lipase-linked cell membrane receptor for pigment epithelium-derived factor.* J Biol Chem, 2006. **281**(49): p. 38022-37.

156. Kaur, G., et al., *Antiangiogenic properties of 17-(dimethylaminoethylamino)-17-demethoxygeldanamycin: an orally bioavailable heat shock protein 90 modulator.* Clinical cancer research : an official journal of the American Association for Cancer Research, 2004. **10**(14): p. 4813-21.

157. Chaudhury, S., T.R. Welch, and B.S. Blagg, *Hsp90 as a target for drug development.* ChemMedChem, 2006. **1**(12): p. 1331-40.

158. Huang, Y., et al., *The angiogenic function of nucleolin is mediated by vascular endothelial growth factor and nonmuscle myosin.* Blood, 2006. **107**(9): p. 3564-71.

159. Keezer, S.M., et al., *Angiogenesis inhibitors target the endothelial cell cytoskeleton through altered regulation of heat shock protein 27 and cofilin.* Cancer Res, 2003. **63**(19): p. 6405-12.

160. Gong, C., K.V. Stoletov, and B.I. Terman, *VEGF treatment induces signaling pathways that regulate both actin polymerization and depolymerization.* Angiogenesis, 2004. **7**(4): p. 313-21.

161. Tzima, E. and P. Schimmel, *Inhibition of tumor angiogenesis by a natural fragment of a tRNA synthetase.* Trends Biochem Sci, 2006. **31**(1): p. 7-10.

162. Wakasugi, K., et al., *A human aminoacyl-tRNA synthetase as a regulator of angiogenesis.* Proc Natl Acad Sci U S A, 2002. **99**(1): p. 173-7.

163. Boja, E.S. and H.M. Fales, *Overalkylation of a protein digest with iodoacetamide.* Anal Chem, 2001. **73**(15): p. 3576-82.

164. Wang, N., et al., *Proteome profile of cytosolic component of zebrafish liver generated by LC-ESI MS/MS combined with trypsin digestion and microwave-assisted acid hydrolysis.* J Proteome Res, 2007. **6**(1): p. 263-72.

165. An, Y., et al., *Solution isoelectric focusing for peptide analysis: comparative investigation of an insoluble nuclear protein fraction.* J Proteome Res, 2005. **4**(6): p. 2126-32.

166. Martinez-Acedo, P., et al., *GELSILOX: Simultaneous High-thoughpout Identification and Quantification of Thiol Redox State and Total Proteomes.* ESF-EMBO Symposium, 2011. **"Glutathione and Related Thiols in Living Cells"**(September, 4-9 2011 (Sant Feliu de Guixols, Spain)).

167. Baty, J.W., M.B. Hampton, and C.C. Winterbourn, *Detection of oxidant sensitive thiol proteins by fluorescence labeling and two-dimensional electrophoresis.* Proteomics, 2002. **2**(9): p. 1261-6.

168. Brennan, J.P., et al., *Detection and mapping of widespread intermolecular protein disulfide formation during cardiac oxidative stress using proteomics with diagonal electrophoresis.* J Biol Chem, 2004. **279**(40): p. 41352-60.

169. Cai, H. and D.G. Harrison, *Endothelial dysfunction in cardiovascular diseases: the role of oxidant stress.* Circ Res, 2000. **87**(10): p. 840-4.

170. Stone, J.R. and S. Yang, *Hydrogen peroxide: a signaling messenger.* Antioxid Redox Signal, 2006. **8**(3-4): p. 243-70.

171. Schroder, E. and P. Eaton, *Hydrogen peroxide as an endogenous mediator and exogenous tool in cardiovascular research: issues and considerations.* Curr Opin Pharmacol, 2008. **8**(2): p. 153-9.

172. Woo, H.A., et al., *Inactivation of peroxiredoxin I by phosphorylation allows localized H(2)O(2) accumulation for cell signaling.* Cell, 2010. **140**(4): p. 517-28.

173. Waypa, G.B., et al., *Hypoxia triggers subcellular compartmental redox signaling in vascular smooth muscle cells.* Circ Res, 2010. **106**(3): p. 526-35.

174. Cadenas, S., J. Aragones, and M.O. Landazuri, *Mitochondrial reprogramming through cardiac oxygen sensors in ischaemic heart disease.* Cardiovasc Res, 2010. **88**(2): p. 219-28.

175. Murphy, E., *Primary and secondary signaling pathways in early preconditioning that converge on the mitochondria to produce cardioprotection.* Circ Res, 2004. **94**(1): p. 7-16.

176. Schulz, R., et al., *Signal transduction of ischemic preconditioning.* Cardiovasc Res, 2001. **52**(2): p. 181-98.

177. Zhu, M., et al., *Ischemic postconditioning protects remodeled myocardium via the PI3K-PKB/Akt reperfusion injury salvage kinase pathway.* Cardiovasc Res, 2006. **72**(1): p. 152-62.

178. Koppenol, W.H., *The basic chemistry of nitrogen monoxide and peroxynitrite.* Free Radic Biol Med, 1998. **25**(4-5): p. 385-91.

179. Szabo, C., et al., *Part I: pathogenetic role of peroxynitrite in the development of diabetes and diabetic vascular complications: studies with FP15, a novel potent peroxynitrite decomposition catalyst.* Mol Med, 2002. **8**(10): p. 571-80.

180. Zou, M.H., R. Cohen, and V. Ullrich, *Peroxynitrite and vascular endothelial dysfunction in diabetes mellitus.* Endothelium, 2004. **11**(2): p. 89-97.

181. Torreilles, F., et al., *Neurodegenerative disorders: the role of peroxynitrite.* Brain Res Brain Res Rev, 1999. **30**(2): p. 153-63.

182. Li, J., et al., *Peroxynitrite induces apoptosis in canine cerebral vascular muscle cells: possible relation to neurodegenerative diseases and strokes.* Neurosci Lett, 2003. **350**(3): p. 173-7.

183. Bouloumie, A., et al., *Endothelial dysfunction coincides with an enhanced nitric oxide synthase expression and superoxide anion production.* Hypertension, 1997. **30**(4): p. 934-41.

184. Belik, J., et al., *Peroxynitrite inhibits relaxation and induces pulmonary artery muscle contraction in the newborn rat.* Free Radic Biol Med, 2004. **37**(9): p. 1384-92.

185. Moncada, S. and E.A. Higgs, *Nitric oxide and the vascular endothelium.* Handb Exp Pharmacol, 2006(176 Pt 1): p. 213-54.

186. Pacher, P., J.S. Beckman, and L. Liaudet, *Physiol Rev.* Physiological reviews, 2007. **87**(1): p. 315-424.

187. Beckman, J.S., et al., *Apparent hydroxyl radical production by peroxynitrite: implications for endothelial injury from nitric oxide and superoxide.* Proc Natl Acad Sci U S A, 1990. **87**(4): p. 1620-4.

188. Yague, J., et al., *Peptide rearrangement during quadrupole ion trap fragmentation: added complexity to MS/MS spectra.* Anal Chem, 2003. **75**(6): p. 1524-35.

189. Graumann, J., et al., *Stable isotope labeling by amino acids in cell culture (SILAC) and proteome quantitation of mouse embryonic stem cells to a depth of 5,111 proteins.* Mol Cell Proteomics, 2008. **7**(4): p. 672-83.

190. D'Ascenzo, M., L. Choe, and K.H. Lee, *iTRAQPak: an R based analysis and visualization package for 8-plex isobaric protein expression data.* Brief Funct Genomic Proteomic, 2008. **7**(2): p. 127-35.

191. Fraterman, S., et al., *Combination of peptide OFFGEL fractionation and label-free quantitation facilitated proteomics profiling of extraocular muscle.* Proteomics, 2007. **7**(18): p. 3404-16.

192. Heller, M., et al., *Added value for tandem mass spectrometry shotgun proteomics data validation through isoelectric focusing of peptides.* J Proteome Res, 2005. **4**(6): p. 2273-82.

193. Horth, P., et al., *Efficient fractionation and improved protein identification by peptide OFFGEL electrophoresis.* Mol Cell Proteomics, 2006. **5**(10): p. 1968-74.

194. Ryan, M.J., et al., *Angiotensin II-induced vascular dysfunction is mediated by the AT1A receptor in mice.* Hypertension, 2004. **43**(5): p. 1074-9.

195. Hamada, K., et al., *The PTEN/PI3K pathway governs normal vascular development and tumor angiogenesis.* Genes Dev, 2005. **19**(17): p. 2054-65.

196. Yang, X.L., P. Schimmel, and K.L. Ewalt, *Relationship of two human tRNA synthetases used in cell signaling.* Trends Biochem Sci, 2004. **29**(5): p. 250-6.

197. Srivastava, M. and H.B. Pollard, *Molecular dissection of nucleolin's role in growth and cell proliferation: new insights.* FASEB J, 1999. **13**(14): p. 1911-22.

198. Zabet-Moghaddam, M., et al., *Electrospray ionization mass spectroscopic analysis of peptides modified with N-ethylmaleimide or iodoacetanilide.* Bioorg Med Chem Lett, 2008. **18**(17): p. 4891-5.

199. Martinez-Ruiz, A., et al., *S-nitrosylation of Hsp90 promotes the inhibition of its ATPase and endothelial nitric oxide synthase regulatory activities.* Proc Natl Acad Sci U S A, 2005. **102**(24): p. 8525-30.

200. Klamt, F., et al., *Oxidant-induced apoptosis is mediated by oxidation of the actin-regulatory protein cofilin.* Nat Cell Biol, 2009. **11**(10): p. 1241-6.

201. Rodriguez-Pascual, F., et al., *Glyceraldehyde-3-phosphate dehydrogenase regulates endothelin-1 expression by a novel, redox-sensitive mechanism involving mRNA stability.* Mol Cell Biol, 2008. **28**(23): p. 7139-55.

202. Murphy, M.P., *How mitochondria produce reactive oxygen species.* Biochem J, 2009. **417**(1): p. 1-13.

203. Kowaltowski, A.J., et al., *Mitochondria and reactive oxygen species.* Free Radic Biol Med, 2009. **47**(4): p. 333-43.

204. Tsutsui, H., S. Kinugawa, and S. Matsushima, *Mitochondrial oxidative stress and dysfunction in myocardial remodelling.* Cardiovasc Res, 2009. **81**(3): p. 449-56.

205. Hofer, T., et al., *Bioenergetics and permeability transition pore opening in heart subsarcolemmal and interfibrillar mitochondria: effects of aging and lifelong calorie restriction.* Mech Ageing Dev, 2009. **130**(5): p. 297-307.

206. Baines, C.P., et al., *Loss of cyclophilin D reveals a critical role for mitochondrial permeability transition in cell death.* Nature, 2005. **434**(7033): p. 658-62.

207. Nakagawa, T., et al., *Cyclophilin D-dependent mitochondrial permeability transition regulates some necrotic but not apoptotic cell death.* Nature, 2005. **434**(7033): p. 652-8.

208. Addabbo, F., et al., *The Krebs cycle and mitochondrial mass are early victims of endothelial dysfunction: proteomic approach.* Am J Pathol, 2009. **174**(1): p. 34-43.

209. Knoops, B., et al., *Peroxiredoxin 5: structure, mechanism, and function of the mammalian atypical 2-Cys peroxiredoxin.* Antioxid Redox Signal, 2011. **15**(3): p. 817-29.

210. Fu, C., et al., *Elucidation of thioredoxin target protein networks in mouse.* Mol Cell Proteomics, 2009. **8**(7): p. 1674-87.

211. Gallien, S., E. Duriez, and B. Domon, *Selected reaction monitoring applied to proteomics.* J Mass Spectrom, 2011. **46**(3): p. 298-312.

212. Miro-Casas, E., et al., *Connexin43 in cardiomyocyte mitochondria contributes to mitochondrial potassium uptake.* Cardiovasc Res, 2009. **83**(4): p. 747-56.

213. Faraci, F.M. and S.P. Didion, *Vascular protection: superoxide dismutase isoforms in the vessel wall.* Arterioscler Thromb Vasc Biol, 2004. **24**(8): p. 1367-73.

214. MacMillan-Crow, L.A. and J.A. Thompson, *Tyrosine modifications and inactivation of active site manganese superoxide dismutase mutant (Y34F) by peroxynitrite.* Arch Biochem Biophys, 1999. **366**(1): p. 82-8.

215. Bayir, H., et al., *Neuronal NOS-mediated nitration and inactivation of manganese superoxide dismutase in brain after experimental and human brain injury.* J Neurochem, 2007. **101**(1): p. 168-81.

216. Xu, S., et al., *Detection of sequence-specific tyrosine nitration of manganese SOD and SERCA in cardiovascular disease and aging.* Am J Physiol Heart Circ Physiol, 2006. **290**(6): p. H2220-7.

217. Guo, W., et al., *Quantitative assessment of tyrosine nitration of manganese superoxide dismutase in angiotensin II-infused rat kidney.* Am J Physiol Heart Circ Physiol, 2003. **285**(4): p. H1396-403.

218. Squadrito, G.L., et al., *Reaction of uric acid with peroxynitrite and implications for the mechanism of neuroprotection by uric acid.* Arch Biochem Biophys, 2000. **376**(2): p. 333-7.

219. Ferrer-Sueta, G. and R. Radi, *Chemical biology of peroxynitrite: kinetics, diffusion, and radicals.* ACS Chem Biol, 2009. **4**(3): p. 161-77.

220. Poole, L.B., et al., *Synthesis of chemical probes to map sulfenic acid modifications on proteins.* Bioconjug Chem, 2005. **16**(6): p. 1624-8.

221. Seo, Y.H. and K.S. Carroll, *Quantification of protein sulfenic acid modifications using isotope-coded dimedone and iododimedone.* Angew Chem Int Ed Engl, 2011. **50**(6): p. 1342-5.

222. Berndt, C., C.H. Lillig, and A. Holmgren, *Thiol-based mechanisms of the thioredoxin and glutaredoxin systems: implications for diseases in the cardiovascular system.* American journal of physiology. Heart and circulatory physiology, 2007. **292**(3): p. H1227-36.

223. Held, J.M., et al., *Targeted quantitation of site-specific cysteine oxidation in endogenous proteins using a differential alkylation and multiple reaction monitoring mass spectrometry approach.* Mol Cell Proteomics, 2010. **9**(7): p. 1400-10.

224. Picotti, P., et al., *Full dynamic range proteome analysis of S. cerevisiae by targeted proteomics.* Cell, 2009. **138**(4): p. 795-806.

ANEXOS

Anexo A.1.- Lista de los péptidos con Cys que aumentan o disminuyen su abundancia en respuesta a la diamida en células endoteliales.

Los valores de z_p negativos corresponden a los péptidos con aumento de abundancia (verde), y las z_p positivas corresponden a las disminuciones (rojo).

Se listan los péptidos con valores de z_p mayores que 2,0 o menores que -2,0.

Los cambios de abundancia estadísticamente significativos con una FDRqp < 0,1 están indicados en azul.

Las modificaciones de las Cys están indicadas por "@" (oxCys) y "^" (redCys).

Nº acceso	Proteína	Secuencia	Xp-Xq	Fold Change		Zp	FDRp
P14618	Pyruvate kinase isozymes M1/M2	C#C#SGAIIVLTK	-3.19	9.1	up	-15.46	0.E+00
P23528	Cofilin-1	HELQANC#YEEVK	-2.38	5.2	up	-12.82	0.E+00
P62258	14-3-3 protein epsilon	LIC#C#DILDVLDK	-2.16	4.5	up	-10.81	0.E+00
Q9Y696	Chloride intrace	IEEFLEEVLC#PPK	-2.06	4.2	up	-10.20	0.E+00
P07858	Cathepsin B	IC#EPGYSPTYK	-1.75	3.4	up	-9.72	0.E+00
P62826	GTP-binding nuclear protein Ran	VC#ENIPIVLC#GNK	-1.79	3.4	up	-9.45	0.E+00
P13639	Elongation factor 2	STLTDSLVC#K	-1.83	3.5	up	-9.04	0.E+00
Q71U36	Tubulin alpha-1A	TIQFVDWC#PTGFK	-1.62	3.1	up	-7.99	5.E-13
P21333	Filamin-A	SPYTVTVGQAC#NPSAC#R	-1.74	3.3	up	-7.93	6.E-13
Q00839	Heterogeneous nuclear ribonucleoprotein U	M*C#LFAGFQR	-1.51	2.9	up	-7.82	1.E-12
P21333	Filamin-A	WC#NEHLK	-1.63	3.1	up	-7.24	9.E-11
Q14315	Filamin-C	LYAQDADGC#PIDIK	-1.49	2.8	up	-6.79	2.E-09
Q06830	Peroxiredoxin-1	HGEVC#PAGWKPGSDTIKPDVQK	-1.43	2.7	up	-6.60	7.E-09
P31948	Stress-induced-phosphoprotein 1	ALSVGNIDDALQC#YSEAIK	-1.29	2.4	up	-6.54	1.E-08
O75369	Filamin-B	GAGTGGLGLTVEGPC#EAK	-1.35	2.6	up	-6.47	1.E-08
P07900	Heat shock protein HSP 90-alpha	LVTSPC#C#IVTSTYGWTANM*ER	-1.39	2.6	up	-6.42	2.E-08
P21333	Filamin-A	APSVANVGSHC#DLSLK	-1.30	2.5	up	-6.34	3.E-08
P09936	Ubiquitin carboxyl-terminal hydrolase isozyme L1	NEAIQAAHDAVAQEGQC#R	-1.16	2.2	up	-6.31	4.E-08
P60953	Cell division control protein 42 homolog	WVPEITHHC#PK	-0.92	1.9	up	-6.15	9.E-08
Q14315	Filamin-C	VGVTEGC#DPTR	-1.33	2.5	up	-6.11	1.E-07
P16070	CD44 antigen	ALSIGFETC#R	-1.16	2.2	up	-6.03	2.E-07
Q8NBS9	Thioredoxin domain-containing protein 5	VDC#TAHSDVC#SAQGVR	-1.17	2.2	up	-6.00	2.E-07
P06733	Alpha-enolase	SC#NC#LLLK	-1.22	2.3	up	-5.94	3.E-07
Q13885	Tubulin beta-2A chain	TAVC#DIPPR	-1.17	2.3	up	-5.93	3.E-07
P62241	40S ribosomal protein S8	NC#IVLIDSTPYR	-1.02	2.0	up	-5.54	3.E-06
O43175	D-3-phosphoglycerate dehydrogenase	NAGNC#LSPAVIVGLLK	-0.81	1.7	up	-5.52	3.E-06
P21333	Filamin-A	AHVVPC#FDASK	-1.23	2.3	up	-5.51	3.E-06
P67775	Serine/threonine-protein phosphatase 2A catalytic subunit alpha isoform	NVVTIFSAPNYC#YR	-0.89	1.9	up	-5.51	3.E-06
P30153	Serine/threonine-protein phosphatase 2A 65 kDa regulatory subunit A alpha isoform	LNIISNLDC#VNEVIGIR	-0.92	1.9	up	-5.35	7.E-06
P60174	Triosephosphate isomerase	DC#GATWVVLGHSER	-1.09	2.1	up	-5.29	9.E-06
Q15365	Poly(rC)-binding protein 1	INISEGNC#PER	-1.00	2.0	up	-5.27	1.E-05
P11940	Polyadenylate-binding protein 1	GFGFVC#FSSPEEATK	-1.06	2.1	up	-4.98	4.E-05
P18124	60S ribosomal protein L7	YGIIC#M*EDLIHEIYTVGK	-0.98	2.0	up	-4.92	5.E-05
Q02543	60S ribosomal protein L18a	DLTTAGAVTQC#YR	-0.92	1.9	up	-4.87	7.E-05
P00558	Phosphoglycerate kinase 1	AC#ANPAAGSVILLENLR	-1.02	2.0	up	-4.85	7.E-05
P09429	High mobility group protein B1	M*SSYAFFVQTC#R	-0.96	1.9	up	-4.84	7.E-05
P07339	Cathepsin D	AIGAVPLIQGEYM*IPC#EK	-1.01	2.0	up	-4.84	7.E-05
Q6ZMR3	L-lactate dehydrogenase A-like 6A	VIGSGC#NLDSAR	-0.69	1.6	up	-4.80	8.E-05
Q71U36	Tubulin alpha-1A	YMAC#C#LLYR	-0.98	2.0	up	-4.77	1.E-04
P02545	Lamin-A/C	AQNTWGC#GNSLR	-1.03	2.0	up	-4.74	1.E-04
P61247	40S ribosomal protein S3a	AC#QSIYPLHDVFVR	-0.84	1.8	up	-4.72	1.E-04
Q16658	Fascin	GEHGFIGC#R	-1.00	2.0	up	-4.71	1.E-04
P27797	Calreticulin	HEQNIDC#GGGYVK	-0.85	1.8	up	-4.71	1.E-04
Q16555	Dihydropyrimidinase-related protein 2	GLYDGPVC#EVSVTPK	-1.04	2.1	up	-4.69	1.E-04
P21333	Filamin-A	ATC#APQHGAPGPGPADASK	-1.07	2.1	up	-4.69	1.E-04
P21980	Protein-glutamine gamma-glutamyltransferase 2	SEGTYC#C#GPVPVR	-0.91	1.9	up	-4.67	1.E-04
P31943	Heterogeneous nuclear ribonucleoprotein H	DLNYC#FSGM*SDHR	-0.92	1.9	up	-4.59	2.E-04
P04406	Glyceraldehyde-3-phosphate dehydrogenase	IISNASC#TTNC#LAPLAK	-0.90	1.9	up	-4.58	2.E-04
P49368	T-complex protein	NLQDAM*QVC#R	-0.91	1.9	up	-4.54	2.E-04
Q71U36	Tubulin alpha-1A	YM*AC#C#LLYR	-0.91	1.9	up	-4.48	3.E-04
P12814	Alpha-actinin-1	EGLLLWC#QR	-0.91	1.9	up	-4.46	3.E-04
P09211	Glutathione S-transferase P	ASC#LYGQLPK	-0.85	1.8	up	-4.44	4.E-04
P12268	Inosine-5'-monophosphate dehydrogenase 2	HGFC#GIPITDTGR	-0.91	1.9	up	-4.39	5.E-04
Q15366	Poly(rC)-binding protein 2	AITIAGIPQSIIEC#VK	-0.81	1.8	up	-4.38	5.E-04
P21333	Filamin-A	THEAEIVEGENHTYC#IR	-0.93	1.9	up	-4.36	5.E-04
P49368	T-complex protein 1 subunit gamma	WSSLAC#NIALDAVK	-0.91	1.9	up	-4.35	5.E-04
P60709	Actin, cytoplasmic	LC#YVALDFEQEMATAASSSSLEK	-0.88	1.8	up	-4.35	5.E-04
P50914	60S ribosomal protein L14	ALVDGPC#TQVR	-0.78	1.7	up	-4.32	6.E-04
Q00610	Clathrin heavy chain	LPVVIGGLLDVDC#SEDVIK	**-0.92**	1.9	up	-4.31	6.E-04
P13489	Ribonuclease inhibitor	LDDC#GLTEAR	-0.87	1.8	up	-4.23	8.E-04

Q13162	Peroxiredoxin-4	HGEVC#PAGWKPGSETIIPDPAGK	-0.80	1.7	up	-4.20	9.E-04
P21980	Protein-glutamine gamma-glutamyltransferase 2	VVSGM*VNC#NDDQGVLLGR	-0.80	1.7	up	-4.03	2.E-03
P21333	Filamin-A	VTYC#PTEPGNYIINIK	-0.84	1.8	up	-4.00	2.E-03
P34932	Heat shock 70 kDa protein 4	KFDEVLVNHFC#EEFGK	-0.84	1.8	up	-3.88	3.E-03
P63241	Eukaryotic translation initiation factor 5A-1	KYEDIC#PSTHNM*DVPNIK	-0.75	1.7	up	-3.85	4.E-03
P49411	Elongation factor Tu, mitochondrial	HYAHTDC#PGHADYVK	-0.88	1.8	up	-3.77	5.E-03
P30041	Peroxiredoxin-6	DFTPVC#TTELGR	-0.86	1.8	up	-3.69	0.01
P11413	Glucose-6-phosphate 1-dehydrogenase	LILDVFC#GSQM*HFVR	-0.81	1.8	up	-3.68	0.01
P23396	40S ribosomal protein S3	GLC#AIAQAESLR	-0.73	1.7	up	-3.67	0.01
P08670	Vimentin	QVQSLTC#EVDALK	-0.83	1.8	up	-3.66	0.01
P14618	Pyruvate kinase isozymes M1/M2	GIFPVLC#K	-0.76	1.7	up	-3.63	0.01
P21333	Filamin-A	VQVQDNEGC#PVEALVK	-0.73	1.7	up	-3.52	0.01
P63244	Guanine nucleotide-binding protein subunit beta-2-like 1	YTVQDESHSEWVSC#VR	-0.70	1.6	up	-3.40	0.02
P11142	Heat shock cognate 71 kDa protein	VC#NPIITK	-0.74	1.7	up	-3.40	0.02
P24534	Elongation factor 1-beta	KLQIQC#VVEDDK	-0.55	1.5	up	-3.40	0.02
P11142	Heat shock cognate 71 kDa protein	GPAVGIDLGTTYSC#VGVFQHGK	-0.68	1.6	up	-3.34	0.02
Q71U36	Tubulin alpha-1A	AYHEQLSVAEITNAC#FEPANQM*VK	-0.69	1.6	up	-3.31	0.02
P68104	Elongation factor 1-alpha 1	DGNASGTTLLEALDC#ILPPTRPTDKPLR	-0.68	1.6	up	-3.22	0.03
P07355	Annexin A2	GLGTDEDSLIEIIC#SR	-0.64	1.6	up	-3.21	0.03
P05388	60S acidic ribosomal protein P0	AGAIAPC#EVTVPAQNTGLGPEK	-0.62	1.5	up	-3.20	0.03
P13489	Ribonuclease inhibitor	WAELLPLLQQC#QVVR	-0.60	1.5	up	-3.17	0.03
P09382	Galectin-1	FNAHGDANTIVC#NSK	-0.61	1.5	up	-3.17	0.03
P07339	Cathepsin D	AIGAVPLIQGEYMIPC#EK	-0.65	1.6	up	-3.16	0.03
P11216	Glycogen phosphorylase, brain form	WLLLC#NPGLADTIVEK	-0.67	1.6	up	-3.13	0.03
P22626	Heterogeneous nuclear ribonucleoproteins A2/B1	LTDC#VVM*R	-0.71	1.6	up	-3.12	0.04
P30050	60S ribosomal protein L12	EILGTAQSVGC#NVDGR	-0.57	1.5	up	-3.10	0.04
P52943	Cysteine-rich protein 2	ASSVTTFTGEPNTC#PR	-0.49	1.4	up	-3.10	0.04
P15121	Aldose reductase	LWC#TYHEK	-0.61	1.5	up	-3.07	0.04
Q32P51	Heterogeneous nuclear ribonucleoprotein A1-like protein 2	SHFEQWGTLTDC#VVM*R	-0.60	1.5	up	-3.01	0.05
P13639	Elongation factor 2	IWC#FGPDGTGPNILTDITK	-0.62	1.5	up	-3.00	0.05
Q9NQC3	Reticulon-4	YSNSALGHVNC#TIK	-0.59	1.5	up	-2.97	0.05
P62753	40S ribosomal protein S6	LNISFPATGC#QK	-0.55	1.5	up	-2.95	0.06
P00491	Purine nucleoside phosphorylase	HRPQVAIIC#GSGLGGLTDK	-0.60	1.5	up	-2.92	0.06
P78527	DNA-dependent protein kinase catalytic subunit	LAGANPAVITC#DELLLGHEK	-0.61	1.5	up	-2.92	0.06
P37837	Transaldolase	ALAGC#DFLTISPK	-0.55	1.5	up	-2.91	0.06
Q15365	Poly(rC)-binding protein 1	LVVPATQC#GSLIGK	-0.53	1.4	up	-2.88	0.07
P12004	Proliferating cell nuclear antigen	DLSHIGDAVVISC#AK	-0.60	1.5	up	-2.85	0.07
P21980	Protein-glutamine gamma-glutamyltransferase 2	VVSGMVNC#NDDQGVLLGR	-0.60	1.5	up	-2.84	0.07
Q15366	Poly(rC)-binding protein 2	LVVPASQC#GSLIGK	-0.52	1.4	up	-2.84	0.07
Q9BUF5	Tubulin beta-6 chain	EIVHIQAGQC#GNQIGTK	-0.53	1.4	up	-2.82	0.08
P62136	Serine/threonine-protein phosphatase PP1-alpha catalytic subunit	HDLDLIC#R	-0.57	1.5	up	-2.78	0.08
P56537	Eukaryotic translation initiation factor 6	LSALGNVTTC#NDYVALVHPDLDR	-0.56	1.5	up	-2.77	0.08
P26641	Elongation factor 1-gamma	WFLTC#INQPQFR	-0.53	1.4	up	-2.76	0.08
P49411	Elongation factor Tu, mitochondrial	GEETPVIVGSALC#ALEGR	-0.54	1.5	up	-2.70	0.10
P45973	Chromobox protein homolog 5	NLDC#PELISEFMK	-0.41	1.3	up	-2.62	0.12
Q32P51	Heterogeneous nuclear ribonucleoprotein A1-like protein	SHFEQWGTLTDC#VVMR	-0.56	1.5	up	-2.61	0.12
P08107	Heat shock 70 kDa protein 1A/1B	FEELC#SDLFR	-0.50	1.4	up	-2.47	0.16
P21796	Voltage-dependent anion-selective channel protein 1	YQIDPDAC#FSAK	-0.55	1.5	up	-2.46	0.16
Q99832	T-complex protein 1 subunit eta	YNFFTGC#PK	-0.57	1.5	up	-2.43	0.17
P60174	Triosephosphate isomerase	IAVAAQNC#YK	-0.47	1.4	up	-2.35	0.20
P17655	Calpain-2 catalytic subunit	RPTEIC#ADPQFIIGGATR	-0.51	1.4	up	-2.33	0.20
P08865	40S ribosomal protein SA	ADHQPLTEASYVNLPTIALC#NTDSPLR	-0.49	1.4	up	-2.29	0.22
O60361	Putative nucleoside diphosphate kinase	GDFC#IQVGR	-0.43	1.3	up	-2.25	0.23
Q9UMS4	Pre-mRNA-processing factor 19	IWSVPNASC#VQVVR	-0.38	1.3	up	-2.22	0.24
P21980	Protein-glutamine gamma-glutamyltransferase 2	TVSYNGILGPEC#GTK	-0.48	1.4	up	-2.21	0.25
P26368	Splicing factor U2AF 65 kDa subunit	SIEIPRPVDGVEVPGC#GK	-0.46	1.4	up	-2.21	0.24
P04406	Glyceraldehyde-3-phosphate dehydrogenase	VPTANVSVVDLTC#R	-0.43	1.3	up	-2.21	0.24
P63241	Eukaryotic translation initiation factor 5A-1	KYEDIC#PSTHNMDVPNIK	-0.49	1.4	up	-2.20	0.25
P13639	Elongation factor 2	C#LYASVLTAQPR	-0.46	1.4	up	-2.17	0.26
Q58FG0	Putative heat shock protein HSP 90-alpha A5	YC#VQQLK	-0.40	1.3	up	-2.15	0.27
P49327	Fatty acid synthase	LSIPTYGLQC#TR	-0.44	1.4	up	-2.14	0.27
Q16222	UDP-N-acetylhexosamine pyrophosphorylase	TNPTEPVGVVC#R	-0.45	1.4	up	-2.13	0.27
Q92841	Probable ATP-dependent RNA helicase DDX17	GDGPIC#LVLAPTR	-0.43	1.3	up	-2.10	0.29
P46782	40S ribosomal protein S5	TIAEC#LADELINAAK	-0.34	1.3	up	-2.05	0.31
P21333	Filamin-A	IVGPSGAAVPC#K	-0.42	1.3	up	-2.04	0.31

P13489	Ribonuclease inhibitor	DSPC#QLEALK	0.42	1.3	down	2.00	0.33
P14618	Pyruvate kinase isozymes M1/M2	AEGSDVANAVLDGADC^IM*LSGETAK	0.46	1.4	down	2.10	0.29
Q15942	Zyxin	C^HQPLAR	0.42	1.3	down	2.19	0.25
P25398	40S ribosomal protein S12	LGEWVGLC^K	0.42	1.3	down	2.27	0.22
P50914	60S ribosomal protein L14	C^MQLTDFILK	0.48	1.4	down	2.44	0.17
P10809	60 kDa heat shock protein, mitochondrial	C^EFQDAYVLLSEK	0.53	1.4	down	2.46	0.16
P12004	Proliferating cell nuclear antigen	C^AGNEDIITLR	0.49	1.4	down	2.49	0.15
Q32P51	Heterogeneous nuclear ribonucleoprotein A1-like protein	SHFEQWGTLTDC^VVM*R	0.61	1.5	down	2.64	0.11
O75083	WD repeat-containing protein 1	LATGSDDNC^AAFFEGPPFK	0.58	1.5	down	3.06	0.04
P37837	Transaldolase	ALAGC^DFLTISPK	0.71	1.6	down	3.36	0.02
P17844	Probable ATP-dependent RNA helicase DDX5	ELAQQVQQVAAEYC^R	0.73	1.7	down	3.36	0.02
P04406	Glyceraldehyde-3-phosphate dehydrogenase	VPTANVSVVDLTC^R	0.71	1.6	down	3.66	0.01
P14618	Pyruvate kinase isozymes M1/M2	AEGSDVANAVLDGADC^IMLSGETAK	0.83	1.8	down	4.19	1.E-03
P08865	40S ribosomal protein SA	ADHQPLTEASYVNLPTIALC^NTDSPLR	0.97	2.0	down	4.35	5.E-04
Q15233	Non-POU domain-containing octamer-binding protein	C^SEGSFLLTTFPR	0.86	1.8	down	4.39	5.E-04
Q6ZMR3	L-lactate dehydrogenase A-like 6A	VIGSGC^NLDSAR	0.70	1.6	down	4.85	7.E-05
Q71U36	Tubulin alpha-1A	AYHEQLSVAEITNAC^FEPANQM*VK	1.02	2.0	down	4.99	4.E-05
P60174	Triosephosphate isomerase	VPADTEVVC^APPTAYIDFAR	0.99	2.0	down	5.06	3.E-05
P12814	Alpha-actinin-1	EGLLLWC^QR	1.10	2.1	down	5.30	9.E-06
Q13885	Tubulin beta-2A chain	NM*M*AAC^DPR	1.08	2.1	down	5.35	7.E-06
P60953	Cell division control protein 42 homolog	C^VVVGDGAVGK	0.86	1.8	down	5.95	3.E-07
Q71U36	Tubulin alpha-1A	AYHEQLSVAEITNAC^FEPANQMVK	1.28	2.4	down	6.36	3.E-08
P14618	Pyruvate kinase isozymes M1/M2	NTGIIC^TIGPASR	1.52	2.9	down	7.46	2.E-11
Q02543	60S ribosomal protein L18a	C^HTPPLYR	2.24	4.7	down	12.31	0.E+00
P23528	Cofilin-1	HELQANC^YEEVK	3.80	13.9	down	20.48	0.E+00

Anexo A.2.- Lista de las proteínas que aumentan o disminuyen su abundancia en respuesta a la diamida en células endoteliales.

Los valores de z_q negativos corresponden a las proteínas con aumento de abundancia (verde), y las z_q positivas corresponden a las disminuciones (rojo).
Se listan las proteínas con valores de z_q mayores que 2,0 o menores que -2,0.
Los cambios de abundancia estadísticamente significativos con una FDRq< 0,1 están indicados en azul.

Nº acceso	Proteína	Xq-X	Fold Change		Zq	FDRq
P08670	Vimentin	-2.08	4.2	up	-20.34	0.E+00
Q15149	Plectin-1	-1.22	2.3	up	-13.58	0.E+00
Q16352	Alpha-internexin	-2.07	4.2	up	-9.05	0.E+00
Q9BXJ5	Complement C1q tumor necrosis factor-related protein 2	-1.97	3.9	up	-8.91	0.E+00
Q09666	Neuroblast differentiation-associated protein AHNAK	-0.80	1.7	up	-8.63	0.E+00
P62932	F-box only protein 40	-1.53	2.9	up	-6.33	4.E-08
O00295	Tubby-related protein 2	-1.25	2.4	up	-5.23	2.E-05
Q9JI55	Plectin-1	-1.19	2.3	up	-4.96	8.E-05
P09525	Annexin A4	-0.73	1.7	up	-4.73	2.E-04
O15355	Protein phosphatase 1G	-1.00	2.0	up	-4.08	3.E-03
Q8IVF2	Protein AHNAK2	-0.76	1.7	up	-4.04	3.E-03
O75436	Vacuolar protein	-0.96	1.9	up	-3.78	0.01
P30049	ATP synthase subunit delta, mitochondrial	-0.85	1.8	up	-3.48	0.02
P46821	Microtubule-associated protein 1B	-0.46	1.4	up	-3.33	0.04
P19096	Fatty acid synthase	-0.74	1.7	up	-3.00	0.10
Q15417	Calponin-3	-0.73	1.7	up	-2.93	0.11
P61019	Ras-related protein Rab-2A	-0.70	1.6	up	-2.82	0.14
P07814	Bifunctional aminoacyl-tRNA synthetase	-0.55	1.5	up	-2.68	0.20
P49327	Fatty acid synthase	-0.28	1.2	up	-2.68	0.20
Q8WWH5	Probable tRNA pseudouridine synthase 1	-0.66	1.6	up	-2.60	0.24
P07942	Laminin subunit beta-1	-0.47	1.4	up	-2.58	0.24
O75643	U5 small nuclear ribonucleoprotein 200 kDa helicase	-0.69	1.6	up	-2.52	0.28
Q13243	Splicing factor, arginine/serine-rich 5	-0.59	1.5	up	-2.52	0.27
P58107	Epiplakin	-0.61	1.5	up	-2.51	0.27
Q07960	Rho GTPase-activating protein 1	-0.59	1.5	up	-2.46	0.29
O95373	Importin-7	-0.32	1.2	up	-2.44	0.31
Q9BZZ5	Apoptosis inhibitor 5	-0.43	1.3	up	-2.38	0.34
P54577	Tyrosyl-tRNA synthase	-0.55	1.5	up	-2.37	0.33
Q92598	Heat shock protein 105 kDa	-0.35	1.3	up	-2.34	0.35
O95905	Protein SGT1	-0.56	1.5	up	-2.33	0.34
Q9Y6N5	Sulfide:quinone oxidoreductase, mitochondrial	-0.59	1.5	up	-2.29	0.36
Q29443	Serotransferrin	-0.73	1.7	up	-2.29	0.36
O14556	Glyceraldehyde-3-phosphate dehydrogenase, testis-specific	-0.52	1.4	up	-2.28	0.35
Q9H4G0	Band 4.1-like protein 1	-0.59	1.5	up	-2.23	0.41
Q16643	Drebrin	-0.41	1.3	up	-2.22	0.40
O60716	Catenin delta-1	-0.38	1.3	up	-2.20	0.41
P06493	Cell division control protein 2 homolog	-0.42	1.3	up	-2.20	0.40
Q9P2E9	Ribosome-binding protein 1	-0.38	1.3	up	-2.19	0.41
P62701	40S ribosomal protein S4, X isoform	-0.27	1.2	up	-2.18	0.40
P15586	N-acetylglucosamine-6-sulfatase	-0.50	1.4	up	-2.17	0.39

Q99426	Tubulin folding cofactor B	-0.34	1.3	up	-2.16	0.40
P54707	Potassium-transporting ATPase alpha chain 2	-0.39	1.3	up	-2.13	0.43
P25490	Transcriptional repressor protein YY1	-0.56	1.5	up	-2.12	0.42
O75369	Filamin-B	-0.20	1.1	up	-2.11	0.43
P12081	Histidyl-tRNA synthetase, cytoplasmic	-0.31	1.2	up	-2.11	0.42
P62195	26S protease regulatory subunit 8	-0.37	1.3	up	-2.09	0.43
P49755	Transmembrane emp24 domain-containing protein 10	-0.50	1.4	up	-2.07	0.45
P21333	Filamin-A	-0.18	1.1	up	-2.06	0.45
P60660	Myosin light polypeptide 6	0.35	1.3	down	2.01	0.49
Q16539	Mitogen-activated protein kinase 14	0.58	1.5	down	2.01	0.50
P55795	Heterogeneous nuclear ribonucleoprotein H2	0.50	1.4	down	2.02	0.48
Q12931	Heat shock protein 75 kDa, mitochondrial	0.33	1.3	down	2.07	0.44
P62857	40S ribosomal protein S28	0.48	1.4	down	2.11	0.42
Q13263	Transcription intermediary factor 1-beta	0.25	1.2	down	2.14	0.42
P0C0S8	Histone H2A type 1	0.36	1.3	down	2.15	0.40
P07910	Heterogeneous nuclear ribonucleoproteins C1/C2	0.34	1.3	down	2.18	0.39
P31483	Nucleolysin TIA-1 isoform p40	0.53	1.4	down	2.19	0.40
Q5NVM5	60 kDa heat shock protein, mitochondrial	0.56	1.5	down	2.20	0.41
O75396	Vesicle-trafficking protein SEC22b	0.39	1.3	down	2.21	0.41
P38919	Eukaryotic initiation factor 4A-III	0.36	1.3	down	2.26	0.38
O43242	26S proteasome non-ATPase regulatory subunit 3	0.41	1.3	down	2.32	0.35
P62805	Histone H4	0.58	1.5	down	2.33	0.35
Q5VYJ4	Putative small nuclear ribonucleoprotein polypeptide E-li	0.41	1.3	down	2.33	0.35
Q86V81	THO complex subunit 4	0.42	1.3	down	2.37	0.34
Q8NBJ7	Sulfatase-modifying factor 2	0.60	1.5	down	2.38	0.33
P62988	Ubiquitin	0.35	1.3	down	2.43	0.30
Q14194	Dihydropyrimidinase-related protein 1	0.60	1.5	down	2.49	0.27
P59998	Actin-related protein 2/3 complex subunit 4	0.47	1.4	down	2.51	0.26
Q9BWX1	PHD finger protein 7	0.64	1.6	down	2.52	0.27
P39019	40S ribosomal protein S19	0.36	1.3	down	2.62	0.23
Q96PK6	RNA-binding protein 14	0.53	1.4	down	2.76	0.16
Q5RFQ4	WD repeat-containing protein 72	0.76	1.7	down	2.85	0.14
P05386	60S acidic ribosomal protein P1	0.63	1.6	down	2.86	0.13
Q96A08	Histone H2B type 1-A	0.69	1.6	down	2.96	0.10
P31943	Heterogeneous nuclear ribonucleoprotein H	0.44	1.4	down	3.00	0.09
O00622	Protein CYR61	0.90	1.9	down	3.04	0.09
P02662	Alpha-S1-casein	0.80	1.7	down	3.09	0.08
P20700	Lamin-B1	0.48	1.4	down	3.14	0.07
P61956	Small ubiquitin-related modifier 2	0.73	1.7	down	3.28	0.04
P52272	Heterogeneous nuclear ribonucleoprotein M	0.43	1.3	down	3.81	0.01
P29627	Hemoglobin subunit beta-Z	0.93	1.9	down	3.94	4.E-03
P05387	60S acidic ribosomal protein P2	0.88	1.8	down	3.97	5.E-03
P02545	Lamin-A/C	0.39	1.3	down	4.17	2.E-03
P05109	Protein S100-A8	0.97	2.0	down	4.21	2.E-03
P62937	Peptidyl-prolyl cis-trans isomerase A	0.57	1.5	down	4.33	1.E-03
P0C2L3	UPF0417 protein FAM163B	1.47	2.8	down	6.13	1.E-07
P16278	Beta-galactosidase	1.51	2.8	down	6.21	9.E-08

Anexo A.3.- Lista de los péptidos con Cys que aumentan o disminuyen su abundancia en respuesta al H_2O_2 en células endoteliales.

Los criterios de filtrado así como el código de colores utilizado y la nomenclatura son los mismos que los que se usaron en el Anexo A.1.

Nº acceso	Proteína	Secuencia	Xp-Xq	Fold Change		Zp	FDRp
Q5E947	Peroxiredoxin-1	HGEVC#PAGWKPGSDTIKPDVQK	-0.86	1.8	up	-6.13	4.E-07
Q2NKY7	Septin-2	TIIC#YIDEQFER	-0.94	1.9	up	-5.95	9.E-07
Q32KN8	Tubulin alpha-3 chain	YM*AC#C@MLYR	-0.67	1.6	up	-4.95	1.E-04
Q3ZBW4	Proliferating cell nuclear antigen	DLSHIGDAVVISC#AK	-0.65	1.6	up	-4.13	3.E-03
O75369	Filamin-B	SGC@IVNNLAEFTVDPK	-0.70	1.6	up	-4.10	4.E-03
Q13177	Serine/threonine-protein kinase PAK 2	EC#LQALEFLHANQVIHR	-0.57	1.5	up	-4.01	5.E-03
P55052	Fatty acid-binding protein, epidermal	VGAM*AKPDC#IITSDGK	-0.66	1.6	up	-3.92	0.01
Q3SYU2	Elongation factor 2	C@LYASVLTAQPR	-0.52	1.4	up	-3.69	0.01
Q76LV2	Heat shock protein HSP 90-alpha	LVTSPC#C#IVTSTYGWTANM*ER	-0.52	1.4	up	-3.51	0.02
Q71SP7	Fatty acid synthase	ALLC#DDPLLSGLLNSPALK	-0.47	1.4	up	-3.25	0.05
Q3ZBT1	Transitional endoplasmic reticulum ATPase	VHLGDVISIQPC#PDVK	-0.47	1.4	up	-3.24	0.06
Q3ZBV8	Threonyl-tRNA synthetase, cytoplasmic	TTPYQIAC#GISQGLADNTVIAK	-0.48	1.4	up	-3.21	0.06
Q1LZA3	Asparagine synthetase [glutamine-hydrolyzing]	IGC#LLSGGLDSSLVAATLLK	-0.36	1.3	up	-3.00	0.09
Q5E947	Peroxiredoxin-1	HGEVC#PAGWK	-0.66	1.6	up	-2.99	0.09
Q58DW5	60S ribosomal protein L5	DIIC#QIAYAR	-0.44	1.4	up	-2.97	0.10
Q5E988	40S ribosomal protein S5	TIAEC#LADELINAAK	-0.36	1.3	up	-2.96	0.10
P11116	Galectin-1	DDNNLC#LHFNPR	-0.37	1.3	up	-2.91	0.11
P21333	Filamin-A	C@SYQPTMEGVHTVHVTFAGVPIPR	-0.46	1.4	up	-2.86	0.12
Q3T0B7	40S ribosomal protein S27-like protein	LTEGC#SFR	-0.44	1.4	up	-2.84	0.12
P63243	Guanine nucleotide-binding protein subunit beta-2-like 1	TNHIGHTGYLNTVTVSPDGSLC#ASGGK	-0.52	1.4	up	-2.82	0.13
Q27975	Heat shock 70 kDa protein 1A	ELEQVC#NPIISR	-0.40	1.3	up	-2.79	0.14
Q562R1	Beta-actin-like protein 2	HQGVMVGMGQKDC@YVGDEAQSK	-0.41	1.3	up	-2.77	0.14
Q3B7N2	Alpha-actinin-1	IC#DQWDNLGALTQK	-0.48	1.4	up	-2.75	0.15
Q56JV9	40S ribosomal protein S3a	NC#LTNFHGMDLTR	-0.38	1.3	up	-2.73	0.15
Q3ZBF7	Prostaglandin E synthase 3	HLNEIDLFHC@IDPNDSK	-0.34	1.3	up	-2.69	0.16
Q6B856	Tubulin beta-2B	LTTPTYGDLNHLVSATM*SGVTTC#LR	-0.42	1.3	up	-2.69	0.16
Q3T0Q6	Cellular nucleic acid-binding protein	C@GETGHVAINC#SK	-0.48	1.4	up	-2.69	0.16
Q6S8J3	POTE ankyrin domain family member E	C#PEALFQPCFLGMESC#GIHETTFNSIM*K	-0.29	1.2	up	-2.64	0.18
P31153	S-adenosylmethionine synthetase isoform type-2	TC#NVLVALEQQSPDIAQGVHLDR	-0.34	1.3	up	-2.59	0.19
P60712	Actin, cytoplasmic 1	LC#YVALDFEQEM*ATAASSSSLEK	-0.60	1.5	up	-2.59	0.19
Q5E9F7	Cofilin-1	AVLFC#LSEDKK	-0.35	1.3	up	-2.46	0.23
P61157	Actin-related protein 3	LGYAGNTEPQFIIPSC#IAIK	-0.38	1.3	up	-2.46	0.23
Q5E958	40S ribosomal protein S8	NC#IVLIDSTPYR	-0.54	1.5	up	-2.45	0.23
P62958	Histidine triad nucleotide-binding protein 1	IIYEDDQC@LAFHDISPQAPTHFLVIPK	-0.30	1.2	up	-2.44	0.23
Q3SYU2	Elongation factor 2	IWC#FGPDGTGPNILTDITK	-0.35	1.3	up	-2.42	0.24
P04075	Fructose-bisphosphate aldolase A	YASIC#QQNGIVPIVEPEILPDGDHDLKR	-0.35	1.3	up	-2.39	0.26
Q5E956	Triosephosphate isomerase	VAHALAEGLGVIAC#IGEK	-0.33	1.3	up	-2.35	0.27
P56965	N(G),N(G)-dimethylarginine dimethylaminohydrolase 1	LTVPDDTAANC#IYLNIPSK	-0.34	1.3	up	-2.31	0.28
P34932	Heat shock 70 kDa protein 4	KFDEVLVNHFC#EEFGK	-0.33	1.3	up	-2.30	0.28
Q3T0P6	Phosphoglycerate kinase 1	AC#ADPAAGSVILLENLR	-0.33	1.3	up	-2.29	0.29
Q3T171	60S ribosomal protein L36	EVC#GFAPYER	-0.27	1.2	up	-2.18	0.36
P79103	40S ribosomal protein S4	EC#LPLIIFLR	-0.29	1.2	up	-2.16	0.37
Q3SWX8	Histone-binding protein RBBP7	HPAKPDPSGEC#NPDLR	-0.28	1.2	up	-2.16	0.37
P10096	Glyceraldehyde-3-phosphate dehydrogenase	VPTPNVSVVDLTC#R	-0.29	1.2	up	-2.13	0.38
Q2NKY7	Septin-2	TIIC@YIDEQFER	-0.32	1.2	up	-2.12	0.39
P56701	26S proteasome non-ATPase regulatory subunit 2	VQQLLHIC#SEHFDSK	-0.38	1.3	up	-2.10	0.39
Q5E9F7	Cofilin-1	HELQANC#YEEVK	-0.29	1.2	up	-2.10	0.39
P55052	Fatty acid-binding protein, epidermal	TQTVC#NFTDGALVQHQEWDGK	-0.28	1.2	up	-2.07	0.41
P68103	Elongation factor 1-alpha 1	DGNASGTTLLEALDC#ILPPTRPTDKPLR	-0.29	1.2	up	-2.07	0.40

Q5E988	40S ribosomal protein S5	TIAEC@LADELINAAK	0.24	1.2	down	2.04	0.41
P62935	Peptidyl-prolyl cis-trans isomerase A	IIPGFMC@QGGDFTR	0.28	1.2	down	2.05	0.41
P67774	Serine/threonine-protein phosphatase 2A catalytic subunit	AHQLVM*EGYNWC@HDR	0.31	1.2	down	2.07	0.41
P04075	Fructose-bisphosphate aldolase A	YASIC#QQNGIVPIVEPEILPDGDHDLK	0.32	1.2	down	2.11	0.39
P17248	Tryptophanyl-tRNA synthetase, cytoplasmic	GIFGFTDSDC@IGK	0.27	1.2	down	2.13	0.38
Q3T0Q6	Cellular nucleic acid-binding protein	TSEVNC@YR	0.36	1.3	down	2.16	0.37
Q5E9F7	Cofilin-1	AVLFC@LSEDKK	0.33	1.3	down	2.22	0.34
O75369	Filamin-B	GAGTGGLGLTVEGPC@EAK	0.32	1.2	down	2.25	0.32
Q3ZCI9	T-complex protein 1 subunit theta	IAVYSC#PFDGM*ITETK	0.37	1.3	down	2.25	0.32
O02675	Dihydropyrimidinase-related protein 2	GLYDGPVC@EVSVTPK	0.50	1.4	down	2.31	0.28
Q0VCK0	Bifunctional purine biosynthesis protein PURH	HVSPAGAAVGIPLSEDEANVC@M*VYDLYK	0.35	1.3	down	2.32	0.28
Q2YDE4	Proteasome subunit alpha type-6	YGYEIPVDMLC@K	0.29	1.2	down	2.32	0.28
P62935	Peptidyl-prolyl cis-trans isomerase A	HTGPGILSM*ANAGPNTNGSQFFIC@TAK	0.33	1.3	down	2.36	0.26
Q3T122	Eukaryotic translation initiation factor 3 subunit D	NLAMEATYINHNFSQQC@LR	0.37	1.3	down	2.40	0.25
Q71SP7	Fatty acid synthase	NC#LLGMEFSGR	0.53	1.4	down	2.44	0.23
Q3SYU2	Elongation factor 2	ETVSEESNVLC@LSK	0.36	1.3	down	2.45	0.23
Q56K03	60S ribosomal protein L27a	NQSFC@PTVNLDK	0.47	1.4	down	2.46	0.23
A1A4J1	6-phosphofructokinase, liver type	LPLMEC@VQM*TKEVQK	0.41	1.3	down	2.48	0.23
P62935	Peptidyl-prolyl cis-trans isomerase A	HTGPGILSMANAGPNTNGSQFFIC@TAK	0.35	1.3	down	2.51	0.21
Q27975	Heat shock 70 kDa protein 1A	ELEQVC@NPIISR	0.33	1.3	down	2.51	0.21
Q6B856	Tubulin beta-2B	TAVC@DIPPR	0.36	1.3	down	2.52	0.22
Q6S8J3	POTE ankyrin domain family member E	C@PEALFQPCFLGMESC@GIHETTFNSIM*K	0.27	1.2	down	2.54	0.21
Q3ZBF7	Prostaglandin E synthase 3	LTFSC@LGGSDNFK	0.47	1.4	down	2.74	0.15
P79136	F-actin-capping protein subunit beta	GC@WDSIHVVEVQEK	0.38	1.3	down	2.81	0.13
A0JN39	Coatomer subunit beta	GALWILGEYC@STK	0.56	1.5	down	3.07	0.08
Q58DW5	60S ribosomal protein L5	IEGDMIVC@AAYAHELPK	0.44	1.4	down	3.14	0.07
P61284	60S ribosomal protein L12	EILGTAQSVGC@NVDGR	0.38	1.3	down	3.14	0.07
P14618	Pyruvate kinase isozymes M1/M2	NTGIIC@TIGPASR	0.60	1.5	down	3.42	0.03
Q3T0Q6	Cellular nucleic acid-binding protein	GFQFVSSSLPDIC@YR	0.50	1.4	down	3.56	0.02
O00622	Protein CYR61	C#NYNC#PHANEAAFPFYR	0.46	1.4	down	3.67	0.01
A7E3Q8	Plastin-3	AVGDGIVLC@K	0.60	1.5	down	3.87	0.01
Q32KN8	Tubulin alpha-3 chain	YMAC@C@MLYR	0.51	1.4	down	3.90	0.01
Q3SZH7	Leukotriene A-4 hydrolase	GSPIEISLPIALC@K	0.51	1.4	down	3.91	0.01
Q5E947	Peroxiredoxin-1	HGEVC@PAGWK	0.69	1.6	down	4.45	1.E-03
Q16658	Fascin	VGKDELFALEQSC@AQVVLQAANER	0.63	1.6	down	4.52	9.E-04
Q3T0K2	T-complex protein 1 subunit gamma	WSSLAC@NIALDAVK	0.63	1.5	down	4.52	9.E-04
Q5E947	Peroxiredoxin-1	HGEVC@PAGWKPGSDTIKPDVQK	0.86	1.8	down	5.87	1.E-06

Anexo A.4.- Lista de las proteínas que aumentan o disminuyen su abundancia en respuesta al H_2O_2 en células endoteliales.

Los criterios de filtrado así como el código de colores utilizado y la nomenclatura son los mismos que los que se usaron en el Anexo A.2.

Nº acceso	Proteína	Xq-X	Fold Change		Zq	FDRq
Q13435	Splicing factor 3B subunit 2;	-1.49	2.8	up	-6.24	4.E-07
O00622	Protein CYR61;	-1.26	2.4	up	-5.70	1.E-05
P18841	Alpha-1B adrenergic receptor;	-0.90	1.9	up	-3.61	0.04
P23246	Splicing factor, proline- and glutamine-rich;	-0.77	1.7	up	-3.52	0.03
A2VDN6	Splicing factor 3 subunit 1;	-0.79	1.7	up	-3.30	0.08
Q08E38	Pre-mRNA-processing factor 19;	-0.75	1.7	up	-3.09	0.13
Q3SZN2	Protein transport protein Sec23B;	-0.71	1.6	up	-2.93	0.17
Q9H0D6	5'-3' exoribonuclease 2;	-0.66	1.6	up	-2.76	0.30
Q56JZ1	60S ribosomal protein L13;	-0.64	1.6	up	-2.66	0.34
Q5E964	26S proteasome non-ATPase regulatory subunit 13;	-0.56	1.5	up	-2.60	0.40
Q12874	Splicing factor 3A subunit 3;	-0.64	1.6	up	-2.56	0.39
Q8WN55	Polypyrimidine tract-binding protein 1;	-0.51	1.4	up	-2.55	0.36
Q3T0C7	Stathmin;	-0.55	1.5	up	-2.51	0.38
Q32L03	Mediator of RNA polymerase II transcription subunit 11;	-0.60	1.5	up	-2.48	0.42
O43390	Heterogeneous nuclear ribonucleoprotein R;	-0.54	1.5	up	-2.47	0.43
Q9H8H2	Probable ATP-dependent RNA helicase DDX31;	-0.62	1.5	up	-2.44	0.42
Q16363	Laminin subunit alpha-4;	-0.59	1.5	up	-2.44	0.42
Q8N163	Protein KIAA1967;	-0.59	1.5	up	-2.40	0.42
Q62148	Retinal dehydrogenase 2;	-0.57	1.5	up	-2.35	0.44
Q04206	Transcription factor p65;	-0.57	1.5	up	-2.34	0.45
A4FV08	Glucosamine-6-phosphate isomerase 1;	-0.60	1.5	up	-2.34	0.43
O46415	Ferritin light chain;	-0.56	1.5	up	-2.31	0.46
P62993	Growth factor receptor-bound protein 2;	-0.56	1.5	up	-2.28	0.48
P97927	Laminin subunit alpha-4;	-0.56	1.5	up	-2.24	0.53
Q3T0I4	THO complex subunit 4	-0.56	1.5	up	-2.22	0.52
Q58DW4	Small nuclear ribonucleoprotein-associated protein B';	-0.51	1.4	up	-2.14	0.63
P09867	Heterogeneous nuclear ribonucleoprotein A1	-0.43	1.3	up	-2.12	0.62
Q1JPJ2	Xaa-Pro aminopeptidase 1;	-0.45	1.4	up	-2.11	0.59
Q1RMR2	U1 small nuclear ribonucleoprotein 70 kDa;	-0.50	1.4	up	-2.07	0.63
Q5KR48	Tropomyosin beta chain;	-0.52	1.4	up	-2.05	0.64
Q96CX2	BTB/POZ domain-containing protein KCTD12;	-0.50	1.4	up	-2.04	0.65
P60661	Myosin light polypeptide 6	-0.41	1.3	up	-2.04	0.65
A6NHL2	Tubulin alpha chain-like 3;	-0.48	1.4	up	-2.01	0.66
Q2HJ60	Heterogeneous nuclear ribonucleoproteins A2/B1;	-0.40	1.3	up	-2.01	0.63
P31408	V-type proton ATPase subunit B, brain isoform;	-0.54	1.5	up	-2.00	0.64

P46778	60S ribosomal protein L21	0.49	1.4	down	2.01	0.66
Q02750	Dual specificity mitogen-activated protein kinase kinase 1	0.59	1.5	down	2.02	0.65
Q3T0R1	40S ribosomal protein S18;	0.42	1.3	down	2.06	0.65
Q2KJ61	Elongator complex protein 3;	0.56	1.5	down	2.09	0.63
Q9UHB9	Signal recognition particle 68 kDa protein	0.53	1.4	down	2.12	0.62
Q3ZBW4	Proliferating cell nuclear antigen;	0.46	1.4	down	2.14	0.60
Q13325	Interferon-induced protein with tetratricopeptide repeats	0.55	1.5	down	2.21	0.53
Q53EL6	Programmed cell death protein 4;	0.55	1.5	down	2.23	0.54
Q562R1	Beta-actin-like protein 2;	0.58	1.5	down	2.36	0.47
P48616	Vimentin;	0.46	1.4	down	2.37	0.46
Q12899	Tripartite motif-containing protein 26;	0.60	1.5	down	2.42	0.44
Q3T0U2	60S ribosomal protein L14;	0.60	1.5	down	2.52	0.41
P33176	Kinesin-1 heavy chain;	0.65	1.6	down	2.58	0.37
Q7TQI3	Ubiquitin thioesterase OTUB1;	0.64	1.6	down	2.69	0.30
Q58DK5	Delta-aminolevulinic acid dehydratase;	0.84	1.8	down	3.03	0.12
Q8CFE5	BTB/POZ domain-containing protein 7;	0.75	1.7	down	3.04	0.15
Q6AY56	Tubulin alpha-8 chain;	0.76	1.7	down	3.15	0.10
P02253	Histone H1.1;	0.82	1.8	down	3.42	0.05
P0C0S9	Histone H2A type 1	0.91	1.9	down	3.86	0.01
Q3T133	Transmembrane emp24 domain-containing protein 9;	0.99	2.0	down	4.10	5.E-03
P62803	Histone H4;	0.90	1.9	down	4.37	3.E-03
Q9BYX7	Beta-actin-like protein 3;	1.30	2.5	down	4.63	8.E-04
Q32LE5	L-asparaginase;	1.44	2.7	down	4.99	1.E-04
Q27991	Myosin-10;	1.19	2.3	down	5.58	2.E-05

Anexo A.5.- Lista de los péptidos con Cys que aumentan o disminuyen su abundancia en respuesta a la hipoxia en células endoteliales.

Los criterios de filtrado así como el código de colores utilizado y la nomenclatura son los mismos que los que se usaron en el Anexo A.1.

Nº acceso	Proteína	Secuencia	Xp-Xq	Fold Change		Zp	FDRp
P05556	Integrin beta-1	DKLPQPVQPDPVSHC#K	-0.72	1.6	up	-2.75	0.49
P08134	Rho-related GTP-binding protein RhoC	HFC#PNVPIILVGNK	-0.54	1.5	up	-2.71	0.52
P08865	40S ribosomal protein SA	ADHQPLTEASYVNLPTIALC#NTDSPLR	-0.63	1.5	up	-2.43	0.64
Q99460	26S proteasome non-ATPase regulatory subunit 1	TPEQC#PSVVSLLSESYNPHVR	-0.58	1.5	up	-2.33	0.68
P00505	Aspartate aminotransferase, mitochondrial	IPEQSVLLLHAC#AHNPTGVDPRPEQWK	-0.64	1.6	up	-2.30	0.69
ROA1	Heterogeneous nuclear ribonucleoprotein A1	SHFEQWGTLTDC#VVM*R	-0.61	1.5	up	-2.25	0.74
P12814	Alpha-actinin-1	IC#DQWDNLGALTQK	-0.61	1.5	up	-2.17	0.81
P62258	14-3-3 protein epsilon	LIC#C#DILDVLDK	-0.57	1.5	up	-2.10	0.85
P68363	Tubulin alpha-1B	AYHEQLSVAEITNAC#FEPANQMVK	-0.56	1.5	up	-2.07	0.86
P11142	Heat shock cognate 71 kDa protein	GPAVGIDLGTTYSC#VGVFQHGK	-0.54	1.5	up	-2.03	0.88
P30044	Peroxiredoxin-5, mitochondrial	GVLFGVPGAFTPGC#SK	-0.51	1.4	up	-2.02	0.88
P63244	Guanine nucleotide-binding protein subunit beta-2-like 1	TNHIGHTGYLNTVTVSPDGSLC#ASGGK	-0.56	1.5	up	-2.01	0.88
P30086	Phosphatidylethanolamine-binding protein 1	APVAGTC@YQAEWDDYVPK	0.51	1.4	down	2.03	0.87
P13639	Elongation factor 2	C@ELLYEGPPDDEAAMGIK	0.59	1.5	down	2.03	0.89
P21980	Protein-glutamine gamma-glutamyltransferase 2	VVSGMVNC@NDDQGVLLGR	0.56	1.5	down	2.06	0.87
P46782	40S ribosomal protein S5	VNQAIWLLC@TGAR	0.50	1.4	down	2.08	0.84
P36578	60S ribosomal protein L4	FC@IWTESAFR	0.56	1.5	down	2.12	0.84
P62826	GTP-binding nuclear protein Ran	VC@ENIPIVLC@GNK	0.57	1.5	down	2.20	0.78
P62829	60S ribosomal protein L23	ISLGLPVGAVINC#ADNTGAK	0.51	1.4	down	2.49	0.62
P07900	Heat shock protein HSP 90-alpha	VFIM*DNC#EELIPEYLNFIR	0.78	1.7	down	2.78	0.49
P13639	Elongation factor 2	C@LYASVLTAQPR	0.74	1.7	down	2.80	0.51
P49327	Fatty acid synthase	LSIPTYGLQC@TR	0.92	1.9	down	3.08	0.65
P68363	Tubulin alpha-1B	AVC@MLSNTTAIAEAWAR	0.90	1.9	down	3.46	1.64

Anexo A.6.- Lista de las proteínas que aumentan o disminuyen su abundancia en respuesta a la hipoxia en células endoteliales.

Los criterios de filtrado así como el código de colores utilizado y la nomenclatura son los mismos que los que se usaron en el Anexo A.2.

Nº acceso	Proteína	Xq-X	Fold Change		Zq	FDRq
Q29443	Serotransferrin	-1.94	3.8	up	-6.60	4.E-08
Q3SZR3	Alpha-1-acid glycoprotein	-2.21	4.6	up	-5.93	8.E-07
Q9Y666	Solute carrier family 12 member 7	-2.09	4.2	up	-5.78	2.E-06
P34955	Alpha-1-antiproteinase	-2.02	4.1	up	-5.55	5.E-06
P69905	Hemoglobin subunit alpha	-1.52	2.9	up	-5.10	3.E-05
P12763	Alpha-2-HS-glycoprotein	-1.49	2.8	up	-4.98	5.E-05
P07108	Acyl-CoA-binding protein	-1.66	3.2	up	-4.52	4.E-04
Q7SIH1	Alpha-2-macroglobulin	-1.03	2.0	up	-3.92	4.E-03
P02788	Lactotransferrin	-1.37	2.6	up	-3.91	4.E-03
P02042	Hemoglobin subunit delta	-1.37	2.6	up	-3.91	4.E-03
P01023	Alpha-2-macroglobulin	-1.23	2.4	up	-3.48	0.02
P61604	10 kDa heat shock protein, mitochondrial	-0.90	1.9	up	-3.25	0.03
P04080	Cystatin-B	-0.89	1.9	up	-3.23	0.03
Q9Y281	Cofilin-2	-0.86	1.8	up	-3.13	0.04
P07858	Cathepsin B	-0.76	1.7	up	-2.95	0.06
P33992	DNA replication licensing factor MCM5	-1.05	2.1	up	-2.84	0.08
P00441	Superoxide dismutase [Cu-Zn]	-0.82	1.8	up	-2.76	0.10
Q96FQ6	Protein S100-A16	-1.05	2.1	up	-2.70	0.11
P09960	Leukotriene A-4 hydrolase	-0.73	1.7	up	-2.70	0.11
Q9UFH2	Dynein heavy chain 17, axonemal	-1.01	2.0	up	-2.69	0.11
P48147	Prolyl endopeptidase	-0.99	2.0	up	-2.62	0.12
P61011	Signal recognition particle 54 kDa protein	-0.98	2.0	up	-2.59	0.13
Q96QK1	Vacuolar protein sorting-associated protein 35	-0.98	2.0	up	-2.59	0.13
P30086	Phosphatidylethanolamine-binding protein 1	-0.68	1.6	up	-2.56	0.14
P01966	Hemoglobin subunit alpha	-0.93	1.9	up	-2.54	0.14
Q9UHD1	Cysteine and histidine-rich domain-containing protein 1	-0.80	1.7	up	-2.50	0.16
P02647	Apolipoprotein A-I	-0.88	1.8	up	-2.49	0.16
Q9UKK3	Poly [ADP-ribose] polymerase 4	-0.94	1.9	up	-2.47	0.16
P99999	Cytochrome c	-0.90	1.9	up	-2.45	0.17
Q06323	Proteasome activator complex subunit 1	-0.60	1.5	up	-2.44	0.17
P10619	Lysosomal protective protein	-0.73	1.7	up	-2.44	0.17
O96019	Actin-like protein 6A	-0.89	1.8	up	-2.43	0.17
Q16531	DNA damage-binding protein 1	-0.68	1.6	up	-2.43	0.16
P11766	Alcohol dehydrogenase class-3	-0.99	2.0	up	-2.43	0.17
P10599	Thioredoxin	-0.86	1.8	up	-2.43	0.16
P78527	DNA-dependent protein kinase catalytic subunit	-0.91	1.9	up	-2.34	0.20
Q99714	3-hydroxyacyl-CoA dehydrogenase type-2	-0.71	1.6	up	-2.32	0.21
P23528	Cofilin-1	-0.61	1.5	up	-2.31	0.21
Q8N543	2-oxoglutarate and iron-dependent oxygenase domain-containing protein 1	-0.92	1.9	up	-2.27	0.22
Q9BVK6	Transmembrane emp24 domain-containing protein 9	-0.85	1.8	up	-2.26	0.22
Q92820	Gamma-glutamyl hydrolase	-0.67	1.6	up	-2.25	0.23
Q15642	Cdc42-interacting protein 4	-0.81	1.8	up	-2.24	0.23
P49755	Transmembrane emp24 domain-containing protein 10	-0.62	1.5	up	-2.23	0.23

Q14320	Protein FAM50A	-0.86	1.8	up	-2.22	0.23
Q9NVJ2	ADP-ribosylation factor-like protein 8B	-0.78	1.7	up	-2.21	0.23
Q9HB71	Calcyclin-binding protein	-0.76	1.7	up	-2.17	0.25
P27816	Microtubule-associated protein 4	-0.60	1.5	up	-2.16	0.26
Q13740	CD166 antigen	-0.59	1.5	up	-2.15	0.26
P29218	Inositol monophosphatase 1	-0.79	1.7	up	-2.15	0.26
Q9H078	Caseinolytic peptidase B protein homolog	-0.82	1.8	up	-2.14	0.26
P09622	Dihydrolipoyl dehydrogenase, mitochondrial	-0.60	1.5	up	-2.12	0.27
Q99584	Protein S100-A13	-0.75	1.7	up	-2.10	0.27
Q92879	CUGBP Elav-like family member 1	-0.89	1.8	up	-2.09	0.27
P11137	Microtubule-associated protein 2	-0.76	1.7	up	-2.08	0.28
P07195	L-lactate dehydrogenase B chain	-0.49	1.4	up	-2.08	0.28
P45974	Ubiquitin carboxyl-terminal hydrolase 5	-0.63	1.6	up	-2.03	0.31
P05455	Lupus La protein	-0.60	1.5	up	-2.01	0.31
P31949	Protein S100-A11	-0.71	1.6	up	-2.01	0.31
P04818	Thymidylate synthase	0.51	1.4	down	2.00	0.32
Q9BUF5	Tubulin beta-6 chain	0.48	1.4	down	2.01	0.32
Q9H4B7	Tubulin beta-1 chain	0.55	1.5	down	2.02	0.31
Q9NZN3	EH domain-containing protein 4	0.56	1.5	down	2.04	0.31
Q00526	Cyclin-dependent kinase 3	0.74	1.7	down	2.06	0.29
P26373	60S ribosomal protein L13	0.55	1.5	down	2.10	0.27
Q99867	Putative tubulin beta-4q chain	0.62	1.5	down	2.11	0.27
P46776	60S ribosomal protein L27a	0.76	1.7	down	2.11	0.27
P84103	Splicing factor, arginine/serine-rich 3	0.75	1.7	down	2.11	0.27
P60842	Eukaryotic initiation factor 4A-I	0.52	1.4	down	2.13	0.26
P07996	Thrombospondin-1	0.78	1.7	down	2.13	0.26
P29692	Elongation factor 1-delta	0.59	1.5	down	2.15	0.26
Q9ULS5	Transmembrane and coiled-coil domains protein 3	0.79	1.7	down	2.19	0.25
Q7L9L4	Mps one binder kinase activator-like 1A	0.82	1.8	down	2.21	0.24
Q14566	DNA replication licensing factor MCM6	0.59	1.5	down	2.21	0.24
Q12905	Interleukin enhancer-binding factor 2	0.57	1.5	down	2.23	0.23
Q13435	Splicing factor 3B subunit 2	0.86	1.8	down	2.24	0.23
P08243	Asparagine synthetase [glutamine-hydrolyzing]	0.63	1.5	down	2.24	0.23
Q96QV6	Histone H2A type 1-A	0.80	1.7	down	2.24	0.23
P49411	Elongation factor Tu, mitochondrial	0.61	1.5	down	2.26	0.23
P12236	ADP/ATP translocase 3	0.79	1.7	down	2.27	0.22
Q13243	Serine/arginine-rich splicing factor 5	0.81	1.8	down	2.30	0.21
O00425	Insulin-like growth factor 2 mRNA-binding protein 3	0.65	1.6	down	2.31	0.21
P49736	DNA replication licensing factor MCM2	0.66	1.6	down	2.32	0.21
Q16629	Splicing factor, arginine/serine-rich 7	0.69	1.6	down	2.33	0.20
Q99729	Heterogeneous nuclear ribonucleoprotein A/B	0.71	1.6	down	2.35	0.20
P63241	Eukaryotic translation initiation factor 5A-1	0.88	1.8	down	2.43	0.16
Q9P2J5	Leucyl-tRNA synthetase, cytoplasmic	0.90	1.9	down	2.44	0.17
O60506	Heterogeneous nuclear ribonucleoprotein Q	0.62	1.5	down	2.46	0.16
Q9H223	EH domain-containing protein 4	0.91	1.9	down	2.47	0.16
P05141	ADP/ATP translocase 2	0.65	1.6	down	2.50	0.15
Q5VW32	BRO1 domain-containing protein BROX	0.94	1.9	down	2.56	0.13
A6NHL2	Tubulin alpha chain-like 3	0.77	1.7	down	2.58	0.13
Q9ULV4	Coronin-1C	0.80	1.7	down	2.59	0.13
Q9NW64	Pre-mRNA-splicing factor RBM22	0.94	1.9	down	2.59	0.13
P42704	Leucine-rich PPR motif-containing protein, mitochondrial	0.80	1.7	down	2.63	0.12
P39656	Dolichyl-diphosphooligosaccharide--protein glycosyltransferase 48 kDa subu	0.74	1.7	down	2.65	0.12
P12235	ADP/ATP translocase 1	0.93	1.9	down	2.67	0.11
O15523	ATP-dependent RN	1.03	2.0	down	2.69	0.11
Q9UGR2	Zinc finger CCCH domain-containing protein 7B	1.01	2.0	down	2.69	0.11

Q13177	Serine/threonine-protein kinase PAK 2	0.99	2.0	down	2.73	0.10
P12956	X-ray repair cross-complementing protein 6	0.73	1.7	down	2.74	0.10
Q7KZF4	Staphylococcal nuclease domain-containing protein 1	0.78	1.7	down	2.74	0.10
O14979	Heterogeneous nuclear ribonucleoprotein D-like	0.81	1.8	down	2.75	0.10
P50579	Methionine aminopeptidase 2	1.03	2.0	down	2.85	0.08
O43390	Heterogeneous nuclear ribonucleoprotein R	0.86	1.8	down	2.85	0.08
P49448	Glutamate dehydrogenase 2, mitochondrial	0.91	1.9	down	2.96	0.06
P35606	Coatomer subunit beta'	0.91	1.9	down	3.04	0.05
P22626	Heterogeneous nuclear ribonucleoproteins A2/B1	0.76	1.7	down	3.09	0.04
P54136	Arginyl-tRNA synthetase, cytoplasmic	0.86	1.8	down	3.09	0.04
P61978	Heterogeneous nuclear ribonucleoprotein K	0.78	1.7	down	3.09	0.04
P39748	Flap endonuclease 1	1.12	2.2	down	3.10	0.04
Q00325	Phosphate carrier protein, mitochondrial	1.10	2.1	down	3.13	0.04
P04908	Histone H2A type 1-B/E	1.19	2.3	down	3.15	0.04
P10398	Serine/threonine-protein kinase A-Raf	1.26	2.4	down	3.18	0.03
O00571	ATP-dependent RNA helicase DDX3X	0.85	1.8	down	3.20	0.03
Q8N4U5	T-complex protein 11-like protein 2	1.17	2.2	down	3.21	0.03
Q08945	FACT complex subunit SSRP1	1.17	2.2	down	3.21	0.03
Q8IVF6	Ankyrin repeat domain-containing protein 18A	1.14	2.2	down	3.27	0.03
Q13263	Transcription intermediary factor 1-beta	1.02	2.0	down	3.28	0.03
P52597	Heterogeneous nuclear ribonucleoprotein F	1.01	2.0	down	3.41	0.02
Q9NY15	Stabilin-1	1.24	2.4	down	3.41	0.02
Q15717	ELAV-like protein 1	1.27	2.4	down	3.44	0.02
P26358	DNA (cytosine-5)-methyltransferase 1	1.28	2.4	down	3.46	0.02
Q15021	Condensin complex subunit 1	1.24	2.4	down	3.49	0.02
Q9H400	Lck-interacting transmembrane adapter 1	1.27	2.4	down	3.51	0.02
P26368	Splicing factor U2AF 65 kDa subunit	1.28	2.4	down	3.52	0.02
Q6ZP68	Putative uncharacterized protein C13orf35	1.33	2.5	down	3.68	0.01
P09651	Heterogeneous nuclear ribonucleoprotein A1	1.02	2.0	down	3.72	0.01
P08670	Vimentin	1.42	2.7	down	3.97	3.E-03
P02545	Lamin-A/C	0.99	2.0	down	4.02	3.E-03
P42331	Rho GTPase-activating protein 25	1.54	2.9	down	4.22	1.E-03
P31942	Heterogeneous nuclear ribonucleoprotein H3	1.57	3.0	down	4.33	8.E-04
P33993	DNA replication licensing factor MCM7	1.23	2.3	down	4.40	6.E-04
P55795	Heterogeneous nuclear ribonucleoprotein H2	1.22	2.3	down	4.46	5.E-04
P07910	Heterogeneous nuclear ribonucleoproteins C1/C2	1.40	2.6	down	4.47	5.E-04
Q00839	Heterogeneous nuclear ribonucleoprotein U	1.20	2.3	down	4.57	3.E-04
Q13283	Ras GTPase-activating protein-binding protein 1	1.26	2.4	down	4.71	2.E-04
P35232	Prohibitin	1.33	2.5	down	5.06	4.E-05
Q9P035	Protein tyrosine phosphatase-like protein PTPLAD1	1.86	3.6	down	5.10	3.E-05
Q15149	Plectin-1	1.84	3.6	down	5.12	4.E-05
Q99623	Prohibitin-2	1.33	2.5	down	5.26	2.E-05
P51991	Heterogeneous nuclear ribonucleoprotein A3	1.40	2.6	down	5.46	8.E-06
Q9H6U8	Alpha-1,2-mannosyltransferase ALG9	2.35	5.1	down	6.48	9.E-08
Q07065	Cytoskeleton-associated protein 4	1.66	3.2	down	6.50	8.E-08

Anexo A.7.- Lista de las péptidos con Cys que aumentan o disminuyen su abundancia en respuesta a la IR en mitocondrias SSM.

Los criterios de filtrado así como el código de colores utilizado y la nomenclatura son los mismos que los que se usaron en el Anexo A.2.

Nº acceso	Proteína	Secuencia	Xp-Xq	Fold Change		Zp	FDRp
Q6P6R2	Dihydrolipoyl dehydrogenase, mitochondrial	NETLGGTC@LNVGC@IPSK	-4.39	20.9	up	-15.13	0.E+00
D3ZA85	Histone cell cycle regulation defective interacting protein 5 (Predicted), isoform CRA_a	LQGSC@TSC@PSSIITLK	-2.33	5.0	up	-10.56	0.E+00
Q5XIH3	NADH dehydrogenase (Ubiquinone) flavoprotein 1	HESC@GQC@TPC@R	-2.93	7.6	up	-9.15	0.E+00
Q9R1Z0	Voltage-dependent anion-selective channel protein 3	LC@QNNFALGYK	-2.73	6.6	up	-9.08	0.E+00
B0BNE6	NADH dehydrogenase (Ubiquinone) Fe-S protein 8 (Predicted), isoform CRA_a	LC@EAIC@PAQAITIEAEPR	-2.59	6.0	up	-8.99	0.E+00
B2RZ24	Sucla2 protein	IC@NQVLVC@ER	-2.57	6.0	up	-8.39	0.E+00
Q66HF1	NADH-ubiquinone oxidoreductase 75 kDa subunit, mitochondrial	VVAAC@AMPVMK	-2.50	5.7	up	-8.26	0.E+00
D3ZCZ9	RCG41951, isoform CRA_a	TGTC@GYC@GLQFK	-1.67	3.2	up	-7.33	6.E-11
P45953	Very long-chain specific acyl-CoA dehydrogenase, mitochondrial	VASGQALAAFC@LTEPSSGSDVASIR	-1.97	3.9	up	-6.38	3.E-08
P81155	Voltage-dependent anion-selective channel protein 2	PIC@IPPPYADLGK	-1.73	3.3	up	-6.02	3.E-07
P85834	Elongation factor Tu, mitochondrial	HYAHTDC@PGHADYVK	-1.78	3.4	up	-5.79	9.E-07
P56574	Isocitrate dehydrogenase [NADP], mitochondrial	SSGGFVWAC@K	-1.68	3.2	up	-5.76	1.E-06
Q66HF1	NADH-ubiquinone oxidoreductase 75 kDa subunit, mitochondrial	VVAAC@AMPVM*K	-1.75	3.4	up	-5.64	2.E-06
B2RZ24	Sucla2 protein	ILAC@DDLDEAAK	-1.76	3.4	up	-5.63	2.E-06
P81155	Voltage-dependent anion-selective channel protein 2	WC@EYGLTFTEK	-1.68	3.2	up	-5.62	2.E-06
D3ZLT1	NADH dehydrogenase (Ubiquinone) 1 beta subcomplex, 7 (Predicted)	HEQHDWDYC@EHQDYVK	-1.62	3.1	up	-5.60	2.E-06
P09605	Creatine kinase S-type, mitochondrial	HNNC#MAEC@LTPTIYAK	-1.67	3.2	up	-5.46	4.E-06
B2RYW3	NADH dehydrogenase (Ubiquinone) 1 beta subcomplex, 9	VPEWC@LDYWHPSEK	-1.50	2.8	up	-5.40	6.E-06
P04041	Glutathione peroxidase 1	YIIWSPVC@R	-1.43	2.7	up	-4.99	4.E-05
Q80W89	NADH dehydrogenase [ubiquinone] 1 alpha subcomplex subunit 11	FFEAYNETPDGTQC@HR	-1.38	2.6	up	-4.99	5.E-05
P09605	Creatine kinase S-type, mitochondrial	LGYILTC@PSNLGTGLR	-1.40	2.6	up	-4.80	1.E-04
P21913	Succinate dehydrogenase [ubiquinone] iron-sulfur subunit, mitochondrial	C@GPMVLDALIK	-1.32	2.5	up	-4.79	1.E-04
Q9ER34	Aconitate hydratase, mitochondrial	DFAPGKPLNC@IIK	-1.45	2.7	up	-4.75	1.E-04
Q9ER34	Aconitate hydratase, mitochondrial	VGLIGSC@TNSSYEDMGR	-1.42	2.7	up	-4.72	1.E-04
D4A311	NADH dehydrogenase (Ubiquinone) 1 alpha subcomplex, 8	FDEC@VLDK	-1.25	2.4	up	-4.69	2.E-04
Q6UPE1	Electron transfer flavoprotein-ubiquinone oxidoreductase, mitochondrial	AAQIGAHTLSGAC@LDPAAFK	-1.43	2.7	up	-4.64	2.E-04
Q6AXV4	Sorting and assembly machinery component 50 homolog	GVSAEYSFPLC@K	-1.41	2.6	up	-4.62	2.E-04
P41565	Isocitrate dehydrogenase [NAD] subunit gamma 1, mitochondrial	TSLDLYANVIHC@K	-1.60	3.0	up	-4.56	3.E-04
Q64428	Trifunctional enzyme subunit alpha, mitochondrial	ALMGLYNGQVLC@K	-1.39	2.6	up	-4.50	3.E-04
P56574	Isocitrate dehydrogenase [NADP], mitochondrial	DLAGC@IHGLSNVK	-1.33	2.5	up	-4.42	5.E-04
Q05962	ADP/ATP translocase 1	GADIMYTGTVDC@WR	-1.35	2.6	up	-4.40	5.E-04
P35738	2-oxoisovalerate dehydrogenase subunit beta, mitochondrial	LGVSC#EVIDLR	-1.13	2.2	up	-4.32	7.E-04
B0BNE6	NADH dehydrogenase (Ubiquinone) Fe-S protein 8 (Predicted), isoform CRA_a	LC@EAIC#PAQAITIEAEPR	-1.19	2.3	up	-4.04	2.E-03
P13437	3-ketoacyl-CoA thiolase, mitochondrial	LC#GSGFQSIVSGC@QEIC#SK	-1.27	2.4	up	-4.04	2.E-03
D3ZL85	Uncharacterized protein Hccs	WEALHAHEC@PC@GPSLVR	-1.13	2.2	up	-4.01	3.E-03
Q5XI78	2-oxoglutarate dehydrogenase, mitochondrial	FGLEGC@EVLIPALK	-1.23	2.3	up	-3.94	4.E-03
P80430	Cytochrome c oxidase subunit 6B1	NC@WQNYLDFHR	-1.04	2.1	up	-3.93	3.E-03
Q9R063	Peroxiredoxin-5, mitochondrial	GVLFGVPGAFTPGC@SK	-1.03	2.0	up	-3.71	0.01
P09650	Mast cell protease 1	GDSGGPLVC@AGVAHGIVSYGR	-0.95	1.9	up	-3.70	0.01
P04636	Malate dehydrogenase, mitochondrial	GC@DVVVIPAGVPR	-1.15	2.2	up	-3.68	0.01
P18886	Carnitine O-palmitoyltransferase 2, mitochondrial	C@LEDIFDALEGK	-1.11	2.2	up	-3.64	0.01
Q9ER34	Aconitate hydratase, mitochondrial	C@TTDHISAAGPWLK	-1.13	2.2	up	-3.62	0.01
Q9R1Z0	Voltage-dependent anion-selective channel protein 3	VC@NYGLIFTQK	-0.99	2.0	up	-3.53	0.01
P13437	3-ketoacyl-CoA thiolase, mitochondrial	LC@GSGFQSIVSGC#QEIC#SK	-0.98	2.0	up	-3.30	0.03
Q9WVK7	Hydroxyacyl-coenzyme A dehydrogenase, mitochondrial	TFESLVDFC@K	-0.90	1.9	up	-3.15	0.04
D3ZLT1	NADH dehydrogenase (Ubiquinone) 1 beta subcomplex, 7 (Predicted)	DSFPNFVAC@K	-0.86	1.8	up	-3.11	0.05
B0K020	CDGSH iron-sulfur domain-containing protein 1	FPFC@DGAHIK	-0.86	1.8	up	-3.08	0.05
P04636	Malate dehydrogenase, mitochondrial	GYLGPEQLPDC@LK	-0.89	1.9	up	-2.96	0.07
Q80W89	NADH dehydrogenase [ubiquinone] 1 alpha subcomplex subunit 11	EKPDDPLNYFIGGC@AGGLTLGAR	-0.80	1.7	up	-2.86	0.09
Q5EBA1	ATP-dependent RNA helicase SUPV3L1, mitochondrial	YLSATSGVYC#GPLK	-0.63	1.5	up	-2.85	0.09
Q920L2	Succinate dehydrogenase [ubiquinone] flavoprotein subunit, mitochondrial	VGSVLQEGC@EK	-0.87	1.8	up	-2.83	0.10
P04636	Malate dehydrogenase, mitochondrial	TIIPLISQC@TPK	-0.81	1.8	up	-2.73	0.13
Q66HF1	NADH-ubiquinone oxidoreductase 75 kDa subunit, mitochondrial	FC@YHER	-0.85	1.8	up	-2.72	0.12
Q05962	ADP/ATP translocase 1	EFNGLGDC@LTK	-0.78	1.7	up	-2.67	0.14
O35854	Branched-chain-amino-acid aminotransferase, mitochondrial	AWIGGVGDC#K	-0.83	1.8	up	-2.53	0.19
B0BNE6	NADH dehydrogenase (Ubiquinone) Fe-S protein 8 (Predicted), isoform CRA_a	LC#EAIC@PAQAITIEAEPR	-0.74	1.7	up	-2.50	0.20
Q66HF1	NADH-ubiquinone oxidoreductase 75 kDa subunit, mitochondrial	M*C@LVEIEK	-0.73	1.7	up	-2.45	0.23
P29411	GTP:AMP phosphotransferase mitochondrial	NLTQC#SWLLDGFPR	-0.71	1.6	up	-2.43	0.23
P16036	Phosphate carrier protein, mitochondrial	GWAPTLIGYSMQGLC#K	-0.69	1.6	up	-2.42	0.24
P14408	Fumarate hydratase, mitochondrial	LLGDASVSFTENC#VVGIQANTER	-0.69	1.6	up	-2.31	0.28
Q920F5	Malonyl-CoA decarboxylase, mitochondrial	VTWHSPC#EVLQK	-0.68	1.6	up	-2.31	0.28
D4A8P9	Uncharacterized protein	VHFVPGWDC#HGLPIETK	-0.67	1.6	up	-2.30	0.28
B2GV06	Succinyl-CoA:3-ketoacid-coenzyme A transferase 1, mitochondrial	NFNLPMC#K	-0.62	1.5	up	-2.23	0.31
P41565	Isocitrate dehydrogenase [NAD] subunit gamma 1, mitochondrial	NIANPTATLLASC#MMLDHLK	-0.66	1.6	up	-2.16	0.35
Q9ER34	Aconitate hydratase, mitochondrial	VGLIGSC@TNSSYEDM*GR	-0.65	1.6	up	-2.09	0.39
Q9ER34	Aconitate hydratase, mitochondrial	C#TTDHISAAGPWLK	-0.62	1.5	up	-2.02	0.42

P09605	Creatine kinase S-type, mitochondrial	LGYILTC#PSNLGTGLR	0.59	1.5	down	2.05	0.41
Q5XHZ0	Heat shock protein 75 kDa, mitochondrial	NIYYLC#APNR	0.60	1.5	down	2.11	0.37
P09605	Creatine kinase S-type, mitochondrial	GLSLPPAC#SR	0.62	1.5	down	2.16	0.34
Q5XIC0	Enoyl-CoA delta isomerase 2, mitochondrial	WLSEEC#INAIM*SFVTR	0.67	1.6	down	2.34	0.27
P09605	Creatine kinase S-type, mitochondrial	LIDDHFLFDKPVSPLLTC#AGM*AR	0.70	1.6	down	2.43	0.23
Q80W89	NADH dehydrogenase [ubiquinone] 1 alpha subcomplex subunit	THSYGTAAIGC#VYM*GTAAALFK	0.79	1.7	down	2.75	0.12
P18163	Long-chain-fatty-acid-CoA ligase 1	ALKPPC#DLSM*QSVEVTGTTEGVR	0.83	1.8	down	2.75	0.12
D3ZL85	Putative uncharacterized protein Hccs	AYEYVEC#PVTGAAAK	0.72	1.6	down	2.79	0.11
Q9R1Z0	Voltage-dependent anion-selective channel protein 3	LC#QNNFALGYK	0.82	1.8	down	2.91	0.08
B2RYS8	NADH dehydrogenase (Ubiquinone) 1 beta subcomplex 8	VDTSPTPVSWDVMC#R	0.83	1.8	down	3.01	0.06
Q9R1Z0	Voltage-dependent anion-selective channel protein 3	VC#NYGLIFTQK	0.89	1.9	down	3.04	0.06
P14408	Fumarate hydratase, mitochondrial	FEALAAHDALVELSGAM*NTTAC#SLM*K	0.93	1.9	down	3.04	0.06
P38718	Brain protein 44	WGLVC#AGLADM*AR	0.77	1.7	down	3.04	0.06
P81155	Voltage-dependent anion-selective channel protein 2	PIC#IPPPYADLGK	1.06	2.1	down	3.26	0.03
P85834	Elongation factor Tu, mitochondrial	GEETPVIVGSALC#ALEQR	0.98	2.0	down	3.30	0.03
Q4V8F9	Hydroxysteroid dehydrogenase-like protein 2	YGM*SM*C#VLGM*AEEFR	0.97	2.0	down	3.39	0.02
B2RYW3	NADH dehydrogenase (Ubiquinone) 1 beta subcomplex, 9	YLAC#LM*R	0.96	1.9	down	3.48	0.02
B2RYS8	NADH dehydrogenase (Ubiquinone) 1 beta subcomplex 8	VDTSPTPVSWDVM*C#R	1.57	3.0	down	5.71	1.E-06
D3ZCZ9	RCG41951, isoform CRA_a	TGTC#GYC#GLQFK	1.47	2.8	down	6.88	1.E-09

Anexo A.8.- Lista de las proteínas que aumentan o disminuyen su abundancia en respuesta a la IR en mitocondrias SSM.

Los criterios de filtrado así como el código de colores utilizado y la nomenclatura son los mismos que los que se usaron en el Anexo A.2.

Nº acceso	Proteína	Xq-X	Fold Change		Zq	FDRq
P23928	Alpha-crystallin B	-2.64	6.2	up	-8.30	0.E+00
P0C169	Histone H2A type 1	-2.07	4.2	up	-5.43	6.E-06
P62630	Elongation factor 1-alpha 1	-1.49	2.8	up	-4.73	1.E-04
P02563	Myosin-6	-1.34	2.5	up	-4.63	2.E-04
P02564	Myosin-7	-1.69	3.2	up	-4.36	5.E-04
P08733	Myosin regulatory light chain 2, ventricular/cardiac muscle isoform	-1.57	3.0	up	-4.10	1.E-03
P60711	Actin, cytoplasmic	-1.24	2.4	up	-3.14	0.04
Q0D2L2	Similar to ribosomal protein, mitochondrial, S22	-1.09	2.1	up	-2.78	0.11
Q64559	Cytosolic acyl coenzyme A thioester hydrolase	-0.82	1.8	up	-2.63	0.16
P16409	Myosin light chain 3	-0.96	1.9	up	-2.39	0.24
Q64591	2,4-dienoyl-CoA reductase, mitochondrial	-0.62	1.5	up	-2.28	0.29
A9UMW2	Ndufa3 protein	-0.72	1.6	up	-2.27	0.29
P04797	Glyceraldehyde-3-phosphate dehydrogenase	-0.86	1.8	up	-2.21	0.32
D3ZZV1	Putative uncharacterized protein Magmas	-0.83	1.8	up	-2.13	0.35
P31399	ATP synthase subunit d, mitochondrial	-0.54	1.4	up	-2.04	0.38
O35796	Complement component 1 Q subcomponent-binding protein, mitochondrial	-0.63	1.5	up	-2.00	0.42
P08050	Gap junction alpha-1 protein	-0.77	1.7	up	-2.00	0.39
Q3B8N9	Biphenyl hydrolase-like (Serine hydrolase)	0.80	1.7	down	2.03	0.39
P21571	ATP synthase-coupling factor 6, mitochondrial	0.79	1.7	down	2.09	0.36
O35257	Prolactin-6A1	0.80	1.7	down	2.11	0.34
B0BNI1	Glutathione S-transferase alpha 3	0.81	1.8	down	2.13	0.33
Q6PCW3	Dcpp2 protein	0.85	1.8	down	2.15	0.34
Q6AY04	Uncharacterized protein C2orf47 homolog, mitochondrial	0.85	1.8	down	2.19	0.31
D3ZXA6	Similar to pyruvate dehydrogenase phosphatase regulatory subunit	0.85	1.8	down	2.20	0.33
B3Y999	Cytochrome b	0.85	1.8	down	2.21	0.32
B0BNJ9	RCG44002, isoform	0.87	1.8	down	2.27	0.30
D4ADS4	Putative uncharacterized protein Mgst3	0.74	1.7	down	2.35	0.26
B1WBP7	Putative uncharacterized protein	0.90	1.9	down	2.37	0.25
Q6PCT8	Succinate dehydrogenase [ubiquinone] cytochrome b small subunit, mitochondrial	0.94	1.9	down	2.42	0.24
P13697	NADP-dependent malic enzyme	0.95	1.9	down	2.45	0.22
P05508	NADH-ubiquinone oxidoreductase chain 4	0.71	1.6	down	2.47	0.22
Q8VHE9	All-trans-retinol 13,14-reductase	0.96	1.9	down	2.47	0.24
P12075	Cytochrome c oxidase subunit 5B, mitochondrial	0.85	1.8	down	2.73	0.12
Q8VGW5	Olfactory receptor 691	1.04	2.1	down	2.73	0.13
P11608	ATP synthase protein 8	1.17	2.3	down	3.08	0.04
Q5EBA1	ATP-dependent RNA helicase SUPV3L1, mitochondrial	1.25	2.4	down	3.22	0.03
P35738	2-oxoisovalerate dehydrogenase subunit beta, mitochondrial	1.07	2.1	down	3.45	0.01
P10888	Cytochrome c oxidase subunit 4 isoform 1, mitochondrial	1.01	2.0	down	3.72	0.01
D3ZB81	Uncharacterized protein	1.50	2.8	down	3.99	2.E-03
Q8BWT1	3-ketoacyl-CoA thiolase, mitochondrial	1.69	3.2	down	4.43	4.E-04
P11662	NADH-ubiquinone oxidoreductase chain 2	1.67	3.2	down	4.43	4.E-04
P11661	NADH-ubiquinone oxidoreductase chain 5	1.82	3.5	down	4.81	8.E-05
P05503	Cytochrome c oxidase subunit 1	1.48	2.8	down	5.20	2.E-05
Q3UQP1	Putative uncharacterized protein	1.71	3.3	down	5.38	8.E-06
P21396	Amine oxidase [flavin-containing] A	1.45	2.7	down	5.65	6.E-06
P03889	NADH-ubiquinone oxidoreductase chain 1	2.17	4.5	down	6.92	2.E-09

Anexo A.9.- Lista de los péptidos con Cys que aumentan o disminuyen su abundancia en respuesta a la IR en mitocondrias IFM.

Los criterios de filtrado así como el código de colores utilizado y la nomenclatura son los mismos que los que se usaron en el Anexo A.2.

Nº acceso	Proteína	Secuencia	Xp-Xq	Fold Change		Zp	FDRp
P00507	Aspartate aminotransferase, mitochondrial	EYLPIGGLADFC@K	-1.70	3.2	up	-10.00	0.E+00
Q920L2	Succinate dehydrogenase [ubiquinone] flavoprotein subunit, mitochondrial	VGSVLQEGC@EK	-1.95	3.9	up	-9.06	0.E+00
P04636	Malate dehydrogenase, mitochondrial	GYLGPEQLPDC@LK	-1.40	2.6	up	-7.56	9.E-12
P56574	Isocitrate dehydrogenase [NADP], mitochondrial	DLAGC@IHGLSNVK	-1.22	2.3	up	-7.08	2.E-10
P04636	Malate dehydrogenase, mitochondrial	TIIPLISQC@TPK	-1.04	2.1	up	-6.29	4.E-08
P04636	Malate dehydrogenase, mitochondrial	GC@DVVVIPAGVPR	-1.09	2.1	up	-4.71	2.E-04
Q05962	ADP/ATP translocase 1	EFNGLGDC@LTK	-0.84	1.8	up	-4.63	3.E-04
B2RZ24	Sucla2 protein	IC#NQVLVC#ER	-0.65	1.6	up	-4.26	2.E-03
Q68FY0	Cytochrome b-c1 complex subunit 1, mitochondrial	LC@TSATESEVTR	-0.71	1.6	up	-3.90	0.01
Q68FU3	Electron transfer flavoprotein subunit beta	EIIAVSC#GPPQC#QETIR	-0.57	1.5	up	-3.68	0.01
P56574	Isocitrate dehydrogenase [NADP], mitochondrial	C@ATITPDEAR	-0.56	1.5	up	-3.20	0.07
P13437	3-ketoacyl-CoA thiolase, mitochondrial	LC#GSGFQSIVSGC#QEIC#SK	-0.45	1.4	up	-2.96	0.15
P56574	Isocitrate dehydrogenase [NADP], mitochondrial	C#ATITPDEAR	-0.47	1.4	up	-2.68	0.25
P08461	Dihydrolipoyllysine-residue acetyltransferase component of pyruvate dehydrogenase complex, mitochondrial	DVPVGSIIC#ITVEKPQDIEAFK	-0.42	1.3	up	-2.54	0.33
P12007	Isovaleryl-CoA dehydrogenase, mitochondrial	GSNTC#ELVFEDC#KVPAANILSQESK	-0.46	1.4	up	-2.44	0.40
B2RZ31	Sirtuin (Silent mating type information regulation 2 homolog) 3	LVEAHGSFVSATC#TVC#R	-0.38	1.3	up	-2.34	0.40
B0BNE6	NADH dehydrogenase (Ubiquinone) Fe-S protein 8 (Predicted), isoform CRA_a	LC#EAIC#PAQAITIEAEPR	-0.32	1.3	up	-2.27	0.43
Q66HF1	NADH-ubiquinone oxidoreductase 75 kDa subunit, mitochondrial	DC#FIVYQGHHGDVGAPIADVILPGAAYTEK	-0.40	1.3	up	-2.23	0.44
Q920L2	Succinate dehydrogenase [ubiquinone] flavoprotein subunit, mitochondrial	AGLPC#QDLEFVQFHPTGIYGAGC#LITEGC#R	-0.52	1.4	up	-2.22	0.44
P26284	Pyruvate dehydrogenase E1 component subunit alpha, somatic form, mitochondrial	NFYGGNGIVGAQVPLGAGIALAC#K	-0.33	1.3	up	-2.19	0.44
P18163	Long-chain-fatty-acid--CoA ligase 1	TKPKPPEPEDLAIIC#FTSGTTGNPK	-0.33	1.3	up	-2.12	0.49
P00507	Aspartate aminotransferase, mitochondrial	TC@GFDFSGALEDISK	-0.39	1.3	up	-2.04	0.55
B1WC61	Acad9 protein	LSSGEHIAAFC#LTEPASGSDAASIQTR	-0.34	1.3	up	-2.03	0.53
Q3V5X8	Endonuclease G	TYQNVYVC#TGPLFLPR	-0.33	1.3	up	-2.01	0.55
P56574	Isocitrate dehydrogenase [NADP], mitochondrial	DLAGC#IHGLSNVK	0.32	1.2	down	2.01	0.54
P04636	Malate dehydrogenase, mitochondrial	TIIPLISQC#TPK	0.32	1.3	down	2.11	0.49
Q3KR86	Mitochondrial inner membrane protein	VSC#SDNEFTQALTAAIPPESLTR	0.36	1.3	down	2.24	0.44
Q68FW7	Threonyl-tRNA synthetase, mitochondrial	GPAGAPEC#PVLIHR	0.39	1.3	down	2.25	0.44
P07633	Propionyl-CoA carboxylase beta chain, mitochondrial	IC#C#DLEVLASK	0.40	1.3	down	2.37	0.38
P56574	Isocitrate dehydrogenase [NADP], mitochondrial	NILGGTVFREPIIC#K	0.47	1.4	down	2.43	0.39
Q63065	[Pyruvate dehydrogenase [lipoamide]] kinase isozyme 1, mitochondrial	KHIGSINPNC#DVVEVIK	0.55	1.5	down	2.63	0.27
D4A311	NADH dehydrogenase (Ubiquinone) 1 alpha subcomplex, 8	LVNGC@ALNFFR	0.52	1.4	down	3.06	0.11
Q9R1Z0	Voltage-dependent anion-selective channel protein 3	VC#NYGLIFTQK	0.53	1.4	down	3.24	0.07
B2RZ24	Sucla2 protein	ILAC#DDLDEAAK	0.69	1.6	down	4.41	8.E-04
D3ZFQ8	Cytochrome c-1 (Predicted), isoform CRA_c	HLVGVC#YTEEEAK	0.73	1.7	down	4.88	1.E-04
Q8BH59	Calcium-binding mitochondrial carrier protein Aralar1	DIPFSAIYFPVYAHC#K	2.45	5.5	down	14.14	0.E+00

Anexo A.10.- Lista de las proteínas que aumentan o disminuyen su abundancia en respuesta a la IR en mitocondrias IFM.

Los criterios de filtrado así como el código de colores utilizado y la nomenclatura son los mismos que los que se usaron en el Anexo A.2.

Nº acceso	Proteína	Xq-X	Fold Change		Zq	FDRq
Q8BH59	Calcium-binding mitochondrial carrier protein Aralar1	-2.98	7.9	up	-13.71	0.E+00
Q9DCZ4	Apolipoprotein O	-1.93	3.8	up	-7.22	2.E-10
P29419	ATP synthase subunit e, mitochondrial	-1.21	2.3	up	-4.38	1.E-03
B2RZ24	Sucla2 protein	-0.78	1.7	up	-3.67	0.01
P63039	60 kDa heat shock protein, mitochondrial	-0.74	1.7	up	-3.58	0.01
D3Z9L0	Similar to putative lipid kinase	-0.97	2.0	up	-3.38	0.03
D3ZDF7	Uncharacterized protein	-0.72	1.6	up	-3.34	0.04
D4A7L4	NADH dehydrogenase (Ubiquinone) 1 beta subcomplex, 11	-0.73	1.7	up	-2.82	0.15
Q4G064	Ubiquinone biosynthesis methyltransferase COQ5, mitochondrial	-0.81	1.8	up	-2.81	0.13
B1H270	RCG56440	-0.61	1.5	up	-2.71	0.17
D3ZWA7	Putative uncharacterized protein ENSRNOP00000063894	-0.76	1.7	up	-2.69	0.15
Q2XTA8	NADH dehydrogenase 1 beta 4	-0.81	1.8	up	-2.65	0.18
A9UMV9	Ndufa7 protein	-0.66	1.6	up	-2.44	0.28
D3ZJX5	Putative uncharac	-0.68	1.6	up	-2.42	0.29
O54937	Pyruvate dehydrogenase [lipoamide]] kinase isozyme 4, mitochondrial	-0.66	1.6	up	-2.36	0.35
Q05962	ADP/ATP translocase 1	-0.49	1.4	up	-2.34	0.31
Q07803	Elongation factor G, mitochondrial	-0.48	1.4	up	-2.13	0.48
Q5M9H2	Acyl-Coenzyme A dehydrogenase, very long chain	-0.55	1.5	up	-2.12	0.50
Q66HC8	Gametogenetin	-0.58	1.5	up	-2.08	0.49
D3Z9X1	Putative uncharacterized protein ENSRNOP00000062065	-0.58	1.5	up	-2.03	0.56
B1WBS7	RGD1562135 protein	-0.57	1.5	up	-2.01	0.55
P07483	Fatty acid-binding protein, heart	0.60	1.5	down	2.17	0.48
D3ZIL6	Enoyl Coenzyme A hydratase domain containing 2	0.83	1.8	down	2.98	0.09
P62898	Cytochrome c, somatic	0.88	1.8	down	3.79	0.01
P21396	Amine oxidase [flavin-containing] A	1.27	2.4	down	5.77	8.E-07

Anexo A.11.- Lista de las péptidos con Cys que aumentan o disminuyen su abundancia en respuesta al IP en mitocondrias SSM.

Los criterios de filtrado así como el código de colores utilizado y la nomenclatura son los mismos que los que se usaron en el Anexo A.2.

Nº acceso	Proteína	Secuencia	Xp-Xq	Fold Change		Zp	FDRp
Q32PX9	Lactation elevated protein 1	ALAVC@HGPLAHYDFLIK	-0.75	1.68	up	-4.32	0.01
P35738	2-oxoisovalerate dehydrogenase subunit beta, mitochondrial	APWGC#VGHGALYHSQSPEAFFAHC#PGIK	-0.47	1.38	up	-3.08	0.26
Q920L2	Succinate dehydrogenase [ubiquinone] flavoprotein subunit, mitochondrial	AGLPC#QDLEFVQFHPTGIYGAGC#LITEGC#R	-0.58	1.50	up	-2.85	0.30
P26284	Pyruvate dehydrogenase E1 component subunit alpha, somatic form, mitochondrial	NFYGGNGIVGAQVPLGAGIALAC#K	-0.45	1.37	up	-2.63	0.33
P56571	ES1 protein homolog, mitochondrial	VVTTPAFM*C#ETELHHIHDGIGAM*VK	-0.46	1.38	up	-2.51	0.35
P45953	Very long-chain specific acyl-CoA dehydrogenase, mitochondrial	MLC#DSWC#IEAATR	-0.52	1.43	up	-2.45	0.36
Q68FY0	Cytochrome b-c1 complex subunit 1, mitochondrial	YFYDQC@PAVAGYGPIEQLSDYNR	-0.53	1.44	up	-2.45	0.37
Q09073	ADP/ATP translocase 2	GTDIM*YTGTLDC#WR	-0.50	1.41	up	-2.42	0.37
Q5XIN6	LETM1 and EF-hand domain-containing protein 1, mitochondria	DTAPVLEGLKGEEITKEEIDILSDAC#SK	-0.45	1.37	up	-2.41	0.37
D3ZTW7	ATP synthase mitochondrial F1 complex assembly factor 2 (Predicted), isoform CRA_c	TAAGTLFVHLC#SESSTVK	-0.41	1.33	up	-2.39	0.38
P13437	3-ketoacyl-CoA thiolase, mitochondrial	LC#GSGFQSIVSGC#QEIC#SK	-0.41	1.33	up	-2.37	0.40
P29147	D-beta-hydroxybutyrate dehydrogenase, mitochondrial	FGVEAFSDC#LR	-0.45	1.36	up	-2.34	0.39
P05708	Hexokinase-1	LGVEPSDVDC#VSVQHIC#TIVSFR	-0.40	1.32	up	-2.29	0.44
B2RYW9	Fumarylacetoacetate hydrolase domain-containing protein 2	VIC#VGLNYADHC#QEQNVR	-0.39	1.31	up	-2.26	0.45
B0BN52	Mitochondrial carrier homolog 2 (C. elegans)	VLQYYQEC@EKPEDLGSANVQK	-0.42	1.34	up	-2.20	0.49
Q6P6R2	Dihydrolipoyl dehydrogenase, mitochondrial	VC#HAHPTLSEAFR	-0.39	1.31	up	-2.16	0.52
Q05962	ADP/ATP translocase 1	EFNGLGDC#LTK	-0.37	1.29	up	-2.16	0.50
Q9ER34	Aconitate hydratase, mitochondrial	DVGGIVLANAC#GPC#IGQWDR	-0.38	1.30	up	-2.12	0.50
Q62651	Delta(3,5)-Delta(2,4)-dienoyl-CoA isomerase, mitochondrial	PVIAAIHGGC#IGGGVDLISAC#DIR	-0.36	1.28	up	-2.10	0.49
Q9ER34	Aconitate hydratase, mitochondrial	VGLIGSC#TNSSYEDMGR	-0.37	1.29	up	-2.08	0.49
Q5XI78	2-oxoglutarate dehydrogenase, mitochondrial	EAQKYPNAELAWC#QEEHK	-0.43	1.34	up	-2.06	0.51
Q01205	Dihydrolipoyllysine-residue succinyltransferase component of 2-oxoglutarate dehydrogenase complex, mitoch	LKEAQNTC#AMLTTFNEVDMSNIQEMR	-0.37	1.30	up	-2.04	0.50
Q09073	ADP/ATP translocase 2	GLGDC#LVK	-0.35	1.28	up	-2.01	0.52
P56574	Isocitrate dehydrogenase [NADP], mitochondrial	NILGGTVFREPIIC#K	0.36	1.28	down	2.03	0.50
P19234	NADH dehydrogenase [ubiquinone] flavoprotein 2, mitochondrial	YHIQVC#TTTPC#MLR	0.41	1.33	down	2.04	0.51
P09605	Creatine kinase S-type, mitochondrial	LGYILTC#PSNLGTGLR	0.37	1.29	down	2.08	0.49
P41565	Isocitrate dehydrogenase [NAD] subunit gamma 1, mitochondrial	NIANPTATLLASC#MMLDHLK	0.40	1.32	down	2.10	0.49
P13437	3-ketoacyl-CoA thiolase, mitochondrial	VVGYFVSGC#DPAIM*GIGPVPAITGALKK	0.44	1.36	down	2.12	0.49
P05708	Hexokinase-1	ATDC#EGHDVASLLR	0.55	1.46	down	2.14	0.50
Q64057	Alpha-aminoadipic semialdehyde dehydrogenase	STC#TINYSTALPLAQGIK	0.33	1.26	down	2.14	0.50
P85834	Elongation factor Tu, mitochondrial	GEETPVIVGSALC#ALEQR	0.40	1.32	down	2.17	0.50
P29147	D-beta-hydroxybutyrate dehydrogenase, mitochondrial	AVLVTGC#DSGFGFSLAK	0.37	1.29	down	2.26	0.46
Q32PX9	Lactation elevated protein 1	ALAVC#HGPLAHYDFLIK	0.41	1.33	down	2.34	0.40
Q66HF1	NADH-ubiquinone oxidoreductase 75 kDa subunit, mitochondrial	VVAAC@AMPVM*K	0.48	1.40	down	2.49	0.36
Q6IRH6	Slc25a3 protein	FFILC#GLGGIISC#GTTHTALVPLDLVK	0.43	1.35	down	2.59	0.33
P49432	Pyruvate dehydrogenase E1 component subunit beta, mitochondrial	PVGHC#LEAAAVLSK	0.47	1.39	down	2.59	0.34
P56571	ES1 protein homolog, mitochondrial	VVTTPAFMC@ETELHHIHDGIGAMVK	0.54	1.46	down	2.69	0.32
D3ZZN3	RCG37494	VAIYM*PVSPLAVAAM*LAC#AR	0.68	1.60	down	2.76	0.27
Q68FY0	Cytochrome b-c1 complex subunit 1, mitochondrial	LC@TSATESEVTR	0.53	1.44	down	2.82	0.28
P15999	ATP synthase subunit alpha, mitochondrial	LYC#IYVAIGQK	0.50	1.41	down	2.85	0.30
P56574	Isocitrate dehydrogenase [NADP], mitochondrial	C@ATITPDEAR	0.59	1.51	down	2.89	0.34
P00507	Aspartate aminotransferase, mitochondrial	NLDKEYLPIGGLADFC#K	0.59	1.51	down	3.13	0.26
P35738	2-oxoisovalerate dehydrogenase subunit beta, mitochondrial	GLLLSC#IEDKNPC#IFFEPK	0.52	1.43	down	3.23	0.21
P45953	Very long-chain specific acyl-CoA dehydrogenase, mitochondrial	LFVALQGC#MDK	0.62	1.54	down	3.27	0.19
Q9ER34	Aconitate hydratase, mitochondrial	VGLIGSC@TNSSYEDM*GR	0.77	1.70	down	3.64	0.09
Q5XIN6	LETM1 and EF-hand domain-containing protein 1, mitochondrial	LFEDELTLDNLTRPQLVALC#K	1.38	2.60	down	7.42	2.E-10
Q561S0	NADH dehydrogenase [ubiquinone] 1 alpha subcomplex subunit 10, mitochondrial	MSEIC#EVLVYSSWEAEDSTK	2.75	6.75	down	14.26	0.E+00

Anexo A.12.- Lista de las proteínas que aumentan o disminuyen su abundancia en respuesta al IP en mitocondrias SSM.

Los criterios de filtrado así como el código de colores utilizado y la nomenclatura son los mismos que los que se usaron en el Anexo A.2.

Nº acceso	Proteína	Xq-X	Fold Change		Zq	FDRq
P23928	Alpha-crystallin B	-1.36	2.57	up	-5.47	2.E-06
Q64591	2,4-dienoyl-CoA reductase, mitochondrial	-0.77	1.70	up	-4.98	3.E-05
P85108	Tubulin beta-2A chain	-1.03	2.04	up	-4.01	2.E-03
Q5U3Z3	Isochorismatase domain-containing protein 2, mitochondrial	-0.79	1.73	up	-3.97	2.E-03
B0BNC0	Ckmt2 protein	-0.52	1.44	up	-2.92	0.06
O35831	Cell division protein kinase 17	-0.69	1.61	up	-2.89	0.06
Q7TQ85	Ac1164	-0.52	1.43	up	-2.87	0.06
Q5XHZ0	Heat shock protein 75 kDa, mitochondrial	-0.56	1.48	up	-2.70	0.10
D3ZI58	Putative uncharacterized protein ENSRNOP00000032974	-0.66	1.58	up	-2.58	0.13
P29147	D-beta-hydroxybutyrate dehydrogenase, mitochondrial	-0.48	1.39	up	-2.45	0.15
O08828	Axonemal dynein heavy chain	0.61	1.53	down	2.48	0.15
P04797	Glyceraldehyde-3-phosphate dehydrogenase	0.51	1.43	down	2.49	0.15
P18163	Long-chain-fatty-acid--CoA ligase 1	0.38	1.30	down	2.57	0.12
Q8C292	Lysyl-tRNA synthetase	0.68	1.61	down	2.70	0.09
B2FDE4	EF-hand calcium binding domain 3	0.68	1.60	down	2.71	0.10
B0BNM1	Apoa1bp protein	0.78	1.72	down	2.96	0.06
D4A311	NADH dehydrogenase (Ubiquinone) 1 alpha subcomplex, 8	0.53	1.44	down	2.98	0.05
P62630	Elongation factor 1-alpha 1	0.58	1.49	down	3.21	0.03
P56391	Cytochrome c oxidase subunit 6B1	0.95	1.94	down	3.70	4.E-03
Q792Z1	MCG140784	1.03	2.04	down	4.30	4.E-04
P16409	Myosin light chain	1.03	2.04	down	4.85	4.E-05
P60711	Actin, cytoplasmic	1.27	2.42	down	4.89	3.E-05
P12847	Myosin-3	1.33	2.51	down	5.22	8.E-06
P08733	Myosin regulatory light chain 2, ventricular/cardiac muscle isoform	1.40	2.64	down	5.90	2.E-07
P48675	Desmin	1.73	3.33	down	6.76	9.E-10
P0C169	Histone H2A type 1	1.72	3.30	down	6.90	5.E-10
P97611	Granzyme J	1.41	2.66	down	7.35	2.E-11
P62738	Actin, aortic smooth muscle	1.33	2.52	down	7.60	9.E-12
P02563	Myosin-6	1.32	2.49	down	8.39	0.E+00

Statistical Model to Analyze Quantitative Proteomics Data Obtained by $^{18}O/^{16}O$ Labeling and Linear Ion Trap Mass Spectrometry

APPLICATION TO THE STUDY OF VASCULAR ENDOTHELIAL GROWTH FACTOR-INDUCED ANGIOGENESIS IN ENDOTHELIAL CELLS*[S]

Inmaculada Jorge‡§, Pedro Navarro‡§, Pablo Martínez-Acedo‡§¶, Estefanía Núñez‡, Horacio Serrano‡, Arántzazu Alfranca‖, Juan Miguel Redondo‖, and Jesús Vázquez‡**

Statistical models for the analysis of protein expression changes by stable isotope labeling are still poorly developed, particularly for data obtained by $^{16}O/^{18}O$ labeling. Besides large scale test experiments to validate the null hypothesis are lacking. Although the study of mechanisms underlying biological actions promoted by vascular endothelial growth factor (VEGF) on endothelial cells is of considerable interest, quantitative proteomics studies on this subject are scarce and have been performed after exposing cells to the factor for long periods of time. In this work we present the largest quantitative proteomics study to date on the short term effects of VEGF on human umbilical vein endothelial cells by $^{18}O/^{16}O$ labeling. Current statistical models based on normality and variance homogeneity were found unsuitable to describe the null hypothesis in a large scale test experiment performed on these cells, producing false expression changes. A random effects model was developed including four different sources of variance at the spectrum-fitting, scan, peptide, and protein levels. With the new model the number of outliers at scan and peptide levels was negligible in three large scale experiments, and only one false protein expression change was observed in the test experiment among more than 1000 proteins. The new model allowed the detection of significant protein expression changes upon VEGF stimulation for 4 and 8 h. The consistency of the changes observed at 4 h was confirmed by a replica at a smaller scale and further validated by Western blot analysis of some proteins. Most of the observed changes have not been described previously and are consistent with a pattern of protein expression that dynamically changes over time following the evolution of the angiogenic response. With this statistical model the ^{18}O labeling approach emerges as a very promising and robust alternative to perform quantitative proteomics studies at a depth of several thousand proteins. ***Molecular & Cellular Proteomics 8:1130–1149, 2009.***

From the ‡Centro de Biología Molecular Severo Ochoa, E-28049 Madrid, Spain and ‖Centro Nacional de Investigaciones Cardiovasculares, E-28029 Madrid, Spain

Received, June 11, 2008, and in revised form, January 14, 2009
Published, MCP Papers in Press, January 29, 2009, DOI 10.1074/mcp.M800260-MCP200

Quantitative proteomics, which may be defined as the study of global changes in the expression level of proteins, is a field that has experienced great development in the last years (1, 2). In these studies two or more protein extracts from tissues, cells, or body fluids in changing environmental or physiological conditions are assayed to determine the presence of proteins exhibiting an alteration in their expression levels. Proteins have traditionally been separated, visualized, and subjected to relative quantification by two-dimensional gel electrophoresis and protein poststaining (3, 4) or prelabeling (5, 6). The spots showing quantitative differences were then excised and proteolyzed, and the resulting peptides were used to identify the proteins by MS (7).

Alternative strategies to the gel-based approaches have emerged in recent years; in these techniques, also called "shotgun proteomics," protein extracts are digested without prior separation, and the complex peptide mixture is separated by multidimensional chromatography coupled to MS/MS analysis (8). The MS/MS spectra are then used for automated identification of protein components in a database. The development of stable isotope labeling protocols has allowed these techniques to produce relative quantitative information (1) and has considerably boosted the field in the last years. Stable isotopic labeling can be achieved by chemical (9, 10), metabolic (11), or enzymatic techniques (12–14). Enzymatic labeling with ^{18}O tags is usually performed after protein digestion by incubating the resulting peptides with a proper endoprotease, usually trypsin (15). The protease catalyzes the incorporation of two ^{18}O atoms at the carboxyl-terminal end of peptides and thus increases their mass by 4 Da. The labeled sample is then combined with the non-labeled one, and the two samples are concurrently processed and analyzed so that peptides are detected in MS as doublets, and the relative intensity of the two signals may be used to estimate the relative concentration of the corresponding proteins in the original samples (12). Because the isotopic patterns of the two peptide forms usually overlap, these analyses have routinely been done by using medium or high resolution MS analyzers. Ion traps can produce medium resolution mass spectra (or "ZoomScans") of selected ions over

a limited *m/z* range, and in our laboratory we have recently demonstrated that using these scanning modes and taking advantage of the high scanning speed of the linear ion trap it is possible to make accurate quantitative measurements without compromising the ability of this machine to perform high throughput peptide identification (16). In a recent refinement of the original technique and on the basis of a kinetic exchange model, quantification was performed by fitting the isotopic envelope composed by the two peptide forms to a theoretical curve, allowing a simultaneous calculation of the relative proportion of peptides in the original samples and of the specific labeling efficiency of each one of the peptide pairs (14). This method eliminates artifacts produced by incomplete oxygen exchange in subsets of peptides that have a low labeling efficiency and may be considered indicative of false expression changes and has been shown to be suitable for the quantification of whole proteomes (14).

Because of the large amounts of differential expression data gathered in these studies, one of the bottlenecks of current quantitative proteomics is determining whether the observed protein expression changes are correct or produced artifactually. Although changes in protein expression may be considered significant when above a specified threshold, it is clearly preferable to use more rigorous statistical methods to establish statistical significance. In this regard, statistics applied to quantitative proteomics are considerably less developed in comparison with those currently applied in the microarray field. The multiple testing problem and the control of the false discovery rate (FDR)[1] or the *q* value (17) on microarray data have been the subject of detailed discussion. A more recent controversy has centered on the validity of the assumption that *p* values generated by commonly used microarray statistics follow a uniform distribution (18). In clear contrast, published studies addressing statistical issues in the quantitative proteomics field are scarce. The majority of published quantitative proteomics studies have used the established two-dimensional gel electrophoresis approach and use the *p* value to identify protein species showing significant expression changes. The need to use robust experimental designs (19) and to control for FDR in differential electrophoresis studies has been claimed only recently (20). The majority of published DIGE studies use the Student's *t* test to identify significant changes in expression (20); however, this test assumes independent sampling, normality of the data, and homogeneity of the variance, and the validity of these assumptions has not been demonstrated in a general context. The situation is not better with expression studies obtained using stable isotope labeling approaches. Although a great effort has been devoted to the development of bioinformatics tools for automated analysis of MS data and calculation of peptide ratios for each one of the several isotope labeling strategies currently available (21, 22), existing analytical methods for the statistical determination of significant expression changes are scarce (for a review, see Ref. 22). Almost all existing methods have in common that statistical significance is calculated assuming an underlying normal distribution for the null hypothesis from which Student's *t* test (23, 24) or *p* values (25) are obtained. However, the general validity of this assumption has not been analyzed in detail. Only recently have studies begun to address the reliability and sources of errors in iTRAQ analysis (26, 27), and a profile likelihood algorithm has been used to estimate confidence intervals of protein abundance ratios determined by $^{14}N/^{15}N$ metabolic labeling (28, 29); however, no specific statistical models have still been proposed to deal with data produced by enzymatic $^{16}O/^{18}O$ labeling. Particularly large scale test studies aimed to establish the distribution of the null hypothesis, similar to those performed with microarray data (18), are lacking.

Angiogenesis, the formation of new blood vessels from a preexisting vascular bed, is determinant for the setup and progress of relevant pathophysiological processes: it is essential in embryo development, the menstrual cycle, wound healing, chronic inflammatory diseases, tumor growth, metastasis formation, and other processes. Angiogenesis comprises a series of finely regulated steps in which endothelial cells play a crucial role. The positive balance between pro- and antiangiogenic factors promotes the acquisition of a proangiogenic phenotype by endothelial cells, therefore triggering the formation of new vessels. Among positive regulators of angiogenesis, members of the vascular endothelial growth factor (VEGF) family are the best characterized. These factors regulate biological functions of endothelial cells involved in new vessel formation, proliferation, survival, migration, extracellular matrix remodeling, and other processes. Endothelial responses to VEGF are elicited through tyrosine kinase receptors among which VEGFR-2 (KDR; Flk-1) is considered the principal mediator of the proangiogenic activity. VEGF binding to this receptor gives rise to the activation of signal transduction routes (30), which ultimately lead to either the transcription of target genes or the posttranslational modification of presynthesized proteins as in the case of endothelial NO synthase (31). Antiangiogenic therapies that interfere directly or indirectly with VEGF production and the mechanisms responsible for its biological activity have already been successfully used in patients (32). Hence the study of mechanisms underlying biological actions promoted by VEGF in endothelial cells may be of great interest for the treatment of angiogenesis-dependent processes. However, to date only a few studies have been performed to analyze the effect of VEGF on endothelial cells by differential expression approaches, mainly by microarray techniques (33–35). Only two

[1] The abbreviations used are: FDR, false discovery rate; HUVEC, human umbilical vein endothelial cell; VEGF, vascular endothelial growth factor; SCX, strong cation exchange; ANXA1, annexin A1; RCN1, reticulocalbin; TB, β-tubulin; iTRAQ, isobaric tags for relative and absolute quantitation; RP, reverse phase; Hsp, heat shock protein.

quantitative proteomics studies have been performed (36, 37); these studies have been done by using differential gel electrophoresis and after exposure of human umbilical vein endothelial cells (HUVECs) to VEGF for considerably long times (24 h or more). Shotgun approaches in conjunction with ICAT labeling have also been applied to study the effect of 24-h incubation of the proangiogenic factor sokotrasterol sulfate on HUVECs (38). These results, obtained after prolonged exposure to the stimuli, might be reflecting variations in protein expression due to indirect effects of the treatments used. Therefore, studies performed at shorter times of treatment would be necessary to minimize the presence of indirect changes induced by VEGF stimulation.

In this work we performed a large scale test experiment using the $^{16}O/^{18}O$ labeling technique on the proteome of HUVECs and developed a random effects statistical model for the null hypothesis that verifies the local assumptions of normality and variance homogeneity. We further demonstrate that with this model it is possible to detect significant and consistent protein expression changes in response to two short time (4- and 8-h) incubations with VEGF. These times were chosen with the idea of detecting effects more directly related to VEGF and to further analyze the dependence of the expression changes with the incubation time. The majority of the changes observed in this work have not been described previously, even using microarray approaches. The detected changes are consistent with a pattern of protein expression that dynamically changes over time following the evolution of the angiogenic response.

EXPERIMENTAL PROCEDURES

Cell Culture and Protein Extraction—HUVECs were isolated from human umbilical cord veins. The vein was cannulated and incubated with 0.1% collagenase (Roche Applied Science). Following removal of the collagenase, cells were pooled and established as primary cultures in medium 199 (BioWhittaker, Walkersville, MD) containing 20% FCS (Invitrogen). HUVECs were grown on dishes coated with 0.5% gelatin (Sigma) in medium 199 supplemented with 20% FCS, 50 μg/ml bovine brain extract, and 100 μg/ml heparin (Sigma). For VEGF treatment, cells were starved overnight in 0.5% FCS and then incubated for different times with 50 ng/ml VEGF (Peprotech, London, UK).

HUVECs (1.5×10^6 cells) were lysed at 4 °C in lysis buffer (50 mM Tris-HCl, pH 7.5, 400 mM NaCl, 1 mM EDTA, 2.5 mM EGTA, 1% Triton X-100, 1 mM DTT, 10 mM β-glycerophosphate, 1 mM sodium vanadate, 1 mM NaF, 1 mM PMSF, 1 μg/ml aprotinin, 1 μg/ml leupeptin, 1 μg/ml pepstatin). For Western blot experiments, proteins (8 μg/lane) were resolved by SDS-PAGE and transferred to nitrocellulose membranes. The membranes were then probed with antibodies anti-annexin A1 (Santa Cruz Biotechnology, Santa Cruz, CA), anti-triosephosphate isomerase (Abcam, Cambridge, UK), anti-reticulocalbin (Bethyl, Montgomery, TX), and anti-β-tubulin (Sigma). Immunoreactive bands were detected by an enhanced chemiluminescent substrate (ECL, GE Healthcare).

In-solution Digestion—Protein concentration in the samples was measured using the Bradford protein assay (39). Samples were desalted and buffer-exchanged on a prepacked PD-10 column (GE Healthcare). After denaturation of proteins with 9 M urea, disulfide bonds from cysteinyl residues were reduced with 10 mM DTT for 1 h at 37 °C, and then thiol groups were alkylated with 50 mM iodoacetamide for 1 h at room temperature in darkness. Samples were diluted to reduce urea concentration below 1.4 M and digested using sequencing grade trypsin (Promega, Madison, WI) overnight at 37 °C using a 1:20 (w/w) trypsin/protein ratio (40). Digestion was stopped by the addition of 1% TFA and by trypsin denaturation by reduction/alkylation as described above.

Trypsin-catalyzed ^{18}O Labeling—Samples containing tryptic peptides were desalted using Oasis HLB (hydrophilic-lipophilic balance) Extraction cartridges (Waters, Milford, MA), dried down, and subjected to labeling with either $H_2{}^{16}O$ or $H_2{}^{18}O$ (95%; Isotec, Miamisburg, OH) in 100 mM ammonium acetate, pH 6.0, 20% CH_3CN in the presence of immobilized trypsin (Pierce) (41) at a 1:200 (v/w) trypsin/protein ratio. Peptides from the control samples were labeled with ^{16}O, and peptides from the VEGF-treated samples were labeled with ^{18}O. Labeling was stopped by addition of 5 mM ammonium formate, pH 3.0. Labeled samples were reduced and alkylated as indicated above, and trypsin beads were removed using a physical filter. The two labeled samples were then mixed and dried down.

Peptide Fractionation by Strong Cation Exchange Liquid Chromatography—Peptides were desalted onto a Vydac C_{18} RP column (4.6 × 250 mm) using a Beckman Gold HPLC system by one-step elution with 40% CH_3CN containing 5 mM ammonium formate, pH 3.0. Clean peptide pools were fractionated by strong cation exchange (SCX) liquid chromatography using a 2.1 × 200-mm BioBasic SCX column (Thermo Electron, Cheshire, UK) operating at 200 μl/min. Peptides were eluted using the following gradient: 0% mobile phase B for 4 min, 0–10% B in 30 min, 10–40% B in 40 min, 40–100% B in 2 min, and 100% B for 8 min (solvent A: 5 mM ammonium formate, pH 3.0, 25% CH_3CN; solvent B: 500 mM ammonium formate, pH 3.0, 25% CH_3CN) (42). Peptides were collected in 1-min fractions.

LC-MS/MS Analysis and Peptide Identification—Each SCX fraction was analyzed by LC-MS/MS using a Surveyor LC system coupled to a linear ion trap mass spectrometer (model LTQ, Thermo Finnigan, San Jose, CA) as described previously with minor modifications (43, 44). Peptides were concentrated and desalted onto an RP precolumn (0.32 × 30 mm, BioBasic C_{18}, Thermo Electron) and eluted on line onto an analytical RP column (0.18 × 150 mm, BioBasic C_{18}, Thermo Electron) operating at 2 μl/min and using the following gradient: 5% B for 15 min, 5–14% B in 15 min, 14–30% B in 155 min, 30–95% B in 7 min, and 95% B for 3 min (solvent A: 0.1% formic acid; solvent B: 0.1% formic acid, 80% CH_3CN). The LTQ was operated in a data-dependent ZoomScan and MS/MS switching mode (45, 46). Zoom target parameters, number of microscans, normalized collision energy, and dynamic exclusion parameters were as described in Lopez-Ferrer *et al.* (16).

Protein identification was carried out as described previously (43). The MS/MS raw files acquired on the mass spectrometer were searched against the human Swiss-Prot database using the SEQUEST algorithm (Bioworks 3.2 package, Thermo Finnigan). The same collection of MS/MS spectra were searched against a pseudo-inverted database constructed from the same database. SEQUEST searches were performed allowing both optional (methionine oxidation and lysine and arginine modification of +4 Da) and fixed modifications (cysteine carboxamidomethylation). Determination of FDR as a measure of statistical significance of peptide identification was performed by using the probability ratio method (47).

Peptide Quantification and Statistics Analysis—Peptide quantification from ZoomScan spectra was performed as described previously (14, 16) using QuiXoT, a program written in C# in our laboratory, that automatically opens the raw files and peptide identification results and sorts out the ZoomScan spectra corresponding to identified peptides (48). The quantification in QuiXoT is performed using an

algorithm described previously (14). Only ZoomScan spectra corresponding to peptide matches with a false discovery rate lower than 5% were used for quantification. ZoomScan spectra were fitted to a theoretical curve so that the best fit parameters allow a simultaneous determination of the peptide concentration in the two samples (*A* and *B*, respectively, expressed in units of area) and of the labeling efficiency *f* (14). The proportion of non-labeled and mono- and dilabeled peptide in the labeled sample (B_0, B_1, and B_2, respectively) can be calculated from these parameters as described previously (14). The theoretical curve used to fit the spectra is a mixed Gaussian/double exponential distribution (14), and their parameters were not constrained during the fitting process. The best fit values of the parameters σ (scale parameter, which determines the half-width of the peak) and β (relative proportion of double exponential component) and of the labeling efficiency *f* were used to eliminate unreliable quantifications. The typical value of σ for the LTQ under the scanning conditions used in this work (16) was around 0.085 Da; an increase in this value indicated that the curve was not consistently fitting an isotopic peak. Similarly values of β or *f* above one were indicative either that the curve cannot be fitted by the theoretical curve or that the relative isotopic peak proportion could not be explained by the superimposition of three peptide components (unlabeled, mono-, and dilabeled), respectively. In the initial filtering step (see Table I) ZoomScans were automatically considered as unreliable and were eliminated when the best fit parameters verified any of the following conditions: $\sigma > 0.12$, $\beta > 1.1$, and $f > 1.2$.

Calculation of Fitting Weights—As described above, ZoomScan spectra were fitted to a theoretical function that depends on peptide concentration in the two samples. Expressing relative peptide concentrations in a base 2 logarithmic scale, if *A* and *B* are the peptide amounts expressed in units of area in the control and treated samples, respectively, the result of a quantification made in scan *s* coming from peptide *p* derived from protein *q* is expressed as $x_{qps} = \log_2(A/B)$. The fitting weight of the scan is calculated using the following formula,

$$v_{qps} = \frac{T^2}{\mathrm{MSDc} + \mathrm{MSDl}} \quad \text{(Eq. 1)}$$

where *T* is a measure of peptide concentration in units of area, MSDc is the mean squared deviation between the experimental and theoretical ZoomScan spectra around a central window spanning the cluster of isotopic peaks, and MSDl is the mean squared deviation around a lateral window at the left or the right of the cluster. If $A + B_0 > B_1 + B_2$ then the lateral window is taken at the left, and $T = A$; otherwise the lateral window is taken at the right, and $T = B$. This procedure ensures that the fitting weight is proportional to the squared value of the peptide concentration and inversely proportional to the variance of the theoretical function; besides it ensures that the weight does not suffer an abrupt decrease when there are large expression changes and also takes into account the presence of adjacent signals when they may artifactually interfere with the quantification. The variance in the $\log_2$ ratio values is calculated from the fitting weight using the following formula: $\sigma^2_{\mathrm{LR}} = k/v_{qps}$ where *k* is a constant that for the LTQ and the scanning conditions used in this work has the value 0.17 (see supplemental information).

Calculation of Averaged Means and Variances at the Scan, Peptide, and Protein Levels—When the peptide amounts in the two samples are identical, $x_{qps} = 0$. Experimental deviations from this value are assumed to come from a systematic error, μ, in the ratio in which the two samples are mixed; from deviations of protein concentration due to biological variability and errors committed during the process of preparation of the protein extracts, ρ_q; from deviations in peptide concentration due to peptide preparation from the protein extracts, β_{qp}; and from errors committed during the quantification of the peptide pair from the scan, ξ_{qps}, giving the following equation.

$$x_{qps} = \mu + \rho_{\mathrm{q}} + \beta_{\mathrm{qp}} + \xi_{qps} \quad \text{(Eq. 2)}$$

Let us assume that β_{qp} and ρ_q are normally distributed, *i.e.* $\beta_{qp} \sim N(0,\sigma^2_{\mathrm{P}})$ and $\rho_q \sim N(0,\sigma^2_{\mathrm{Q}})$, and that the peptide and protein variances, σ^2_{P} and σ^2_{Q}, respectively, are constant. Let us also assume that ξ_{qps} is normally distributed according to $\xi_{qps} \sim \mathrm{N}(0,\sigma^2_{\mathrm{S}} + k/v_{qps})$ where σ^2_{S} is the scan variance, v_{qps} is the fitting weight, and *k* is the constant described in the previous section.

The $\log_2$ ratio value associated to each peptide is calculated as a weighted average of the scans used to quantify the peptide, and the value associated to each protein is similarly the weighted average of its peptides. Besides a grand mean is calculated as a weighted average of the protein values. The statistical weight associated to each scan, peptide, and protein is the inverse of their local variances, whereas the inverse of the variances of the averaged values is the sum of the inverses of variances of the values used to calculate the average. Hence the statistical weights are given by the following.

$$w_{qps} = \frac{1}{\frac{k}{v_{qps}} + \sigma^2_{\mathrm{S}}} \quad \text{(Eq. 3)}$$

$$w_{qp} = \frac{1}{\frac{1}{\sum_s w_{qps}} + \sigma^2_{\mathrm{P}}} \quad \text{(Eq. 4)}$$

$$w_q = \frac{1}{\frac{1}{\sum_p w_{qp}} + \sigma^2_{\mathrm{Q}}} \quad \text{(Eq. 5)}$$

And the peptide and protein averages and the grand mean, which is an estimate of μ, are given, respectively, by the following.

$$x_{qp} = \frac{\sum_s w_{qps} x_{qps}}{\sum_s w_{qps}} \quad \text{(Eq. 6)}$$

$$x_q = \frac{\sum_p w_{qp} x_{pq}}{\sum_p w_{qp}} \quad \text{(Eq. 7)}$$

$$x = \frac{\sum_q w_q x_q}{\sum_q w_q} \quad \text{(Eq. 8)}$$

To take into account the systematic error μ of the experiment, protein ratios are normalized by subtracting the grand mean. The algorithm used to estimate the values of σ^2_{S}, σ^2_{P}, and σ^2_{Q} as well as their associated confidence intervals is described in the supplemental information.

As commented above, the local variances of the scan determinations and of the peptide and protein averages are the inverse of the scan weights in Equations 3–5, respectively. These variances may be used to determine whether a particular value significantly deviates from average more than expected according to the assumed normal distribution. Defining $P(\mu,\sigma^2,x_t)$ as the two-tailed probability that the

TABLE I
Identification and quantification statistics of the three large scale experiments

	Test	VEGF	
		4 h	8 h
SCX fractions[a]	71	64	92
MS/MS spectra obtained	142,585	134,590	149,713
MS/MS spectra yielding a peptide match[b]	13,701	9,171	12,196
Number of unique peptides identified	4,878	4,806	3,876
Number of unique proteins identified	2,461	1,982	2,085
Scans remaining after initial filtering[c]	9,786	7,315	8,145
Scans used for the analysis[d]	7,640	5,097	4,391
Number of unique peptides quantified	2,271	2,556	1,218
Number of unique proteins quantified	1,246	1,278	890
Scan variance (σ_S^2) (95% C.I.[e])	0.018 (0.016–0.020)	0.024 (0.022–0.026)	0.031 (0.028–0.034)
Peptide variance (σ_P^2) (95% C.I.)	0.021 (0.014–0.028)	0.019 (0.014–0.026)	0.014 (0.006–0.023)
Protein variance (σ_Q^2) (95% C.I.)	0.0007 (0–0.009)	0.004 (0–0.012)	0.003 (0–0.011)
Significant expression changes ($FDR_q \leq 5\%$)	1	26	37
Significant expression changes ($FDR_q \leq 10\%$)	1	32	46

[a] Fractions where peptides are detected.
[b] With an FDR of identification equal or lower than 5%, calculated using the probability ratio method (see "Experimental Procedures").
[c] "Scans" refer to ZoomScan spectra. Initial filtering was made using the following criteria: $\sigma < 0.12$, $\beta < 1.1$, $f < 1.2$, and $v_{qps} > 3.1$.
[d] Remaining after second filtering: elimination of scans from C-terminal peptides and peptides containing methionine residues and missed cleavage sites, and subpeptides from the latter.
[e] C.I., confidence interval.

value x_t taken from sample t deviates from a normal distribution with mean μ and variance σ^2, the probabilities that a given scan, peptide, or protein measurement is an outlier with respect to the corresponding average may be estimated, respectively, by the following.

$$p_{qps} = P(x_{qp}, w_{qps}^{-1}, x_{qps}) \quad \text{(Eq. 9)}$$

$$p_{qp} = P(x_q, w_{qp}^{-1}, x_{qp}) \quad \text{(Eq. 10)}$$

$$p_q = P(x, w_q^{-1}, x_q) \quad \text{(Eq. 11)}$$

Detection of the presence of outliers is made by using multiple hypothesis testing and controlling for the FDR (49–52), defined as the proportion of values expected to deviate by chance alone within the population of observed outliers. Because the number of expected random changes is the product of the probability, as defined in Equations 9–11, multiplied by the total number of determinations at each level, the FDR at each one of the three levels is calculated by

$$FDR_{qps} = \frac{p_{qps} \cdot NS}{O(p_{qps})} \quad \text{(Eq. 12)}$$

$$FDR_{qp} = \frac{p_{qp} \cdot NP}{O(p_{qp})} \quad \text{(Eq. 13)}$$

$$FDR_q = \frac{p_q \cdot NQ}{O(p_q)} \quad \text{(Eq. 14)}$$

where NS, NP, and NQ are the total number of scans, peptides, and proteins, respectively, and $O(p)$ is the observed number of values detected in each population with a probability equal to or less than p.

RESULTS

Strategy for Quantitative Proteomics by $^{16}O/^{18}O$ Labeling and Analysis by Linear Ion Trap Mass Spectrometry—In this work, ^{18}O-based quantitative proteomics analyses were performed to determine protein expression changes induced by the proangiogenic factor VEGF in HUVECs. For this purpose, we performed three large scale experiments using 1 mg of total protein extracts from untreated and VEGF-treated cells. In the two first experiments the cells were incubated in the presence of VEGF for 4 and 8 h, respectively. As a positive control of VEGF stimulation, cells were routinely checked for VEGF-induced increase in COX-2 expression and ERK-1,2 activation by Western blot analysis of these cell extracts (not shown) (53). In the third experiment two identical aliquots from a total HUVEC protein extract containing 1 mg of protein each were compared; this large scale control experiment was used to test for the null hypothesis and to study the robustness of the statistical model used to interpret the quantitative data. Finally a replica of the 4-h VEGF stimulation experiment was also performed at a smaller scale using 100 μg of each HUVEC protein extract.

The protein extracts were trypsin-digested in solution, and the resulting peptides were labeled postdigestion with either ^{16}O or ^{18}O in the presence of trypsin. The control and stimulated samples were then mixed and separated by SCX chromatography. Each fraction was analyzed by RP HPLC on line with an LTQ linear ion trap mass spectrometer using large gradients of 170 min; hence each one of the experiments took several weeks to complete. As described in a previous work (16), the LTQ was programmed to perform a ZoomScan spectrum and then an MS/MS spectrum over the most intense ions detected; the first scan was used to quantify the $^{16}O/^{18}O$-labeled peptide pair, and the second scan was used to identify the peptide in a human database. About 10,000 MS/MS spectra were assigned to peptide sequences at an FDR of 5% using the probability ratio method (47), corresponding to around 4000 unique peptides and 2000 unique proteins in each one of the three large scale experiments (Table I). A typical distribution of identified peptides and proteins along the SCX fractions is illustrated in Fig. 1*A*. Proteins identified

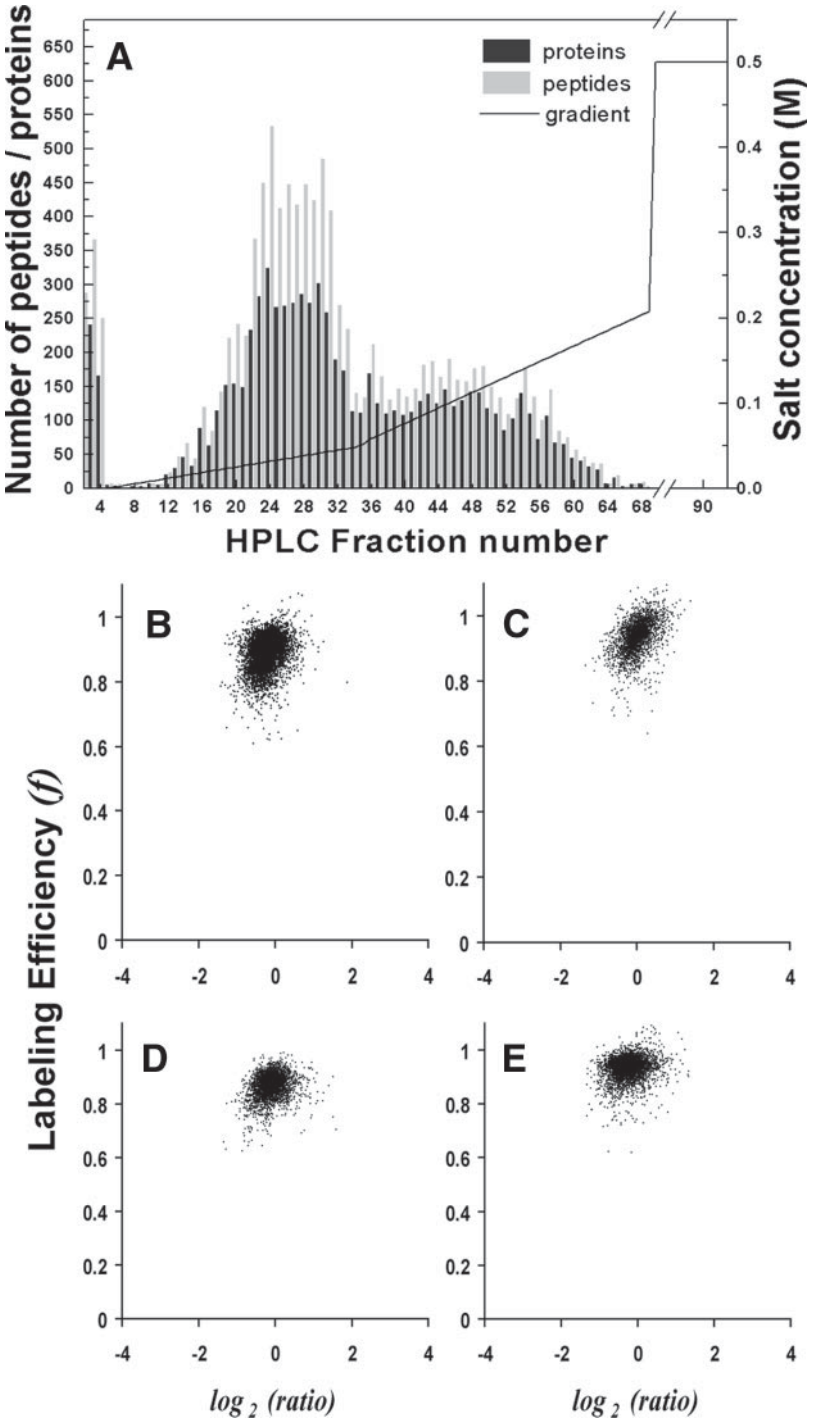

FIG. 1. **Peptide fractionation profile by HPLC-SCX chromatography and analysis of labeling efficiencies.** *A*, peptide and protein yields in the different fractions in the 4-h VEGF incubation experiment. *B–E*, distribution of labeling efficiencies as a function of $\log_2$ ratios in the test experiment (*B*), small scale 4-h VEGF incubation experiment (*C*), and the two large scale 4- and 8-h VEGF incubation experiments (*D* and *E*, respectively).

in these experiments showed a considerable but not complete overlap (not shown), and combining the four experiments a total of 3878 unique proteins could be identified in this study.

Quantification was performed on the ZoomScan spectra corresponding to identified peptides only using a method previously developed in our laboratory that allowed control of labeling efficiency of each one of the peptides (14). In this method ZoomScan spectra were fitted to a theoretical curve, and the peptide concentration (in units of area) in the two samples and the labeling efficiency were determined simultaneously (14). As explained under "Experimental Procedures," the best fit parameters were used as an initial criterion to automatically filter out unreliable quantifications. As indicated in Table I, in this initial filtering step about 20% of the scans corresponding to identified peptides were considered as un-

reliable. Scans corresponding to peptides not containing a basic residue in the carboxyl-terminal position, corresponding to peptides located at the carboxyl-terminal end of proteins, were also eliminated at this initial filtering step; these scans were present in a very low proportion with respect to the total number of spectra.

Monitoring of labeling efficiency at the individual peptide level was critical to achieve trustable quantification results in these large scale experiments. In initial attempts using previously published protocols (14, 16) we observed a slow but significant $^{16}O/^{18}O$ back-exchange over the time needed to analyze all SCX fractions. This phenomenon was not originally observed when performing shorter experiments. It was necessary to improve labeling conditions until peptides remained stably labeled even after being stored for several months (not shown). In our hands it was critical to achieve a complete inactivation of residual trypsin activity, which was in part responsible for the slow back-exchange as observed by other authors (54). This was efficiently accomplished by using trypsin covalently bound to cross-linked agarose beads, which are eliminated by filtration, and by subjecting the filtered material to reduction and alkylation. Besides acidic hydrolysis of labeled peptides (54) was carefully avoided by maintaining pH at 3.0. Under these conditions all the peptides remained effectively labeled, having a labeling efficiency higher than 0.8 in all cases as illustrated in Fig. 1, *B–E*.

Analysis of the Null Hypothesis—To analyze the null hypothesis we studied the distribution of $\log_2$ ratios obtained in the large scale test experiment where a proteome was compared against itself. We observed that peptides containing missed cleavage sites or oxidized methionine residues tended to deviate frequently from the expected 1:1 ratio, suggesting that these peptides did not reliably reflect protein concentration. To avoid these potential artifacts from altering the distribution of data under the null hypothesis, a second filtering step was performed, eliminating peptides that were partially digested or peptides containing oxidized methionines and also subpeptides belonging to the former and peptides containing non-oxidized methionine residues (Table I); the behavior of these peptides was analyzed later in more detail (see below). Partially digested peptides were assumed to be those containing at least one missed cleavage site that did not contain a proline residue after the arginine or lysine residues. The distribution of $\log_2$ ratio values of filtered data is presented as a frequency histogram in Fig. 2*A*. As shown, the data were symmetrically distributed and had a Gaussian-like shape. The presence of outliers was inspected by fitting the histogram to a normal distribution and counting how many peptide pairs had a ratio that deviated from the mean value at a $p < 0.05$ confidence level. Using this commonly used criterion, more than 200 peptides were detected as having significant expression changes, corresponding to 72 proteins. The number of significantly altered proteins decreased when the FDR was used as a criterion; thus, more than 40 peptides, corresponding to 20 proteins, were detected as outliers at a 5% FDR.

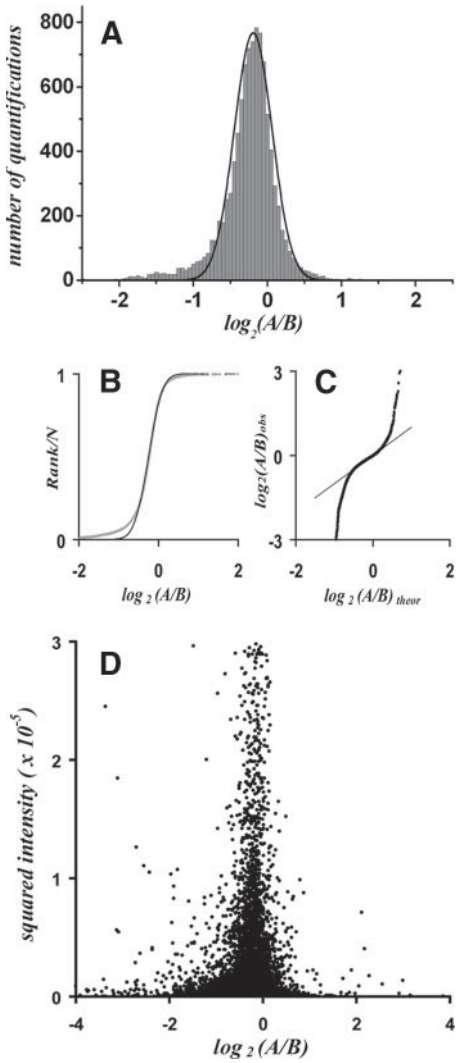

FIG. 2. **Analysis of the null hypothesis by using a normal distribution.** *A*, frequency histogram of $\log_2$ ratios in the test experiment. *B*, cumulative frequency plot (*gray points*) showing the best fit obtained by using a normal distribution (*black line*). *C*, normal probability plot (the *thin line* represents the results expected for a normal distribution). *D*, distribution of squared peak intensities as a function of $\log_2$ ratio.

As these results were unacceptable because application of these criteria to the real experiments would have resulted in a large number of false expression changes, we analyzed in more detail whether the normal distribution was a good model for this kind of data. For this end, a cumulative normalized frequency plot was constructed and fitted to the theoretical curve corresponding to a Gaussian function; as shown, clear deviations were evident between the theoretical curve and the experimental data points (Fig. 2*B*). Besides the data were analyzed using a normal probability plot (Fig. 2*C*); in this kind of plot the ordered observations are represented against the inverse of the standard normal cumulative and

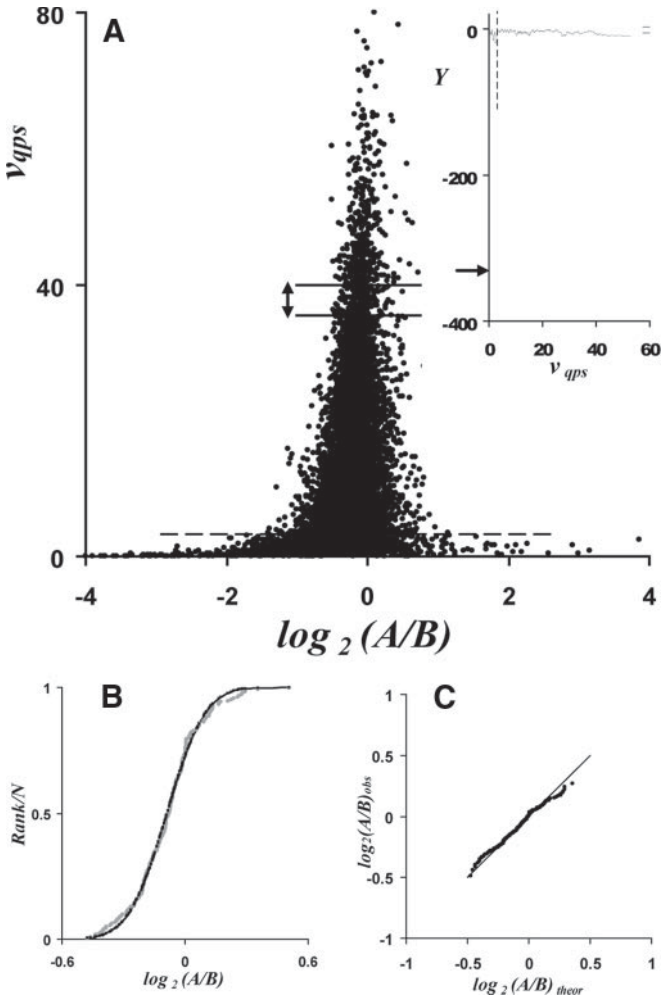

FIG. 3. **Classification of data into normal populations according to the fitting weight.** *A*, distribution of fitting weights as a function of $\log_2$ ratios. *Inset*, results of the D'Agostino normality test (56) applied in sliding windows of 200 points ranked according to fitting weight; shown are values taken by the *Y* parameter (56) as a function of the median fitting weight in each window. 99% confidence levels for *Y* values for a normal distribution (2.9 to −5.6) are indicated in the *inset*. For comparison, the *arrow* in the *y axis* of the *inset* indicates the *Y* value (−330) obtained by applying the test to the entire population. The minimum fitting weight threshold used in this study (3.1) is indicated by *discontinuous lines* in the main figure and in the *inset*. *B* and *C* are cumulative frequency and normal probability plots, respectively, as in Fig. 2, corresponding to the window indicated in *A*.

are very useful to detect sources of deviation of normality (55). As shown, the data considerably deviated from the expected values (Fig. 2*C*, *straight line*) and showed the characteristic shape indicative of leptokurtosis (55). Finally the data failed to pass a normality test (56) (Fig. 3*A*, *inset*, *arrow*). These findings demonstrated that the Gaussian distribution, which is the statistical model most commonly used to analyze this kind of data, is not adequate to describe the behavior of the null hypothesis.

A Random Effects Statistical Model for the Null Hypothesis: Calculation of Variance Components and of Peptide and Protein Averages—We hypothesized that the failure to follow a normal distribution was due to the presence of peptide pairs that were quantified with different accuracy so that the variance in the entire population of data was not homogeneous. With this idea in mind, we analyzed whether the data could be classified into discrete categories having homogeneous variance. For this purpose, we considered that quantifications performed with peaks having a larger intensity, and hence a larger peak area, should be more accurate than those performed with low intensity peaks; hence a plot of the squared intensity against the $\log_2$ ratio values was constructed. As shown in Fig. 2*D*, the dispersion of ratio values around the mean ratio clearly diminished when peak intensity increased, suggesting that the accuracy of quantification and hence the variance was intensity-dependent. We also observed the presence of numerous peptide pairs having a relatively high intensity that showed significant deviations from the expected value, indicating that the squared intensity alone could not be used as a criterion to classify data into homogeneous categories.

Because quantification of peptide pairs was made by fitting each ZoomScan spectrum to a theoretical function (14), deviations from the computed curve are indicative of errors committed in the calculation of the ratios from the fitted parameters. As explained under "Experimental Procedures," it is possible to estimate the variance of the $\log_2$ ratio values from the mean squared deviation of the fitted curve. The influence of contaminating peaks adjacent to the peptide pair peaks was also estimated from the mean squared deviations computed in narrow windows at the left and right of the main isotopic peaks. These mean squared deviations together define a statistical parameter, v_{qps}, defined as the *fitting weight* of scan *s* coming from peptide *p* derived from protein *q* (Equation 1). The fitting weight, in a $\log_2$ ratio scale, is expected to be inversely proportional to the variance produced by deviations between the theoretical and the experimental spectrum profiles. Because this parameter contains the squared peak intensity, spectra having higher intensity peaks have higher fitting weights than those displaying lower signal to noise ratios. In addition, the fitting weights tend to acquire lower values when the theoretical isotopic envelope fails to describe the experimental peaks or when co-eluting peaks are superimposed or adjacent to the main isotopic peaks. In Fig. 3*A* the fitting weights are plotted *versus* $\log_2$ ratio values; as shown, an excellent correlation between $\log_2$ ratio dispersion and fitting weight was obtained. The data were ranked according to decreasing fitting weights, and the normality test was then applied in sliding windows containing 200 ZoomScan spectra each. As shown in Fig. 3*A*, *inset*, the normality test was satisfactorily passed for all scan weights above a minimum threshold value. Besides the cumulative frequency distributions within each window could be satisfactorily fitted by Gaussian curves (Fig. 3*B*), and the shape of the curves in normal probability plots did not indicate apparent deviations

from normality (Fig. 3*C*). This result strongly suggested that, above the minimum threshold, the fitting weight may be used to classify the data set into discrete categories having homogeneous variance; in other words, that scans having similar fitting weights have similar $\log_2$ ratio variances. Besides these variances may be directly calculated from the fitting weights (see "Experimental Procedures"). In addition, this criterion allows using the minimum threshold value as an efficient cutoff parameter to eliminate low quality quantifications whose variance cannot be statistically controlled (Fig. 3*A*, *horizontal dashed line*, and Fig. 3*A*, *inset*, *vertical dashed line*).

During the analysis of the relation between fitting weight and scan variance, we observed that the variance tended to be a constant, non-zero value when fitting weight increased (supplemental Fig. S1). This finding indicated the presence of a constant residual scan variance component, termed σ_S^2, that was independent of the curve fitting; in other words, that a "perfect" quantification (in terms of the goodness of fitting and signal to noise ratio of ZoomScan spectra) still retains a constant error source that is independent of scan quality and hence of signal intensity. This is due to variations in the signal produced by the MS detector; this variance component is approximately constant because of the logarithmic nature of the scale used to analyze peptide ratios. To further analyze the behavior of this error source, we selected a subpopulation of data containing high quality quantifications only by choosing an arbitrary fitting weight threshold (supplemental information) above which the effect of curve fitting errors was expected to be negligible. We observed that this population passed the normality test, suggesting that the error source produced by the MS detector is homogeneous and can be reasonably modeled by a Gaussian distribution (not shown). In addition, errors are also expected at the peptide level because not all the peptides derived from the same protein produce exactly the same quantitative result. Similarly a further error source has to be considered at the protein level because not all the proteins are produced at exactly the same concentration due to the manipulation of the sample. These three error sources were analyzed by assuming a random effects, hierarchical statistical model. Because the population of high quality quantifications was found to display a normal behavior, we thought it reasonable to assume that in this population these three error sources have a constant variance and are normally distributed. Finally because the fitting weight is a property that only depends on the spectrum profile and is not related to the peptide and protein nature, we also found it reasonable to assume that peptide and protein variances are constant for all the scans in the population. The mathematical details of the statistical model are described under "Experimental Procedures."

Because as explained above quantifications at the scan level have a variance component due to curve fitting whose magnitude depends on the fitting weight, not all the quantifications are made with the same accuracy. Therefore when different quantifications from the same peptide are considered together they have to be weighted to estimate the averaged peptide ratio; this is done by using as statistical weight the inverse of the scan variance (Equations 3 and 6). In turn, averaging of different scans increases the accuracy of the peptide mean so that, in the absence of other error sources, the inverse of the peptide variance may be calculated by adding up the inverses of scan variances; this is equivalent to adding up scan weights. Note that this is the general procedure to calculate the variance of a weighted mean and that if there are *N* scans and all of them have the same variance then the variance of the mean takes the well known form, *i.e.* the scan variance divided by *N*. The final expression for the statistical weight associated to each peptide that measures accuracy of quantification at the peptide level is finally calculated by taking into account the contribution of errors at the scan level and the error produced by peptide preparation, which are measured by the peptide variance σ_P^2 (Equations 4 and 7). Similar considerations explain the formulas used to calculate the weighted average and the statistical weight at the protein level (Equations 5 and 8).

To apply the model to the practice it is not only necessary to estimate the variance components at the scan, peptide, and protein levels but also to determine how reliable these estimations are. This was accomplished in each one of the experiments, as explained in the supplemental information, by using the subset of high quality quantifications described in the previous section and applying an algorithm to estimate the variance components that best explain the structure of the data. The algorithm was tested by constructing data sets of similar size and structure, introducing normally distributed random errors having preset variance components, and checking that the estimated variances coincide with the original ones (supplemental Fig. S3). These simulations were particularly critical to ensure that the variance estimates were non-biased due to the particular structure of these data where most of the peptides and proteins were quantified by one or two scans and peptides, respectively (supplemental Fig. S3). These simulations were also used to calculate the 95% confidence intervals of the estimated variances.

Application of the algorithm to the three large scale experiments gave the results presented in Table I. As shown, an excellent agreement was found in the scan and peptide variances among the different experiments. The protein variances were not significantly different from zero in any of the cases, suggesting that the experimental design of the comparative study was adequate to determine the presence of significant expression changes at the protein level. In general, these results indicate that the three variance components can be efficiently calculated from the data and hence that the random effects model is in practice suitable for these kind of studies.

Analysis of Outliers at the Scan and Peptide Levels—As explained before, the scan populations having the same fitting weight (Fig. 3*A*) behaved as normal distributions. This as-

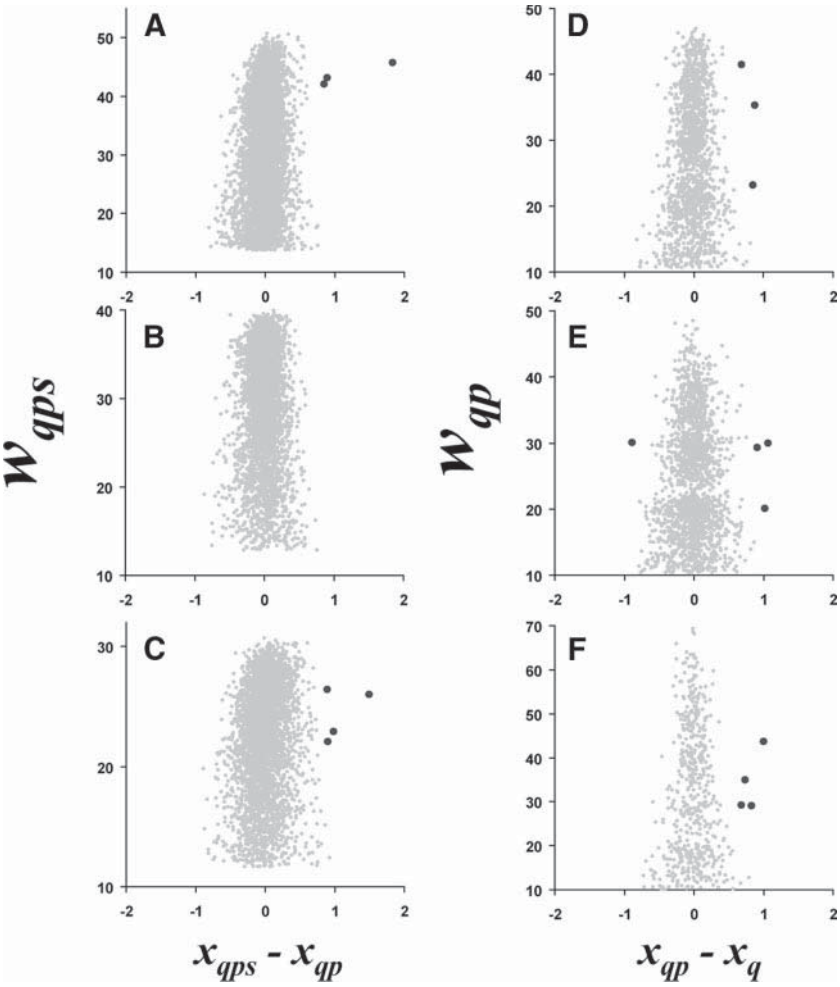

FIG. 4. **Analysis of outliers at the scan (*A–C*) and peptide (*D–F*) levels.** *Dark points* indicate outliers at the scan ($FDR_{qps} < 5\%$) or peptide levels ($FDR_{qp} < 5\%$) in the test experiment (*A* and *D*) and the 4-h (*B* and *E*) and 8-h VEGF incubation experiments (*C* and *F*).

sumption was further checked by analyzing the presence of outliers. For this end, the variances estimated in the previous section were used to calculate peptide and protein averages and the grand mean using Equations 3–8. In this step the population of scans remaining after the second filtering was used, and hence scans belonging to peptides containing missed cleavage sites or subpeptides derived from these or peptides containing methionine residues were not taken into account. The presence of outliers at the scan level was analyzed by checking for the presence of scans having a deviation from the peptide average higher than that expected by chance alone. The probability that a scan deviates from the peptide average was calculated using Equation 9 and the corresponding error rate (FDR_{qps}) using Equation 12. Determinations having an FDR_{qps} lower than 5% were visually inspected. In this step some scan outliers appeared whose deviation from the peptide average was explained by the presence of other isobaric peptides or contaminants, elevated background noise, or poor curve fitting. After eliminating these artifacts, the number of true scan outliers was extremely low (Fig. 4, *left panels*); only a maximum of four outliers per experiment was detected among several thousand scans. A similar analysis was performed to detect peptide quantifications that significantly deviated from the corresponding protein averages; this was done using as a criterion the parameter FDR_{qp} (Equations 10 and 13). The number of true peptide outliers was again almost negligible (Fig. 4, *right panels*).

As commented above, an additional source of variability at the peptide level was due to methionine oxidation and partial protein digestion; because these factors were found with some frequency to introduce considerable deviations in the ratios, they were analyzed in more detail. Oxidation of methionines occurs spontaneously, and this process may take place at different extents in the two samples so that the relative proportion of oxidized and non-oxidized peptides may deviate from the true peptide ratio. To check this phenomenon, the dispersion from protein averages in the $\log_2$ ratio values corresponding to peptides containing non-oxidized methionines was compared with those of methionine-oxidized peptides (Fig. 5, *A–C*). A visual inspection of this figure immediately suggested that with some frequency both oxidized and non-oxidized forms of methionine-containing peptides tended in general to deviate from their corresponding protein averages. Partial protein digestion was also an impor-

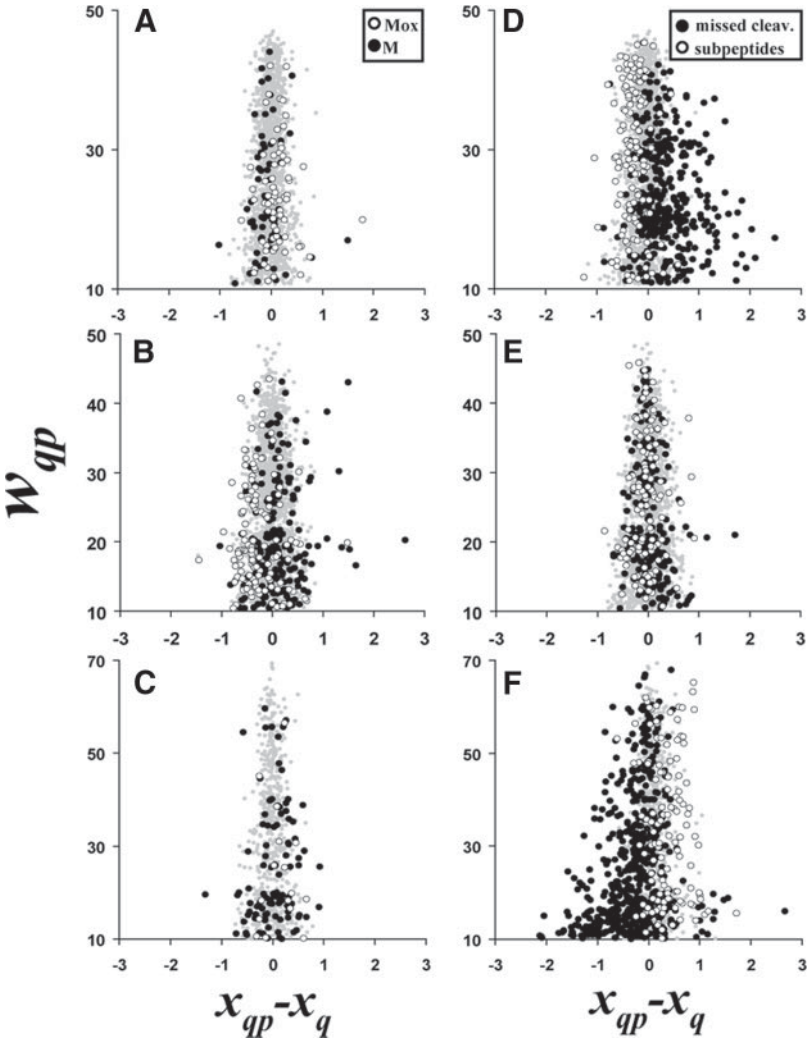

FIG. 5. **Effect of methionine oxidation and partial digestion on relative peptide quantification.** In *A–C*, scans corresponding to peptides containing oxidized (*Mox*) and non-oxidized methionines (*M*) are indicated by *black points* and *white circles*, respectively. In *D–F*, scans corresponding to peptides containing missed cleavage (*cleav.*) sites, except those with a proline after the basic residue, are indicated by a *black point*; subpeptides derived from a partially digested peptide identified in the same experiment are indicated by a *white circle*. Results correspond to the test experiment (*A* and *D*) and the 4-h (*B* and *E*) and 8-h VEGF incubation experiments (*C* and *F*).

tant source of deviations at the peptide level because partially digested peptides may not accurately reflect the protein concentration in the two samples. A similar approach was used to analyze this effect. The $\log_2$ ratios corresponding to peptides containing a missed cleavage were superimposed with those of completely digested peptides and also with subpeptides whose sequence is located inside a larger quantified peptide of the same protein. As shown in Fig. 5, *D–F*, the ratios of partially digested peptides were displaced from the expected values, whereas those of subpeptides tended to be displaced to opposite values. In general these kind of artifacts due to oxidation and digestion are easily detected as outliers by using the parameter FDR_{qp} as in Fig. 4; in this work we have judged these data as unreliable for protein quantification and have therefore eliminated them from the analysis.

As shown in Table I, once poor quality determinations and partially digested and methionine-containing peptides were discarded, the number of scans used for the quantitative analysis was considerably lower than the number of MS/MS spectra yielding a positive peptide identification. It is important to note here that this is not due to the ^{18}O labeling technique by itself because, as shown in Fig. 1, the labeling efficiency is well controlled in these experiments. Similarly it is not due to the statistical model used in this work because the number of outliers at the scan and peptide levels is negligible. Most of the poor quality scans eliminated in the first filtering are due to the limited resolving power of the ZoomScan mode in the linear ion trap, whereas the methionine oxidation and partial digestion effects are inherent to peptidecentric quantification approaches based on postdigestion labeling.

Analysis of Outliers at the Protein Level in the Test Experiment, and Symmetry and Consistency of Detected Expression Changes—From a purely statistical viewpoint, outliers at the protein level are significant expression changes and are detected by using the same strategy as that used at the scan and peptide levels; protein outliers present in the test experiment should, however, be considered as true artifacts. The outliers were analyzed by inspecting for the presence of protein values with an FDR_q lower than 10%. Only one outlier was identified among more than 1200 proteins in the test experi-

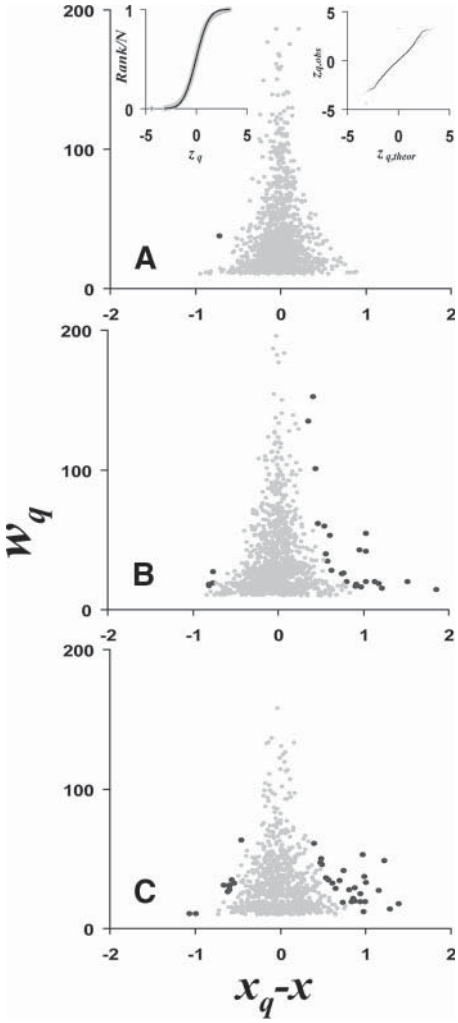

FIG. 6. **Analysis of statistically significant protein expression changes.** Outliers at the protein level ($FDR_q < 10\%$) were detected in the test experiment (*A*) and the 4-h (*B*) and 8-h VEGF incubation experiments (*C*) and are indicated by *black points*. The two *insets* in *A* are the cumulative frequency (*left*) and normal probability plots (*right*) of the standardized variable (z_q); the *black lines* are drawn according to the normal distribution $N(0,1)$. *theor*, theoretical.

ment. A further validation was done by studying the protein $\log_2$ ratio distribution according to the estimated variance of each one of the proteins. For this purpose $\log_2$ ratios at the protein level (x_q) were converted to standard normal values (z_q) by subtracting the grand mean and dividing by the standard deviation, *i.e.* $z_q = (x_q - x)\sqrt{w_q}$. As shown in Fig. 6*A*, *left inset*, the normalized cumulative frequency distribution of the standardized variable behaved according to the expected standard normal distribution $z_q \sim N(0,1)$, and in the corresponding normal probability plot (Fig. 6*A*, *right inset*) no deviations from normality become apparent. These findings provided a final and conclusive support of the validity of the statistical model.

Once the statistical model was validated, a set of experiments was performed to check the robustness of the new labeling protocol and the accuracy and symmetry of calculated protein ratios. One experiment addressed the consistency of results when the labeling protocol inverted the sample that was subjected to ^{18}O labeling. In this experiment no bias was found toward the sample being labeled with ^{18}O, and the data showed a good symmetry (supplemental Fig. S4A). In another experiment the theoretical and experimental protein ratios were compared in two aliquots from the same proteome doped with a set of proteins at different ratios; an excellent agreement was found between the expected and calculated values (supplemental Fig. S4B).

Finally the consistency of the method was analyzed by comparing the expression changes induced by VEGF after 4-h incubation in the large scale experiment and its technical replica at a smaller scale. As expected, not all the proteins quantified in the large experiment could be detected in the small experiment; however, among the proteins quantified in the two experiments, all the proteins displaying significant expression changes in the large experiment were observed to maintain an expression change of the same sign and similar extent in the small experiment even when the significance threshold was relaxed to a 35% FDR (Fig. 7). Hence the method showed an excellent consistency among two technical replicas.

Analysis of Protein Expression Changes Induced by VEGF Treatment in Endothelial Cells—In clear contrast with the test experiment, significant expression changes could be detected when cells were subjected to VEGF incubation for 4 and 8 h (Fig. 6, *B* and *C*, and Tables II and III). Some of the observed changes were moderate, although they were statistically significant. The protein values having the highest protein weights in the plots of Fig. 6 corresponded mainly to proteins quantified by several peptides. For instance, the von Willebrand factor showed only a 1.33-fold decrease after 4-h incubation; however, this protein was quantified by 12 peptides so that the expression change was associated with an FDR lower than 0.01%. Other proteins detected as statistically significant were quantified by a lower number of peptides but showed a larger expression change.

In this study, 32 and 46 proteins were found to be differentially expressed after VEGF treatment for 4 and 8 h, respectively. Most of the differentially expressed proteins in cells treated with VEGF for 4 h were down-regulated (84%) rather than up-regulated (16%) at 4 h (Fig. 6). The difference between the proportions of down- and up-regulated proteins was less remarkable (65 *versus* 35%, respectively) in cells treated with VEGF for 8 h, suggesting a biphasic expression pattern. This finding was consistent with the fact that the majority of proteins showing expression changes were different at 4 and 8 h. According to the Gene Ontology annotations, most of the differentially expressed proteins at 4 h are cytoplasmic and seem to be implicated in protein folding, whereas at 8 h the majority of changing proteins are distributed not only in the cytoplasm but also in the intracellular membrane-

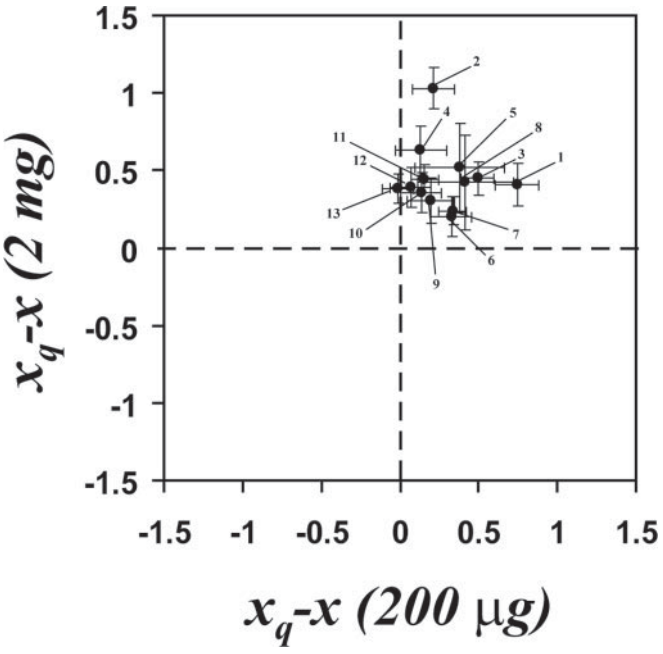

FIG. 7. **Consistency of protein expression changes in the two 4h VEGF experiments.** The list of proteins showing a significant expression change at the $FDR_q < 35\%$ level ($p_q < 0.02$) in the 4-h VEGF experiment was compared with those quantified in the small scale replica, and the x_q values in one experiment are plotted against those observed in the other. *Error bars* represent standard deviations of protein averages ($\sqrt{w_q^{-1}}$). *Numbers* in the figure refer to the following proteins: *1*, von Willebrand factor precursor (P04275); *2*, calreticulin precursor (P27797); *3*, 14-3-3 protein ζ/δ (P63104); *4*, phosphoglycerate mutase 1 (P18669); *5*, Rab GDP dissociation inhibitor α (P31150); *6*, ubiquitin-like modifier-activating enzyme 1 (P22314); *7*, vimentin (P08670); *8*, thioredoxin-dependent peroxide reductase, mitochondrial precursor (P30048); *9*, heat shock protein Hsp90-β (P08238); *10*, heat shock protein Hsp90-α (P07900); *11*, annexin A1 (P04083); *12*, 14-3-3 protein θ (P27348); and *13*, triose-phosphate isomerase (P60174).

bound organelle part, being primarily implicated in the cellular response to diverse stimulus.

Among the three experiments the relative proportion of a total of 1319 unique proteins was quantified in response to VEGF stimulus for 4 or 8 h. Among these proteins we found the majority of HUVEC proteins previously reported to show significant expression changes in response to VEGF (36, 37) or the angiogenic factor sokotrasterol sulfate (38), but very few of the proteins previously reported as differentially expressed were found to change their expression levels in our study. Among the proteins detected as differential expression events in this study, annexin A1 (ANXA1) (37), reticulocalbin (RCN1) (36), and triose-phosphate isomerase (38) were reported previously, but the changes were in the opposite sign, and only the change in Ran GTPase-activating protein and heat shock protein 70 (Hsp70) (36, 37) coincided with our results.

To validate some of the expression changes detected by isotope labeling and further investigate the expression changes that did not agree with those reported previously, expression levels of ANXA1, RCN1, and triose-phosphate isomerase were analyzed by Western blotting after incubating HUVECs with VEGF for 4 h and also for 8, 16, and 24 h. β-Tubulin (TB) levels were also analyzed as an internal control for protein loading (Fig. 8*A*). Although the expression changes detected by MS were moderate (2-fold or less) and hence difficult to analyze by Western blotting, the bands corresponding to RCN1 and ANXA1 after 4-h VEGF incubation clearly diminished in relation to the corresponding controls (Fig. 8*A*). Although no appreciable changes in triose-phosphate isomerase band at this incubation time could be detected upon a direct inspection of the blot, a densitometric analysis of all the bands over the entire time course revealed a relative expression pattern that was consistent with the MS data. As shown in Fig. 8*B*, the three proteins behaved in the same manner, appearing down-regulated at short VEGF incubation times and tending to recover their levels toward a slight up-regulation at longer times, whereas TB levels remained unaltered (Fig. 8*B*). Taking into account that the expression changes of triose-phosphate isomerase and ANXA1 at 4-h VEGF incubation were also confirmed in the small scale replica (Fig. 7), all these findings indicate that the expression patterns detected in this work reflect a specific short term response of the endothelial cellular machinery that cannot be directly compared with previous studies. Consistently some of the proteins showing differential expression changes by VEGF at 4 or 8 h in this study and that have not been observed previously are known to play an important role in processes implicated in angiogenesis; these include adipose triglyceride lipase (57), Hsp90 (58, 59), nucleolin (60), cofilin-2 (61, 62), tyrosyl-tRNA synthetase, and tryptophanyl-tRNA synthetase (63, 64).

DISCUSSION

In this work we describe the largest proteomics study performed to date in HUVECs. More than 3800 unique proteins were identified among four different experiments; from these, we were able to quantify more than 1300 unique proteins using stable ^{18}O labeling and linear ion trap mass spectrometry. These results conclusively demonstrate the suitability of the ZoomScanning technique in the linear ion trap for relative peptide quantification using this labeling approach. The scanning conditions necessary to perform alternate ZoomScan and MS/MS spectra were described in a previous work (16), and the algorithm we have developed to control and correct for the labeling efficiency has also been published previously (14). Controlling labeling efficiency for each one of the quantified peptides was particularly critical to develop an appropriate labeling protocol for these long lasting high throughput studies and to achieve consistent quantitative results. It should be noted that isotope labeling performance has also been claimed as potentially problematic in other labeling approaches. For instance, efficient using of stable isotope label-

TABLE II
Significant protein expression changes after VEGF incubation for 4 h

Protein name	Accession number	$(x_q - x) \pm$ S.D. (n)	-Fold change	p_q	FDR_q
					%
Calreticulin (precursor)	P27797	1.03 ± 0.14 (2)	2.04 down	3.3e−14	0.00
Cofilin-2	Q9Y281	1.86 ± 0.26 (1)	3.62 down	2.1e−12	0.00
Tyrosyl-tRNA synthetase, cytoplasmic	P54577	1.53 ± 0.22 (1)	2.88 down	8.9e−12	0.00
Triose-phosphate isomerase	P60174	1.03 ± 0.16 (2)	2.04 down	3.3e−11	0.00
Calumenin (precursor)	O43852	0.96 ± 0.15 (2)	1.94 down	4.3e−10	0.00
von Willebrand factor (precursor)	P04275	0.41 ± 0.08 (12)	1.33 down	4.3e−07	0.01
UDP-glucose:glycoprotein glucosyltransferase 1 (precursor)	Q9NYU2	1.13 ± 0.23 (1)	2.20 down	4.8e−07	0.01
Multifunctional protein ADE2	P22234	1.18 ± 0.23 (1)	2.27 down	4.0e−07	0.01
Rho GTPase-activating protein 29	Q52LW3	1.22 ± 0.26 (1)	2.33 down	2.1e−06	0.04
Annexin A1	P04083	0.44 ± 0.10 (5)	1.36 down	8.3e−06	0.1
Eukaryotic translation initiation factor 5B	O60841	0.61 ± 0.14 (3)	1.53 down	7.7e−06	0.1
Reticulocalbin-1 (precursor)	Q15293	0.55 ± 0.13 (3)	1.46 down	2.5e−05	0.3
Heat shock protein Hsp90-α	P07900	0.36 ± 0.09 (9)	1.28 down	3.0e−05	0.3
γ-Interferon-inducible protein Ifi-16	Q16666	0.77 ± 0.20 (1)	1.71 down	7.6e−05	0.6
YTH domain family protein 2	Q9Y5A9	0.97 ± 0.25 (1)	1.97 down	8.7e−05	0.7
Flotillin-1	O75955	0.92 ± 0.24 (1)	1.89 down	9.7e−05	0.7
Lupus La protein	P05455	0.75 ± 0.20 (1)	1.68 down	0.0002	1.1
RRP1-like protein B	Q14684	0.91 ± 0.25 (1)	1.88 down	0.0002	1.3
T-complex protein 1 subunit θ	P50990	0.47 ± 0.13 (3)	1.38 down	0.0002	1.5
Obg-like ATPase 1	Q9NTK5	0.56 ± 0.16 (2)	1.48 down	0.0004	2.4
Coatomer subunit β'	P35606	0.59 ± 0.17 (2)	1.50 down	0.0006	3.4
Phosphoglycerate mutase 1	P18669	0.63 ± 0.19 (1)	1.55 down	0.0009	4.5
Cation-dependent mannose 6-phosphate receptor (precursor)	P20645	0.77 ± 0.23 (1)	1.70 down	0.0011	5.1
Cytochrome b-c_1 complex subunit 1, mitochondrial (precursor)	P31930	0.54 ± 0.17 (2)	1.45 down	0.0014	5.9
tRNA (cytosine-5-)-methyltransferase NSUN2	Q08J23	0.80 ± 0.25 (1)	1.74 down	0.0014	6.1
Carbonyl reductase (NADPH) 1	P16152	0.76 ± 0.25 (1)	1.69 down	0.0021	8.3
Staphylococcal nuclease domain-containing protein 1	Q7KZF4	0.41 ± 0.13 (3)	1.33 down	0.0022	8.7
Proteasome subunit α type-3	P25788	−0.76 ± 0.19 (1)	1.70 up	7.6e−05	0.6
Replication protein A 14-kDa subunit	P35244	−0.81 ± 0.24 (1)	1.75 up	0.0006	3.1
α-Endosulfine	O43768	−0.80 ± 0.24 (1)	1.75 up	0.0009	4.3
Squamous cell carcinoma antigen recognized by T-cells 3	Q15020	−0.76 ± 0.23 (1)	1.69 up	0.0010	4.6
Methionine adenosyltransferase 2 subunit β	Q9NZL9	−0.73 ± 0.23 (1)	1.65 up	0.0017	6.7

ing by amino acids in cell culture (SILAC) requires careful checking of the extent of metabolic incorporation of labeled amino acids into the cultures and controlling potential sources of unlabeled amino acids and other effects such as arginine to proline conversions (65). In other recent work, an algorithm to calculate the labeling efficiency of iTRAQ reagents was proposed (66), and its application revealed not only the presence of a noticeable proportion of partially labeled peptides but also a differential incorporation efficiency in the four quadruplex reagents. Labeling analysis on these last two techniques, however, can only be performed on a global basis on the entire population of peptides, whereas our algorithm allows calculating efficiency at the individual peptide level. Calculation of labeling efficiency in the ^{18}O case is possible because of the two-step nature of the kinetics involved and seems to be specific for this technique (14). Although iTRAQ incorporation may also be considered a two-step process in peptides containing extra reactive residues such as Lys, the amount of non-labeled peptide is not quantified in this approach, making this kind of kinetic algorithm unsuitable.

Detection of significant expression changes in endothelial cells in response to VEGF was possible by the development of a new statistical model for the analysis of peptide and protein expression changes. The model is characterized by three main features. First, the model considers that not all relative quantifications of peptide pairs are performed with the same accuracy. Therefore, the variance cannot be assumed to be homogeneous in the entire population, and it is necessary to classify the data into subsets where measurements have the same variance. This is efficiently done using the fitting weight, a parameter that measures the dispersion in the $\log_2$ ratio values due solely to the fitting of the theoretical curve to the isotope envelope. We not only demonstrated that $\log_2$ ratio subsets corresponding to scans having the same fitting weight behave as normal distributions but also that the variance of these populations can be directly estimated from the fitting weight. As a consequence, it is possible to assign a variance due to quantification from the isotopic envelope to each one of the scan measurements. Other works using $^{14}N/^{15}N$ metabolic label-

TABLE III
Significant protein expression changes after VEGF incubation for 8 h

Protein name	Accession number	$(x_q - x) \pm$ S.D. (n)	-Fold change	p_q	FDR_q
					%
Tryptophanyl-tRNA synthetase, cytoplasmic	P23381	1.22 ± 0.14 (1)	2.34 down	0.0e+00	0.00
Purine-nucleoside phosphorylase	P00491	0.97 ± 0.14 (1)	1.95 down	2.7e−12	0.00
Echinoderm microtubule-associated protein-like 3	Q32P44	1.16 ± 0.19 (1)	2.23 down	2.0e−09	0.00
Ubiquitin carboxyl-terminal hydrolase 5	P45974	1.40 ± 0.24 (1)	2.63 down	4.3e−09	0.00
High mobility group protein B2	P26583	0.99 ± 0.16 (1)	1.99 down	1.8e−09	0.00
Lamin-B1	P20700	1.01 ± 0.17 (1)	2.01 down	7.8e−09	0.00
Mitochondrial inner membrane protein	Q16891	0.74 ± 0.16 (1)	1.68 down	1.7e−06	0.02
Probable palmitoyltransferase ZDHHC13	Q8IUH4	1.29 ± 0.27 (1)	2.45 down	2.0e−06	0.03
Nucleolin	P19338	0.94 ± 0.20 (1)	1.92 down	2.9e−06	0.03
Interferon-induced transmembrane protein 3	Q01628	0.88 ± 0.19 (1)	1.84 down	2.5e−06	0.03
Myotrophin	P58546	1.00 ± 0.23 (1)	1.99 down	1.4e−05	0.1
Cofilin-2	Q9Y281	0.81 ± 0.19 (1)	1.75 down	2.4e−05	0.2
Nuclear receptor-binding factor 2	Q96F24	0.94 ± 0.23 (1)	1.92 down	5.0e−05	0.3
Casein kinase II subunit β	P67870	0.70 ± 0.17 (1)	1.62 down	4.9e−05	0.4
CDGSH iron-sulfur domain-containing protein 2	Q8N5K1	0.86 ± 0.22 (1)	1.81 down	8.5e−05	0.5
Zinc transporter 1	Q9Y6M5	0.88 ± 0.23 (1)	1.84 down	0.0001	0.7
Pirin	O00625	0.84 ± 0.23 (1)	1.79 down	0.0002	1.3
Glutaredoxin-3	O76003	0.61 ± 0.18 (1)	1.53 down	0.0005	2.3
Transcription intermediary factor 1-β	Q13263	0.65 ± 0.19 (1)	1.57 down	0.0005	2.4
Serpin H1 (precursor)	P50454	0.48 ± 0.14 (1)	1.40 down	0.0007	3.0
Superoxide dismutase (Cu-Zn)	P00441	0.98 ± 0.29 (1)	1.97 down	0.0009	3.1
UBX domain-containing protein 8	Q96CS3	0.57 ± 0.17 (1)	1.48 down	0.0009	3.2
Ran GTPase-activating protein 1	P46060	0.49 ± 0.15 (1)	1.41 down	0.0009	3.3
Interleukin enhancer-binding factor 2	Q12905	0.54 ± 0.17 (1)	1.45 down	0.0012	3.5
40 S ribosomal protein S14	P62263	0.48 ± 0.15 (1)	1.39 down	0.0011	3.5
Fas-associated death domain protein	Q13158	0.74 ± 0.23 (1)	1.67 down	0.0017	4.5
ATP-dependent RNA helicase DDX39	O00148	0.40 ± 0.13 (2)	1.32 down	0.0019	4.8
Enoyl-CoA hydratase, mitochondrial (precursor)	P30084	0.47 ± 0.15 (1)	1.39 down	0.0023	5.2
Protein-L-isoaspartate (D-aspartate) *O*-methyltransferase	P22061	0.76 ± 0.25 (1)	1.70 down	0.0022	5.2
Translation initiation factor eIF-2B subunit δ	Q9UI10	0.76 ± 0.26 (1)	1.69 down	0.0045	8.9
Leucine-rich repeat flightless-interacting protein 1	Q32MZ4	−0.66 ± 0.18 (1)	1.58 up	0.0003	1.3
Eukaryotic translation initiation factor 2A	Q9BY44	−0.45 ± 0.13 (3)	1.37 up	0.0003	1.4
Patatin-like phospholipase domain-containing protein 2	Q96AD5	−1.06 ± 0.31 (1)	2.09 up	0.0005	2.3
Succinate dehydrogenase (ubiquinone) flavoprotein subunit, mitochondrial (precursor)	P31040	−0.57 ± 0.17 (2)	1.48 up	0.0008	3.0
Δ^1-Pyrroline-5-carboxylate synthetase	P54886	−0.59 ± 0.18 (2)	1.51 up	0.0010	3.1
Eukaryotic translation initiation factor 3 subunit E	P60228	−0.60 ± 0.18 (1)	1.51 up	0.0010	3.1
Palmdelphin	Q9NP74	−0.99 ± 0.31 (1)	1.99 up	0.0012	3.5
Periodic tryptophan protein 1 homolog	Q13610	−0.60 ± 0.19 (1)	1.52 up	0.0015	4.2
Matrin-3	P43243	−0.61 ± 0.20 (1)	1.53 up	0.0017	4.5
Protein ERGIC-53 (precursor)	P49257	−0.54 ± 0.18 (1)	1.46 up	0.0020	4.6
Vacuolar protein sorting-associating protein 4A	Q9UN37	−0.46 ± 0.15 (2)	1.37 up	0.0020	5.0
Mitofusin-2	O95140	−0.49 ± 0.16 (1)	1.40 up	0.0027	6.0
Protein-disulfide isomerase A4 (precursor)	P13667	−0.39 ± 0.13 (2)	1.31 up	0.0034	7.2
Myosin-Id	O94832	−0.39 ± 0.13 (2)	1.31 up	0.0038	8.1
Heat shock 70-kDa protein 1	P08107	−0.66 ± 0.23 (1)	1.58 up	0.0040	8.5
Synaptic vesicle membrane protein VAT-1 homolog	Q99536	−0.39 ± 0.14 (2)	1.31 up	0.0044	8.7

ing have also described that peptide quantification variance is not homogeneous but correlated with signal to noise ratio (28, 29); that observation is in agreement with the results presented in this work because scan variance decreases as a function of the fitting weight, which in turn is proportional to the square of peptide peak area (Equation 1), a parameter that reflects the effect of peak intensity in a manner similar to the signal to noise ratio.

Second, the model takes into account three additional sources of error at each one of the quantitative levels: scan, peptide, and protein. This is done by applying a hierarchical, random effects model and calculating the peptide and protein averages as well as their deviations taking into account the error contributions from each one of the three sources. Peptide and protein averages are calculated as weighted means using as statistical weights the inverse of variances of the

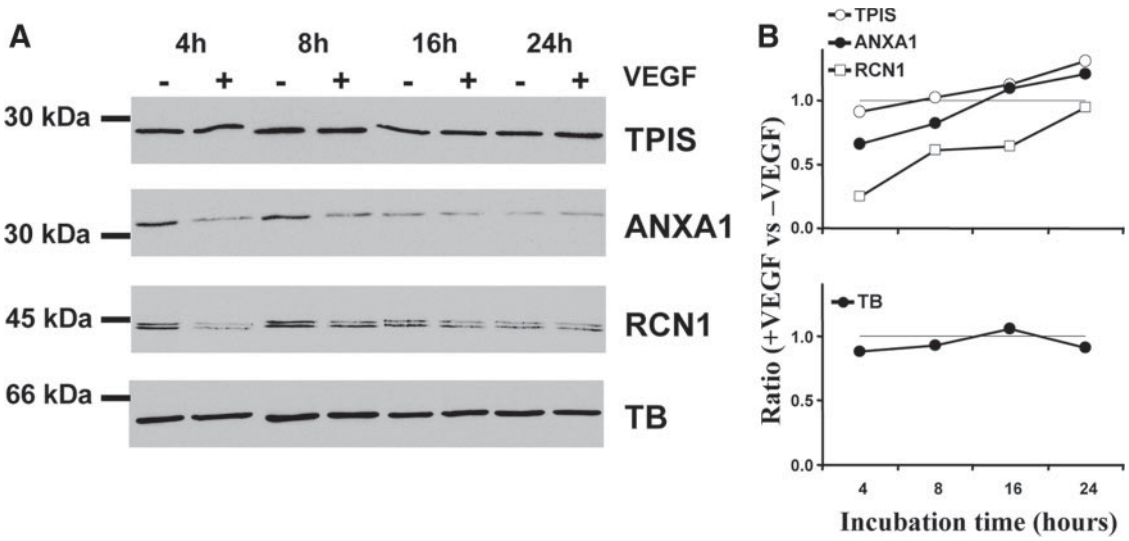

FIG. 8. **Western blot analysis of expression changes of some of the proteins quantified in this study.** *A*, protein extracts from HUVECs incubated in the absence or presence of VEGF for various times as indicated were separated by SDS-PAGE, blotted, and analyzed using specific antibodies against ANXA1 (37), RCN1 (36), triose-phosphate isomerase (*TPIS*), and TB. The position of molecular mass standards are indicated at the *left*. In *B* the stained bands were quantified by densitometry, and the resulting data were plotted as the ratio of band intensities obtained in the presence and absence of VEGF. Statistical analysis by conventional regression methods indicated the existence of a significant correlation between protein ratio and incubation time ($p < 0.02$) for ANXA1, RCN1, and triose-phosphate isomerase; in the case of TB the correlation was not statistically significant ($p > 0.3$).

values from which the average is calculated, and their variances are similarly calculated by integrating the variance at each level with the variances of the data used to calculate the average. This procedure is not only sound from the statistical viewpoint but also integrates the results in a coherent and intuitive manner. Thus, the averaged values are skewed toward the determinations that are more accurate (*i.e.* that have lower variance), and lower quality determinations have little effect on the average and hence do not need to be eliminated. Besides the model takes naturally into account the fact that quantifications at any of the higher levels (peptide or protein) are more reliable when they are calculated from two or more quantifications from the lower levels (scans or peptides, respectively). Moreover peptide and protein measurements are assumed to have their own source of error, and this error remains despite that the error transmitted from lower levels is decreased by extensive scan and peptide averaging, respectively. If these higher level errors are not taken into account, the peptides measured with a very large number of scans would have an almost negligible error, and protein averages would be completely skewed toward these peptides. In clear contrast, our hierarchical model assigns a similar weight to two peptides when they are measured by at least one good scan with little influence of the actual number of scans with which they are measured. Quality weights that are the inverse of variances have recently been used in the microarray field; by assigning lower weights to less reproducible arrays in different experiments the power to detect differential expression was reported to increase (67).

The model also address two of the most controversial points in quantitative proteomics: what is the minimum number of peptides required to consider protein quantification reliable, and what is the lowest expression change that may be considered statistically significant? In our model the accuracy of quantification is measured by its associated variance, which depends not only on the number of peptides with which it is measured but also on the accuracy of each one of the peptide measurements. Hence a protein quantified by two peptide measurements with low accuracy may have a higher variance than a protein quantified by only one peptide with higher accuracy. The statistical analysis will then produce a population of proteins with large heterogeneity with regard to their number of peptides and their associated variance, and the general rule will then be that a protein expression change may be called as significant when its ratio significantly deviates from the global distribution above the expected limits imposed by its own accuracy. It can be argued that a protein expression change is less prone to artifacts when it is detected by more than one peptide; however, in the experiments presented here all the peptides analyzed, except for a remarkably negligible number of exceptions, show a ratio dispersion that lies within the limits expected according to their variance. In such a context of absence of outliers it is reasonable to call as significant an expression change for proteins quantified by only one peptide.

Two main sources of peptide outliers are methionine oxidation and variations in protein digestion. Oxidation of methionines may take place at a different extent in the two samples, and this source of error is technically very difficult if not

impossible to control. For the same reason, peptides containing missed cleavage sites indicate incomplete trypsin digestion at these sites, the extent of which may again be different in the two samples, making protein quantification unreliable. Although these two potential sources of artifacts are obvious, they have not been analyzed before and were apparently not taken into account in the studies devoted to protein quantification by stable isotope labeling.

A very useful graphical interpretation of the quantitative results is obtained by plotting protein weights (*i.e.* the inverse of protein variances) *versus* $\log_2$ ratio values (Fig. 6). As shown in this figure and in Tables II and III, there are proteins displaying very moderate expression changes that are highly significant due to their higher protein weight, whereas others, displaying higher expression changes, cannot be considered significant because they have lower protein weights. The protein weight is expected to increase with protein concentration due to an increase in the number of quantified peptides; therefore these peptidecentric methods will naturally tend to produce better results with higher abundance proteins. Not surprising, in this work we were able to detect moderate protein expression changes that were not detected as significant by microarray approaches.

The third characteristic feature of our model is the assumption that the variances associated to the three error sources at the different levels are constant and common for the entire population of scans, peptides, and proteins in the same experiment. This viewpoint comes from a global approach in contrast with the local Student's *t* test approach commonly used in microarray or two-dimensional gel electrophoresis experiments where even being measured by the same number of determinations each protein is assumed to have a different variance. In the microarray field several groups have suggested that estimates of variance from individual genes are unreliable (18, 68, 69), and it has been pointed out that when the variance from each gene is truly unknown it makes sense to consider all of the genes on the array as arising from a single, normal distribution (18). In our case variance homogeneity at the three levels is convincingly supported by several lines of evidence. First, the population of scans having a large fitting weight (*i.e.* that have negligible errors due to curve fitting) pass the normality test; because the fitting weight is completely independent of the scan, peptide, and protein variances, such a result would not have been obtained if one of the error sources is not normally distributed. Second, the variances obtained at the three levels in several different experiments take essentially the same values, and their dispersion, calculated by computer simulation, indicates that they can be estimated with good accuracy. Third, the numbers of outliers at the scan and peptide levels are negligible; this result indicates that all the scans belonging to one peptide and all the peptides belonging to one protein display the same expression change. This result would have not been obtained if the error sources were not homogeneous. It should be noted that it is a common practice to eliminate scan or peptide outliers using criteria such as Dixon's (23, 25, 70). Fourth, the distribution of protein ratios standardized according to its variance (z_q values) can be convincingly modeled by a Gaussian function having a standard deviation of one; this result strongly indicates that variance integration at the three levels has been properly estimated and hence that the mathematical details of the model are sound. A final result that supports the validity of the method is given by the practical absence of false protein expression changes in the test experiment. Although these kinds of tests have been reported in the microarray field (see for instance Fodor *et al.* (18)), the number of test experiments published supporting the validity of statistical models using stable isotope labeling data are almost non-existent in the literature. A further point that remains to be studied is whether the global variance approach, and in general the statistical model presented in this work, could be applied to quantitative experiments performed using other isotope labeling methods such as iTRAQ. In this regard, it should be noted that only the error sources at the fitting and scan levels seems to be specific for the ^{18}O labeling method and the linear ion trap analyzer used in this study; whereas the error sources at the peptide and protein levels are expected to depend only on sample preparation and protein digestion, provided that labeling efficiency effects are properly controlled. This suggests that by introducing an appropriate model for scan variance under the null hypothesis the random effects statistical model proposed here could be used to analyze iTRAQ data and also other isotope labeling methods.

Application of the statistical model to the analysis of the VEGF effect on endothelial cells allowed the detection of significant expression changes at 4- and 8-h incubations. Because of the large number of proteins quantified, the expression changes were detected as significant by controlling for the FDR. Interestingly the majority of detected proteins were down-regulated in response to VEGF after 4-h incubation. This behavior has also been observed in other studies using the same cells; thus, when HUVECs were stimulated with cancer cell-conditioned medium, a model expected to resemble tumor angiogenesis better than VEGF alone, most differentially expressed proteins (88%) were also down-regulated (37). We also observed that the expression changes were more equilibrated at 8 h, the detected proteins were different from those observed at 4 h, and the classification of proteins according to Gene Ontology categories followed a different pattern; all these results are consistent with a biphasic process. The fact that almost all the proteins showing significant expression changes are different from those observed in other works (36–38) where cells were incubated for longer times with the proangiogenic factor and the results obtained by Western blotting with a selected set of proteins using different incubation times are together consistent with a pattern of protein expression that dynamically changes over

time following the evolution of the angiogenic response. The exposure to proangiogenic stimuli could give rise either to posttranslational modifications of preexisting proteins or to *de novo* synthesis of angiogenesis regulators. These mediators would then act in an autocrine fashion, thus amplifying the angiogenic response at later times. We cannot, however, discard the possibility that the differences between this work and previously published works may in part be due to the much more rigorous statistical criterion used in this work to establish significant expression changes, including not only a validated null hypothesis model but also the use of FDR and not *p* values or -fold changes alone.

It is interesting to note that the majority of significant expression changes detected in this study have not been described before even by microarray approaches and hence give novel information about the molecular processes involved in the response to VEGF at earlier stages. Some of these proteins have been directly or indirectly associated with angiogenesis in endothelial cells. In addition to Hsp70, a chaperone reported to display down-regulation in HUVECs exposed to VEGF (36, 37), we also found a down-regulation of Hsp90, and some studies show that inhibitors of this protein have antiangiogenic activity *in vivo* (58, 59). Down-regulation of adipose triglyceride lipase is also consistent with a proangiogenic event because this protein acts as a receptor for pigment epithelium-derived factor (57), a strong endogenous inhibitor of angiogenesis (71). Similarly Ran GTPase-activating protein regulates the nuclear localization of PTEN, a tumor suppressor gene product that is also closely associated with angiogenesis (72), suggesting that down-regulation of Ran GTPase-activating protein by VEGF might suppress the nuclear translocation of PTEN. Our study also revealed a down-regulation of cofilin-2 both at 4 and 8 h of incubation, and it is interesting to note that VEGF has been reported to stimulate cofilin phosphorylation in HUVECs (62). Of the two aminoacyl-tRNA synthetases displaying expression changes in this study, tyrosyl-tRNA synthetase, which was detected after 4-h incubation with VEGF, has been described as a proangiogenic factor on HUVECs (73), whereas tryptophanyl-tRNA synthetase, which was detected after 8-h incubation with VEGF, has been shown to inhibit HUVEC migration and angiogenesis (64). Finally previous studies reporting that localization of nucleolin at the cell surface is modulated by VEGF in the process of angiogenesis (60) and the finding that casein kinase 2 regulates cellular processes, such as organization of nucleolar chromatin where nucleolin plays a fundamental role (74), are also in agreement with the implication of these two proteins in angiogenesis.

In conclusion, the results presented in this work suggest that the ^{18}O labeling approach and analysis by linear ion trap mass spectrometry in conjunction with a computational algorithm that allow a precise control of labeling efficiency and a robust and validated statistical model provide a promising and semiautomated alternative to perform large scale studies of differential expression of proteins by stable isotope labeling. With this approach we were able to identify novel protein expression changes in HUVECs in response to incubations with the proangiogenic factor VEGF for short periods of time.

Acknowledgment—We thank Aurora García-Dorado for helpful discussion on analysis of variance.

* This work was supported in part by Grants BIO2006-10085 and SAF 2006-8348 from Spain's Ministerio de Educación y Ciencia, by Grant CAM BIO/0194/2006 from Comunidad de Madrid, by Grant LSHM-CT-2004-005033-EICOSANOX from the European Union, by the Fondo de Investigaciones Sanitarias (Ministerio de Sanidad y Consumo, Instituto Salud Carlos III, RECAVA Grant RD06/0014), and by an institutional grant from Fundación Ramón Areces (to Centro de Biología Molecular Severo Ochoa).

S The on-line version of this article (available at http://www.mcponline.org) contains supplemental material.

§ These authors contributed equally to this work.

¶ Recipient of a fellowship from the Comunidad Autónoma de Madrid (supported by the European Social Fund).

** To whom correspondence should be addressed: Centro de Biología Molecular Severo Ochoa, CSIC-Universidad Autónoma de Madrid, 28049 Cantoblanco, Madrid, Spain. Tel.: 34-91-196-4628; Fax: 34-91-196-4420; E-mail: jvazquez@cbm.uam.es.

REFERENCES

1. Aebersold, R., and Mann, M. (2003) Mass spectrometry-based proteomics. *Nature* **422,** 198–207
2. Hanash, S. (2003) Disease proteomics. *Nature* **422,** 226–232
3. Fievet, J., Dillmann, C., Lagniel, G., Davanture, M., Negroni, L., Labarre, J., and de Vienne, D. (2004) Assessing factors for reliable quantitative proteomics based on two-dimensional gel electrophoresis. *Proteomics* **4,** 1939–1949
4. Smejkal, G. B., Robinson, M. H., and Lazarev, A. (2004) Comparison of fluorescent stains: relative photostability and differential staining of proteins in two-dimensional gels. *Electrophoresis* **25,** 2511–2519
5. Yan, J. X., Devenish, A. T., Wait, R., Stone, T., Lewis, S., and Fowler, S. (2002) Fluorescence two-dimensional difference gel electrophoresis and mass spectrometry based proteomic analysis of Escherichia coli. *Proteomics* **2,** 1682–1698
6. Hu, Y., Wang, G., Chen, G. Y., Fu, X., and Yao, S. Q. (2003) Proteome analysis of Saccharomyces cerevisiae under metal stress by two-dimensional differential gel electrophoresis. *Electrophoresis* **24,** 1458–1470
7. Shevchenko, A., Jensen, O. N., Podtelejnikov, A. V., Sagliocco, F., Wilm, M., Vorm, O., Mortensen, P., Shevchenko, A., Boucherie, H., and Mann, M. (1996) Linking genome and proteome by mass spectrometry: large-scale identification of yeast proteins from two dimensional gels. *Proc. Natl. Acad. Sci. U. S. A.* **93,** 14440–14445
8. Yates, J. R., III, Eng, J. K., McCormack, A. L., and Schieltz, D. (1995) Method to correlate tandem mass spectra of modified peptides to amino acid sequences in the protein database. *Anal. Chem.* **67,** 1426–1436
9. Gygi, S. P., Rist, B., Gerber, S. A., Turecek, F., Gelb, M. H., and Aebersold, R. (1999) Quantitative analysis of complex protein mixtures using isotope-coded affinity tags. *Nat. Biotechnol.* **17,** 994–999
10. Ross, P. L., Huang, Y. N., Marchese, J. N., Williamson, B., Parker, K., Hattan, S., Khainovski, N., Pillai, S., Dey, S., Daniels, S., Purkayastha, S., Juhasz, P., Martin, S., Bartlet-Jones, M., He, F., Jacobson, A., and Pappin, D. J. (2004) Multiplexed protein quantitation in Saccharomyces cerevisiae using amine-reactive isobaric tagging reagents. *Mol. Cell. Proteomics* **3,** 1154–1169
11. Ong, S. E., Blagoev, B., Kratchmarova, I., Kristensen, D. B., Steen, H., Pandey, A., and Mann, M. (2002) Stable isotope labeling by amino acids in cell culture, SILAC, as a simple and accurate approach to expression proteomics. *Mol. Cell. Proteomics* **1,** 376–386
12. Mirgorodskaya, O. A., Kozmin, Y. P., Titov, M. I., Korner, R., Sonksen, C. P., and Roepstorff, P. (2000) Quantitation of peptides and proteins by matrix-assisted laser desorption/ionization mass spectrometry using ^{18}O-

labeled internal standards. *Rapid Commun. Mass Spectrom.* **14,** 1226–1232
13. Yao, X., Freas, A., Ramirez, J., Demirev, P. A., and Fenselau, C. (2001) Proteolytic ^{18}O labeling for comparative proteomics: model studies with two serotypes of adenovirus. *Anal. Chem.* **73,** 2836–2842
14. Ramos-Fernandez, A., Lopez-Ferrer, D., and Vazquez, J. (2007) Improved method for differential expression proteomics using trypsin-catalyzed ^{18}O labeling with a correction for labeling efficiency. *Mol. Cell. Proteomics* **6,** 1274–1286
15. Yao, X., Afonso, C., and Fenselau, C. (2003) Dissection of proteolytic ^{18}O labeling: endoprotease-catalyzed ^{16}O-to-^{18}O exchange of truncated peptide substrates. *J. Proteome Res.* **2,** 147–152
16. Lopez-Ferrer, D., Ramos-Fernandez, A., Martinez-Bartolome, S., Garcia-Ruiz, P., and Vazquez, J. (2006) Quantitative proteomics using $^{16}O/^{18}O$ labeling and linear ion trap mass spectrometry. *Proteomics* **6,** Suppl. 1, S4–S11
17. Storey, J. D., and Tibshirani, R. (2003) Statistical significance for genome-wide studies. *Proc. Natl. Acad. Sci. U. S. A.* **100,** 9440–9445
18. Fodor, A. A., Tickle, T. L., and Richardson, C. (2007) Towards the uniform distribution of null P values on Affymetrix microarrays. *Genome Biol.* **8,** R69
19. Karp, N. A., and Lilley, K. S. (2007) Design and analysis issues in quantitative proteomics studies. *Proteomics* **7,** Suppl. 1, 42–50
20. Karp, N. A., McCormick, P. S., Russell, M. R., and Lilley, K. S. (2007) Experimental and statistical considerations to avoid false conclusions in proteomics studies using differential in-gel electrophoresis. *Mol. Cell. Proteomics* **6,** 1354–1364
21. Mueller, L. N., Brusniak, M. Y., Mani, D. R., and Aebersold, R. (2008) An assessment of software solutions for the analysis of mass spectrometry based quantitative proteomics data. *J. Proteome Res.* **7,** 51–61
22. Lau, K. W., Jones, A. R., Swainston, N., Siepen, J. A., and Hubbard, S. J. (2007) Capture and analysis of quantitative proteomic data. *Proteomics* **7,** 2787–2799
23. MacCoss, M. J., Wu, C. C., Liu, H., Sadygov, R., and Yates, J. R., III (2003) A correlation algorithm for the automated quantitative analysis of shotgun proteomics data. *Anal. Chem.* **75,** 6912–6921
24. Wang, G., Wu, W. W., Pisitkun, T., Hoffert, J. D., Knepper, M. A., and Shen, R. F. (2006) Automated quantification tool for high-throughput proteomics using stable isotope labeling and LC-MSn. *Anal. Chem.* **78,** 5752–5761
25. Li, X. J., Zhang, H., Ranish, J. A., and Aebersold, R. (2003) Automated statistical analysis of protein abundance ratios from data generated by stable-isotope dilution and tandem mass spectrometry. *Anal. Chem.* **75,** 6648–6657
26. Gan, C. S., Chong, P. K., Pham, T. K., and Wright, P. C. (2007) Technical, experimental, and biological variations in isobaric tags for relative and absolute quantitation (iTRAQ). *J. Proteome Res.* **6,** 821–827
27. Boehm, A. M., Putz, S., Altenhofer, D., Sickmann, A., and Falk, M. (2007) Precise protein quantification based on peptide quantification using iTRAQ. *BMC Bioinformatics* **8,** 214
28. Pan, C., Kora, G., McDonald, W. H., Tabb, D. L., VerBerkmoes, N. C., Hurst, G. B., Pelletier, D. A., Samatova, N. F., and Hettich, R. L. (2006) ProRata: a quantitative proteomics program for accurate protein abundance ratio estimation with confidence interval evaluation. *Anal. Chem.* **78,** 7121–7131
29. Pan, C., Kora, G., Tabb, D. L., Pelletier, D. A., McDonald, W. H., Hurst, G. B., Hettich, R. L., and Samatova, N. F. (2006) Robust estimation of peptide abundance ratios and rigorous scoring of their variability and bias in quantitative shotgun proteomics. *Anal. Chem.* **78,** 7110–7120
30. Carmeliet, P. (2000) Mechanisms of angiogenesis and arteriogenesis. *Nat. Med.* **6,** 389–395
31. Papapetropoulos, A., Garcia-Cardena, G., Madri, J. A., and Sessa, W. C. (1997) Nitric oxide production contributes to the angiogenic properties of vascular endothelial growth factor in human endothelial cells. *J. Clin. Investig.* **100,** 3131–3139
32. Shih, T., and Lindley, C. (2006) Bevacizumab: an angiogenesis inhibitor for the treatment of solid malignancies. *Clin. Ther.* **28,** 1779–1802
33. Abe, M., and Sato, Y. (2001) cDNA microarray analysis of the gene expression profile of VEGF-activated human umbilical vein endothelial cells. *Angiogenesis* **4,** 289–298
34. Minami, T., Horiuchi, K., Miura, M., Abid, M. R., Takabe, W., Noguchi, N., Kohro, T., Ge, X., Aburatani, H., Hamakubo, T., Kodama, T., and Aird, W. C. (2004) Vascular endothelial growth factor- and thrombin-induced termination factor, Down syndrome critical region-1, attenuates endothelial cell proliferation and angiogenesis. *J. Biol. Chem.* **279,** 50537–50554
35. Yang, S., Toy, K., Ingle, G., Zlot, C., Williams, P. M., Fuh, G., Li, B., de Vos, A., and Gerritsen, M. E. (2002) Vascular endothelial growth factor-induced genes in human umbilical vein endothelial cells: relative roles of KDR and Flt-1 receptors. *Arterioscler. Thromb. Vasc. Biol.* **22,** 1797–1803
36. Pawlowska, Z., Baranska, P., Jerczynska, H., Koziolkiewicz, W., and Cierniewski, C. S. (2005) Heat shock proteins and other components of cellular machinery for protein synthesis are up-regulated in vascular endothelial cell growth factor-activated human endothelial cells. *Proteomics* **5,** 1217–1227
37. Katanasaka, Y., Asai, T., Naitou, H., Ohashi, N., and Oku, N. (2007) Proteomic characterization of angiogenic endothelial cells stimulated with cancer cell-conditioned medium. *Biol. Pharm. Bull.* **30,** 2300–2307
38. Karsan, A., Pollet, I., Yu, L. R., Chan, K. C., Conrads, T. P., Lucas, D. A., Andersen, R., and Veenstra, T. (2005) Quantitative proteomic analysis of sokotrasterol sulfate-stimulated primary human endothelial cells. *Mol. Cell. Proteomics* **4,** 191–204
39. Bradford, M. M. (1976) A rapid and sensitive method for the quantitation of microgram quantities of protein utilizing the principle of protein-dye binding. *Anal. Biochem.* **72,** 248–254
40. Villar, M., Ortega-Perez, I., Were, F., Cano, E., Redondo, J. M., and Vazquez, J. (2006) Systematic characterization of phosphorylation sites in NFATc2 by linear ion trap mass spectrometry. *Proteomics* **6,** Suppl. 1, S16–S27
41. Sevinsky, J. R., Brown, K. J., Cargile, B. J., Bundy, J. L., and Stephenson, J. L., Jr. (2007) Minimizing back exchange in $^{18}O/^{16}O$ quantitative proteomics experiments by incorporation of immobilized trypsin into the initial digestion step. *Anal. Chem.* **79,** 2158–2162
42. Liu, T., Qian, W. J., Strittmatter, E. F., Camp, D. G., II, Anderson, G. A., Thrall, B. D., and Smith, R. D. (2004) High-throughput comparative proteome analysis using a quantitative cysteinyl-peptide enrichment technology. *Anal. Chem.***76,** 5345–5353
43. Lopez-Ferrer, D., Martinez-Bartolome, S., Villar, M., Campillos, M., Martin-Maroto, F., and Vazquez, J. (2004) Statistical model for large-scale peptide identification in databases from tandem mass spectra using SEQUEST. *Anal. Chem.* **76,** 6853–6860
44. Ortega-Perez, I., Cano, E., Were, F., Villar, M., Vazquez, J., and Redondo, J. M. (2005) c-Jun N-terminal kinase (JNK) positively regulates NFATc2 transactivation through phosphorylation within the N-terminal regulatory domain. *J. Biol. Chem.* **280,** 20867–20878
45. Serrano, H., Jorge, I., Martínez-Acedo, P., Navarro, P. J., Pérez-Hernández, D., Miró Casas, E., García-Dorado, D., and Vázquez, J. (2007) Quantitative proteomics of mitochondrial membrane proteins by sodium dodecyl sulphate polyacrylamide gel electrophoresis, 16O/18O stable isotope labeling and linear ion trap mass spectrometry. *Proteomica* **0,** 29–34
46. Jorge, I., Casas, E. M., Villar, M., Ortega-Perez, I., Lopez-Ferrer, D., Martinez-Ruiz, A., Carrera, M., Marina, A., Martinez, P., Serrano, H., Canas, B., Were, F., Gallardo, J. M., Lamas, S., Redondo, J. M., Garcia-Dorado, D., and Vazquez, J. (2007) High-sensitivity analysis of specific peptides in complex samples by selected MS/MS ion monitoring and linear ion trap mass spectrometry: application to biological studies. *J. Mass Spectrom.* **42,** 1391–1403
47. Martinez-Bartolome, S., Navarro, P., Martin-Maroto, F., Lopez-Ferrer, D., Ramos-Fernandez, A., Villar, M., Garcia-Ruiz, J. P., and Vazquez, J. (2008) Properties of average score distributions of SEQUEST: the probability ratio method. *Mol. Cell. Proteomics* **7,** 1135–1145
48. Navarro, P. J., Martínez-Acedo, P., Serrano, H., Jorge, I., and Vázquez, J. (2007) A full automated and integrated bioinformatic toolset for large-scale peptide identification and quantification by ^{18}O stable isotope labeling, in the *2nd Congress of the SEProt and 1st Meeting of the European Proteomics Association, Valencia, March 13, 2007*, p. 119, Sociedad Española de Proteómica (SEProt), Valencia, Spain
49. Choi, H., and Nesvizhskii, A. I. (2008) False discovery rates and related statistical concepts in mass spectrometry-based proteomics. *J. Proteome Res.* **7,** 47–50
50. Kall, L., Storey, J. D., MacCoss, M. J., and Noble, W. S. (2008) Assigning

significance to peptides identified by tandem mass spectrometry using decoy databases. *J. Proteome Res.* **7,** 29–34
51. Tabb, D. L. (2008) What's driving false discovery rates? *J. Proteome Res.* **7,** 45–46
52. Fitzgibbon, M., Li, Q., and McIntosh, M. (2008) Modes of inference for evaluating the confidence of peptide identifications. *J. Proteome Res.* **7,** 35–39
53. Hernandez, G. L., Volpert, O. V., Iniguez, M. A., Lorenzo, E., Martinez-Martinez, S., Grau, R., Fresno, M., and Redondo, J. M. (2001) Selective inhibition of vascular endothelial growth factor-mediated angiogenesis by cyclosporin A: roles of the nuclear factor of activated T cells and cyclooxygenase 2. *J. Exp. Med.* **193,** 607–620
54. Staes, A., Demol, H., Van Damme, J., Martens, L., Vandekerckhove, J., and Gevaert, K. (2004) Global differential non-gel proteomics by quantitative and stable labeling of tryptic peptides with oxygen-18. *J. Proteome Res.* **3,** 786–791
55. D'Agostino, R. B., Belanger, A., and D'Agostino, R. B. J. (1990) A suggestion for using powerful and informative tests of normality. *Am. Stat.* **44,** 316–321
56. D'Agostino, R. B. (1971) An omnibus test of normality for moderate and large size samples. *Biometrika* **58,** 341–348
57. Notari, L., Baladron, V., Aroca-Aguilar, J. D., Balko, N., Heredia, R., Meyer, C., Notario, P. M., Saravanamuthu, S., Nueda, M. L., Sanchez-Sanchez, F., Escribano, J., Laborda, J., and Becerra, S. P. (2006) Identification of a lipase-linked cell membrane receptor for pigment epithelium-derived factor. *J. Biol. Chem.* **281,** 38022–38037
58. Kaur, G., Belotti, D., Burger, A. M., Fisher-Nielson, K., Borsotti, P., Riccardi, E., Thillainathan, J., Hollingshead, M., Sausville, E. A., and Giavazzi, R. (2004) Antiangiogenic properties of 17-(dimethylaminoethylamino)-17-demethoxygeldanamycin: an orally bioavailable heat shock protein 90 modulator. *Clin. Cancer Res.* **10,** 4813–4821
59. Chaudhury, S., Welch, T. R., and Blagg, B. S. (2006) Hsp90 as a target for drug development. *Chem. Med. Chem.* **1,** 1331–1340
60. Huang, Y., Shi, H., Zhou, H., Song, X., Yuan, S., and Luo, Y. (2006) The angiogenic function of nucleolin is mediated by vascular endothelial growth factor and nonmuscle myosin. *Blood* **107,** 3564–3571
61. Keezer, S. M., Ivie, S. E., Krutzsch, H. C., Tandle, A., Libutti, S. K., and Roberts, D. D. (2003) Angiogenesis inhibitors target the endothelial cell cytoskeleton through altered regulation of heat shock protein 27 and cofilin. *Cancer Res.* **63,** 6405–6412
62. Gong, C., Stoletov, K. V., and Terman, B. I. (2004) VEGF treatment induces signaling pathways that regulate both actin polymerization and depolymerization. *Angiogenesis* **7,** 313–321
63. Tzima, E., and Schimmel, P. (2006) Inhibition of tumor angiogenesis by a natural fragment of a tRNA synthetase. *Trends Biochem. Sci.* **31,** 7–10
64. Wakasugi, K., Slike, B. M., Hood, J., Otani, A., Ewalt, K. L., Friedlander, M., Cheresh, D. A., and Schimmel, P. (2002) A human aminoacyl-tRNA synthetase as a regulator of angiogenesis. *Proc. Natl. Acad. Sci. U. S. A.* **99,** 173–177
65. Graumann, J., Hubner, N. C., Kim, J. B., Ko, K., Moser, M., Kumar, C., Cox, J., Scholer, H., and Mann, M. (2008) Stable isotope labeling by amino acids in cell culture (SILAC) and proteome quantitation of mouse embryonic stem cells to a depth of 5,111 proteins. *Mol. Cell. Proteomics* **7,** 672–683
66. D'Ascenzo, M., Choe, L., and Lee, K. H. (2008) iTRAQPak: an R based analysis and visualization package for 8-plex isobaric protein expression data. *Brief. Funct. Genomics Proteomics* **7,** 127–135
67. Ritchie, M. E., Diyagama, D., Neilson, J., van Laar, R., Dobrovic, A., Holloway, A., and Smyth, G. K. (2006) Empirical array quality weights in the analysis of microarray data. *BMC Bioinformatics* **7,** 261
68. Baldi, P., and Long, A. D. (2001) A Bayesian framework for the analysis of microarray expression data: regularized t-test and statistical inferences of gene changes. *Bioinformatics* **17,** 509–519
69. Allison, D. B., Cui, X., Page, G. P., and Sabripour, M. (2006) Microarray data analysis: from disarray to consolidation and consensus. *Nat. Rev. Genet.* **7,** 55–65
70. Park, S. K., Venable, J. D., Xu, T., and Yates, J. R., III (2008) A quantitative analysis software tool for mass spectrometry-based proteomics. *Nat. Methods* **5,** 319–322
71. Dawson, D. W., Volpert, O. V., Gillis, P., Crawford, S. E., Xu, H., Benedict, W., and Bouck, N. P. (1999) Pigment epithelium-derived factor: a potent inhibitor of angiogenesis. *Science* **285,** 245–248
72. Ueda, S., Basaki, Y., Yoshie, M., Ogawa, K., Sakisaka, S., Kuwano, M., and Ono, M. (2006) PTEN/Akt signaling through epidermal growth factor receptor is prerequisite for angiogenesis by hepatocellular carcinoma cells that is susceptible to inhibition by gefitinib. *Cancer Res.* **66,** 5346–5353
73. Yang, X. L., Schimmel, P., and Ewalt, K. L. (2004) Relationship of two human tRNA synthetases used in cell signaling. *Trends Biochem. Sci.* **29,** 250–256
74. Srivastava, M., and Pollard, H. B. (1999) Molecular dissection of nucleolin's role in growth and cell proliferation: new insights. *FASEB J.* **13,** 1911–1922

Supplementary Information

Statistical model to analyze quantitative proteomics data obtained by $^{18}O/^{16}O$ labeling and linear ion trap mass spectrometry:

Application to the study of VEGF-induced angiogenesis in endothelial cells

Inmaculada Jorge[1#], Pedro Navarro[1#], P. Martínez-Acedo[1#], Estefanía Núñez[1], Horacio Serrano[1], Arántzazu Alfranca[2], Juan Miguel Redondo[2] and Jesús Vázquez[1*]

[1]Centro de Biología Molecular Severo Ochoa, Madrid, Spain

[2]Centro Nacional de Investigaciones Cardiovasculares, Madrid, Spain

Fitting weight and variance due to curve fitting

According to error propagation theory the variance in the $\log_2$-ratio values σ_{LR}^2 is related to the variances in peptide concentrations (in unit of peak area) due to curve fitting, σ_A^2 and σ_B^2, by:

$$\sigma_{LR}^2 = \frac{1}{(\ln 2)^2}\left[\frac{\sigma_A^2}{A^2} + \frac{\sigma_B^2}{B^2}\right] \approx \frac{2}{(\ln 2)^2}\frac{\sigma_T^2}{T^2} \qquad (S1)$$

And since the variance in peptide concentration is proportional to the mean squared deviation between observed and theoretical ZoomScan spectra, from Eq. 1 of the main text it is evident that

$$\sigma_{LR}^2 = \frac{k}{v_{qps}} \qquad (S2)$$

To calculate *k*, scans coming from peptides quantified by three or more scans were selected, and the fitting weights plotted against the difference between scan and peptide values (Fig. S1); this was done to eliminate the potential contribution of peptide and protein variances to the total $\log_2$-ratio variance. Scans were ranked according to decreasing fitting weights and the mean squared deviation (MSD) was calculated in sliding windows containing 200 values; this was done using a robust method in order to eliminate the effects of potential outliers. MSDs were then plotted against the median value of fitting weight in each window (Fig. S1, inset). The value of *k* was obtained by fitting the points to a hyperbolic curve. The same value of 0.17 was obtained in the three large-scale experiments used in this work.

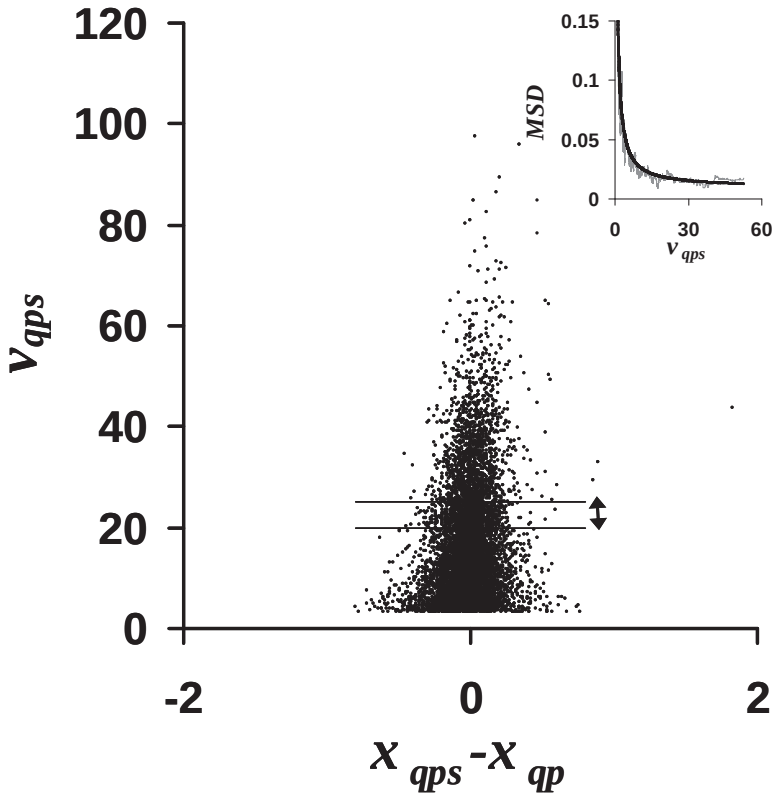

Fig.S1.- Determination of the *k* constant. Fitting weights are plotted against the differences between scan values and peptide averages for peptides measured by three or more scans. Inset: mean squared deviation (MSD) in sliding windows containing 200 points plotted as a function of median fitting weight in each window (grey lines) for the test experiment. The curve (black line) corresponds to the best fit to a hyperbolic curve and is drawn using $k = 0.17$.

Determination of the variance components

Let`s assume that we analyze *NQ* proteins, each protein being quantified by n_q different peptides, and each peptide being measured by n_{qp} scans. Let $NS = \sum_q \sum_p n_{qp}$ and $NP = \sum_q n_q$ be the total number of scans and peptides, respectively.

The scan, peptide and protein variance components are calculated using a population containing high-quality scans where errors due to curve fitting can be assumed to be negligible. This population is constructed by selecting scans whose fitting weight v_{qps} is higher than 30. This subpopulation of scans was normally distributed in the three large-scale experiments of this work. Since in this population scan variance may be assumed to be constant, all scans contribute equally to peptide averages. Hence, in this subpopulation peptide averages may be calculated as non-weighted means:

$$x_{qp} = \frac{\sum_s x_{qps}}{n_{qp}} \qquad (S3)$$

Let

$$SSS = \sum_q \sum_p \sum_s (x_{qps} - x_{qp})^2 \qquad (S4)$$

be the sum of squares due to differences in scans within each peptide. This sum may be used to estimate the variance component at the scan level as in the conventional ANOVA method:

$$\frac{E(SSS)}{NS - NP} = \sigma_s^2 \qquad (S5)$$

To calculate peptide variance an iterative method is used. An initial value of $\sigma_{\mathbf{P}}^2$, for instance zero, is used to calculate peptide weights, and protein averages are calculated as weighted means of peptides:

$$w_{qp} = \frac{1}{\frac{\sigma_{\mathbf{S}}^2}{n_{qp}} + \sigma_{\mathbf{P}}^2} \qquad (S6); \quad x_q = \frac{\sum_p w_{qp} x_{pq}}{\sum_p w_{qp}} \qquad (S7)$$

The weighted sum of squares due to differences in peptides within each protein

$$SSP = \sum_q \sum_p w_{qp} (x_{qp} - x_q)^2 \qquad (S8)$$

is used to calculate the variance at peptide level by using the following formula:

$$\sigma_{\mathbf{P}}^2 = \frac{E(SSP)}{\sum_q W_q} - \frac{\sigma_{\mathbf{S}}^2 \sum_q \sum_p \frac{w_{qp}}{n_{qp}}}{\sum_q \sum_p w_{qp}} \qquad (S9)$$

where

$$W_q = \sum_p w_{qp} - \frac{\sum_p w_{qp}^2}{\sum_p w_{qp}} \qquad (S10)$$

are the degrees of freedom. This factor ensures that the estimation of local peptide variance from the sum of squares due to differences within each protein is unbiased when the number of peptides per protein is low, as it is the usual case (Fig. S2). The new value of $\sigma_{\mathbf{P}}^2$ is used as initial estimate, and the process repeated until a

stable value is obtained. The process converges to the same final value irrespective of the initial value used.

The variance at the protein level is similarly computed by taking an initial estimate of $\sigma_{\mathbf{Q}}^2$ to calculate protein weights and then estimating the grand mean as a weighted average of proteins:

$$w_q = \frac{1}{\frac{1}{\sum_p w_{qp}} + \sigma_{\mathbf{Q}}^2} \qquad (S11); \quad x = \frac{\sum_q w_q x_q}{NQ} \qquad (S12)$$

The weighted sum of squares due to differences between proteins and the grand mean

$$SSQ = \sum_q w_q (x_q - x)^2 \qquad (S13)$$

is used to calculate the variance at the protein level from the formula

$$\sigma_{\mathbf{Q}}^2 = \frac{E(SSQ)}{\sum_q w_q - \frac{\sum_q w_q^2}{\sum_q w_q}} - \frac{\sum_q w_q^2}{\sum_q w_q} \qquad (S14)$$

And the process is iterated until a stable value of $\sigma_{\mathbf{Q}}^2$ is reached.

Confidence intervals of estimated variances are determined by computer simulation using a Monte Carlo approach. This was done by generating random datasets containing trees of scans/peptides/proteins with the same size and distribution of the number of scans per peptide and peptides per protein (Fig. S2) than the original data, and containing random, normally distributed errors at the scan, peptide and

protein levels according to the preset variances. Typically, 100 datasets were generated to determine confidence intervals of variances estimated in each experiment. An example is shown in Fig. S3.

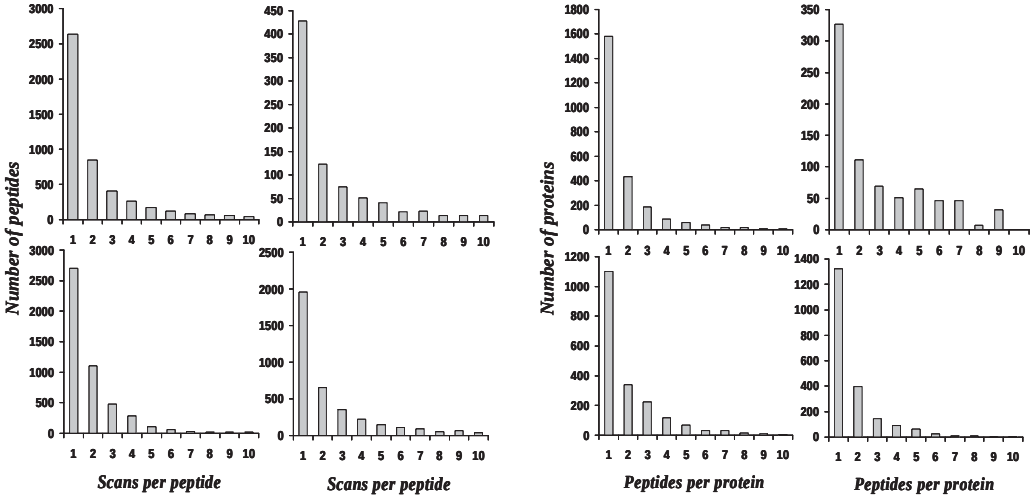

Fig. S2.- Distribution of the number of scans per peptide (left panels) and the number of peptides per protein (right panels) in the four experiments analyzed in this study.

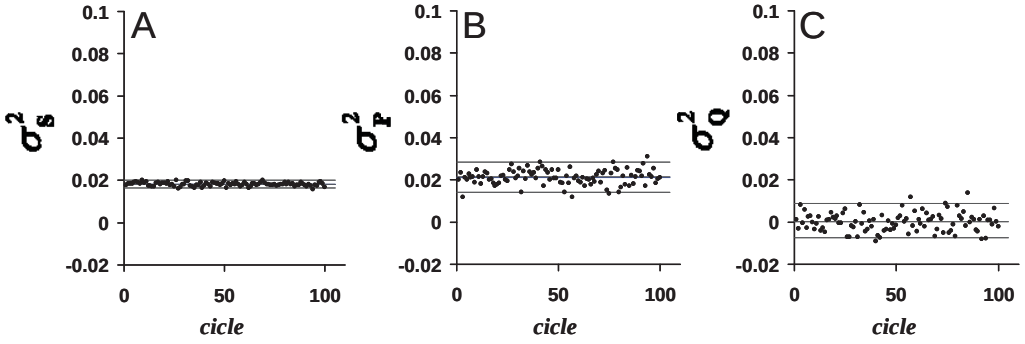

Fig. S3.- Example of determination of confidence intervals of variances by Monte Carlo simulation. Preset variances used for the simulation were $\sigma^2_S = 0.018$, $\sigma^2_P = 0.021$ and $\sigma^2_Q = 0.000$ and correspond to the central horizontal lines. The upper and lower lines indicate 95% confidence intervals in each case.

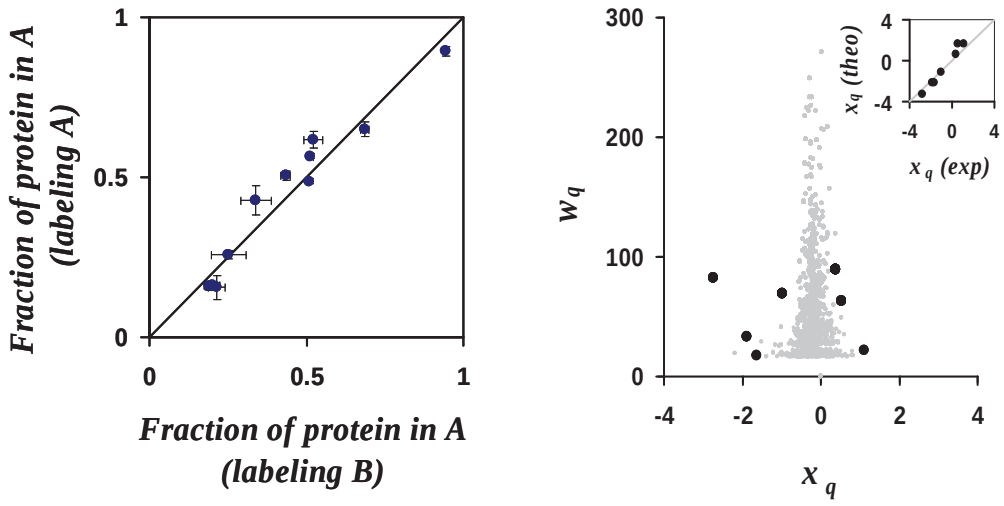

Fig. S4.- Left panel: results obtained in a reverse labeling experiment**.** Two samples A and B containing eleven proteins at different proportions were labeled with ^{18}O and ^{16}O, respectively, in one experiment, and with ^{16}O and ^{18}O, respectively, in other experiment, and the quantifications obtained in the two experiments are compared in the figure. Right panel: an *Escherichia coli* proteome was split into two identical aliquots and each one was doped with seven proteins at different known relative proportions. The doped proteomes were digested, labeled with $^{16}O/^{18}O$, mixed and subjected to relative quantification. Quantifications at the protein level are shown in the figure; the black points are the ratios corresponding to the doped proteins, while the grey points belong to the quantified proteins of the proteome. Inset: plot of the expected protein $\log_2$-ratios against the observed values.

This paper is available on line at http://www.mcponline.org

A Robust Method for Quantitative High-throughput Analysis of Proteomes by ^{18}O Labeling*[S]

Elena Bonzon-Kulichenko‡, Daniel Pérez-Hernández‡, Estefanía Núñez‡, Pablo Martínez-Acedo‡, Pedro Navarro‡, Marco Trevisan-Herraz‡, María del Carmen Ramos§, Saleta Sierra§, Sara Martínez-Martínez¶, Marisol Ruiz-Meana‖, Elizabeth Miró-Casas‖, David García-Dorado‖, Juan Miguel Redondo¶, Javier S. Burgos§, and Jesús Vázquez‡**

MS-based quantitative proteomics plays an increasingly important role in biological and medical research and the development of these techniques remains one of the most important challenges in mass spectrometry. Numerous stable isotope labeling approaches have been proposed. However, and particularly in the case of ^{18}O-labeling, a standard protocol of general applicability is still lacking, and statistical issues associated to these methods remain to be investigated. In this work we present an improved high-throughput quantitative proteomics method based on whole proteome concentration by SDS-PAGE, optimized in-gel digestion, peptide ^{18}O-labeling, and separation by off-gel isoelectric focusing followed by liquid chromatography-LIT-MS. We demonstrate that the off-gel technique is fully compatible with ^{18}O peptide labeling in any pH range. A recently developed statistical model indicated that partial digestions and methionine oxidation do not alter protein quantification and that variances at the scan, peptide, and protein levels are stable and reproducible in a variety of proteomes of different origin. We have also analyzed the dynamic range of quantification and demonstrated the practical utility of the method by detecting expression changes in a model of activation of Jurkat T-cells. Our protocol provides a general approach to perform quantitative proteomics by ^{18}O-labeling in high-throughput studies, with the added value that it has a validated statistical model for the null hypothesis. To the best of our knowledge, this is the first report where a general protocol for stable isotope labeling is tested in practice using a collection of samples and analyzed at this degree of statistical detail. ***Molecular & Cellular Proteomics 10: 10.1074/mcp.M110.003335, 1–14, 2011.***

The analysis of differential protein expression is fundamental for the understanding of biological processes and plays an increasingly important role in biological and medical research (1). In recent years, numerous stable isotope labeling (SIL)[1] techniques have emerged as alternatives to the historically used two-dimensional-based approaches for semiquantitative proteomic studies. In these techniques the quantification is done in the same mass spectrometer where peptides are analyzed by tandem mass spectrometry (MS/MS), so relative quantification and peptide identification is performed at the same time. The differences among the several existing SIL approaches are mainly related to the way labels are introduced and the method used to perform the quantification by MS. Thus, in the SILAC method (2) labels are introduced metabolically at the protein level before peptides are generated from protein by enzymatic digestion, minimizing variability introduced by peptide preparation, whereas in the others labeling is performed postdigestion at the peptide level, either chemically in the iTRAQ method (3), or enzymatically in the ^{18}O labeling method (4–6). In the iTRAQ method, quantification is made at the MS/MS level, allowing the possibility of performing multiplexed comparisons (7) whereas in SILAC and ^{18}O methods peptides are quantified at the MS level and are mainly used for pairwise comparisons. In other SIL approaches, such as the ICAT method (8), labeled peptides are specifically recovered after an affinity purification approach; this allows reducing peptide complexity, which is particularly appropriate to selectively analyze peptide subpopulations, such as reduced or oxidized cys-containing peptides (9). The ^{18}O labeling method has the advantage that labels are intro-

From the ‡Laboratory of Protein Chemistry and Proteomics, Centro de Biología Molecular "Severo Ochoa" (CSIC-UAM), Madrid, E-28049, Spain, §Neuron Biopharma S.A. Parque tecnológico de ciencias de la salud de Granada, Granada, 18100, Spain, ¶Department of Vascular Biology and Inflammation, Centro Nacional de Investigaciones Cardiovasculares, Madrid, E-28029, Spain, ‖Laboratorio de Cardiología Experimental, Servicio de Cardiología, Hospital Universitari Vall d'Hebron, Barcelona, Spain

Received September 3, 2010, and in revised form, September 6, 2010

Published, MCP Papers in Press, DOI 10.1074/mcp.M110.003335

[1] The abbreviations used are: SIL, stable isotope labeling; MS/MS, tandem MS; RP-HPLC, reverse phase-high pressure liquid chromatography; IEF, isoelectric focusing; pI, isoelectric point; FDR, false discovery rate.

duced enzymatically using trypsin, so that eventually any kind of protein sample may be labeled, the same mass shift is introduced in all the peptides and secondary reactions inherent to chemical labeling are avoided. In addition, the reagent needed (^{18}O-labeled water) is extremely stable and, because of its relatively low price, labeling of peptides produced from large amounts of sample is possible. However, ^{18}O labeling is considered a more delicate and less robust technique than the others, and if it is not carefully controlled, the complete ^{18}O labeling of peptides is not always attained, producing quantitative artifacts. In addition, ^{18}O labels are pH-sensitive (10, 11) and hence not all peptide manipulation steps are fully compatible with this labeling method. These problems have hindered the widespread use of this technique in comparison with the other SIL methods. Not surprising, a wide repertoire of sample preparation, proteome digestion, and ^{18}O labeling protocols may be found in the literature. The quantitative analysis of proteomes from human cells at the depth of several thousand proteins using this method has recently been demonstrated by our laboratory (10), showing that a full ^{18}O incorporation is possible in very complex samples. However, we also reported the existence of a number of potential artifacts related to the method used, including incomplete proteome digestion and differential methionine oxidation. Clearly, a universal, robust, and high-throughput ^{18}O labeling protocol, capable of attaining a full ^{18}O incorporation, which avoids ^{18}O unlabeling and that minimizes digestion and oxidation artifacts is currently needed. Such a method would put the wide application of this promising technique at the same level as its other SIL counterparts.

Protein digestion is most commonly performed in solution after protein denaturation in the presence of high urea concentrations (12, 13, 10). The use of centrifuge spin filters to wash away contaminants that might hinder subsequent MS analysis has also been demonstrated (14, 15). In-solution digestion is thought to be particularly adequate in studies concerning post-translational modifications (16); (17), where as much as possible from the protein sequence should be recovered for analysis. In-solution digestion is commonly followed by a first step of peptide fractionation by cation-exchange chromatography, which is done prior to reverse phase-high pressure liquid chromatography (RP-HPLC)-MS analysis (18). We (10) and previously others (12) have shown that this approach is fully compatible with ^{18}O labeling. An alternative to in-solution digestion of proteins followed by peptide fractionation is protein fractionation by one-dimensional-SDS-PAGE followed by in-gel digestion and RP-HPLC-MS peptide analysis of each fraction separately. This method may not only be more effective for the analysis of hydrophobic proteins, such as membrane proteins, but by trapping the proteins within the gel matrix it also allows the effective removal of detergents and other contaminants that might hinder subsequent trypsin digestion or may be difficult to eliminate from the peptide pool to avoid interferences with MS analysis. In conjunction with SILAC labeling and previous subcellular fractionation, in-gel digestion of SDS-PAGE-separated proteins allowed the quantification of whole proteomes from cell cultures at a depth of several thousand proteins (19, 20). Very recently a method has been described that combines the advantages of SDS protein solubilization with in-solution digestion in presence of urea, using centrifuge spin filters (21).

Protein separation by SDS-PAGE prior to ^{18}O labeling of peptides has also been used to study the differential complex formation around the NFkB transcription factor p65 upon TNF-α stimulation (22). Lane *et al.* 2007 (23) employed a similar approach to perform a comparative analysis of microsomal P450 proteins in liver from control and drug-treated mice. Although the combination of SDS-PAGE protein separation and ^{18}O labeling was demonstrated to attain femtomolar sensitivity (22), the variability introduced by protein preparation in a postdigestion method like ^{18}O when the peptides were quantified by MS has never been investigated.

A recent alternative for peptide fractionation is isoelectric focusing (IEF) (24, 13), which presents an excellent resolution and provides another criterion, the peptide isoelectric point (pI), to validate peptide identifications (25). The off-gel technique uses IPG strips conventionally used for two-dimensional electrophoresis protein separation and maintains IEF-separated peptides in solution (26). This technique has been demonstrated to be highly efficient and reproducible in resolving complex peptide samples (27–29). By subjecting whole cell extracts to in-solution digestion and off-gel separation, the same depth of analysis was obtained as with subcellular fractionation followed by the one-dimensional-SDS-PAGE approach (29), but with less time and effort. IEF separation of ^{18}O labeled peptides in the pH range 3–11 was used to compare the relative abundances of nuclear proteins from a drug resistant MCF-7 cancer cell line with those from the drug susceptible parent cell line (24). However, extreme pH values have been reported to cause acid- or base-catalyzed oxygen back-exchange (4) and in that work the stability of ^{18}O peptide labeling was not addressed. Therefore, it still remains unclear whether the off-gel is fully compatible with protein quantitation by ^{18}O labeling.

In a recent work, a method to determine the extent of individual ^{18}O labeling of each one of the peptides quantified in a paired comparison of proteomes was demonstrated in our laboratory (30). Using this procedure to control for labeling efficiency, we demonstrated the precise ^{18}O quantification of proteomes at a depth of several thousand proteins (10). In that work, a statistical model was also developed for the analysis of results obtained by ^{18}O labeling and linear ion trap mass spectrometry (10). The model decomposes the sources of variance at the scan, peptide and protein levels, allowing their separate analysis. Although variance at the scan level is mainly dependent on the MS setup and at the protein level on the preparation of protein samples, at the peptide level it

measures the dispersion of quantitative values obtained from different peptides belonging to the same protein. Because this dispersion depends critically on the procedure used for peptide preparation and labeling, analysis of variance at the peptide level would not only inform about the accuracy associated to the protocol but also indicate the existence of quantification artifacts. Using this statistical framework, in a previous work we were able to detect systematic errors associated to protein digestion and differential methionine oxidation, which are factors whose effect on quantification accuracy have not been analyzed previously (10). Taken together, the existence of computational tools for a systematic control of ^{18}O labeling efficiency and for the analysis of variance at the peptide level opens the way to the development of peptide preparation procedures that optimize labeling efficiency, are fully compatible with ^{18}O labels, and at the same time maintain protein quantification accuracy.

In this work we apply these tools to demonstrate the existence of quantification problems associated to the combination of one-dimensional-SDS-PAGE protein fractionation and postdigestion ^{18}O labeling. Also, we present a robust method that combines the advantages of both the SDS-PAGE and off-gel approaches, attains a full degree of ^{18}O labeling, maintains ^{18}O label stability, and keeps at a low and constant level peptide variance for proteomes obtained from a wide range of biological sources. According to our knowledge, this is the first systematic study of quantification error sources produced in a general sample preparation method for SIL.

EXPERIMENTAL PROCEDURES

Cell Culture and Protein Extraction—HepG2 and SK-N-MC human cell lines were obtained from American Type Culture Collection (ATCC no. HB-8065 and HTB-10TM). Cells were grown in MEM supplemented with 10% FBS, 2 mM L-glutamine, 1 mM sodium pyruvate, 0.1 mM nonessential aminoacids, and 0.05 mg/ml gentamicin, at 37 °C and 5% CO_2. After trypsinization cells were plated out from 175-mm^2 flasks to 100-mm dishes (Corning, Elmira, NY) at 3×10^6 cells/dish. After 24 h the cell pellet was washed twice with ice-cold phosphate-buffered saline, resuspended and incubated for 30 min in 350 μl ice-cold phosphate-buffered saline with 1% triton X-100 and EDTA-free Protease Inhibitor Mixture (Roche Applied Science) during 30 min at 4 °C. The suspension was homogenized in a Potter-Elvehjem homogenizer and centrifuged at 200 $\times$ *g* for 5 min to remove cell debris. The supernatants were collected and protein concentration was determined by Bradford (Bio-Rad) using BSA as standard. The complete lysates were obtained after adding 5$\times$ SDS-sample buffer (50% glycerol, 10% SDS, 25% β-mercapto-ethanol, 0.05% bromphenol blue, and 250 mM Tris, pH 6.8).

Cardiac mitochondria were isolated from rat hearts by differential centrifugation and Percoll-gradient ultracentrifugation as described previously (31). The purity of the mitochondrial preparations was controlled by Western blot analysis using antibodies for other cellular compartments. Protein concentration in mitochondrial extracts was measured using the Bradford protein assay.

Jurkat T cells were grown in RPMI (GIBCO, Invitrogen) containing 10% fetal calf serum (Sigma) supplemented with L-glutamine plus antibiotics (100 units/ml penicillin and 100 μg/ml streptomycin) until 300×10^6 cells were obtained, at 37 °C and 5% CO_2. Cells were washed three times with serum-free RPMI and left to culture at 2×10^6 cells/ml in RPMI without serum. After 12 h, the conditioned medium was eliminated by three washes with phosphate-buffered saline and replaced by RPMI without serum. After 8 h conditioned media from two 150 ml flasks were combined, centrifuged at 200 $\times$ *g* for 5 min to remove cell debris and then at 100,000 $\times$ *g* for 1 h to remove intracellular vesicles. Supernatants were lyophilized, resuspended in 2.5 ml 25 mM ammonium bicarbonate, pH 8.8, desalted on PD-10 columns (GE Healthcare) equilibrated with the same buffer and lyophilized. Samples were taken up in 200 μl water and protein concentration was assayed by the Bradford method.

The cytosolic fraction of Jurkat T cells stimulated with phorbol 12-myristate 13-acetate and calcium ionophore A23187 (Io) was obtained as described in (29). Briefly, after culturing cells for 12 h in RPMI without serum as described above, cells were washed thrice with phosphate-buffered saline and incubated for 8 h in RPMI without serum, supplemented with 20 ng/ml phorbol 12-myristate 13-acetate, 1 μM Io (Sigma). Control cells were cultured in serum-free media containing vehicle (dimethylsulfoxide). The cell pellet was incubated for 10 min in 800 μl ice-cold lysis buffer (10 mM HEPES, pH 7.9, 1.5 mM $MgCl_2$, 10 mM KCl, 0.2% N-octylglucoside, and EDTA-free Protease Inhibitor Mixture). The suspension was homogenized in a Potter-Elvehjem homogenizer and centrifuged at 400 $\times$ *g* for 15 min to obtain a supernatant containing predominantly cytoplasmic proteins.

Protein Quantification by Proteome Separation on SDS-PAGE and Postdigestion ^{18}O Labeling—A 300-μg aliquot of paired protein extracts were suspended in 100 μl sample buffer (5% (w/v) SDS, 10% (v/v) glycerol, 25 mM Tris-Cl, pH 6.8, 10 mM dithiotreitol, and 0.01% (w/v) bromphenol blue), separated on different lanes of a 1.5 mm thick, 10% SDS-PAGE gel, and visualized by Coomassie Brilliant Blue R-250 staining. Gel lanes were horizontally cut into 10 slices and each gel slice was cut into cubes (2×2 mm). The gel cubes were pooled in a tube and subjected to a standard overnight in-gel digestion at 37 °C (32) with 600 μl of 0.01 μg/μl sequencing grade trypsin (Promega, Madison, WI, USA) in 50 mM ammonium bicarbonate, pH 8.8. The resulting tryptic peptides were extracted twice by 1-h incubation at room temperature using 400 μl of 12 mM ammonium bicarbonate, pH 8.8. Trifluoroacetic acid was added to a final concentration of 1% and samples were desalted on OMIX C18 tips (Varian) and dried-down.

Peptides from each gel slice were differentially labeled with either $H_2{}^{16}O$ or $H_2{}^{18}O$ (95%, Isotec, Miamisburg, OH) as previously described (10). After labeling, trypsin beads were removed using a physical filter (Wizard minicolumns; Promega, Madison, WI). The filtered samples were reduced with 10 mM dithiotreitol for 1 h at room temperature, and remaining trypsin activity was eliminated by alkylation by incubating with 50 mM iodoacetamide for 1 h at room temperature on the dark. The paired labeled samples from the corresponding gel fractions were then mixed, diluted to 2.5% acetonitrile (ACN), pH adjusted to 3 with 1 M ammonium formate, pH 3, and desalted onto C18 Oasis HLB Extraction cartridges (Waters, Milford, MA) using as elution solution 50% ACN in 5 mM ammonium formate, pH 3. The resulting peptides from each gel slice were dried down and analyzed separately by RP-HPLC-LIT.

Protein Quantification by One-Step In-Gel Digestion, Peptide ^{18}O Labeling, and IEF Fractionation—The paired protein extracts, containing from 0.25 to 1 mg protein, were suspended in a volume up to 300 μl of sample buffer, and then applied onto 2.8-cm wide wells of a conventional SDS-PAGE gel (0.5 mm-thick, 4% stacking, and 10% resolving). The run was stopped as soon as the front entered 3 mm into the resolving gel, so that the whole proteome became concentrated in the stacking/resolving gel interface (Fig. 1). The unseparated protein bands were visualized by Coomassie staining, excised, cut into cubes (2×2 mm), and digested overnight at 37 °C with 60 ng/μl trypsin at 5:1 protein:trypsin (w/w) ratio in 50 mM ammonium bicar-

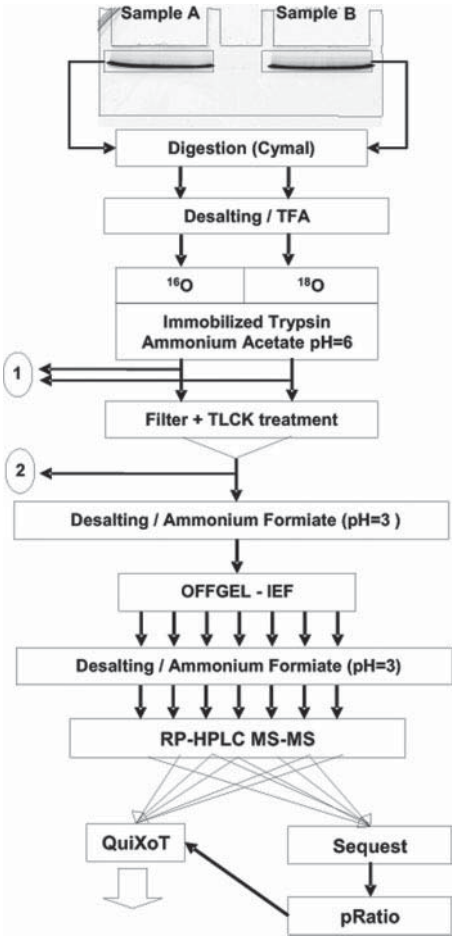

FIG. 1. **Scheme of the proposed ^{18}O-based quantification protocol.** For further details see the text. Numbers 1 and 2 indicate control points to check for labeling efficiency.

bonate, pH 8.8 containing 10% (v/v) ACN and 0.01% (w/v) 5-cyclohexyl-1-pentyl-β-D-maltoside (33). The resulting tryptic peptides from each proteome were extracted by 1-h incubation in 12 mM ammonium bicarbonate, pH 8.8. Trifluoroacetic acid was added to a final concentration of 1% and the peptides were finally desalted onto C18 OASIS cartridges and dried-down.

Dried peptides from the paired samples were subjected to differential $^{16}O/^{18}O$-labeling in 100 mM ammonium acetate, pH 6, 20% ACN, at 1:200 (v:w) immobilized trypsin/protein ratio (10). For the cytosolic fraction of Jurkat T cells, peptides from control cells were labeled with ^{16}O, whereas peptides from activated cells were labeled with ^{18}O. The extent of labeling reaction may be monitored at this point by taking up small aliquots, mixing them up and immediately analyzing them by HPLC-MS/MS. After labeling, trypsin activity was eliminated by removing trypsin beads using a physical filter (Wizard minicolumns, Promega) and by adding to the filtrate the irreversible trypsin inhibitor TLCK at a final concentration of 1 mM from a 50 mg/ml stock solution in methanol and incubating for 1 h at 37 °C. Control of trypsin inactivation may be performed by taking up small aliquots from each sample and checking that no oxygen back-exchange takes place after dilution in nonlabeled water. The two labeled samples were mixed, diluted to 2% ACN and pH adjusted to 3 with 1 M ammonium formate, pH 3, desalted onto C18 Oasis cartridges using as elution solution 50% ACN in 5 mM ammonium formate pH 3, and dried down. Aliquots (5 μg protein) were taken before and after the labeling step to control poor labeling or unlabeling, respectively (Fig. 1). The peptide pools were taken up in focusing buffer (5% glycerol and 2% IPG buffer pH 3–10 or 4–7 (GE Healthcare)) loaded onto 24 wells over a 24 cm long Immobiline DryStrip, pH3–10 or 4–7 (GE Healthcare) and separated by IEF on a 3100 OFFgel fractionator (Agilent, Santa Clara, CA), using the standard method for peptides recommended by the manufacturer. The recovered fractions were acidified with 20 μl of 1 M ammonium formate, pH 3, and the peptides were desalted using OMIX C18 tips. After elution with 50% ACN in 5 mM ammonium formate, pH 3, the peptides were dried-down prior to RP-HPLC-LIT analysis.

For the experiments aimed to analyze the effect of activation on cytoplasmic proteins of Jurkat T cells, peptide samples differentially labeled with $^{16}O/^{18}O$ were desalted separately on C18 Oasis cartridges, mixed at different ratios (1:1, 2:1, 4:1, 8:1, 1:2, 1:4, and 1:8) at a final content of 200 μg of peptides and dried-down. Each one of the peptide mixtures was taken up in 400 μl of 25% ACN in 5 mM ammonium formate pH 3, loaded onto MCX Oasis cartridges (Waters), eluted thrice with 100 μl 25% ACN in 1 M ammonium formate pH 3, twice with 100 μl 25% ACN in 2 M ammonium formate pH 3, and dried-down prior to RP-HPLC-LIT analysis.

LC-MS/MS Analysis and Peptide Identification—All samples were analyzed by LC-MS/MS using a Surveyor LC system coupled to a linear ion trap mass spectrometer model LTQ (Thermo-Finnigan, San Jose, CA) as previously described (34, 35). The LTQ was operated in a data-dependent ZoomScan- and MS/MS-switching mode (36). Zoom target parameters, number of microscans, normalized collision energy, and dynamic exclusion parameters were as previously described (34). Protein identification was carried out as previously described (34) using SEQUEST algorithm (Bioworks 3.2 package, Thermo Finnigan), allowing optional (methionine oxidation, lysine and arginine modification of +4 Da) and fixed modifications (cysteine carboxamidomethylation), two missed cleavages, 2 atomic mass units, or 1.2 atomic mass units mass tolerance for precursor or fragment ions, respectively. The MS/MS raw files from brain (SK-N-MC) and liver (HepG2) cell samples were searched against the Human Swissprot database (Uniprot release 14.0, 19929 sequence entries for human) supplemented with porcine trypsin, whereas those from rat samples were searched against the Mammal Swissprot database (Uniprot release 54.4, 56413 sequence entries for mammal). The same collections of MS/MS spectra were also searched against inverted databases constructed from the same target databases. SEQUEST results were analyzed using the probability ratio method (37) and false discovery rates (FDR) of peptide identifications were calculated from the search results against the inverted databases using the refined method (38).

When the off-gel technique was used to separate peptide pools, we used an improved version of the probability ratio method that took into account the isoelectric point (pI) of the peptides to improve peptide identification. The peptides were first identified by the conventional method using FDR$<$0.01 as a criterion and the median pI of the corresponding peptides was then calculated in each off-gel fraction. An arbitrary window around the mean pI is then applied so that peptides whose pI are outside this window are considered as false identifications and a new peptide identification *versus* FDR curve is constructed. The width of the pI window is then iteratively varied and the FDR curves recalculated until an optimum FDR value is obtained. An example of the improved efficiency in peptide separation obtained using this algorithm can be found in Supplementary Fig. S1. This procedure is robust against potential problems arising during IEF peptide separation, because in no case the final performance is lower than the one obtained without the pI information. The procedure has been implemented into our probability ratio software, which is freely available upon request.

Peptide Quantification and Statistics—Peptide quantification from ZoomScan spectra and calculation of labeling efficiencies of all the identified peptides with a FDR lower than 5% were performed as described (39, 30) using QuiXoT, a program written in C# in our laboratory. Statistical analysis of the data was done on the basis of a novel random-effects model recently developed in our laboratory that includes four different sources of variance: at the spectrum-fitting, scan, peptide, and protein levels (10). The $\log_2$-ratio of peptide concentration in samples A (nonlabeled) and B (labeled) determined by scan *s* coming from peptide *p* derived from protein *q* is expressed as $x_{qps}=\log_2(A/B)$. The statistical weight associated to the scan, w_{qps}, is calculated from the spectrum fitting and the scan variance, σ^2_s, as described (10). The $\log_2$-ratio value associated to each peptide, x_{qp}, is calculated as a weighted average of the scans used to quantify the peptide, and the value associated to each protein, x_q, is similarly the weighted average of its peptides. Besides, a grand mean, x, is calculated as a weighted average of the protein values. In turn, the statistical weight associated to each peptide, w_{qp}, is calculated from the corresponding scan weights and the peptide variance, σ^2_P, and that of each protein, w_q, is calculated from the corresponding peptide weights and the protein variance, σ^2_Q. In all cases the statistical weights are the inverses of variances. Outliers at the scan and peptide levels are detected by calculating the probability that the measurements deviate from the expected average according to their respective variances, and controlling for the false discovery rate at each level, FDR_{qps}, and FDR_{qp}, respectively. Details about the statistical model and the algorithm used to calculate the variances at the scan, peptide, and protein levels can be found in our previous work (10). Raw quantification data may be found at: ftp://150.244.205.155/raw_quantif_data/raw_quantif_data.xls.

RESULTS

Quantitative Analysis of Proteomes by One-Dimensional SDS-PAGE Fractionation, In-Gel Digestion and ^{18}O Labeling—We first analyzed whether one-dimensional-SDS-PAGE protein separation was suitable to perform a relative quantification of two protein preparations by ^{18}O labeling. Two different proteome extracts from rat heart mitochondria, prepared under the same conditions, were separated by SDS-PAGE in two adjacent gel lanes and each protein lane was horizontally cut into 10 pieces at the same places. The 20 resulting gel pieces were subjected to in-gel trypsin digestion separately and the peptides were extracted, desalted, and subjected to trypsin-catalyzed labeling, as described under "Experimental Procedures," the peptides from one sample in the presence of unlabeled water and those from the other in the presence of ^{18}O-labeled water. To assure a complete elimination of residual trypsin activity, a step critical to avoid oxygen back-exchange of labeled peptides in the presence of nonlabeled water (11), we used a two-step procedure. First, immobilized trypsin beads were used for labeling, and the beads were separated by filtration; second, the potentially remaining trypsin activity in the filtrate was inhibited by reduction followed by alkylation. The two peptide samples corresponding to each gel fraction were then mixed and the resulting $^{16}O/^{18}O$-labeled peptide pairs analyzed by RP-HPLC-MS/MS in a LTQ linear ion trap mass spectrometer, making a total of 10 HPLC runs. The LTQ was programmed to perform a Zoom scan spectrum and then an MS/MS spectrum over the six most intense ions detected in a survey MS scan, as described (39). The first scan was used for $^{16}O/^{18}O$-labeled peptide pair quantification, and the second scan for peptide identification. ^{18}O labeling efficiency of each one of the quantified peptide pairs was calculated automatically using an algorithm described previously (30).

As shown in Fig. 2*A*, using this procedure the majority of peptides were labeled with an efficiency of 0.9, and only a small amount had an efficiency lower than 0.8; this result was representative of several different experiments performed using this protocol. Because labeling efficiency is defined as the fraction of labeled oxygen atoms, in these conditions the remaining fraction of nonlabeled peptide belonging to the labeled sample was lower than 0.04; therefore the effect of labeling efficiency on the calculated ratio was in no case superior to 4% and could be efficiently corrected (30).

However, in the same figure it was observed that the cloud of quantifications had a greater dispersion in the $\log_2$-ratio scale than that usually observed in previous analysis using in-solution digestion (10). When quantifications from different gel fractions were analyzed separately, we observed that each fraction's cloud of points was slightly displaced in relation to the others (Fig. 2*A*, black points), thus explaining the increased overall dispersion of quantifications in relation to the grand mean. Although this effect could be partially alleviated by subtracting to the quantifications in each fraction its own grand mean, this procedure introduced numerical errors and consistently produced higher variances than those observed when all the proteins were digested together in-solution (data not shown).

The sources of error associated to this protocol were studied in more detail by using a statistical random-effects model developed for the analysis of ^{18}O labeling data by linear ion trap mass spectrometry (10). This model assigns to every scan (*i.e.* individual quantitative measurement) a different variance, calculated from the fitting of a theoretical isotope profile to the ZoomScan spectra (10); peptide means and variances are then calculated from the different scans by which each peptide is quantified and finally protein means and variances from the different peptides belonging to the same protein (10). One of the advantages of this method is that the variances at the scan level can be used to detect the presence of outliers, *i.e.* of scans that deviate from peptide mean more than expected from their estimated variance. With this protocol we routinely found a striking large proportion of scan outliers (15% of the total number of scans in the example presented in Fig. 2*B*, see black points). A detailed analysis of these outliers revealed that they were produced by peptides coming from proteins that were quantified in different fractions because the proteins were located in the frontier between two adjacent gel slices. Accordingly, when proteins identified in different fractions were statistically treated as if they were

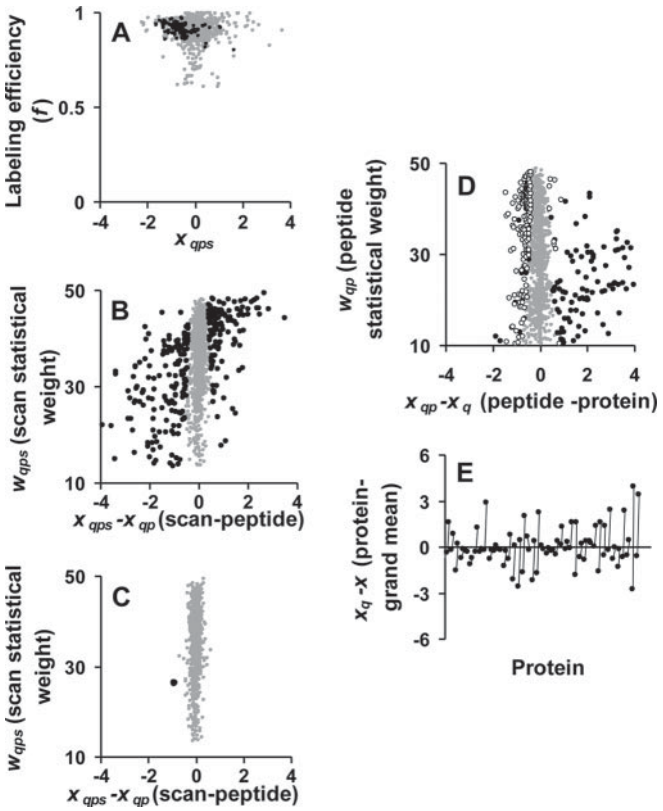

FIG. 2. **Analysis of quantification artifacts associated to ^{18}O labeling by the SDS-PAGE protein fractionation technique.** *A*, Distribution of labeling efficiencies as a function of log2-ratios in a representative experiment (gray points). Scans corresponding to a representative gel fraction are indicated by black points. *B* and *C*, Analysis of outliers at the scan level. The statistical weight associated to each quantification is plotted against the difference between the scan measurement and their corresponding peptide average in order to highlight the presence of outliers. Black points indicate outliers at the scan level (FDRqps $<$ 5%). In (*C*) the peptides and proteins which were quantified in different gel fractions were considered as a different species. *D*, Effect of alkylation on quantifications at the peptide level. The statistical weight associated to each peptide is plotted against the difference between the peptide and their corresponding protein average. Peptides that were acetylated in Lys are indicated by black points, while these that were also found in non-acetylated form are indicated by white points. *E*, Analysis of proteins quantified in more than one gel fraction. The plot shows the protein averages corrected for the grand mean, assuming that the proteins which were quantified in different gel fractions are different entities; the lines join averages from the same protein when they were quantified in different fractions. For all the proteins, the averages having higher protein weights are plotted first. Note that the lines cross the horizontal axis when the protein log-ratios have different sign in the gel fractions.

different entities, the number of scan outliers became negligible, just as observed in a previous work (10) (Fig. 2*C*), indicating that these outliers were not consequence of measurement errors but were produced by the "gel-cutting effect." Further evidence of this effect was provided by plotting the $\log_2$-ratios of proteins that were quantified separately in adjacent fractions (Fig. 2*E*). As shown, in most cases the protein ratios in one fraction were clearly different to those in the other. We have observed this effect to occur systematically in all experiments performed following this protocol, even when the two samples were checked in advance to have the same electrophoretic behavior and the cuts were carefully performed in gel zones where no proteins were detected by Coomassie staining (data not shown).

A further technical problem associated to this protocol is that it requires two reduction/alkylation steps, being the first one necessary to achieve a good yield during in-gel trypsin digestion, and the second to inactivate residual trypsin activity after the labeling step. To analyze whether the double alkylation treatment affected amine groups, known to react to a certain extent with iodoacetyl moieties, and whether these secondary reactions could affect protein quantification at the peptide level, the database search was repeated by setting as variable modification carbamidomethylation at Lys residues and N-terminal peptide ends. We observed that a surprisingly large proportion (20%) of these amine groups was alkylated. Furthermore, peptides containing alkylated amino groups were often detected as peptide outliers, because they tended to produce a ratio significantly different from other peptides belonging to the same protein (Fig. 2*D*). Clearly, an alternative, artifact-free method was also required to attain trypsin inactivation.

Quantitative Analysis of Proteomes by One-Step In-Gel Digestion, ^{18}O-Labeling and Off-Gel Peptide fractionation: Digestion and Labeling Efficiencies—To circumvent the above mentioned limitations, we devised a new strategy, which kept the SDS-PAGE protein treatment step but avoided the gel-cutting effect. In the new protocol, schematized in Fig. 1, voltage was stopped when the front of the run entered 3 mm into the resolving part of the gel, so that all proteins got inside the stacking gel but remained unseparated forming a single band around the stacking and resolving gel interface. The bands from each sample were then cut into pieces and subjected to in-gel trypsin digestion in one single tube per sample. The resulting peptides were then extracted, $^{16}O/^{18}O$-labeled and mixed together.

In-gel digestion conditions were performed using always the same gel geometry, protein concentration, and volume, and protein:trypsin ratios, as described under "Experimental Procedures." To optimize the efficiency of in-gel digestion as much as possible, the detergent 5-cyclohexyl-1-pentyl-β-D-maltoside was also added to the digestion buffer (33). In test experiments, we observed that the presence of 5-cyclohexyl-1-pentyl-β-D-maltoside not only increased the number of peptides that could be identified in the extract, but also the relative proportion of larger peptides (data not shown). Digestion efficiency was assessed by calculating the proportion of identified peptides containing one or more missed cleavages, *i.e.* non-C-terminal Arg or Lys residues not flanked by Pro residues. The new in-gel digestion approach produced a proportion of missed cleavages lower than 10% (Table I), which

TABLE I

Digestion efficiencies and variances calculated at the scan, peptide, and protein levels obtained from the quantitative analysis by ^{18}O-labeling of several proteomes using the proposed protocol. Taken from [10]. The abbreviations used are: H, HepG2 cells; S, SK-N-MC cells; Sec, Jurkat T-cell secretome; Mit, rat heart mitochondria; HUVEC, human umbilical vascular endothelial cells

proteomes	H1	H2	S1	S2	Sec	Mit	HUVEC
% partial digestion[a]	5.3	4.2	2.8	4.6	6.7	8.0	12.9–39.8
Scan variance (σ^2_S) (95% C.I.)	0.011 (0.010–0.012)	0.019 (0.018–0.020)	0.017 (0.015–0.019)	0.015 (0.018–0.020)	0.012 (0.010–0.013)	0.019 (0.017–0.021)	0.018–0.031
Peptide variance (σ^2_P) (95% C.I.)	0.024 (0.019–0.031)	0.018 (0.015–0.021)	0.018 (0.007–0.026)	0.019 (0.015–0.021)	0.023 (0.014–0.029)	0.031 (0.020–0.040)	0.014–0.021
Protein variance (σ^2_Q) (95% C.I).	0.005 (0–0.011)	0.005 (0–0.009)	0.008 (0–0.021)	0.006 (0–0.009)	0.003 (0–0.012)	0.006 (0–0.019)	0.0007–0.004

[a] Partially digested peptides were assumed to be those containing at least one missed cleavage site that did not contain a proline residue after the Arg or Lysine residue.

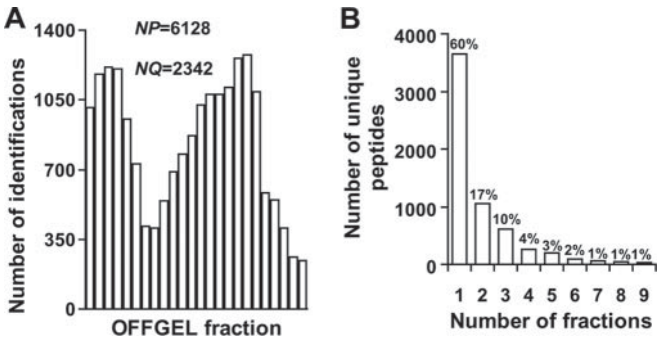

FIG. 3. **Analysis of peptide identifications by the IEF off-gel technique.** *A*, Peptide fractionation profile, *B,* distribution of peptides according to the number of different fractions where they were identified in a representative experiment. These results were obtained from the analysis of a protein extract from HepG2 cells, whose labeled peptides were fractionated into a 4 to 7 pH range. Figures indicate the number of unique peptides (*NP*) and proteins (*NQ*) identified.

was lower than that obtained using the in-solution digestion protocol in the presence of urea (10) (Table I). This digestion efficiency was consistently maintained when proteomes from a variety of different sources, including those rich in membrane proteins, were analyzed, demonstrating the good reproducibility of the protocol (Table I).

After digestion, peptide labeling was performed at pH 6 using ammonium acetate as a buffer (Fig. 1). After the labeling step, and to avoid secondary reactions of residues other than Cys during the alkylation step, in the new protocol trypsin inactivation was achieved by incubating the labeled peptides with the irreversible trypsin inhibitor TLCK (Fig. 1). This procedure was found to be effective to prevent label back-exchange reactions because of residual trypsin activity (see also below).

In the new protocol the pool of labeled peptides were desalted and IEF-separated into 24 fractions (Fig. 1) using the off-gel technique. Because this technique allows an efficient separation of peptides according to their pI, this parameter was used as an additional criterion to improve peptide identification (see Experimental Procedures and Supplemental Fig. S1). A representative distribution of identified peptides along a 4–7 pI range is presented in Fig. 3 *A*; we observed that this pI distribution of peptides was essentially similar when proteomes from other sources were analyzed using this protocol (data not shown) and agreed well with previously published studies (26, 27, 40). We also noticed that the peptide desalting step before off-gel fractionation (Fig. 1) was highly advisable to optimize the IEF peptide separation. In these conditions, more than 65% of the identified peptides were found in only one fraction and more than 75% in one or two fractions (Fig. 3*B*). The peptide redundancy, defined as the ratio of peptides that are identified adding up all the fractions by the final number of unique peptides, was usually lower than two.

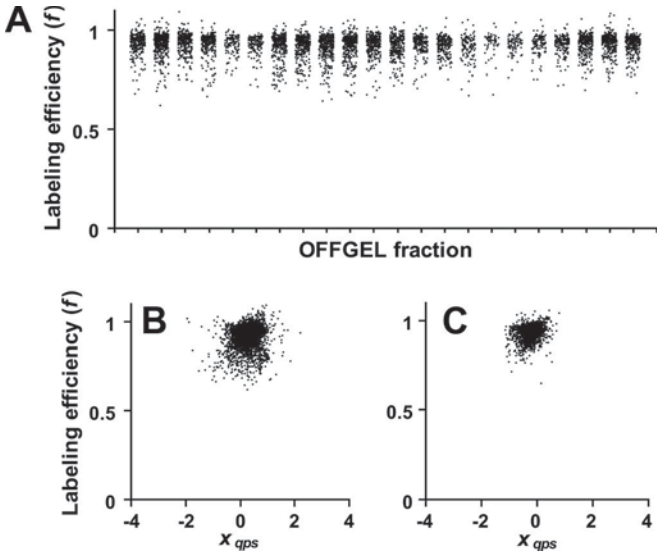

FIG. 4. **Analysis of ^{18}O labeling efficiency of peptides separated by the off-gel technique.** *A*, Plot of individual labeling efficiencies as a function of the IEF fraction. *B*, Plot of labeling efficiencies as a function of the $\log_2$-ratio. These results were obtained using protein extracts from a Jurkat T cell secretome fractionated into a 3 to 10 pH range (*A* and *B*) or protein extracts from HepG2 cells fractionated into a 4 to 7 pH range (*C*).

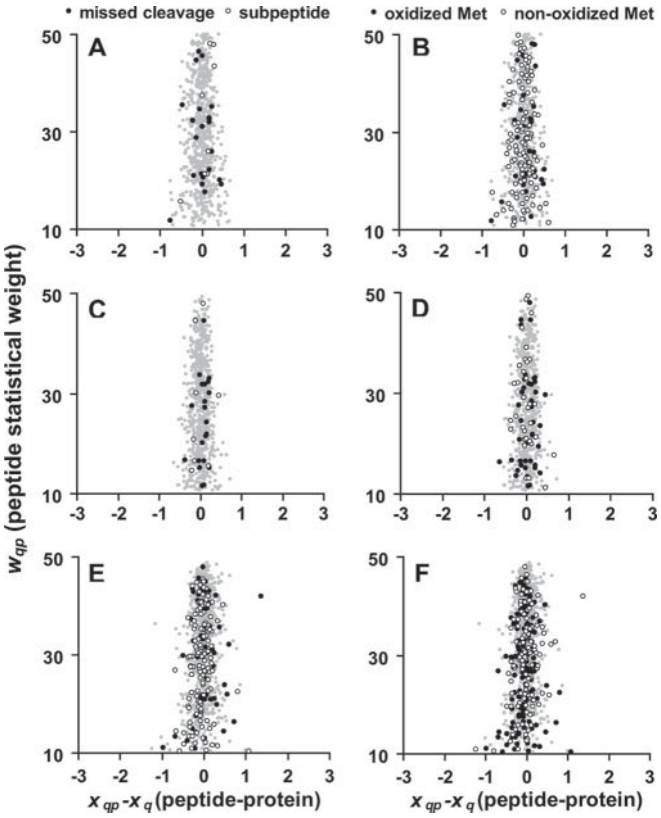

FIG. 5. **Effect of partial digestion and methionine oxidation on relative quantification at the peptide level.** Protein extracts from HepG2 cells (*A*, *B*), SK-N-MC cells (*C*, *D*) and rat heart mitochondria (*E*, *F*) were used as test samples. (*A*, *C*, *E*) Scans corresponding to peptides containing missed cleavage sites, except those with proline after the basic residue, are indicated by black points; subpeptides derived from a partially digested peptide identified in the same experiment are indicated by white circles. (*B*, *D*, *F*) Scans corresponding to peptides containing oxidized methionines (Mox) and nonoxidized methionines (M) are indicated by black points and white circles, respectively.

The compatibility of this protocol to separate ^{18}O-labeled peptides was then investigated by analyzing the labeling efficiency of all the quantified peptides. The procedure included two desalting steps that were performed at a controlled pH 3.0 using ammonium formate buffer (Fig. 1); this pH was low enough to allow quantitative recovery of peptides from C18 solid-phase extraction cartridges and at the same time was high enough to avoid acid-catalyzed oxygen back-exchange reactions. As shown in Fig. 4, the peptides remained effectively labeled during the two desalting steps and all the time needed to run the off-gel fractionations, even when pI ranges of 3 to 10 were used. In addition no tendency to acid or base-catalyzed unlabeling was observed even at the more extreme pH fractions (Fig. 4). The distribution of labeling efficiencies obtained using the new protocol was remarkably similar to the one obtained using the previously proposed protocol (Fig. 4*B* and *C*). These results demonstrate for the first time that the off-gel peptide separation method is fully compatible with ^{18}O labeling.

Quantitative Analysis of Proteomes by One-Step In-Gel Digestion, ^{18}O-Labeling, and Off-Gel Peptide Fractionation: Analysis of Variances—To assess the sources of variability of the new method we applied the statistical model previously developed for ^{18}O quantification by linear ion trap MS (10). We observed that the proportion of scan outliers was negligible (typically no more than three scan outliers among 1300 scans), in agreement with the results obtained previously (10). Besides, and as shown in Table I (second row), the scan variances obtained from a number of different proteomes were all similar to those obtained in a previous work (10). Also, as shown in Table I (fourth row), in none of the proteomes analyzed in this study was the protein variance significantly different from zero. This result just indicated that the different cell cultures and subproteome fractionations used in this study were performed in a way that did not introduce appreciable error sources for relative comparison of protein levels.

Analysis of the variance at the peptide level, a parameter more critical to judge the suitability of the proposed method based on postdigestion SIL, was then performed in detail for each one of the proteomes analyzed in Table I. As shown in Fig. 5, left panels, the peptide quantifications containing missed cleavage sites (black points) or completely digested subpeptides derived from the former (white points) did not show an appreciable deviation from the rest of the peptides, indicating that in all cases the digestion was reproducible in the two samples that were compared. A similar result was obtained when the quantifications of peptides containing ei-

ther nonoxidized (white points) or oxidized Met residues (black points) were analyzed (Fig. 5, *right* panels), indicating that no quantification artifacts were introduced by the protocol because of differential Met oxidation in the two samples. Similar results to those presented in Fig. 5 were obtained with the other proteomes listed in Table I (data not shown). In consistency with these results, the number of peptide outliers yielding a $\log_2$-ratio significantly displaced from the protein average, as judged by the analysis of the FDR_p parameter (see Experimental Procedures) was found to be negligible (less than four per every 1800 quantified peptides) in all the proteomes analyzed. Moreover, and as shown in Table I (third row), the calculated variances at the peptide level were remarkably similar in all proteomes studied and essentially identical to those obtained by in-solution digestion and labeling (10).

The accuracy of the null hypothesis associated to the statistical model was tested in the proteomes analyzed. This was done, as in our previous work (10), by plotting the distribution of protein $\log_2$-ratios standardized according to their estimated variances (z_q values) and fitting the curves to Gaussian functions. As shown in Fig. 6, the standard deviations of the curves were in no case significantly different from one, as expected. In addition, no deviations from normality were detected in any of the corresponding normal probability plots (Fig. 6, inset). Therefore, the errors produced by the proposed protocol were reproducible, well-controlled, and in good agreement with the null hypothesis of the statistical model used and the variance parameters in Table I.

Application of the Technique to Study Cytoplasmic Activation of Jurkat T cells and Analysis of Dynamic Range—To determine the dynamic range of quantification and at the same time demonstrate the utility of the technique for the analysis of protein expression changes within a physiological context, we used as a model cytosolic extracts of either control or phorbol 12-myristate 13-acetate +Io-stimulated Jurkat T cells. These extracts were digested using the one-step in-gel protocol and the resulting peptides from the control and activated cells were labeled with either ^{16}O or ^{18}O, respectively. The two samples were then mixed at different ratios (1:1, 2:1, 4:1, 8:1, 1:2, 1:4, and 1:8), fractionated, and analyzed, so that the quantitative results from these seven independent experiments could be compared in terms of variances and of statistical significance of expression changes.

In each experiment the grand mean (x) was calculated as the weighted mean of the $\log_2$-ratios of all quantified proteins (10). When the grand mean estimations were compared with the expected values, a good agreement was obtained in the entire range except for a slight underestimation of the expected value at the 8:1 ratio (Supplementary Fig. S2*A*). This effect is expected, since at these ratios the isotopic cluster peaks of ^{16}O-labeled peptides significantly interfere with their ^{18}O-labeled peptide counterparts, diminishing the accuracy

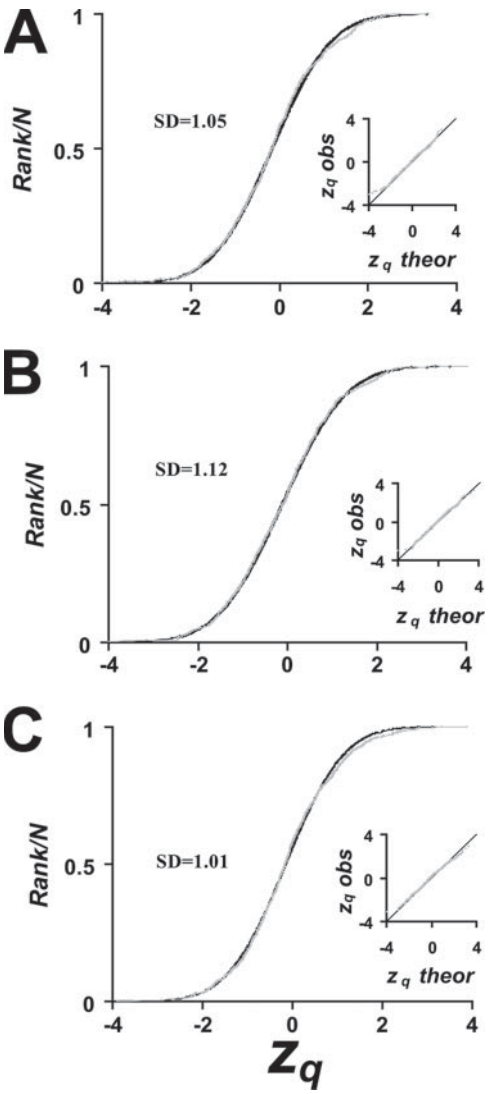

FIG. 6. **Analysis of normality of the quantifications at the protein level in several experiments.** The three panels show the cumulative frequency distributions of the standardized variable z_q (gray points); the insets show the corresponding normal probability plots. Data were obtained from the comparative analysis of protein extracts from HepG2 cells (*A*, *B*) and SK-N-MC cells (*C*). The curves were fitted by least squares to a normal distribution (black lines); the figures indicate the standard deviation (S.D.) corresponding to the best fit.

of the estimated ratios. Accordingly, variances at the scan, peptide, and protein levels remained reasonably stable, and were similar to those obtained with the other proteomes analyzed at 1:1 ratios, except at the peptide level in the case of the 4:1 and 8:1 ratios, where, for the same reason, they showed a tendency to increase (Supplementary Table S1). The distributions of standardized $\log_2$-ratios, however, were in all cases in excellent agreement with the expected curves for a normal distribution with a variance of one, even at the two most extreme sample ratios (Supplementary Fig. S2*B–D*), demonstrating the validity of the null-hypothesis model in the entire dynamic range tested.

TABLE II

Comparative analysis of differential expression events upon Jurkat T cell activation when control and treated samples are mixed at different ratios

Accesion Number	Protein Description[a]	Corrected log_2-ratio[b]								-Fold change[d]		z_q[c]								FDR_q[d]
		1:1	1:2	2:1	1:4	4:1	1:8	8:1	All			1:1	1:2	2:1	1:4	4:1	1:8	8:1	All	
P11021	GRP78 78 kDa glucose-regulated protein precursor	-0.54	-0.54	-0.41	-0.63	-0.40	-0.77	-0.58	-0.56	1.47	up	-5.23	-5.37	-2.51	-5.99	-1.74	-3.77	-1.90	-10.8	1.E-24
P08670	VIME Vimentin	-0.55	-0.49	-0.47	-0.58	-0.38	-0.65	-0.20	-0.52	1.43	up	-5.99	-4.78	-2.84	-5.28	-1.44	-3.24	-0.74	-10.2	3.E-22
P17661	DESM Desmin	-0.60	-0.64	-0.47	-0.66	-0.42	-0.67	-0.01	-0.58	1.50	up	-3.36	-3.30	-1.57	-3.17	-0.97	-2.26	-0.02	-6.23	8.E-08
P43490	NAMPT Nicotinamide phosphoribosyltransferase		-0.75	-0.75	-0.65		0.09		-0.60	1.52	up		-3.77	-2.75	-3.01		0.29		-5.04	5.E-05
Q16891	IMMT Mitochondrial inner membrane protein	-0.49	-0.35	-0.72	-0.26				-0.39	1.31	up	-2.74	-2.95	-2.55	-1.46				-4.74	2.E-04
P30520	PURA2 Adenylosuccinate synthetase isozyme 2	-0.78	-0.49						-0.69	1.61	up	-4.16	-1.86						-4.47	0.001
Q9UJZ1	STML2 Stomatin-like protein 2	-0.53	-0.28	-0.34	-0.35				-0.36	1.28	up	-3.01	-2.28	-1.49	-2.08				-4.42	0.001
P21796	VDAC1 Voltage-dependent anion-selective channel protein 1		-0.53		-0.35				-0.49	1.40	up		-4.18		-1.61				-4.41	0.001
Q9UQ80	PA2G4 Proliferation-associated protein 2G4	-0.84	0.01	-0.71	-0.16	-0.91	-0.85	-0.93	-0.33	1.26	up	-4.60	0.09	-2.49	-0.73	-2.12	-2.57	-1.78	-4.15	0.002
P34932	HSP74 Heat shock 70 kDa protein 4	-0.60	-0.14	-0.09	-0.23	-0.34	-0.29	-0.21	-0.27	1.21	up	-4.37	-1.30	-0.44	-1.06	-0.83	-1.41	-0.73	-4.12	0.002
Q00325	MPCP Phosphate carrier protein	-0.50	-0.23	-0.29	-0.45	-0.35		0.03	-0.35	1.27	up	-2.84	-1.40	-1.04	-2.06	-0.78		0.06	-3.72	0.008
P41219	PERI Peripherin		-0.60	-0.59					-0.60	1.51	up		-2.99	-2.10					-3.66	0.01
Q9Y4L1	HYOU1 Hypoxia up-regulated protein 1 precursor	-0.15	-0.22	-0.49	-0.15	0.07	-0.49	-0.15	-0.22	1.16	up	-1.31	-2.17	-2.13	-1.10	0.18	-2.04	-0.29	-3.57	0.01
P45880	VDAC2 Voltage-dependent anion-selective channel protein 2	-0.50	-0.27						-0.37	1.30	up	-2.75	-1.70						-3.09	0.05
P42025	ACTY Beta-centractin		-0.46	-0.76					-0.59	1.50	up		-1.78	-2.62					-3.07	0.05
P62899	RL31 60S ribosomal protein L31		-0.28		-0.67				-0.48	1.40	up		-1.20		-3.02				-3.02	0.06
P25705	ATPA ATP synthase subunit alpha	-0.23	-0.14	-0.02	-0.16	-0.23	-0.51	0.03	-0.17	1.13	up	-1.79	-1.21	-0.09	-1.32	-0.83	-2.02	0.08	-2.83	0.10
P62988	UBIQ Ubiquitin	0.284	0.173	0.18	0.27	-0.02	0.256	-0.09	0.215	1.16	down	1.643	1.132	0.678	1.66	-0.04	0.799	-0.17	2.61	0.11
P60174	TPIS Triosephosphate isomerase	0.347	-0.04	0.228	-0.08	0.51	0.038	0.552	0.166	1.12	down	3.408	-0.32	1.231	-0.5	1.664	0.119	1.464	2.7	0.09
O60234	GMFG Glia maturation factor gamma		0.485	-0.12			0.94	-1.12	0.349	1.27	down		2.895	-0.42			2.979	-2.11	2.73	0.09
Q9NVI1	FANCI Fanconi anemia group I protein		0.21		0.71				0.36	1.29	down		1.38		2.99				2.80	0.08
Q9P2J5	SYLC Leucyl-tRNA synthetase		0.20	-0.10	0.44	0.51		0.31	0.26	1.20	down		1.62	-0.32	2.57	1.24		0.56	2.84	0.08
Q16643	DREB Drebrin	0.47	0.18	0.27	0.21				0.27	1.21	down	2.58	1.27	0.94	0.99				2.9	0.06
Q8TCS8	PNPT1 Polyribonucleotide nucleotidyltransferase 1		0.05		0.91		0.57		0.41	1.33	down		0.25		3.53		1.81		2.92	0.06
P17252	KPCA Protein kinase C alpha type		0.53	0.40					0.48	1.40	down		2.60	1.39					2.93	0.06
O00767	ACOD Acyl-CoA desaturase		0.49	0.44					0.47	1.39	down		2.45	1.61					2.93	0.06
P54819	KAD2 Adenylate kinase isoenzyme 2		0.13	-0.16	0.74		0.82		0.35	1.28	down		0.67	-0.55	3.31		2.56		2.94	0.06
P62917	RL8 60S ribosomal protein L8	0.37	0.24			0.68			0.31	1.24	down	1.94	1.87			1.68			2.98	0.06
Q9NR28	DBLOH Diablo homolog		0.80	0.12					0.54	1.46	down		3.62	0.44					3.11	0.04
Q6UXN9	WDR82 WD repeat-containing protein 82	0.42	0.34	0.31				0.48	0.38	1.30	down	2.25	1.74	1.08				0.95	3.15	0.04
Q14165	K0152 Uncharacterized protein KIAA0152 precursor		0.63	-0.32			1.37		0.52	1.43	down		2.77	-1.07			4.04		3.27	0.03
P20700	LMNB1 Lamin-B1	0.34	0.54						0.43	1.34	down	1.96	2.75						3.29	0.03
P16949	STMN1 Stathmin	0.47	0.23	0.29	0.13	0.38	0.12	0.20	0.27	1.20	down	2.86	1.55	1.35	0.77	0.95	0.37	0.40	3.4	0.02
P06400	RB Retinoblastoma-associated protein		0.37	0.47				0.39	0.39	1.31	down		2.85	1.64				1.05	3.44	0.02
P58546	MTPN Myotrophin		0.47				0.79	0.88	0.57	1.48	down		2.44				2.23	1.61	3.54	0.01
P60981	DEST Destrin		0.36		0.78				0.54	1.45	down		1.84		3.36				3.58	0.01
Q7L9L4	MOL1A Mps one binder kinase activator-like 1A	0.29	0.45	0.66	0.33	0.53	0.42	0.58	0.41	1.33	down	1.70	2.36	2.43	1.58	1.32	1.43	1.17	4.5	4.E-04
P31350	RIR2 Ribonucleoside-diphosphate reductase subunit M2	0.63	0.36	0.26	0.52	-0.12	0.42	-0.13	0.40	1.32	down	3.70	2.59	1.18	2.45	-0.29	1.27	-0.26	4.92	6.E-05
P62805	H4 Histone H4	0.40	0.26	0.59	0.18	0.80	0.07	0.78	0.35	1.27	down	3.04	1.83	2.98	1.09	2.57	0.28	1.99	5.05	3.E-05
P01733	TVB1 T-cell receptor beta chain V region YT35 precursor		0.93	0.52		0.93		0.97	0.81	1.75	down		4.03	1.78		2.15		1.82	5.09	3.E-05
P61604	CH10 10 kDa heat shock protein	0.41	0.32	0.63	0.06	0.58	0.78		0.37	1.29	down	3.16	2.51	3.22	0.37	1.33	2.55		5.23	2.E-05
P37268	FDFT Squalene synthetase		1.07	0.81					1.02	2.03	down		7.62	2.91					8.11	1.E-13

[a] Proteins quantified in two or more experiments.

[b] Log_2-ratios were corrected by subtracting the grand mean value obtained in each experiment.

[c] Standardized normal values were obtained by dividing protein log_2-ratios by their variance, as described [10].

[d] The fold change and the FDR_q (false discovery rate at the protein level) were calculated by analyzing as a whole all the results from the seven experiments. Proteins are sorted by z_q. The magnitudes of expression change and of the standardized variable are shown according to the color scales on the top.

Further information about the performance of the method along the dynamic range was obtained by comparing the expression changes induced by activation of Jurkat T cells at the seven sample ratios. As shown in Table II, an excellent agreement in the magnitude and sign of the most significant expression changes was obtained in all the experiments. In addition, although the statistical significance of expression changes (expressed in terms of the standardized variable z_q in Table II) showed a tendency to diminish at the more extreme sample ratios, as expected, the significance results were highly consistent in all the experiments.

The statistical model that bases our method allows accurate estimations of the dispersion of each one of the measurements at the scan, peptide, or protein levels by just calculating the variance as the inverse of the statistical weight (10). For illustrative purposes the dispersions of the log_2-ratios obtained by using the proposed method are presented in Fig. 7. Note that these are typical results, because, as shown in Table I (and also Supplemental Table S1), the general variances are obtained in a reproducible manner in different kinds of samples. As shown, the total dispersion of log_2-ratios tend to diminish at higher weights, but even the less accurate measurements rarely deviates more than twofold from the expected value (Fig. 7*A*). The dispersions of individual scans from their peptide mean (Fig. 7*B*) and of peptides from their protein mean (Fig. 7*C*) are very narrow and because of the effect of averaging produce an even narrower distribution of proteins around the grand mean (Fig. 7*D*). In these conditions,

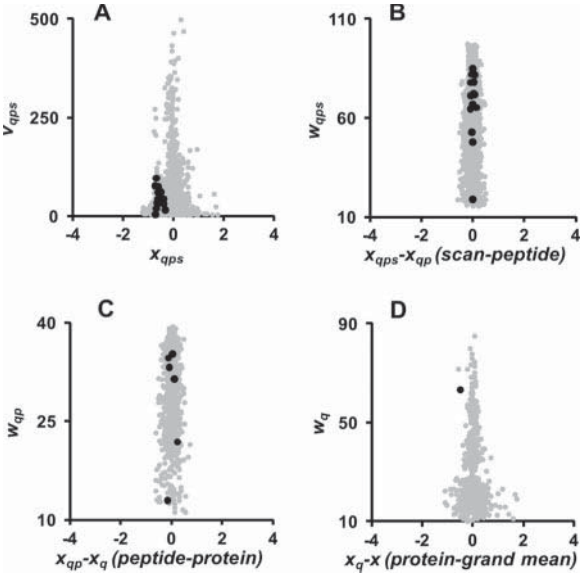

FIG. 7. **Accuracy of quantifications at the scan, peptide and protein levels.** The four graphs show the total dispersion of $\log_2$-ratios (*A*), the dispersion of scans from their peptide mean (*B*), the dispersion of peptides from their protein mean (*C*) and the dispersion of proteins from the grand mean (*D*). The *y* axis are the fitting weight (*A*) or the weights at each one of the three levels (*B*, *C*, *D*), whose inverses can be used as estimates of local variances. These results are taken from the quantitative analysis of cytosolic extracts of control and activated Jurkat T cells mixed at 1:1 (^{16}O:^{18}O) ratio. Black points correspond to quantifications associated to the protein vimentin.

expression changes as small as those of the protein vimentin (1.4-fold increase, Table II) are clearly rendered as statistically significant (Fig. 7, black points).

To determine what proteins showed significant expression changes after stimulation of Jurkat T cells, we analyzed as a whole the results obtained in all the experiments. Using a 10% FDR_q threshold, corresponding to less than two false expression changes, 17 proteins were found up-regulated and 25 down-regulated (Table II). Among these, several proteins are known be involved in T-cell signaling. Thus, NAMPT, STML-2, PA2G4, and PURA2, proteins playing a role in T-cell activation (41–45), were increased. The actin-binding protein Drebrin also decreased in the cytosolic fraction of activated Jurkat T cells, in line with recent findings demonstrating relocalization of this protein toward the immunological synapse at the plasma membrane in activated human T cells (46). In addition, a long-time treatment with phorbol 12-myristate 13-acetate plus Io has also been reported to induce apoptosis in Jurkat T cells (47); accordingly, a number of proteins known for participating in the cellular response to stress conditions were found increased in this analysis, including the ER-stress sensors GRP78 and HYOU1 (48, 49); a subunit of the ATP synthase complex, ATPA (50), and the mitochondria-mediated apoptosis proteins VDAC1 (51), VDAC2 (52), and IMMT (53). Some of the proteins whose levels decreased in the cytoplasm of our cells (H4 and KPCA) have recently been reported to increase in the lipid raft fraction of apoptotic Jurkat T cells (54). In these cells, KPCA disappears from the cytoplasm and is redistributed to lipid rafts of plasma membrane (54). Such relocalization of KPCA under apoptotic conditions is consistent with the reduction of KPCA in our cytosolic extracts. The list of down-regulated proteins also includes cytoskeletal proteins (DEST, LMNB1, STMN1, and MTPN), proteins playing a role in energy (TPIS) and lipid metabolism (ACOD, FDFT), and in protein synthesis and degradation (UBIQ, SYLC, and RL8 60S). All these results indicate that, although some accuracy is lost in the detection of changes taking place at high ratios, the proposed protocol allows full control over the sources of variance and accurate estimation of statistical significances for the detection of protein expression changes of physiological relevance in a dynamic range spanning about two orders of magnitude.

DISCUSSION

In this work we present a general protocol for ^{18}O-based labeling tested on a set of samples of different nature. During optimization of experimental conditions in order to minimize quantification artifacts because of digestion, methonine oxidation, and incomplete labeling, this protocol was subjected to a profound statistical analysis on the basis of a previously published statistical model (10). As a first step toward this general ^{18}O-labeling protocol, we performed a detailed statistical analysis of the widely used in-gel digestion method of SDS-PAGE-separated proteins (19, 20). SDS-solubilized proteins are known to be readily digested in-gel after SDS-PAGE protein separation and SDS elimination from the gel matrix. We reasoned that this kind of approach based on protein solubilization using SDS would be compatible with most kinds of proteomes, including those containing hydrophobic and membrane proteins. However, our data clearly demonstrates that although this protocol is satisfactory from the point of view of labeling efficiency, it suffers from an increased quantification variance, because each fraction has to be digested and labeled separately. This manipulation introduces systematic effects that are impossible to control at exactly the same extent in all the fractions. Moreover, even when the gel is cut into fractions at gel zones where proteins are not detected by staining, it is very difficult, if not impossible, to cut all proteins into fractions having exactly the same proportion in the two samples, especially in the case of proteins located at the cutting point between two adjacent gel slices. This makes unreliable the quantification of a protein located in adjacent fractions. Our data uncovers for the first time the "gel-cutting" effect associated to the one-dimensional-SDS-PAGE protein separation, demonstrating the problems encountered when this protocol is used with postdigestion SIL techniques. Also, we demonstrate that the reduction/alkylation step traditionally used for trypsin inactivation after ^{18}O-labeling, modified a significant proportion of peptide amino groups, introducing an

additional source of quantification artifacts at the peptide level. This effect was produced because, being amine alkylation a minor reaction, it is highly unlikely that it takes place at exactly the same extent in the two protein samples.

Taking into account these results we designed an improved high-throughput semiquantitative proteomics protocol, based on protein concentration on SDS-PAGE, followed by one-step in-gel digestion and peptide ^{18}O-labeling. Because reproducibility and efficiency of the digestion step is critical to achieve a robust and artifact-free peptide-centric quantification, the in-gel digestion step was optimized, obtaining higher and more reproducible digestion efficiencies with proteomes of different nature, including membrane proteomes, compared with in-solution digestion. To minimize eventual losses of long peptides, which have been associated to in-gel digestion procedures (see for instance 55), the detergent 5-cyclohexyl-1-pentyl-β-D-maltoside was added to the digestion mixture. This detergent has been described to improve recovery of large hydrophobic peptides, reducing the risk of entrapment of proteolytic peptides within the gel matrix (33). Moreover, the good digestion efficiency of the new protocol was checked as not to be because of a bias against longer peptides partially retained by the gel matrix, because with this protocol long peptides containing missed cleavage sites were sometimes detected in higher amounts during the optimization of experimental conditions (not shown). After the labeling, the reduction/alkylation step was substituted by treatment with the irreversible trypsin inhibitor TLCK, a modification that was found to be effective in preventing label back-exchange throughout all the time of analysis. This step avoided the possibility of uncontrolled chemical modifications introducing quantification artifacts. Fractionation of labeled peptides was performed by off-gel IEF, a method that gave very satisfactory results in terms of reproducibility and peptide quantification performance, in agreement with other recent works (27, 28, 29), This method also allowed using the pI as an additional criterion to validate peptide identifications (25). As we show in the supplemental information, the number of peptides identified at the same error rate increased typically by 5%–7%, depending on the pH range used, being this effect more pronounced at narrow pH ranges. By analyzing the labeling efficiency of each one of the quantified peptides, we could demonstrate that the off-gel separation is fully compatible with ^{18}O peptide labeling, even at rather extreme pH values of 3 or 10. Although ^{18}O labels are long known to be pH-sensitive (10, 11) and off-gel IEF have been used before by others to fractionate ^{18}O-labeled peptides (24), to the best of our knowledge the label stability as a source of potential artifacts has not been analyzed before and was not taken into account in previous studies devoted to protein quantification by SIL.

The suitability of a stable isotope labeling method for quantitative proteomics can only be established by analyzing the accuracy with which proteins are quantified, using an appropriate statistical framework. After analyzing a set of proteomes of different nature, together with a proteome exhibiting differential expression of proteins in which the control and treated samples are mixed at different relative proportions, we demonstrate that the variance at the scan level was essentially identical for all of them. Although this similarity was foreseen, because quantifications were made using the same MS method described before (39), we should note that this result reinforces the robustness of the statistical algorithm used to analyze this kind of data. On the other hand, the two main sources of variability at the peptide level are the partial digestions and methionine oxidation, which may occur at different extents in the two samples, making protein quantification unreliable. We demonstrate that in the novel protocol these two potential sources of quantification artifacts do not increase the variability for individual peptide quantification, rendering practically identical variances at the peptide level for all the proteomes analyzed. The variability because of the residual degree of partial digestion was minimized thanks to the efficient and reproducible in-gel digestion achieved in the new protocol. Also the new approach involved less sample manipulation and only about a third of the mass spectrometric analysis time compared with previous conditions (10), which probably might be the cause for the absence of Met oxidation artifacts. Hence, the new protocol allowed the inclusion in the analysis of all scans corresponding to partially digested and Met-containing peptides, which may amount up to 25% of those yielding positive peptide identification, thus increasing the number of quantified peptides without compromising protein quantification accuracy. We also analyze the dynamic range of quantification and demonstrate the utility of the method in the practice by showing the consistent detection of expression changes in a model of activated T cells. At the protein level, the source of variance is related to the method used to prepare the biological samples and to extract the proteins, and has little, if any, relation with the MS method used for protein quantification. The variance at the protein level was also similar among all the analyzed proteomes and close to zero, indicating that no biases were introduced during sample preparation from cell cultures, tissues, or subcellular fractionations. Finally, the distribution of quantified proteins, normalized according to its estimated variance, could be very accurately explained by a Gaussian function with a standard deviation of one in all the cases. This final and definitive result indicates that the variance integration at the three quantification levels was properly performed to calculate the final protein variances, which behaved as expected according to the statistical model.

Taken together, all these results demonstrate that the proposed protocol for protein digestion and ^{18}O labeling is suitable for performing quantitative studies on a wide variety of protein preparations. To the best of our knowledge, this is the first time that a general protocol for stable isotope labeling is tested in practice using a collection of samples of different origin and analyzed at this degree of statistical detail. The

development and testing of such protocol was possible thanks to the algorithm that calculates the individual ^{18}O-labeling efficiency of all the peptides (30) and also to the existence of a statistical model for the null hypothesis (10) against which the different levels of variance associated to the experimental procedure can be tested. The similarity of the variances also suggest that following carefully the experimental conditions described here the null-hypothesis model defined by these variances can be considered as a good approach to detect the presence of significant expression changes in true quantitative experiments obviating the need for a careful adjustment of variances in each experiment. This would speed up the time required to interpret quantitative data generated in large-scale experiments. Similarly, the set of variances presented in this work can be used as reference for the detection of additional sources of error and artifacts. In our experience we have found some instances where an increase in variance at the scan level was indicative of malfunctions in the mass spectrometer, whereas at the peptide level they warned us against problems in the digestion step. We have also been able to detected significant increases in the variance at the protein level when experiments were performed trying to compare samples that required many steps of protein preparation (data not shown).

In summary, in this work we present a new protocol based on SDS-PAGE protein concentration, one-step in-gel digestion, peptide ^{18}O-labeling, and fractionation by off-gel IEF. This protocol, together with our previously developed computational algorithm that allows semi-automated data analysis (30), could become a general approach to perform large-scale semiquantitative proteomic studies by ^{18}O labeling and linear ion trap mass spectrometry. We believe that with these developments the ^{18}O-labeling technique has reached its maturity, attaining the same level of reproducibility and stability than other SIL methods, with the added value that it has a validated statistical model for the null hypothesis. With these technical advances it is now possible to exploit on a routine basis the advantages of the ^{18}O labeling procedure, including its universal applicability, absence of background reactions, and the possibility of labeling large amounts of protein material.

* This work was supported by grants BIO2006-10085, SAF 2009–03736 and SAF 2006-8348 from Spain's Ministerio de Educación y Ciencia, CAM BIO/0194/2006 from Comunidad de Madrid, the Fondo de Investigaciones Sanitarias (Ministerio de Sanidad y Consumo, Instituto Salud Carlos III, RECAVA RD06/0014), and by an institutional grant by Fundación Ramón Areces to CBMSO (Centre of Molecular Biology "Severo Ochoa").

[S] This article contains supplemental Fig. S1 and Table S1.

** To whom correspondence should be addressed: Jesús Vázquez, Centro de Biología Molecular Severo Ochoa, CSIC-Universidad Autónoma de Madrid, 28049 Cantoblanco, Madrid, Spain. Tel.: +34 91 196 4628; Fax: +34 91 196 4420; E-mail: jvazquez@cbm.uam.es.

REFERENCES

1. Li, X.J., H. Zhang, J.A. Ranish, and R. Aebersold, (2003) Automated statistical analysis of protein abundance ratios from data generated by stable-isotope dilution and tandem mass spectrometry. *Anal Chem*, **75,** 6648–57
2. Ong, S.E., B. Blagoev, I. Kratchmarova, D.B. Kristensen, H. Steen, A. Pandey, and M. Mann, (2002) Stable isotope labeling by amino acids in cell culture, SILAC, as a simple and accurate approach to expression proteomics. *Mol Cell Proteomics*, **1,** 376–86
3. Griffin, T.J., H. Xie, S. Bandhakavi, J. Popko, A. Mohan, J.V. Carlis, and L. Higgins, (2007) iTRAQ reagent-based quantitative proteomic analysis on a linear ion trap mass spectrometer. *J Proteome Res*, **6,** 4200–9
4. Schnolzer, M., P. Jedrzejewski, and W.D. Lehmann, (1996) Protease-catalyzed incorporation of 18O into peptide fragments and its application for protein sequencing by electrospray and matrix-assisted laser desorption/ionization mass spectrometry. *Electrophoresis*, **17,** 945–53
5. Yao, X., A. Freas, J. Ramirez, P.A. Demirev, and C. Fenselau, (2001) Proteolytic 18O labeling for comparative proteomics: model studies with two serotypes of adenovirus. *Anal Chem*, **73,** 2836–42
6. Mirgorodskaya, O.A., Y.P. Kozmin, M.I. Titov, R. Korner, C.P. Sonksen, and P. Roepstorff, (2000) Quantitation of peptides and proteins by matrix-assisted laser desorption/ionization mass spectrometry using (18)O-labeled internal standards. *Rapid Commun Mass Spectrom*, **14,** 1226–32
7. Pierce, A., R.D. Unwin, C.A. Evans, S. Griffiths, L. Carney, L. Zhang, E. Jaworska, C.F. Lee, D. Blinco, M.J. Okoniewski, C.J. Miller, D.A. Bitton, E. Spooncer, and A.D. Whetton, (2008) Eight-channel iTRAQ enables comparison of the activity of six leukemogenic tyrosine kinases. *Mol Cell Proteomics*, **7,** 853–63
8. Gygi, S.P., B. Rist, S.A. Gerber, F. Turecek, M.H. Gelb, and R. Aebersold, (1999) Quantitative analysis of complex protein mixtures using isotope-coded affinity tags. *Nat Biotechnol*, **17,** 994–9
9. Leichert, L.I., F. Gehrke, H.V. Gudiseva, T. Blackwell, M. Ilbert, A.K. Walker, J.R. Strahler, P.C. Andrews, and U. Jakob, (2008) Quantifying changes in the thiol redox proteome upon oxidative stress in vivo. *Proc. Natl. Acad. Sci. U.S.A.*, **105,** 8197–202
10. Jorge, I., P. Navarro, P. Martinez-Acedo, E. Nunez, H. Serrano, A. Alfranca, J.M. Redondo, and J. Vazquez, (2009) Statistical model to analyze quantitative proteomics data obtained by 18O/16O labeling and linear ion trap mass spectrometry: Application to the study of VEGF-induced angiogenesis in endothelial cells. *Mol Cell Proteomics*, **8,** 1130–49
11. Staes, A., H. Demol, J. Van Damme, L. Martens, J. Vandekerckhove, and K. Gevaert, (2004) Global differential non-gel proteomics by quantitative and stable labeling of tryptic peptides with oxygen-18. *J Proteome Res*, **3,** 786–91
12. Blonder, J., M.L. Hale, K.C. Chan, L.R. Yu, D.A. Lucas, T.P. Conrads, M. Zhou, M.R. Popoff, H.J. Issaq, B.G. Stiles, and T.D. Veenstra, (2005) Quantitative profiling of the detergent-resistant membrane proteome of iota-b toxin induced vero cells. *J Proteome Res*, **4,** 523–31
13. Wang, N., L. Mackenzie, A.G. De Souza, H. Zhong, G. Goss, and L. Li, (2007) Proteome profile of cytosolic component of zebrafish liver generated by LC-ESI MS/MS combined with trypsin digestion and microwave-assisted acid hydrolysis. *J Proteome Res*, **6,** 263–72
14. Manza, L.L., S.L. Stamer, A.J. Ham, S.G. Codreanu, and D.C. Liebler, (2005) Sample preparation and digestion for proteomic analyses using spin filters. *Proteomics*, **5,** 1742–5
15. Liebler, D.C., and A.J. Ham, *Spin filter-based sample preparation for shotgun proteomics.* Nat Methods, 2009; **6(11):** p. 785; author reply 785–6
16. Kaji, H., Y. Yamauchi, N. Takahashi, and T. Isobe, (2006) Mass spectrometric identification of N-linked glycopeptides using lectin-mediated affinity capture and glycosylation site-specific stable isotope tagging. *Nat Protoc*, **1,** 3019–27
17. Smith, J.R., M. Olivier, and A.S. Greene, (2007) Relative quantification of peptide phosphorylation in a complex mixture using 18O labeling. *Physiol Genomics*, **31,** 357–63
18. Washburn, M.P., D. Wolters, and J.R. Yates, 3rd, *Large-scale analysis of the yeast proteome by multidimensional protein identification technology*. Nat Biotechnol, **19(3):** p. 242–7, 2001
19. de Godoy, L.M., J.V. Olsen, J. Cox, M.L. Nielsen, N.C. Hubner, F. Frohlich, T.C. Walther, and M. Mann, (2008) Comprehensive mass-spectrometry-based proteome quantification of haploid versus diploid yeast. *Nature*, **455,** 1251–4

20. de Godoy, L.M., J.V. Olsen, G.A. de Souza, G. Li, P. Mortensen, and M. Mann, *Status of complete proteome analysis by mass spectrometry: SILAC labeled yeast as a model system*. Genome Biol, 2006; **7(6):** p. R50
21. Wisniewski, J.R., A. Zougman, N. Nagaraj, and M. Mann, (2009) Universal sample preparation method for proteome analysis. *Nat Methods*, **6,** 359–62
22. Bantscheff, M., B. Dumpelfeld, and B. Kuster, (2004) Femtomol sensitivity post-digest (18)O labeling for relative quantification of differential protein complex composition. *Rapid Commun Mass Spectrom*, **18,** 869–76
23. Lane, C.S., Y. Wang, R. Betts, W.J. Griffiths, and L.H. Patterson, (2007) Comparative cytochrome P450 proteomics in the livers of immunodeficient mice using 18O stable isotope labeling. *Mol Cell Proteomics*, **6,** 953–62
24. An, Y., Z. Fu, P. Gutierrez, and C. Fenselau, (2005) Solution isoelectric focusing for peptide analysis: comparative investigation of an insoluble nuclear protein fraction. *J Proteome Res*, **4,** 2126–32
25. Chenau, J., S. Michelland, J. Sidibe, and M. Seve, *Peptides OFFGEL electrophoresis: a suitable pre-analytical step for complex eukaryotic samples fractionation compatible with quantitative iTRAQ labeling*. Proteome Sci, 2008. **6:** p. 9
26. Horth, P., C.A. Miller, T. Preckel, and C. Wenz, (2006) Efficient fractionation and improved protein identification by peptide OFFGEL electrophoresis. *Mol Cell Proteomics*, **5,** 1968–74
27. Fraterman, S., U. Zeiger, T.S. Khurana, N.A. Rubinstein, and M. Wilm, (2007) Combination of peptide OFFGEL fractionation and label-free quantitation facilitated proteomics profiling of extraocular muscle. *Proteomics*, **7,** 3404–16
28. Heller, M., M. Ye, P.E. Michel, P. Morier, D. Stalder, M.A. Junger, R. Aebersold, F. Reymond, and J.S. Rossier, (2005) Added value for tandem mass spectrometry shotgun proteomics data validation through isoelectric focusing of peptides. *J Proteome Res*, **4,** 2273–82
29. Graumann, J., N.C. Hubner, J.B. Kim, K. Ko, M. Moser, C. Kumar, J. Cox, H. Scholer, and M. Mann, (2008) Stable isotope labeling by amino acids in cell culture (SILAC) and proteome quantitation of mouse embryonic stem cells to a depth of 5,111 proteins. *Mol Cell Proteomics*, **7,** 672–83
30. Ramos-Fernandez, A., D. Lopez-Ferrer, and J. Vazquez, (2007) Improved method for differential expression proteomics using trypsin-catalyzed 18O labeling with a correction for labeling efficiency. *Mol Cell Proteomics*, **6,** 1274–86
31. Boengler, K., G. Dodoni, A. Rodriguez-Sinovas, A. Cabestrero, M. Ruiz-Meana, P. Gres, I. Konietzka, C. Lopez-Iglesias, D. Garcia-Dorado, F. Di Lisa, G. Heusch, and R. Schulz, (2005) Connexin 43 in cardiomyocyte mitochondria and its increase by ischemic preconditioning. *Cardiovasc Res,* **67,** 234–44
32. Shevchenko, A., H. Tomas, J. Havlis, J.V. Olsen, and M. Mann, (2006) In-gel digestion for mass spectrometric characterization of proteins and proteomes. *Nat Protoc*, **1,** 2856–60
33. Katayama, H., T. Tabata, Y. Ishihama, T. Sato, Y. Oda, and T. Nagasu, (2004) Efficient in-gel digestion procedure using 5-cyclohexyl-1-pentyl-beta-D-maltoside as an additive for gel-based membrane proteomics. *Rapid Commun Mass Spectrom*, **18,** 2388–94
34. Lopez-Ferrer, D., S. Martinez-Bartolome, M. Villar, M. Campillos, F. Martin-Maroto, and J. Vazquez, (2004) Statistical model for large-scale peptide identification in databases from tandem mass spectra using SEQUEST. *Anal Chem*, **76,** 6853–60
35. Ortega-Perez, I., E. Cano, F. Were, M. Villar, J. Vazquez, and J.M. Redondo, (2005) c-Jun N-terminal kinase (JNK) positively regulates NFATc2 transactivation through phosphorylation within the N-terminal regulatory domain. *J. Biol. Chem.*, **280,** 20867–78
36. Jorge, I., E.M. Casas, M. Villar, I. Ortega-Perez, D. Lopez-Ferrer, A. Martinez-Ruiz, M. Carrera, A. Marina, P. Martinez, H. Serrano, B. Canas, F. Were, J.M. Gallardo, S. Lamas, J.M. Redondo, D. Garcia-Dorado, and J. Vazquez, (2007) High-sensitivity analysis of specific peptides in complex samples by selected MS/MS ion monitoring and linear ion trap mass spectrometry: application to biological studies. *J Mass Spectrom*, **42,** 1391–403
37. Martinez-Bartolome, S., P. Navarro, F. Martin-Maroto, D. Lopez-Ferrer, A. Ramos-Fernandez, M. Villar, J.P. Garcia-Ruiz, and J. Vazquez, (2008) Properties of average score distributions of SEQUEST: the probability ratio method. *Mol Cell Proteomics*, **7,** 1135–45
38. Navarro, P., and V.Z. JS, *A refined method to calculate False Discovery Rates for peptide identification using decoy databases*. J Proteome Res, **8(4):** p. 1792–6, 2009
39. Lopez-Ferrer, D., A. Ramos-Fernandez, S. Martinez-Bartolome, P. Garcia-Ruiz, and J. Vazquez, *Quantitative proteomics using 16O/18O labeling and linear ion trap mass spectrometry*. Proteomics, 2006. **6 Suppl 1:** p. S4–11
40. Cargile, B.J., D.L. Talley, and J.L. Stephenson, Jr., *Immobilized pH gradients as a first dimension in shotgun proteomics and analysis of the accuracy of pI predictability of peptides*. Electrophoresis, **25(6):** p. 936–45, 2004
41. Feske, S., J. Giltnane, R. Dolmetsch, L.M. Staudt, and A. Rao, (2001) Gene regulation mediated by calcium signals in T lymphocytes. *Nat Immunol*, **2,** 316–24
42. Rongvaux, A., R.J. Shea, M.H. Mulks, D. Gigot, J. Urbain, O. Leo, and F. Andris, (2002) Pre-B-cell colony-enhancing factor, whose expression is up-regulated in activated lymphocytes, is a nicotinamide phosphoribosyltransferase, a cytosolic enzyme involved in NAD biosynthesis. *Eur. J. Immunol.*, **32,** 3225–34
43. Kirchhof, M.G., L.A. Chau, C.D. Lemke, S. Vardhana, P.J. Darlington, M.E. Marquez, R. Taylor, K. Rizkalla, I. Blanca, M.L. Dustin, and J. Madrenas, (2008) Modulation of T cell activation by stomatin-like protein 2. *J. Immunol.*, **181,** 1927–36
44. Sun, H., N. Li, X. Wang, T. Chen, L. Shi, L. Zhang, J. Wang, T. Wan, and X. Cao, *Molecular cloning and characterization of a novel muscle adenylosuccinate synthetase, AdSSL1, from human bone marrow stromal cells.* Mol Cell Biochem., 2005. **269(1–2):** p. 85–94
45. Clark, L., J.R. Matthews, and R.T. Hay, (1990) Interaction of enhancer-binding protein EBP1 (NF-kappa B) with the human immunodeficiency virus type 1 enhancer. *J. Virol.*, **64,** 1335–44
46. Perez-Martinez, M., M. Gordon-Alonso, J.R. Cabrero, M. Barrero-Villar, M. Rey, M. Mittelbrunn, A. Lamana, G. Morlino, C. Calabia, H. Yamazaki, T. Shirao, J. Vazquez, R. Gonzalez-Amaro, E. Veiga, and F. Sanchez-Madrid, *F-actin-binding protein drebrin regulates CXCR4 recruitment to the immune synapse.* J. Cell Sci. 2010. **123(Pt 7):** p. 1160–70
47. Rodriguez-Tarduchy, G., A.G. Sahuquillo, B. Alarcon, and R. Bragado, (1996) Apoptosis but not other activation events is inhibited by a mutation in the transmembrane domain of T cell receptor beta that impairs CD3zeta association. *J. Biol. Chem.*, **271,** 30417–25
48. Lopez-Anton, N., A. Rudy, N. Barth, M.L. Schmitz, G.R. Pettit, K. Schulze-Osthoff, V.M. Dirsch, and A.M. Vollmar, (2006) The marine product cephalostatin 1 activates an endoplasmic reticulum stress-specific and apoptosome-independent apoptotic signaling pathway. *J. Biol. Chem.*, **281,** 33078–86
49. Sanson, M., N. Auge, C. Vindis, C. Muller, Y. Bando, J.C. Thiers, M.A. Marachet, K. Zarkovic, Y. Sawa, R. Salvayre, and A. Negre-Salvayre, (2009) Oxidized low-density lipoproteins trigger endoplasmic reticulum stress in vascular cells: prevention by oxygen-regulated protein 150 expression. *Circ. Res.*, **104,** 328–36
50. Singh, S., and A. Khar, (2005) Differential gene expression during apoptosis induced by a serum factor: role of mitochondrial F0-F1 ATP synthase complex. *Apoptosis*, **10,** 1469–82
51. Godbole, A., J. Varghese, A. Sarin, and M.K. Mathew, *VDAC is a conserved element of death pathways in plant and animal systems*. Biochim Biophys Acta, 2003. **1642(1–2):** p. 87–96
52. Roy, S.S., A.M. Ehrlich, W.J. Craigen, and G. Hajnoczky, (2009) VDAC2 is required for truncated BID-induced mitochondrial apoptosis by recruiting BAK to the mitochondria. *EMBO Rep*, **10,** 1341–7
53. John, G.B., Y. Shang, L. Li, C. Renken, C.A. Mannella, J.M. Selker, L. Rangell, M.J. Bennett, and J. Zha, (2005) The mitochondrial inner membrane protein mitofilin controls cristae morphology. *Mol. Biol. Cell*, **16,** 1543–54
54. Solstad, T., E. Bjorgo, C.J. Koehler, M. Strozynski, K.M. Torgersen, K. Tasken, and B. Thiede, *Quantitative proteome analysis of detergent-resistant membranes identifies the differential regulation of protein kinase C isoforms in apoptotic T cells*. *Proteomics*. **10(15):** p. 2758–68, 2010
55. Villar, M., I. Ortega-Perez, F. Were, E. Cano, J.M. Redondo, and J. Vazquez, *Systematic characterization of phosphorylation sites in NFATc2 by linear ion trap mass spectrometry*. Proteomics, 2006. **6 Suppl 1:** p. S16–27

Supplemental Information

A robust method for quantitative high-throughput analysis of proteomes by ^{18}O labeling

Elena Bonzon-Kulichenko, Daniel Pérez-Hernández, Estefanía Núñez, Pablo Martínez-Acedo, Pedro Navarro, Marco Trevisán-Herraz, María del Carmen Ramos, Saleta Sierra, Sara Martínez-Martínez, Marisol Ruiz-Meana, Elizabeth Miró-Casas, David García-Dorado, Juan Miguel Redondo, Javier S. Burgos and Jesús Vázquez

Figure S1. Improved peptide identification performance by using the isoelectric point (pI) after OFFGEL separation. Paired protein extracts from HepG2 cells (A,C) and Jurkat T-cell secretome (B,D) were processed for stable isotope labeling quantification using the single one-step in-gel digestion, peptide ^{18}O labeling and IEF fractionation protocol. Peptide identification performance was improved as explained in Experimental Procedures by taking advantage of the fact that peptides focused in each fraction tend to have similar pI values. (A) and (B) show the distribution of pI, calculated from peptide sequence, as a function of the OFFGEL fraction where the peptides were identified (grey dots). The black lines represent the pI supplier's specifications of the 24–cm IPG strips at each pH range. The optimum pI windows used to delimit the valid peptide identifications are represented by error bars. (C) and (D) show the identification/FDR curves of each experiment, obtained by using the probability ratio method and taking into account (grey dots) or not (black dots) the peptide-pI information. The final percent of improvement in the number of peptide-spectrum matches is shown.

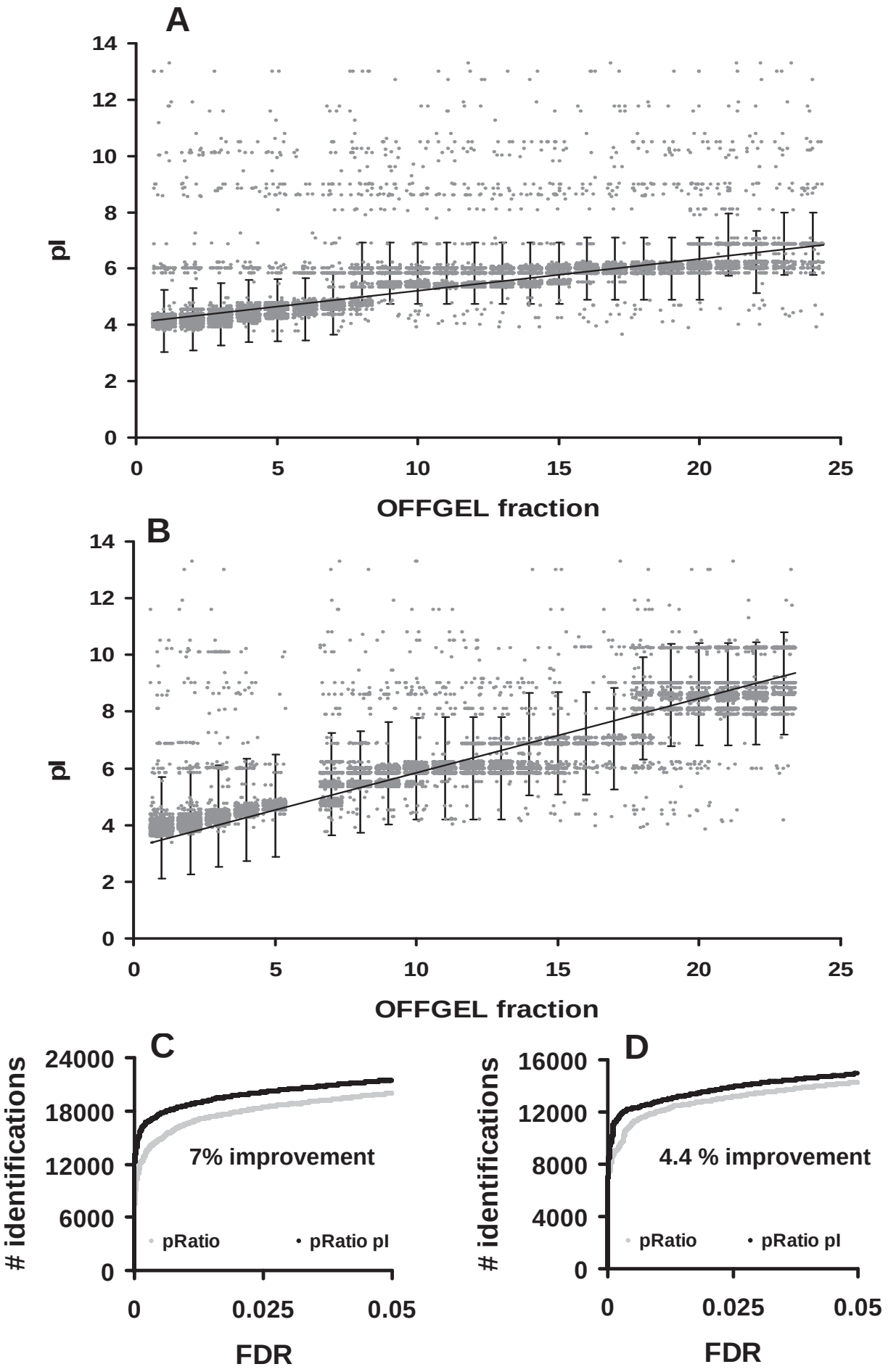
A
pI
OFFGEL fraction
B
pI
OFFGEL fraction
C
identifications
7% improvement
pRatio
pRatio pI
FDR
D
identifications
4.4 % improvement
pRatio
pRatio pI
FDR

Figure S2. Analysis of dynamic range. Cytosolic extracts of control and activated Jurkat T-cells were in-gel concentrated, digested, labeled with ^{16}O and ^{18}O, respectively, mixed at several ratios (1:1, 1:2, 1:4, 1:8, 2:1, 4:1, 8:1) and subjected to relative quantification. (A) Comparison of observed and expected grand mean values; the straight line represents the identity between x- and y-values. (B-D) Cumulative frequency distributions of the standardized variable z_q (grey points) for 1:1, 8:1 and 1:8 (^{16}O:^{18}O) sample ratios. The curves were fitted by least squares to a normal distribution (black lines). The standard deviation (SD) corresponding to the best fit is shown.

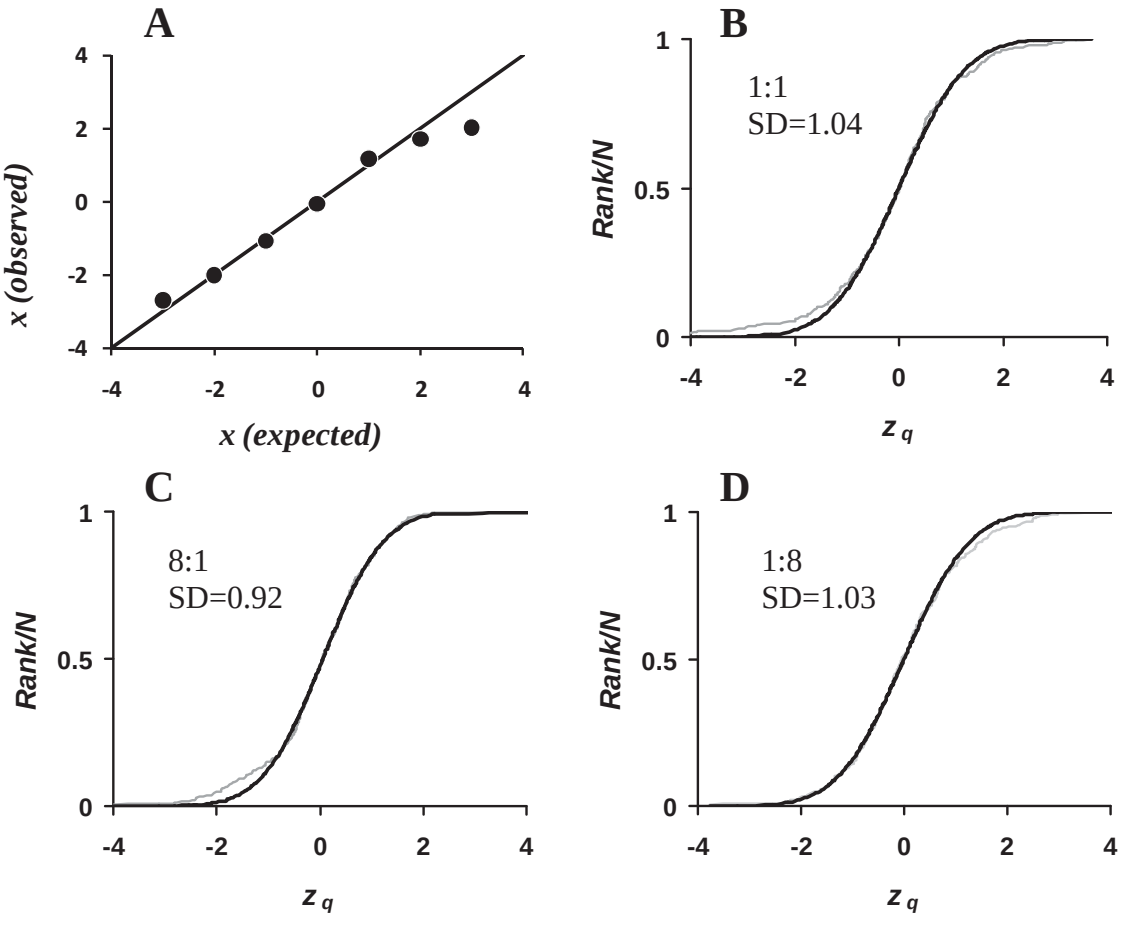

Table S1

Scan, peptide and protein variances obtained from the Jurkat T-cell experiment when control and treated samples are mixed at different ratios

Sample ratio	Scan variance (σ^2_S) (95% C.I.)	Peptide variance (σ^2_P) (95% C.I.)	Protein variance (σ^2_Q) (95% C.I.)
1:1	0.019 (0.016-0.024)	0.020 (0.019-0.044)	0.004 (0.000-0.010)
1:2	0.010 (0.008-0.015)	0.026 (0.022-0.031)	0.008 (0.000-0.010)
2:1	0.027 (0.024-0.029)	0.045 (0.037-0.053)	0.019 (0.008-0.032)
1:4	0.022 (0.005-0.024)	0.031 (0.030-0.039)	0.008 (0.000-0.010)
4:1	0.015 (0.011-0.017)	0.084 (0.071-0.098)	0.027 (0.013-0.039)
1:8	0.027 (0.023-0.031)	0.054 (0.042-0.071)	0.024 (0.006-0.044)
8:1	0.027 (0.020-0.034)	0.19 (0.16-0.24)	0.026 (0.000-0.060)

JOURNAL OF MASS SPECTROMETRY
J. Mass Spectrom. 2007; **42**: 1391–1403
Published online in Wiley InterScience
(www.interscience.wiley.com) DOI: 10.1002/jms.1314

JMS

SPECIAL FEATURE: PERSPECTIVE

High-sensitivity analysis of specific peptides in complex samples by selected MS/MS ion monitoring and linear ion trap mass spectrometry: Application to biological studies

Inmaculada Jorge,[1] Elisabet Miró Casas,[2] Margarita Villar,[1] Inmaculada Ortega-Pérez,[3] Daniel López-Ferrer,[1] Antonio Martínez-Ruiz,[3] Mónica Carrera,[5] Anabel Marina,[1] Pablo Martínez,[1] Horacio Serrano,[1,6] Benito Cañas,[7] Felipe Were,[3] José Manuel Gallardo,[5] Santiago Lamas,[4] Juan Miguel Redondo,[3] David García-Dorado[2] and Jesús Vázquez[1]*

[1] Protein Chemistry and Proteomics Laboratory, Centro de Biología Molecular Severo Ochoa, CSIC, Madrid, Spain
[2] Servicio de Cardiologia, Hospital Vall d'Hebron, Barcelona, Spain
[3] Centro Nacional de Investigaciones Cardiovasculares, Madrid, Spain
[4] Centro de Investigaciones Biológicas, CSIC, Madrid, Spain
[5] Instituto de Investigaciones Marinas, CSIC, Vigo, Spain
[6] Universidad de Puerto Rico en Arecibo, Puerto Rico, Spain
[7] Analytical Chemistry Department, Universidad Complutense de Madrid, Spain

Received 9 July 2007; Accepted 22 August 2007

Mass spectrometry (MS) is a technique of paramount importance in Proteomics, and developments in this field have been possible owing to novel MS instrumentation, experimental strategies, and bioinformatics tools. Today it is possible to identify and determine relative expression levels of thousands of proteins in a biological system by MS analysis of peptides produced by proteolytic digestion. In some situations, however, the precise characterization of a particular peptide species in a very complex peptide mixture is needed. While single-fragment ion-based scanning modes such as selected ion reaction monitoring (SIRM) or consecutive reaction monitoring (CRM) may be highly sensitive, they do not produce MS/MS information and their actual specificity must be determined in advance, a prerequisite that is not usually met in a basic research context. In such cases, the MS detector may be programmed to perform continuous MS/MS spectra on the peptide ion of interest in order to obtain structural information. This selected MS/MS ion monitoring (SMIM) mode has a number of advantages that are fully exploited by MS detectors that, like the linear ion trap, are characterized by high scanning speeds. In this work, we show some applications of this technique in the context of biological studies. These results were obtained by selecting an appropriate combination of scans according to the purpose of each one of these research scenarios. They include highly specific identification of proteins present in low amounts, characterization and relative quantification of post-translational modifications such as phosphorylation and *S*-nitrosylation and species-specific peptide identification.

KEYWORDS: proteomics; tandem mass spectrometry; linear ion trap; ion monitoring; post-translational modifications; protein identification

INTRODUCTION

The term proteome was first coined to describe the set of proteins encoded by a particular genome.[1] Proteomics is concerned with determining the structure, expression, localization, biochemical activity, interactions, and cellular roles of as many proteins as possible. There has been a great progress owing to novel instrumentation, experimental strategies, and bioinformatics tools.[2] Two decades after the discovery of electrospray ionization (ESI) and matrix-assisted laser desorption ionization (MALDI), which, at last, allowed the gentle ionization of large biomolecules, mass

*Correspondence to: Jesús Vázquez, Centro de Biología Molecular Severo Ochoa, Universidad Autónoma de Madrid, 28049 Cantoblanco, Madrid, Spain. E-mail: jvazquez@cbm.uam.es

spectrometry (MS) has become a powerful tool in protein analysis and the key technology in Proteomics.[3] The development and increased use of MS are broadly impacting research in biology and medicine.[4] Recent advances illustrate the role of MS-based Proteomics as an indispensable tool for molecular and cellular biology and for the emerging field of systems biology.[5] These include study of protein–protein interactions via isolation of affinity-based protein complexes on a small and proteome-wide scale,[6–8] mapping of numerous organelles,[9] and generation of quantitative protein profiles from diverse species.

The success of MS is driven by both innovative instrumentation designs, especially those operating on the time-of-flight or ion-trapping principles, and large-scale biochemical strategies, which use MS for the detection and identification of proteins. The precise identification of thousands of proteins from complex samples is now possible: any human protein can now be identified directly using the information contained in genome databases on the basis of minimal data retrieved by MS. Similar to what took place before in genomics, the increase in the automation of sample handling, analysis, and interpretation of results is generating a great number of qualitative and quantitative proteomic data.[10] Entire protein complexes, signaling pathways, and whole organelles are being characterized. Post-translational modifications remain difficult to analyze but efficient generic strategies are presently emerging.[11]

The quantification of protein expression is also possible by MS, frequently using the information provided by the fragmentation spectra taken in triple quadrupole or ion trap instruments. MS/MS is required because the coelution of isobaric peptides is not uncommon when LC/MS is applied to very complex peptide mixtures. Quantification using only Full Scan MS, although possible, suffers from lack of specificity, especially, for experiments with very complex matrices like blood. MS/MS fragmentation usually provides unique characteristic fragment ions for a given peptide, which combined with the specific precursor m/z value and the retention time, may be used for the selective monitoring and quantification of the peptides under study.

LC/MS data may be acquired using the diverse operating scanning procedures attainable with most of the tandem mass spectrometers used in proteomics: Full Scan, Selected Ion Monitoring (SIM), Selected Ion Reaction Monitoring (SIRM), and Consecutive Reaction Monitoring (CRM). In the Full Scan analysis, analyzer voltages change continuously to allow the selection of ions with diverse m/z. Consequently, only a fraction of a given ion is detected. Full Scan chromatograms are usually represented as the Total Ion Current (TIC) of a wide m/z range *versus* time in a plot giving information about the m/z of the ions eluting from the column at any given retention time. TIC chromatograms are much like UV traces except for the richness in information provided by MS when compared to UV. Information about the m/z, and hence the mass from LC eluting compounds is deduced from TIC plots. Nevertheless, it is important to keep in mind that the intact mass of a compound is not a unique identifier. Using the mass spectrometer in the Full Scan mode, specific compounds can be monitored and their elution time and ion intensity represented in selective m/z plots.

However, a much more sensitive detection is possible when the MS analyzers are concentrated to analyze only one ion of interest; this kind of scan is termed SIM. In a quadrupole, this is achieved by fixing the voltages so that the passage of ions is restricted to those with a given m/z value. When ion traps are used, only ions in a very narrow range of m/z are trapped. As the mass range set is narrower, the specificity of the SIM experiment increases. Plotting the TIC intensity for this reduced range *versus* time constitutes the SIM chromatogram. Only compounds with a given m/z value are detected and plotted, making the detection very selective. Visualized peaks in the SIM plot may be minor components in the Full Scan TIC chromatogram. Nevertheless, in the SIM plots there is no structural information about the selected ion, leaving some uncertainty about the identity of the monitored compound. This uncertainty may be critical when SIM plots are taken from very complicated samples, since several peptides may produce ions with similar m/z under ESI ionization, making selective detection unreliable. In any case, higher sensitivity may be attained by the SIM scan mode than with the Full Scan experiment because the mass spectrometer dwells for a much longer time over a smaller mass range.

SIRM is the method used by the majority of scientists to perform highly specific and accurate peptide quantification by MS. The SIRM experiment is accomplished by selecting the m/z of the precursor ion for MS/MS fragmentation and specifically monitoring only one of the fragment ions produced. One could think of this operation as the SIM of a fragment ion. SIRM experiments deliver the trace of a unique fragment ion that can be monitored and quantified in the midst of a very complex matrix. This characteristic makes the SIRM plot most suitable for sensitive and specific quantification. SIRM plots are very simple, usually containing only a single peak. The combination of the m/z values from a given precursor ion and from one of the fragment ions produced by it, is known as a 'transition' and is represented as (precursor mass → fragment mass). In some MS detectors, like ion traps, multiple transitions may be programmed so that one of the daughter ions resulting from precursor fragmentation may be further fragmented, obtaining a MS^3 spectrum. CRM can then be achieved by selectively monitoring one of the MS^3 fragment ions. Specificity greatly increases at the expense of sensitivity, since a certain proportion of ions are lost in each of the fragmentation/trapping events. However, by adjusting the trapping mass windows and the fragmentation energies a good compromise may usually be attained that allows a highly specific identification of the compound of interest.

While SIRM and CRM are the most sensitive scanning modes for peptide identification, they do not produce MS/MS or MS^n spectra. Hence it is necessary that the peptide has been previously identified and that the fragments used for monitoring have been checked to be specific for these peptide species. Hence, they are only applicable to peptides previously identified and the fragments used for monitoring must be specific for the precursor peptides. However, when

DOI: 10.1002/jms

dealing with very complex samples, sometimes, it is difficult to find a specific fragment ion. In such cases, the MS/MS spectrum of the peptide under study is of paramount importance to confirm the nature of the species identified, to detect alterations in the sequence, or to find the exact site of a post-translational modification. Nevertheless, obtaining an interpretable MS/MS spectrum is not always possible when the MS detector is programmed to fragment the most intense species eluting from the column. Sample complexity may be too high to allow the fragmentation of all the peptide species eluting at a given retention time, or the peptide concentration too low to be detected in the Full Scan spectrum as signal may be masked by background noise. In these circumstances, the MS detector may be programmed to perform continuous MS/MS scans on the selected precursor along the gradient. This operating mode, to which we refer to here as 'selected MS/MS ion monitoring' (SMIM) has a number of advantages over other conventional scanning modes: an increased sensitivity is possible by averaging a large number of MS/MS scans over a narrow elution time and 'virtual' SIM chromatogram traces for the different fragment ions can be obtained. These advantages are particularly evident with MS detectors, like linear ion traps (LITs), which have a high scanning speed. In the last years, we had successfully applied in our laboratory, this kind of scanning mode for the study of peptide species in the context of several research projects. Some representative examples are presented in this work.

EXPERIMENTAL PROCEDURES

For connexin 43 (Cx43) identification, a protein extract from cardiomyocyte membranes (100 μg), prepared as described,[12] was redissolved in a 40-μl buffer consisting of 8% (w/v) SDS, 10% (v/v) glycerol, 25 mM Tris–HCl (pH 6.8), 5% (v/v) β-mercaptoethanol, 0.01% (w/v) bromophenol blue, and was separated by SDS-PAGE (10% polyacrylamide gel, 8 × 8 cm). The gel was stained with Coomassie Brilliant Blue R-250 (Bio-Rad). The gel lanes were cut into five pieces (containing approximately 20 μg of protein each), and the piece corresponding to the 37–50 kDa region was subjected to digestion with porcine trypsin (Promega) at a substrate/protease ratio of 20:1 (w/w), and the peptides were extracted as previously described.[13]

Identification of phosphorylation sites of NFATc2 by p38 kinase was carried out as follows. As much as 50 ng of constitutively active MKK6 (SIGMA), 3 μg of GST-p38, and 10 μg of GST-HA-mouse NFATc2-(amino acid 4–385)[14] which were kindly provided by Dr J. Han (The Scripps Research Institute) were incubated at 37 °C for 30 min in a kinase buffer containing 20 mM HEPES (pH 7.9), 25 mM β-glycerophosphate, 20 mM $MgCl_2$, 0.1 mM sodium orthovanadate, and 2 mM dithiothreitol. The reaction took place in the presence of 250 μM ATP. Assays were stopped with Laemmli sample buffer and loaded onto a 7% SDS-PAGE gel or alternatively frozen for 'in solution' digestion.

Characterization of Hsp90 *S*-nitrosylation sites in crude cell extracts was performed as follows: EA.hy926 cells were grown and treated with *S*-nitroso-L-cysteine as described.[15,16] For preparing cell protein extracts, confluent cells were scrapaed and resuspended in nondenaturing lysis solution [(50 mM Tris–HCl (pH 7.4), 300 mM NaCl, 5 mM EDTA, 0.1 mM neocuproine, and 1% Triton X-100 plus protease inhibitor cocktail)], incubated in ice for 15 min, and centrifuged at 10 000 g, for 15 min at 4 °C. Supernatants were collected and protein-quantified with the Bradford reagent (Bio-Rad), and subjected to trypsin digestion 'in solution', as described[17] or separated by SDS-PAGE using 7.5% gel in refrigeration, under darkness. Pure Hsp90 was included in SDS-PAGE gel in separate lanes as a control of the electrophoretic mobility. 'In-gel' digestion was performed as described,[13] under darkness.

For species identification from crude fish extracts, sarcoplasmic protein extracts from white muscle of each of species were prepared according to a previous work.[18] The resulting complex protein mixture was subjected to an 'in solution' digestion with trypsin (Promega, Madison, WI, USA) at 1:50 protease-to-protein ratio for at least 12 h at 37 °C. Digests were individually desalted and concentrated using in-tip reverse-phase resins (ZipTip C18, Millipore) and directly analyzed by HPLC-MS/MS.

MS analysis of peptides was performed by using a Surveyor HPLC system coupled to an LTQ LIT mass spectrometer (Thermo-Fisher) as described previously,[14,15] with minor modifications. Peptides were concentrated and desalted on an RP precolumn (0.32 × 30 mm, BioBasic-18, Thermo Electron) and on-line eluted on an analytical RP column (0.18 × 150 mm BioBasic-18, Thermo Fisher), operating at 2 μl/min and using a 170-min gradient from 5% to 40% B [solvent A: 0.1% formic acid (v/v), solvent B: 0.1% formic acid (v/v), and 80% acetonitrile (v/v)]. The LIT was programmed to perform a different set of scans per cycle according to each experiment, as described in the text. Normalized collision energy was set to 35% and a 3-Da mass window was used to fragment selected parent ions. Protein identification in *Rattus norvegicus*-uniprot.fasta database was carried out as described using SEQUEST,[17] and statistical analysis and determination of error rates were performed after doing a normal and inverted database search by using the Probability Ratio method.[19]

RESULTS AND DISCUSSION

Combination of scanning modes in the linear ion trap

Peptide analysis in electrospray-based mass spectrometers are usually performed by HPLC separation on-line with MS detection; the detector is programmed so that a suitable scanning mode is applied according to the purpose of the analysis. In the 3D ion traps, a popular combination of scanning modes is the so-called 'triple-play' method (Scheme 1(A)). In this method a survey scan (or 'Full Scan') is firstly used to detect the presence of potential peptide ions at low resolutions, and then one of the ions is automatically selected for further analysis. A higher resolution scan is then performed in a short mass range around the selected ion ('Zoom Scan') and then an MS/MS spectrum is triggered in order to produce fragment information for peptide identification or characterization. Automatic ion selection

DOI: 10.1002/jms

from the Full Scan is performed on the most intense species according to a set of rules that are applied to avoid a repeated fragmentation of the same peptide or contaminant ion (usually referred to as 'dynamic exclusion' (DE); see Scheme 1). Zoom Scans are performed to determine peptide mass of the precursor ion with a mass accuracy better than that obtained in the Full Scan, and when isotopic peaks are well separated (as is the usual case for peptides with three or lower charges); it also serves to determine charge state. This information is sometimes very useful for a better interpretation of the MS/MS spectra. Zoom Scan spectra in the 3D trap are often omitted in order to obtain a higher number of peptide fragmentations at the expense of mass accuracy; in such cases, a cycle of three consecutive MS/MS scans is usually performed (Scheme 1(B)).

The LIT has a considerably higher scanning speed than the 3D traps;[20] hence, a considerably higher number of scans can be programmed in each cycle. For instance, the LIT allows performance of six consecutive Zoom Scan–MS/MS combinations per cycle (Scheme 1(C)). This method is particularly useful for large-scale peptide quantification by stable isotope labeling; Zoom Scan spectra are used to resolve peptide peaks from different isotopes, thus allowing relative peptide quantification, and the subsequent MS/MS spectra are used for peptide identification. Quantification and identification are thus afforded at the same time. In previous works, the practical utility of this method of quantification applied to $^{16}O/^{18}O$ stable isotope labeling has been demonstrated in our laboratory.[21,22] When the highest performance in peptide identification of very complex samples is pursued, the LIT may be programmed to perform a large number of consecutive MS/MS scans per cycle (Scheme 1(D)) by using dynamic exclusion-based programs; this method is particularly useful for the analysis of very complex peptide mixtures, such as those produced by the digestion of entire proteomes.

In biological studies, the characterization of specific peptide species is often pursued. Besides, the concentration of the protein under study is frequently very low making it impossible to detect any peptide from the protein above background noise. In some occasions, the ion is masked by adjacent ions having higher intensity, or the sample complexity is too high for this ion to be selected for fragmentation among a complex pool of coeluting peptide ions. In such cases, when the m/z of the precursor ion is known *a priori*, the MS/MS detector may be programmed to trigger a blind, continuous fragmentation over the peptide ion along the RP gradient; in this work we refer to this kind of analysis as SMIM. Note that the SMIM concept, as defined here, does not refer to a new kind of scanning mode, but to a conventional MS/MS scan on a fixed precursor ion that is selected *a priori* and performed along the entire LC run. Since most of the chemical noise due to electrospray ionization is eliminated when performing MS/MS fragmentation, interpretable MS/MS spectra may be obtained even in cases where the precursor ion is not detected in the Full Scan spectrum. Besides, several MS/MS spectra may be averaged together along the peptide elution peak, thus increasing the signal-to-noise ratio.[23] Multiple peptides may also be selected for monitoring, so that the detector performs in each cycle, sequential MS/MS scans over a list of prefixed peptide ions. The LIT is particularly suitable for this kind of scanning modes due to its high scanning speed; in a recent work, we demonstrated that the continuous monitoring of 30 different peptide species is possible, obtaining more than three interpretable MS/MS spectra per cycle.[24] This combination of scanning modes is illustrated in Scheme 1(E), where the 'S' subindex denotes that the mass of the precursor ion to be fragmented is selected *a priori*.

Mixed combinations of automatic fragmentations triggered according to ions detected in the Full Scan, together with SMIM scans may also be programmed in the same scanning cycle. For instance, in Scheme 1(F) a survey scan is programmed followed by a dependent MS/MS scan that serves to make a general identification of the peptides present in the sample; this scan is useful to detect potential problems that arise from sample preparation. The dependent scan is then followed by SMIM scans over two different peptide species; however, by repeating the scans more than once over the same peptide ion, the MS detector may be made to spend more time scanning over one of the precursors. This may be useful when the concentration of one of the species is lower than that of the other and a more extensive spectrum averaging is required for this specie in order to produce interpretable MS/MS spectra. Besides, multiple fragmentations over the same ions are also possible; for instance, Scheme 1(G) shows a scanning mode where two peptide species are continuously monitored by performing an MS/MS spectrum followed by two MS^3 spectra over two fragments selected *a priori*. Some examples of the application of these scanning modes to resolve a range of problems encountered in biology are presented in the following sections.

Identification of connexin 43 in a crude preparation of membrane proteins

Connexin is a family of proteins of paramount biological importance whose most important and best known function is to form transmembrane channels, known as connexons or hemichannels, at the gap junctions.[25–28] Gap junctions are involved in propagation of electrical impulse in myocardium[28,29] as well as chemical communication in many other cell types and tissues.[30–34] Within the heart, ventricular cardiomyocytes express almost exclusively a connexin isoform with a molecular weight of 43 kDa (Cx43), which is one of the most important connexin isoforms.[35] Several studies have shown that Cx43 can participate in important cell process by mechanisms independent from gap junction-mediated cell-to-cell communication.[36,37] Recent studies have shown that Cx43 can be located in intracellular membranes, as the nuclear membrane[38] and, in particular, the inner mitochondrial membrane.[39] The exact localization, molecular interactions, regulation, mechanisms of translocation, and functions of Cx43 in membranes outside gap junction areas are the subject of an intense research effort. So far, studies aimed to answer these questions have been almost exclusively based on antibody-based techniques, including immunoelectrophoresis, immunoprecitation, immunohistochemistry, and gold

DOI: 10.1002/jms

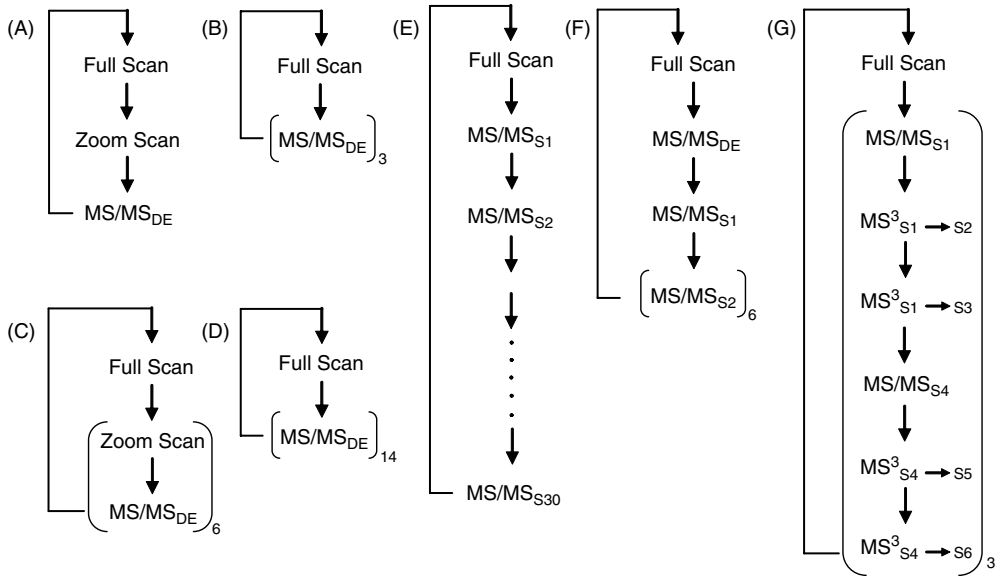

Scheme 1. Some possible combinations of scanning modes in the linear ion trap.

labelled immuno-electron microscopy. In this context, the analysis of Cx43 by direct techniques such as MS in purified membrane fractions, multiprotein aggregates, and other preparations should be an invaluable research tool.

In a previous work, we analyzed the protein composition of a preparation of rat membrane proteins by subjecting the sample to SDS-PAGE, cutting the gel lane into pieces and performing an 'in-gel' tryptic digestion; the resulting peptides were identified by HPLC-MS/MS using an LIT MS as described.[40] The MS/MS spectra were then searched against a rat protein database. In this experiment, the peptide TYIISILFK from Cx43 was found to give a match in first position with one of the MS/MS spectra from a precursor ion at m/z 549.1; however, the SEQUEST scores (Xcorr = 1.913, DCn = 0.42) were not considered as statistically significant at the 5% FDR identification level. Besides, a close inspection of the MS/MS spectrum was not conclusive, and it remained unclear whether this peptide was correctly identified or not (not shown). Another Cx43 peptide gave even a worse match with MS/MS spectra over a precursor ion at m/z 514.3, yielding an Xcorr = 1.927 and a DCn = 0.087. Since no other peptides from Cx43 were detected in this preparation, these results did not allow to establish whether Cx43 was present in the sample or not.

In order to confirm unambiguously the presence of Cx43 in the preparation of membrane proteins, an identical fraction from the same gel was analyzed by SMIM programming the LIT as schematized in Scheme 1(G). An m/z 400–1600 Full Scan was first performed in order to check for the presence of digested peptides as well as peptide separation along the gradient. Then, one selected MS/MS ion monitoring was programmed on the doubly-charged precursor ion at m/z 549.1 and two additional MS^3 spectra were programmed on ions at m/z 720.5 and 833.6, two of the most intense fragments in the MS/MS spectrum recorded in the previous experiment. A group of scans with the same structure was also programmed for ion at m/z 514.3, and the two scan groups were repeated three times per cycle (see Scheme 1(G)).

The results of this experiment are shown in Fig. 1. The base peak chromatogram trace of the survey scans revealed the presence of abundant ionic species as well as a good peak resolution (Fig. 1(A)), suggesting that the digestion was performed with good yield and there were no chromatographic problems. The chromatogram trace at m/z 549.1 of the survey scans also revealed the presence of several ionic species having this mass (Fig. 1(B)); however, the MS/MS spectra of these precursors at the most intense peaks were completely different to the spectrum detected in the previous experiment, indicating that none of these prominent species corresponded to the putative Cx43 peptide. After a careful inspection of all the MS/MS spectra obtained along the time course, an MS/MS spectrum resembling that obtained previously was found at a retention time around 42 min (Fig. 1(F)). This MS/MS spectrum revealed a prominent fragment at m/z 833.6; a chromatogram trace was then drawn by plotting the intensity of this fragment *versus* the retention time (Fig. 1(C)). This trace was completely different to that obtained for the precursor peptide ion from the survey scan (compare with Fig. 1(B)), revealing the presence of a prominent, single species at this retention time. Since this ion corresponded to the $y''_3{}^+$ fragment from peptide TYIISILFK, we assumed that the peak in Fig. 1(B) was indicative of peptide elution at this retention time. Averaging of the MS/MS scans on precursor ion at m/z 549.1 around the peak apex produced a fragment spectrum where the signal-to-noise ratio was improved (Fig. 1(G)). Most of the fragments detected in this spectrum could be assigned to y''- or b-ion series; however, some of the fragments could not be interpreted as arising from this peptide (indicated by arrows in Fig. 1(G)). The spectrum was then filtered by subtracting adjacent MS/MS spectra from the same precursor (shown in Fig. 1(H) and (I)) in order to minimize nonspecific background noise. The resulting spectrum was fully consistent with the peptide sequence and all the significant peaks in the spectrum could be assigned (Fig. 1(J)).

DOI: 10.1002/jms

JMS

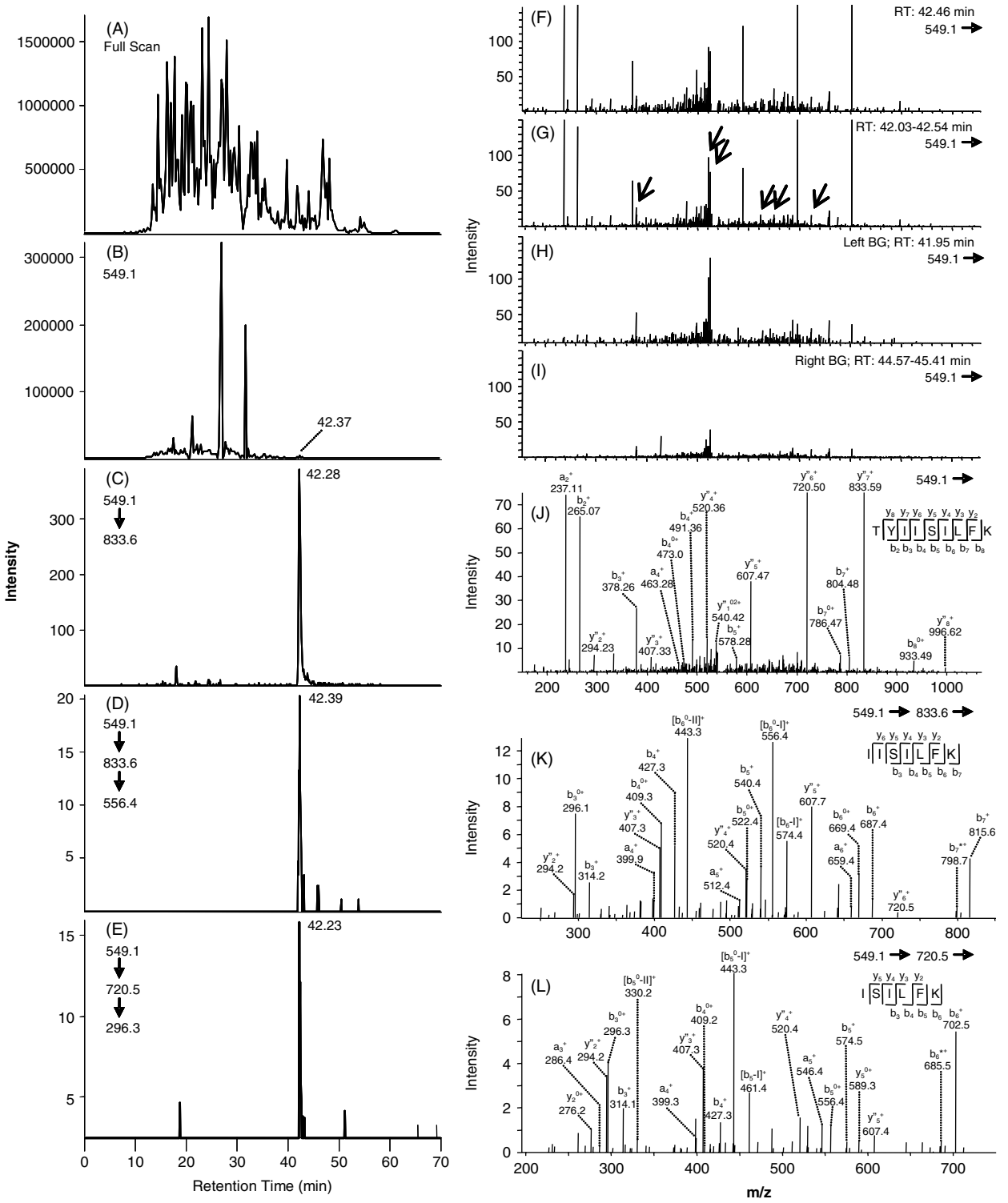

Figure 1. Identification of peptide TYIISILFK from connexin 43 in a preparation of membrane proteins by selected MS^n ion monitoring. A crude preparation of membrane proteins was separated by SDS-PAGE and the region around 43 kDa was cut and trypsin-digested. The resulting peptides were analyzed by HPLC on-line with LIT- MS as described in the text. The left panels show the chromatograms corresponding to the base peak signals of most intense precursor ions (A) and daughter ions originating from the continuous fragmentation of precursor ion at *m/z* 549.1 which corresponds with the doubly-charged ion of the peptide (B) as well as the MS/MS and MS^3 traces from selected peptide fragments (C)–(E). Panels (F) – (J) show the raw MS/MS spectrum from the same ion at the peak apex (F), the averaged spectra of scans around the peak (G), the background MS/MS spectra just before (H) and after the peak (I), and the final averaged and background-corrected MS/MS spectrum (J). Two averaged, uncorrected MS^3 spectra from the same ion are shown in (K) and (L). Fragments corresponding to the loss of internal amino acids from *b* ions in (K) and (L) are indicated with the same nomenclature used previously[41].

DOI: 10.1002/jms

The peptide identity was unambiguously confirmed by inspecting the two MS^3 spectra, which were also averaged around the peak in Fig. 1(C). As shown in Fig. 1(K) and (L), fragmentation of the two selected y'' ions was very rich and allowed the confirmation of their entire subsequence. Interestingly, some intense fragments were detected corresponding to the loss of internal amino acids from *b* ions. Fragments of this kind are observed with some frequency and their formation is thought to arise from cyclation of *b* ions, as previously demonstrated in our laboratory[41]; these ions are usually very intense, a property that is attributed to enhanced stability due to cyclation.[41] Interpretation of the same results corresponding to the 514.0 ion failed to demonstrate that this ion was produced by sequence VAQTDGVNVEMHLK of Cx43, indicating that this method can also be used to detect false positive assignations. Finally, as shown in Fig. 1(D) and (E), a very clean trace of the presence of the Cx43 peptide could be constructed by plotting the intensity of one of the most intense fragments detected in the MS^3 spectra. Taken together, the three traces shown in Fig. 1(C), (D), and (E) can be used as a diagnostic signal characteristic of the presence of this peptide and hence of Cx43, in the sample. When this trace is detected, the final and unambiguous confirmation of the presence of Cx43 is achieved by checking that the corresponding MS/MS and MS^3 spectra are as shown in Fig. 1(J)–(L) This SMIM experiment demonstrates for the first time that Cx43 can be unequivocally identified in crude extracts of membrane preparations, and opens the way to the study of this important protein at the proteomics level.

Characterization of *in vitro* phosphorylation sites in NFATc2 by p38 kinase

Characterization of phosphorylation sites in proteins is one of the most challenging tasks in modern proteomics due to the low stoichiometry of these modifications. The Nuclear Factor of Activated T cells (NFAT) family of transcription factors regulates the transcription of many genes that are active in different cell systems including the immune, cardiovascular, and nervous systems.[42] It comprises of four members termed as NFATc1, c2, c3, and c4, whose activity is modulated by the calcium-activated phosphatase calcineurin. In resting cells, NFAT is present in the cytosol in a highly phosphorylated form. When intracellular calcium levels rise, NFAT *N*-terminal domain is rapidly dephosphorylated by calcineurin, leading to its nuclear translocation and enhancing its transcriptional activity. Once the calcium levels are restored, NFAT is exported to the cytoplasm[42–44] in a process dependent on phosphorylation by different protein kinases including c-jun NH_2-terminal kinase (JNK), p38, CK1,GSK3, PKA, MEKK1, CK1, and DYRK.[45–53] However, the exact identification of the modified residues has been difficult to document largely because of the technical difficulties, and to date it is still unclear how the activity of NFAT can be orchestered in a scenario of more that 30 possible phosphorylation sites.

High sensitivity characterization of phosphorylation sites can be performed by SMIM of prefixed ions known to be potentially phosphorylated. We have recently used this approach to specifically detect a dynamic phosphorylation site in NFATc2 by JNK in cell cultures.[14,24] Phosphorylation sites may in theory be detected with higher sensitivity using a triple-quadrupole MS detector when scanning is concentrated on a single daughter ion characteristic of phosphopeptides (single reaction monitoring or SRM) or by monitoring neutral loss of phosphate group. However, these scanning modes do not produce an MS/MS spectrum and hence no structural information is obtained. For this reason, these scans are usually followed by an MS/MS spectrum that is only triggered when a precursor ion of certain intensity is detected. Hence, if the aim of the experiment is to obtain structural phosphopeptide information by MS/MS, better results should be expected by selected ion MS/MS monitoring in an ion trap, since this latter approach combines the higher trapping efficiency of this detector for fragment ions after collision-induced dissociation (CID) with the possibility of performing extensive spectrum averaging, as shown in the previous section. An example of the highly specific degree of structural information that can be attained by SMIM of phosphopeptides is shown in Fig. 2. In order to characterize phosphorylation sites of NFATc2 by p38 kinase, a preparation of recombinant NFATc2 was subjected to *in vitro* phosphorylation in the presence of the kinase and the protein was digested with trypsin. Among other sites, two potential sites suspected to be phosphorylated by this kinase are present in tryptic peptide TSPDPTPVSTAPSK. To analyze whether these sites are phosphorylated, the peptides resultant from tryptic digestion of the phosphorylated protein were analyzed by the SMIM technique by a scanning method similar to that of Scheme 1(E). The scanning cycle contained a Full Scan followed by 22 MS/MS scans on a set of ions corresponding to nonphosphorylated and suspected phosphorylated peptides from NFATc2. Among these, one MS/MS scan was programmed on the nonphosphorylated form of peptide TSPDPTPVSTAPSK (m/z 692.8), to confirm the presence of the nonphosphorylated form of the peptide, which was used as internal control, and other on the mono-phosphorylated form (m/z 732.8). To detect the presence of the modified peptide, scans were averaged using a sliding time window of about 1 min, and the resulting averaged spectra were manually analyzed. Fragment spectra in good agreement with peptide sequence were detected at a retention time of 2 min; however, two different MS/MS spectra were detected at slightly different retention times (Fig. 2). At 2.04 min, the averaged MS/MS spectrum was consistent with a phosphorylation at the second Thr residue (Fig. 2(D)); while at 3.23 min the averaged fragment spectrum indicated a phosphorylation at the first Ser residue (Fig. 2(E)). In both cases a prominent y''_{10} fragment was observed, probably due to the presence of a Pro residue in 5th position, which favored *N*-terminal peptide cleavage at this position. Luckily, this fragment contained the phosphorylated residue in one case, but not in the other; hence this fragment ion was 80 Da higher in the first case (compare Fig. 2(D) and (E)). Plotting of the chromatogram traces of the respective y''_{10} fragments served to locate the exact retention times of each one of the phosphorylated species (Fig. 2(B) and (C)). Interestingly, the trace peak intensity of the phospho-Thr peptide was considerably higher than that of the

DOI: 10.1002/jms

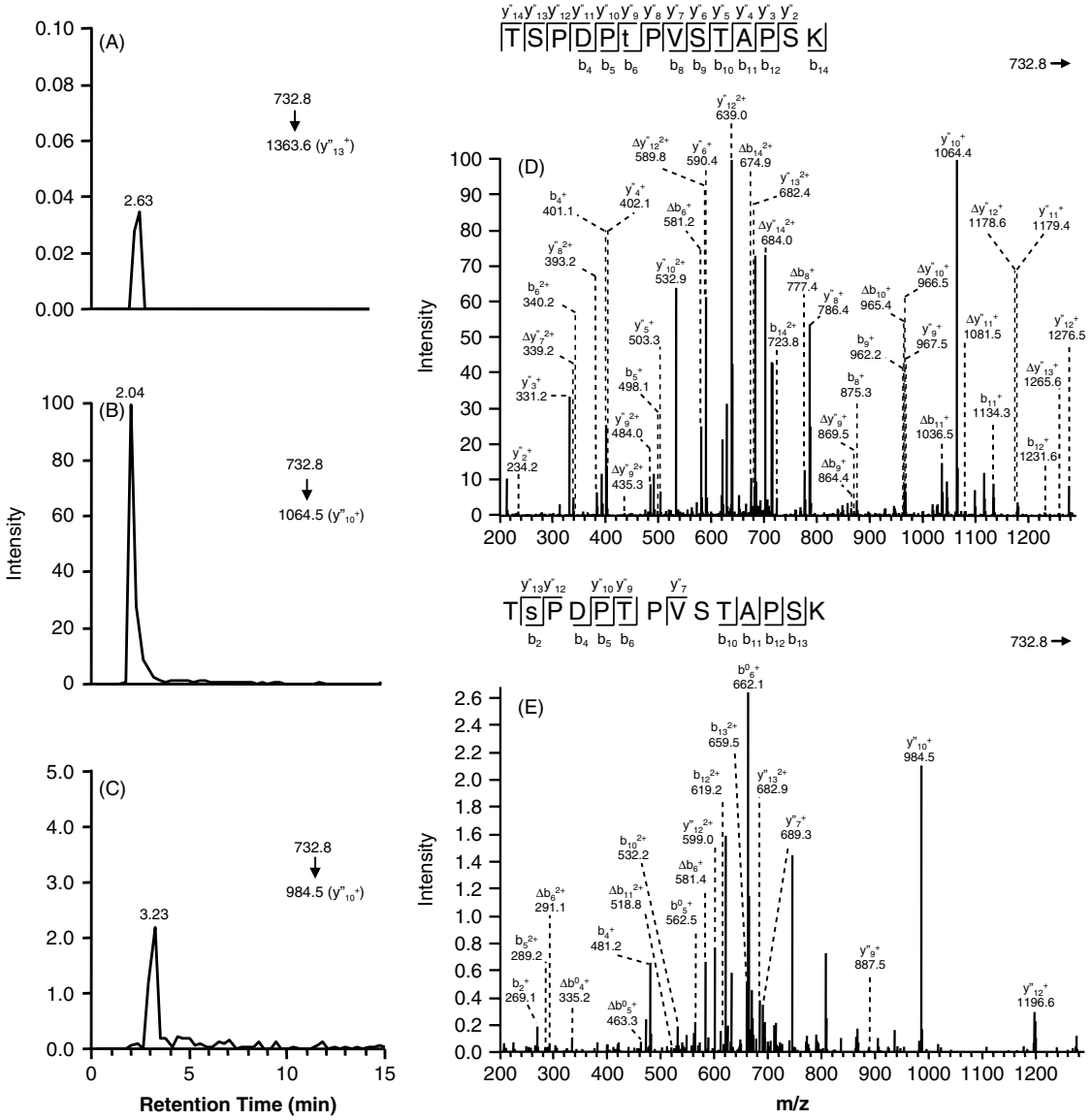

Figure 2. Characterization of two sites of phosphorylation by p38 kinase in the same peptide of NFATc2. A preparation of recombinant NFATc2 was subjected to *in vitro* phosphorylation in the presence of p38 kinase and the protein was digested with trypsin and analyzed by LIT-MS/MS as described in the Material and Methods section. A selected MS/MS monitoring was programmed on the doubly-charged precursor ion corresponding to the mono-phosphorylated form of peptide TSPDPTPVSTAPSK (*m/z* 732.8). The MS/MS trace of fragments at *m/z* 1363.6, 1064.5 and 984.5, are shown in the left panels (A)–(C). Averaged MS/MS spectra around the retention times of 2.04 min (D) and 3.23 min (E) are shown in the right panels. These spectra correspond to two different sites of phosphorylation in the same peptide.

phospho-Ser peptide. Although the direct comparison of these traces must be done with caution, since the position of the phosphate moiety at the sequence backbone may affect peptide fragmentation, in this case the intensity differences are so evident that a reasonable conclusion from the experiment is that p38 mediates NFATc2 phosphorylation preferentially at the Thr residue. This information is very useful to direct further experiments aimed to demonstrate the functional role of phosphorylation at this residue on NFATc2 regulation.

Characterization of *S*-nitrosylation sites in crude cell extracts

The formation of a thionitrite, R–S–N═O in a cysteine thiol, a protein modification called *S-nitrosylation* or *S-nitrosation* is increasingly being considered as a new paradigm of cell signaling due to its particular features as a nonenzymatic post-translational modification produced by nitric oxide (NO) and related reactive nitrogen species.[54,55] One of the features that makes it so interesting for cell signaling is its easy reversibility in cellular environments by several biochemical reactions. At the same time this is also one of the major limitations for its detection as it is very labile in many of the standard analytical processes (including many of the processes of sample preparation for peptide identification by MS) and further improvements in analytical techniques are needed to get a deeper insight into the functional roles of this modifications in (patho) physiological settings. Indeed, the modification is specifically lost in standard MALDI ionization,[56] probably

DOI: 10.1002/jms

due to its characteristic absorption band around 350 nm. A derivatization method has been used to identify proteins and peptides that are *S*-nitrosylated by substituting this modification by a more stable biotinylation.[57] However, this is an indirect method, which relies on a series of successive chemical steps, and a compromise has to be reached between sensitivity and specificity[58] in order to avoid possible artifacts. We have characterized the *S*-nitrosylation of Hsp90, a chaperone involved in the activation of one of the NO-producing enzymes, endothelial nitric oxide synthase (eNOS).[15] This modification inhibits the capacity of Hsp90 to activate eNOS and it can be the molecular basis of a negative feedback loop regulating NO production. Using ESI-MS/MS we characterized a cysteine residue in Hsp90 that was *S*-nitrosylated *in vitro* and were able to describe by complementary methods the presence of the modification in endothelial cells treated with a nitrosothiol and, more subtly, with eNOS agonists.[15] However, further insight into the molecular mechanisms underlying these events requires the direct characterization of these *S*-nitrosylated sites in cellular extracts and without using chemical derivatization steps. Some encouraging results in this regard were obtained by using the SMIM approach and are described as follows.

An initial attempt to characterize *S*-nitrosylation events in crude, unseparated cell extracts were performed by tryptic digestion of the crude extracts followed by direct SMIM analysis of the peptide digest, concentrating the MS detector on the *S*-nitrosylated peptide of Hsp90 previously characterized. For this purpose the scanning method of Scheme 1(F) was used. It included a Full Scan followed by one MS/MS scan, triggered on the most intense ions detected in the previous scan using dynamic exclusion, one MS/MS scan on the non-nitrosylated peptide, and six MS/MS scans on the putatively nitrosylated peptide. The first dependent MS/MS scan served to identify the most abundant peptides produced by protein digestion; this information was useful to check digestion yield and also sequence coverage (not shown); a higher number of scans were programmed on the modified peptide to concentrate the MS detector most of the time on the fragmentation of this specie. In these experiments we were able to produce a good MS/MS spectrum that unequivocally demonstrated the presence of the nonmodified peptide (not shown), suggesting that the method was sensitive enough to characterize potential modifications of this specie. Unluckily, when the MS/MS spectra produced from the fragmentation of the *S*-nitrosylated peptide were analyzed, a prominent contaminant was detected having the same precursor mass and retention time (not shown) making the characterization of the *S*-nitrosylated peptide impossible. This potential interference was expected due to the extremely high complexity of the peptide mixture obtained after tryptic digestion of a whole proteome.

Since the analysis of the MS/MS spectrum from the contaminant suggested that it was produced by single peptide specie (not shown), we tried to separate the contaminant protein by a single prefractionation step. For this end the crude cellular extract was subjected to SDS-PAGE separation and the gel region corresponding to the electrophoretic mobility of Hsp90 was sliced, cut into pieces and subjected to 'in-gel' tryptic digestion. The peptide digest was then analyzed by the SMIM technique using the same scanning method. Results from this experiment are presented in Fig. 3. The nonmodified peptide was detected at a retention time of 48.5 min, and the averaged scan had a good signal-to-noise ratio, allowing the identification of this peptide (Fig. 3(D)). The *S*-nitrosylated form of this peptide was detected at a retention time of 50 min, and the MS/MS spectra was very similar, except for the expected displacement of the series due to the modification (Fig. 3(E)), and also confirmed unequivocally the presence of an *S*-nitrosylation in the second Cys residue at position 7. Plotting of the trace chromatogram of fragment $y''_{12}{}^{+}$ produced very clear peaks that were specific for both the control and the modified peptides (Fig. 3(B) and (C)). Since the NO- moiety was not expected to have a significant influence on the pattern of peptide fragmentation (a supposition supported on the similarity of MS/MS spectra in Fig. 3(D) and (E)) the differences in intensity of these peaks suggested that only 7.1% of the peptide was in *S*-nitrosylated form, illustrating how the SMIM approach can in some cases be used to yield relevant quantitative information of the *S*-nitrosylation status of a protein. Note that *S*-nitrosylation is a rather labile modification and that in this calculation we ignore the possibility that the modification is partially lost during the preparation of the sample. In general, relative quantifications of modifications, in relation to the control protein concentrations, can be potentially achieved by the SMIM approach; these experiments would require the detector to spend the same time on the analysis of the control and modified peptides, and a previous knowledge of the relative intensity of the fragments, obtained by analyzing exact amounts of synthetic peptides. Note that we are also assuming that ion intensity is proportional to peptide concentration, but we do not presently know the actual linear dynamic range of protein quantification that we are achieving with the SMIM approach.

Species-specific identification by selected MS/MS ion monitoring in crude fish extracts

Conventional identification of unprocessed fish is done by the examination of their morphological characteristics. However, owing to the development of the fishing industry, marine products can be processed, making the appreciation of their external morphological features often impossible. To avoid cases of substitution of certain fish species by others with less commercial value, a number of global regulations have been implemented.[59] As a consequence, these regulations make the development of the necessary analytical tools to make possible distinguishing between closely related species highly recommendable. DNA-based[60,61] and protein identification methodologies[18,62] have been used with authentication purposes, but today these techniques are tedious and time-consuming. In this sense, the coupling between the separation power of liquid chromatography and the ability of MS using the SMIM scanning mode, have provided a rapid and reliable method for the species identification in complex mixtures.[63–65]

DOI: 10.1002/jms

JMS

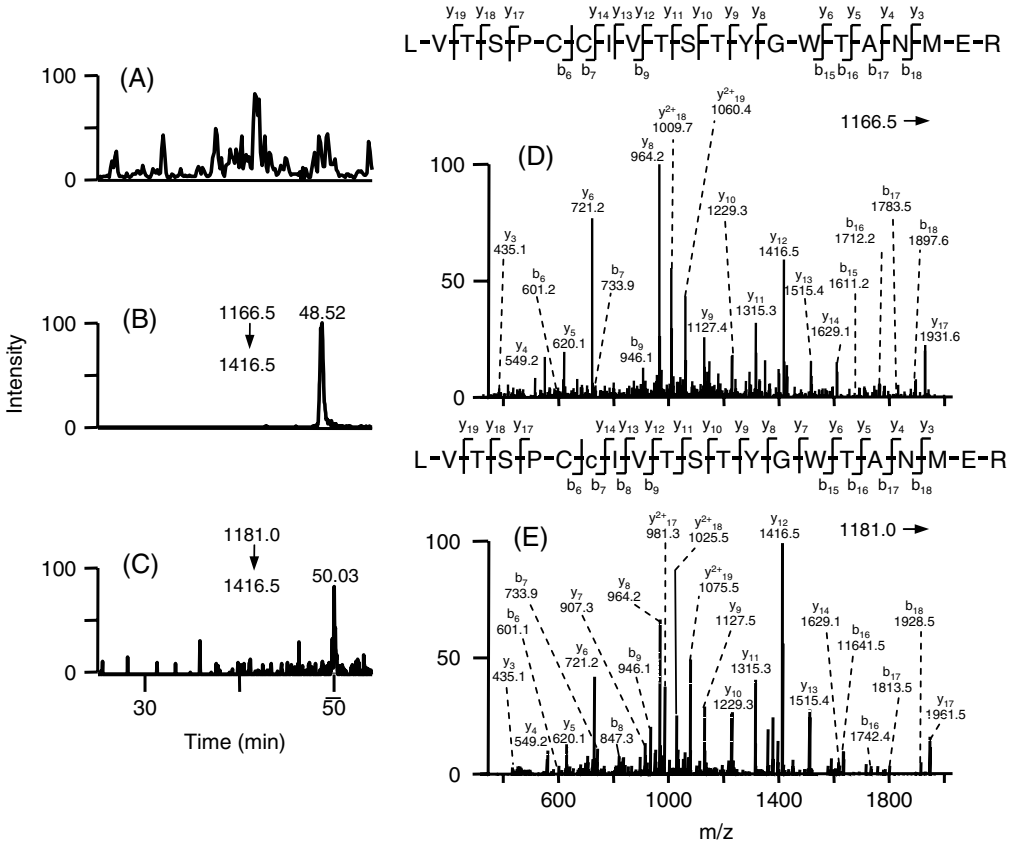

Figure 3. Characterization of Hsp90 *S*-nitrosylation in a crude protein extract from endothelial cells.- A crude protein extract from EA.hy926 cells treated with *S*-nitroso-L-cysteine was subjected to SDS-PAGE and the gel was Coomassie-Blue-stained. The region of the gel corresponding to the position of Hsp90 was cut and subjected to 'in-gel' digestion with trypsin. The peptides were then directly analyzed by LIT-MS/MS as described in the Material and Methods section. The scanning program corresponded to that in Scheme 1(F). The selected MS/MS spectra were programmed on the doubly charged precursor ion corresponding to unmodified peptide LVTSPCCIVTSTYGWTANMER (*m/z* 1166.5), as well as on the *S*-nitrosylated form of the same peptide (*m/z* 1181.0). The base peak profile corresponding to Full Scan spectra is shown in (A). The traces of fragment at *m/z* 1416.5 ($y''_{12}{}^{+}$) from the control and from the modified peptide are shown in (B) and (C), respectively. Averaged MS/MS spectra around the peaks in (B) and (C) are shown in (D) and (E). The absolute intensity of peaks from the nonmodified peptide form (D) and *S*-nitrosylated peptide form (E) were 2.45E6 and 1.75E5, respectively. The *S*-nitrosylated Cys residue is indicated by a lowercase letter.

In this section, we present an example of the application of SMIM approach to the rapid and accurate differentiation of two closely-related hake species, which coexist in the same fishing ground (Cape hakes). For this end, crude protein extracts from fish meat extracted from individuals belonging to these two hake species were directly subjected to trypsin digestion and the resulting peptide pool was analyzed by SMIM. In this experiment the scanning method was similar to that of Scheme 1(E), but only two precursor ions at m/z 590.3 and 597.3 were selected for monitoring, corresponding to the doubly-charged ions from two peptides that have the same sequence except for a single Asp to Glu substitution in position 4 (Fig. 4). These were species-specific peptides from the protein parvalbumin, a heat-stable sarcoplasmic protein that we had sequenced in these two species in previous studies.[66] As shown in Fig. 4(B), when the averaged MS/MS spectra produced by SMIM monitoring of the first precursor ion from *Merluccius paradoxus* extracts was analyzed, a very clear MS/MS spectrum was obtained around a retention time of 56.2 min, which gave a perfect agreement with the peptide sequence. Tracing of the $y''_8{}^{+}$ fragment at m/z 910.3 of this precursor ion produced a highly specific peptide peak at the exact retention time (Fig. 4(A)). A similar result was obtained with the second precursor ion in the extracts from *Merluccius capensis*; in this sample the specific peptide eluted at a retention time of 56.46 min, and the averaged MS/MS also corresponded clearly with the peptide sequence (Fig. 4(D)). The MS/MS was very similar to that produced by the other peptide, and the trace of the corresponding $y''_8{}^{+}$ fragment (m/z 924.3) also produced a highly specific peak (Fig. 4(C)).

In clear contrast, the MS/MS spectrum corresponding to the second peptide could not be detected in the sample from *M. paradoxus*. This is illustrated by a chromatogram trace where no sign could be detected of the presence of this peptide (Fig. 4(A)). The same negative result was obtained when the MS/MS spectrum characteristic of the first peptide was searched in the analysis of the sample from *M. capensis* (Fig. 4(C)).

These results illustrate how peptide fragment chromatograms produced by specific precursor ions can be used as highly specific traces measuring the presence of

DOI: 10.1002/jms

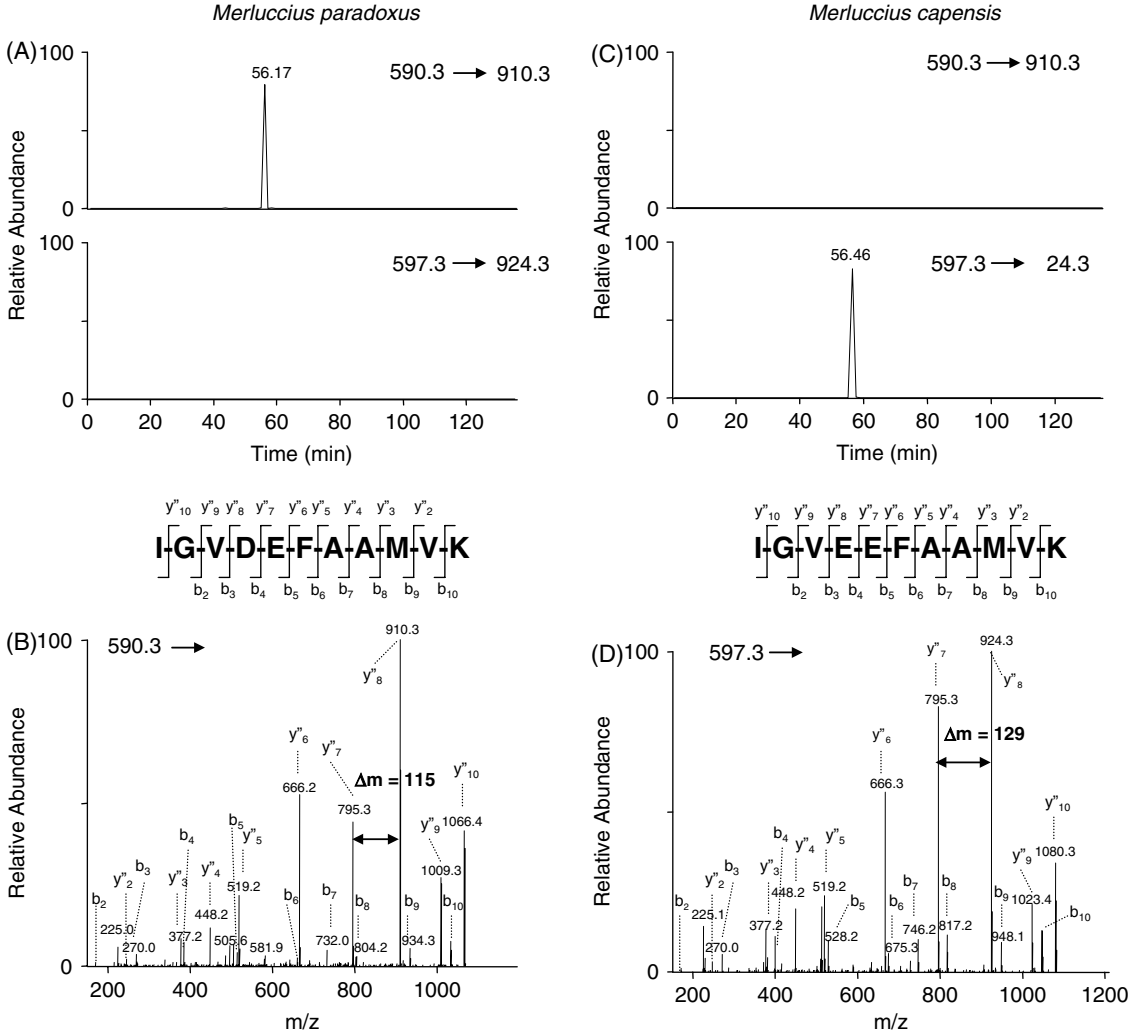

Figure 4. Discrimination of two closely-related hake species (*Merluccius paradoxus* and *Merluccius capensis*) by SMIM of two parvalbumin species-specific tryptic peptides in crude fish extracts. The protein extracts were digested with trypsin 'in solution' and directly analyzed by HPLC-MS/MS. The IT detector was set to perform a continuous operation in the MS/MS mode, being fragmented only the doubly-charged ions corresponding to specific peptides at *m/z* 590.3 and 597.3. The traces of fragment $y''_8{}^+$ (*m/z* 910.3 and 924.3, respectively) as a function of retention time are plotted in the upper chromatograms. The MS/MS spectra obtained at each of the peaks are shown in the lower panels. The selected species-specific peptides corresponded to the same peptide sequence differing in only one amino acid. Note that the relative abundance scale is the same in all the panels.

protein sequences belonging to particular hake species, and suggest that a broad range of species could be monitored simultaneously in a single LC-MS/MS experiment using the SMIM approach. In cases where the number of ionic species that are monitored is small (two to four), this scanning method can also be performed by using a conventional 3D ion trap; we have extensively used this approach using an LCQ Deca XP (Thermo Fisher) with good results regarding identification of species-specific peptides.[65,66] This approach can be easily automated and even used to quantify the presence of small amounts of contaminating species in seafood products. The methodology provides a rapid, sensitive, and effective identification tool that could be used by the authorities responsible for the supervision of safety, quality, and labeling to guarantee an appropriate composition of the foodstuffs to the consumers and even to avoid problems of disloyal competition.

CONCLUSIONS

In this paper, we report an array of results obtained from the application of the selected MS/MS ion monitoring technique to different biological problems. The SMIM approach can be performed in the LIT using different combination of scans up to 30 scans per cycle. By combining free MS/MS scans with Zoom Scans and selected MS/MS and MS^n ion scans and adjusting the number of times each scan is performed, analysis of peptide species can be performed in a number of research scenarios. These include unequivocal identification of membrane proteins in crude membrane extracts and the characterization of relevant post-translational modifications such as phosphorylation and *S*-nitrosylation sites *in vitro* and *in vivo*. Finally, the technique is also particularly suitable for performing a rapid and highly specific identification of species in unseparated protein extracts.

DOI: 10.1002/jms

Acknowledgements

The authors wish to thank to Joaquín Abián for his helpful comments. This work was supported by grants BIO2003-01805, BIO2006-10085, GR/SAL/0141/2004 (CAM), CAM BIO/0194/2006, the Fondo de Investigaciones Sanitarias (Ministerio de Sanidad y Consumo, Instituto Salud Carlos III, RECAVA), and by an institutional grant by Fundación Ramón Areces to CBMSO.

REFERENCES

1. Wilkins MR, Pasquali C, Appel RD, Ou K, Golaz O, Sanchez JC, Yan JX, Gooley AA, Hughes G, Humphery-Smith I, Williams KL, Hochstrasser DF. From proteins to proteomes: large scale protein identification by two-dimensional electrophoresis and amino acid analysis. *Biotechnology (N Y)* 1996; **14**: 61.
2. de Hoog CL, Mann M. Proteomics. *Annual Review of Genomics and Human Genetics* 2004; **5**: 267.
3. Lane CS. Mass spectrometry-based proteomics in the life sciences. *Cell and Molecular Life Sciences* 2005; **62**: 848.
4. Aebersold R, Mann M. Mass spectrometry-based proteomics. *Nature* 2003; **422**: 198.
5. Tyers M, Mann M. From genomics to proteomics. *Nature* 2003; **422**: 193.
6. Neubauer G, Gottschalk A, Fabrizio P, Seraphin B, Luhrmann R, Mann M. Identification of the proteins of the yeast U1 small nuclear ribonucleoprotein complex by mass spectrometry. *Proceedings of National Academy of Sciences of the United States of America* 1997; **94**: 385.
7. Neubauer G, King A, Rappsilber J, Calvio C, Watson M, Ajuh P, Sleeman J, Lamond A, Mann M. Mass spectrometry and EST-database searching allows characterization of the multi-protein spliceosome complex. *Nature Genetics* 1998; **20**: 46.
8. Rout MP, Aitchison JD, Suprapto A, Hjertaas K, Zhao Y, Chait BT. The yeast nuclear pore complex: composition, architecture, and transport mechanism. *Journal of Cell Biology* 2000; **148**: 635.
9. Andersen JS, Mann M. Organellar proteomics: turning inventories into insights. *EMBO Reports* 2006; **7**: 874.
10. Mann M, Hendrickson RC, Pandey A. Analysis of proteins and proteomes by mass spectrometry. *Annual Review of Biochemistry* 2001; **70**: 437.
11. Reinders J, Lewandrowski U, Moebius J, Wagner Y, Sickmann A. Challenges in mass spectrometry-based proteomics. *Proteomics* 2004; **4**: 3686.
12. Ruiz-Meana M, Garcia-Dorado D, Hofstaetter B, Piper HM, Soler-Soler J. Propagation of cardiomyocyte hypercontracture by passage of Na(+) through gap junctions. *Circulation Research* 1999; **85**: 280.
13. Shevchenko A, Tomas H, Havlis J, Olsen JV, Mann M. In-gel digestion for mass spectrometric characterization of proteins and proteomes. *Nature Protocol* 2006; **1**: 2856.
14. Ortega-Perez I, Cano E, Were F, Villar M, Vazquez J, Redondo JM. c-Jun N-terminal kinase (JNK) positively regulates NFATc2 transactivation through phosphorylation within the N-terminal regulatory domain. *Journal of Biological Chemistry* 2005; **280**: 20867.
15. Martinez-Ruiz A, Villanueva L, Gonzalez de Orduna C, Lopez-Ferrer D, Higueras MA, Tarin C, Rodriguez-Crespo I, Vazquez J, Lamas S. S-nitrosylation of Hsp90 promotes the inhibition of its ATPase and endothelial nitric oxide synthase regulatory activities. *Proceedings of the National Academy of Sciences of the United States of America* 2005; **102**: 8525.
16. Martinez-Ruiz A, Lamas S. Detection and proteomic identification of S-nitrosylated proteins in endothelial cells. *Archives of Biochemistry and Biophysics* 2004; **423**: 192.
17. Lopez-Ferrer D, Martinez-Bartolome S, Villar M, Campillos M, Martin-Maroto F, Vazquez J. Statistical model for large-scale peptide identification in databases from tandem mass spectra using SEQUEST. *Analytical Chemistry* 2004; **76**: 6853.
18. Carrera M, Canas B, Pineiro C, Vazquez J, Gallardo JM. Identification of commercial hake and grenadier species by proteomic analysis of the parvalbumin fraction. *Proteomics* 2006; **6**: 5278.
19. Martínez-Bartolomé S, Martín-Maroto F, Navarro PJ, López-Ferrer D, Ramos-Fernández A, Villar M, García-Ruiz JP, Vázquez J. Properties of average score distributions of SEQUEST: the Probability ratio method. *Molecular and Cellular Proteomics* 2007; submitted.
20. Mayya V, Rezaul K, Cong YS, Han D. Systematic comparison of a two-dimensional ion trap and a three-dimensional ion trap mass spectrometer in proteomics. *Molecular and Cell Proteomics* 2005; **4**: 214.
21. Lopez-Ferrer D, Ramos-Fernandez A, Martinez-Bartolome S, Garcia-Ruiz P, Vazquez J. Quantitative proteomics using (16)O/(18)O labeling and linear ion trap mass spectrometry. *Proteomics* 2006; **6** (**Suppl. 1**): S4.
22. Ramos-Fernandez A, Lopez-Ferrer D, Vazquez J. Improved method for differential expression proteomics using trypsin-catalyzed 18O labeling with a correction for labeling efficiency. *Molecular and Cell Proteomics* 2007; **6**: 1274.
23. Marina A, Garcia MA, Albar JP, Yague J, Lopez de Castro JA, Vazquez J. High-sensitivity analysis and sequencing of peptides and proteins by quadrupole ion trap mass spectrometry. *Journal of Mass Spectrometry* 1999; **34**: 17.
24. Villar M, Ortega-Perez I, Were F, Cano E, Redondo JM, Vazquez J. Systematic characterization of phosphorylation sites in NFATc2 by linear ion trap mass spectrometry. *Proteomics* 2006; **6** (**Suppl. 1**): S16.
25. Harris AL. Emerging issues of connexin channels: biophysics fills the gap. *Quarterly Reviews of Biophysics* 2001; **34**: 325.
26. Sosinsky GE, Nicholson BJ. Structural organization of gap junction channels. *Biochimica et Biophysica Acta-Biomembranes* 2005; **1711**: 99.
27. Saez JC, Berthoud VM, Branes MC, Martinez AD, Beyer EC. Plasma membrane channels formed by connexins: their regulation and functions. *Physiological Reviews* 2003; **83**: 1359.
28. Sohl G, Willecke K. Gap junctions and the connexin protein family. *Cardiovascular Research* 2004; **62**: 228.
29. van Veen AA, van Rijen HV, Opthof T. Cardiac gap junction channels: modulation of expression and channel properties. *Cardiovascular Research* 2001; **51**: 217.
30. Dermietzel R, Hertberg EL, Kessler JA, Spray DC. Gap junctions between cultured astrocytes: immunocytochemical, molecular, and electrophysiological analysis. *Journal of Neuroscience* 1991; **11**: 1421.
31. Dermietzel R, Spray DC. Gap junctions in the brain: where, what type, how many and why?. *Trends in Neurosciences* 1993; **16**: 186.
32. Duval N, Gomes D, Calaora V, Calabrese A, Meda P, Bruzzone R. Cell coupling and Cx43 expression in embryonic mouse neural progenitor cells. *Journal of Cell Science* 2002; **115**: 3241.
33. Iino S, Asamoto K, Nojyo Y. Heterogeneous distribution of a gap junction protein, connexin43, in the gastroduodenal junction of the guinea pig. *Autonomic Neuroscience* 2001; **93**: 8.
34. Rozental R, Srinivas M, Gokhan S, Urban M, Dermietzel R, Kessler JA, Spray DC, Mehler MF. Temporal expression of neuronal connexins during hippocampal ontogeny. *Brain Research Reviews* 2000; **32**: 57.
35. Severs NJ. The cardiac gap junction and intercalated disc. *International Journal of Cardiology* 1990; **26**: 137.
36. Jiang JX, Gu S. Gap junction- and hemichannel-independent actions of connexins. *Biochimica et Biophysica Acta-Biomembranes* 2005; **1711**: 208.
37. Stout C, Goodenough DA, Paul DL. Connexins: functions without junctions. *Current Opinion in Cell Biology* 2004; **16**: 507.
38. Dang X, Doble BW, Kardami E. The carboxy-tail of connexin-43 localizes to the nucleus and inhibits cell growth. *Molecular and Cellular Biochemistry* 2003; **242**: 35.
39. Rodriguez-Sinovas A, Boengler K, Cabestrero A, Gres P, Morente M, Ruiz-Meana M, Konietzka I, Miro E, Totzeck A, Heusch G, Schulz R, Garcia-Dorado D. Translocation of connexin 43 to the inner mitochondrial membrane of

cardiomyocytes through the heat shock protein 90-dependent TOM pathway and its importance for cardioprotection. *Circulation Research* 2006; **99**: 93.
40. Serrano H, Jorge I, Martinez-Acedo P, Navarro PJ, Pérez-Hernández D, Miró E, García-Dorado D, Vázquez J. Quantitatives proteomics of mitochondrial membrane proteins by sodium dodecyl sulphate polyacrylamide gel electrophoresis, 16O/18O stable isotope labeling and linear ion trap mass spectrometry. *Proteómica* 2007; **0**: 29.
41. Yague J, Paradela A, Ramos M, Ogueta S, Marina A, Barahona F, Lopez de Castro JA, Vazquez J. Peptide rearrangement during quadrupole ion trap fragmentation: added complexity to MS/MS spectra. *Analytical Chemistry* 2003; **75**: 1524.
42. Horsley V, Pavlath GK. NFAT: ubiquitous regulator of cell differentiation and adaptation. *Journal of Cell Biology* 2002; **156**: 771.
43. Crabtree GR. Calcium, calcineurin, and the control of transcription. *Journal of Biological Chemistry* 2001; **276**: 2313.
44. Hogan PG, Chen L, Nardone J, Rao A. Transcriptional regulation by calcium, calcineurin, and NFAT. *Genes and Development* 2003; **17**: 2205.
45. Chow CW, Rincon M, Cavanagh J, Dickens M, Davis RJ. Nuclear accumulation of NFAT4 opposed by the JNK signal transduction pathway. *Science* 1997; **278**: 1638.
46. Beals CR, Sheridan CM, Turck CW, Gardner P, Crabtree GR. Nuclear export of NF-ATc enhanced by glycogen synthase kinase-3. *Science* 1997; **275**: 1930.
47. Zhu J, Shibasaki F, Price R, Guillemot JC, Yano T, Dotsch V, Wagner G, Ferrara P, McKeon F. Intramolecular masking of nuclear import signal on NF-AT4 by casein kinase I and MEKK1. *Cell* 1998; **93**: 851.
48. Graef IA, Mermelstein PG, Stankunas K, Neilson JR, Deisseroth K, Tsien RW, Crabtree GR. L-type calcium channels and GSK-3 regulate the activity of NF-ATc4 in hippocampal neurons. *Nature* 1999; **401**: 703.
49. Chow CW, Davis RJ. Integration of calcium and cyclic AMP signaling pathways by 14-3-3. *Molecular and Cellular Biology* 2000; **20**: 702.
50. Porter CM, Havens MA, Clipstone NA. Identification of amino acid residues and protein kinases involved in the regulation of NFATc subcellular localization. *Journal of Biological Chemistry* 2000; **275**: 3543.
51. Neal JW, Clipstone NA. Glycogen synthase kinase-3 inhibits the DNA binding activity of NFATc. *Journal of Biological Chemistry* 2001; **276**: 3666.
52. Sheridan CM, Heist EK, Beals CR, Crabtree GR, Gardner P. Protein kinase A negatively modulates the nuclear accumulation of NF-ATc1 by priming for subsequent phosphorylation by glycogen synthase kinase-3. *Journal of Biological Chemistry* 2002; **277**: 48664.
53. Gwack Y, Sharma S, Nardone J, Tanasa B, Iuga A, Srikanth S, Okamura H, Bolton D, Feske S, Hogan PG, Rao A. A genome-wide Drosophila RNAi screen identifies DYRK-family kinases as regulators of NFAT. *Nature* 2006; **441**: 646.
54. Martinez-Ruiz A, Lamas S. S-nitrosylation: a potential new paradigm in signal transduction. *Cardiovascular Research* 2004; **62**: 43.
55. Hess DT, Matsumoto A, Kim SO, Marshall HE, Stamler JS. Protein S-nitrosylation: purview and parameters. *Nature Reviews Molecular Cell Biology* 2005; **6**: 150.
56. Kaneko R, Wada Y. Decomposition of protein nitrosothiolsin matrix-assisted laser desorption/ionization and electrospray ionization mass spectrometry. *Journal of Mass Spectrometry* 2003; **38**: 526.
57. Jaffrey SR, Erdjument-Bromage H, Ferris CD, Tempst P, Snyder SH. Protein S-nitrosylation: a physiological signal for neuronal nitric oxide. *Nature Cell Biology* 2001; **3**: 193.
58. Martinez-Ruiz A, Lamas S. Proteomic identification of S-nitrosylated proteins in endothelial cells. *Methods in Molecular Biology* 2007; **357**: 215.
59. Law 121/2004, 23rd January, Ministry of Agriculture, Fish, and Food of Spain. B.O.E. 2004; **31**: 4864–4868.
60. Perez M, Vieites JM, Presa P. ITS1-rDNA-based methodology to identify world-wide hake species of the Genus Merluccius. *Journal of Agricultural and Food Chemistry* 2005; **53**: 5239.
61. Quinteiro J, Vidal R, Izquierdo M, Sotelo CG, Chapela MJ, Perez-Martin RI, Rehbein H, Hold GL, Russell VJ, Pryde SE, Rosa C, Santos AT, Rey-Mendez M. Identification of Hake species (Merluccius Genus) using sequencing and PCR-RFLP analysis of mitochondrial DNA control region sequences. *Journal of Agricultural and Food Chemistry* 2001; **49**: 5108.
62. Pineiro C, Vazquez J, Marina AI, Barros-Velazquez J, Gallardo JM. Characterization and partial sequencing of species-specific sarcoplasmic polypeptides from commercial hake species by mass spectrometry following two-dimensional electrophoresis. *Electrophoresis* 2001; **22**: 1545.
63. Lopez JL, Marina A, Alvarez G, Vazquez J. Application of proteomics for fast identification of species-specific peptides from marine species. *Proteomics* 2002; **2**: 1658.
64. Lo AA, Hu A, Ho YP. Identification of microbial mixtures by LC-selective proteotypic-peptide analysis(SPA). *Journal of Mass Spectrometry* 2006; **41**: 1049.
65. Carrera M, Cañas B, Piñeiro C, Vázquez J, Gallardo JM. De novo mass spectrometry sequencing and characterization of species-specific peptides from nucleoside diphosphate kinase B (NDK B) for the classification of commercial fish species belonging to the family Merlucciidae. *Journal of Proteome Research* 2007; **6**: 3070.
66. Carrera M, Gallardo JM, Pineiro C, Cañas B, López-Ferrer D, Vázquez J. Procedure for the identification of the commercial species from the Merlucciidae family, necessary elements and applications. CSIC registration number 200603287, Patent approval pending, 2006.

Cardiovascular Research (2010) **87**, 356–365
doi:10.1093/cvr/cvq028

Cyclosporine A-induced nitration of tyrosine 34 MnSOD in endothelial cells: role of mitochondrial superoxide

Mariano Redondo-Horcajo[1,6], Natalia Romero[2], Pablo Martínez-Acedo[3], Antonio Martínez-Ruiz[4], Celia Quijano[2], Catia F. Lourenço[7], Nieves Movilla[5], Jose Antonio Enríquez[5], Fernando Rodríguez-Pascual[1,6], Eduardo Rial[1], Rafael Radi[2], Jesús Vázquez[3], and Santiago Lamas[1,6]*

[1]Departamento Medicina Celular y Molecular, Centro de Investigaciones Biológicas, Consejo Superior de Investigaciones Científicas (CIB-CSIC), Madrid, Spain; [2]Departamento Bioquímica and Center for Free Radical and Biomedical Research, Facultad de Medicina Universidad de la República, Montevideo, Uruguay; [3]Centro Biología Molecular Severo Ochoa (CMB-CSIC), Madrid, Spain; [4]Servicio de Inmunología, Hospital de La Princesa, Madrid, Spain; [5]Departamento Bioquímica y Biología Molecular y Celular, Universidad de Zaragoza, Zaragoza, Spain; [6]Laboratorio Mixto CSIC-FRIAT de Fisiopatología Vascular y Renal, Centro de Investigaciones Biológicas (CIB-CSIC), Fundación Renal Iñigo Alvarez de Toledo, Ramiro Maeztu 9, Madrid 28040, Spain; and [7]Faculdade de Farmácia, Universidade de Coimbra, Coimbra, Portugal

Received 17 July 2009; revised 30 December 2009; accepted 22 January 2010; online publish-ahead-of-print 27 January 2010

Time for primary review: 49 days

Aims Cyclosporine A (CsA) has represented a fundamental therapeutic weapon in immunosupression for the past three decades. However, its clinical use is not devoid of side effects, among which hypertension and vascular injury represent a major drawback. Endothelial cells are able to generate reactive oxygen and nitrogen species upon exposure to CsA, including formation of peroxynitrite. This may result in endothelial cell toxicity and increased tyrosine nitration. We have now studied the subcellular origin of superoxide formation in endothelial cells treated with CsA and the biochemical consequences for the function of mitochondrial enzymes.

Methods and results By using electron spin resonance and endothelial cells lacking functional mitochondria, we showed that superoxide anion is generated in mitochondria. This was associated with an effect of CsA on bioenergetic parameters: increased mitochondrial membrane potential and inhibition of cellular respiration. In addition, CsA inhibited the activity of the mitochondrial enzymes aconitase and manganese superoxide dismutase (MnSOD). The use of murine lung endothelial cells deficient in endothelial nitric oxide synthase (eNOS) and NOS/peroxynitrite inhibitors allowed us to establish that the presence of eNOS and concomitant NO synthesis and peroxynitrite formation were essential for CsA induced nitration and inhibition of MnSOD activity. As the latter has been shown to become inactivated by nitration, we sought to identify this modification by mass spectrometry analysis. We found that CsA induced specific MnSOD tyrosine 34 nitration both in the recombinant protein and in endothelial cells overexpressing MnSOD.

Conclusion We propose that CsA induced endothelial damage may be related to increased mitochondrial superoxide formation and subsequent peroxynitrite-dependent nitroxidative damage, specifically targeting MnSOD. The inactivation of this key antioxidant enzyme by tyrosine nitration represents a pathophysiological cellular mechanism contributing to self-perpetuation and amplification of CsA-related vascular toxicity.

Keywords Peroxynitrite • Calcineurin inhibitors • Reactive nitrogen species • Vascular toxicity • Nitroxidative stress

1. Introduction

Cyclosporine A (CsA) has been for many years an essential therapeutic tool in the fields of solid organ transplantation and autoimmune diseases. Its mechanism of action, based on the inhibition of the phosphatase calcineurin upon CsA binding to cyclophilin proteins, is now well known and shared in part by other immunosuppressors such as Tacrolimus.[1,2] However, serious side effects associated to

* Corresponding author. Centro de Biologia Molecular "Severo Ochoa", Nicolas Cabrera 1, campus UAM, Madrid 28049, Spain. Tel: +34 91 196 4455; fax: +34 91 196 4420, Email: slamas@cbm.uam.es

its clinical use still promote significant morbidity and dictate changes in therapeutic strategies. Among them, vascular injury is an important one as it is reflected in post-transplant hypertension, accelerated atherosclerosis, and occasionally in the appearance of thrombotic microangiopathy.[3] Several reports point to the importance of oxidative stress as a pathogenetic mechanism responsible for this undesired damage (see[4] for review). Oxidative stress is the result of the action of reactive oxygen species (ROS)[5] on different molecular targets and it is now accepted that the latter do not only participate in pathophysiological responses but are also important signals for some homeostatic cellular functions.[6] In addition, reactive nitrogen species (RNS) such as nitric oxide or peroxynitrite may have a dual physiological and pathophysiological role, and hence the term nitroxidative stress has been coined.[7,8] Vascular injury associated to the clinical use of CsA is pathogenetically related to endothelial dysfunction[9] promoted by increased nitroxidative stress.[10–13] Cellular sources generating ROS and RNS in endothelial cells are multiple, including several enzymatic systems and the mitochondrial electron transport chain. The contribution of mitochondria to ROS generation has received increasing attention in recent years and this is especially noticeable in endothelial cells and vascular pathophysiology.[14]

In previous work from our laboratory, we found that CsA promotes the generation of superoxide and peroxynitrite in the vascular endothelium and that this effect is associated with increased protein tyrosine nitration which may be prevented by the concomitant use of antioxidant agents.[15] Among these proteins, manganese superoxide dismutase (MnSOD) appeared as a strong candidate, given the fact that tyrosine nitration specifically inactivates its catalytic activity[16–18] by a Mn-catalyzed nitration of tyrosine 34 (Tyr34).[19] Nevertheless, several important questions remain to be answered including: (i) the subcellular topology of ROS generation mediated by CsA, (ii) the functional consequences of CsA treatment on the activity of MnSOD in endothelial cells, and (iii) the identification of specific tyrosine residues which undergo nitration induced by CsA. In this manuscript, we provide data demonstrating the mitochondrial generation of CsA induced superoxide in vascular endothelial cells, the inhibition of MnSOD activity by CsA and the specific nitration of Tyr34 promoted by CsA in this same enzyme.

2. Methods

An expanded version of Material and Methods can be found as Supplementary material online.

2.1 Cells

Bovine aortic endothelial cells (BAEC) were obtained from aortas donated by a local slaughterhouse and cultured as described.[20] Mouse lung endothelial cells (MLEC) were isolated as described.[21] All protocols used conform to the Guide for the Care and Use of Laboratory Animals published by the US National Institutes of Health (NIH publication No. 85-23).

2.2 Flow cytometry

An EPICS XL analyser was used to quantitate fluorescence at the single-cell level. Data are expressed as percentage of signal related to the control.

2.3 MitoSOX-Red fluorescence and confocal microscopy

Images were collected with a Leica TCS SP2 AOBS confocal microscope (Mannheim, Germany).

2.4 Electron spin resonance experiments

Electron spin resonance (ESR) signals were detected with a Miniscope MS 200 Magnetech GmbH.

2.5 O_2 consumption

Mitochondrial oxygen consumption was measured at 37°C using a Clark-type oxygen electrode (Hansatech Instruments, King's Lynn, England).

2.6 Aconitase activity

Aconitase activity in the mitochondrial and cytosolic fractions was determined spectrophotometrically using the coupled assay with porcine heart isocitrate dehydrogenase, as described.[22]

2.7 MnSOD activity

MnSOD activity was determined in cellular lysates by measuring the inhibition of superoxide-dependent cytochrome c reduction generated by xanthine oxidase/xanthine in the presence of 3 mM potassium cyanide.[23]

2.8 Western blot analysis

Western blot analysis was performed as described.[15]

2.9 MnSOD nitration

For recombinant human MnSOD nitration experiments, the protein was incubated with conditioned media from BAEC treated with CsA (10 μM, 2 h), its vehicle or nitrating buffer[18] and then processed as described.[15]

2.10 Mass spectrometry

MS analysis of peptides was performed by using a Surveyor high performance liquid chromatography (HPLC) system coupled to an LTQ linear ion trap mass spectrometer (ThermoScientific, San Jose, CA, USA) as described.[24]

2.11 Nitric oxide determination

$^{\bullet}$NO release was monitorized using an $^{\bullet}$NO electrode (ISO-NOP; World Precision Instruments, Stevenage, Herts, UK).

2.12 Statistics

Unless otherwise specified, data are expressed as means ± SEM with the number (*n*) of experiments indicated. Statistical analysis was performed by unpaired Student's *t*-test, or non-parametric tests as appropriate.

3. Results

3.1 Detection of mitochondrial-derived superoxide radical in endothelial cells exposed to CsA

ESR is considered a highly specific method for the detection of superoxide. Reaction of superoxide and hydoxyl radicals with the spin trap 5,5 dimethyl-1-pyrroline N-oxide (DMPO) yield the DMPO-OOH adduct ($t_{1/2} < 1$ min) that rapidly decays in the cellular medium to the more stable adduct DMPO-OH. As shown in *Figure 1A*, when BAEC were incubated with CsA (10 μM, 2 h), an ESR signal with the characteristic spectral properties of DMPO-OH adduct was observed (1:2:2:1 pattern and $a^N = a^H = 14.9$ G), and the signal was

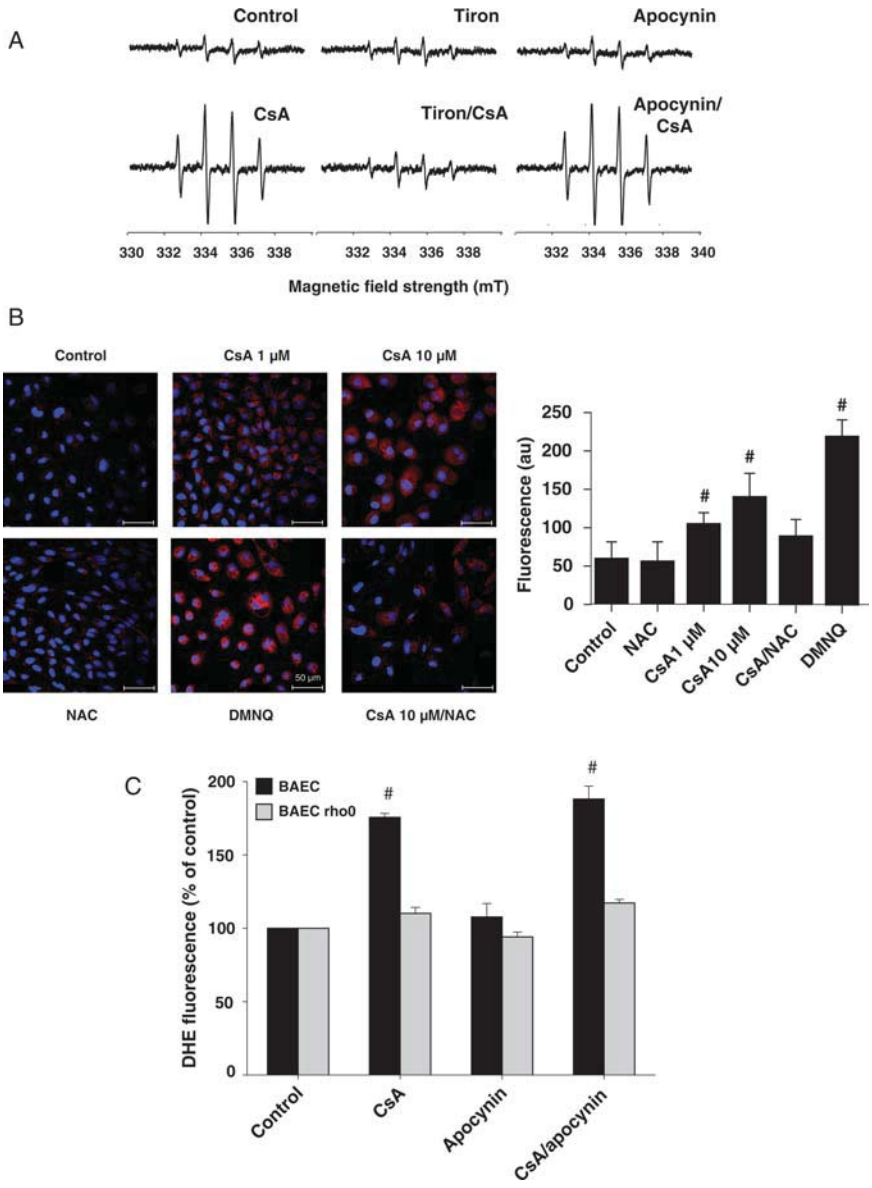

Figure 1 Cyclosporine A generates superoxide anion through mitochondria. (*A*) BAEC were treated with CsA (10 μM, 2 h), Tiron (1 mM, 30 min pre-incubation), apocynin (100 μM, 30 min pre-incubation), or combinations as indicated and ESR detection of superoxide anion was performed as described in Methods section. The ESR 'signature' 1:2:2:1 is depicted. A representative experiment from $n = 4$ is shown. (*B*) BAEC were treated with CsA, 2,3-dimethoxy-1,4-naphthoquinone (25 μM 1 h), NAC (3 mM, 30 min pre-incubation), or combinations as indicated and mitochondrial generation of superoxide was detected with MitoSOX fluorescent probe (red); nuclear staining by DAPI is shown in blue. A representative experiment from $n = 3$ is shown. (*C*) Native or mitochondrial-deficient (rho0) BAEC were exposed to CsA, apocynin, or combinations as indicated. Superoxide production was evaluated by DHE fluorescence as described in Methods section. ($n = 7$, $^{\#}P < 0.05$ vs. control).

significantly abrogated in the presence of the superoxide scavenger Tiron (1 mM),[25] strongly suggesting that superoxide radical is being formed after exposure of BAEC to CsA. The NADPH oxidase inhibitor, apocynin, was unable to quench the CsA induced ESR signal (*Figure 1A*). An identical signal was obtained when BAEC were incubated with the redox cycling agent 2,3-dimethoxy-1,4-naphthoquinone (DMNQ) (25 μM), a known intracellular superoxide generator (see Supplementary material online, *Figure S1*).

The fluorescent probe MitoSOX Red[26] was used in order to investigate if mitochondria are the source of CsA-dependent superoxide production. As shown in *Figure 1B*, treatment of BAEC with both CsA (10 μM, 2 h) and DMNQ (25 μM, 1 h) results in a significant increment of cellular fluorescence, compatible with a mitochondrial localization (see Supplementary material online, *Figure S2*), suggesting that an increase in superoxide and other mitochondrial-derived oxidants are being formed after treatment with CsA. Pre-incubation of cells with the general antioxidant *N*-acetylcysteine (3 mM) markedly reduced the CsA-dependent MitoSOX-Red fluorescent signal. In order to confirm the important contribution of mitochondrial sources to superoxide generation in endothelial cells, we studied the effect of CsA on BAEC which have been deprived of functional mitochondria (rho0). As shown in *Figure 1C*, when cells were incubated with dihydroethidine

(DHE) as the fluorescent probe, a significant increase in oxidized DHE fluorescence was detected only in native BAEC and not in rho0 cells upon exposure to CsA, whereas apocynin failed to have any significant effect in both cell types. BAEC treated with DMNQ followed a similar behaviour as those exposed to CsA (see Supplementary material online, *Figure S3*). We take this set of results as strongly supporting that treatment of endothelial cells with CsA increases mitochondrial-derived superoxide and/or oxidant production.

3.2 Mitochondrial bioenergetic profile of BAEC treated with CsA

The relationship between cell respiration rate, mitochondria membrane potential ($\Delta\Psi$m), and ROS production is a complex one. In general, it is accepted that when mitochondria are respiring in state 3, there is a limited generation of superoxide anion. However, when ADP has been phosphorylated and $\Delta\Psi$m is high, respiratory rates are low and there is an increased superoxide generation by complexes I and III.[27] We sought to study the influence of CsA on several bioenergetic parameters in BAEC. As shown in *Figure 2A*, CsA caused a significant increase in $\Delta\Psi$m (measured as the fluorescence intensity of the $DiOC_6$ {3} probe) that was associated with a decrease in the respiration rate (*Figure 2B*), a slight reduction in intracellular ATP levels ($21 \pm 10\%$ compared with control) and an increase in the production of superoxide as detected with the fluorescent probe DHE (*Figure 2C*). As expected, the protonophore carbonyl cyanide-p-trifluoromethoxyphenyhydrazone (FCCP) lowered $\Delta\Psi$m, stimulated respiration (*Figure 2A* and *B*) and lowered the mitochondrial production of superoxide (see Supplementary material online, *Figure S4A* and *B*). In an effort to identify the relative contribution of complex I or complex III to CsA-associated superoxide production, we performed experiments in the presence of specific electron transport inhibitors for these two complexes. The addition of different respiratory chain inhibitors (rotenone, myxothiazol, or antimycin A) lead to an increase in superoxide production. The addition of CsA resulted in a further increment in superoxide levels when rotenone or antimycin A were present but not when combined with myxothiazol (*Figure 2C*–E). In order to exclude a direct effect of CsA on complex III, we determined its activity in the presence and absence of CsA and we found no significant differences (data not shown).

3.3 Functional significance of CsA induced ROS and RNS generation: inhibition of mitochondrial-related enzymatic activities

Previous reported work from our laboratory showed that CsA promotes the generation of peroxynitrite in endothelial cells by favouring spatio-temporal conditions of interaction between superoxide and $^{\bullet}NO$[12,28] to yield the strong oxidant peroxynitrite. Intracellular peroxynitrite formation has consequences for endothelial viability, in general promoting oxidation and nitration of cellular targets. Inhibition of aconitase activity (an enzyme present in both mitochondrial and cytosolic compartment) has been widely used as a sensitivity assay for measuring superoxide cellular-compartment levels.[22,29] Other species such as peroxynitrite or carbonate radical are able to react with and inactivate aconitase, but their production is also a consequence of an increase in superoxide steady-state level. In addition, the mitochondrial enzyme MnSOD becomes inactivated upon nitration. Taking into account these considerations, we were now interested in identifying the functional relevance of CsA treatment on the activities of these mitochondrial enzymes. *Figure 3A* shows that both the mitochondrial superoxide generator DMNQ and CsA significantly reduced mitochondrial aconitase and MnSOD activities after short-term exposure to CsA. The effect on MnSOD activity was also documented after 24 h of CsA treatment (*Figure 3B*). The antioxidant Tiron and the tyrosine nitration inhibitor uric acid[30] inhibited or partially prevented the effect of CsA on MnSOD activity, (*Figure 3C* and *D*, respectively). A similar preventive effect of Tiron was observed on aconitase activity ($n = 2$ by duplicate, data not shown). Aconitase activity was also reduced in cytosolic fractions (data not shown) even when no significant contamination of mitochondria in the cytosolic fractions was detected, as determined by western blot against MnSOD (see Supplementary material online, *Figure S5*).

To prove that the nitration induced by CsA was NOS dependent and that NOS inhibition prevented CsA induced enzymatic inactivation, we performed two types of experiments. First, we studied tyrosine nitration in MLEC arising from both wild-type and endothelial nitric oxide synthase (eNOS) deficient animals. CsA induced tyrosine nitration only in wild-type MLEC as opposed to the peroxynitrite exogenous generator SIN-1 (1,3-morpholino sydnonimine), which also had an effect in MLEC from eNOS-deficient animals (*Figure 4A*). The nitration pattern correlated well with the levels of nitrite (NO_2^-) in the extracellular medium, as it was determined using a selective NO electrode (*Figure 4B*). In addition, the NOS inhibitor 2-amino-4-methylpyridine significantly abrogated the effect of CsA on MnSOD activity (*Figure 4C*). These data imply that the generation of superoxide and peroxynitrite by CsA has important functional consequences for the activities of mitochondrial aconitase and MnSOD, both enzymes with a mitochondrial localization. In addition, CsA induced an increase in peroxynitrite generation (as determined by DHR123 flow cytometry experiments) which was only present in wild-type MLEC (*Figure 4D*).

3.4 Identification of Tyr34 as the nitrated residue of MnSOD in endothelial cells treated with CsA

Tyr34 has been identified as a critical target for the *in vitro* nitration and inactivation of MnSOD with functional consequences also *in vivo*.[31,32] Thus, it was important to find out if treatment of endothelial cells with CsA could specifically affect this residue. We first set up the conditions for characterizing Tyr34 nitration by mass spectrometry in a preparation of rHuMnSOD exposed to a nitrating buffer.[18] This was accomplished by selected MS/MS ion monitoring (SMIM) using a HPLC-linear ion trap mass spectrometer.[24,33,34] The detector was programmed to perform multiple fragmentations of the ions corresponding to the non-modified and Tyr-nitrated forms of the tryptic peptide HHAAY[34]VNNLNVTEEK from MnSOD. By monitoring the fragmentation of the precursor ions and the subfragmentation of one of the most intense fragments, we could demonstrate the nitration at Tyr34 (data not shown). Once the conditions for specifically detecting Tyr34 nitration by SMIM were optimized, we applied the technique to the analysis of rHuMnSOD incubated in the presence of conditioned medium of cells exposed to CsA. The fragmentation patterns and the presence of specific fragments for the non-modified and nitro-Tyr forms of the peptide demonstrated that incubation of the recombinant protein with the conditioned medium produced nitration at the Tyr34 residue of

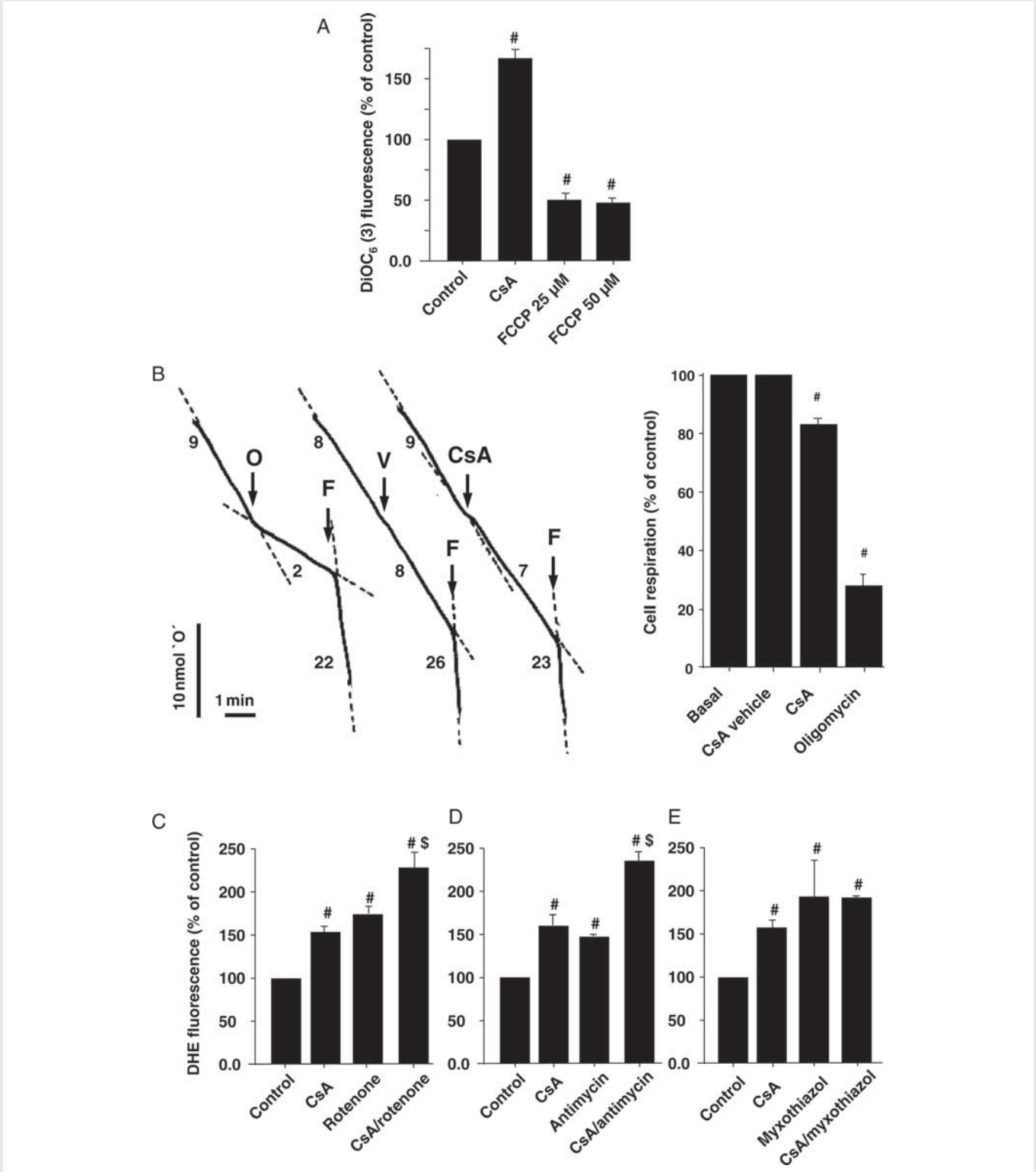

Figure 2 Cyclosporine A modifies the mitochondrial bioenergetic profile consistently with increased superoxide production. (*A*) Effect of CsA on membrane potential as determined with the $DiOC_6$ {3} probe. BAEC were treated with CsA or the protonophore FCCP as a control which induces membrane uncoupling ($n = 4$, $^{\#}P < 0.05$ vs. control). (*B*) Effect of CsA on the oxygen consumption of BAEC. Left panel: representative oxygen electrode traces of the effect of CsA 10 μM, oligomycin (O, 2 mg/mL) or its vehicle (V) and the uncoupler FCCP (F; 10 μM). It represents the respiratory rates expressed as nmol 'O' min^{-1} 10^6 $cells^{-1}$. Right panel: histogram with the summary of the effects of the agents on BAEC respiration ($n = 4$, $^{\#}P < 0.05$ vs. basal or CsA vehicle). (*C–E*) Effect of complex I and III inhibitors on CsA induced superoxide generation. BAEC were pre-treated with the complex I inhibitor Rotenone (4 μM, 30 min) or the complex III inhibitors myxothiazol (10 μM, 30 min) or antimycin (2 μM, 30 min) and then treated with CsA (10 μM, 2 h) as described in Methods section. Superoxide production was evaluated by DHE fluorescence. (*C*) $n = 10$, $^{\#}P < 0.05$ vs. control; $^{\$}P < 0.05$ vs. CsA. (*D*) $n = 3$, $^{\#}P < 0.05$ vs. control; $^{\$}P < 0.05$ vs. CsA. (*E*) $n = 4$, $^{\#}P < 0.05$ vs. control.

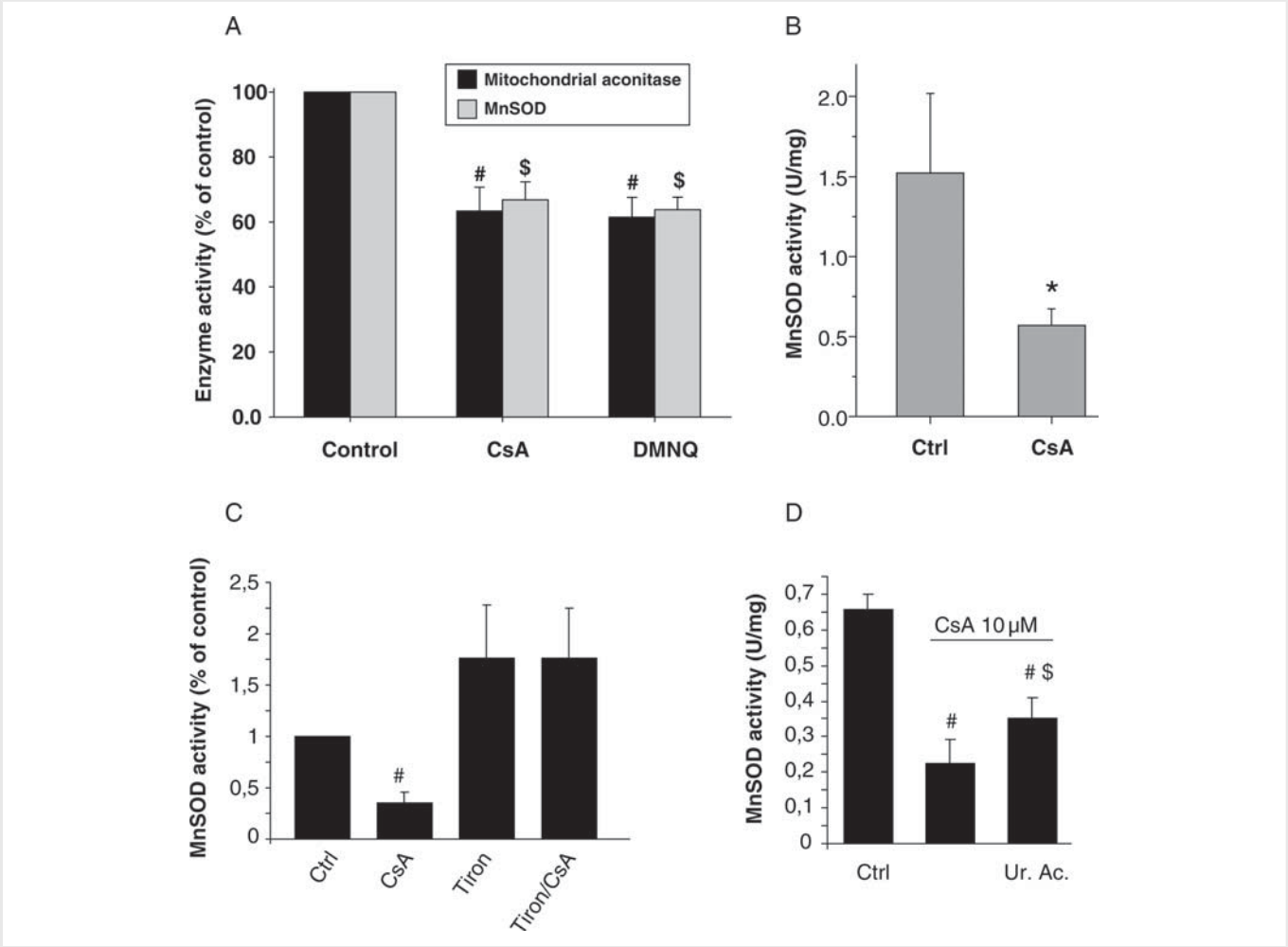

Figure 3 Cyclosporine A causes functional inactivation of Mn-superoxide dismutase and aconitase. (*A*) BAEC were treated with CsA (10 μM, 2 h) or DMNQ (25 μM, 1 h) and mitochondrial aconitase and MnSOD activities were determined as described in Methods section ($n = 4$ for each enzyme, $^{\#}P < 0.05$ vs. control; $^{\$}P < 0.05$ vs. control). (*B*) BAEC were exposed to CsA (1 μM, 24 h), and MnSOD activity was determined ($n = 3$, $^{*}P < 0.05$). (*C*) Effect of Tiron on the prevention of CsA-associated inhibition of MnSOD activity. BAEC were exposed to Tiron (1 mM, 30 min pre-incubation), and then treated as described in (*A*) ($n = 3$, $^{\#}P < 0.05$ vs. control). (*D*) Effect of uric acid (160 μM) on the prevention of CsA-associated inhibition of MnSOD activity. BAEC were treated with CsA (10 μM, 2 h) alone or in the presence of uric acid (160 μM), and then MnSOD activity was determined as described in Methods section ($n = 3$, $^{\#}P < 0.05$ vs. control, $^{\$}P < 0.05$ vs. treatment with CsA).

MnSOD (see Supplementary material online, *Figure S6*). Finally, the same approach was followed to analyse this modification in endothelial cells treated with CsA. For this purpose, whole protein extracts from BAEC infected with adenoviral constructs bearing MnSOD were used to perform the same analysis. These infections did not modify the capacity of CsA to induce protein nitration (see Supplementary material online, *Figure S7*). As shown in *Figure 5B*, the chromatogram trace of specific fragment ions revealed that the modified peptide was present at a negligible proportion in the extracts from vehicle-treated cells. In clear contrast, when the cells were treated with CsA, the intensity of the non-modified peptide decreased (*Figure 5A*), whereas that of the modified peptide increased (*Figure 5B*). The MS/MS and MS^3 fragment spectra obtained at the elution times of these peaks demonstrated unequivocally the sequence of the peptide and the presence of a modification by 45 Da in Tyr34 (*Figure 5C* and *D*), consistent with Tyr-nitration at this site. Altogether, these data provide strong evidence suggesting that CsA is able to promote MnSOD nitration in endothelial cells precisely at the residue which is essential for a correct catalytic activation of the enzyme, hence identifying a specific biochemical target for CsA induced endothelial toxicity.

4. Discussion

This study provides molecular insight into the mechanism of endothelial toxicity associated to CsA. Data presented here strongly support that superoxide production is mainly of mitochondrial origin and that CsA causes a change in membrane potential that leads to a decrease in the respiratory rate and increased ROS generation. This results in a functional inactivation of the mitochondrial enzymes aconitase and MnSOD. Finally, tyrosine nitration of MnSOD by CsA is assigned to a specific residue (Tyr34) which is essential for its catalytic function on superoxide elimination.

The association between CsA treatment and increased oxidative stress has been accepted for several years based not only on experimental data but also on clinical observations. In fact, CsA induced

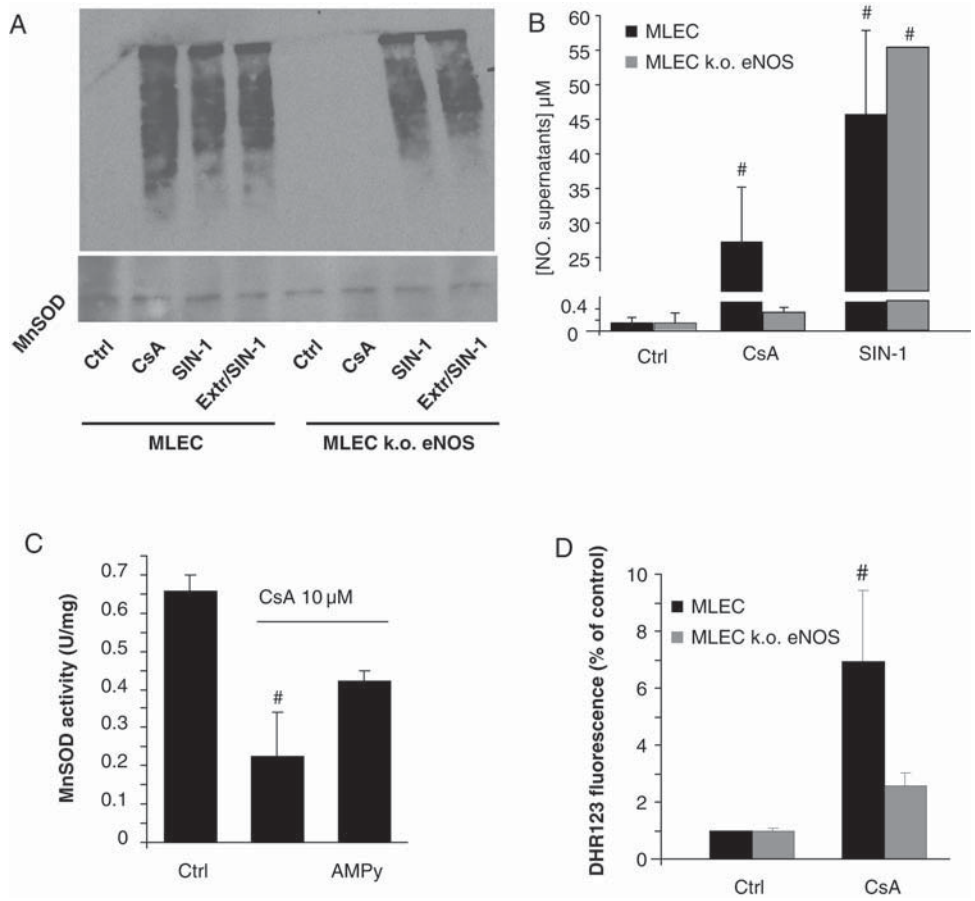

Figure 4 The eNOS pathway is necessary for CsA-dependent nitration and peroxynitrite formation. (*A*) MLEC wild-type and knockout (KO) for eNOS were exposed to CsA (10 μM, 2 h) or the generator of peroxynitrite SIN-1 (100 μM, 2 h), and protein lysates were processed as described in Methods section. Control cellular extracts were exogenously treated with the same concentration of SIN-1 for 1 h (extr/SIN-1). Tyrosine nitration was evaluated by immunoblot. (*B*) NO_2^- accumulation was determined with a selective NO electrode in supernatants of MLEC exposed to CsA or SIN-1, in the conditions described above ($n = 3$, $^{\#}P < 0.05$ vs. control). (*C*) BAEC were treated with CsA (10 μM, 2 h) alone or in the presence of AMPy (100 μM), and then MnSOD activity was determined as described in Methods section ($n = 3$, $^{\#}P < 0.05$ vs. control). (*D*) Peroxynitrite formation in MLEC (wild-type or KO) was evaluated by flow cytometry using DHR123 fluorescence ($n = 3$, $^{\#}P < 0.05$ vs. control).

hypertension is related to increased ROS production.[35] We and others have provided evidence for the presence of nitroxidative stress in cells from the vascular wall.[5,15,36] Data herein presented demonstrate unequivocally by using ESR and fluorescent probes that endothelial cells generate ROS under exposure to CsA. Although it is possible that hydroxyl radical could account for the characteristic ESR signal, abrogation by Tiron and overwhelming evidence on the production of superoxide by mitochondria make this scenario unlikely. Few studies have addressed the issue of the source of ROS in endothelial cells. This work clearly shows that endothelial mitochondria are potential generators of superoxide anion in the presence of CsA (*Figure 1B*). The general nicotinamide adenine dinucleotide phosphate oxidase inhibitor, apocynin, did not result in an inhibition of superoxide production, thus excluding NADPH oxidase as a fundamental source of CsA induced oxidative stress in BAEC. However, the fact that cytosolic aconitase is also partially inhibited by CsA does not completely exclude the possibility of other superoxide sources aside from mitochondria. Besides, results obtained in cells with the absence of functional mitochondria revealed that these organelles are critical for CsA-associated production of superoxide. However, other authors have found that other endothelial cell types may behave differently in response to CsA.[37] In addition, uncoupling of eNOS has also been suggested as a mechanism for CsA induced superoxide generation in animal models.[38] In our study, the presence of eNOS was clearly necessary for the generation of peroxynitrite and induction of nitration (*Figure 4*), thus suggesting that this mechanism could also be contributing to superoxide generation.

The effects of CsA on mitochondrial function need to be interpreted in the context of established actions of this drug on the mitochondrial permeability transition pore (PTP). Among CsA direct actions, binding to cyclophilin D in the mitochondrial matrix leads to the inhibition of the PTP. PTP opens under a variety of conditions related to mitochondrial dysfunction like ROS-induced damage, an elevation of mitochondrial calcium and phosphate, depletion of pyridine nucleotides, or high levels of fatty acids. Prolonged PTP opening leads to matrix swelling and disruption of the outer membrane with the concomitant release of pro-apoptotic factors. The inhibition of PTP opening by CsA can be used to increase the cell viability and prevent, for example, cell death after ischaemia–

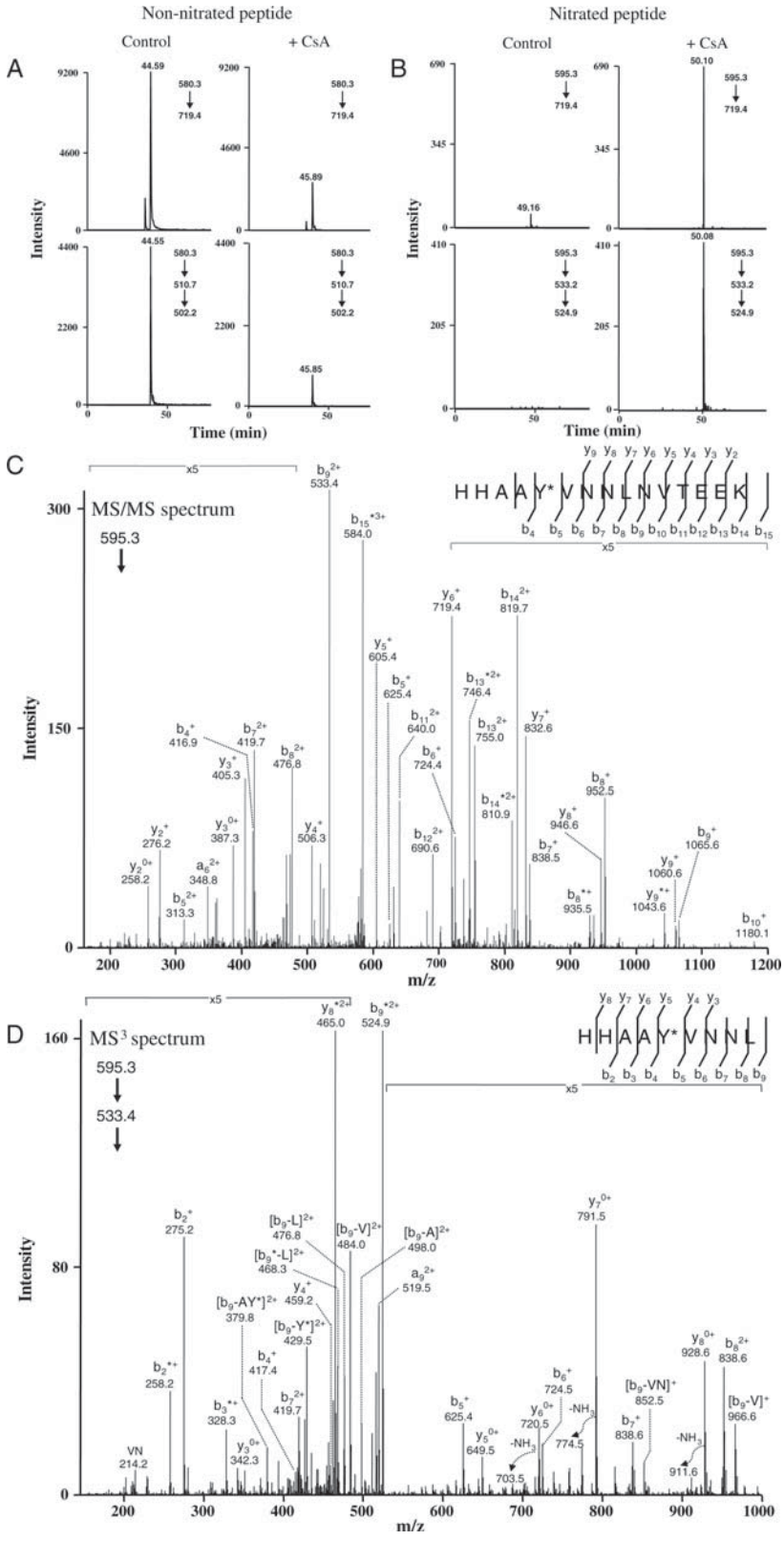

Figure 5 Cyclosporine A induces nitration of Tyr34 in MnSOD. Identification of the MnSOD peptide HHAAYVNNLNVTEEK nitrated at Tyr34 (*A*, *B*) MS/MS (upper panels) and MS^3 (lower panels) traces from selected peptide fragments corresponding to the non-nitrated (*A*) and the nitrated peptide (*B*) from protein extracts from BAEC infected with adenoviral constructs bearing human MnSOD and treated with either vehicle (control) or CsA. The upper panels correspond to the trace of fragment y_6^+ and the lower panels to the trace of subfragment b_9^{*2+} originated from fragment b_9^{2+}. (*C* and *D*) MS/MS and MS^3 spectra of the peptide species at the elution times of peaks detected in (*B*). The MS^3 spectrum in (*D*) was obtained from the doubly charged ion b_9^{2+} detected in (*C*). Fragments corresponding to the loss of internal amino acids from *b* ions are indicated with the same nomenclature used previously.[53] Note that fragments of this kind are observed with some frequency upon refragmentation and their formation is thought to arise from cyclation of intense *b* ions.[53] Spectra correspond to a representative experiment repeated twice.

reperfusion.[39] However, electrophysiological studies have shown that the PTP can also open transiently (in the millisecond range) and this channel activity is referred to as 'conductance flickerings'.[40] These transient openings are also CsA sensitive and probably related to fluctuations in physiological parameters such as matrix pH or to physiological activities like protein import or fast calcium release. The flickering of the PTP is therefore a physiological event that does not necessarily lead to the dramatic effects due to the permanent opening of the PTP.[41] We have observed a CsA induced increase in $\Delta\Psi$m that could be due to the inhibition of the flickering of the pore (*Figure 2A*). The observed decrease in respiration (*Figure 2B*) would also be a consequence of the increased efficiency of the oxidative phosphorylation and higher $\Delta\Psi$m.

The effect of the two modes of PTP opening would have different consequences on the mitochondrial production of superoxide. It has been reported that prolonged opening of the PTP is associated with increased levels of H_2O_2 in mitochondria due to a specific conformational change in complex I.[42] The loss of cytochrome c, due to the rupture of the outer mitochondrial membrane, has also been considered a cause of both the inhibition of respiration and the concomitant increase in ROS production due to the opening of the PTP.[43,44] However, recent studies in cardiomyocytes subjected to ischaemia–reperfusion have shown that the production of ROS increase when the PTP is inhibited by CsA,[45] in keeping with data presented here. We believe that the marked increase in DHE fluorescence that we have observed in the presence of CsA is consistent with a possible non-permanent inhibition of the PTP.

MnSOD (SOD-2) is a mitochondrial enzyme considered to be essential as a first-line superoxide detoxifier. In the vascular wall, this enzyme has been shown to play a crucial role in vascular protection.[46] MnSOD converts superoxide into hydrogen peroxide plus molecular oxygen. This conversion has several purposes including the protection of $^{\bullet}$NO and mitochondrial proteins such as aconitase or fumarase from inactivation by superoxide.[46] The Mn atom is essential for redox cycling and the Tyr34 residue lies in close proximity to this atom and hence to the active site.[47] Nitration of this residue was demonstrated more than 10 years ago and it is widely accepted that this modification involves enzymatic inactivation.[8] Moreover, peroxynitrite is the only known biological oxidant competent to inactivate MnSOD enzymatic activity.[47] Several studies have highlighted the pathophysiological importance of MnSOD nitration in a panoply of disease models, including chronic renal allograft rejection,[16] traumatic brain injury,[48] ageing,[49] and angiotensin II-induced hypertension.[50] We now provide evidence for the functional inactivation of MnSOD by CsA together with a repercussion on the function of an exquisitely sensitive enzyme to superoxide, aconitase (*Figure 3*). Also, and for the first time to our knowledge, we show that CsA induced nitration of MnSOD takes place precisely at Tyr34, thus offering a biochemical explanation for MnSOD inactivation (*Figure 5*). Furthermore, the protection from MnSOD inactivation by treatment of the cells with uric acid, a well known anti-nitrating compound via scavenging of peroxynitrite-derived radicals,[51,52] further supports a direct link between CsA toxicity and mitochondrial nitroxidative stress. Although we attempted to quantitate the amount of nitration of MnSOD, experiments using an antibody specifically directed against nitrated MnSOD (nY-34)[49] were inconclusive (data not shown). Nitration of Tyr34 in MnSOD can lead to a fully inactivated enzyme;[19] the fact that we only observed about 40% inhibition of MnSOD in the presence of CsA supports that only a fraction of the total MnSOD pool becomes nitrated in the critical tyrosine upon CsA exposure. Indeed, fractional MnSOD nitration/inactivation under cellular conditions will depend on both the overall production of peroxynitrite over the incubation period and the competing reactions with other targets and detoxification systems. Given these considerations, one can conclude that peroxynitrite formation in the system under study was large, as it significantly dropped the activity of MnSOD, typically present at 10–20 μM concentrations in mitochondria.[29] In addition, experiments performed in BAEC infected with adenoviral constructs bearing a MnSOD expression plasmid strongly suggest that CsA induced Tyr34 nitration is operative in endothelial cells. Of interest, the concentrations of CsA used in this study (1–10 μM) are slightly above the high limit of the therapeutic range of concentrations found in renal transplant patients treated with these agents, and hence expected to be found in the context of vascular toxicity. Thus, it is tempting to speculate that a reduced catalytic activity of endothelial MnSOD would contribute to amplify nitroxidative stress and to promote the self-perpetuation of endothelial damage.

Supplementary material

Supplementary Material is available at *Cardiovascular Research online*.

Acknowledgements

Please see Supplementary material online.

Conflict of interest: none declared.

Funding

This work was supported by grants [SAF 2006-02410] and Consolider [CSD-2007-0020]. Network of Excellence for the Research on Oxidative Stress in Spain, Reactive Oxygen Species and Systems (ROSAS) from Plan Nacional de I + D + I; CARDIOVREP from Comunidad de Madrid; an Accion Integrada [2007UY0018 CSIC], Spain- Universidad de la Republica, Uruguay; a grant from the Sociedad Española de Nefrología and Fundación Renal Iñigo Alvarez de Toledo to S.L.; a 'Miguel Servet' grant [CP07/00143] from Instituto de Salud Carlos III (Spain) to A.M.-R.; a grant from Fundación de Investigación Médica Mutua Madrileña to F.R.-P.; by grants [BIO2006-10085, GR/SAL/0141/2004 (CAM), CAM BIO/0194/2006], from the Fondo de Investigaciones Sanitarias (Ministerio de Sanidad y Consumo, Instituto Salud Carlos III, RECAVA) and by an institutional grant by Fundación Ramón Areces to CBMSO to J.V. N.R. received grant support from Fondo Clemente Estable/Agencia Nacional de Investigación e Innovación-Uruguay and R.R. from the Howard Hughes Medical Institute and the International Centre for Genetic Engineering and Biotechnology.

References

1. Flanagan WM, Corthésy B, Bram RJ, Crabtree GR. Nuclear association of a T-cell transcription factor blocked by FK-506 and cyclosporin A. *Nature* 1991;**352**:803–807.
2. Liu J, Farmer JD Jr, Lane WS, Friedman J, Weissman I, Schreiber SL. Calcineurin is a common target of cyclophilin–cyclosporin A and FKBP–FK506 complexes. *Cell* 1991;**66**:807–815.
3. Miller LW. Cardiovascular toxicities of immunosuppressive agents. *Am J Transplant* 2002;**2**:807–818.
4. Lamas S. Cellular mechanisms of vascular injury mediated by calcineurin inhibitors. *Kidney Int* 2005;**68**:898–907.
5. Ramzy D, Rao V, Tumiati LC, Xu N, Miriuka S, Delgado D *et al*. Role of endothelin-1 and nitric oxide bioavailability in transplant-related vascular injury: comparative effects of rapamycin and cyclosporine. *Circulation* 2006;**114**:I214–I219.
6. D'Autreaux B, Toledano MB. ROS as signalling molecules: mechanisms that generate specificity in ROS homeostasis. *Nat Rev Mol Cell Biol* 2007;**8**:813–824.

7. Lancaster JR Jr. Nitroxidative, nitrosative, and nitrative stress: kinetic predictions of reactive nitrogen species chemistry under biological conditions. *Chem Res Toxicol* 2006;**19**:1160–1174.
8. Peluffo G, Radi R. Biochemistry of protein tyrosine nitration in cardiovascular pathology. *Cardiovasc Res* 2007;**75**:291–302.
9. Roullet JB, Xue H, McCarron DA, Holcomb S, Bennett WM. Vascular mechanisms of cyclosporin-induced hypertension in the rat. *J Clin Invest* 1994;**93**:2244–2250. Issn: 0021-9738.
10. Diederich D, Yang Z, Lüscher TF. Chronic cyclosporine therapy impairs endothelium-dependent relaxation in the renal artery of the rat. *J Am Soc Nephrol* 1992;**2**: 1291–1297.
11. Morris ST, McMurray JJ, Rodger RS, Farmer R, Jardine AG. Endothelial dysfunction in renal transplant recipients maintained on cyclosporine. *Kidney Int* 2000;**57**: 1100–1106.
12. Navarro-Antolín J, López-Muñoz MJ, Klatt P, Soria J, Michel T, Lamas S. Formation of peroxynitrite in vascular endothelial cells exposed to cyclosporine A. *FASEB J* 2001; **15**:1291–1293.
13. Ovuworie CA, Fox ER, Chow CM, Pascual M, Shih VE, Picard MH *et al*. Vascular endothelial function in cyclosporine and tacrolimus treated renal transplant recipients. *Transplantation* 2001;**72**:1385–1388.
14. Zhang DX, Gutterman DD. Mitochondrial reactive oxygen species-mediated signaling in endothelial cells. *Am J Physiol Heart Circ Physiol* 2007;**292**:H2023–H2031.
15. Navarro-Antolín J, Redondo-Horcajo M, Zaragoza C, Alvarez-Barrientos A, Fernández AP, León-Gómez E *et al*. Role of peroxynitrite in endothelial damage mediated by Cyclosporine A. *Free Radic Biol Med* 2007;**42**:394–403.
16. MacMillan-Crow LA, Crow JP, Kerby JD, Beckman JS, Thompson JA. Nitration and inactivation of manganese superoxide dismutase in chronic rejection of human renal allografts. *Proc Natl Acad Sci USA* 1996;**93**:11853–11858.
17. MacMillan-Crow LA, Crow JP, Thompson JA. Peroxynitrite-mediated inactivation of manganese superoxide dismutase involves nitration and oxidation of critical tyrosine residues. *Biochemistry* 1998;**37**:1613–1622.
18. Yamakura F, Taka H, Fujimura T, Murayama K. Inactivation of human manganese-superoxide dismutase by peroxynitrite is caused by exclusive nitration of tyrosine 34 to 3-nitrotyrosine. *J Biol Chem* 1998;**273**:14085–14089.
19. Quijano C, Hernandez-Saavedra D, Castro L, McCord JM, Freeman BA, Radi R. Reaction of peroxynitrite with Mn-superoxide dismutase. Role of the metal center in decomposition kinetics and nitration. *J Biol Chem* 2001;**276**:11631–11638.
20. López-Ongil S, Saura M, Rodríguez-Puyol D, Rodríguez-Puyol M, Lamas S. Regulation of endothelial NO synthase expression by cyclosporin A in bovine aortic endothelial cells. *Am J Physiol* 1996;**271**:H1072–H1078.
21. Genis L, Gonzalo P, Tutor AS, Galvez BG, Martinez-Ruiz A, Zaragoza C *et al*. Functional interplay between endothelial nitric oxide synthase and membrane type 1 matrix metalloproteinase in migrating endothelial cells. *Blood* 2007;**110**:2916–2923.
22. Gardner PR. Aconitase: sensitive target and measure of superoxide. *Methods Enzymol* 2002;**349**:9–23.
23. Flohe L, Otting F. Superoxide dismutase assays. *Methods Enzymol* 1984;**105**:93–104.
24. Villar M, Ortega-Pérez I, Were F, Cano E, Redondo JM, Vázquez J. Systematic characterization of phosphorylation sites in NFATc2 by linear ion trap mass spectrometry. *Proteomics* 2006;**6** (Suppl. 1):S16–S27.
25. Ledenev AN, Konstantinov AA, Popova E, Ruuge EK. A simple assay of the superoxide generation rate with Tiron as an EPR-visible radical scavenger. *Biochem Int* 1986; **13**:391–396.
26. Mukhopadhyay P, Rajesh M, Yoshihiro K, Hasko G, Pacher P. Simple quantitative detection of mitochondrial superoxide production in live cells. *Biochem Biophys Res Commun* 2007;**358**:203–208.
27. Adam-Vizi V, Chinopoulos C. Bioenergetics and the formation of mitochondrial reactive oxygen species. *Trends Pharmacol Sci* 2006;**27**:639–645.
28. Navarro-Antolín J, López-Muñoz MJ, Soria J, Lamas S. Superoxide limits cyclosporine-A-induced formation of peroxynitrite in endothelial cells(2). *Free Radic Biol Med* 2002;**32**:702–711.
29. Quijano C, Castro L, Peluffo G, Vález V, Radi R. Enhanced mitochondrial superoxide in hyperglycemic endothelial cells: direct measurements and formation of hydrogen peroxide and peroxynitrite. *Am J Physiol Heart Circ Physiol* 2007;**293**:H3404–H3414.
30. Teng RJ, Ye YZ, Parks DA, Beckman JS. Urate produced during hypoxia protects heart proteins from peroxynitrite-mediated protein nitration. *Free Radic Biol Med* 2002;**33**: 1243–1249.
31. Quijano C, Romero N, Radi R. Tyrosine nitration by superoxide and nitric oxide fluxes in biological systems: modeling the impact of superoxide dismutase and nitric oxide diffusion. *Free Radic Biol Med* 2005;**39**:728–741.
32. Radi R. Nitric oxide, oxidants, and protein tyrosine nitration. *Proc Natl Acad Sci USA* 2004;**101**:4003–4008.
33. Jorge I, Casas EM, Villar M, Ortega-Pérez I, López-Ferrer D, Martínez-Ruiz A *et al*. High-sensitivity analysis of specific peptides in complex samples by selected MS/MS ion monitoring and linear ion trap mass spectrometry: application to biological studies. *J Mass Spectrom* 2007;**42**:1391–1403.
34. Martínez-Ruiz A, Villanueva L, González de Orduña C, López-Ferrer D, Higueras MA, Tarín C *et al*. S-nitrosylation of Hsp90 promotes the inhibition of its ATPase and endothelial nitric oxide synthase regulatory activities. *Proc Natl Acad Sci USA* 2005; **102**:8525–8530.
35. Calo LA, Davis PA, Giacon B, Pagnin E, Sartori M, Riegler P *et al*. Oxidative stress in kidney transplant patients with calcineurin inhibitor-induced hypertension: effect of ramipril. *J Cardiovasc Pharmacol* 2002;**40**:625–631.
36. Krauskopf A, Lhote P, Petermann O, Ruegg UT, Buetler TM. Cyclosporin A generates superoxide in smooth muscle cells. *Free Radic Res* 2005;**39**:913–919.
37. Krotz F, Keller M, Derflinger S, Schmid H, Gloe T, Bassermann F *et al*. Mycophenolate acid inhibits endothelial NAD(P)H oxidase activity and superoxide formation by a Rac1-dependent mechanism. *Hypertension* 2007;**49**:201–208.
38. Reis F, Rocha-Pereira P, Teixeira de Lemos E, Parada B, Baptista S, Figueiredo A *et al*. Oxidative stress in cyclosporine-induced hypertension: evidence of beneficial effects or tolerance development with nitrate therapy. *Transplant Proc* 2007;**39**: 2494–2500.
39. Bernardi P, Krauskopf A, Basso E, Petronilli V, Blachly-Dyson E, Di Lisa F *et al*. The mitochondrial permeability transition from *in vitro* artifact to disease target. *FEBS J* 2006;**273**:2077–2099.
40. Szabo I, Zoratti M. The giant channel of the inner mitochondrial membrane is inhibited by cyclosporin A. *J Biol Chem* 1991;**266**:3376–3379.
41. Rasola A, Bernardi P. The mitochondrial permeability transition pore and its involvement in cell death and in disease pathogenesis. *Apoptosis* 2007;**12**:815–833.
42. Batandier C, Leverve X, Fontaine E. Opening of the mitochondrial permeability transition pore induces reactive oxygen species production at the level of the respiratory chain complex I. *J Biol Chem* 2004;**279**:17197–17204.
43. Kroemer G, Galluzzi L, Brenner C. Mitochondrial membrane permeabilization in cell death. *Physiol Rev* 2007;**87**:99–163.
44. Zorov DB, Filburn CR, Klotz LO, Zweier JL, Sollott SJ. Reactive oxygen species (ROS)-induced ROS release: a new phenomenon accompanying induction of the mitochondrial permeability transition in cardiac myocytes. *J Exp Med* 2000;**192**:1001–1014.
45. West MB, Rokosh G, Obal D, Velayutham M, Xuan YT, Hill BG *et al*. Cardiac myocyte-specific expression of inducible nitric oxide synthase protects against ischemia/reperfusion injury by preventing mitochondrial permeability transition. *Circulation* 2008;**118**:1970–1978.
46. Faraci FM, Didion SP. Vascular protection: superoxide dismutase isoforms in the vessel wall. *Arterioscler Thromb Vasc Biol* 2004;**24**:1367–1373.
47. MacMillan-Crow LA, Thompson JA. Tyrosine modifications and inactivation of active site manganese superoxide dismutase mutant (Y34F) by peroxynitrite. *Arch Biochem Biophys* 1999;**366**:82–88.
48. Bayir H, Kagan VE, Clark RS, Janesko-Feldman K, Rafikov R, Huang Z *et al*. Neuronal NOS-mediated nitration and inactivation of manganese superoxide dismutase in brain after experimental and human brain injury. *J Neurochem* 2007;**101**:168–181.
49. Xu S, Ying J, Jiang B, Guo W, Adachi T, Sharov V *et al*. Detection of sequence-specific tyrosine nitration of manganese SOD and SERCA in cardiovascular disease and aging. *Am J Physiol Heart Circ Physiol* 2006;**290**:H2220–H2227.
50. Guo W, Adachi T, Matsui R, Xu S, Jiang B, Zou MH *et al*. Quantitative assessment of tyrosine nitration of manganese superoxide dismutase in angiotensin II-infused rat kidney. *Am J Physiol Heart Circ Physiol* 2003;**285**:H1396–H1403.
51. Squadrito GL, Cueto R, Splenser AE, Valavanidis A, Zhang H, Uppu RM *et al*. Reaction of uric acid with peroxynitrite and implications for the mechanism of neuroprotection by uric acid. *Arch Biochem Biophys* 2000;**376**:333–337.
52. Ferrer-Sueta G, Radi R. Chemical biology of peroxynitrite: kinetics, diffusion, and radicals. *ACS Chem Biol* 2009;**4**:161–177.
53. Yagüe J, Paradela A, Ramos M, Ogueta S, Marina A, Barahona F *et al*. Peptide rearrangement during quadrupole ion trap fragmentation: added complexity to MS/MS spectra. *Anal Chem* 2003;**75**:1524–1535.

Materials and Methods

Materials. CsA was a gift from Dr. D. Rodríguez-Puyol (Hospital Príncipe de Asturias, Alcalá de Henares, Madrid, Spain). Dihydroethidium (also named hydroethidine) (DHE), acetylated-low-density lipoprotein (diI-Ac-LDL), Dihydrorhodamine 123 (DHR 123), Mitosox and Mitotracker were from Molecular Probes (Eugene, OR); 2,3-Dimethoxy-1,4-naphthoquinone (DMNQ) was from Calbiochem (San Diego, CA); N-Acetylcysteine, uridin, sodium pyruvate, apocynin, rotenone, antimycin-A, myxothiazol, uric acid and all other reagents were from Sigma-Aldrich (St. Louis, MO). Purified MnSOD protein was from Jena Bioscience (Jena, Germany). The spin trap DMPO was from Dojindo (Kumamoto, Japan). Mn SOD antibody was from Stressgen Bioreagents (Victoria, BC). Nitrotyrosine antibody was from Millipore (MA). Cell culture mediums were from Invitrogen (Carlsbad, CA). Decyl Analogue of coenzyme Q DBH2 (2,3 –dimethoxy-5-methyl-6-n-decyl-1,4 benzoquinone) was a gift from Dr. D Rafael Garesse (Instituto Investigaciones Biomédicas, Madrid, Spain). Amino methyl piridine (AMPy), Iron (III) tetrakis (N-methyl-4´-pyridil) porphyrin and 1,3-morpholino sydnonimine (SIN-1) was from Alexis (Farmingdale, NY).

Bovine Aortic Endothelial Cell Culture and preparation of Mitochondrial DNA-depleted BAEC (rho0) cells. To prepare rho0, BAEC cells were exposed continuously to 5μg/ml of ethidium bromide in a rho0-permissive medium consisting of RPMI, 10% FBS, 1% Penicillin/Streptomycin, 50 μg/ml uridine, and 0.11g/l sodium pyruvate, for 7-10 weeks, until the complete absence of endogenous mtDNA was demonstrated. The amount of mtDNA was monitored periodically by Real Time PCR using specific mtDNA sequences. The test sequences were as follows: a) a fragment in the bovine mtDNA D-loop spanning nucleotides 16020-16040

and 16161-16137; b) a fragment in the bovine nuclear SDH spanning nucleotides 102725-102744 and 102848-102868). The rho0 status was confirmed by the inability of the cells to grow in absence of uridine. The endothelial phenotype of rho0 cells was confirmed by flow cytometry using a fluorescently labelled acetylated-low-density lipoprotein (diI-Ac-LDL). Medium was routinely changed twice a week and on the previous day of the experiments.

Mouse Lung Endothelial Cells preparation. Lungs from C57BL/6 wild type and knock out for endothelial nitric oxide sinthase (eNOS) were used at passages 2–4. eNOS $^{-/-}$ and eNOS$^{+/+}$ C57BL6 mice were purchased from Jackson Laboratories (Bar Harbor, ME, USA). Mice were provided by our animal facility and prepared as described [1]. All protocols used conform to the Guide for the Care and Use of Laboratory Animals published by the U.S. National Institutes of Health (NIH publication No. 85-23). eNOS expression was checked in MLECs from different genotypes by Western Blot.

Flow cytometry. 80% confluent BAEC or BAEC rho0 cells were incubated in serum-free RPMI without phenol red for 2.5 h, unless otherwise indicated. Where indicated, at t = 0, inhibitors (apocynin, rotenone, antimycin-A, myxothiazol) were added. At t = 30 minutes, inhibitors were discarded and CsA (10 μM) or its vehicle (0.01% ethanol) were added. At t = 1.5 h, DMNQ (25 μM) was added. The last hour, a non-limiting concentration of the probe DHE (5 μM) was added. Controls for the specificity of this probe have been previously published [2]. An EPICS XL analyzer was used to quantify fluorescence at the single-cell level. The excitation wavelength was 488 nm and the emission wavelength filter was 625 nm (red fluorescence). Data are expressed as percentage of signal related to the control. In the case of DHR123 the concentration used was 2 μM and the excitation wavelength was 510 nm and the emission wavelength filter was 540 nm. For the measurement of mitochondrial membrane potential ($\Delta\Psi m$), BAEC were incubated with CsA or the mitochondrial uncoupling agent FCCP (carbonyl cyanide p-trifluoromethoxyphenyhydrazone; 25 or 50 μM) for 30 min, and then

$DiOC_6$ {3} probe (3,3′-dihexyloxacarbocyanine iodide, 1 nM final concentration) was added. In this case, data are expressed as a percentage of uncoupling under control conditions. For the characterization of rho0 BAEC, cells were incubated with Alexa Fluor 488 Ac-LDL for 1 h. All incubations were done in the dark.

MitoSOX-Red fluorescence and confocal microscopy: BAEC were prepared as described above with the exception that they were grown on cover slides in 24-well-plates. Where indicated, at t = 0, N-acetyl-cysteine (NAC) was added. At t = 30 minutes, NAC was discarded and CsA or its vehicle (0.01% ethanol) were added. At t = 1.5 h, DMNQ was added. After treatment, cells were washed with RPMI medium and incubated with 3 µM MitoSOX-Red for 10 min, washed with PBS and then fixed with 3.5% paraformaldehyde and visualized by confocal microscopy. Images were collected with a Leica TCS SP2 AOBS confocal microscope (Mannheim, Germany) with 20X and 63X oil immersion optics. Laser line at 561 nm for excitation of oxidized MitoSOX was provided by a DPSS laser. To co-localize oxidized MitoSOX and mitochondria, cells were incubated with MitoFluor green for 45 min (488 nm for excitation provided by an Ar laser) prior to incubation with MitoSOX. Detection ranges were set to eliminate crosstalk between fluorophores.

ESR experiments: BAEC were culture in 6-well plates as described before. The spin trap DMPO (5,5 dimethyl-1- pyrroline N-oxide) was added for the final 15 min of the treatment period, and kept at 37º C in the darkness. Forty µL of each supernatant were placed in 100 µL capillary tubes and ESR signals were detected in a Miniscope MS 200 Magnetech GmbH using the following instrumental conditions: 150 mG modulation amplitude**,** 10 mW microwave power, 5 receiver gain, 60s sweep time, 80G sweep width and 5 scans accumulation.

O_2 consumption. BAEC were trypsinized and resuspended in RPMI at a density of two million cells per ml. BAEC were incubated with oligomycin (2.0 mg/ml) for ATPase inhibition or CsA (10 µM) or its vehicle. Mitochondrial oxygen consumption was measured at 37°C using a

Clark-type oxygen electrode. Experiments were terminated with addition of the uncoupler FCCP (10 µM). There were no differences between basal and vehicle conditions.

Aconitase activity. To measure aconitase activity in subcellular fractions, cells were grown in 140-mm-diameter culture dishes in RPMI containing 10% Calf serum. After confluence, cells were treated with DMNQ, CsA or its vehicle, in free serum RPMI without phenol red as described above and then collected and processed for subcellular fractionation as previously described [3]. After processing, aconitase activity in the mitochondrial and cytosolic fractions was immediately determined spectrophotometrically using the coupled assay with porcine heart isocitrate dehydrogenase, as described [4]. Purity of the subcellular fractions was evaluated by immunoblot using an anti-Mn SOD antibody. Spectrophotometric studies were simultaneously done using a Ultrospec 4000 UV/Visible Spectrophotometer (Pharmacia Biotech, UK).

Complex III activity. BAEC were treated with CsA (10 µM, 2h) or its vehicle and processed for subcellular fractionation as previously described [3]. The activity of mitochondrial respiratory chain complex III was determined spectrophotometrically (550 nm) from the antimycin-sensitive rate of reduction of cytochrome c using decyl ubiquinol (50 µM) as substrate, in the conditions described [5].

$^{\cdot}$NO determination: $^{\cdot}$NO released under CsA or SIN-1 treatments were measured in supernatants of BAEC or MLEC in 5 ml of activating solution (0,5 M H_2SO_4 + 0.1 M KI) in gas-tight vessels, gently agitated, and kept at room temperature using an $^{\cdot}$NO electrode (ISO-NOP; World Precision Instruments, Stevenage, Herts, UK). A media of three measures were done for each sample, at different volumes. The $^{\cdot}$NO electrode was also calibrated with $NaNO_2$ under the same reducing conditions (KI/H_2SO_4).

ATP measures: BAEC were incubated in 100-mm-diameter plates with CsA or its vehicle for 2 hours and whole lysates were collected. ATP measures were performed according to the

instructions of the manufacturer of the ATP Bioluminiscence Assay Kit HS II (&Roche, Mannheim, Germany). This kit is used for highly sentitive and quantitative determination of ATP using the ATP dependency of the light emitting luciferase catalyzed oxidation of luciferin for the measurement of low concentrations of ATP.

MnSOD activity. BAEC were prepared as described above for aconitase activity except that 100-mm-diameter plates were used and no subcellular fractionation was performed. MnSOD activity was determined in cellular lysates by measuring the inhibition of superoxide-dependent cytochrome *c* reduction generated by xanthine oxidase/xanthine in the presence of 3 mM potassium cyanide [6] in order to inhibit cytosolic Cu-Zn SOD.

Western blot analysis. Western blot analysis was performed as described[7].

MnSOD nitration. For recombinant human MnSOD nitration experiments, the protein was incubated with conditioned media from BAEC treated with CsA (10 μM, 2 h), its vehicle or nitrating buffer [8] and then processed as described [7]. For cellular MnSOD nitration experiments, BAEC cells were serum-deprived during 16 h and then infected with MnSOD adenoviral vector (Gene Transfer Vector Core, University of Iowa) at a multiplicity of infection (moi) of 100 over 2 h. Viruses were then washed-off and the cells were incubated with complete medium for 22 h. Finally, BAEC cells were treated with CsA (10 μM, 2 h) or its vehicle and protein extracts collected.

Mass spectrometry . To characterize the specific nitration of Tyr^{34} in MnSOD, the samples were separated by SDS-PAGE and the gel band corresponding to the expected molecular size of MnSOD was cut and subjected to trypsin digestion as described [9]. Digestion was stopped by the addition of 1 % TFA. Briefly, peptides were concentrated and desalted on an RP precolumn (0.32 x 30 mm, BioBasic-18, ThermoScientific) and on-line eluted on an analytical RP column (0.18 x 150 mm BioBasic-18, ThermoScientific), operating at 2 μl/min and using a 40-min gradient from 0% to 40% solvent B [solvent A: 0.1% formic acid (v/v), solvent B: 0.1% formic

acid (v/v), and 80% acetonitrile (v/v)]. The LTQ was programmed in the 'selected MS/MS ion monitoring' (SMIM) mode [10]. An *m/z* 400-1600 survey scan was firstly performed in order to check for the presence of digested peptides as well as peptide separation along the gradient. This survey scan is followed by a dependent MS/MS scan that fragments the most intense ions to make a general identification of the peptides present in the sample. Subsequent MS/MS spectra were programmed on the ion at *m/z* 580.3, corresponding to the triply-charged precursor ion of peptide HHAAYVNNLNVTEEK and on the ion at *m/z* 595.3, corresponding to the triply-charged precursor ion of the Tyr-nitrated form of the same peptide. Two additional MS^3 spectra were programmed on ions at *m/z* 510.7 and 533.20, produced from the fragmentation of the non-modified peptide and the nitrated one, respectively. The scan group was repeated twice per cycle.

Acknowledgments

We want to thank Dr. Javier Navarro-Antolín for all his previous contributions to this topic as a former lab member and Dr. Diego Rodríguez Puyol for supplying us with CsA. We also thank Dr. Pedro Lastres, Maria Teresa Seisdedos and Yolanda Olmos for their valuable assistance with flow-cytometry, confocal microscopy and amplification of adenoviruses, respectively. We are grateful to Dr. Richard Cohen and members of his laboratory and to all the members of our laboratory for helpful discussions. We are especially indebted to Maria Angeles Higueras and Oscar Busnadiego for the isolation and culture of MLEC used in this work.

References

[1] Genis L, Gonzalo P, Tutor AS, Galvez BG, Martinez-Ruiz A, Zaragoza C *et al.* Functional interplay between endothelial nitric oxide synthase and membrane type 1 matrix metalloproteinase in migrating endothelial cells. *Blood* 2007;**110**:2916-2923.

[2] Navarro-Antolín J, López-Muñoz MJ, Klatt P, Soria J, Michel T, Lamas S. Formation of peroxynitrite in vascular endothelial cells exposed to cyclosporine A. *Faseb J* 2001;**15**:1291-1293.

[3] Quijano C, Castro L, Peluffo G, Vález V, Radi R. Enhanced mitochondrial superoxide in hyperglycemic endothelial cells: direct measurements and formation of hydrogen peroxide and peroxynitrite. *Am J Physiol Heart Circ Physiol* 2007;**293**:H3404-3414.

[4] Gardner PR. Aconitase: sensitive target and measure of superoxide. *Methods Enzymol* 2002;**349**:9-23.

[5] Lisa C. Heather CAC, Daniel J. Stuckey, Simon Pope, Karl J. Morten, Emma E. Carter, lindsay M. Edwards, and Kieran Clarke. Critical role of complex III in the early metabolic changes following myocardial infarction. *Cardiovascular Research* 2010;**85**:127-136.

[6] Flohe L, Otting F. Superoxide dismutase assays. *Methods Enzymol* 1984;**105**:93-104.

[7] Navarro-Antolín J, Redondo-Horcajo M, Zaragoza C, Alvarez-Barrientos A, Fernández AP, León-Gómez E *et al.* Role of peroxynitrite in endothelial damage mediated by Cyclosporine A. *Free Radic Biol Med* 2007;**42**:394-403.

[8] Yamakura F, Taka H, Fujimura T, Murayama K. Inactivation of human manganese-superoxide dismutase by peroxynitrite is caused by exclusive nitration of tyrosine 34 to 3-nitrotyrosine. *J Biol Chem* 1998;**273**:14085-14089.

[9] Villar M, Ortega-Pérez I, Were F, Cano E, Redondo JM, Vázquez J. Systematic characterization of phosphorylation sites in NFATc2 by linear ion trap mass spectrometry. *Proteomics* 2006;**6 Suppl 1**:S16-27.

[10] Jorge I, Casas EM, Villar M, Ortega-Pérez I, López-Ferrer D, Martínez-Ruiz A *et al.* High-sensitivity analysis of specific peptides in complex samples by selected MS/MS ion monitoring and linear ion trap mass spectrometry: application to biological studies. *J Mass Spectrom* 2007;**42**:1391-1403.

Legends of supplementary figures

Supplementary Fig. 1: The superoxide generator DMNQ induces an ESR signal similar to that obtained after CsA treatment. BAEC were treated with CsA (10 µM, 2 h) or DMNQ (25 µM, 1 h) as indicated and ESR detection of superoxide anion was performed as described in Methods. The ESR "signature" 1:2:2:1 is depicted. A representative experiment from n=4 is shown.

Supplementary Fig 2: Superoxide-induced CsA is predominantly localized in mitochondria. Images show the overlap in brown of fluorescence of MitoSox Red and MitoFluor Green suggesting the mitochondrial origin of ROS after CsA or DMNQ treatment of BAEC, as described in Methods. A representative experiment from n=3 is shown.

Supplementary Fig. 3: Mitochondria-depleted rho0 BAEC cells do not respond with increased formation of DMNQ-derived superoxide. Native or mitochondrial-deficient BAEC (rho0) were exposed to the superoxide generator DMNQ (25 µM, 1 h) vs control. Superoxide production was evaluated by DHE fluorescence as described in Methods. (n=3, #: $p < 0.05$ vs control).

Supplementary Fig.4: A: Effect of CsA and oligomycin on membrane potential as determined with the $DiOC_6$ {3} probe. BAEC were treated with CsA (10 µM), oligomycin (2 mg/ml), or the protonophore FCCP as a control (n=4, #: $p < 0.05$ vs control). B: Effect of oligomycin on mitochondria superoxide generation. BAEC were treated as described above, and superoxide radical was detected by DHE probe (n=4, #: $p < 0.05$ vs control).

Supplementary Fig. 5: MnSOD localization in the mitochondrial fraction. Mitochondrial and cytosolic fractions of BAEC (5 µg) were analyzed by Western blot with an anti-MnSOD antibody. Rh MnSOD (0.5 µg) was loaded for control.

Supplementary Fig. 6: The conditioned medium from BAEC exposed to CsA (see Methods for details) is able to nitrate MnSOD at Tyr^{34}. Spectra correspond to a representative experiment repeated twice.

Supplementary Fig. 7: Effect of CsA- induced nitration on BAEC with and without infection of adenoviral constructs bearing MnSOD. BAEC were infected as described in materials and methods, treated with CsA and whole lysates analyzed by Western Blot. Three infections for CsA and two for control are shown. CsA is able to induce apparently the same nitration pattern also in cells overexpressing MnSOD. A representative experiment of two is shown.

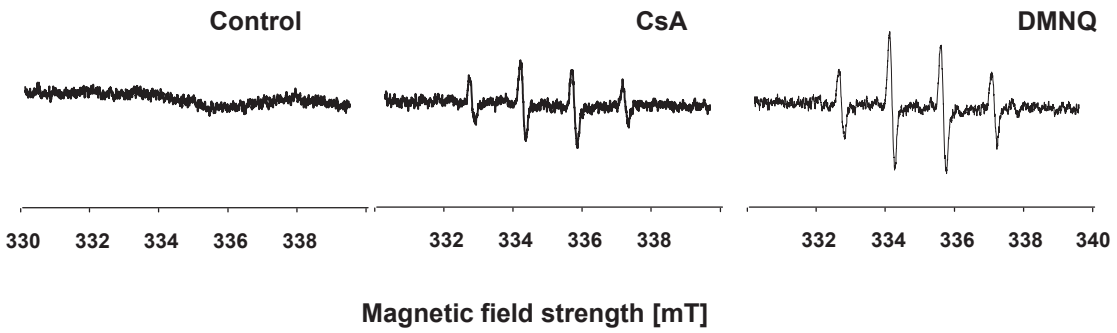

Supplementary Figure 1

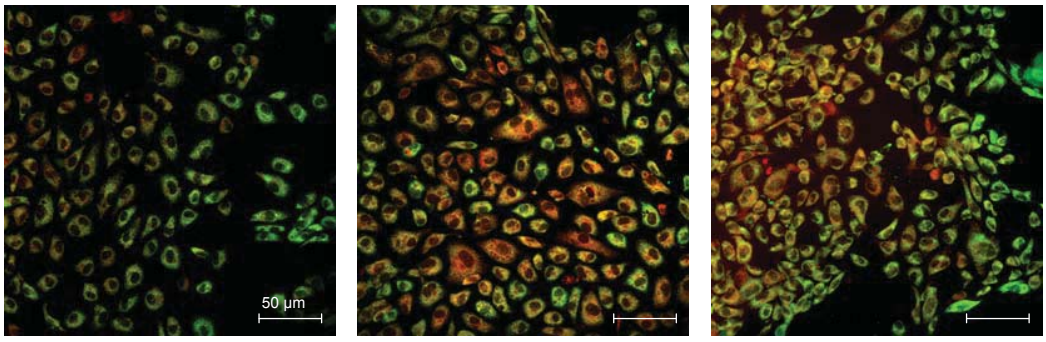

Control **CsA 1 µM** **DMNQ 25 µM**

Supplementary Figure 2

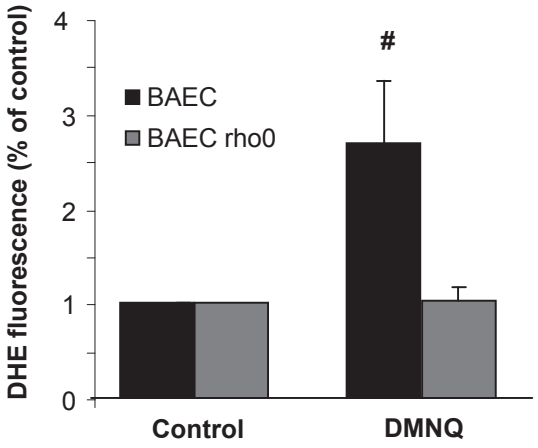

Supplementary Figure 3

A

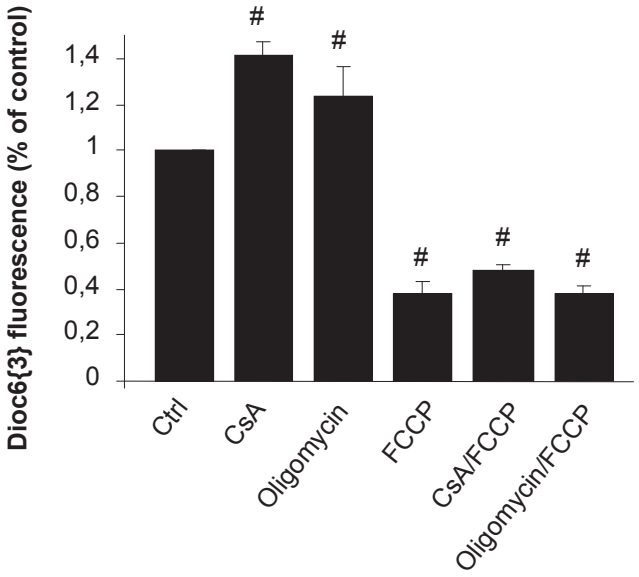

B

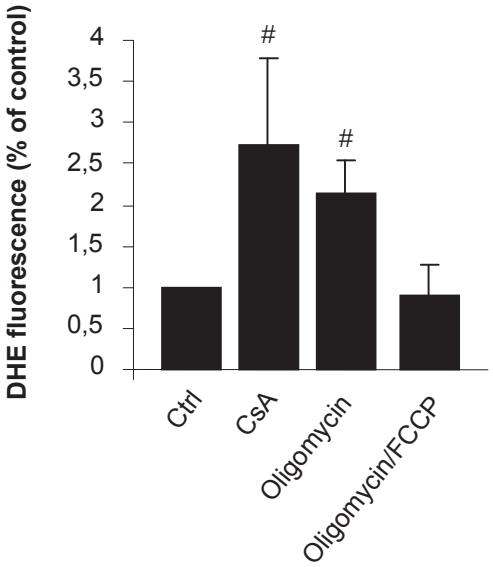

Supplementary Figure 4

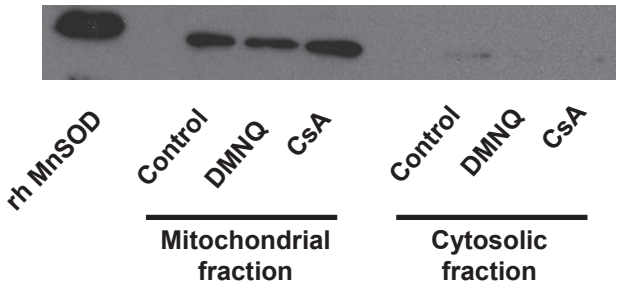

Supplementary Figure 5

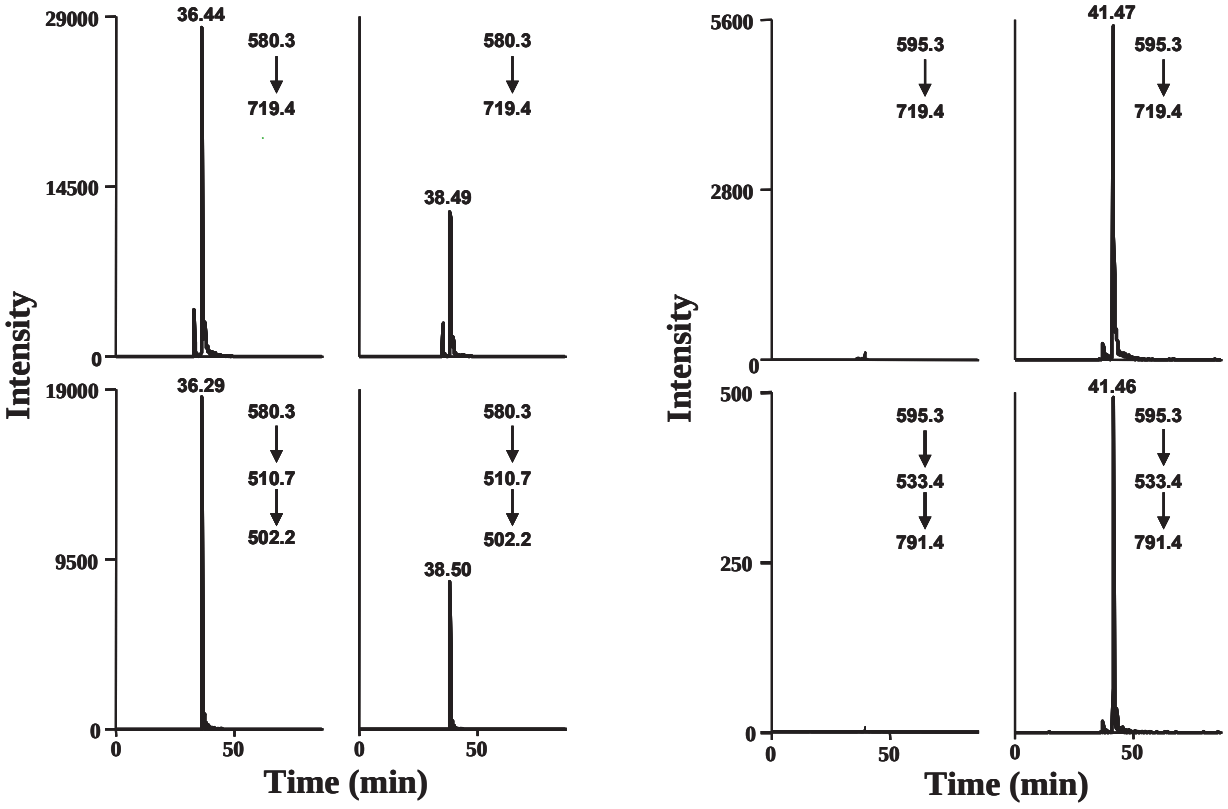

Supplementary Figure 6

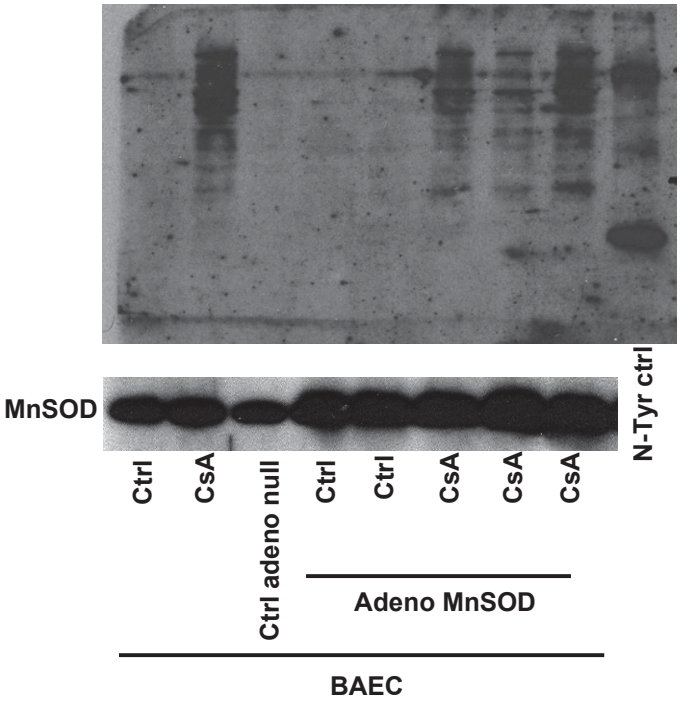

Supplementary Figure 7